R77AEG229

NASA CR-135117

QUIET CLEAN SHORT-HAUL EXPERIMENTAL ENGINE

(QCSEE)

Acoustic Performance of a 50.8-cm (20-inch) Diameter Variable-Pitch Fan and Inlet, Test Results and Analysis

Volume I

by

K.R. Bilwakesh
A. Clemons
D.L. Stimpert

RAL ELECTRIC COMPANY

APRIL 1979

Prepared For

utics and Space Administration

NASA-Lewis Research Center
Contract NAS3-18021

1. Report No.	2. Government Accession No.	3. Recipient's Catalog No.
CR 135117		

4. Title and Subtitle	5. Report Date
QUIET CLEAN SHORT-HAUL EXPERIMENTAL ENGINE (QCSEE). Acoustic Performance of a 50.8-cm (20-inch) Diameter Variable Pitch Fan and Inlet, Test Results and Analysis, Volume I.	April 1979
	6. Performing Organization Code
7. Author(s)	8. Performing Organization Report No.
K.R. Bilwakesh, A. Clemons, D.L. Stimpert	R77AEG229
	10. Work Unit No.
9. Performing Organization Name and Address	11. Contract or Grant No.
General Electric Company Aircraft Engine Group 1, Jimson Road, Cincinnati, Ohio 45215	NAS3-18021
	13. Type of Report and Period Covered
12. Sponsoring Agency Name and Address	Contractor Report
National Aeronautics and Space Administration Washington, D.C. 20546	14. Sponsoring Agency Code

15. Supplementary Notes

Final Report, Project Manager, C.C. Ciepluch, QCSEE Project Office
Technical Adviser, D.A. Sagerser
NASA Lewis Research Center, Cleveland, Ohio 44135

16. Abstract

This is the first of a two-volume final report presenting the results from acoustic tests on a 50.8-cm (20-inch) diameter, variable-pitch fan and inlet simulator for the QCSEE Under-The-Wing (UTW) engine. Tests were run both in forward- and in reverse-thrust modes with a bellmouth inlet, five accelerating inlets (one hard wall and four treated) with a design throat Mach number of 0.79 at the takeoff condition, and four low Mach inlets (one hard wall and three treated) with a design throat Mach number of 0.6 at the takeoff condition. Unsuppressed- and suppressed-inlet-radiated noise levels were measured at conditions representative of QCSEE takeoff, approach, and reverse-thrust operations. Measured aerodynamic performance of the accelerating inlet is also included in this report.

This volume describes in detail the objectives, test facility, test configurations, data analysis, results, and comparisons. Volume II of this report contains tabulation of one-third-octave-band acoustic data for the model size on the measured 5.2-m (17-ft) arc and scaled data (scaled to full QCSEE size, 71:20) on a 152.4-m (500-ft) sideline.

17. Key Words (Suggested by Author(s))	18. Distribution Statement
Acoustics Inlet Treatments Variable Pitch Fan Accelerating Inlet Acoustics Low Mach Number Inlet Acoustics	[redacted]

19. Security Classif. (of this report)	20. Security Classif. (of this page)	21. No. of Pages	22. Price*
Unclassified	Unclassified	282	

[redacted]

NASA-C-168 (Rev. 6-71)

FOREWORD

Acknowledgment is made to the following contributors:

Project Engineer	K.R. Bilwakesh
Test Engineers	K. Bekofske R. Sheer R. Warren
Fan Aerodynamics	R. Giffin R. McFalls
Inlet Aerodynamics	W. Ruehr
Inlet Acoustic Treatments	A. Clemons
Overall Program Manager	H. Sowers

TABLE OF CONTENTS

TABLE OF CONTENTS (Concluded)

LIST OF ILLUSTRATIONS

LIST OF ILLUSTRATIONS (Continued)

LIST OF ILLUSTRATIONS (Continued)

LIST OF ILLUSTRATIONS (Continued)

LIST OF ILLUSTRATIONS (Continued)

LIST OF ILLUSTRATIONS (Continued)

LIST OF ILLUSTRATIONS (Continued)

LIST OF ILLUSTRATIONS (Continued)

LIST OF ILLUSTRATIONS (Continued)

LIST OF ILLUSTRATIONS (Continued)

LIST OF ILLUSTRATIONS (Continued)

LIST OF ILLUSTRATIONS (Continued)

LIST OF ILLUSTRATIONS (Continued)

LIST OF ILLUSTRATIONS (Continued)

LIST OF ILLUSTRATIONS (Concluded)

LIST OF TABLES

NOMENCLATURE

Symbol or Abbreviation	Definition	Units
A	Area	m^2 (ft^2)
A_{th}	Inlet physical throat area	m^2 (ft^2)
A_{18}	Fan exhaust nozzle area	m^2 (ft^2)
BPF	Blade passing frequency	Hz
C	Speed of sound	m/sec (ft/sec)
D_F	Fan diameter	m (ft)
D_{HL}	Inlet highlight diameter	m (ft)
D_{max}	Maximum inlet flow-path diameter	m (ft)
D_{th}	Inlet throat diameter	m (ft)
DV	Discharge valve setting	---
EPNL	Effective Perceived Noise Level	EPNdB
F_n	Net thrust	N (lbf)
L	Inlet length	m (ft)
M_{cruise}	Cruise Mach number	---
M_{th}	Throat Mach number	---
$M_{th\ max\ cr}$	Maximum cruise one-dimensional throat Mach number	---
$M_{th\ T/O}$	Takeoff average one-dimensional throat Mach number	---
MPT	Multiple pure tones	---
N, N_P	Fan speed (Physical)	rpm
N_{FC}	Corrected fan speed	rpm
OGV	Outlet guide vane	---
P_S	Static pressure	N/m^2 (psi)
P_T	Total pressure	N/m^2 (psi)
P_{T_0}	Ambient total pressure	N/m^2 (psi)
P_{T_2}	Total pressure at station 2	N/m^2 (psi)
P_{T4}	Station 14 total pressure	N/m^2 (psia)
PNL	Perceived noise level	PNdB
PWL	Sound power level re 10^{-13} watt	dB

NOMENCLATURE (Concluded)

Symbol or Abbreviation	Definition	Units
R_{th}	Inlet throat radius	m (ft)
SPL	Sound pressure level re 0.0002 microbars	dB
T_T	Total temperature	K (° R)
V	Aircraft velocity	m/sec (ft/sec)
W	Weight flow	kg/sec (lbm/sec)
X	Axial length	m (in.)
x	Acoustic reactance	rayls
β	Rotor pitch or blade angle	degrees
δ	Ambient to reference pressure ratio	---
η	Diffuser total pressure recovery	---
η_{14}	Fan adiabatic efficiency	---
θ	Ambient to reference temperature ratio	---
θ	Acoustic angle relative to inlet	degrees
θ_{eq}	Equivalent conical diffusion angle	degrees
θ_{max}	Maximum diffusion angle	degrees
ρ	Density	kg/m^3 (lbm/ft^3)

1.0 SUMMARY

As part of the Quiet, Clean, Short-Haul, Experimental Engine (QCSEE) program sponsored by the NASA Lewis research Center, a series of acoustic tests were conducted on a scale model of the Under-The-Wing (UTW) variable-pitch fan. The model fan was 50.8 cm (20 in.) in diameter and was a 1:35 scale of the full-size fan. Tests were run both in forward- and reverse-thrust modes with a bellmouth inlet; five accelerating inlets (one hard-wall and four treated) with a design throat Mach number of 0.79 at the takeoff condition, and four low Mach inlets (one hard-wall and three treated) with a design throat Mach number of 0.6 at the takeoff condition. Unsuppressed- and suppressed-inlet, radiated-noise levels were measured at conditions representative of QCSEE takeoff, approach, and reverse-thrust operations. Measured aerodynamic performance of the accelerating inlet is also included in this report.

2.0 INTRODUCTION

The General Electric Company is currently engaged in the Quiet, Clean, Short-Haul, Experimental Engine (QCSEE) program under Contract NAS3-18021 to NASA Lewis Research Center. A major objective of the QCSEE program is to develop and demonstrate the technology required to meet the stringent noise requirements anticipated for commercial short-haul turbofan aircraft. The specific goal is a maximum noise level of 95 EPNdB including powered-lift noise at 152.5-m (500-ft) sideline during all portions of the airplane trajectory. For noise-prediction purposes, the airplane is defined to have 400 kN (90,000 lbf) installed thrust and to be designed for a 610-m (2,000-ft) runway. A second noise objective is 100 PNdB maximum on a 152.4-m (500-ft) sideline during reverse thrust. The QCSEE program explores a wide range of pertinent technology involving both a variable-pitch, under-the-wing (UTW) and a fixed-pitch, over-the-wing (OTW) propulsion system. An overview of the QCSEE program is given in Reference 1.

The UTW 50.8-cm (20-inch) Simulator Test Program was designed to evaluate aerodynamic performance of the fan and inlet acoustic performance from a 1:3.55 scale model of the variable pitch UTW fan.

2.1 FAN AERODYNAMIC PERFORMANCE OBJECTIVES

- Obtain base operating maps of the bypass and core portions of the fan at several forward-thrust, rotor-pitch settings.
- Determine the effect of off-design bypass ratio on performance.
- Determine degree of circumferential flow distortion induced by nonaxisymmetric bypass OGV and pylon configuration.
- Obtain fan performance in an acoustically treated, accelerating-inlet environment.
- Evaluate fan-performance sensitivity to a tip radial inlet distortion.
- Determine reverse-thrust performance through both flat-pitch and stall-pitch settings.
- Obtain core duct recovery and distortion characteristics during reverse-pitch operation.

2.2 FAN INLET ACOUSTIC PERFORMANCE OBJECTIVES

- Obtain the basic, unsuppressed, acoustic signature of the fan stage with a bellmouth inlet.

- Measure suppression provided by a treated accelerating inlet designed for a throat Mach number of 0.79 at the takeoff condition. The suppression objective at the takeoff condition is 13 PNdB.

- Measure suppression provided by the treated, accelerating inlet at the approach condition. The suppression objective is 8 PNdB at this condition.

- Measure suppression with the accelerating inlet by different treatments in the reverse-thrust mode of operation. These treatments were designed to provide 3 PNdB in the reverse-thrust mode.

- Measure suppression provided by different wall treatments at the takeoff, approach, and reverse-thrust conditions with low Mach inlets designed for a throat Mach number of approximately 0.6 at takeoff. This inlet design was considered a backup design in the event the accelerating inlet was found unacceptable.

- Compare static acoustic performance of the inlet with (1) a flight lip, representative of the full-scale flight inlet, and (2) an aeroacoustic lip designed to simulate inlet-flow conditions typical of a 41-m/sec (80-knot) forward velocity.

The fan aerodynamic performance test results were presented and discussed in Reference 2. This report presents, in two volumes, the results of acoustic performance and aerodynamic performance testing of the inlet. Volume I presents the test configurations, test faciility, vehicle, data acquisition and reduction procedures, detailed data analysis, results, and comparisons. Volume II presents 1/3-octave-band data for all configurations. The data are given for the model size at a 5.18-cm (17-ft) arc and for scaled-to-QCSEE full size (3.55:1) on a 152.4-m (500-ft) sideline.

3.0 TEST FACILITY

The tests were conducted in the anechoic environment of the General Electric Corporate Research and Development Aero/Acoustic Facility in Schenectady, New York. An overview of the facility is shown in Figure 1. A photograph of the facility with the UTW simulator installed is presented in Figure 2. It is comprised of:.

1. A 1.86-MW (2500-hp) drive system for speeds up to 15,000 rpm.

2. An anechoic chamber approximately 10.67-m (35-ft) wide by 7.62-m (25-ft) long by 3.05-m (10-ft) high designed for less than $\pm$ 1 dB standing-wave ratio at 200 Hz. All walls, floor, and ceiling are covered with an array of 71.1-cm (28-in.) polyurethane foam wedges.

3. Porous walls for minimum in-flow distortion to the fan when measuring inlet-radiated noise.

4. Capability to install the fan for evaluation of both forward-radiated and exhaust-radiated noise.

5. Far-field noise measurement on a 5.2-m (17-ft) arc from 0° to 110° relative to the inlet for inlet-radiated noise.

The sound field is set up with the center of the arc located such as to assume the source location to be at the fan face during tests of inlet-radiated-noise levels.

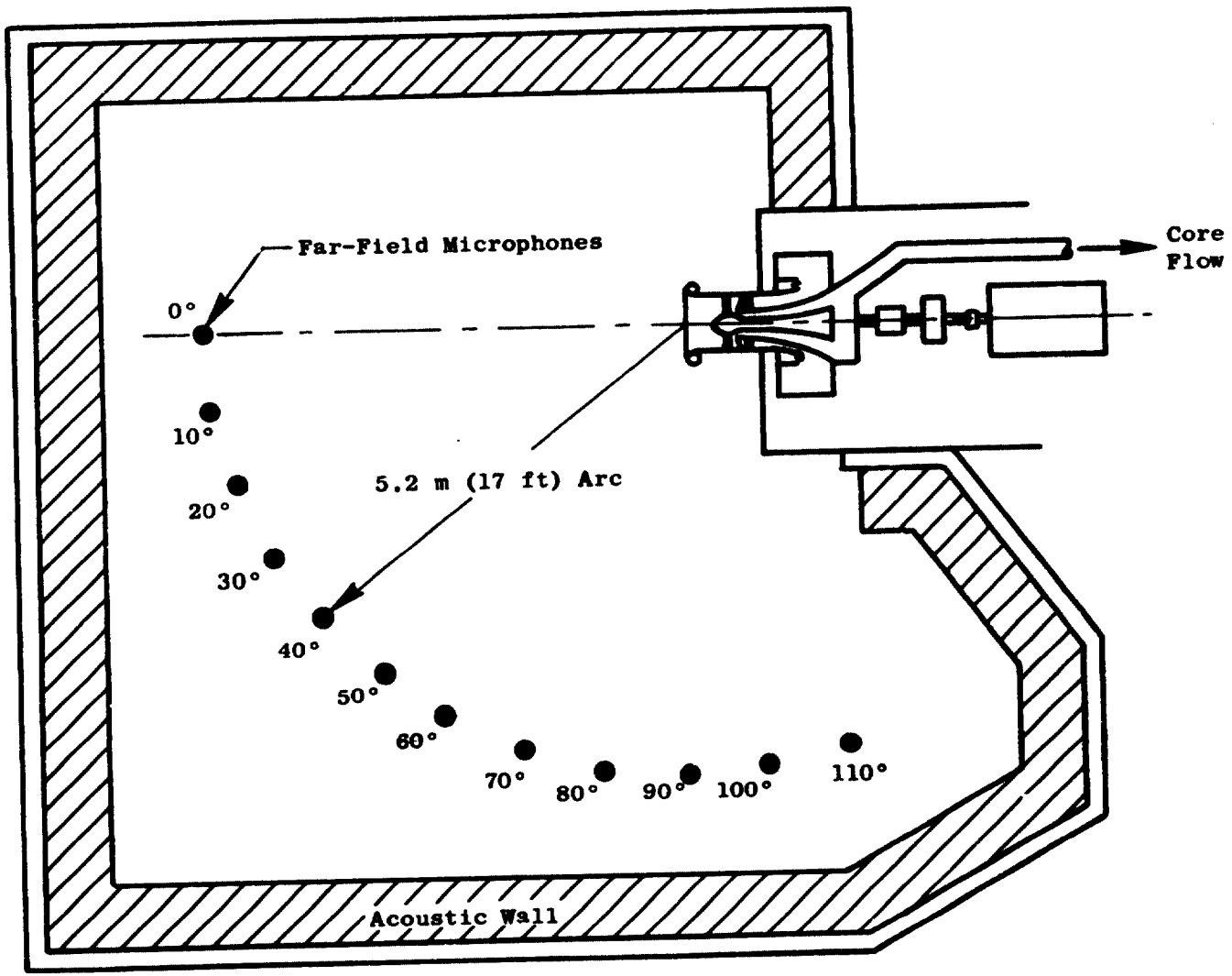

Figure 1. Schematic of General Electric Research and Development Center Anechoic Chamber.

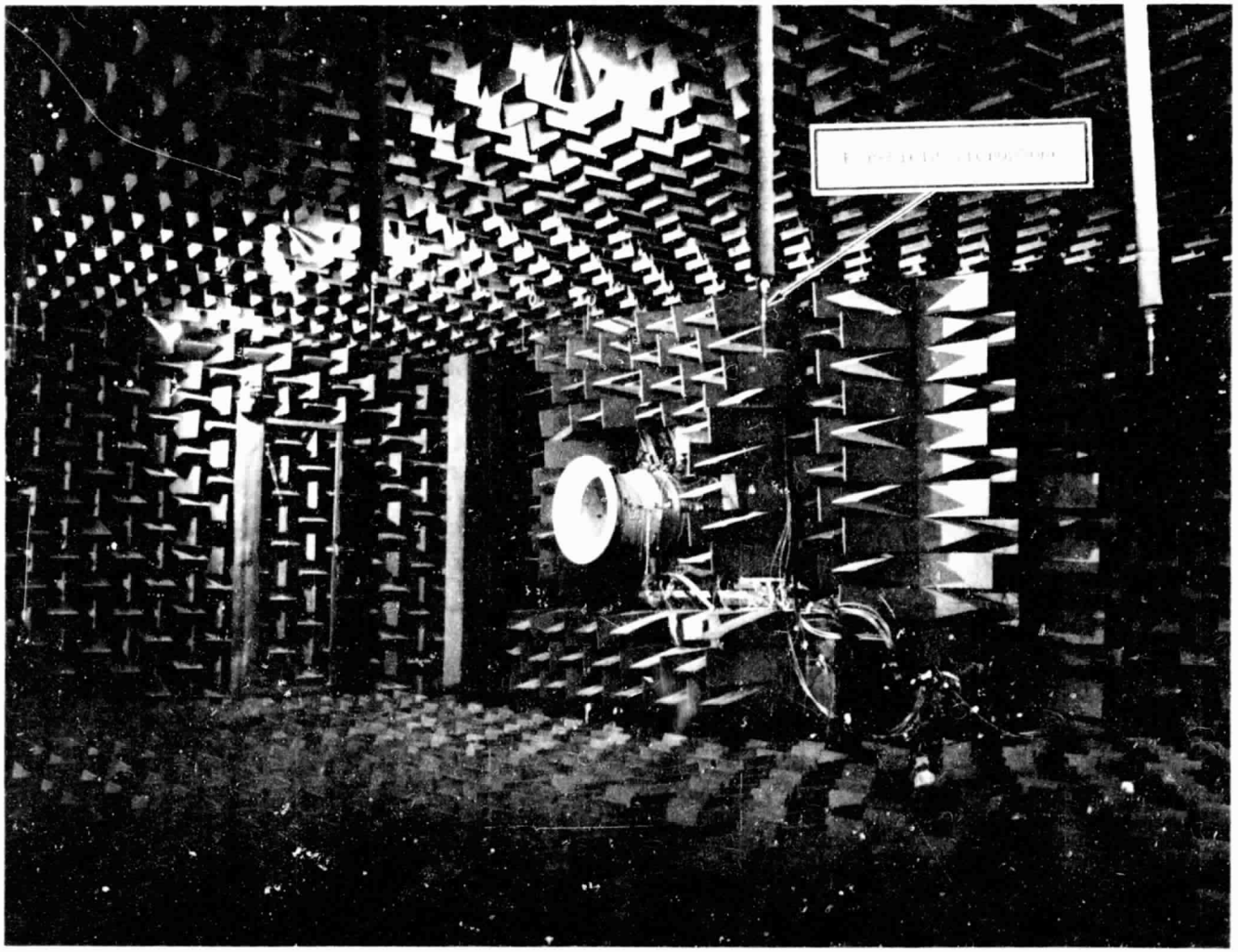

Figure 2. Photograph of General Electric Company Anechoic Chamber.

4.0 TEST VEHICLE

The test vehicle was an adjustable-pitch, 50.8-cm (20-in.)-diameter, exact-linear-scale model (scale factor 20.0:71.0) of the QCSEE Under-The-Wing (UTW) variable-pitch fan. The scale model included the rotor, the nonaxisymmetric bypass OGV and pylon, the core stator, and the transition duct for the core flow. The 50.8-cm (20-in.) stage characteristics are given in Table I.

A cross section of the UTW model fan as assembled on the test stand is shown in Figure 3. There were 18 variable-pitch rotor blades with a solidity of 0.95 at the outer diameter and 0.98 at the inner diameter. Circumferentially grooved casing treatment was incorporated over the rotor tip. The engine bypass OGV's performed the dual function of an outlet guide vane for the bypass flow and a frame support for the engine components and nacelle. They were integrated with the pylon, which protruded forward into the vane row. The vane frame was positioned at an axial distance downstream of the rotor trailing edge equal to 1.5 true rotor-tip chords. The 33 vanes in the vane frame consisted of five different geometries around the annulus to minimize flow distotions that would otherwise be imposed by the pylon. The vane/blade ratio was 1.8 (33/18). Immediately following the rotor, in the hub region, was an annular ring or island. The 96 OGV's for the fan hub flow were in the annular space between the underside of the island and the hub. A full-circumferential axial gap separated the island trailing edge from the splitter leading edge. The splitter divided the flow into a bypass portion and a core portion. There were six struts in the core inlet duct. The island configuration was selected specifically to permit the attainment of a high hub-supercharging pressure ratio during forward-pitch operation without causing a large core-flow induction pressure loss during reverse-pitch operation.

The design rotor tip relative Mach number was 1.13. The outer portion of the blade employed a profile shape that was specifically tailored to minimize excessive shock losses on the suction surface and still be compatible with the requirements governing the inlet flow and energy addition. The blade mean-line shape and point-of-maximum-thickness varied radially. The blade shape was similar to a double circular-arc profile in the hub region. Profile shapes at other radii were generally similar in appearance to the NASA multiple circular-arc sections, in which a small percentage of the overall camber occurs in the forward portion of the blade. A photograph of the rotor is shown in Figure 4.

A conventional OGV system turned the incoming flow to axial. However, the housing requirements of the pylon dictated a geometry in which the OGV's underturn approximately 10° on one side and overturn approximately 10° on the other side. To avoid excessive costs, five vane-geometry groups were deemed sufficient. Figure 5 shows an unwrapped section at the inner diameter of the vane to illustrate the different vane groupings; it shows an approximate streamline pattern derived from an analysis of the circumferential flow field. A more complete description of the aerodynamic and mechanical design of the UTW engine is reported in Reference 3.

Table I. UTW 50.8-cm (20-in.) Simulator Fan - Stage Design Characteristics.

• Inlet guide vanes	None
• Fan diameter	50.8 cm (20 in.)
• Number of rotor blades	18
• Number of stators	33 (32 + pylon)
• Number rotor/stator spacing	1.5 true rotor tip chords
• Hub/tip-radius ratio	0.443
• Rotor pitch angle	Adjustable
• Fan Design Point	
• Corrected tip speed	306.3 m/sec (1005 ft/sec)
• Corrected fan speed	11,520 rpm (100%)
• Fan bypass pressure ratio	1.34
• Fan core pressure ratio	1.23
• Corrected fan weight flow	32.4 kg/sec (71.4 lbm/sec)
• Bypass ratio	11.3
• Specific flow	199 kg/sec-m^2 (40.8 lbm/sec-ft^2)
• Objective adiabatic efficiency	
• Bypasss	88%
• Core	78%
• Design Takeoff Condition	
• Corrected tip speed	289.6 m/sec (950 ft/sec)
• Corrected fan speed	10,886 rpm (94.5%)
• Fan bypass pressure ratio	1.27
• Corrected fan weight flow	32.2 kg/sec (71 lbm/sec)
• Bypass ratio	13.15
• Rotor pitch angle	0° (design)

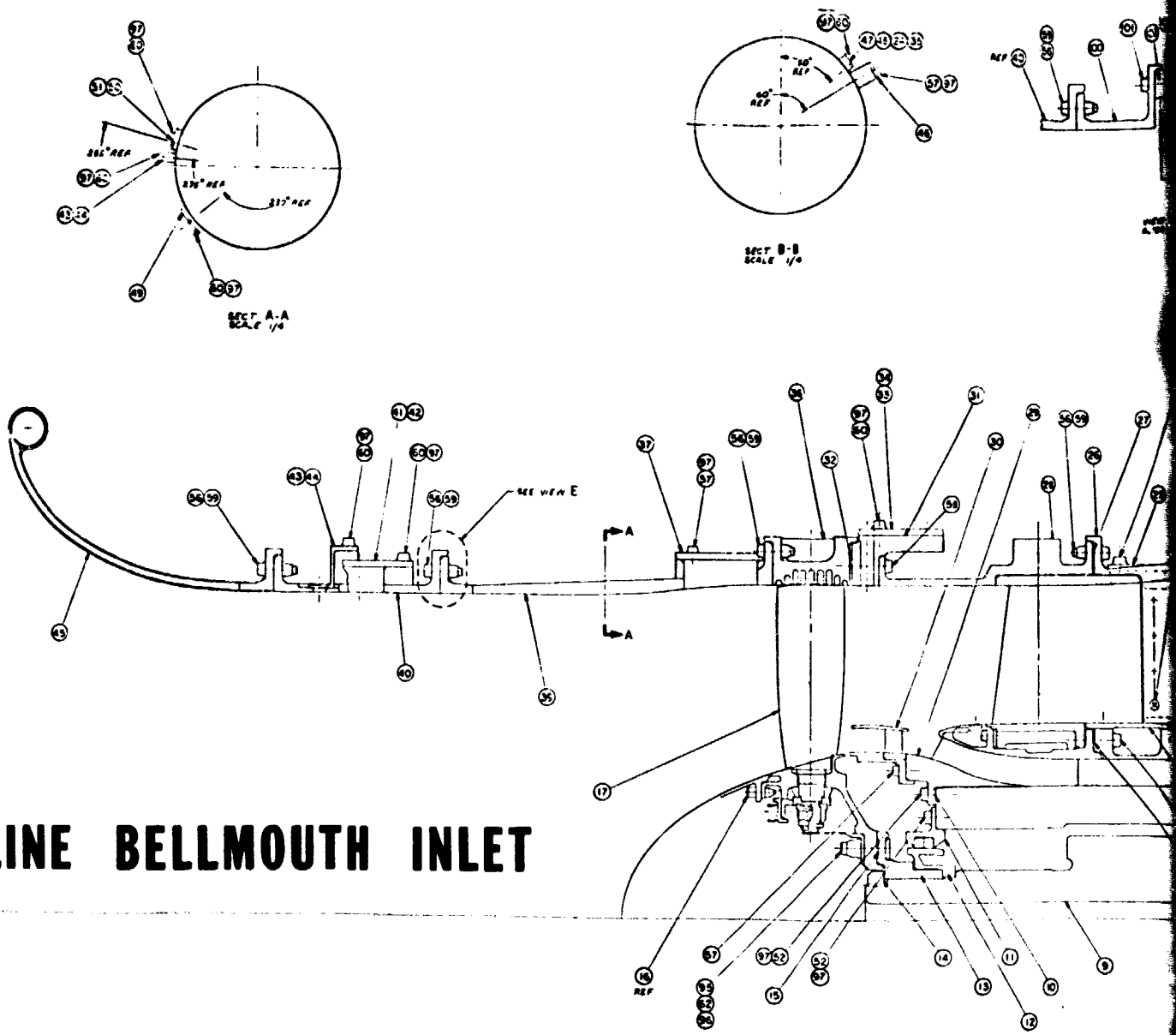

BASELINE BELLMOUTH INLET

Figure 3. UTW Model Fan As

FOLDOUT FRAME

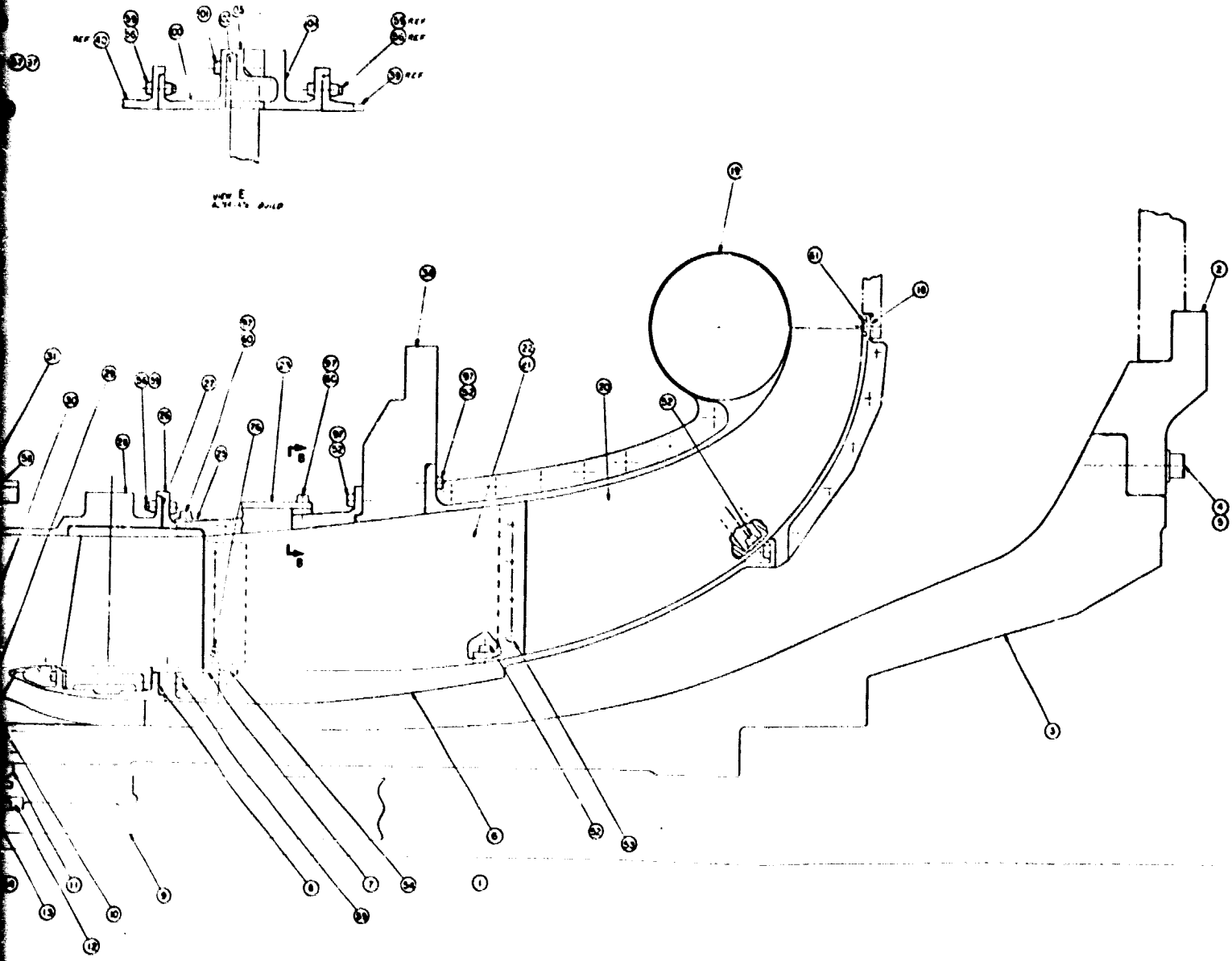

UTW Model Fan Assembly Drawing.

FOLDOUT FRAME

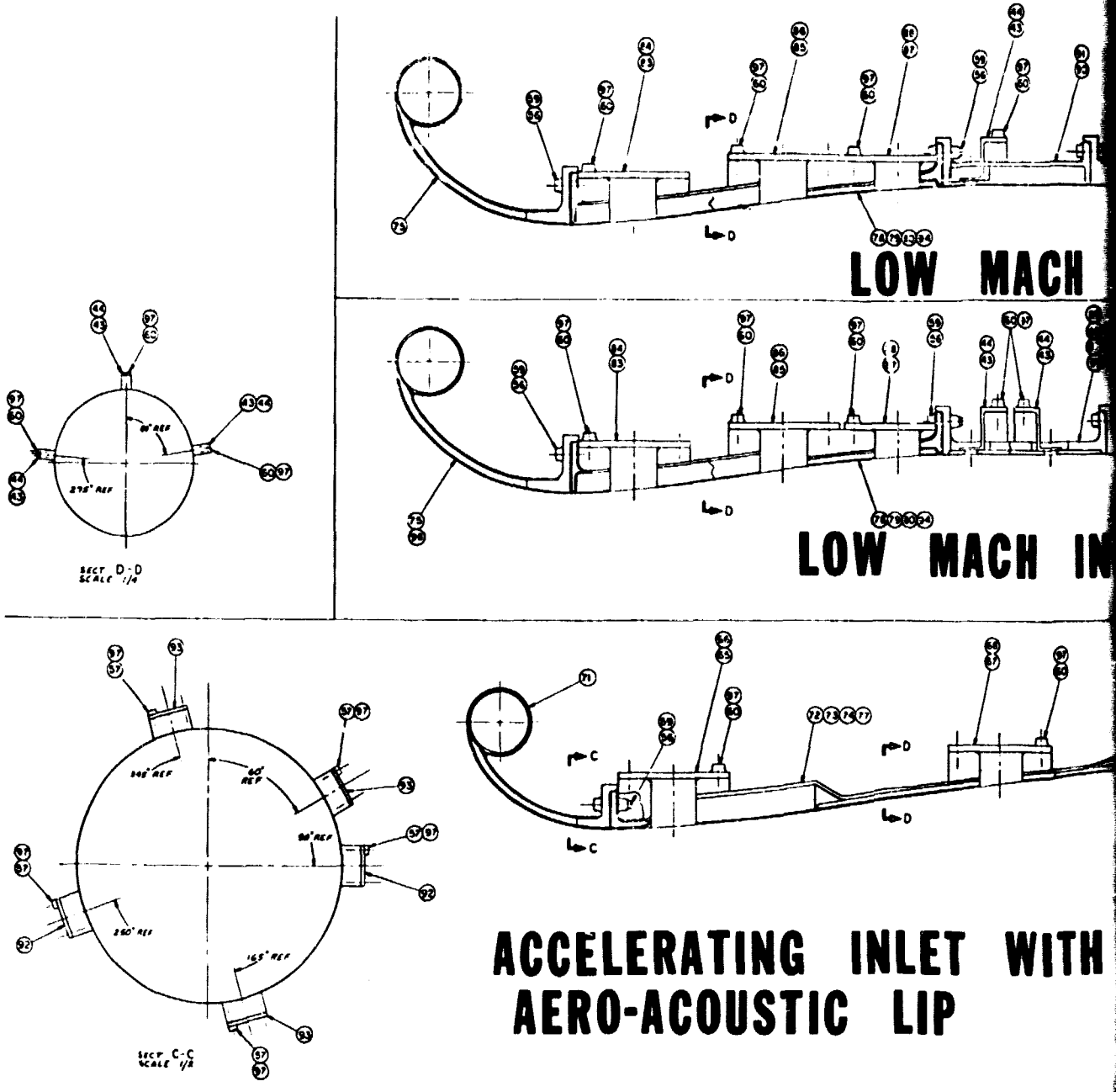

Figure 3. UTW Model Fan Assembly Dr

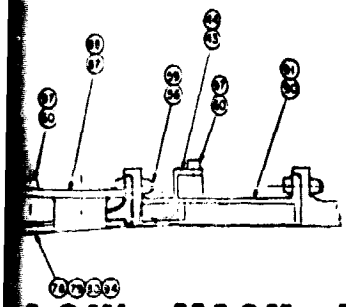

LOW MACH INLET

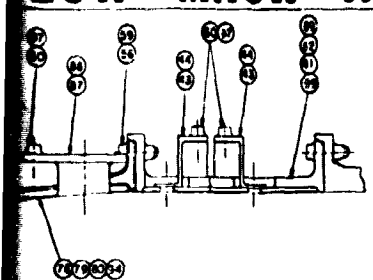

W MACH INLET

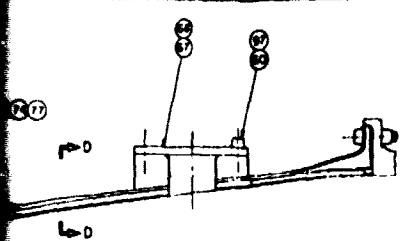

INLET WITH
LIP

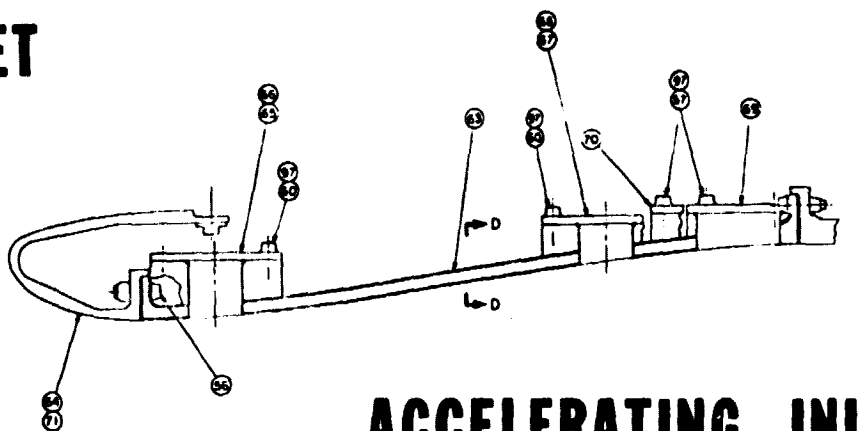

ACCELERATING INLET
WITH FLIGHT LIP

Model Fan Assembly Drawing (Concluded).

2

FOLDOUT FRAME

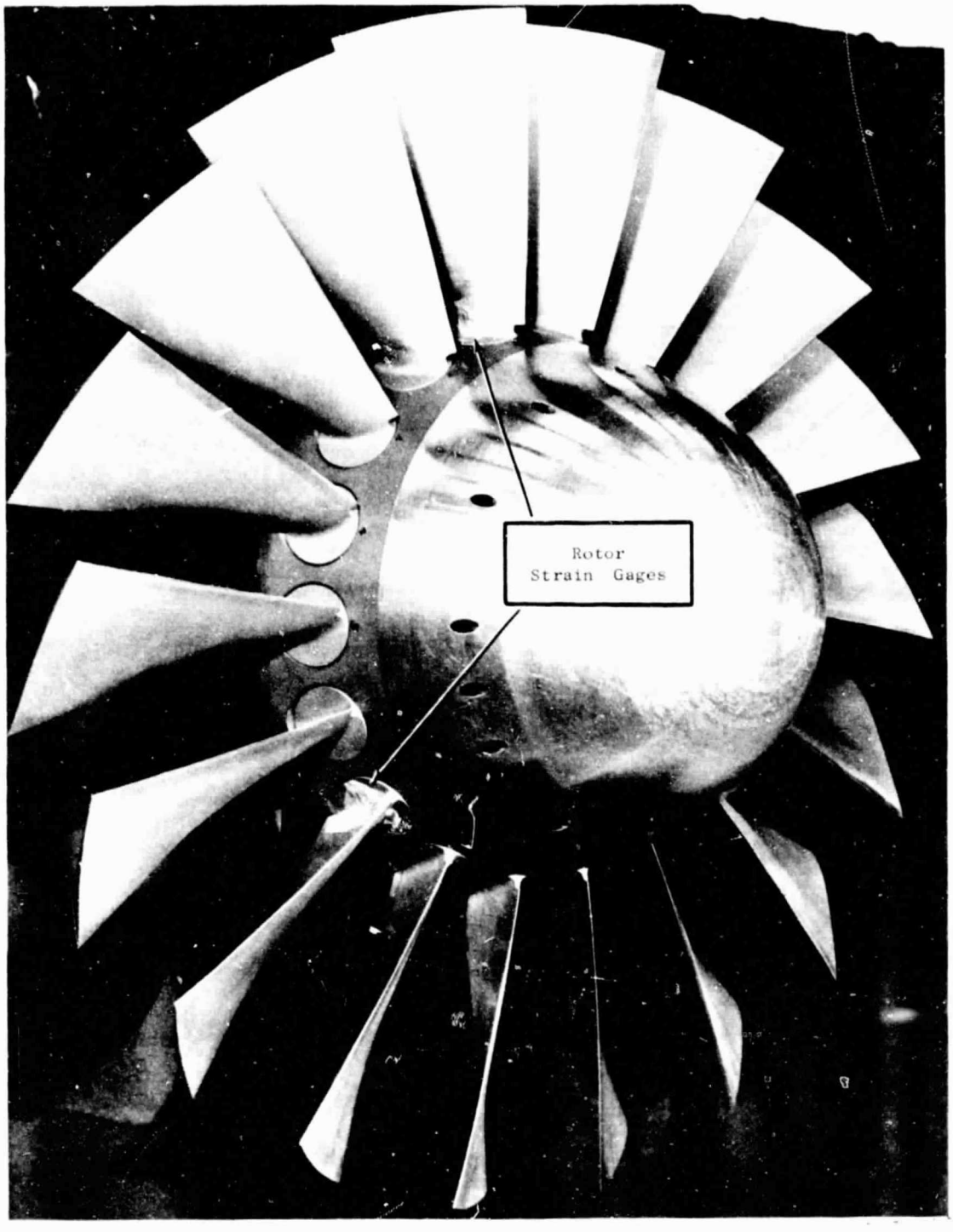

Figure 4. Photograph of the 50.8-cm (20-in.) Scale-Model UTW Variable-Pitch Fan.

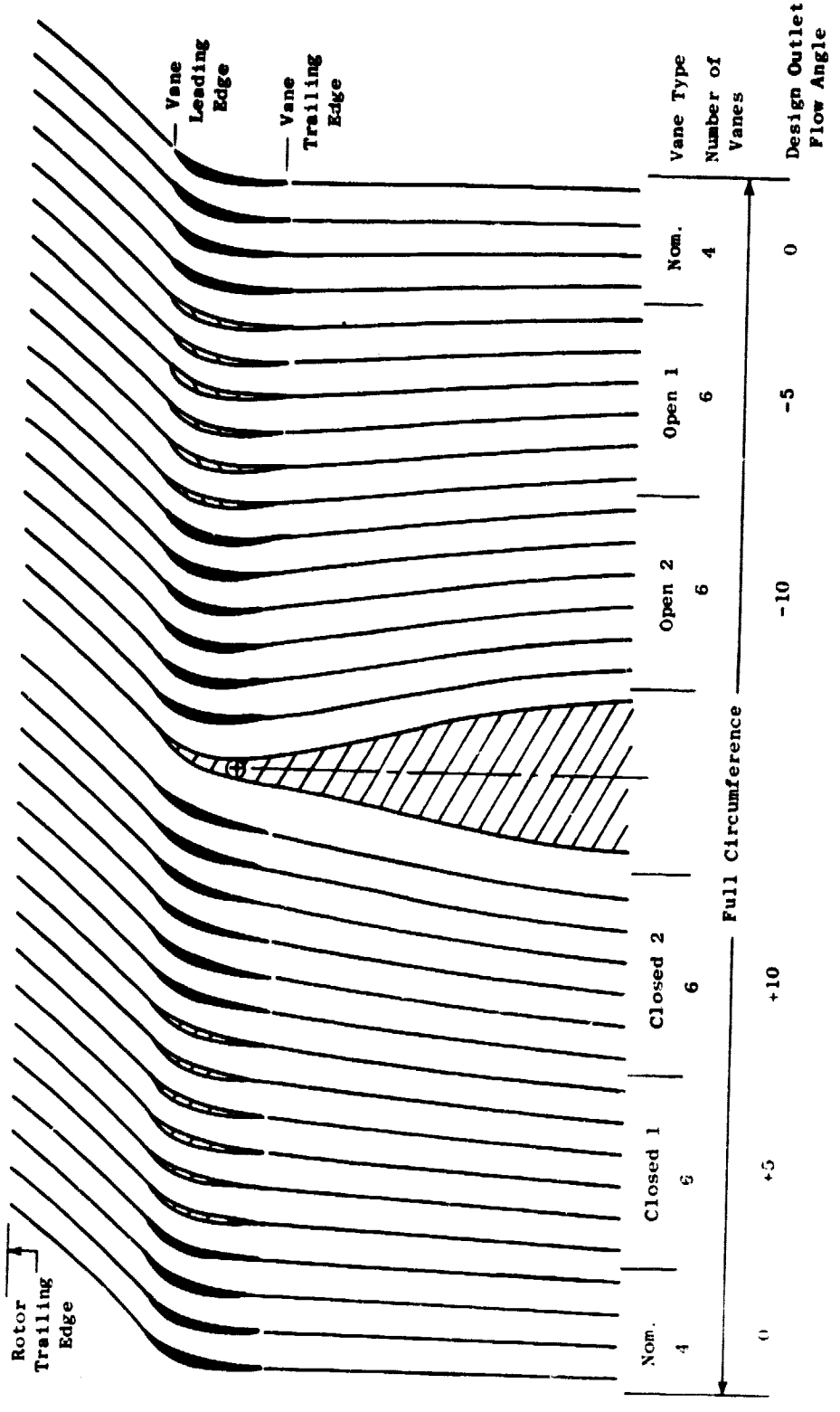

Figure 5. Vane Frame Unwrapped Section at the Inner Flow Path.

A fully adjustable discharge valve (DV) was used to vary the bypass exhaust nozzle area. The core flow was controlled separately by suction through two Fuller pumps.

5.0 INLET CONFIGURATIONS AND TREATMENTS

One of the major objectives of this test program was to select a suitable inlet-wall acoustic treatment for the full-size UTW engine. The principle of obtaining reduction in inlet-radiated noise (reduction relative to a constant-cross-sectional bellmouth) by accelerating the flow at the inlet had been well established from past experience for high-tip-speed fans (Reference 3). Little data was available, however, for fans operating at subsonic tip speeds. Adding acoustic-absorption treatment to the accelerating inlet wall was expected to yield a nacelle that could provide suppression capability, particularly at the approach and reverse-thrust conditions. The overall inlet suppression objectives for the system under different operating conditions were:

Takeoff	13 PNdB
Approach	8 PNdB
Reverse Thrust	3 PNdB

Using the design philosophy discussed in References 3 and 4, a baseline bellmouth inlet, a hard-wall accelerating inlet (with a design throat Mach number of 0.79 at the takeoff conditions), four treated accelerating inlets (with the same internal flow path as the hard-wall inlet), a hard-wall low Mach number inlet (design throat Mach number of 0.6 at takeoff conditions), and three treated low Mach inlets were chosen for the tests. In addition, one of the treated accelerating inlets was also tested with two different lips: a flight lip, representative of the full-scale flight inlet, and an aero-acoustic lip which simulated inlet-flow conditions typical of an 41-m/sec (80-knot) forward velocity. The qualitative test objectives with the various inlet configurations are shown below.

1.	Scale-model bellmouth	-	Reference noise level for comparison with suppression inlets. Scale model of bellmouth to be tested on full-scale engine.
2.	Accelerating inlet with hard-wall, aero-acoustic lip	-	Determine suppression due to throat Mach number.
3.	Accelerating inlet with treated wall, aero-acoustic lip	-	Determine combined suppression due to Mach number and wall treatment.
4.	Accelerating inlet with treated wall, flight lip	-	Compare flight lip and aero-acoustic lip forward-thrust noise levels. If there is a significant difference, both

lips will be built. the aero-acoustic lip for acoustic and the flight lip for aerodynamic testing.

5. Low Mach inlet, hard wall - Reference noise level for comparison with treated low Mach inlets. Also compare to bell-mouth levels.

6. Low Mach inlet, treated wall - Determine suppression due to wall treatment.

The details of the four treatments for the accelerating inlet are given in Table II. Figure 6 is a photograph of the accelerating inlet and the flight lip. The details of the three low Mach treatments are given in Table III. A photograph of the low Mach inlet is shown in Figure 7. The reader is also referred to Figure 3 which shows the various inlets and flight lips.

5.1 ACCELERATING INLETS

The accelerating inlets were designed to reduce forward-radiated fan noise by accelerating the flow upstream of the fan. The accelerating inlets for this program were designed to achieve a throat Mach number of 0.79 at the takeoff condition. This throat Mach number was selected on the basis of both acoustic and aerodynamic design criteria. Acoustically this throat Mach number was estimated to provide sufficient suppression to satisfy the noise goals. Higher throat Mach numbers would obviously provide higher suppression; however, aerodynamic tests (Reference 5) had shown the inlet recovery to be unacceptable above this Mach number, after allowing for control and engine-variation tolerances. Each inlet was constructed with a flange at the throat to permit testing with either a flight lip or an aero-acoustic lip. A total of five accelerating inlets were built, one with a hard wall and four with treatment, all having the same wall contour. Three of them (hard wall, treatment B, and treatment D) were tested in the reverse-thrust acoustic mode. Table IV gives pertinent aerodynamic design parameters for the accelerating inlets, and Table V gives the coordinates for the inlet contours including the spinner.

5.1.1 Accelerating Inlet Treatment Configurations

A summary of the different accelerating inlet treatment configurations is given in Table II. Four designs are defined; each configuration had the following features.

- Three sections of different depths
- Total treated-length/fan-diameter ratio of 0.74
- Treatment designed for reverse-thrust noise spectrum

Table II. Accelerating Inlet Treatment Designs.

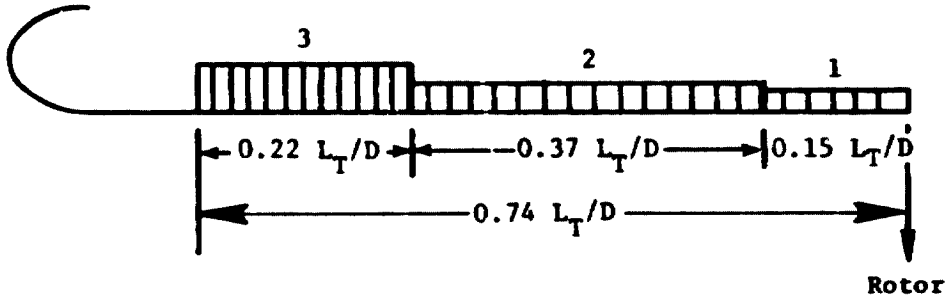

Design	Section	Cavity Depth		Faceplate					Tuning Frequency Reverse Thrust, Hz	
				Porosity	Hole Diameter		Thickness			
		cm	in.	%	cm	in.	cm	in.	Full Scale	Model
Treatment A	1	0.312	0.123	24	0.06	0.024	0.081	0.032	3150	11,182
	2	0.57	0.225	24	0.06	0.024	0.081	0.032	2000	7100
	3	1.72	0.680	24	0.06	0.024	0.081	0.032	1000	3550
Treatment B	1	0.312	0.123	9.2	0.11	0.045	0.0508	0.020	3150	11,182
	2	0.57	0.225	9.2	0.11	0.045	0.0508	0.020	2000	7100
	3	1.72	0.680	9.2	0.11	0.045	0.0508	0.020	1000	3550
Treatment C	1	0.134	0.053	3.6	0.158	0.0625	0.0508	0.020	3150	11,182
	2	0.325	0.128	3.6	0.158	0.0625	0.0508	0.020	2000	7100
	3	1.42	0.560	3.6	0.158	0.0625	0.0508	0.020	1000	3550
Treatment D	1	0.246	0.097	7.2	0.083	0.033	0.0508	0.020	3150	11,182
	2	0.744	0.293	14.4	0.055	0.022	0.0508	0.020	2000	7100
	3	2.06	0.812	28.0	0.114	0.045	0.0508	0.020	1000	3550

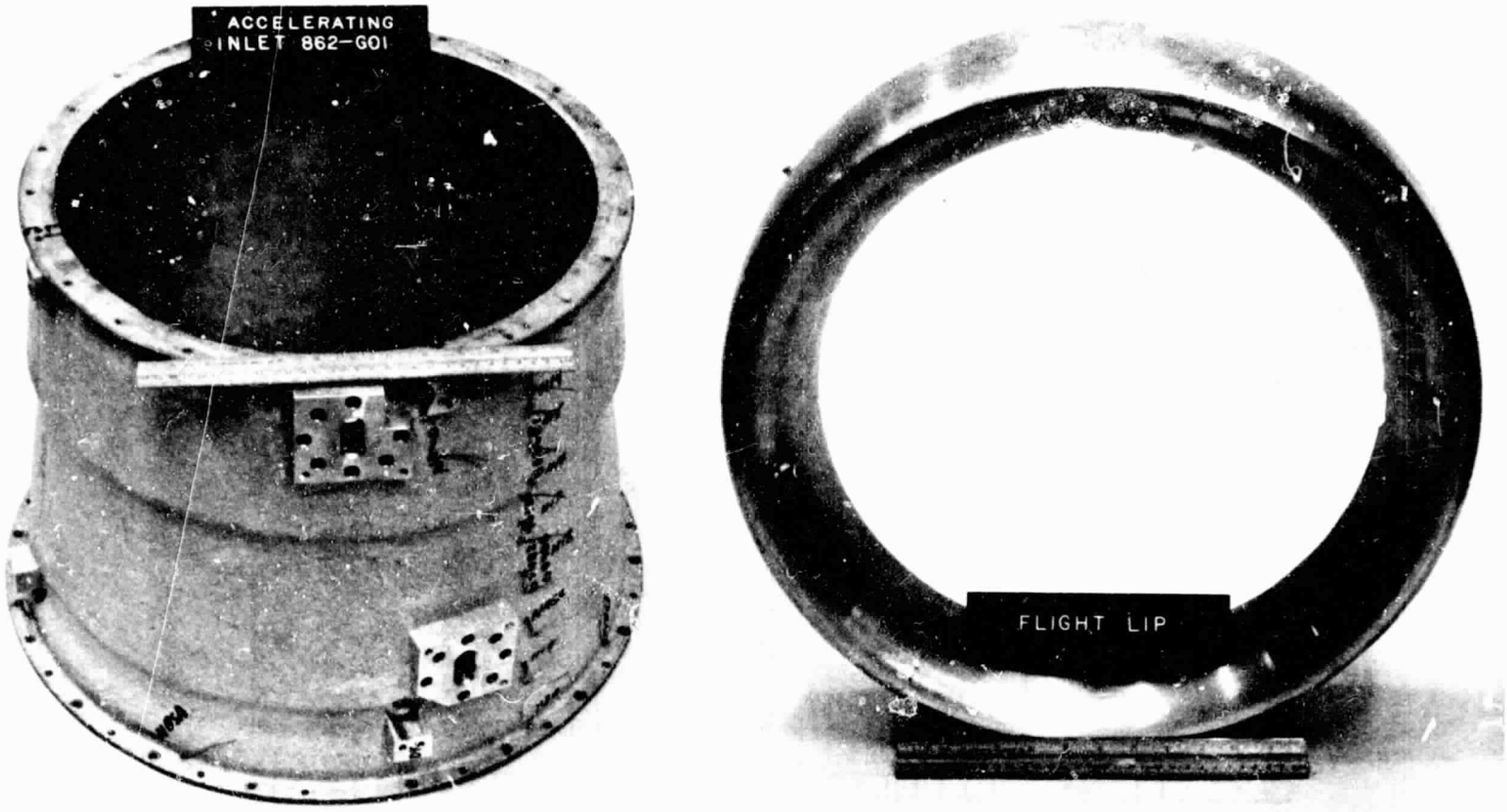

Figure 6. Accelerating Inlet and Flight Lip.

Table III. Low Mach Inlet Treatment Designs.

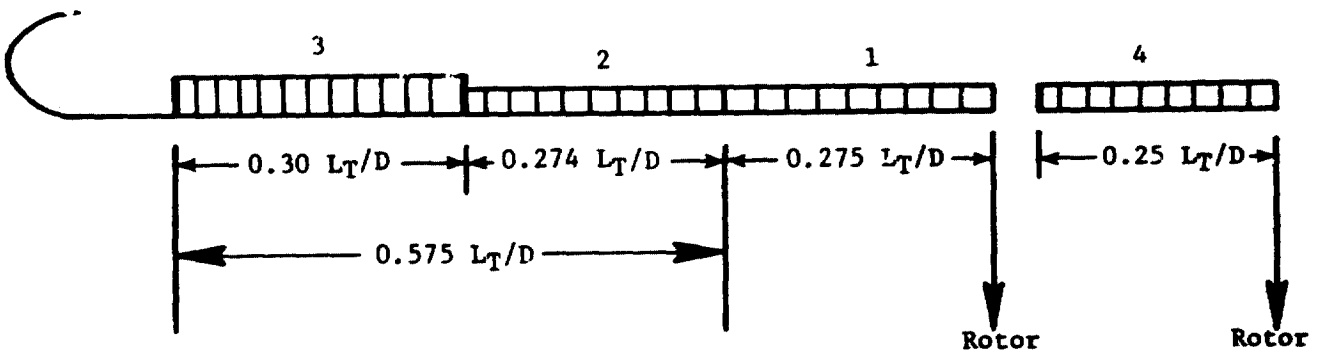

Design	Section	Cavity Depth		Faceplate					Tuning Frequency Forward Thrust, Hz	
				Porosity	Hole Diameter		Thickness			
		cm	in.	%	cm	in.	cm	in.	Full Scale	Model
Treatment A	2	0.381	0.15	10	0.114	0.0450	0.081	0.032	2000	7100
	3	1.42	0.56	10	0.114	0.0450	0.081	0.032	1000	3550
	4	0.147	0.058	10	0.114	0.0450	0.081	0.032	3150	11,182
Treatment B (Scottfelt)	1	1.27	0.5	28	0.158	0.0625	0.051	0.020	Broadband Characteristics	
	2	1.27	0.5	28	0.158	0.0625	0.051	0.020		
	3	1.27	0.5	28	0.158	0.0625	0.051	0.020		
Treatment C	2	0.134	0.053	3.6	0.158	0.0625	0.051	0.020	2800	9940
	3	0.393	0.155	3.6	0.158	0.0625	0.051	0.020	1550	5500
	4	0.200	0.080	3.6	0.158	0.0625	0.051	0.020	2253	8000

Figure 7. Low Mach Inlet.

Table IV. Inlet Aerodynamic Design Parameters.

	Accelerating Inlet		Low Mach Inlet
	Flight Lip	Aero-Acoustic Lip	Aero-Acoustic Lip
Fan diameter, D_F	50.8 cm (20 in.)	50.8 cm (20 in.)	50.8 cm (20 in.)
Nondimensional inlet length, L/D_F	1.029	1.081	1.125
Diffuser area ratio, $(D_F/D_{th})^2$	1.466	1.466	1.283
Equivalent conical diffusion angle, $2\theta_{eq}$	11.6°	11.6°	11.6°
Maximum diffusion angle, θ_{max}	8.7°	8.7°	8.7°
Inlet contraction ratio, D_{HL}/D_{th}	1.21	1.394	1.45
Ellipse ratio	2.0	1.382	1.382
Highlight to maximum diameter ratio, D_{HL}/D_{max}	0.900	---	---
Nondimensional external forebody length, X/D_{max}	0.219	---	---
Cruise Mach number, M_{cruise}	0.7	0.7	0.555
Takeoff average one-dimensional throat Mach number, $M_{th_{T/O}}$	0.79	0.79	0.60
Maximum cruise average one-dimensional throat Mach number, $M_{th_{max\ cr}}$	0.79	0.79	0.60

Table V. Accelerating Inlet Coordinates.

Aero-Acoustic				Flight Lip				Spinner				Diffuser			
Axial Station		Radius		Axial Station		Radius		Axial Station		Radius		Axial Station		Radius	
cm	in.	cm	in.	cm	in.	cm	in.	cm	in.	cm	in.	cm	in.	cm	in.
-54.89	-21.611	29.24	11.512	-39.93	-15.719	28.20	11.102	-11.77	-4.634	0	0	-43.47	-17.114	20.9	8.258
-54.87	-21.604	28.79	11.336	-48.08	-18.929	27.80	10.819	-11.18	-4.403	3.03	1.194	0	0	25.40	10.000
-54.74	-21.552	27.90	10.986	-51.85	-20.412	26.17	10.302	-10.57	-4.163	4.27	1.682		(Fan Face)		
-54.48	-21.447	27.03	10.642	-52.23	-20.563	25.65	10.099	-9.94	-3.915	5.20	2.048				
-53.84	-21.195	25.77	10.146	-52.58	-20.582	25.38	9.992	-9.01	-3.549	7.58	2.986				
-52.92	-20.836	24.60	4.686	-52.27	-20.577	25.14	9.898	-5.51	-2.169	8.99	3.538				
-51.76	-20.379	23.56	9.274	-51.96	-20.456	24.20	9.528	-3.86	-1.521	9.85	3.876				
-48.27	-19.002	21.74	8.559	-51.25	-20.178	23.32	9.180	-2.47	-0.972	10.44	4.110				
-45.93	-18.081	21.17	8.334	-49.17	-19.359	22.02	8.670	-1.23	-0.479	10.90	4.290				
-43.47	-17.114	20.98	8.258	-44.89	-17.675	21.03	8.281	0	0	11.27	4.437				
(Throat)															

Table II also gives the faceplate definition for each configuration including hole diameter, porosity, and thickness.

5.1.2 Treatment Design Procedure

The treatment configurations as given in Table III were designed for reverse-thrust operation because the desired suppression levels at takeoff power were assumed to be achievable primarily from the high throat Mach number produced with the accelerating inlet design. This assumption was based on high Mach inlet data from previous tests. The predicted noise spectrum for the reverse-thrust mode is given in Figure 8. The spectrum is based on engine data (found in Reference 6) from tests of a 1.83-m (6-ft) diameter, variable-pitch, 1.2 pressure-ratio fan, and is scaled to the full-size UTW engine. The Noy-weighted, unsuppressed spectrum is also given and indicates that the spectrum requires broadband suppression characteristics in order to obtain significant PNL suppression. Thus, the inlet treatment of each configuration has three thicknesses to provide the different tuning frequencies as defined in Table II. The Noy-weighted, unsuppressed spectrum indicates that tuning at these frequencies should provide a balanced design.

The suppression requirements at approach power were also considered. Estimates indicated that the suppression requirements could be achieved with the treatment design for reverse thrust.

The required treatment depths and faceplate parameters needed to give the tuning frequencies were determined using analytical methods to predict the acoustic reactance and the optimum reactance required in designing for the reverse-thrust mode. Treatments A, B, and C were designed for the lowest order radial mode with a 10th-order, spinning, lobe pattern. Treatment D was designed for the 15th-order, spinning, lobe pattern. The analytical model used for determining the optimum reactance is presented by Rice in Reference 7 and predicted panel reactance values were made using the analytical relations given in Reference 8.

Figure 9 gives the predicted optimum reactance for the 10th-order lobe pattern as a function of frequency for reverse- and forward-thrust conditions, plus the predicted reactance for treatments A and B. Figure 10 gives the same type of information for treatments C and D. The intersection of the optimum reactance curve with the predicted reactance curve determines the tuning frequencies for each section of treatment. A comparison of the optimum reactance versus the predicted reactance shows that the panel designs have the optimum reactance within the previously defined 1/3-octave-band tuning frequencies for reverse-thrust operation.

The faceplate porosities for treatments A, B, and C were selected to give a wide range of acoustic resistance values. Cavity depths were changed as required to maintain the same tuning frequencies for each design. The results from this type of test matrix provide essential data for the optimization of acoustic liner faceplates.

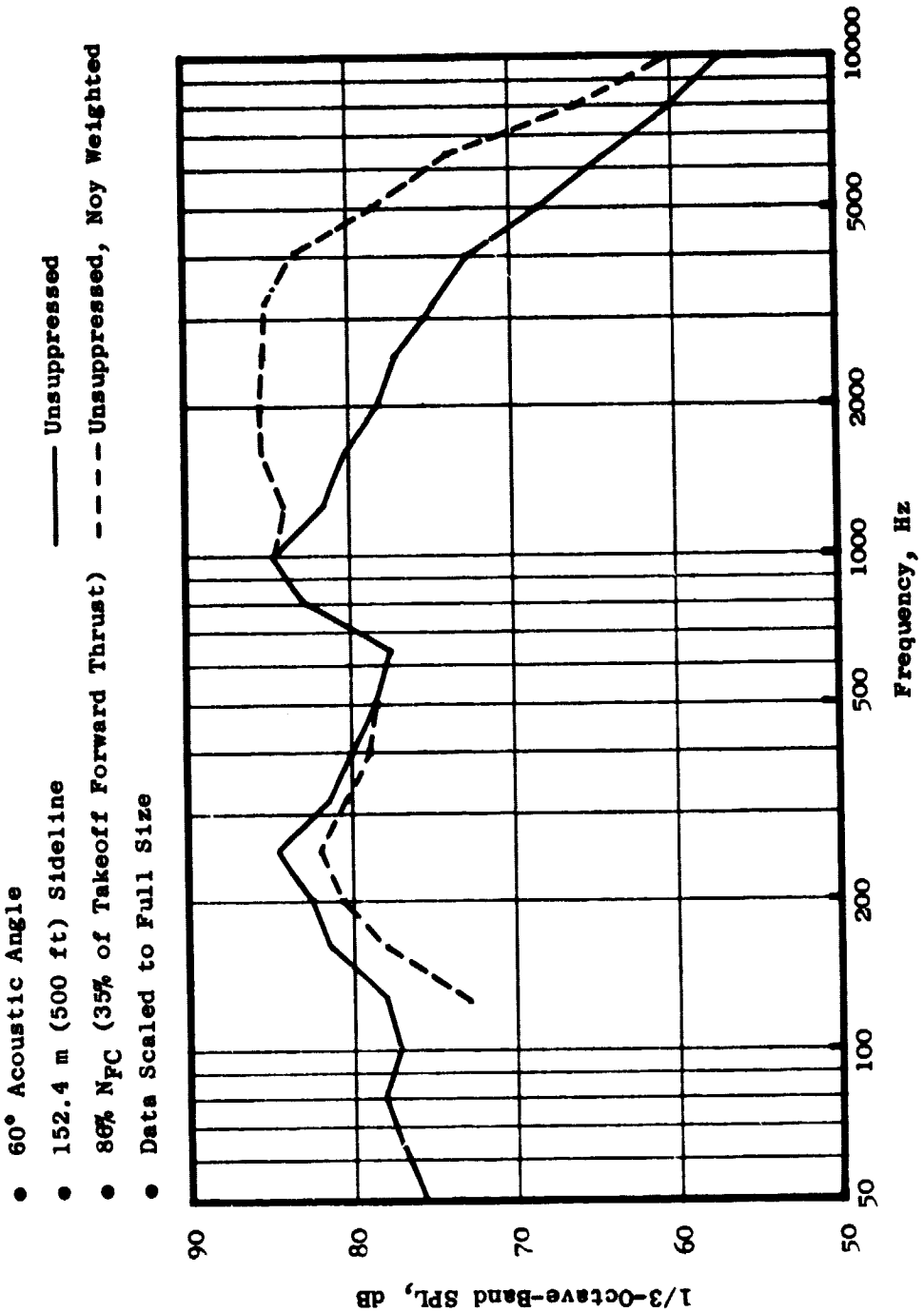

Figure 8. Predicted Reverse-Thrust UTW Engine Noise Spectra at 86% N_{FC} at 60°.

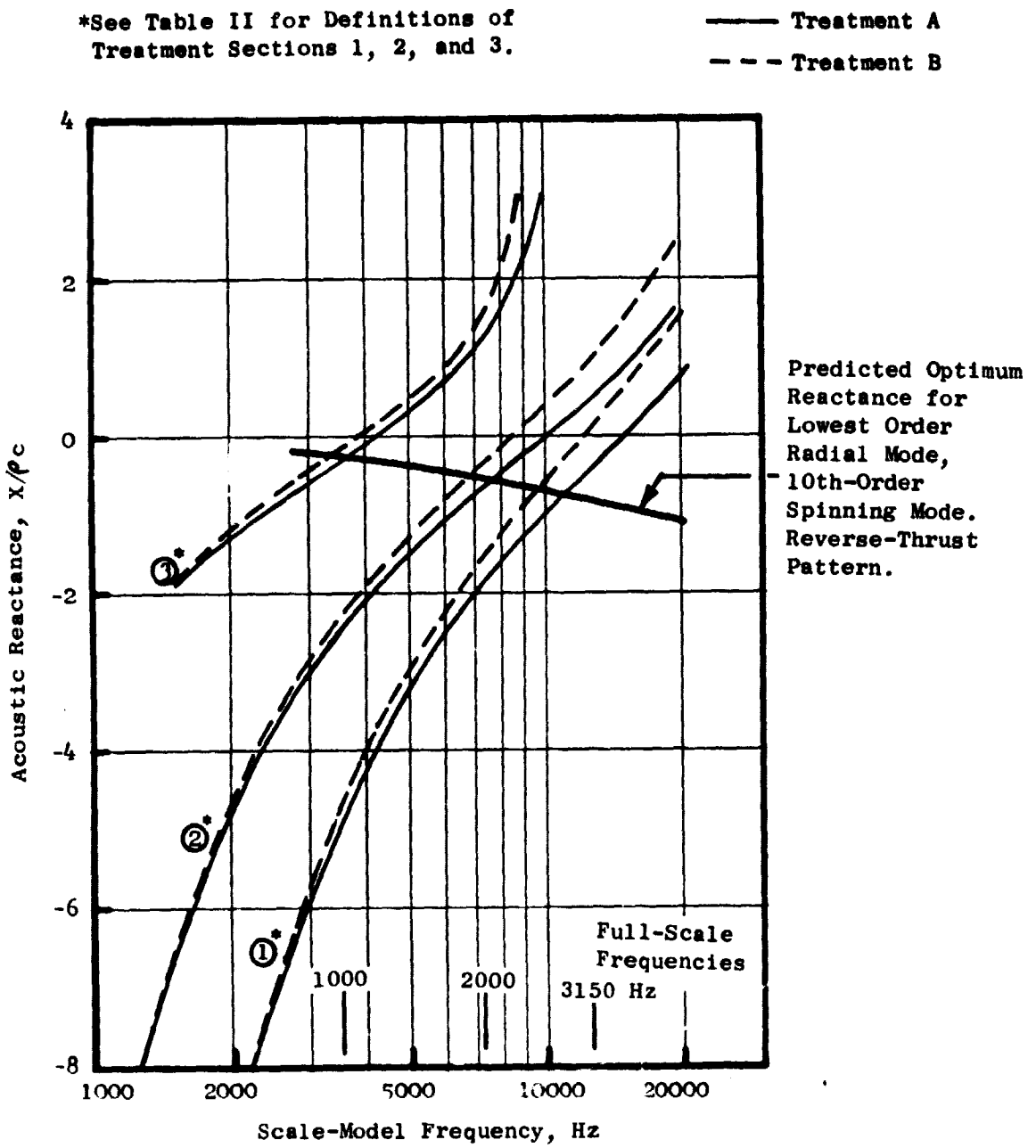

Figure 9. Reverse-Thrust Acoustic Reactance Vs. Frequency for Accelerating Inlet Treatments A and B.

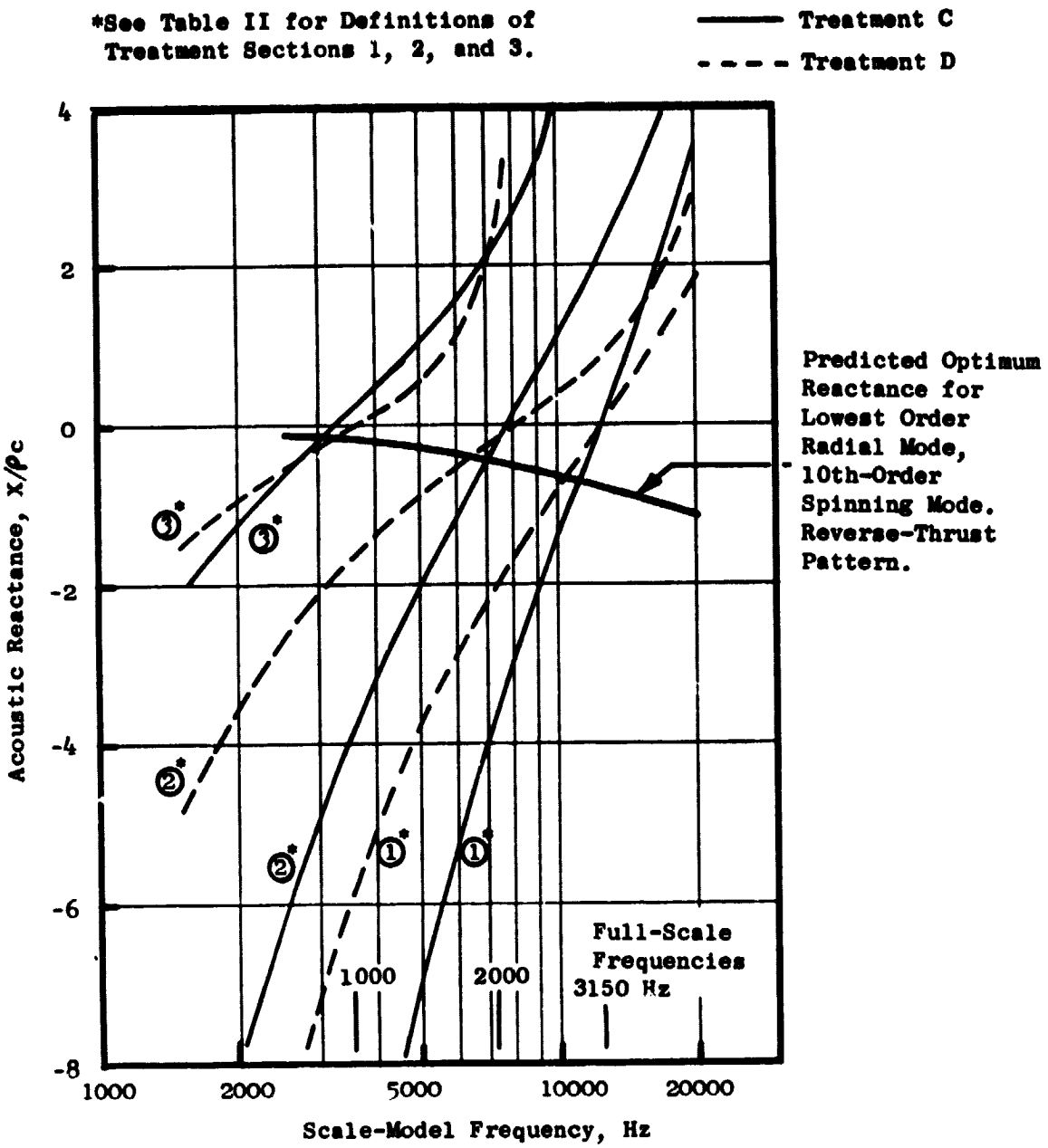

Figure 10. Reverse-Thrust Acoustic Reactance Vs. Frequency for Accelerating Inlet Treatments C and D.

The faceplate porosity is different for each of the three treatment sections to optimize the resistance for each of the different tuning frequencies corresponding to each section of treatment. This order of porosities is optimum for reverse flow but off-design for forward flow. The analytical methods used in the faceplate selection are presented in Reference 7.

5.1.3 Predicted Characteristics in Forward Thrust

The unsuppressed fan-noise spectrum as predicted for the forward-thrust operation at takeoff power (94.5% N_{FC}) is given in Figure 11. Also shown is the Noy-weighted, unsuppressed spectrum; this indicates that the noise level in terms of PNdB peaks at 1000 Hz and 3150 Hz. A significant but somewhat smaller contribution is seen at the 2000-Hz 1/3-octave-band frequency. Thus, for effective PNL suppression, broadband suppression is necessary. The predicted acoustic reactance for inlets A and B are given in Figure 12. The same information for inlets C and D is shown in Figure 13. These predictions are based on the analytical procedure given in Reference 8. Also shown is the predicted optimum reactance versus frequency based on the analytical relations presented in Reference 7. The predicted optimum reactance is for the lowest order radial mode (10th-order, spinning, lobe pattern). The intersection of this curve with the reactance for each section of treatment determines the optimum tuning frequency for that section.

The full-scale, forward-thrust, tuning frequencies for each inlet are summarized below.

Accelerating Inlet Treatment	Section and 1/3-Octave-Band Tuning Frequency (Hz)		
	1	2	3
A	2000	1600	800
B	2000	1600	800
C	2500	1600	800
D	2500	1250	800

Comparing these predicted tuning frequencies with the 1000 and 3150-Hz frequencies from Figure 11, which are required for optimum PNL suppression, shows that none of the configurations are optimized for this condition.

5.2 LOW MACH INLETS

The low Mach inlet (M_{th} = 0.6 at design flow) featured a reduced throat Mach number via a larger throat radius. As indicated in Table IV, the low Mach inlet diffuser contour maintained the same average diffusion angle ($2\theta_{eq}$) and inlet length (L/D_F) as the accelerating inlet. This was achieved

- 60° Acoustic Angle
- 152.4 m (500 ft) Sideline at 61 m (200 ft) Altitude
- 100% N_{FC}
- Full-Scale Data

—— Unsuppressed

- - - - Unsuppressed, Noy Weighted

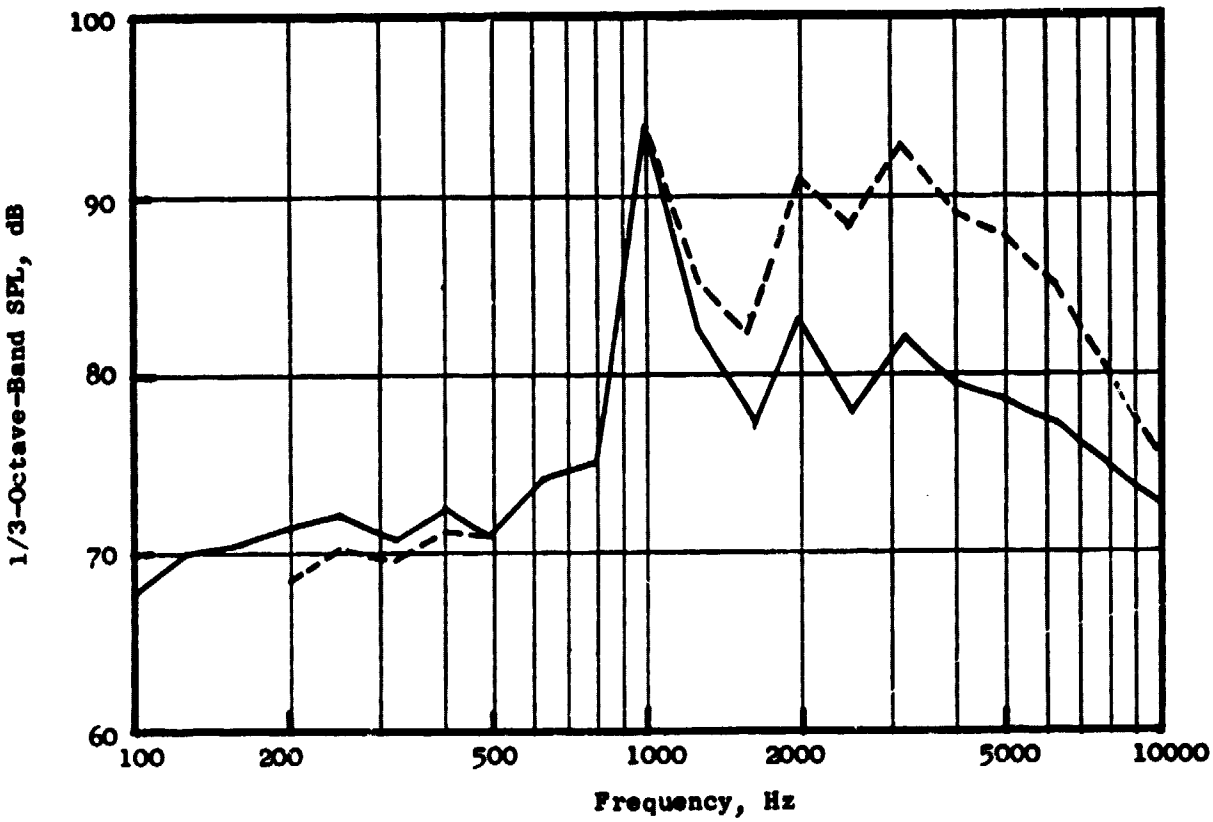

Figure 11. Predicted Unsuppressed Forward-Thrust UTW Fan Spectra at 100% N_{FC} at 60°.

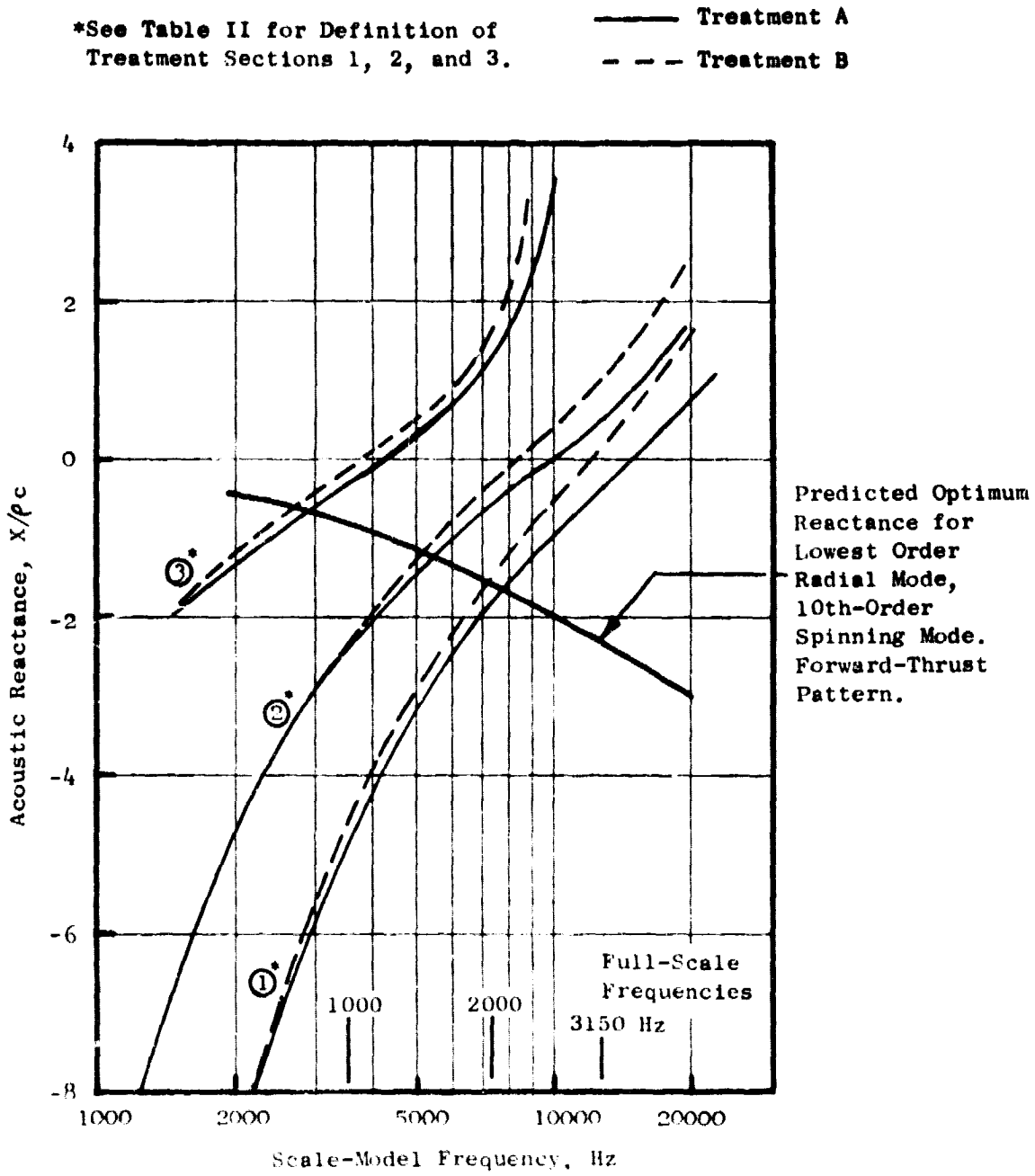

Figure 12. Forward-Thrust Acoustic Reactance Vs. Frequency for Accelerating Inlet Treatments A and B.

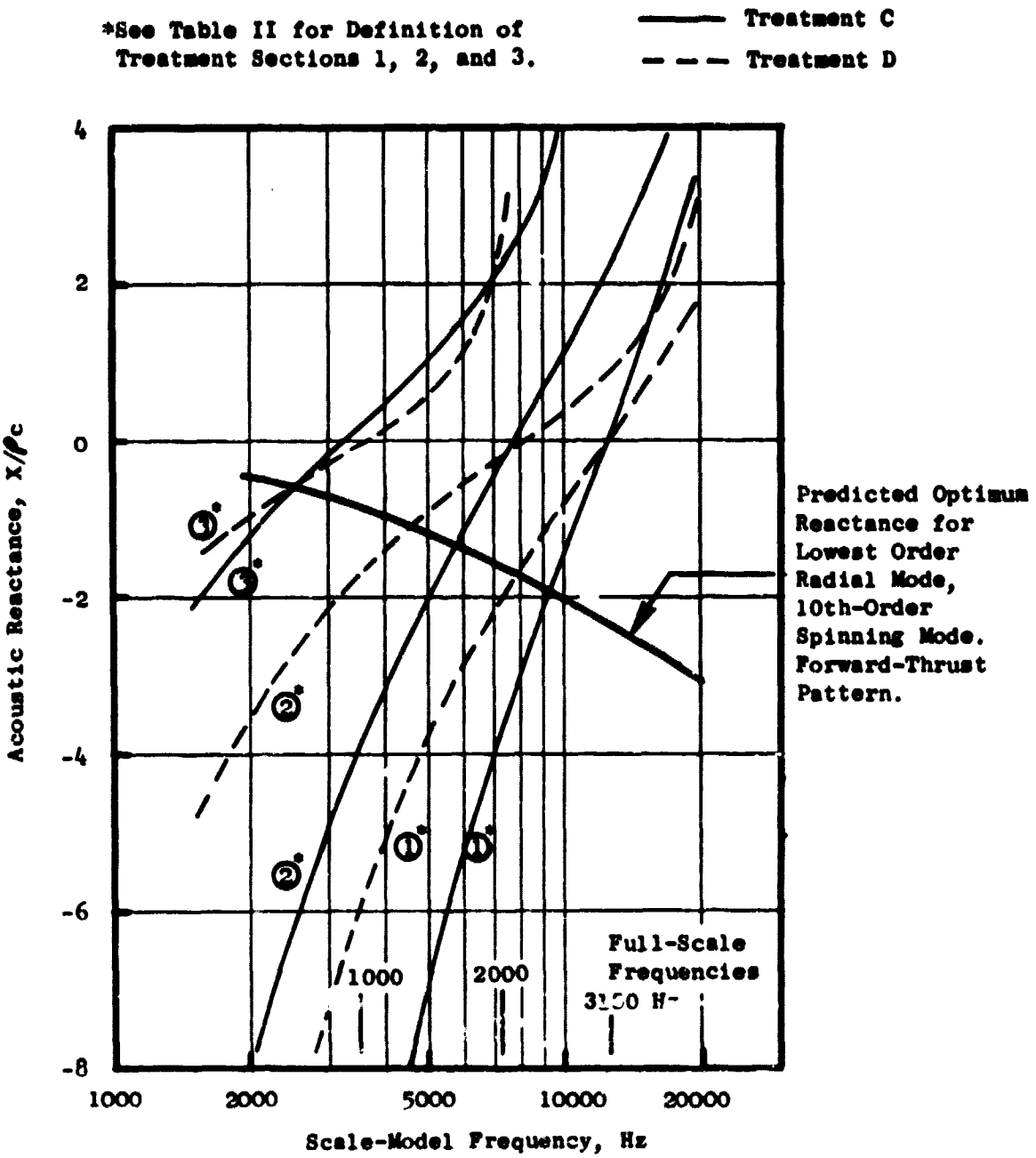

Figure 13. Forward-Thrust Acoustic Reactance Vs. Frequency for Accelerating Inlet Treatments C and D.

by inserting a 13.9-cm (5.506-in.), cylindrical spool piece between the diffuser exit and the fan casing. Considering the relatively low inlet wall Mach numbers (a consequence of low throat Mach number and the cylindrical spool piece), it was anticipated that the desired fan-noise attenuation could be achieved with treatment alone in the low Mach inlet. No attenuations due to Mach number was expected at the M_{th} = 0.6 design point. The coordinates for the low Mach inlet are given in Table VI.

A hard-wall, low Mach inlet and three treated inlets, all to the same contour, were tested. The details of the treatment design are discussed below.

5.2.1 Low Mach Inlet Treatment Configurations

The low Mach number, treated-inlet configurations are defined in Table III. Two of these three configurations are single-degree-of-freedom (SDOF), resonator-type designs while the third utilizes the bulk absorber concept. The faceplate dimensions for each of the configurations are given in Table III.

5.2.2 Treatment Design Procedure

The treatment configurations as defined in Table III were designed to give the optimum suppression with the fan operating in the forward-thrust mode. The unsuppressed and the unsuppressed, Noy-weighted spectra are given in Figure 11. The Noy-weighted spectrum indicates the unsuppressed PNL is controlled at 1000 and 3150 Hz with some contribution also from the 2000-Hz 1/3-octave band. Thus, from this spectrum, it is obvious that an optimum treatment design in terms of PNL suppression requires broadband suppression characteristics. With this in mind, the two treated-inlet configurations with resonator treatment (configurations A and C) were designed to give the three different tuning frequencies as given in Table III. The bulk absorber inlet design (configuration B) has a constant depth of 1.27 cm (0.5 inches). This design selection was based on the performance of previous suppression data obtained from bulk-type materials that demonstrated wide suppression characteristics.

Figure 14 gives the predicted acoustic reactance for the A and C inlet liner designs described in Table III. Also shown is the predicted optimum reactance versus frequency for the lowest order radial mode and 10th-order, spinning, lobe pattern. The intersection of the reactance lines with this curve determines the optimum tuning frequency for each liner section for treatments A and C. The desired tuning frequencies for the liner sections as determined from the Noy-weighted spectrum in Figure 11 are 1000, 2000, and 3150 Hz. The inlet A design gives these tuning frequencies; however, the tuning for treatment C is somewhat different: tuning frequencies are

Table VI. Low Mach Inlet Coordinates.

Aero-Acoustic Lip				Diffuser			
Axial Station		Radius		Axial Station		Radius	
cm	in.	cm	in.	cm	in.	cm	in.
-57.13	-22.492	32.52	12.804	-43.18	-17.000	22.43	8.830
-57.11	-22.484	31.98	12.589	-13.99	-5.506	25.40	10.000
-56.95	-22.420	30.89	12.161	0	0	25.40	10.000
-56.62	-22.292	29.82	11.741	(Fan Face)			
-56.14	-22.102	28.79	11.333				
-55.50	-21.852	27.80	10.943				
-54.28	-21.372	26.41	10.399				
-52.77	-20.777	25.19	9.919				
-51.01	-20.082	24.17	9.515				
-48.34	-19.033	23.14	9.112				
-45.31	-17.839	22.56	8.882				
-43.18	-17.000	22.43	8.830				
(Throat)							

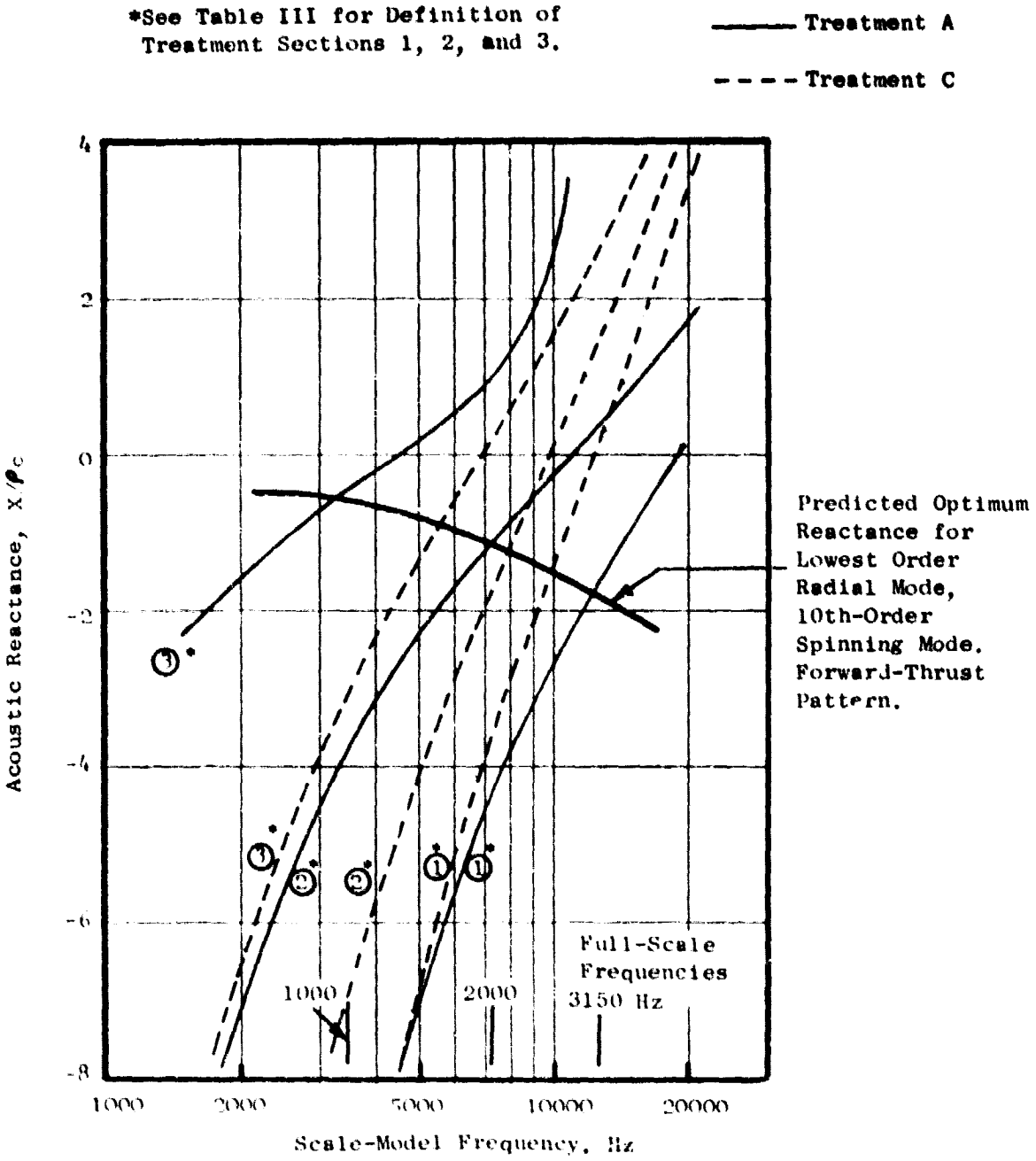

Figure 14. Forward-Thrust Acoustic Reactance Vs. Frequency for Low Mach Inlet Treatments A and C.

1600, 2500, and 3150 Hz. These tuning frequencies are due to the combination of the low-porosity selection and the faceplate materials.

Inlets A and C have constant faceplate porosities of 10% and 3.6% respectively. These porosity values were selected on the basis of previous fan data (Reference 9 for 8% and 2.5%) showing good suppression results for the liner designs with these porosity values.

5.2.3 Predicted Characteristics in Reverse Thrust

As previously discussed, the low Mach inlet configurations were designed for forward-thrust operation. Figure 15 gives the predicted acoustic reactance for the lowest order radial mode and 10th-order, spinning, lobe pattern at the reverse-thrust condition. These predictions result from the analytical methods given in References 7 and 8. The intersection of the predicted optimum reactance with the reactance curve for each section of treatment determines the optimum tuning frequency of each section.

Treatment A full-scale, predicted, 1/3-octave-band tuning frequencies for the reverse-thrust condition are 800, 2500, and 4000 Hz. For treatment C the predicted 1/3-octave-band tuning frequencies are 1600, 2500, and 3150 Hz. No tuning frequency is shown for treatment B because previous data from tests with bulk-type absorber liners have rather flat broadband-noise-suppression characteristics. Since the low Mach inlets were designed for forward thrust, it is not surprising to see that the predicted tuning frequencies do not correspond to the optimum reverse-thrust design frequencies of 1000, 2000, and 3150 Hz. However, the frequencies are reasonably close; thus, good PNL suppression was expected for each design.

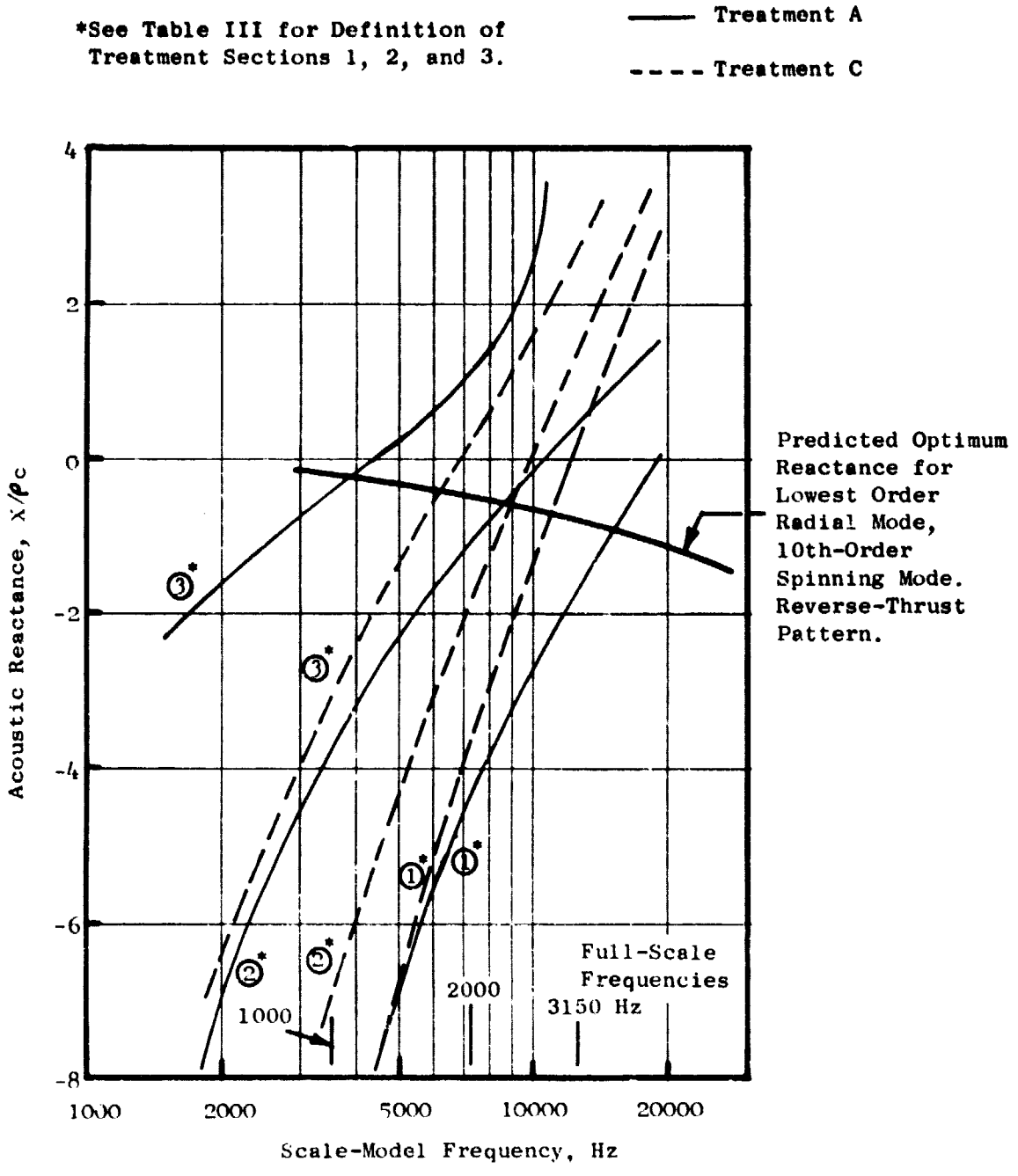

Figure 15. Reverse-Thrust Acoustic Reactance Vs. Frequency for Low Mach Inlet Treatments A and C.

6.0 INSTRUMENTATION AND DATA ACQUISITION

The overall instrumentation was installed for fan aerodynamic-performance measurements and for acoustic measurements. Figure 16 shows the schematic for the vehicle instrumentation. In addition, there were 12 microphones in the anechoic chamber for acoustic far-field measurements, as shown in Figure 1.

6.1 FAN AERODYNAMIC PERFORMANCE INSTRUMENTATION

This was discussed in detail in Reference 2. A brief summary is given below.

6.1.1 Radial Rakes

There were three inlet radial rakes of five total pressure and five total temperature elements each. For reverse-thrust aerodynamic testing, these were reversed and moved forward to the inlet throat. Once the aerodynamic performance map was established and operating lines determined, the rakes were removed from the vehicle; they were not present during acoustic tests.

Three radial rakes of five P_T and five T_T elements each were located in the bypass duct just downstream of the OGV. These rakes were also reversed for reverse-thrust aerodynamic testing and removed from the vehicle during acoustic testing.

Three radial rakes of four P_T and four T_T elements each were located in the core duct. These were not removed from the vehicle for acoustic tests.

6.1.2 Traverse Rakes

Two traversing (arc) rakes with 13 P_T and 13 T_T elements each were located in the bypass duct approximately 3/4-chord downstream of the OGV. These were removed from the vehicle for acoustic tests.

6.1.3 Traverse Probes

Provisions for cobra-probe (P_T and T_T) traverses were incorporated into the vehicle at three different locations. In reverse-pitch aerodynamic operation, a cobra and a wedge probe simultaneously traversed the throat region of the accelerating inlet to provide data for reverse-thrust and exhaust-swirl determination. These traverse probes were removed from the vehicle for acoustic testing.

6.1.4 Static Pressures

Static pressure instrumentation was provided for four purposes: determining airflow, assessing circumferential flow distortion, determining axial profiles, and monitoring vehicle operation during acoustic testing with all rakes (except core duct rakes) removed.

Static pressure taps were located in the inlet, bypass duct exit, and core duct for airflow determination. Inlet weight flow and Mach number profile determination during acoustic tests relied very heavily on a series of static pressure taps in the inlet. The location of these taps and the special method used to accurately determine inlet throat Mach number based on these static taps are discussed in detail in the Appendix.

The procedure for acquisition of fan aerodynamic data (specifically with radial rakes, traversing rakes, etc.) is discussed in Reference 2. In general, the instrumentation and data reduction were coordinated to stay within the following constraints:

- Scannivalve limitations (96 ports, 8 of them alloted to reference pressure, leaving a total of 88 for fan aerodynamics)
- Fan aerodynamic temperature limited to 44

Since the acoustic tests were carried out with all the rakes removed, an additional 20 wall static pressures were monitored and recorded.

6.2 FAN INLET ACOUSTIC INSTRUMENTATION

6.2.1 Far-Field Microphones

Twelve 0.64-cm (0.25-in.) diameter Bruel and Kjaer microphones were located in the facility on a 5.2-m (17-ft) radius from 0° to 110° relative to the inlet axis. The locations are shown schematically in Figure 1. During reverse-thrust testing the microphones at 0° and 10°, and in some cases at 20°, were removed because they would have had exhaust air impinging on them. At the start of each test day, the microphones were calibrated with a pistonphone, and the calibration was recorded on magnetic tape.

6.2.2 Wall Kulites

Four wall Kulites were located at four axial locations on the inlet wall, between the throat and fan face, at a single circumferential orientation. One Kulite was located aft of the bypass OGV. All the Kulites were calibrated at the beginning of each test day. Kulite phase-shift-relation calibrations were determined two ways: first, by applying a pressure on each Kulite simultaneously and observing the direction of the d.c. shift; second, by inserting a clipped sine wave signal into the amplifiers of all Kulites simultaneously and recording the results on magnetic tape.

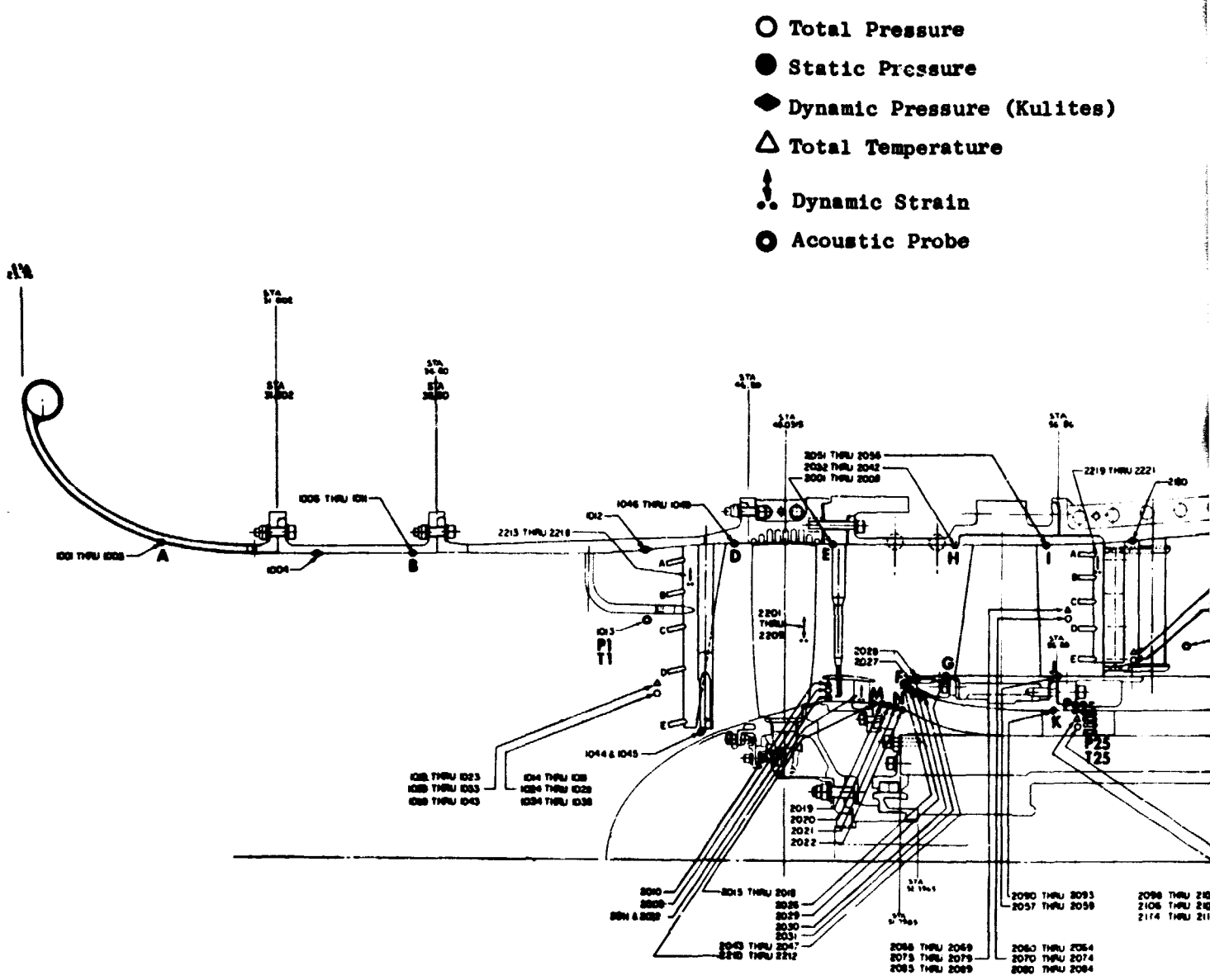

Figure 16. Instrumentation Schematic for UTW Simulator

FOLDOUT

ORIGINAL PAGE
OF POOR QUALITY

otal Pressure

tatic Pressure

ynamic Pressure (Kulites)

otal Temperature

ynamic Strain

coustic Probe

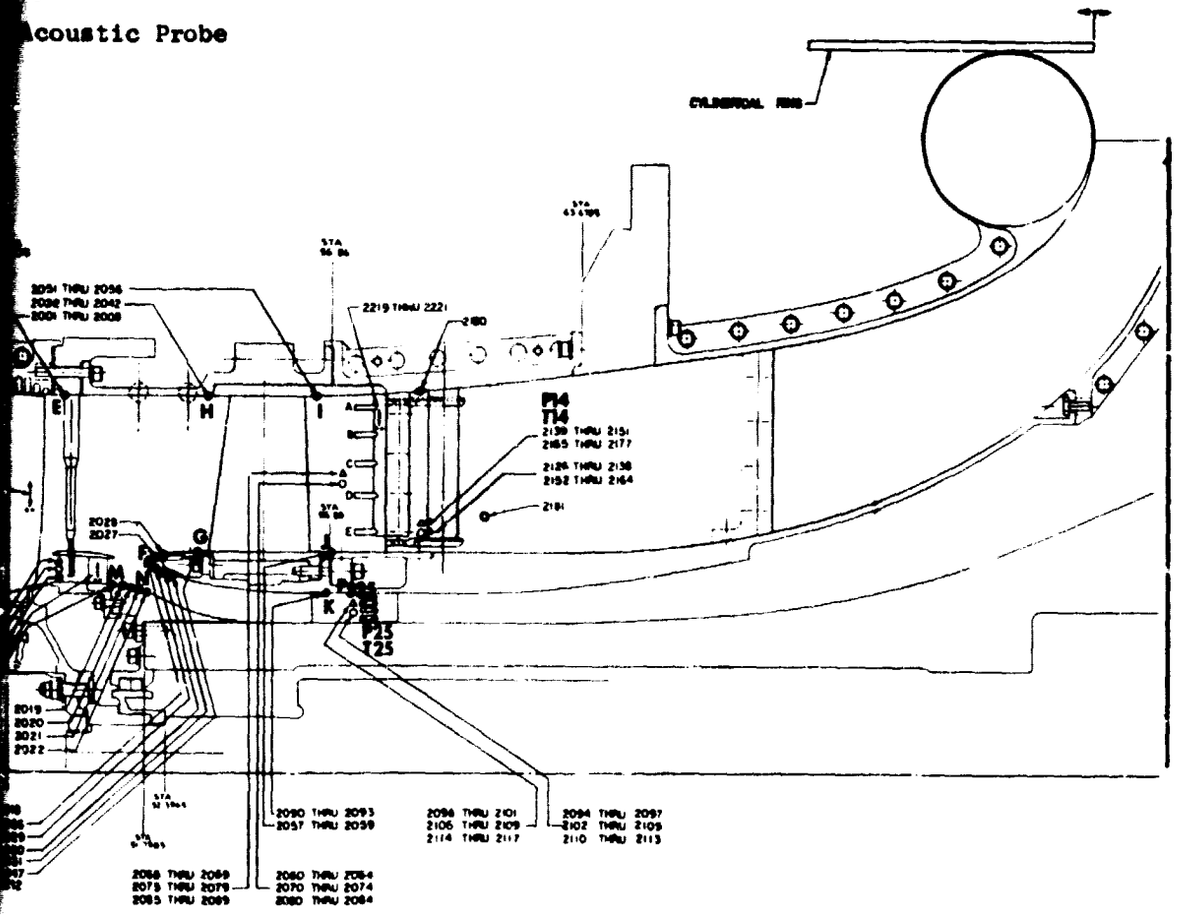

tation Schematic for UTW Simulator Tests.

The acoustic data from the far-field microphones and the Kulites were recorded simultaneously for 60 seconds at each data point on a 28-track, Sangamo Sabre IV recorder which has a 40-kHz capability in the FM mode at 152 cm/sec (60 in./sec). All the microphone and Kulite signals were continuously monitored on oscilloscopes during all the acoustic tests. In addition, the output from one of the microphones (generally the one at 60° to the inlet) was processed through a General Radio analyzer and log converter, and the SPL spectrum was plotted on-line. In addition to providing a check on the test data acquisition, this allowed quick, on-line comparison of configurations, a capability which was useful in making changes to the test plan.

6.2.3 Sound-Separation Probe

General Electric has developed special sound-separation probes for installation in flowing ducts to obtain data for discrimination between acoustic and aerodynamic pressure fluctuations. One of these sound-separation probes was built for the QCSEE simulator test and is shown schematically in Figure 17 mounted in the accelerating inlet for traversing across the stream. The probe was pointed aft to keep the tip from interfering with the high Mach throat region of the inlet.

These probes contain two pressure sensors flush-mounted in the probe tip and axially separated by 2.54 cm (1 in.). The sensors are immersed in the flow to provide a flat frequency response (Figure 18) and phase retention between signals. The sensors are covered with a millipore screen to prevent damage and are separately reloadable in the event of sensor failure.

6.3 MECHANICAL INSTRUMENTATION

The rotor blades, bypass vanes, core vanes, inlet radial rakes, and bypass duct radial rakes were instrumented with strain gages. The strain gages were monitored on a 14-channel recording and monitoring system for all critical testing. Details of the mechanical instrumentation, as well as observations and results, are presented in Reference 2.

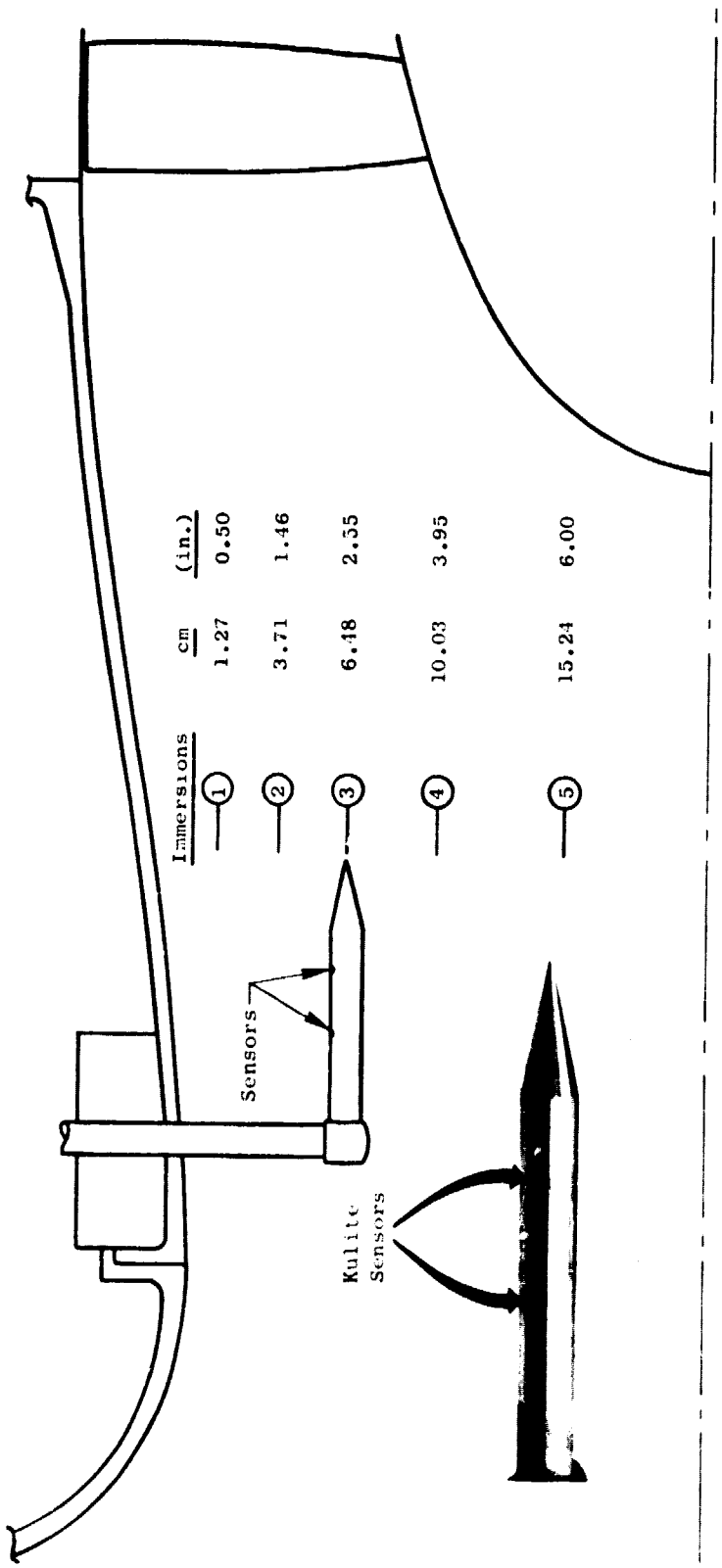

Figure 17. QCSEE Simulator Accelerating Inlet and Sound-Separation Probe.

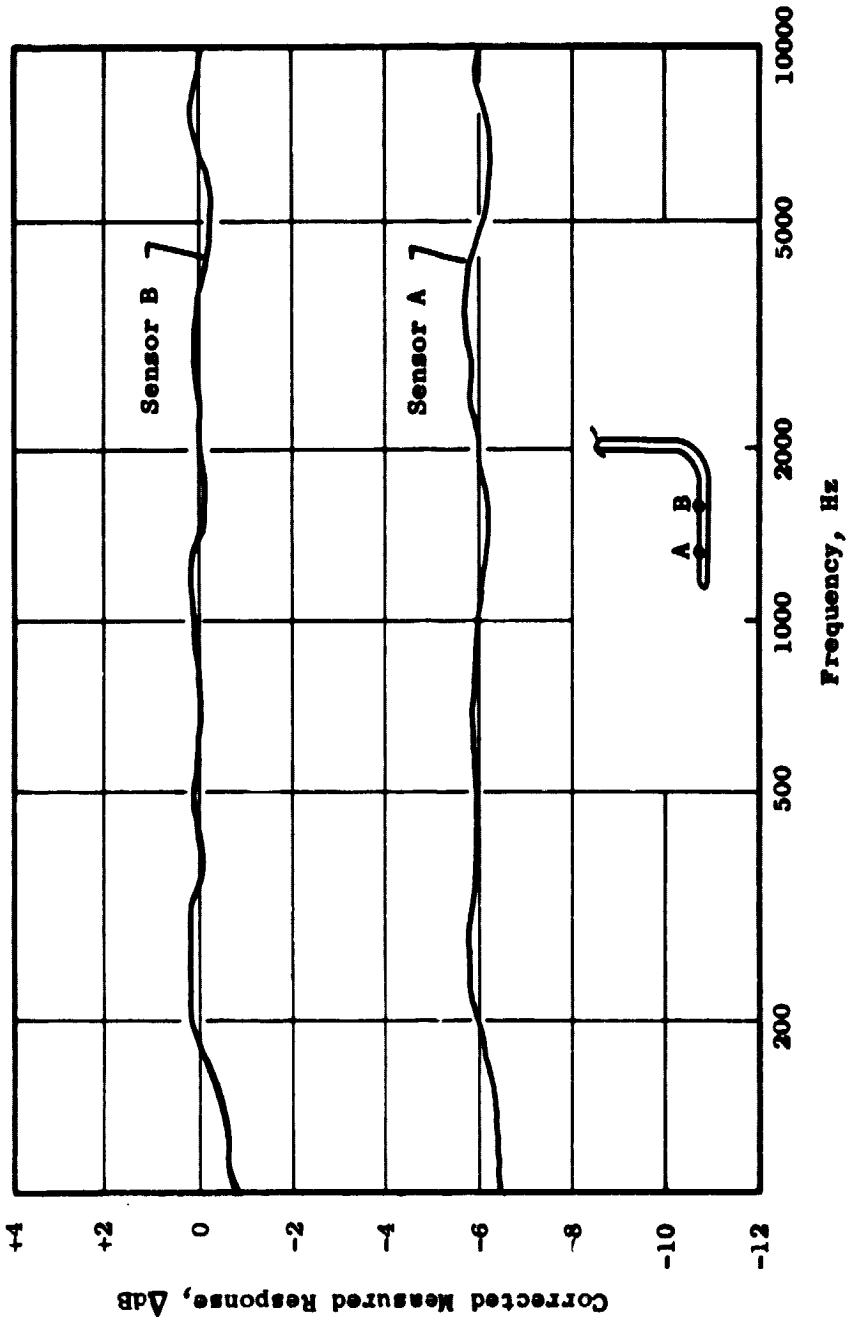

Figure 18. Typical Frequency Response of a Sound-Separation Probe.

7.0 TEST MATRIX

The test program was divided into two segments: fan aerodynamic performance tests and fan acoustic tests. This separation was needed because all the rakes which were needed in the inlet and in the fan bypass for the aerodynamic performance testing had to be removed for the acoustic tests to prevent generation of noise by these flow-path obstructions. A complete listing of all the aerodynamic performance test readings taken is given in Reference 2. After initial vehicle-shakedown tests, the fan performance at nominal rotor blade angle setting (0°) was mapped out with the baseline bellmouth. The discharge valve (DV) setting (related to the exit nozzle area), blade speed, and blade angle are the independent parameters that uniquely determine a fan aerodynamic test condition. Accordingly, it is appropriate and convenient to identify a given test condition by the DV setting once the blade angle and speed are fixed. The fan aerodynamic performance map for the baseline bellmouth inlet at 0° (nominal) blade angle setting is shown in Figure 19. The operating line through the takeoff condition was at a DV setting of 7.7. This corresponds to a full-scale nozzle area of 1.60 m^2 (2480 $in.^2$). Numerically higher DV settings correspond to higher fan back pressure (towards stall) - that is, lower nozzle area, and numerically lower DV settings correspond to lower fan back pressure (toward choke) - that is, at larger nozzle areas. Figure 20 gives a plot of full-size-engine nozzle area as a function of DV setting. Most of the forward-thrust acoustic tests for inlet and treatment evaluation at nominal rotor pitch angle were conducted at the takeoff DV setting of 7.7. Approach-condition testing at +5° blade angle and reverse-thrust testing were conducted at different DV settings, and the choice of DV setting is discussed in the appropriate sections.

The core flow is collected in a manifold and exhausted through two pipes, one on either side of the vehicle, to a set of suction pumps. The pumps are outside the test chamber and independently control the core flow to maintain the desired bypass-ratio schedule for a given discharge valve (DV) setting.

The corrected fan speed (as percent of design speed), DV setting, blade angle setting, and configuration (inlet and treatment) for each acoustic-data point are given in Table VII.

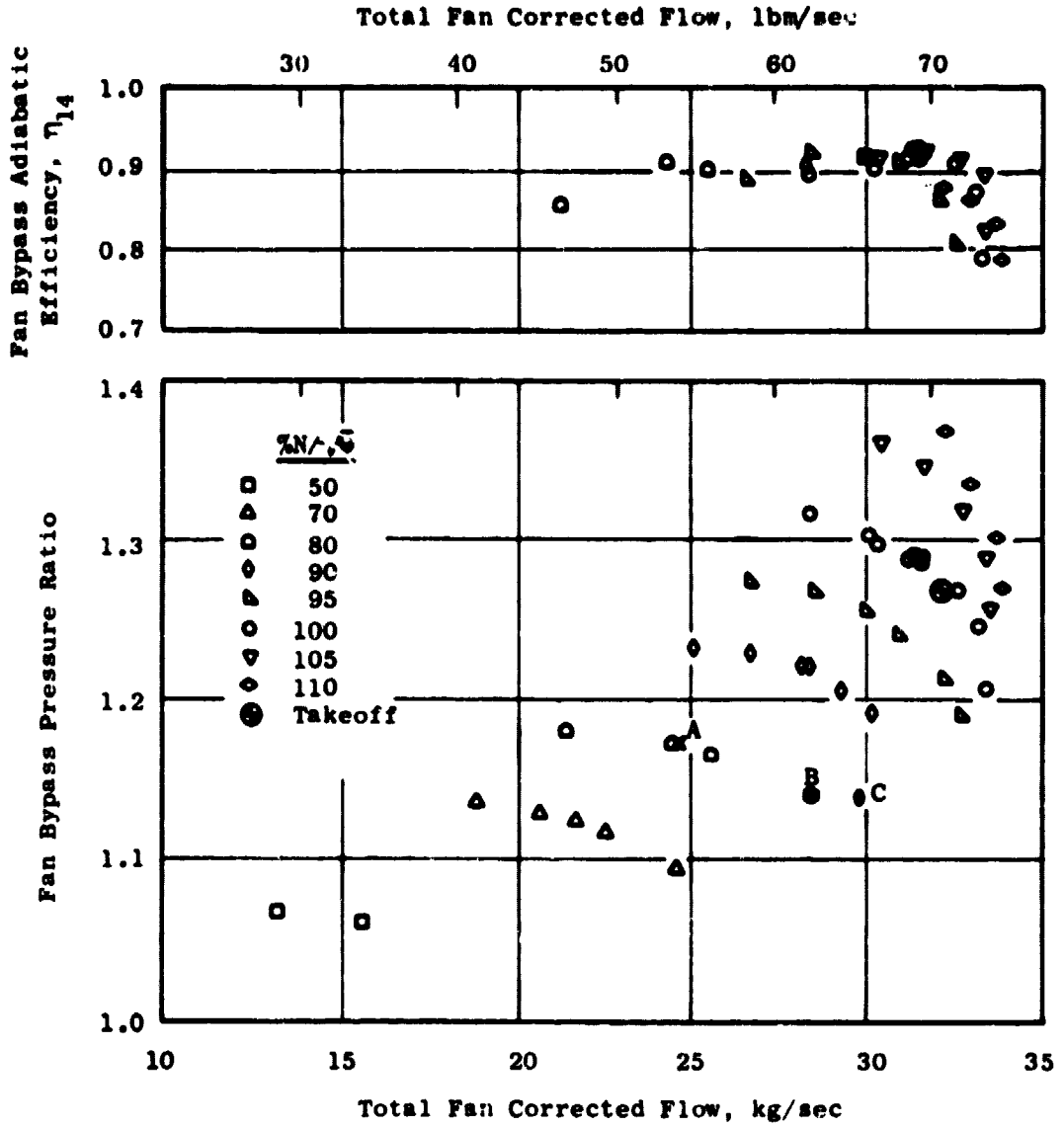

Figure 19. Fan Performance Map, 0° Blade Angle.

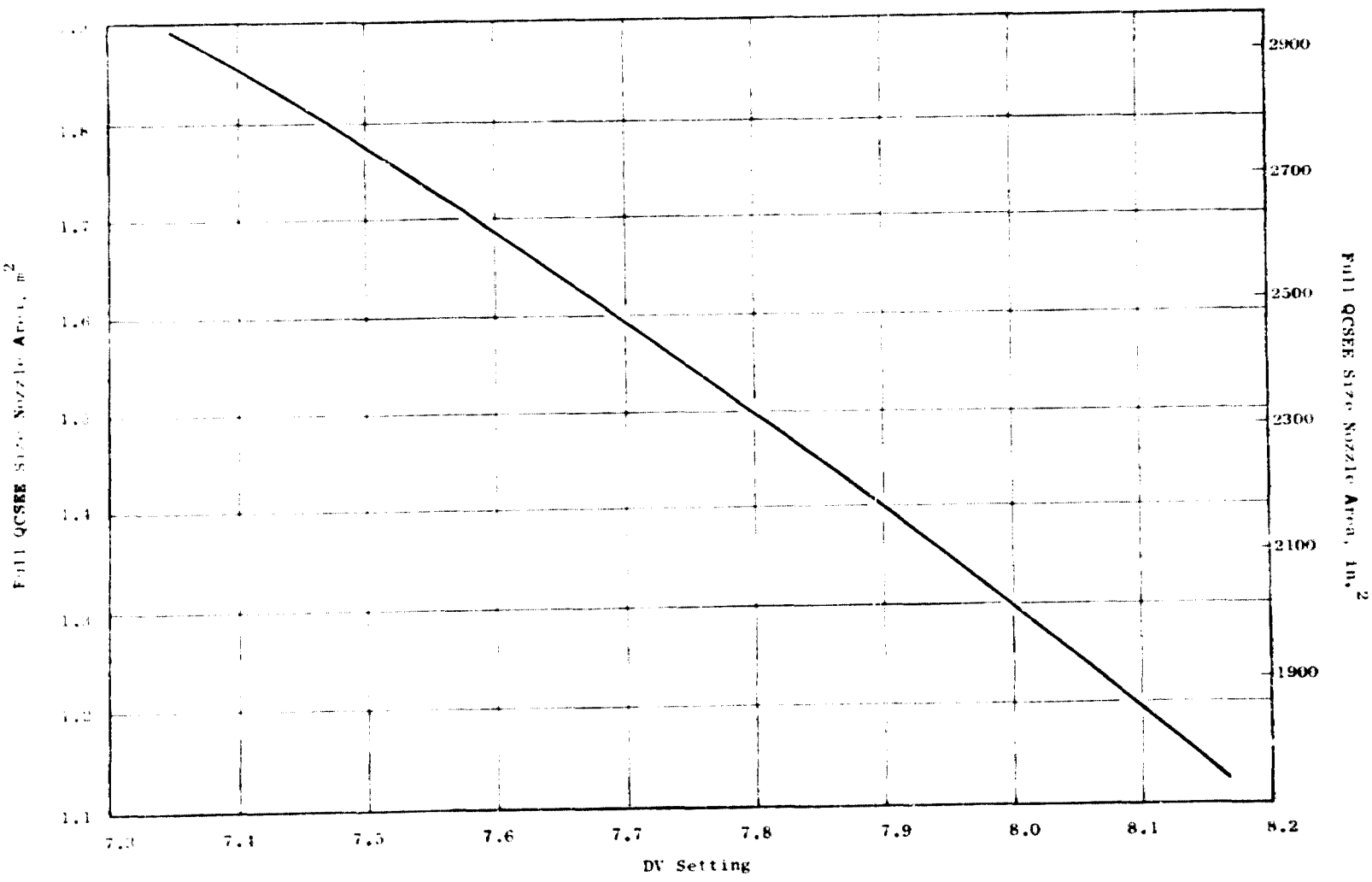

Figure 20. Full-Size Nozzle Area Vs. Discharge Valve (DV) Setting.

Table VII. Tabulation of Acoustic Test Conditions.

Run	Configuration	Thrust Mode and Blade Angle	Reading	Discharge Valve	Percent Speed	Immersion Number
2	Baseline Bellmouth	Forward 0°	6	7.7	70	
			7	7.7	78	
			8	7.7	90	
			9	7.7	95	
			10	7.7	98	
			11	7.7	102	
			12	7.7	105	
			13	7.4	102	
			14	7.4	95	
			15	7.4	90	
			16	7.4	78	
			17	7.9	78	
			18	7.9	90	
			19	7.9	95	
			20	7.9	100	
			21	7.9	102	
4	Accelerating Inlet, Hard Wall	Forward 0°	5	7.75	70	
			6	7.75	78	
			7	7.75	90	
			8	7.75	93.5	
			9	7.75	96	
			10	7.75	98.5	
			11	7.75	99.5	
			12	7.75	100.5	
			13	7.75	101.5	
			14	7.75	103	
			15	7.75	99	
			16	7.7	97.1	
5	Accelerating Inlet, Treatment B	Forward 0°	4	7.75	70	
			5	7.75	78	
			6	7.75	90	
			7	7.75	93.5	
			8	7.75	96	
			9	7.75	98.5	
			10	7.75	99.5	
			11	7.75	100.5	
			12	7.75	101.5	
			13	7.75	103	
			14	7.75	99	
			15	7.7	97.7	

Table VII. Tabulation of Acoustic Test Conditions. (Continued)

Run	Configuration	Thrust Mode and Blade Angle	Reading	Discharge Valve	Percent Speed	Immersion Number
12	Baseline Bellmouth	Forward +5°	4	7.40	83	
			5	7.78	90.5	
			6	7.65	91.5	
			7	7.5	92.5	
			8	7.9	95	
			9	7.65	95	
			10	7.4	95	
			11	7.78	98	
			12	7.4	98.5	
			13	7.78	105	
			14	7.4	105	
			15	7.4	110	
			16	7.78	110	
			17	7.9	100	
			18	7.5	100	
			19	7.9	80	
			20	7.78	80	
13	Accelerating Inlet, Treatment B (Sound Separation Probe Run)	Forward +5°	4	7.78	90.5	1
			5	7.78	90.5	2
			6	7.78	90.5	3
			7	7.78	90.5	4
			8	7.78	90.5	5
			9	7.4	110	1
			10	7.4	110	2
			11	7.4	110	3
			12	7.4	110	4
			13	7.4	110	5
			14	7.5	92.5	1
			15	7.5	92.5	2
			16	7.5	92.5	3
			17	7.5	92.5	4
			18	7.5	92.5	5
			19	7.78	98	1
			20	7.78	98	2
			21	7.78	98	3
			22	7.78	98	4
			23	7.78	98	5

Table VII. Tabulation of Acoustic Test Conditions. (Continued)

Run	Configuration	Thrust Mode and Blade Angle	Reading	Discharge Valve	Percent Speed	Immersion Number
14	Accelerating Inlet, Treatment B	Forward +5°	4	7.4	83	
			5	7.78	90.5	
			6	7.65	91.5	
			7	7.5	92.5	
			8	7.9	95	
			9	7.65	95	
			10	7.4	95	
			11	7.78	98	
			12	7.4	98.5	
			13	7.78	105	
			14	7.4	105	
			15	7.4	110	
			16	7.4	110	
			17	7.78	110	
			18	7.9	100	
			19	7.5	100	
			20	7.9	80	
			21	7.78	80	
19	Accelerating Inlet, Treatment B, Flight Lip	Forward 0°	4	7.75	70	
			5	7.75	78	
			6	7.75	90	
			7	7.75	93.5	
			8	7.75	96	
			9	7.75	98.5	
			10	7.75	99	
			11	7.75	99.5	
			12	7.75	100.5	
			13	7.75	101.5	
			14	7.75	103	
			15	7.75	99	
			16	7.75	78	
26	Accelerating Inlet, Treatment B	Reverse -100°	4	6.37	60	
			5	6.37	80	
			6	6.37	90	
			7	6.37	100	
			8	6.37	86	
			9	6.37	83	
			10	6.37	75	

Table VII. Tabulation of Acoustic Test Conditions. (Continued)

Run	Configuration	Thrust Mode and Blade Angle	Reading	Discharge Valve	Percent Speed	Immersion Number
27	Accelerating Inlet, Hard Wall	Reverse -100°	1	6.37	60	
			2	6.37	80	
			3	6.37	90	
			4	6.37	100	
			5	6.37	86	
			6	6.37	83	
			7	6.37	75	
28	Accelerating Inlet, Treatment A	Reverse -100°	1	6.37	83	
			2	6.37	86	
			3	6.37	90	
			4	6.37	100	
			5	6.37	80	
			6	6.37	75	
			7	6.37	60	
29	Accelerating Inlet, Treatment C	Reverse -100°	4	6.37	83	
			5	6.37	86	
			6	6.37	90	
			7	6.37	100	
				6.37	80	
			9	6.37	75	
30	Accelerating Inlet, Treatment D	Reverse -100°	1	6.37	83	
			2	6.37	86	
			3	6.37	90	
			4	6.37	100	
			5	6.37	80	
			6	6.37	75	
			7	6.37	60	
31	Accelerating Inlet, Hard Wall	Reverse -95°	4	6.37	100	
			5	6.37	90	
			6	6.37	85	
			7	6.37	80	
			8	6.37	75	
			9	6.37	70	
			10	6.37	60	

Table VII. Tabulation of Acoustic Test Conditions. (Continued)

Run	Configuration	Thrust Mode and Blade Angle	Reading	Discharge Valve	Percent Speed	Immersion Number
32	Accelerating Inlet, Treatment D	Reverse -95°	1	6.37	75	
			2	6.37	80	
			3	6.37	85	
			4	6.37	90	
			5	6.37	100	
			6	6.37	70	
			7	6.37	60	
33	Accelerating Inlet, Treatment D	Reverse -105°	1	6.37	60	
			2	6.37	70	
			3	6.37	75	
			4	6.37	80	
			5	6.37	85	
			6	6.37	90	
			7	6.37	100	
34	Accelerating Inlet, Hard Wall	Reverse -105°	4	6.37	60	
			5	6.37	70	
			6	6.37	75	
			7	6.37	80	
			8	6.37	85	
			9	6.37	90	
			10	6.37	100	
35	Accelerating Inlet, Treatment D	Forward 0°	1	7.75	70	
			2	7.75	78	
			3	7.75	90	
			4	7.75	93.5	
			5	7.75	96	
			6	7.75	98.5	
			7	7.75	99.5	
			8	7.75	100.5	
			9	7.75	101.5	
			10	7.75	103	
			11	7.75	99	
			12	7.7	97.1	
36	Baseline Bellmouth (Rerun)	Forward 0°	4	7.7	70	
			5	7.7	78	
			6	7.7	90	
			7	7.7	95	
			8	7.7	98	
			10	7.7	102	
			11	7.7	105	

Table VII. Tabulation of Acoustic Test Conditions. (Continued)

Run	Configuration	Thrust Mode and Blade Angle	Reading	Discharge Valve	Percent Speed	Immersion Number
39	Low Mach Inlet, Treatment A	Forward 0°	4	7.75	60	
			5	7.75	70	
			6	7.75	80	
			7	7.75	90	
			8	7.75	95	
			9	7.75	98.5	
			10	7.75	99.5	
			11	7.75	103	
40	Low Mach Inlet B	Forward 0°	4	7.75	60	
			5	7.75	70	
			6	7.75	80	
			7	7.75	90	
			8	7.75	95	
			9	7.75	98.5	
			10	7.75	99.5	
			11	7.75	103	
41	Low Mach Inlet C	Forward 0°	1	7.75	60	
			2	7.75	70	
			3	7.75	80	
			4	7.75	90	
			5	7.75	95	
			6	7.75	98.5	
			7	7.75	99.5	
			8	7.75	103	
42	Low Mach Inlet Hard wall	Forward 0°	1	7.75	60	
			2	7.75	70	
			3	7.75	80	
			4	7.75	90	
			5	7.75	95	
			6	7.75	98.5	
			7	7.75	99.5	
			8	7.75	103	

Table VII. Tabulation of Acoustic Test Conditions. (Concluded)

Run	Configuration	Thrust Mode and Blade Angle	Reading	Discharge Valve	Percent Speed	Immersion Number
43	Low Mach Inlet A	Reverse 100°	4	6.37	60	
			5	6.37	75	
			6	6.37	80	
			7	6.37	83	
			8	6.37	86	
			9	6.37	90	
			10	6.37	100	
			11	0.53	100	
			12	0.53	90	
			13	0.53	86	
			14	0.53	83	
			15	0.53	80	
			16	0.53	75	
			17	0.53	60	
44	Low Mach Inlet B	Reverse 100°	4	6.37	60	
			5	6.37	75	
			6	6.37	80	
			7	6.37	83	
			8*	6.37	83	
			9	6.37	86	
			10	6.37	90	
			11	6.37	100	
*No acoustic data.						
45	Low Mach Inlet C	Reverse -100°	1	6.37	60	
			2	6.37	75	
			3	6.37	80	
			4	6.37	83	
			5	6.37	86	
			6	6.37	90	
			7	6.37	100	
46	Low Mach Inlet, Hard Wall	Reverse -100°	1	6.37	60	
			2	6.37	75	
			3	6.37	80	
			4	6.37	83	
			5	6.37	86	
			6	6.37	90	
			7	6.37	100	
			8	0.54	100	
			9	0.54	90	
			10	0.54	80	
			11	0.54	60	

8.0 DATA REDUCTION

Data-reduction procedures were specified for the seven data modes described below:

Fan Aerodynamic Performance Tests

Mode 1 - Conventional-pitch test mode with all fixed, radial rakes installed

Mode 1 (Mod) - Conventional-pitch traverse mode for cobra and/or wedge probes

Mode 2 - Conventional-pitch test mode for traversing the bypass OGV with both arc rakes simultaneously

Mode 4 - Reverse-pitch test mode with all fixed, radial rakes installed

Mode 5 - Reverse-pitch test mode for simultaneous cobra and wedge-probe traverse of inlet throat

Fan Acoustic Tests

Mode 6 - Conventional-pitch test mode for operating-line monitoring for acoustic testing with fixed rakes removed

Mode 7 - Reverse-pitch test mode for monitoring vehicle acoustic testing.

In Mode 6, the mode for forward-thrust acoustic testing, the axial profile of static pressures measured in the inlet was used to obtain inlet flow and throat Mach number. The procedure used is explained in the Appendix.

In Mode 6 and 7, the mode for reverse-thrust acoustic testing, the core flow was measured by an orifice in the core suction system. The bypass flow was obtained by measurements of wall static pressures aft of the OGV (between the OGV and the discharge value) and total pressure and total temperature measurements in the stack leading to the discharge valve.

Acoustic data, recorded on a 28-channel Sangamo Sabre IV tape recorder, was processed using a General Radio 1927 real-time analyzer for digital output that was run through a Full-Scale Data Reduction (FSDR) Program. Corrections for microphone responses were done in this program as was data extrapolation using appropriate atmospheric-absorption corrections. Scaling

of the model data to full size included (1) an adder of 10 times the logarithm of the weight/flow ratio between model and full size, plus (2) a 1/3-octave-band frequency shift based upon the blade passing frequency of the 1/3-octave bands which contain the model and full-scale blade passing frequencies. The printout from the FSDR program (contained in Volume II) consisted of measured model SPL on the 5.2-m (17-ft) arc and full-size QCSEE (71:20) data on 61-m (200-ft) and 162-m (500-ft) sidelines. A schematic of the acoustic data system is given in Figure 21. The repeatability of the entire data-reduction system (at Evendale, at R&DC, and between the two facilities) was within $\pm$0.5 dB. Narrowbands of 20-Hz bandwidth were obtained for selected cases using a Federal Scientific UA-6A Ubiquitous Spectrum Analyzer. The methods used for reducing the data from the sound-separation probe are discussed in Section 9.5.

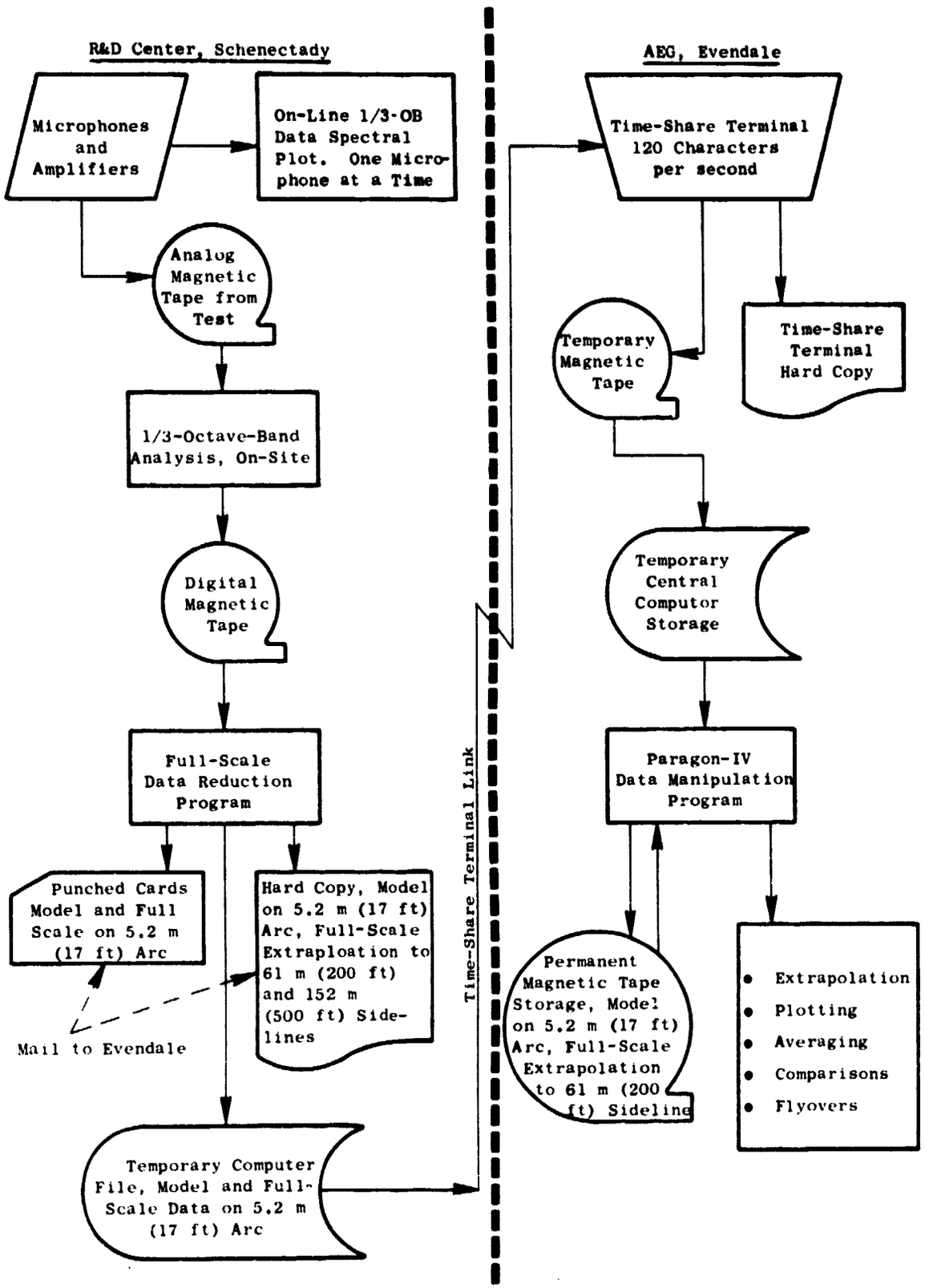

Figure 21. Schematic of Acoustic Data-Reduction System.

9.0 FORWARD-THRUST RESULTS

9.1 BASELINE BELLMOUTH INLET

9.1.1 Summary of Fan Aerodynamic Performance

After the initial mechanical shakedown tests of the facility and vehicle, a complete aerodynamic-performance test was conducted in order to determine the fan performance characteristics and define the operating conditions at which acoustic data were to be taken. Figure 19 shows the fan aerodynamic-performance map at nominal rotor blade setting (0°) with the bellmouth inlet.

Along a fixed-area operating line through the aerodynamic design point (the design speed and nominal blade angle), measured flow of 30.6 kg/sec (67.5 lbm/sec) and bypass pressure ratio of 1.30 are, respectively, 5.5% and 3.0% less than the design values of 32.4 kg/sec (71.4 lb/sec) and pressure ratio of 1.34. The bypass adiabatic efficiency is 0.87 which occurs on a operating line approximately 4% more open than design.

Measured performance of the fan hub flow, Figure 22, is close to the design-point objective. Comparison is made at design speed and nominal blade angle at a flow of 30.6 kg/sec (67.5 lbm/sec). This flow is significant because it is the measured flow along an operating line through the design point on the fan bypass map. The measured hub pressure ratio slightly exceeds the design-point objective of 1.23. The core adiabatic efficiency of 0.84 is six points higher than the predicted value of 0.78.

Fan performance tests were also run at +5° (closed) and -5° (open) rotor pitch settings. Figures 23 and 24 show the performance maps for these two conditions respectively. Fan performance at +5° (closed) and -5° (open) rotor pitch angles exhibit expected trends. Speed lines shift to higher flow when the rotor pitch is opened from nominal and shift to lower flow as the rotor is closed. Peak efficiency is slightly higher for the closed-pitch angles at comparable speeds but drops significantly as the rotor is opened. Peak efficiency occurs at or near 100% N_{FC} for the +5° (closed) blade angle and drops off less rapidly with overspeed than for the nominal blade angle. For the -5° (open) pitch setting, peak efficiency occurs at about 95% speed and appears to fall off more rapidly with speed increase than for the nominal pitch setting. Also, a deterioration in peak efficiency is noted at lower speeds.

To meet the required takeoff fan flow, bypass pressure ratio, and corrected speed (94.5%) the rotor must be opened approximately 3° from nominal rather than the pretest estimate of 1° open. Increased speed at a less open-pitch setting however, would also satisfy the thrust and flow requirements and would additionally improve efficiency because of the efficiency trend

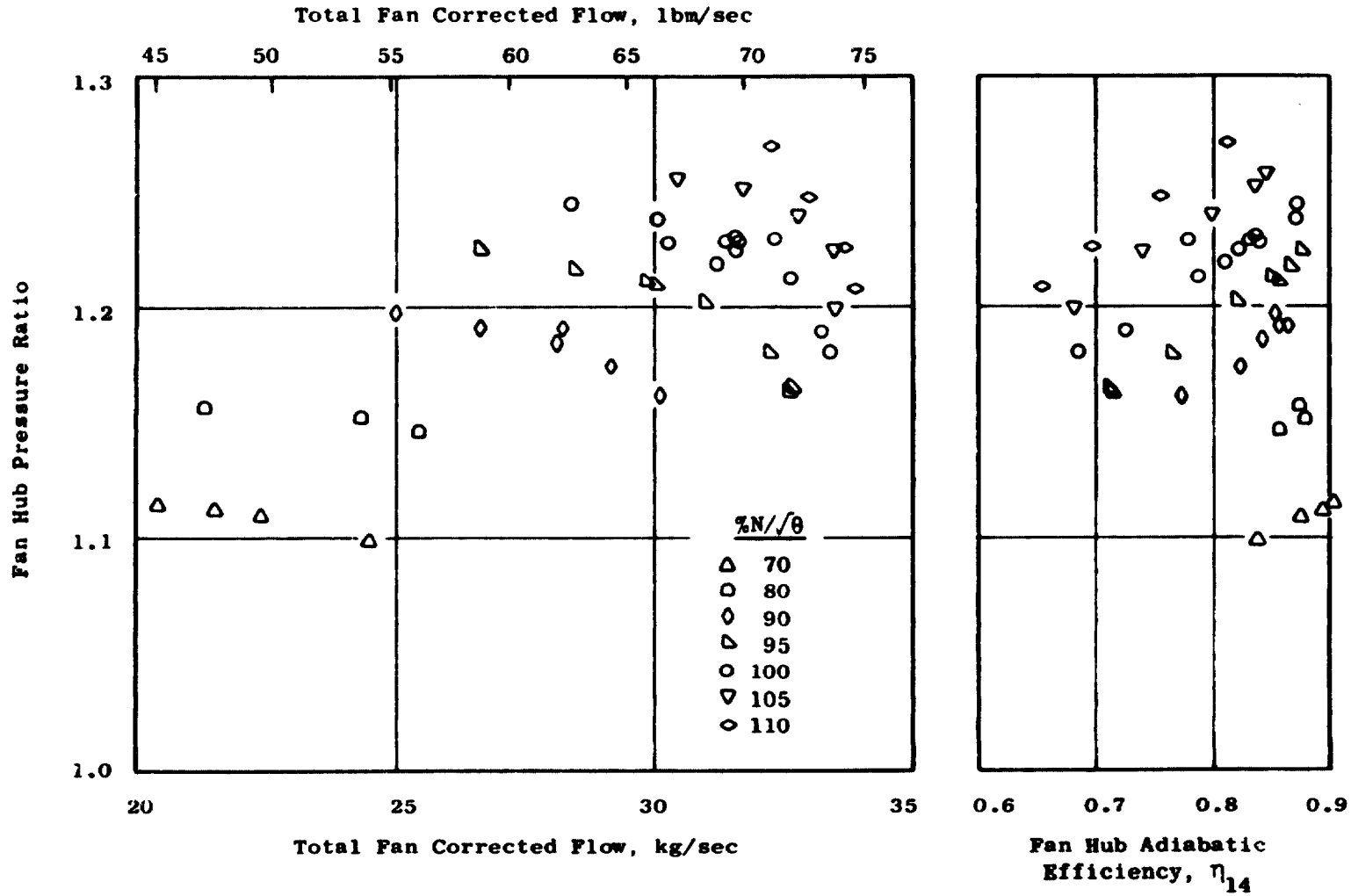

Figure 22. Fan Hub Performance Map, 0° (Nominal) Blade Angle.

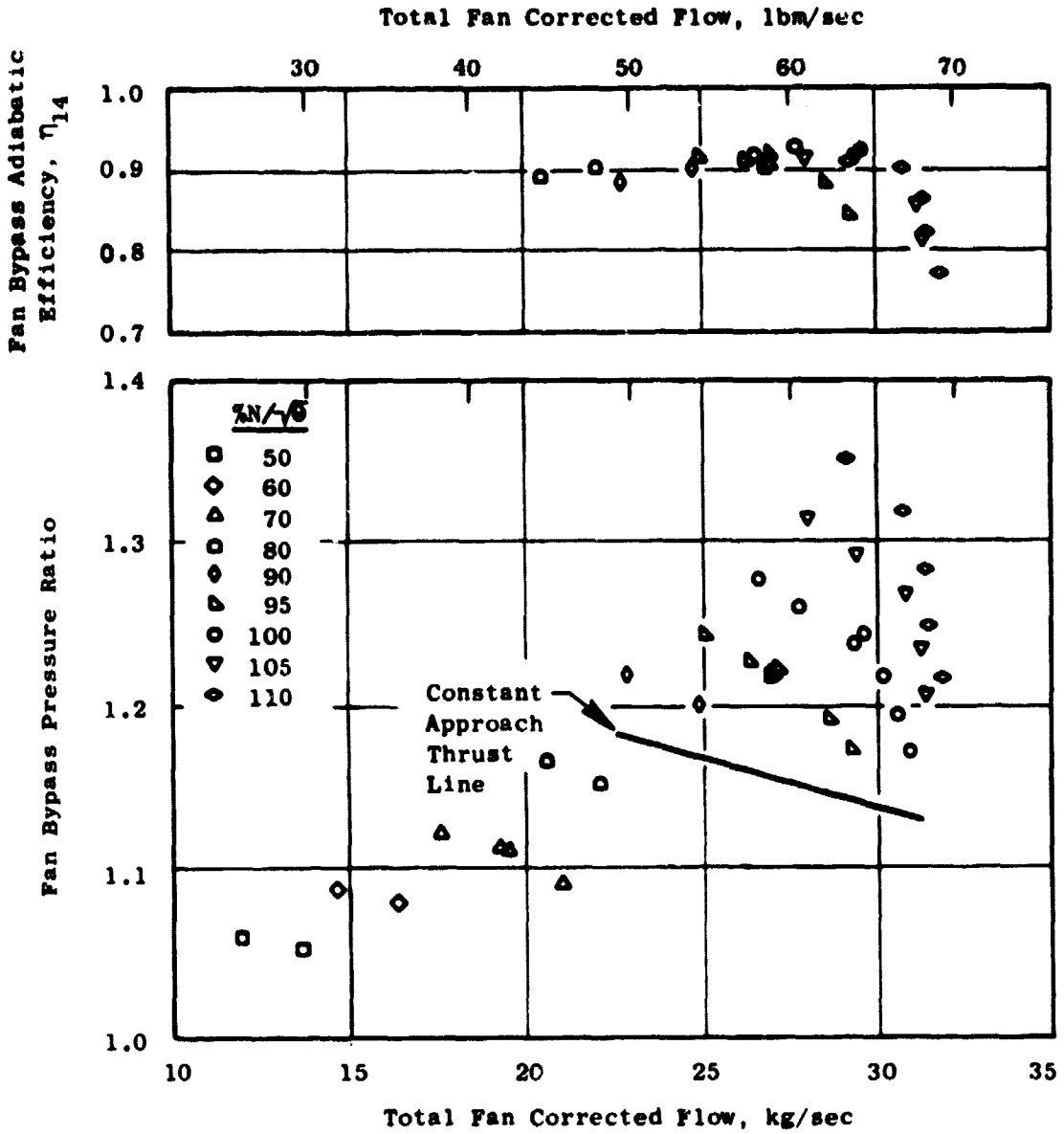

Figure 23. Fan Performance Map, +5° (Closed) Blade Angle.

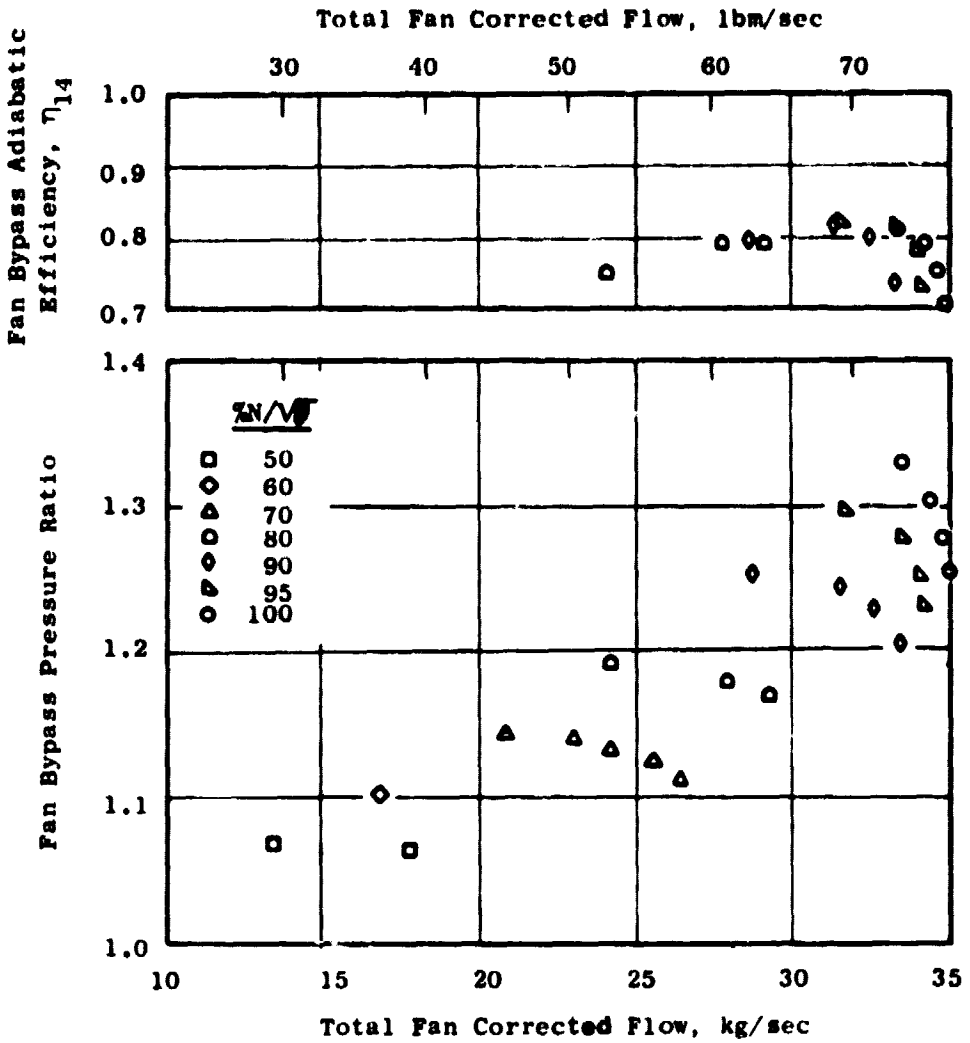

Figure 24. Fan Performance Map, -5° (Open) Blade Angle.

with pitch angle noted earlier. Therefore, from the fan-performance standpoint, it was felt desirable to match the required takeoff flow and pressure ratio with the least open rotor setting possible. The potential impact of the resulting higher fan speed on the acoustic signature needs to be weighed carefully. Acoustic data, discussed in later sections, tend to show that while the baseline bellmouth PNL satisfied the original prediction even at higher speeds, the suppression due to acceleration is increased with increasing speed (at nominal pitch angle) making the higher speed operation (higher throat Mach number) at takeoff more attractive. The limiting factor would be inlet recovery, which shows a steep drop after $M_{th} = 0.9$.

For QCSEE the thrust at approach is defined as 65% of the takeoff thrust. With a variable-pitch fan such as the UTW, approach thrust can be set by closing down the blades and holding high fan speeds for quick response in the event of a missed approach condition. Figure 23 shows a constant-approach-thrust line on the fan map. No aerodynamic-performance analysis was done at approach; however, acoustic performance for the approach condition will be discussed in a later section. Further details of the fan aerodynamic performance are discussed in Reference 2.

9.1.2 Acoustic Results at Nominal Pitch

Since takeoff represented one of the critical acoustic-test conditions, most of the acoustic tests were conducted along an operating line through the takeoff condition; this occurs at a DV setting of 7.7 at 98.5% speed. The DV setting of 7.7 is identified in all the pertinent acoustic figures as A_{18} = takeoff [corresponding to a QCSEE full-size takeoff nozzle area of 1.6 m^2 2480 $in.^2$]. Additional data with the bellmouth inlet were also taken at DV = 7.4 [A_{18} = 1.73 m^2 (2680 $in.^2$)] and DV = 7.9 [A_{18} = 1.40 m^2 (2170 $in.^2$)] (full size).

Most of the data presented in the rest of this volume are for the full-size QCSEE, 1.8-m (71-in.) diameter fan, scaled from the 50.8-cm (20-in.) diameter simulator fan. Sideline data presented are generally for a 152.4-m (500-ft) sideline.

Variation with fan corrected speed for full-size, 152.4-m (500-ft) sideline, perceived noise level (PNL) at 60° to the inlet and at the nominal blade-angle setting is shown in Figure 25 for three DV settings: DV = 7.4, 7.7, and 7.9. The trend shows that the PNL is slightly higher at the higher operating line; this corresponds to a higher pressure ratio for a given speed. One noteworthy aspect of the plot is the rather flat profile with varying speed.

Plots of PNL directivity [full-size, 152.4-m (500-ft) sideline] at DV = 7.4 are shown in Figure 26 for 70%, 98%, and 105% fan speeds. At the peak angle (60° to inlet), the measured (scaled and extrapolated) PNL was 94 dB for the takeoff condition. Figures 27 through 29 show the 1/3-octave band SPL

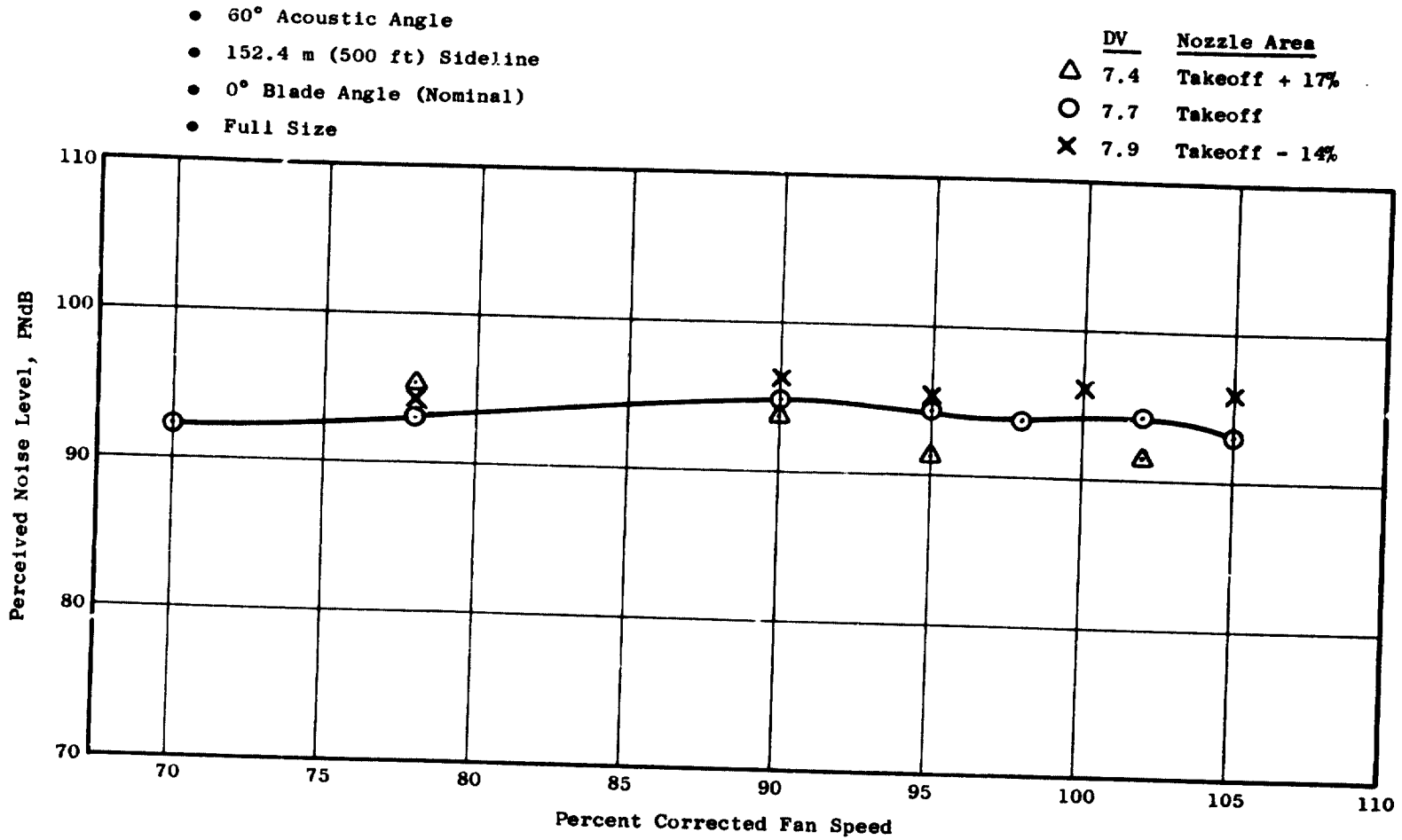

Figure 25. Variation of PNL with Fan Speed - Baseline Bellmouth Inlet.

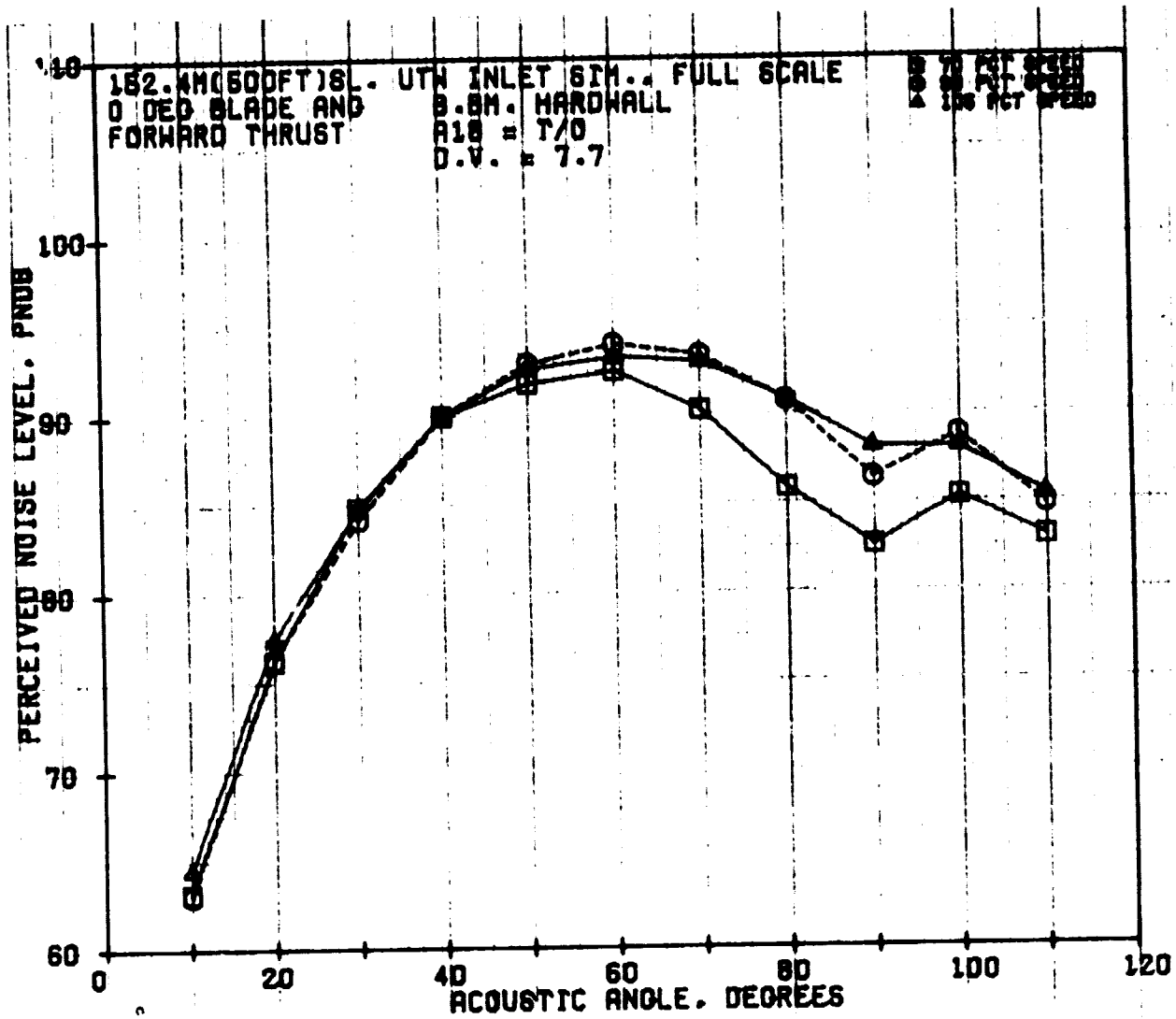

Figure 26. PNL Directivity - Baseline Bellmouth at 70%, 98%, and 105% N_{FC}.

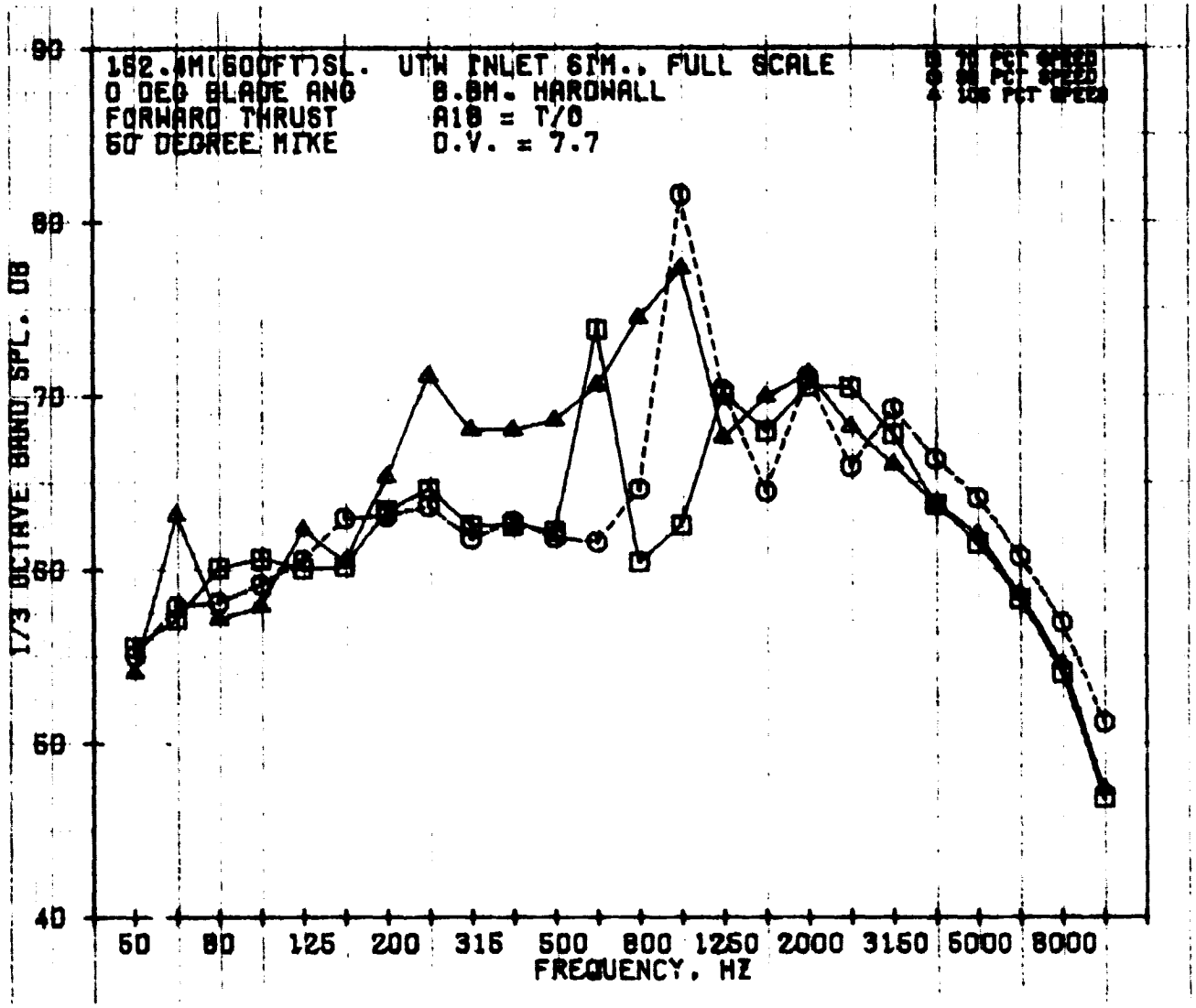

Figure 27. Baseline Bellmouth Inlet 1/3-Octave-Band SPL at 70%, 98%, and 105% N_{FC} at 50°.

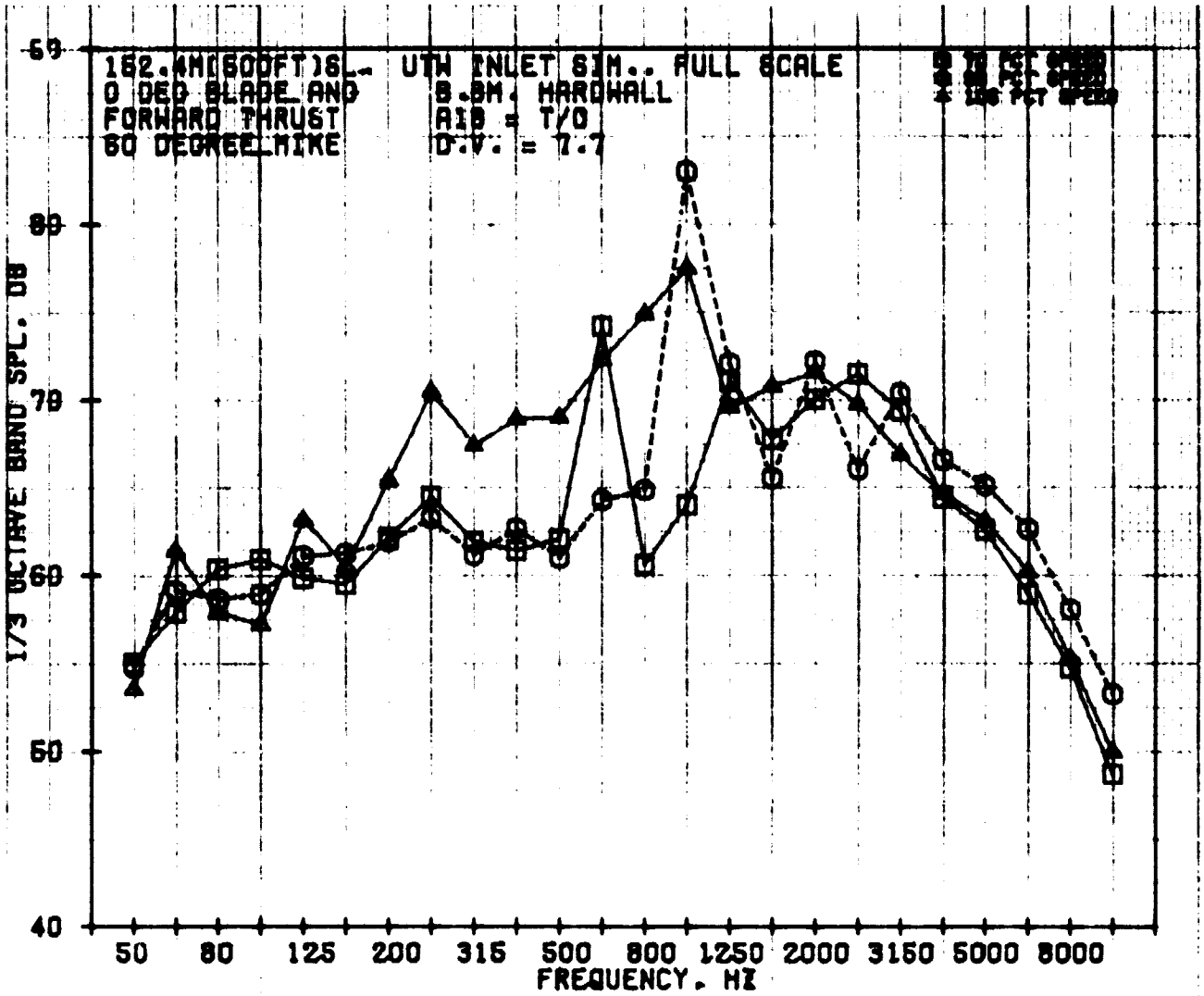

Figure 28. Baseline Bellmouth Inlet 1/3-Octave-Band SPL at 70%, 98%, and 105% N_{FC} at 60°.

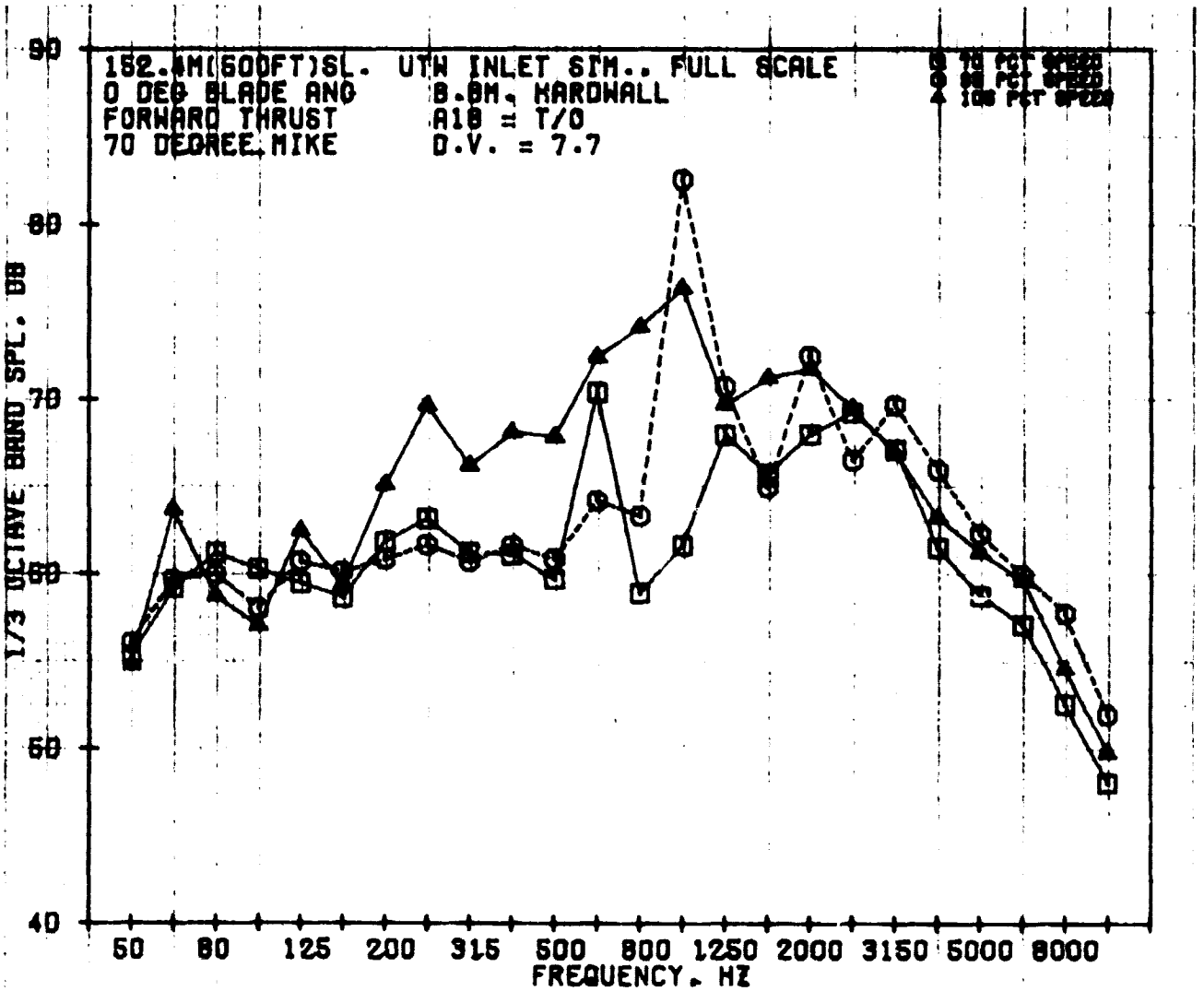

Figure 29. Baseline Bellmouth Inlet 1/3-Octave-Band SPL at 70%, 98%, and 105% N_{FC} at 70°.

spectra for these three speeds at 50°, 60°, and 70° to the inlet respectively. The 1/3-octave-band, power-level spectra for these three speeds are shown in Figure 30. While the tone fundamental level (BPF) and levels beyond the third harmonic are higher for the 98.5% speed, the 105% speed spectra indicate a very high incidence of lower frequency noise. In order to explore the possibility of the presence of multiple pure tones (MPT's) at the higher speeds, 20-Hz bandwidth narrowbands were generated with the model-size data.

The 20-Hz narrowbands from the 60° microphone for the model-size data at 70%, 98%, 102%, and 105% N_{FC} are shown in Figures 31, 32, 33, and 34 respectively. The relative tip Mach numbers for the four speeds were 0.75, 1.06, 1.17, and 1.21 respectively. The fan speed and corresponding shaft frequency are listed in each of the figures. The 1/3-octave-band model data are also shown in each of the figures plotted at the band center frequencies. One immediate observation is that the narrowband spectrum is dominated by broadband noise at 70% N_{FC}, and the tones at the BPF and the second harmonic, but at higher speeds where the tip relative Mach numbers are greater than 1.0, the MPT's are dominating the 1/3-octave-band levels below the BPF, and the broadband noise dominates the 1/3-octave-band levels above the BPF. Translating these results back to Figure 30 and performing the frequency shift required due to the scale (71:30 diameter), it is apparent that the high levels at 105% between 250 Hz and 1000 Hz in Figure 30 are the result of high MPT content.

Figures 35 and 36 give directivities of the blade passing frequency and the second harmonic of the BPF on a 152.4-m (500-ft) sideline. The degradation of the BPF with the onset of strong MPT's is seen in Figure 35.

The takeoff condition for QCSEE occurs on the nominal-blade-angle, fan-performance map at 98.5% corrected seed (Figure 19). The measured, unsuppressed PNL, scaled to full-size QCSEE and extrapolated to 152.4-m (500-ft) sideline, at this condition was 94 dB in Figure 25, agreeing with the earlier prediction (Reference 10).

9.2 ACCELERATING INLETS AT NOMINAL PITCH

9.2.1 Fan Aerodynamics

Prior to the acoustic tests with accelerating inlets, a series of fan aerodynamic tests were run in order to determine the fan aerodynamic characteristics and the inlet diffusion characteristics with the accelerating inlet. From these tests, it was determined that the operating line through the takeoff condition was at a DV setting of 7.75; hence, all the forward-thrust acoustic tests with the accelerating and the low Mach inlets were conducted at a DV setting of 7.75.

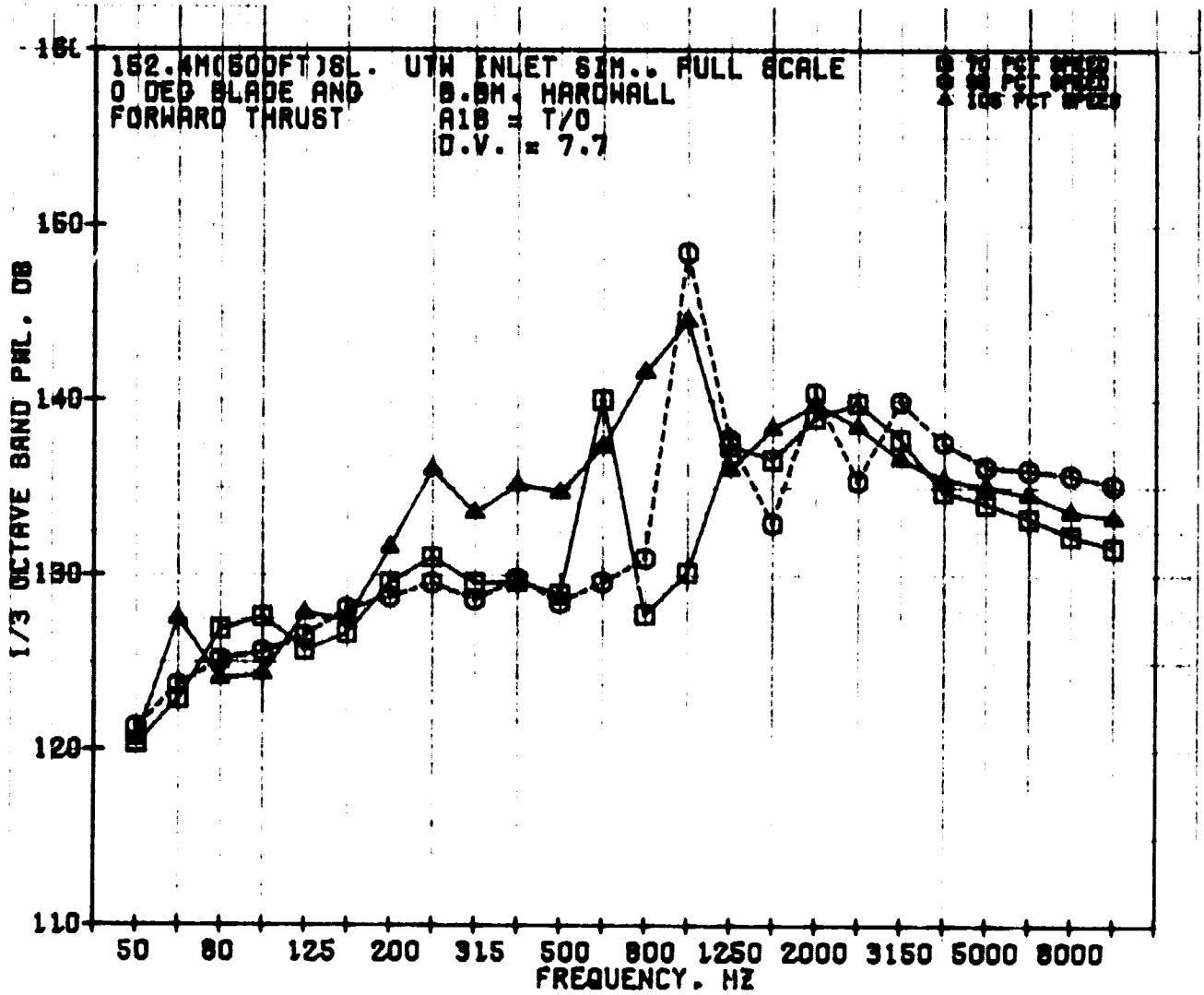

Figure 30. Baseline Bellmouth Inlet 1/3-Octave-Band PWL at 70%, 98%, and 105% N_{FC}.

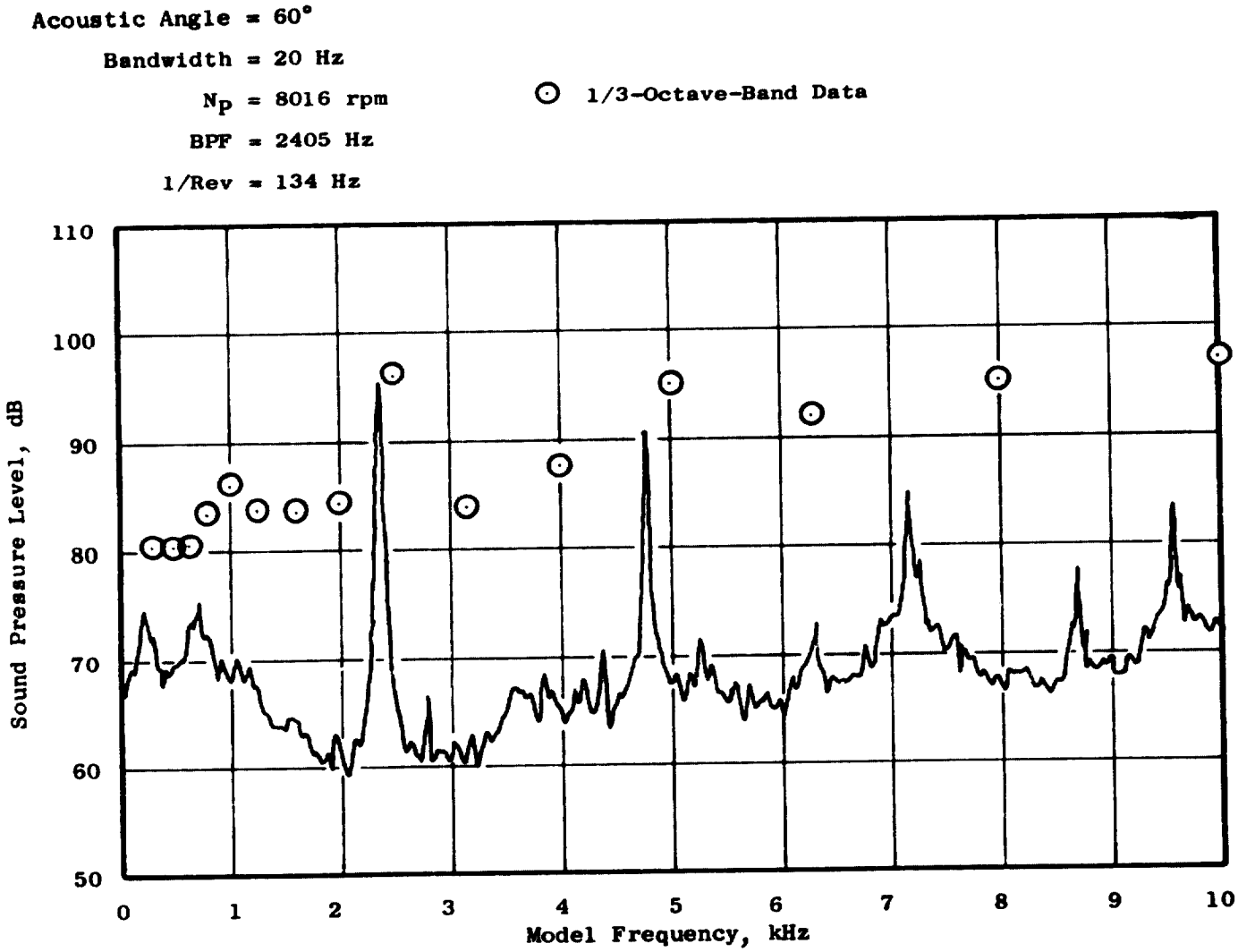

Figure 31. Narrowband SPL Spectrum - Baseline Bellmouth, Nominal Pitch, 70% N_{FC}.

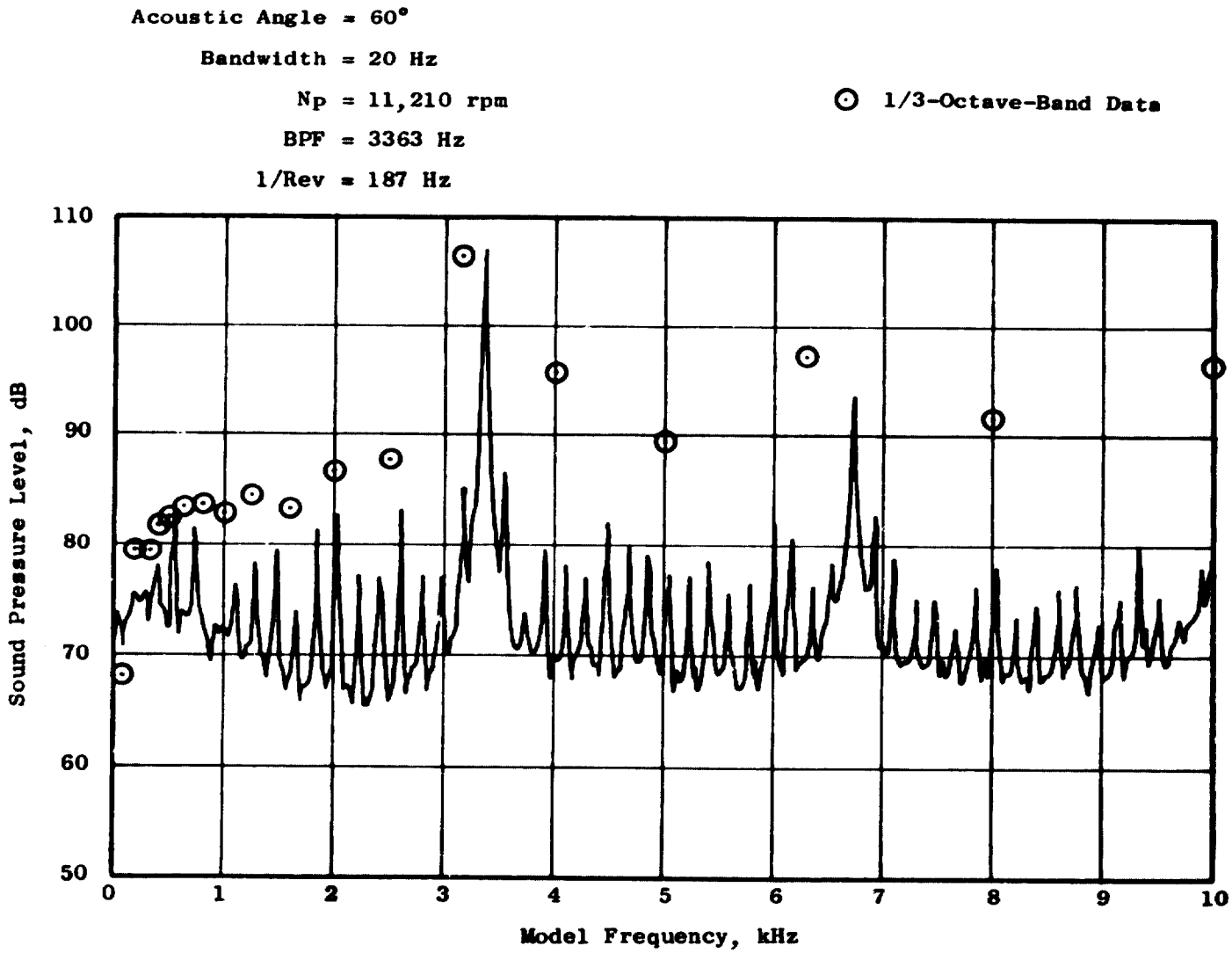

Figure 32. Narrowband SPL Spectrum - Baseline Bellmouth, Nominal Pitch, 98% N_{FC}.

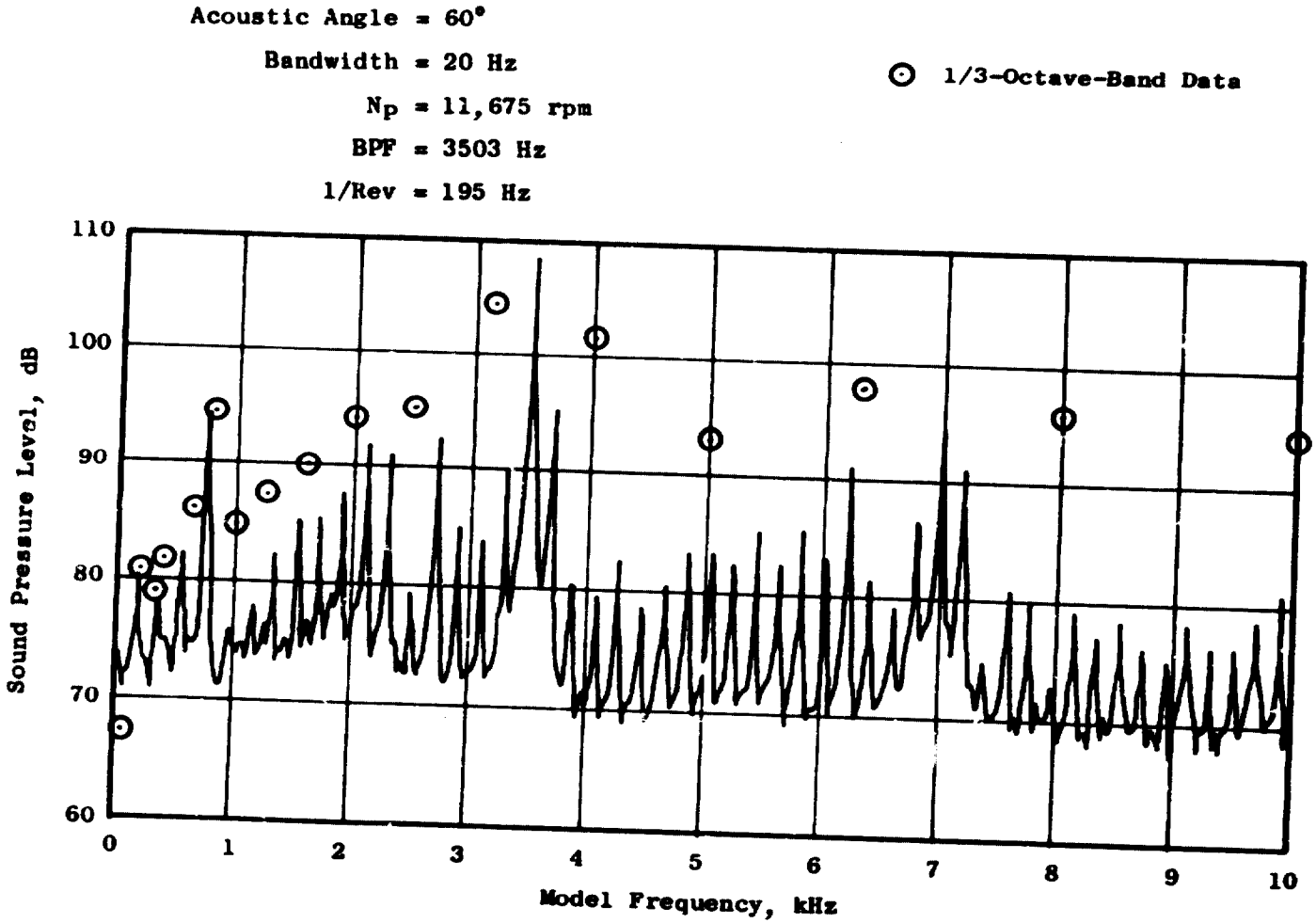

Figure 33. Narrowband SPL Spectrum - Baseline Bellmouth, Nominal Pitch, 102% N_{FC}.

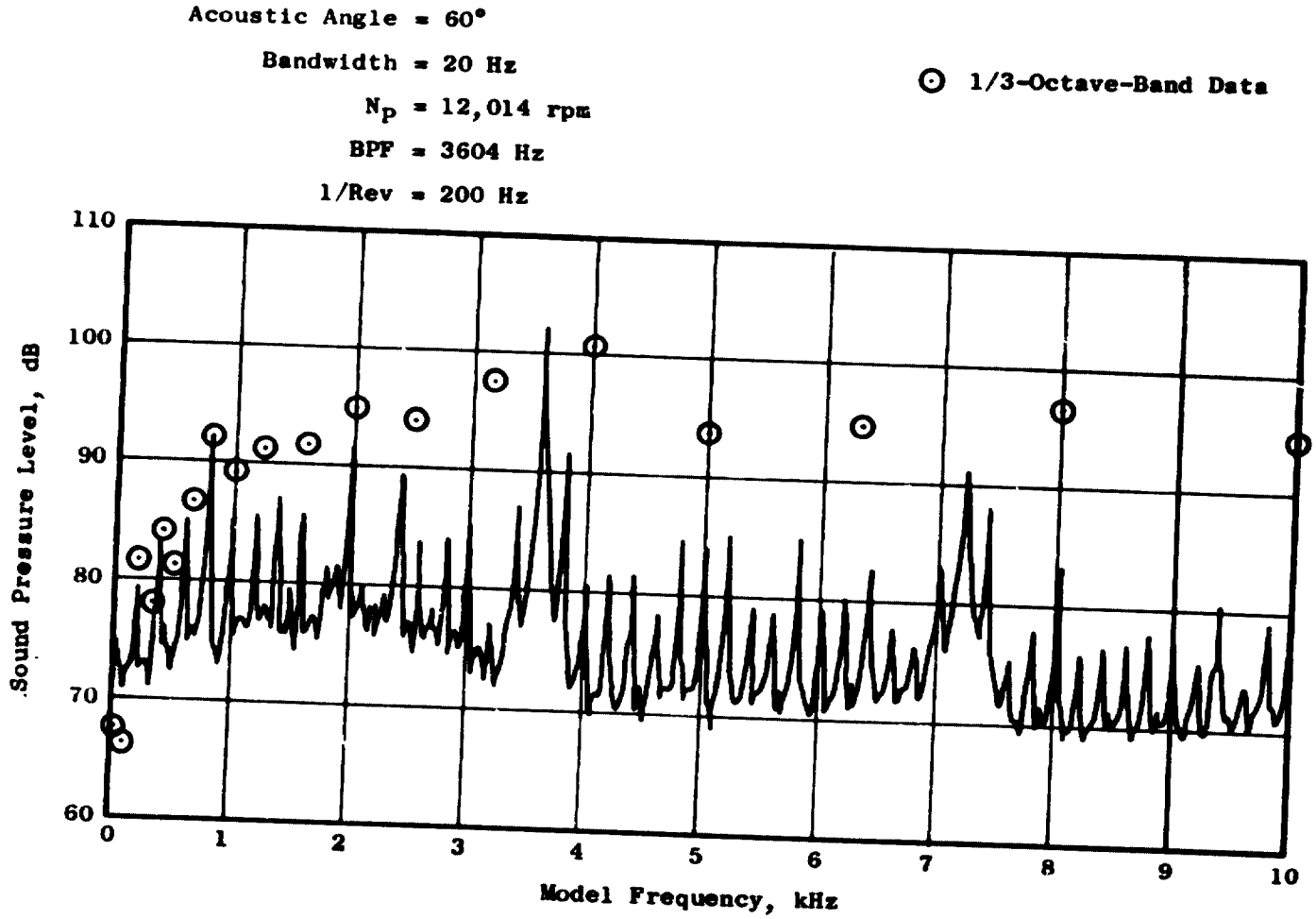

Figure 34. Narrowband SPL Spectrum - Baseline Bellmouth, Nominal Pitch, 105% N_{FC}.

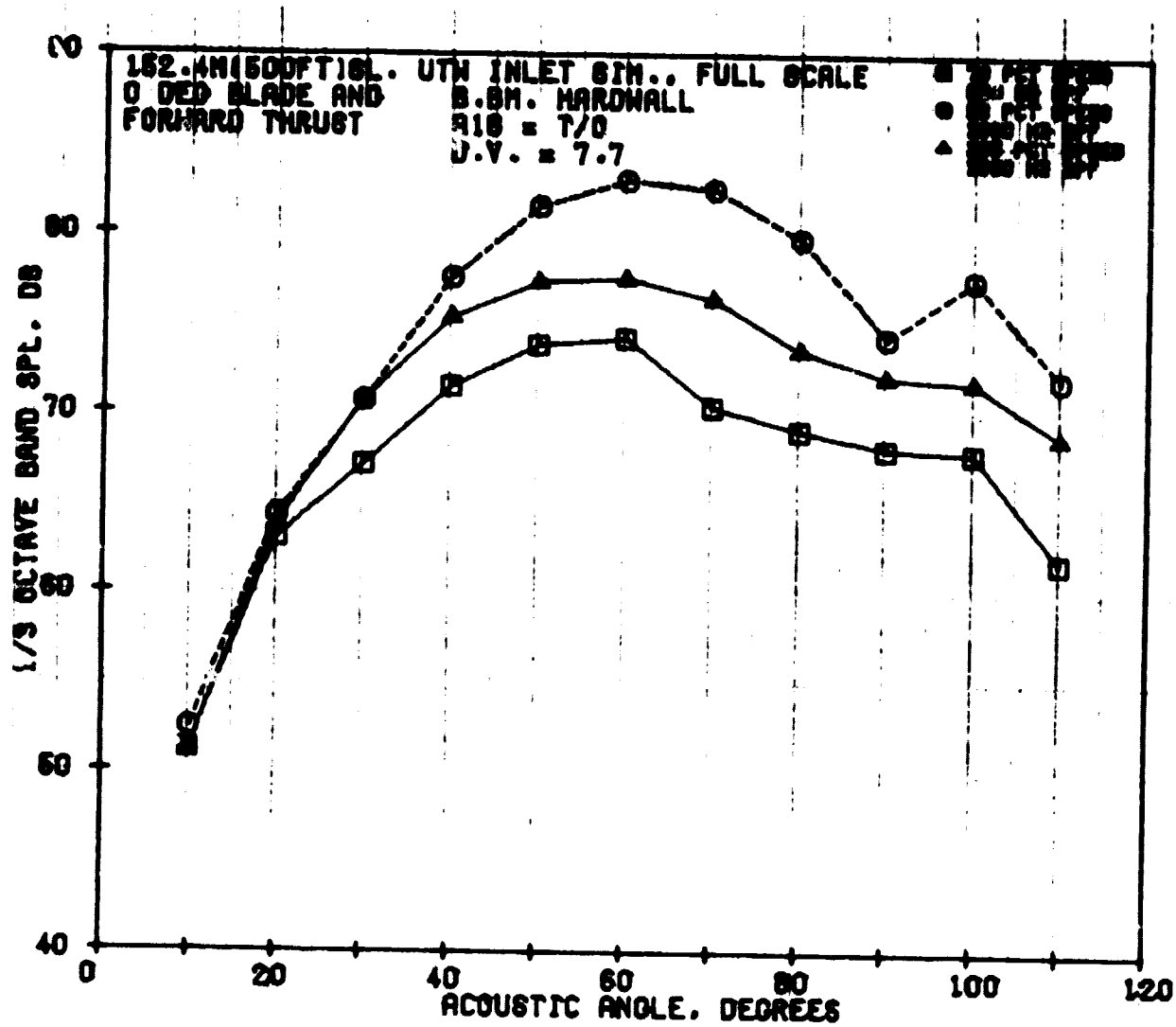

Figure 35. One-Third-Octave-Band SPL Directivity of Blade Passing Frequency - Baseline Bellmouth Inlet at 70%, 98%, and 105% NFC.

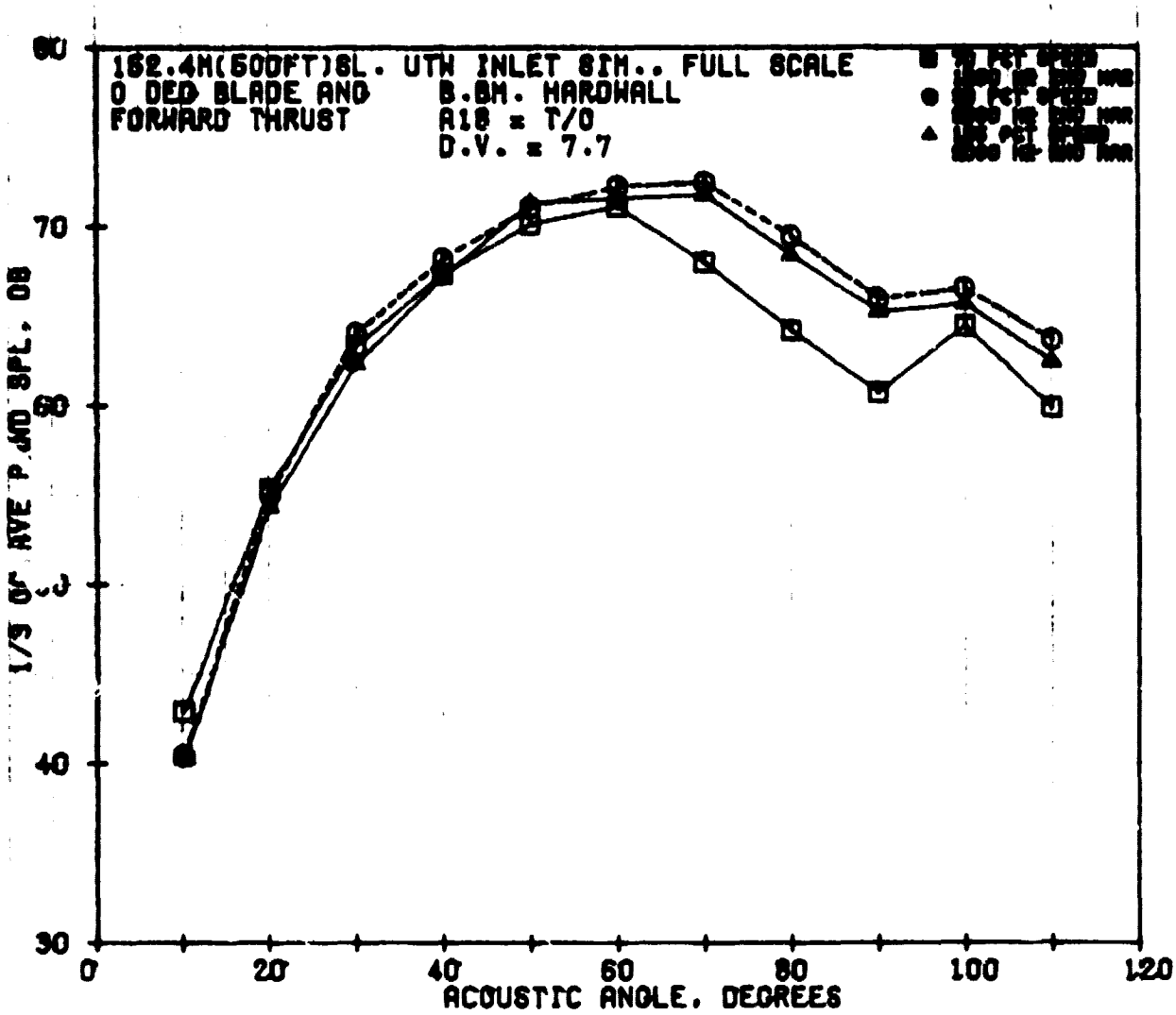

Figure 36. One-Third-Octave-Band SPL Directivity of Second Harmonic - Baseline Bellmouth Inlet at 70%, 98%, and 105% N_{FC}.

9.2.2 Inlet Aerodynamics

Acoustic tests in the forward-thrust mode were conducted with three accelerating-inlet diffuser configurations: hard-wall, treatment B, and treatment D. Treatment B was tested with both an aero-acoustic lip and a flight lip while the hard-wall and treatment D were tested only with the aero-acoustic lip. Due to the fact that all inlet and fan-exhaust rakes were removed from the airstream during acoustic testing, the aerodynamic performance of the inlet, including throat Mach number determination to set operating condition, was monitored by means of a series of wall static pressure taps located on the inlet lip and diffusers. The methods for determining inlet throat Mach number and for adjusting the prediction for viscosity are described in the Appendix.

The inlet aerodynamic performance pertaining to the hard wall (with aero-acoustic lip) and the treatment B (with aero-acoustic and flight lips) configurations is discussed in this section. Since the acoustic results from inlet D presented some special problems, the inlet aerodynamic performance of treatment D is discussed separately along with corresponding acoustic data.

The hard-wall, accelerating inlet was tested with an aero-acoustic lip designed (using a streamtube curvature program, Reference 11) to simulate inlet flow conditions typical of a 41-m/sec (80-knot) forward velocity. A flight lip, representative of the full-scale flight inlet, was also designed but was tested only with treated accelerating inlet B. Figure 37 is a geometric comparison of the two lips. Figure 38 compares inviscid streamtube curvature (STC) computer predictions (Reference 16) of the wall Mach number distributions for the aero-acoustic lip at a static condition and for the flight lip at a 41-m/sec (80-knot) forward velocity. The results indicate that the aero-acoustic lip provides a very similar wall Mach number distribution in terms of both the peak wall Mach number and the rate of diffusion.

In Figure 39 measured data are compared to the STC-predicted viscous wall Mach number distribution for the aero-acoustic inlet at the design takeoff throat Mach number (0.79). With a few exceptions, the wall static pressure data are in good agreement with predictions. At Stations -17.4 and -17.5, in the vicinity of the throat where there is a steep gradient of Mach number versus axial station, static taps at two circumferential locations indicated significantly different Mach numbers. This could have resulted either from a surface discontinuity at the lip/diffuser interface or from a static tap installation problem. Figure 40 presents the M_{th} versus fan percent design speed relationship for the accelerating inlets; design takeoff M_{th} (0.79) occurs at 98.5% with the hard-wall, accelerating inlet; inlet B requires 99.5% speed, and inlet D requires 100.5% speed. Typically, an increase in the corrected fan speed needed to produce a given throat Mach number suggests a decrease in inlet recovery. However, the variability in resetting the fan blade angles ($\pm 1^\circ$) introduced an additional factor to be considered. The hard-wall and the treatment B diffuser inlets were tested

C-2

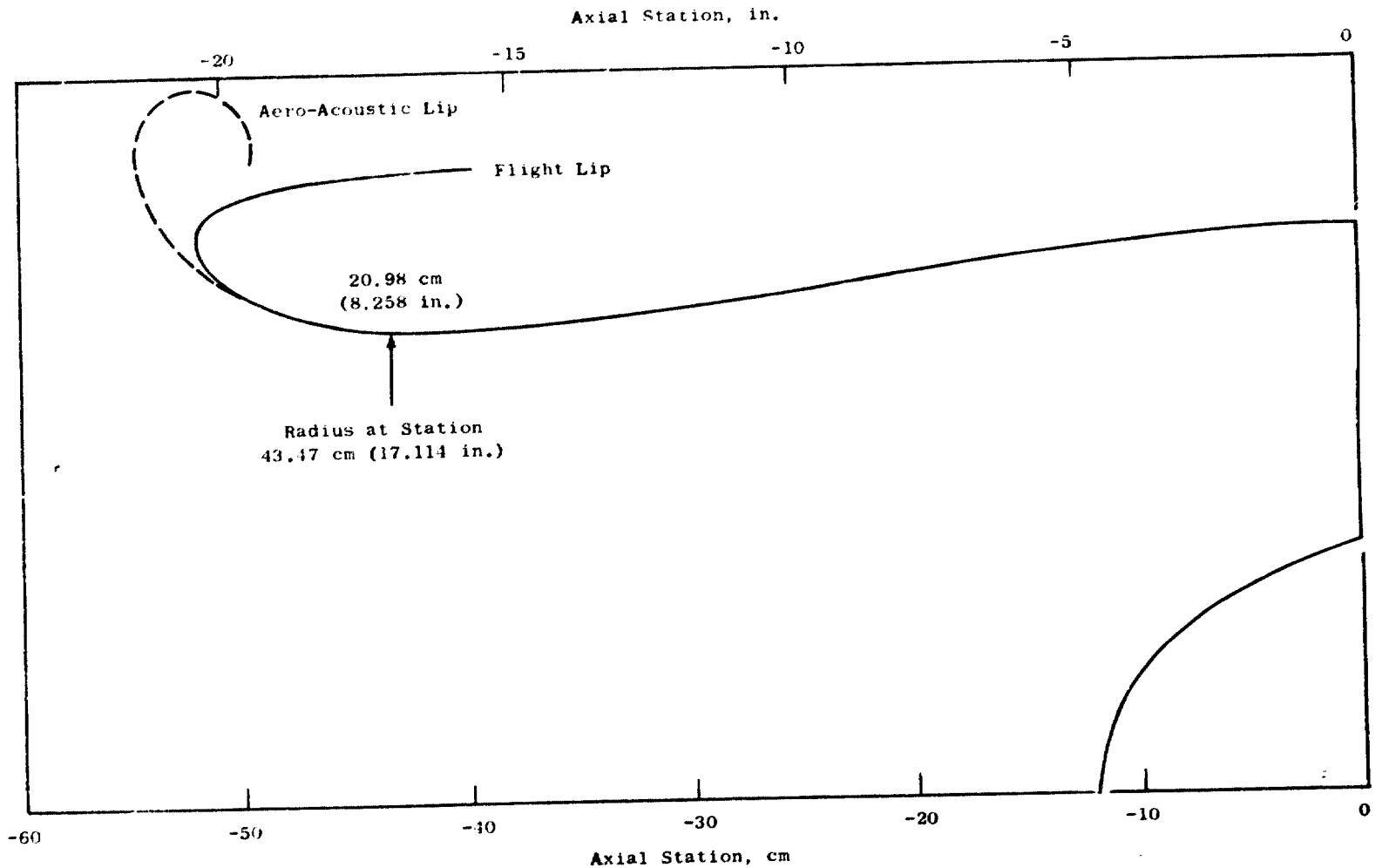

Figure 37. UTW Simulator Accelerating Inlet - Flight Lip and Aero-Acoustic Lips.

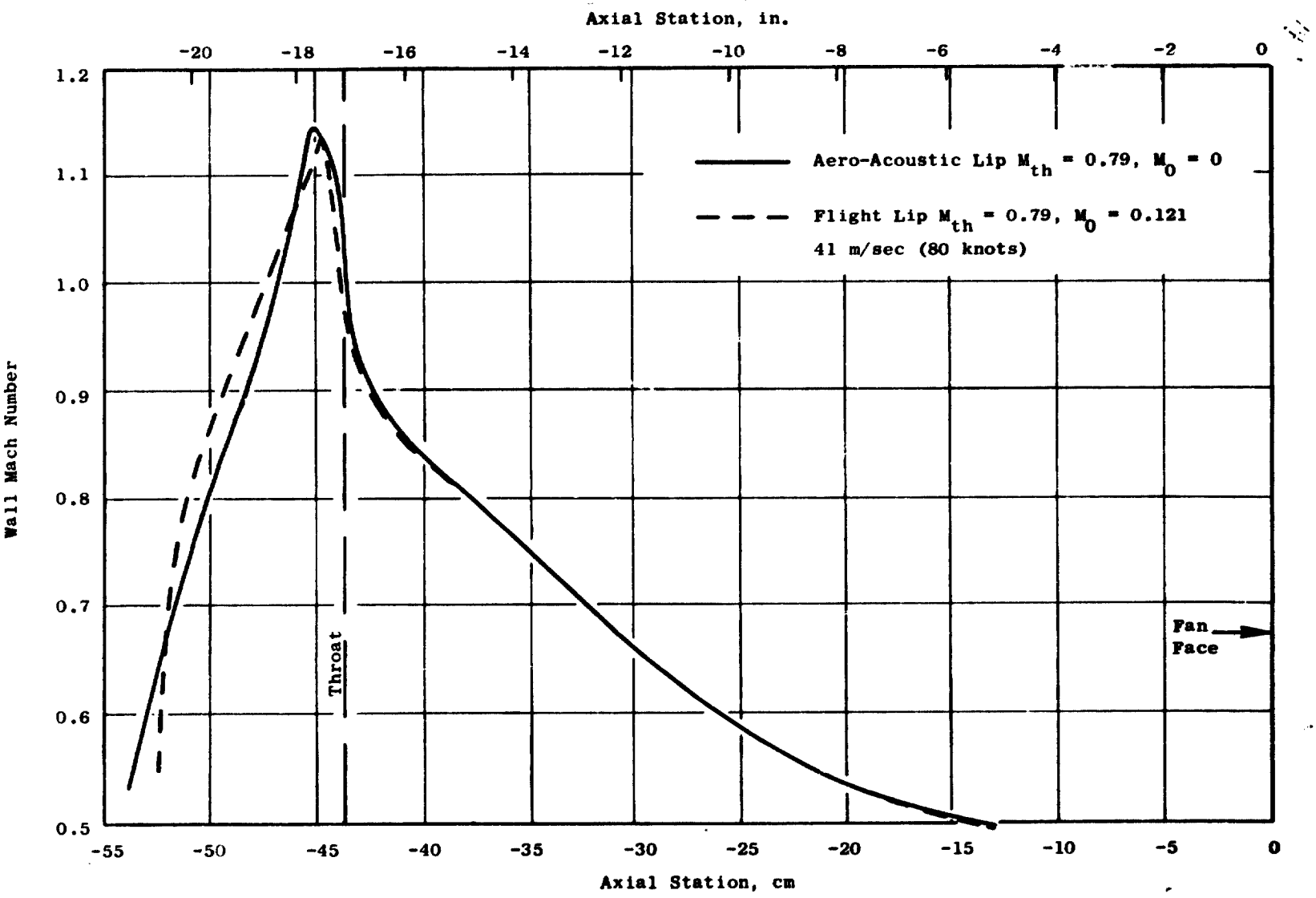

Figure 38. Comparison of Flight Lip and Aero-Acoustic Lip - Predicted Wall Mach Number Distributions.

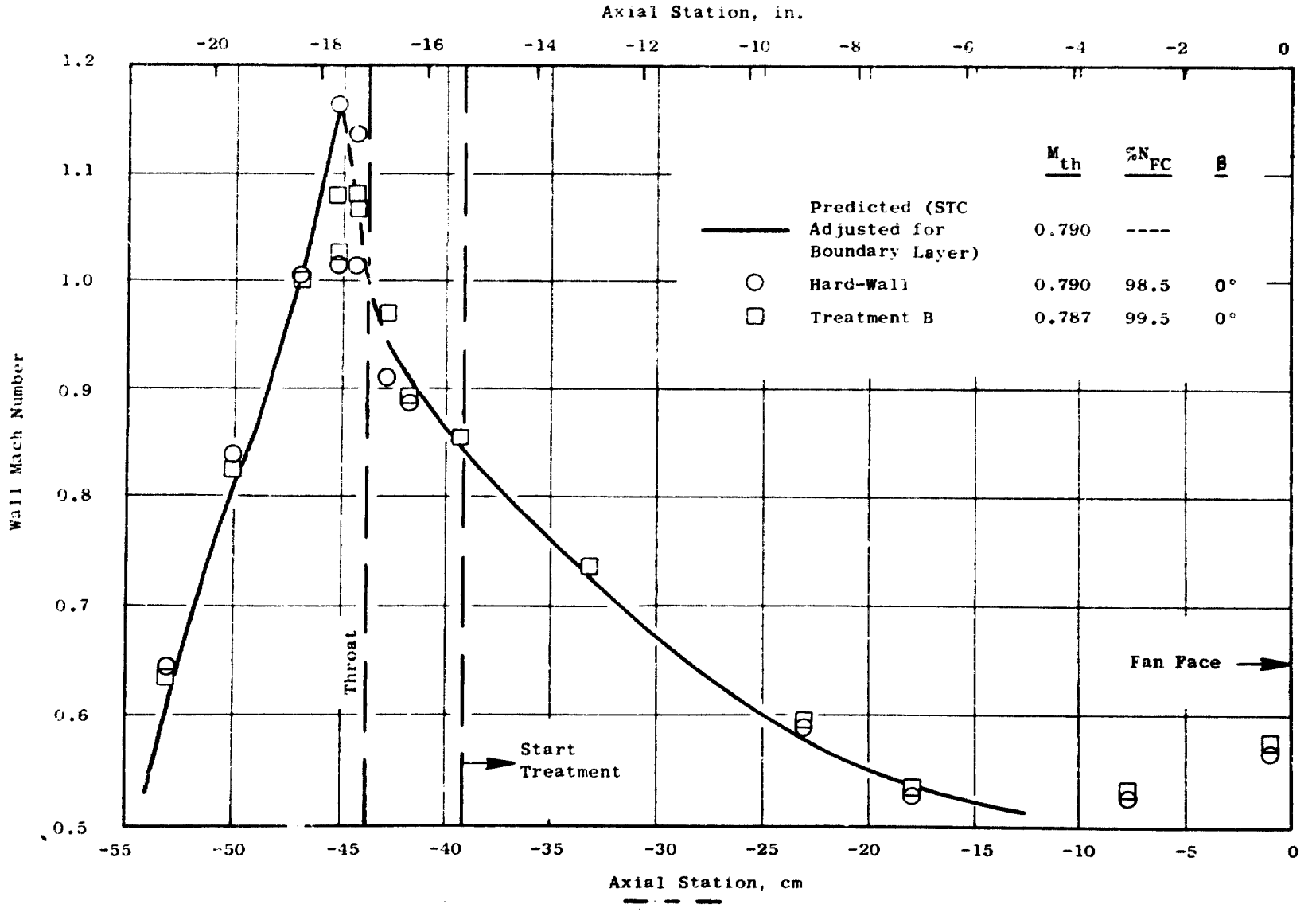

Figure 39. Aero-Acoustic Lip - Accelerating Inlet Wall Mach Number Distributions, $M_{th} \approx 0.79$.

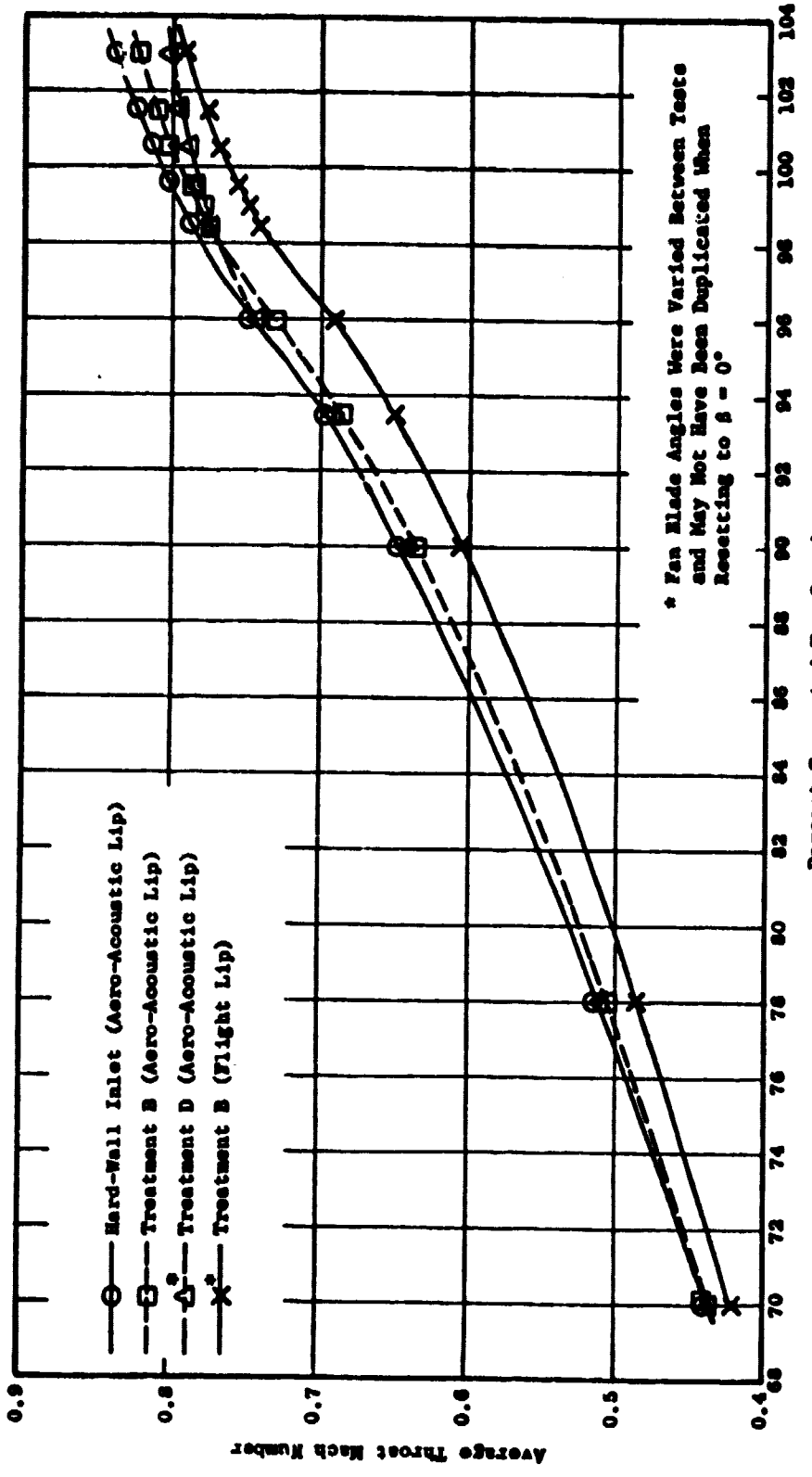

Figure 40. UTW Accelerating Inlet Average Throat Mach Number as a Function of Fan Speed.

with no intervening blade-angle changes. Therefore, the observed difference in throat Mach number at a given fan speed is likely due to additional inlet total pressure losses caused by the perforated treatment faceplate. On this basis, treatment B appears to contribute 0.6% additional inlet recovery loss relative to the hard-wall inlet at the design takeoff flow (M_{th} = 0.79). In terms of fan speed, the treated inlet requires about 1% higher corrected speed to attain the design throat Mach number. The treatment recovery loss inferred from Figure 40 data cannot be independently verified because total pressure rakes, adequate for measuring inlet recovery, were not installed in the inlet.

The variation of inlet M_{th} with percent fan speed, shown in Figure 40 for inlet B with the two lips, indicates that a substantially reduced flow was observed with the flight lip. Careful investigation revealed that several blade-angle changes had been made between the acoustic tests with the two lips. The data from the aerodynamic tests also showed that when the nominal (0°) blade angle was reset by hand for the baseline bellmouth, the ± blade angle repeatability and intervening discharge valve repair work had slightly changed the fan flow/speed characteristics. The 2.5% flow reduction measured with the flight lip was well within the flow variation possible with a ±0.5 blade-angle setting repeatability.

Figure 41 compares measured wall Mach number distribution at 103% speed with STC calculations at M_{th} = 0.79. A similar comparison is shown in Figure 42 at M_{th} = 0.79 and measured data at 99.5% speed for the aeroacoustic lip.

9.2.3 Inlet Acoustics

9.2.3.1 Hard-Wall, Accelerating Inlet

The variation of full-size, 152-m (500-ft) sideline PNL (at 60° to inlet) with fan corrected speed is presented in Figure 43 for the hard-wall, accelerating inlet. Also shown, for comparison, are the data with the baseline bellmouth inlet. The suppression due to acceleration begins to show at the 93.5% speed condition. Figure 44 shows the same PNL data plotted versus throat Mach number for the accelerating inlet. The abcissa for the bellmouth data is plotted on an equal-tip-speed basis with inlet B. It is now seen from Figure 44 that the suppression due to acceleration shows a monotonic increase from about M_{th} = 0.69. At the takeoff flow condition (M_{th} = 0.79), the suppression obtained was 9.5 PNdB with the hard-wall, accelerating inlet. The objective suppression at the takeoff condition was 13 PNdB with a treated inlet, and data presented in a later section will show that this objective was met with treatment B. The variation of suppression with throat Mach number for the hard-wall, accelerating inlet (baseline bellmouth - hard-wall accelerating inlet) is shown in Figure 45. The band shown along with the current data represents results from 18 other configurations (Reference 3).

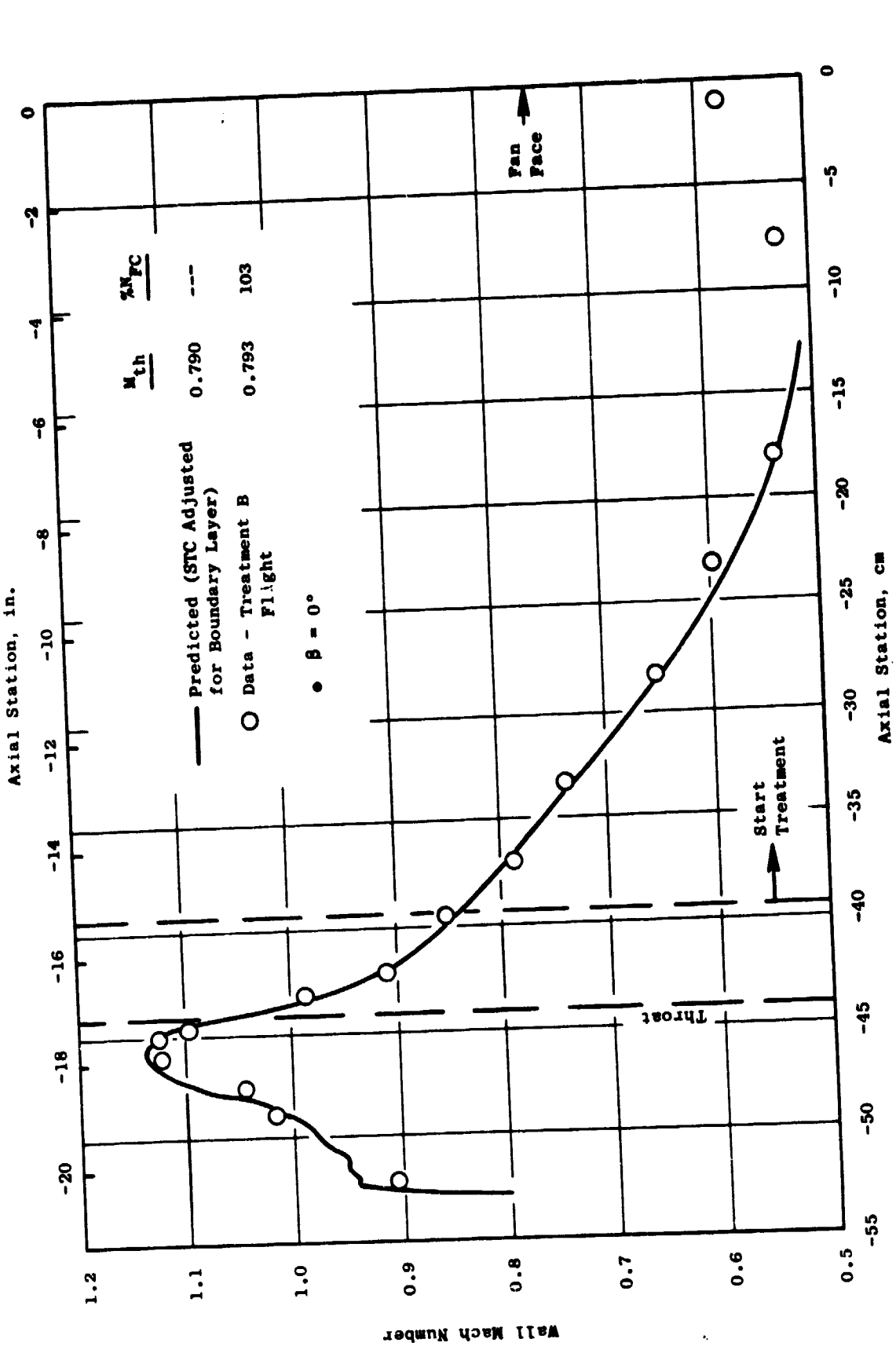

Figure 41. Flight Lip - Accelerating Inlet Wall Mach Number Distributions, M_{th} = 0.79.

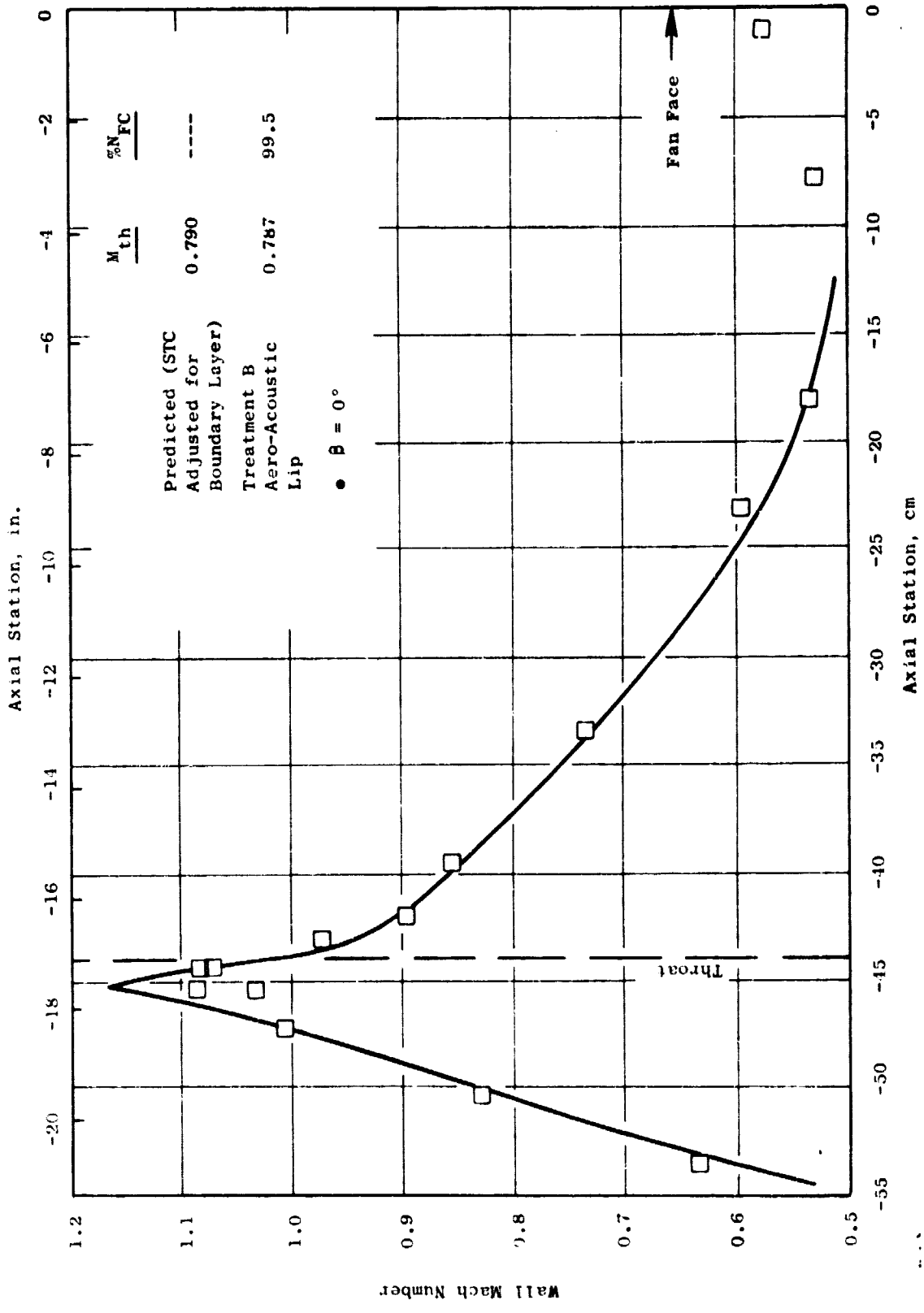

Figure 42. Aero-Acoustic Lip - Predicted Versus Measured Wall Mach Number Distributions, Mth = 0.79.

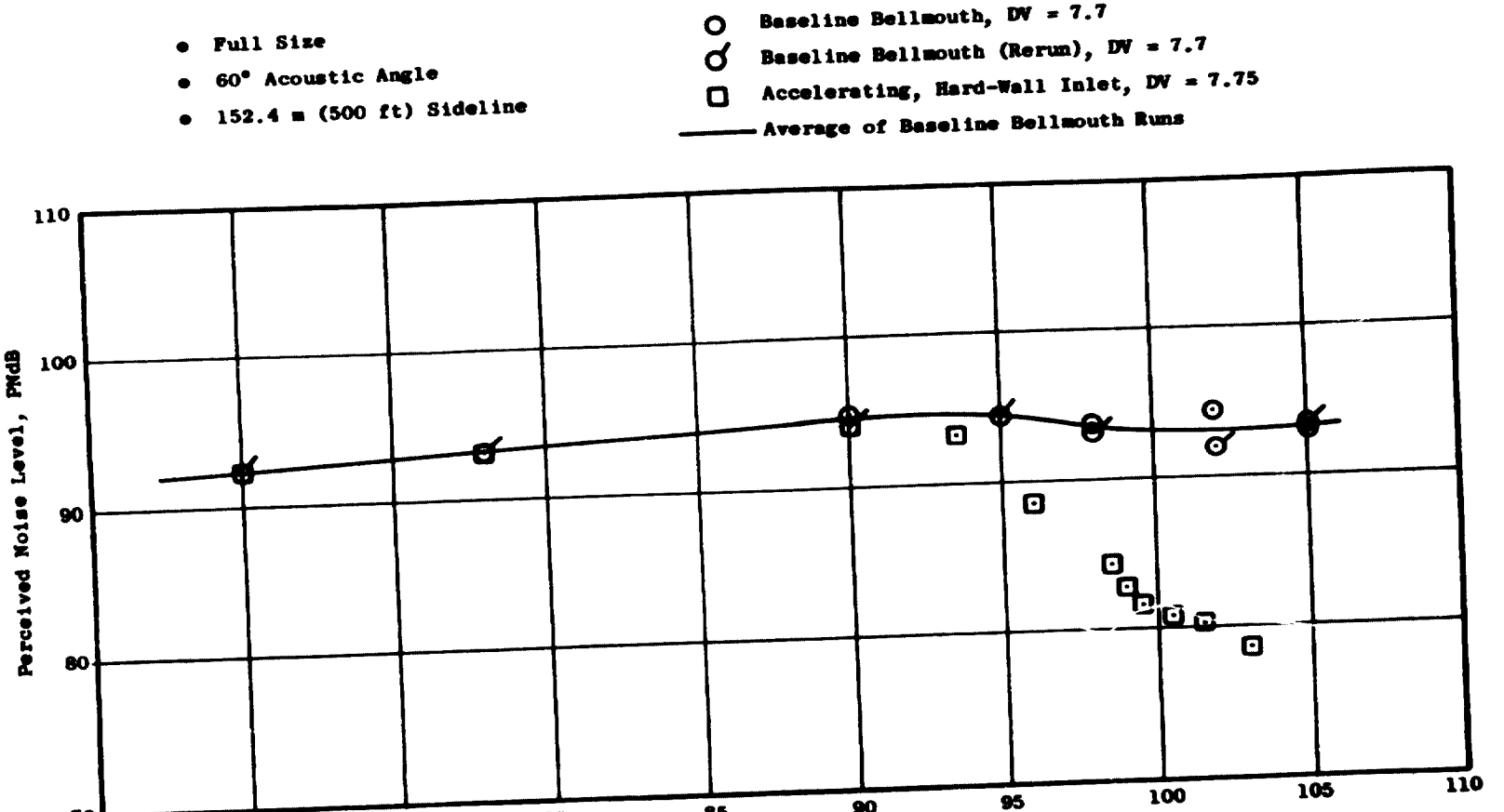

Figure 43. PNL Vs. Percent Corrected Fan Speed; Baseline Bellmouth and Hard-Wall Accelerating Inlets.

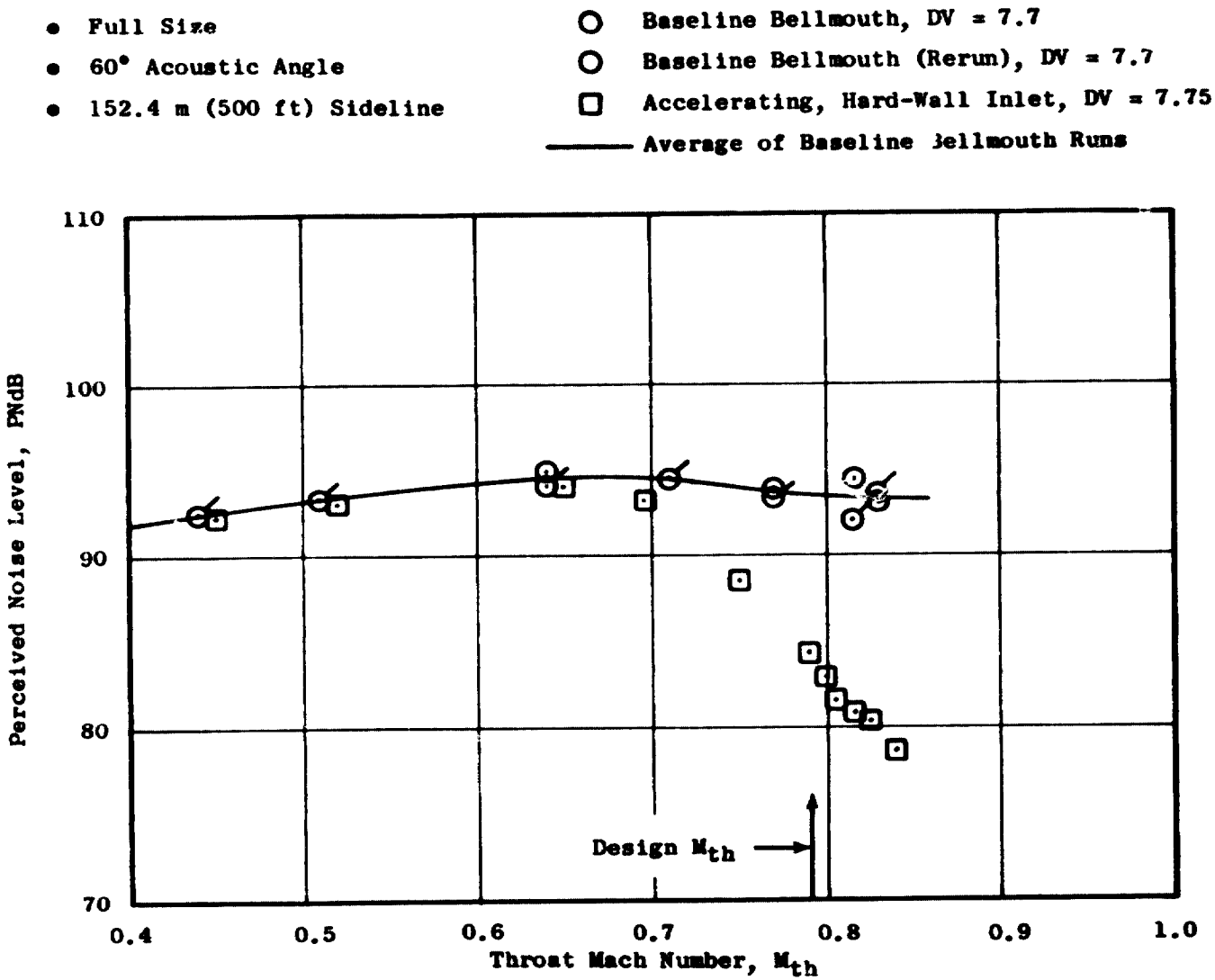

Figure 44. PNL Vs. Throat Mach Number; Baseline Bellmouth and Hard-Wall Accelerating Inlets.

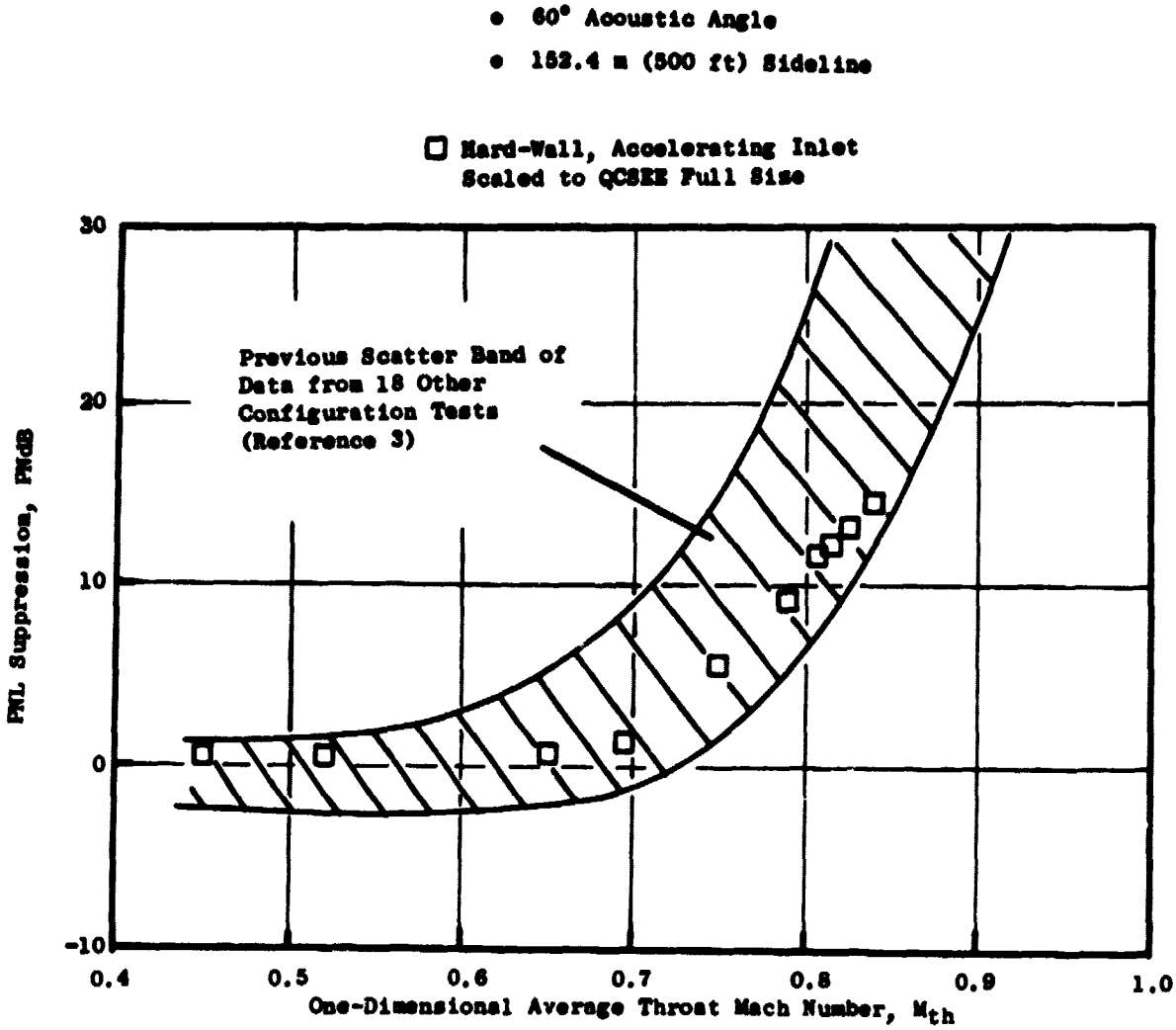

Figure 45. PNL Suppression Vs. Average Throat Mach Number of Hard-Wall, Accelerating Inlet.

Figure 46 shows the PNL directivities [full-size, 152-m (500-ft) sideline] at the takeoff condition (98.5% speed, M_{th} = 0.79) with the baseline bellmouth inlet and the hard-wall, accelerating inlet. Both patterns peak at 60° to the inlet where the suppression was 9.5 PNdB. The 1/3-octave-band SPL spectra for the two inlets at 98.5% speed are compared in Figures 47, 48, and 49 at 50°, 60°, and 70° to the inlet respectively. The suppression contributing to PNL is seen to be achieved at and above blade passing frequency. A certain amount of suppression of the MPT's is also observed at the lower frequencies. This can be seen more readily from Figures 50 to 52, which show the 20-Hz narrowband compared for the two inlets at 50°, 60°, and 70° respectively. The narrowbands are for unscaled data measured on a 5.2-m (17-ft) arc; however, an approximate scale is also shown in the figures to adjust for shifting the frequencies to full QCSEE size. Figures 53 and 54 show the 1/3-octave-band SPL directivities of the blade passing frequency and the second harmonic of the BPF; a stronger attenuation is indicated of the BPF than of the second harmonic. The 1/3-octave-band PWL spectra comparison at the takeoff speed is shown in Figure 55.

At low speeds the hard-wall, accelerating inlet should be expected to give an acoustic signature similar to that of a baseline bellmouth inlet. This, to some extent, can be seen by comparing the PNL directivity at 70% speed, shown in Figure 56 for the two inlets. While the excellent agreement between 10° and 70° is as expected, the reason for the deviation between 80° and 110° is not clear. Figure 57 shows the 1/3-octave-band SPL spectra at 60° to the two inlets. The spectra are quite similar in character and comparable in levels except for the higher BPF level with the hard-wall, accelerating inlet. The directivity of the BPF shown in Figure 58 indicates that the BPF level is about 5 dB, or more, higher for the hard-wall, accelerating inlet than for the baseline bellmouth in the 30° to 100° range. The second-harmonic level shown in Figure 59 indicates that the hard-wall, accelerating inlet is about 3 PNdB higher from 10° to 70° and 6 PNdB higher at 80° and 90°.

The effect of increasing the fan corrected speed (and thus the throat Mach number) with the hard-wall, accelerating inlet is seen in Figure 60; the full-size, 152-m (500-ft) sideline, PNL directivities at 70%, 98.5%, and 101.5% speeds are shown. The reduction in PNL continues with higher speed, increasing by as much as 5 dB between 98.5% (M_{th} = 0.79) and 101.5% (M_{th} = 0.82) at the peak angle of 60° to the inlet. This points to the attractiveness, from an acoustic standpoint, of setting takeoff at a higher speed and choosing a lower operating line (a more open DV) to adjust to a lower pressure ratio and maintain takeoff thrust. This consideration may, however, be accompanied by other engine operating constraints pertaining to the engine cycle and inlet recovery. The 1/3-octave-band, SPL spectra at the three speeds (70%, 98.5%, and 101.5%) are shown in Figures 61 through 63 respectively for 50°, 60°, and 70° to the inlet. The PNL suppression that results from acceleration is dominated by the high-frequency suppression (at and above BPF). However, a considerable degree of low-frequency suppression is observed between 70% and 98.5% speeds. The 1/3-octave-band PWL spectra for these three speeds are shown in Figure 64.

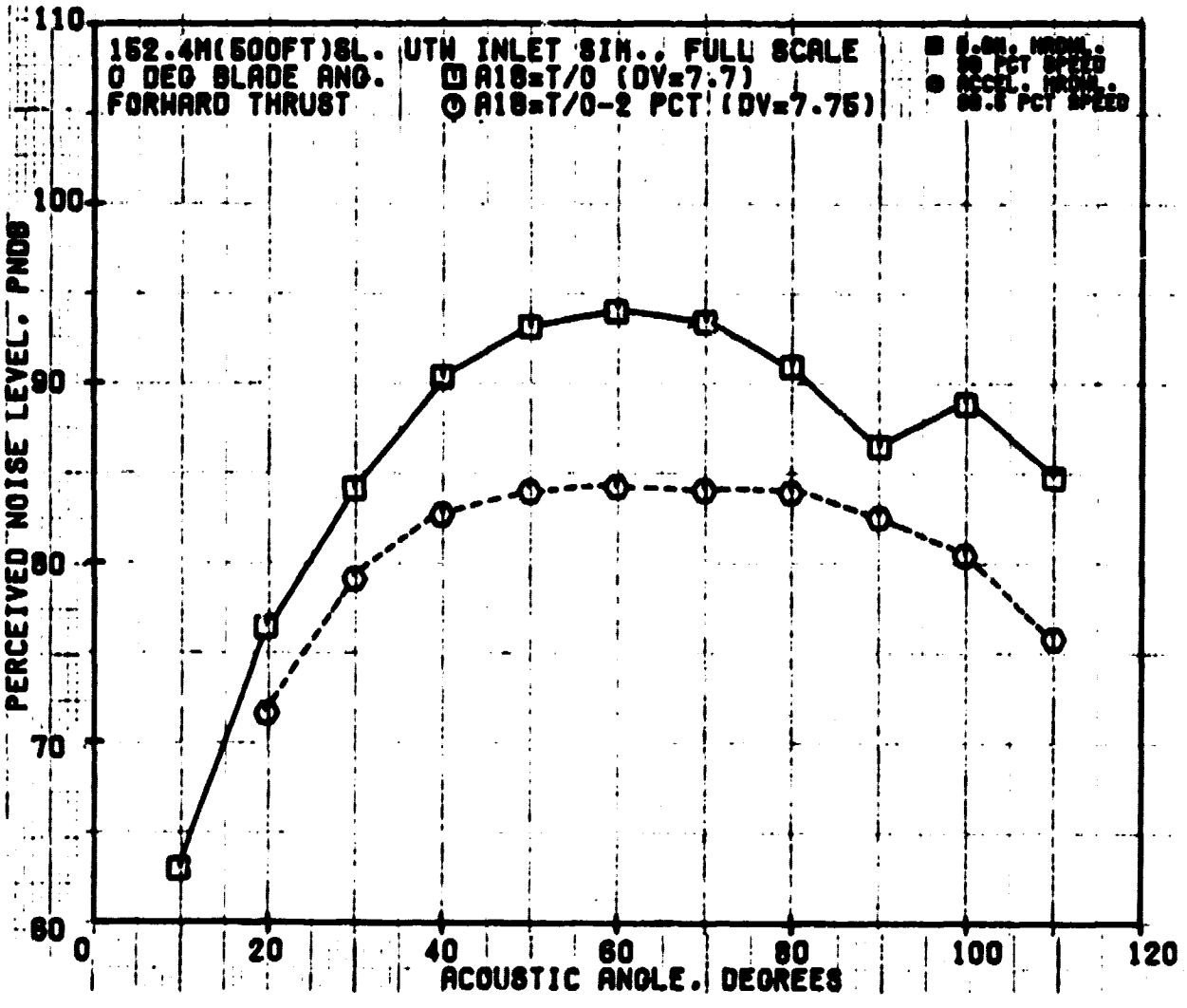

Figure 46. Forward-Thrust, PNL Directivity - Baseline Bellmouth and Accelerating Hard-Wall Inlets at 0.79 Throat Mach Number.

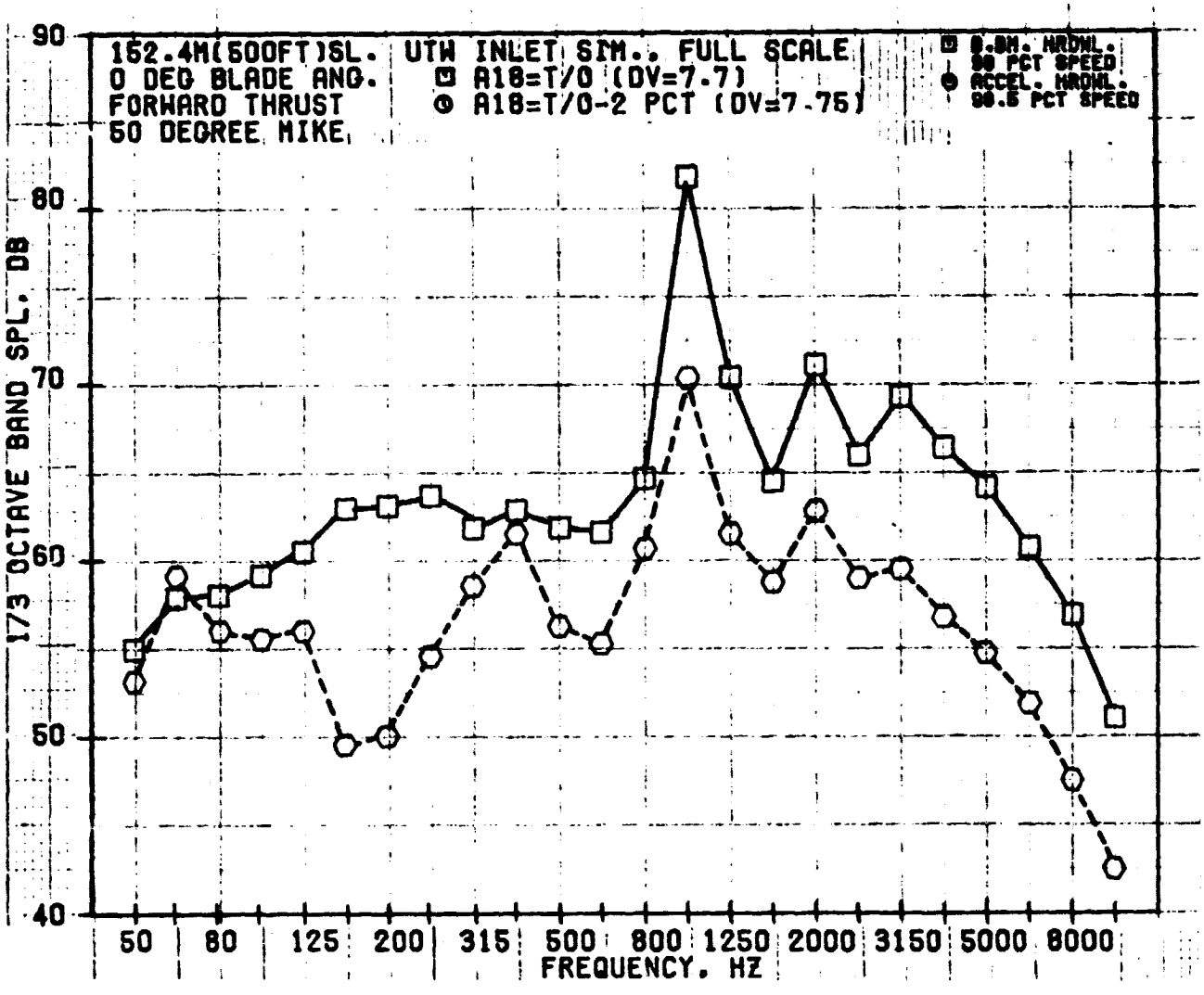

Figure 47. Forward-Thrust, 1/3-Octave-Band, SPL Spectra - Baseline Bellmouth and Accelerating Hard-Wall Inlets at 0.79 Throat Mach Number at 50°.

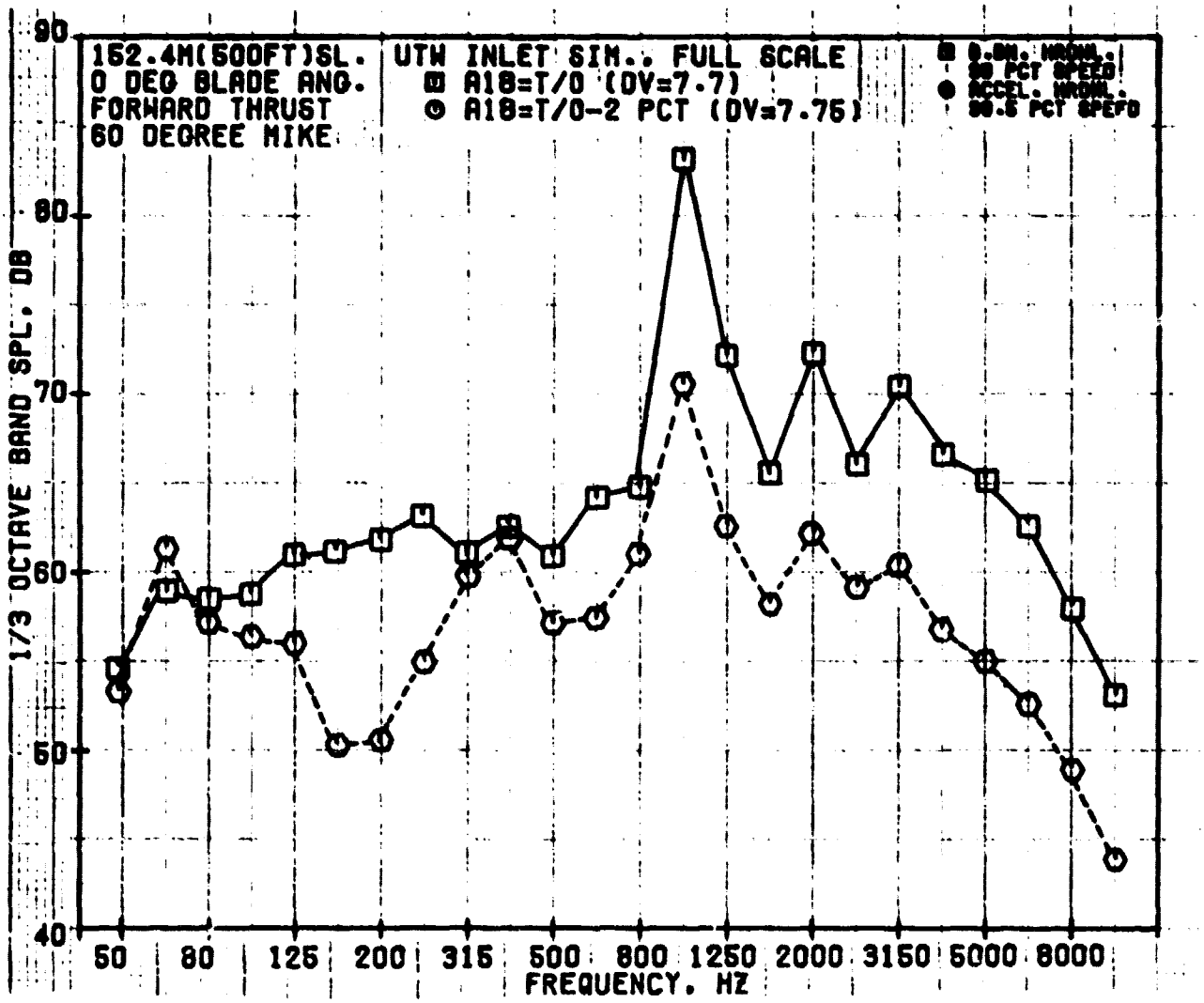

Figure 48. Forward-Thrust, 1/3-Octave-Band, SPL Spectra - Baseline Bellmouth and Accelerating Hard-Wall Inlets at 0.79 Throat Mach Number at 60°.

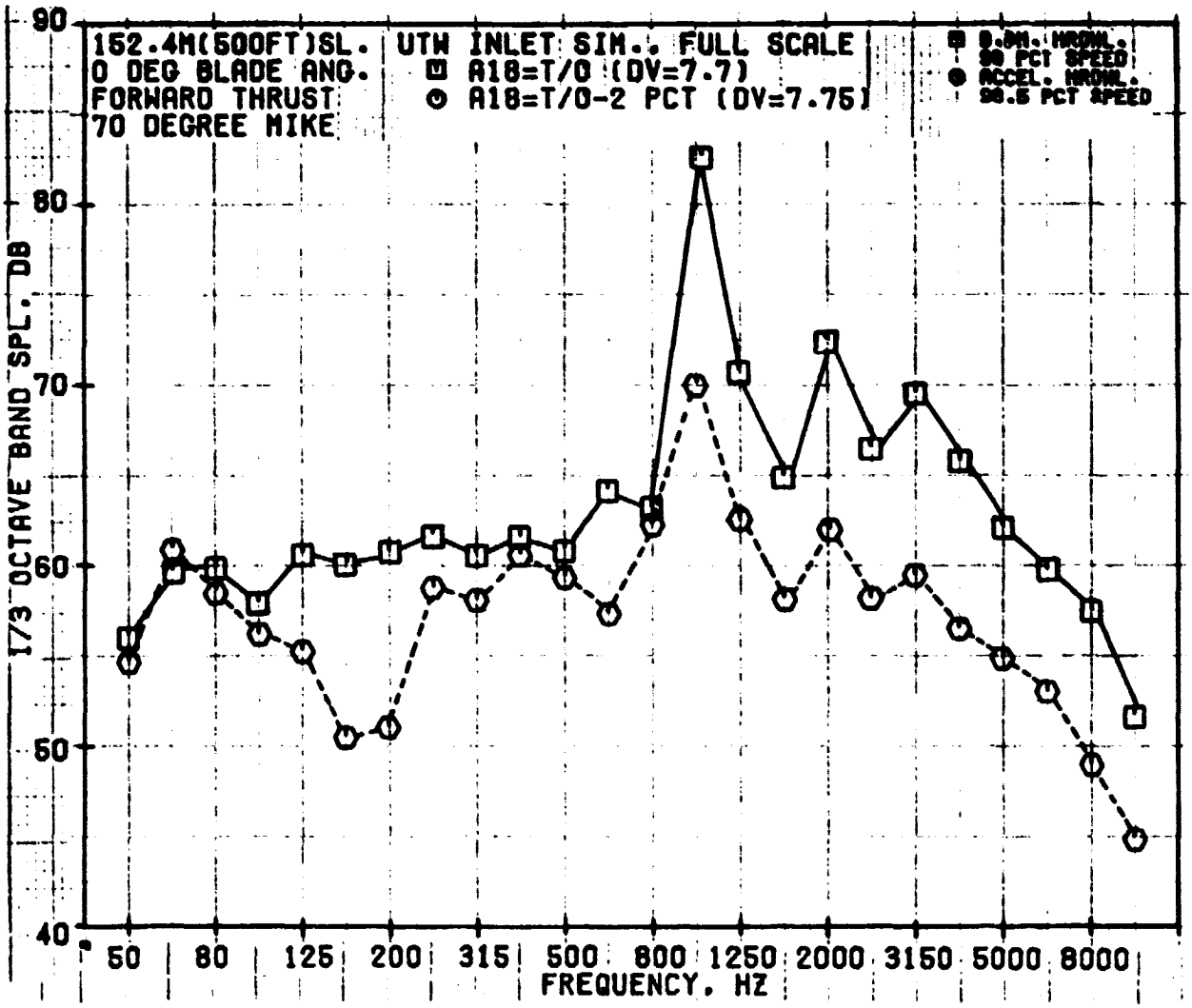

Figure 49. Forward-Thrust, 1/3-Octave-Band, SPL Spectra - Baseline Bellmouth and Accelerating Hard-Wall Inlets at 0.79 Throat Mach Number at 70°.

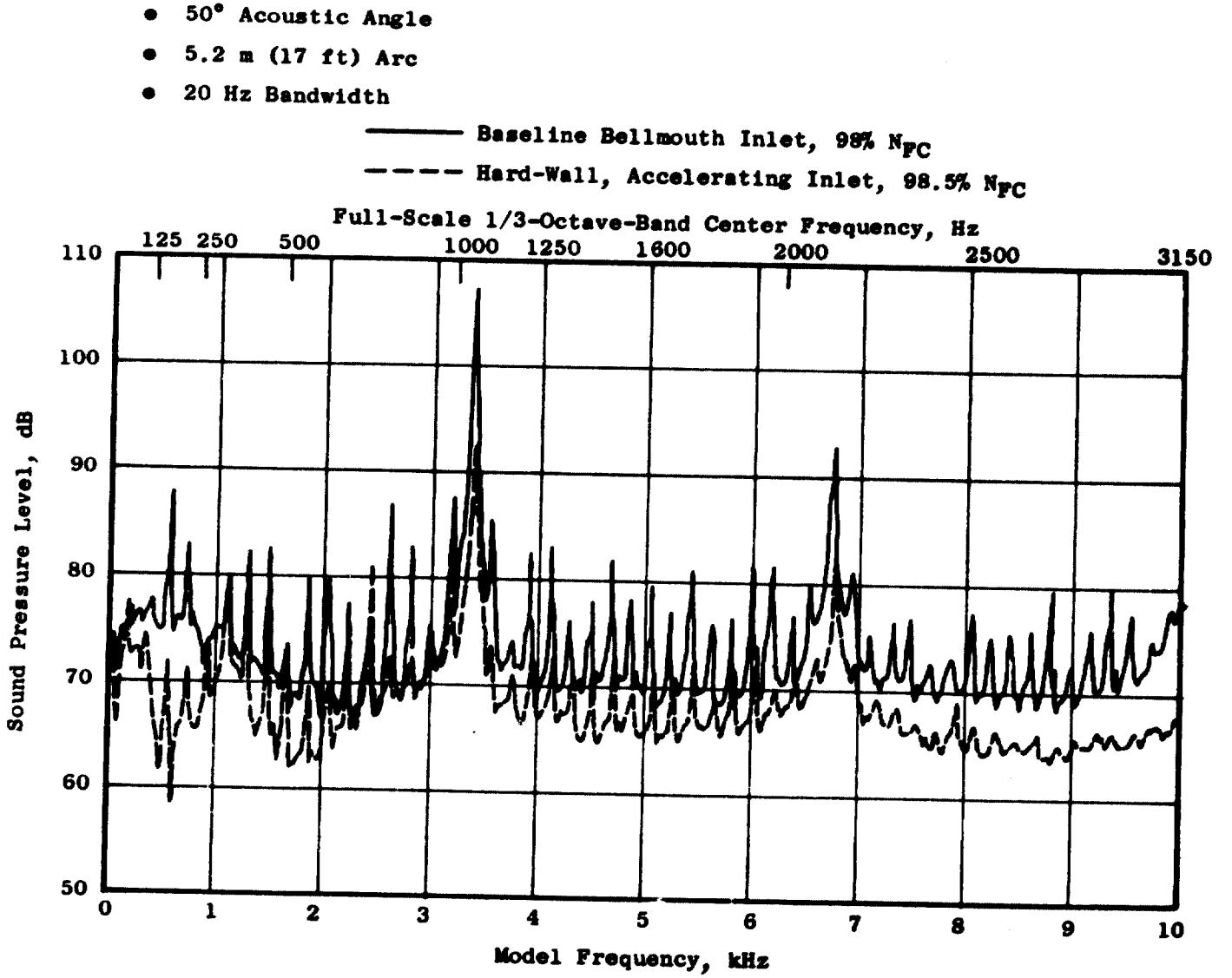

Figure 50. Narrowband SPL Spectra - Baseline Bellmouth and Hard-Wall Accelerating Inlet at 0.79 Throat Mach Number at 50°.

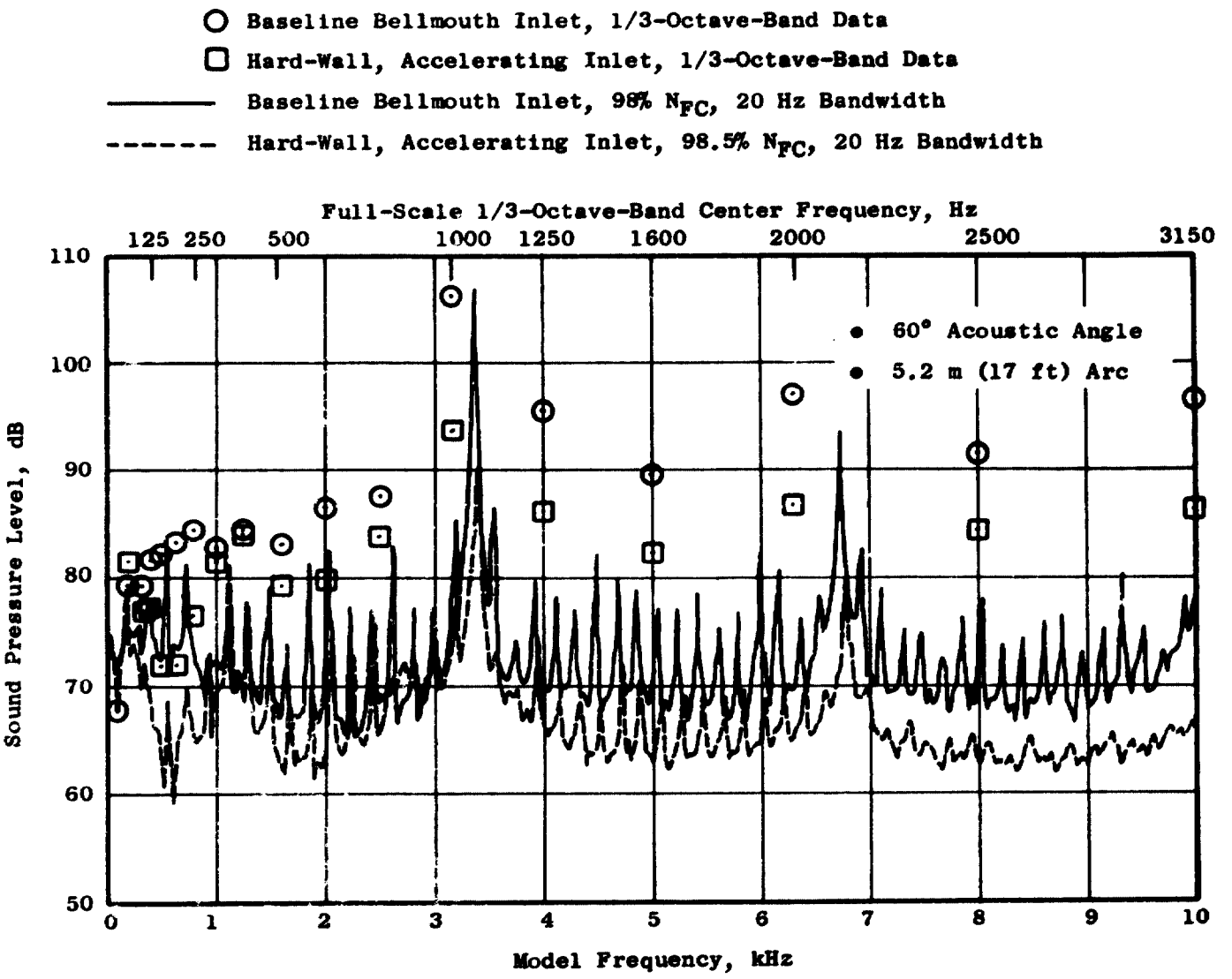

Figure 51. Narrowband SPL Spectra - Baseline Bellmouth and Hard-Wall Accelerating Inlet at 0.79 Throat Mach Number at 60°.

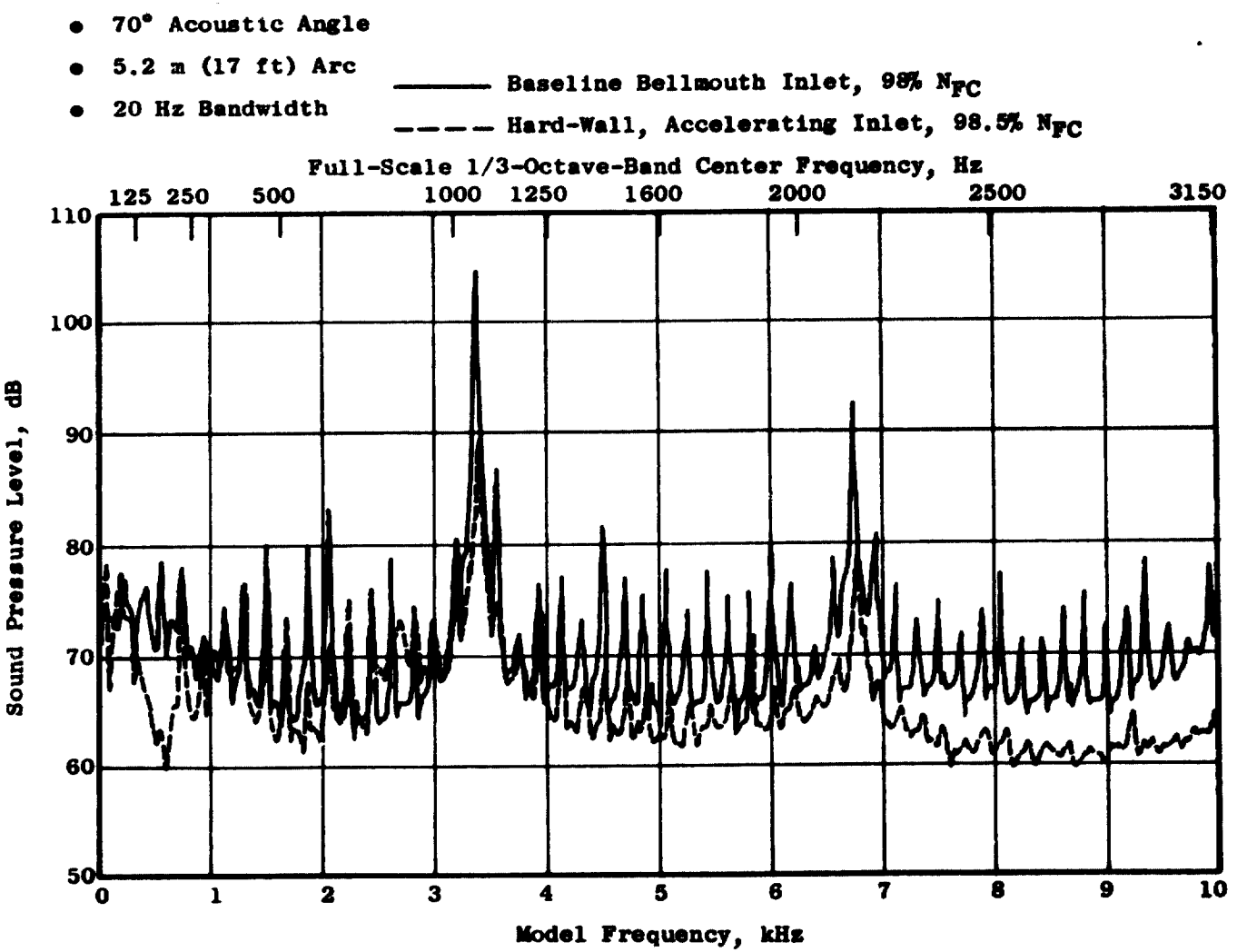

Figure 52. Narrowband SPL Spectra - Baseline Bellmouth and Hard-Wall Accelerating Inlet at 0.79 Throat Mach Number at 70°.

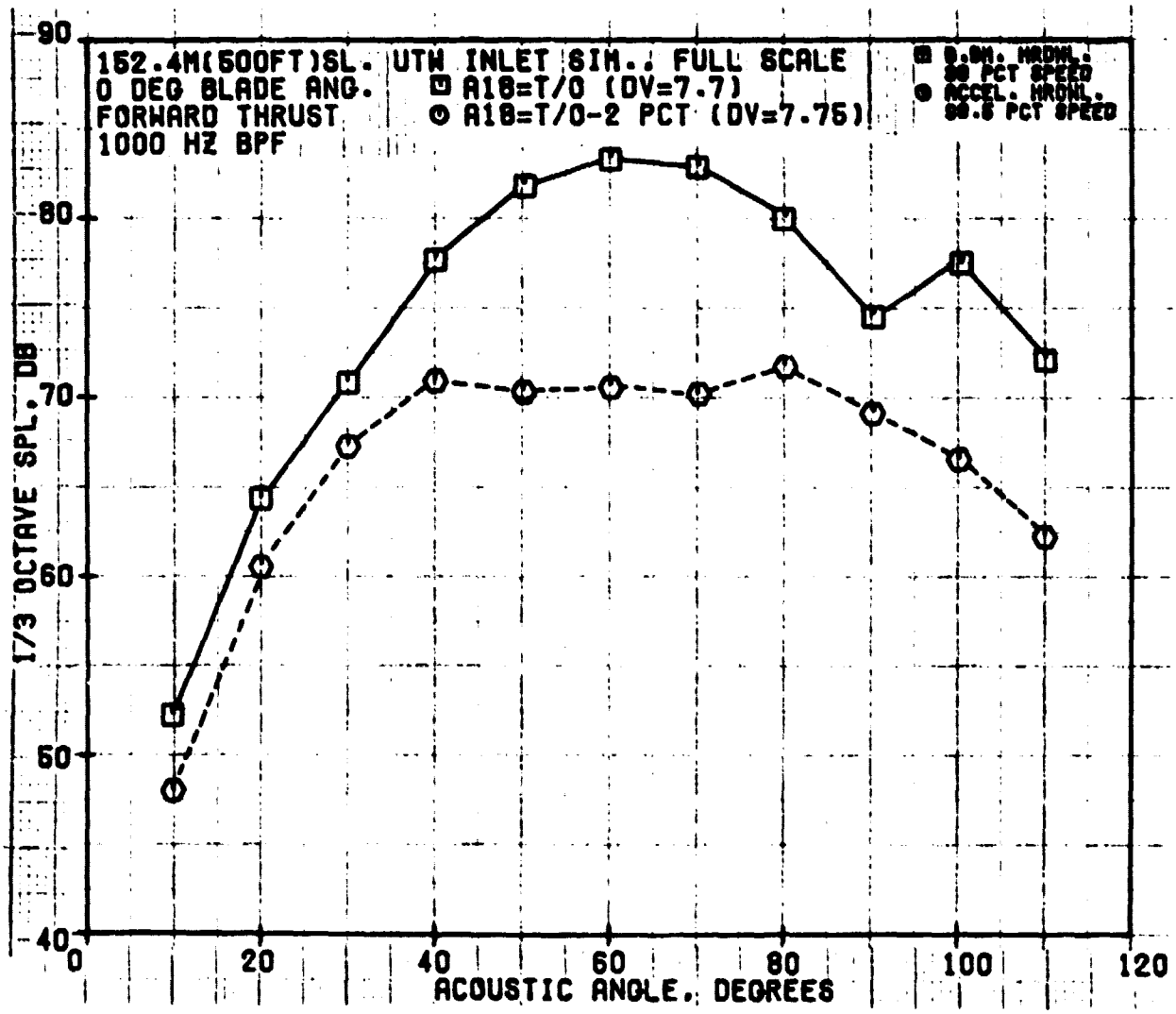

Figure 53. Forward-Thrust, 1/3-Octave-Band, SPL Directivity of Blade Passing Frequency - Baseline Bellmouth and Accelerating Hard-Wall Inlets at 0.79 Throat Mach Number.

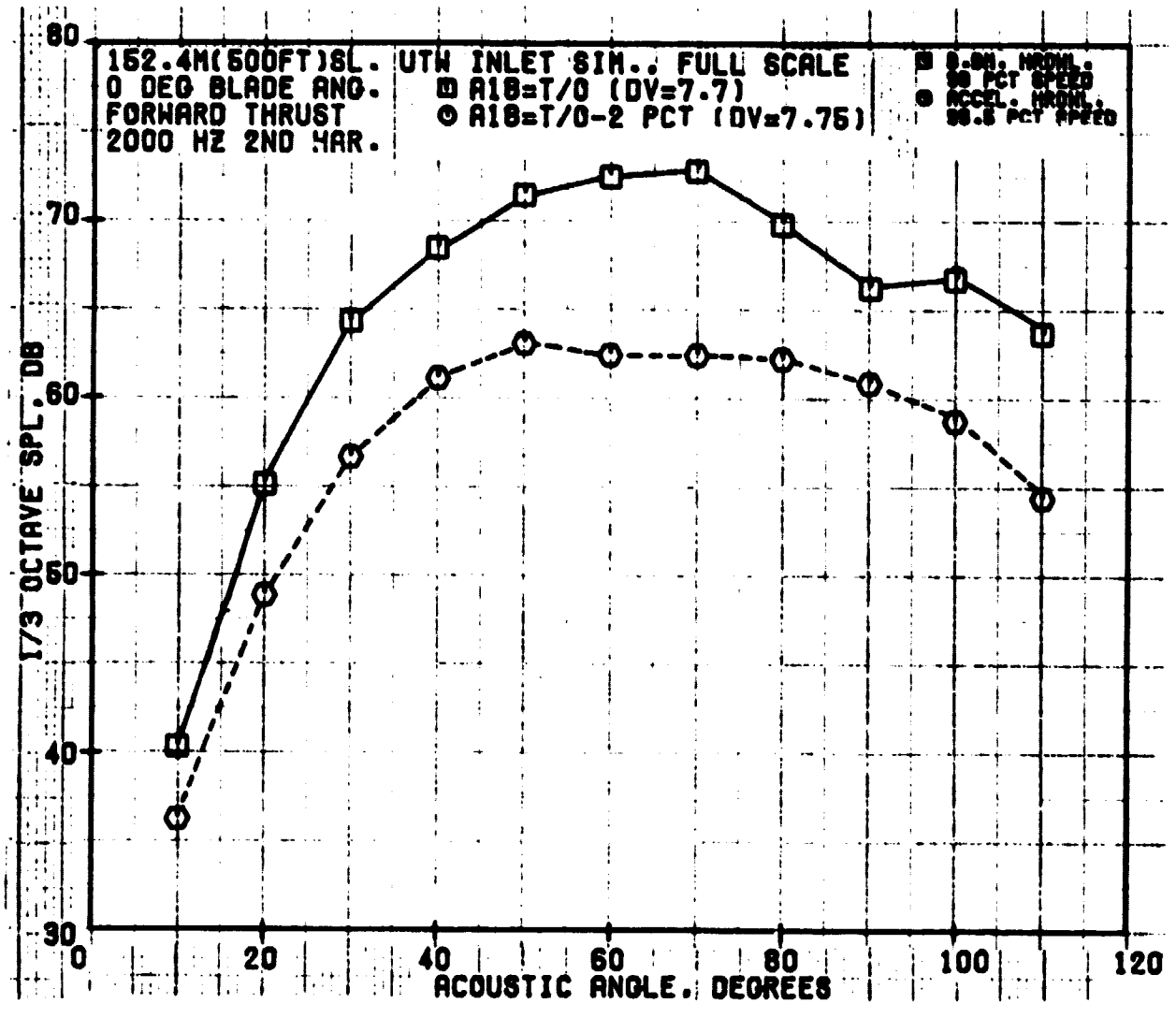

Figure 54. Forward-Thrust, 1/3-Octave-Band, SPL Directivity of Second Harmonic - Baseline Bellmouth and Accelerating Hard-Wall Inlets at 0.79 Throat Mach Number.

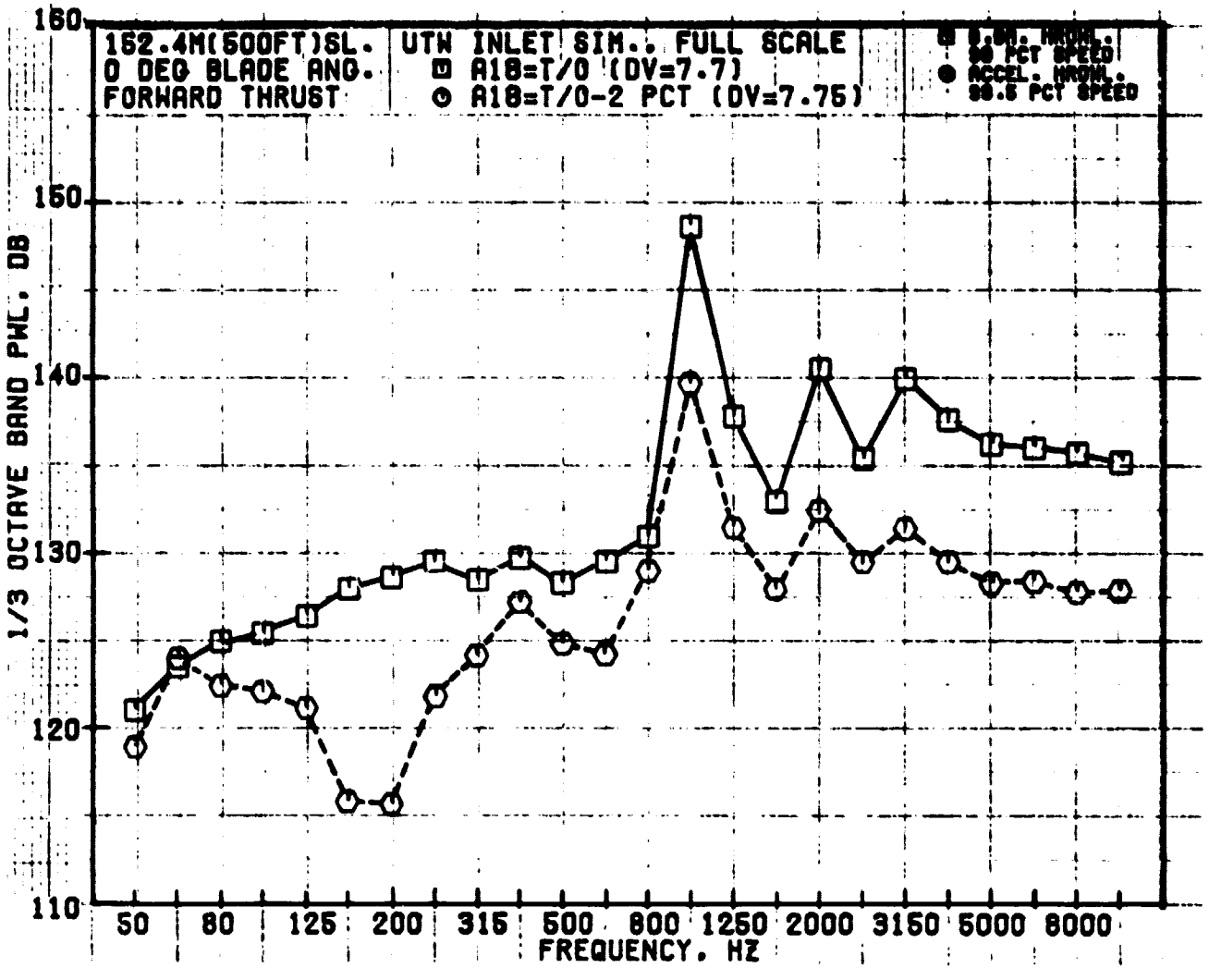

Figure 55. Forward-Thrust, PNL Directivity - Baseline Bellmouth and Accelerating Hard-Wall Inlets at 70% N_{FC}.

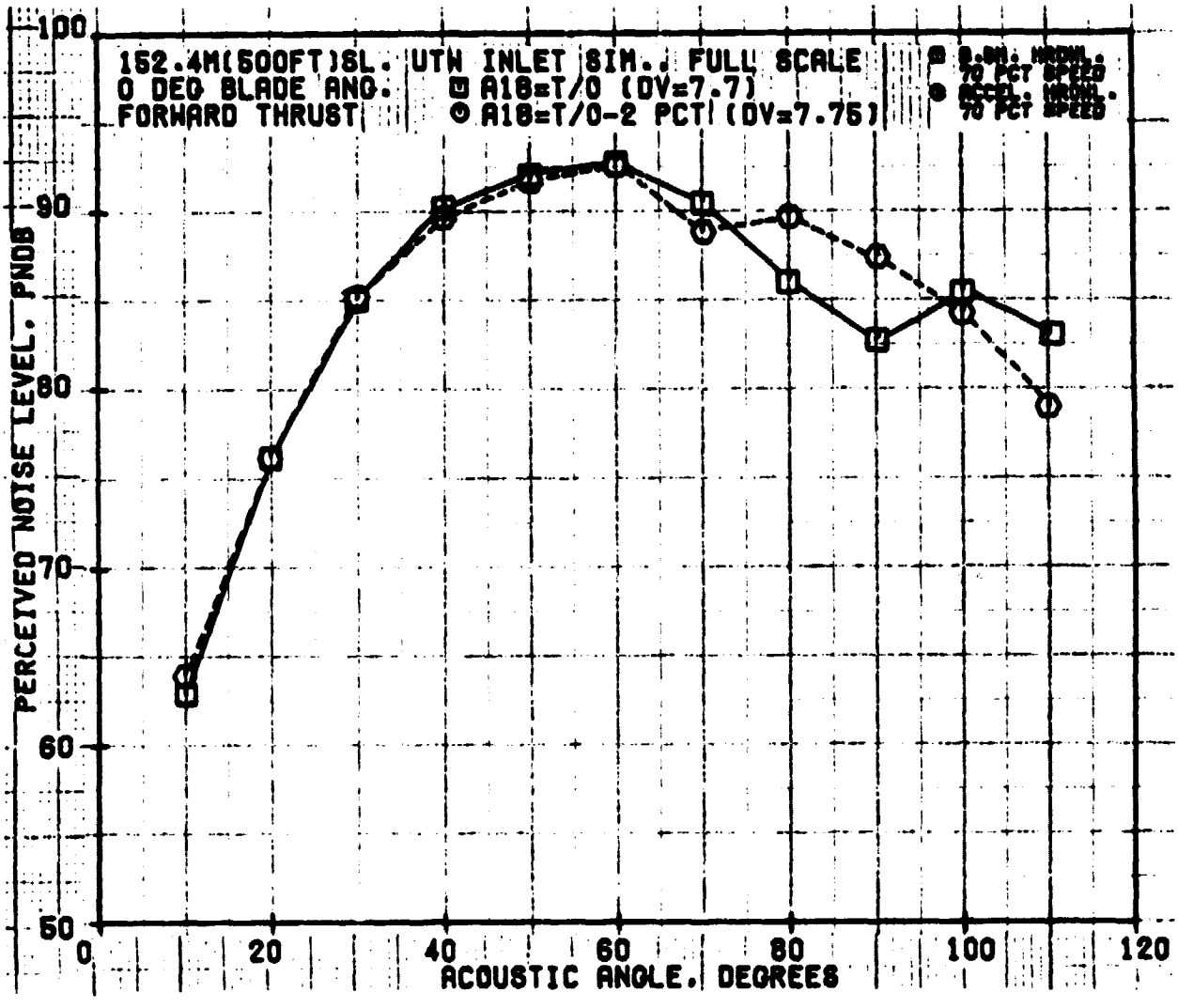

Figure 56. Forward-Thrust, PNL Directivity - Baseline Bellmouth and Accelerating Hard-Wall Inlets at 70% N_{FC}.

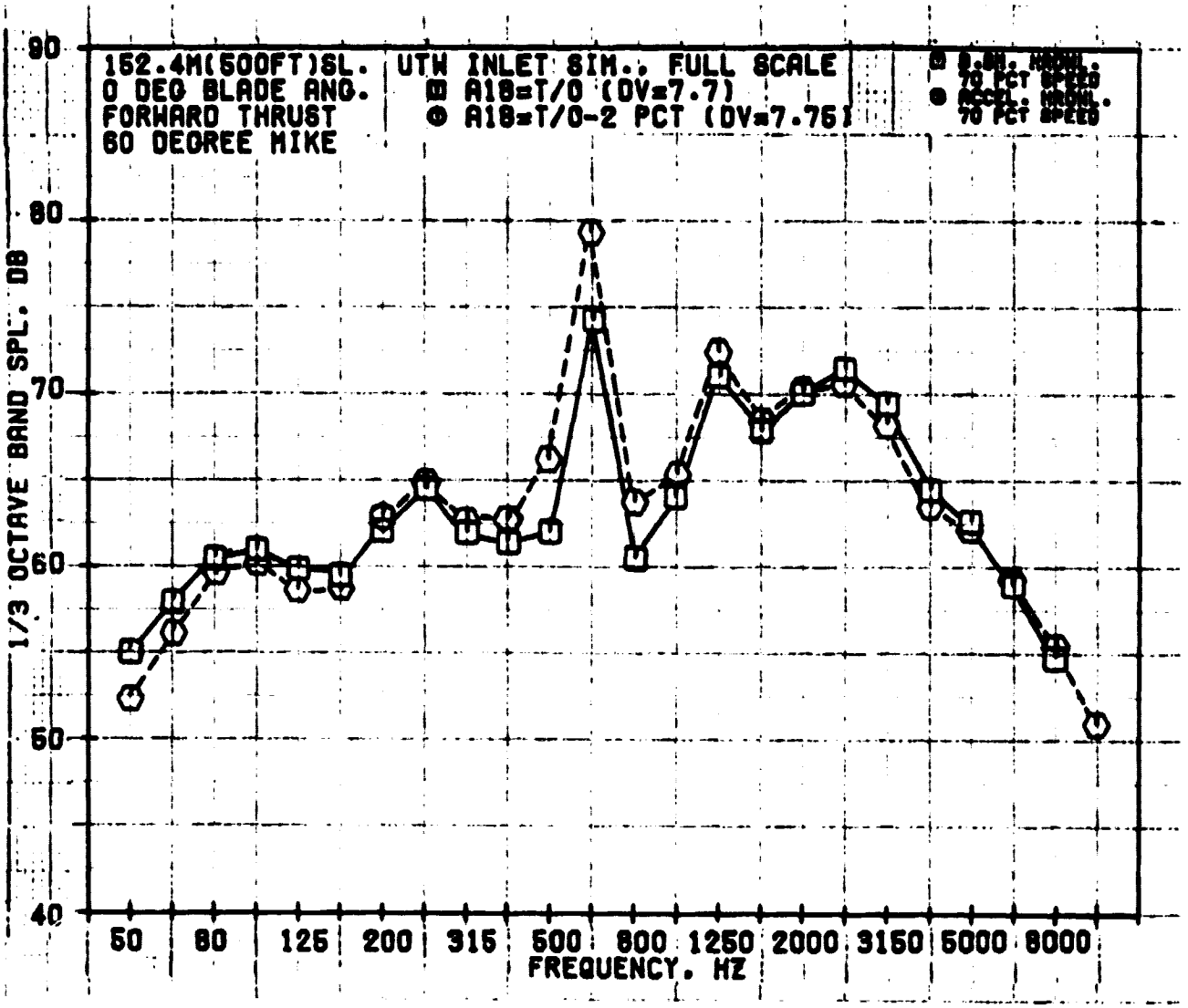

Figure 57. Forward-Thrust, 1/3-Octave-Band, SPL Spectra - Baseline Bellmouth and Accelerating Hard-Wall Inlets at 70% N_{FC} at 60°.

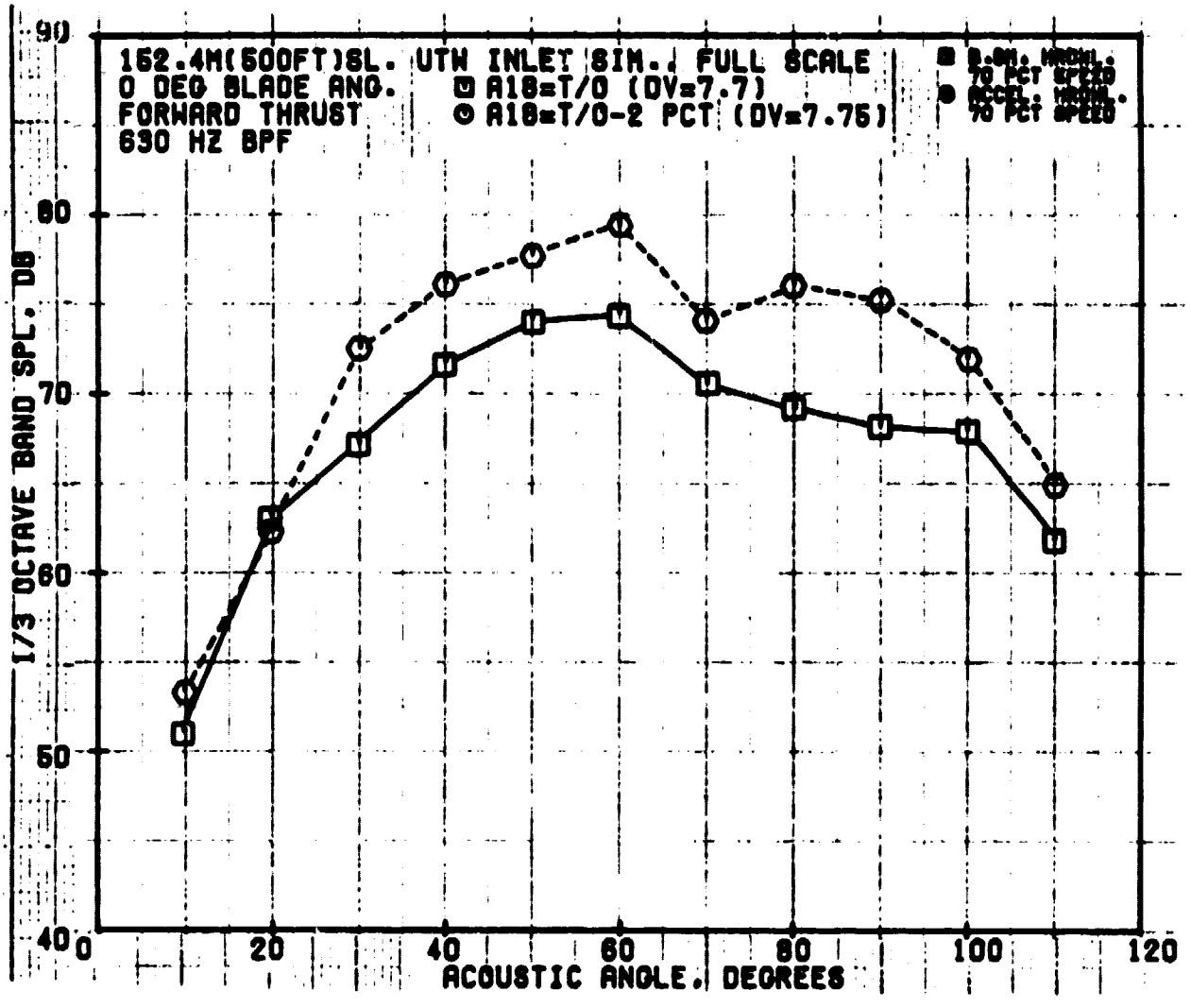

Figure 58. Forward-Thrust, 1/3-Octave-Band, SPL Directivity of Blade Passing Frequency for Baseline Bellmouth and Hard-Wall Accelerating Inlets at 70% N_{FC}.

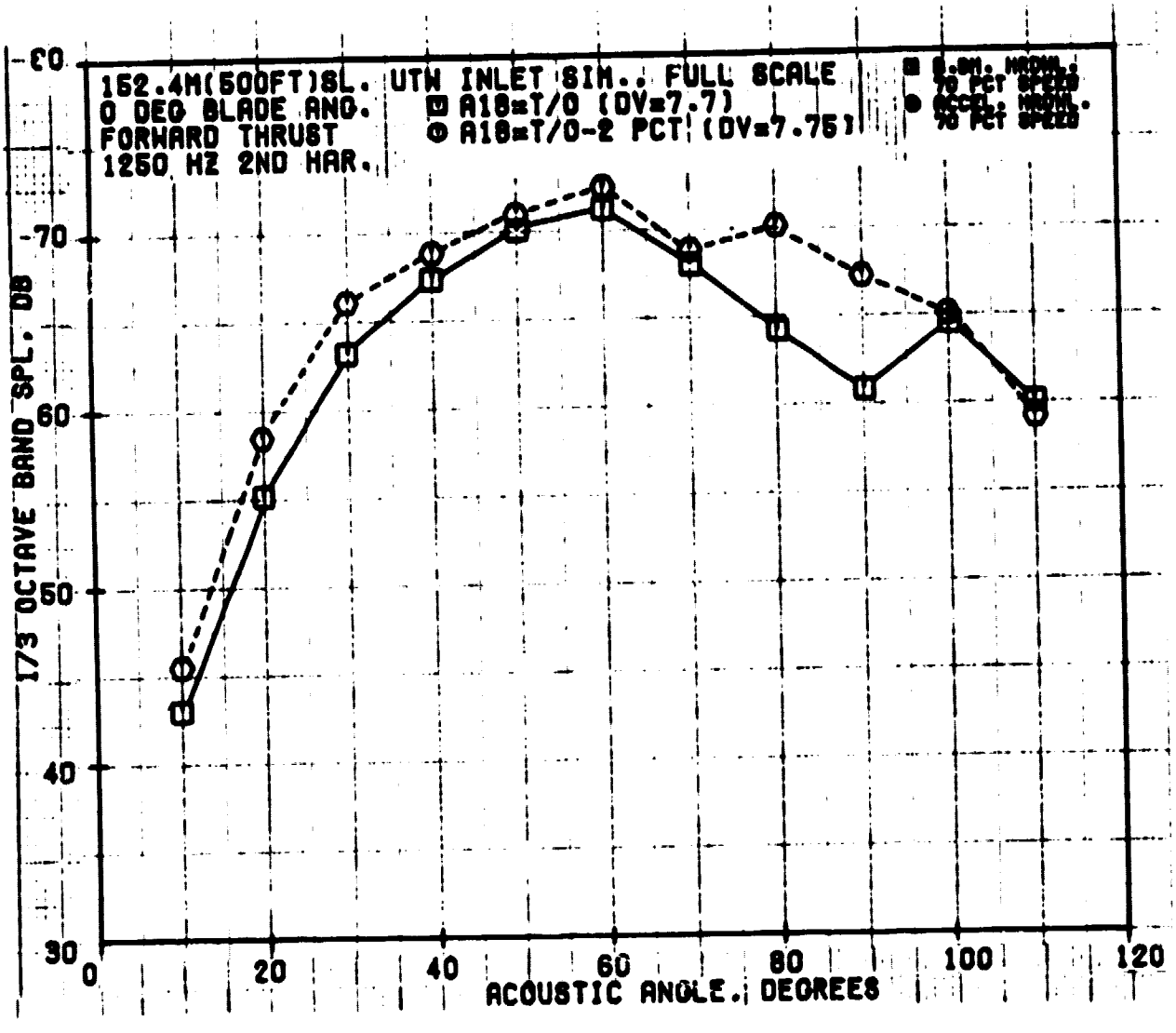

Figure 59. Forward-Thrust, 1/3-Octave-Band, SPL Directivity of Second Harmonic for Baseline Bellmouth and Accelerating Hard-Wall Inlets at 70% N_{FC}.

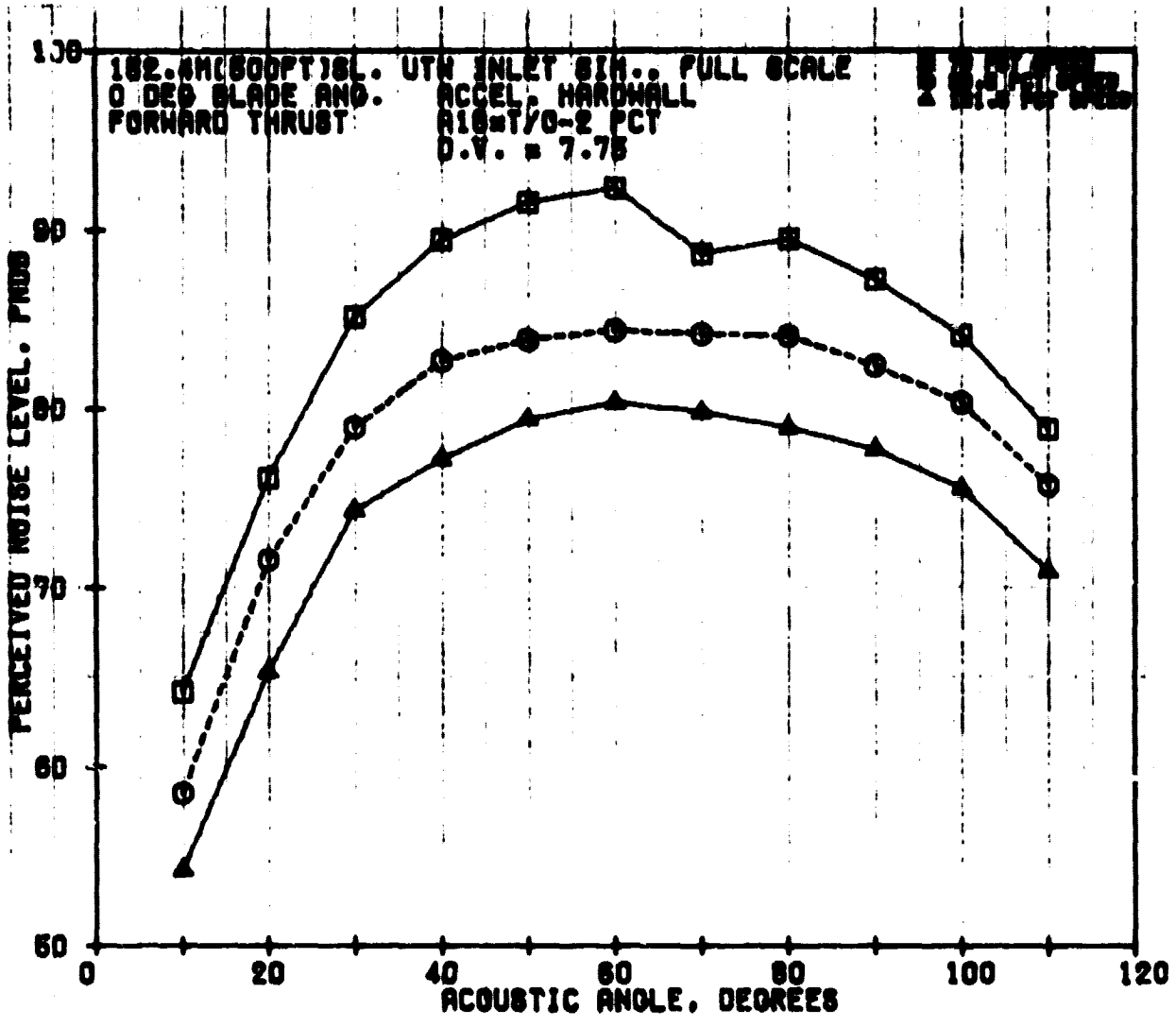

Figure 60. Forward-Thrust, PNL Directivity for Accelerating, Hard-Wall Inlet at 70%, 98.5%, and 101.5% N_{FC}.

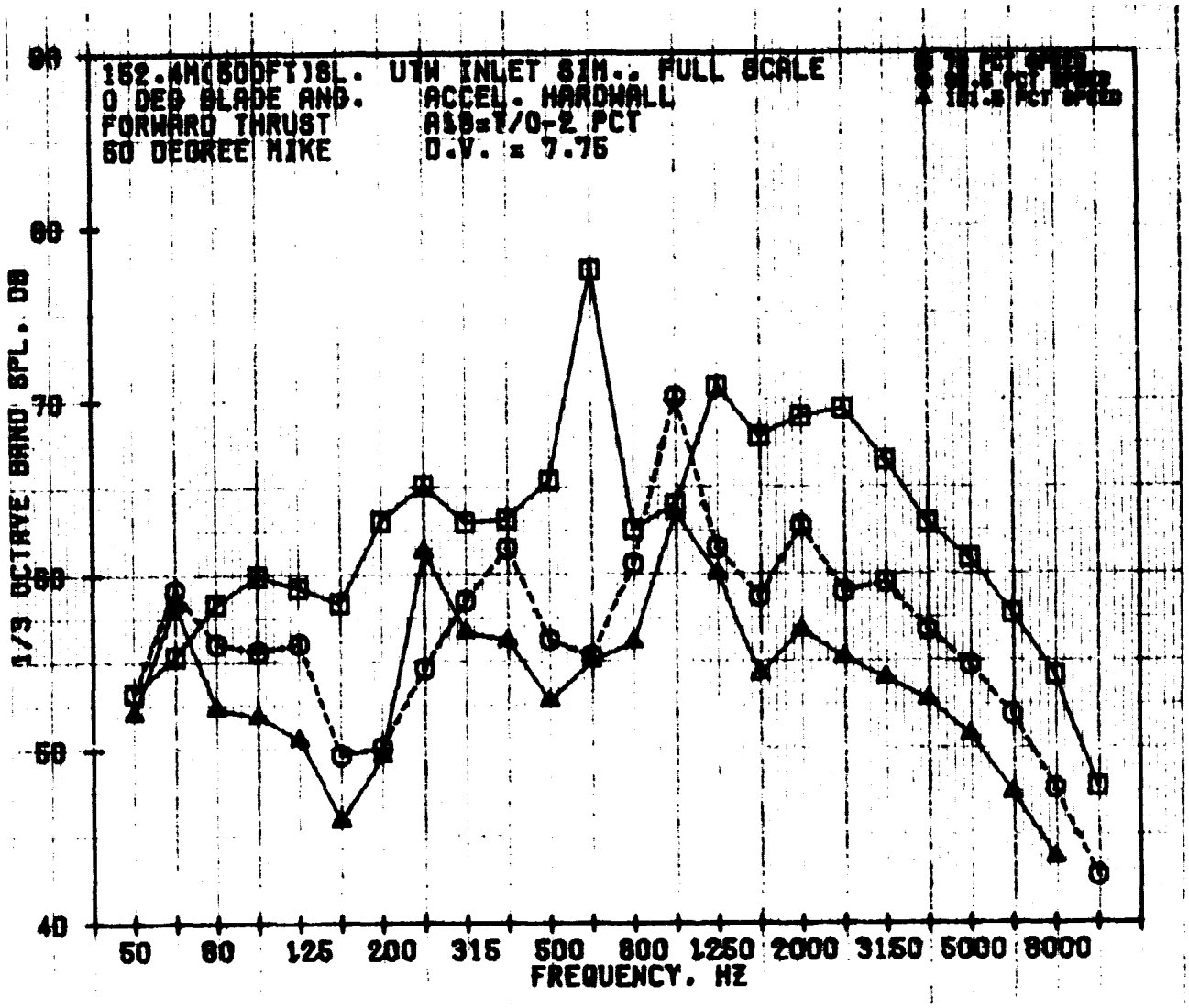

Figure 61. Forward-Thrust, 1/3-Octave-Band, SPL Spectra for the Accelerating, Hard-Wall Inlet at 70%, 98.5%, and 101.5% N_{FC} at 50°.

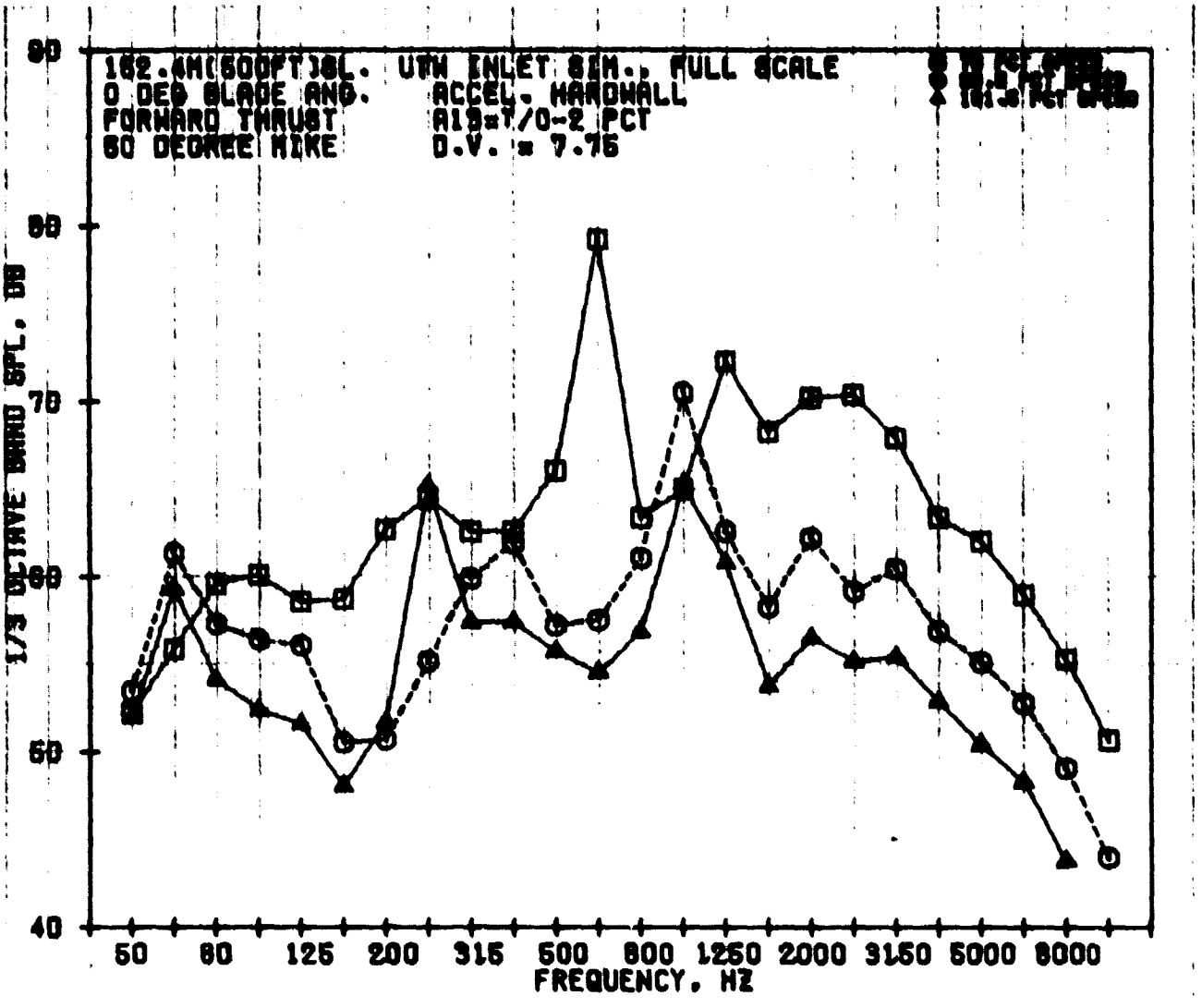

Figure 62. Forward-Thrust, 1/3-Octave-Band, SPL Spectra for the Accelerating, Hard-Wall Inlet at 70%, 98.5%, and 101.5% N_{FC} at 60°.

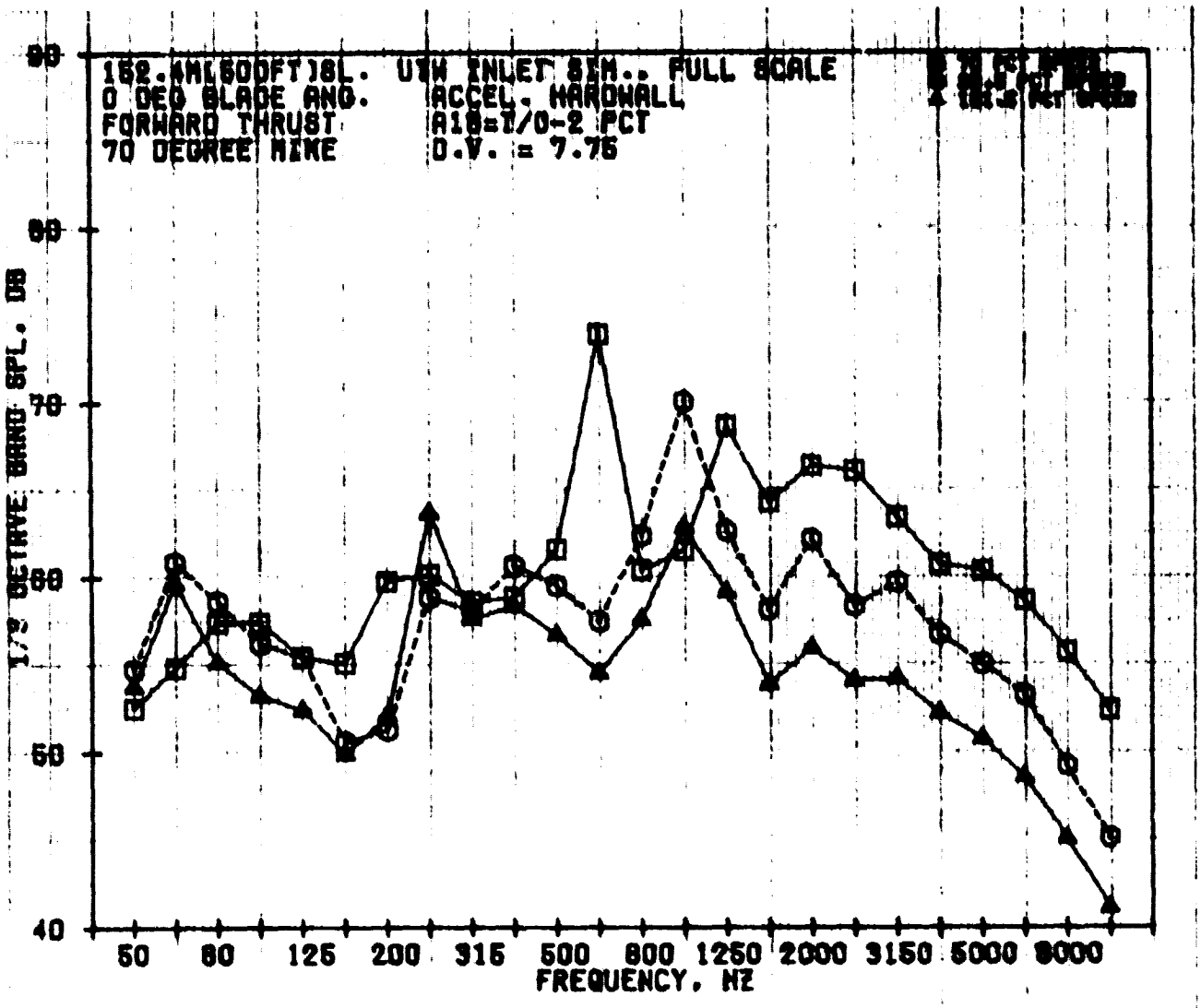

Figure 63. Forward-Thrust, 1/3-Octave-Band, SPL Spectra for the Accelerating, Hard-Wall Inlet at 70%, 98.5%, and 101.5% N_{FC} at 70°.

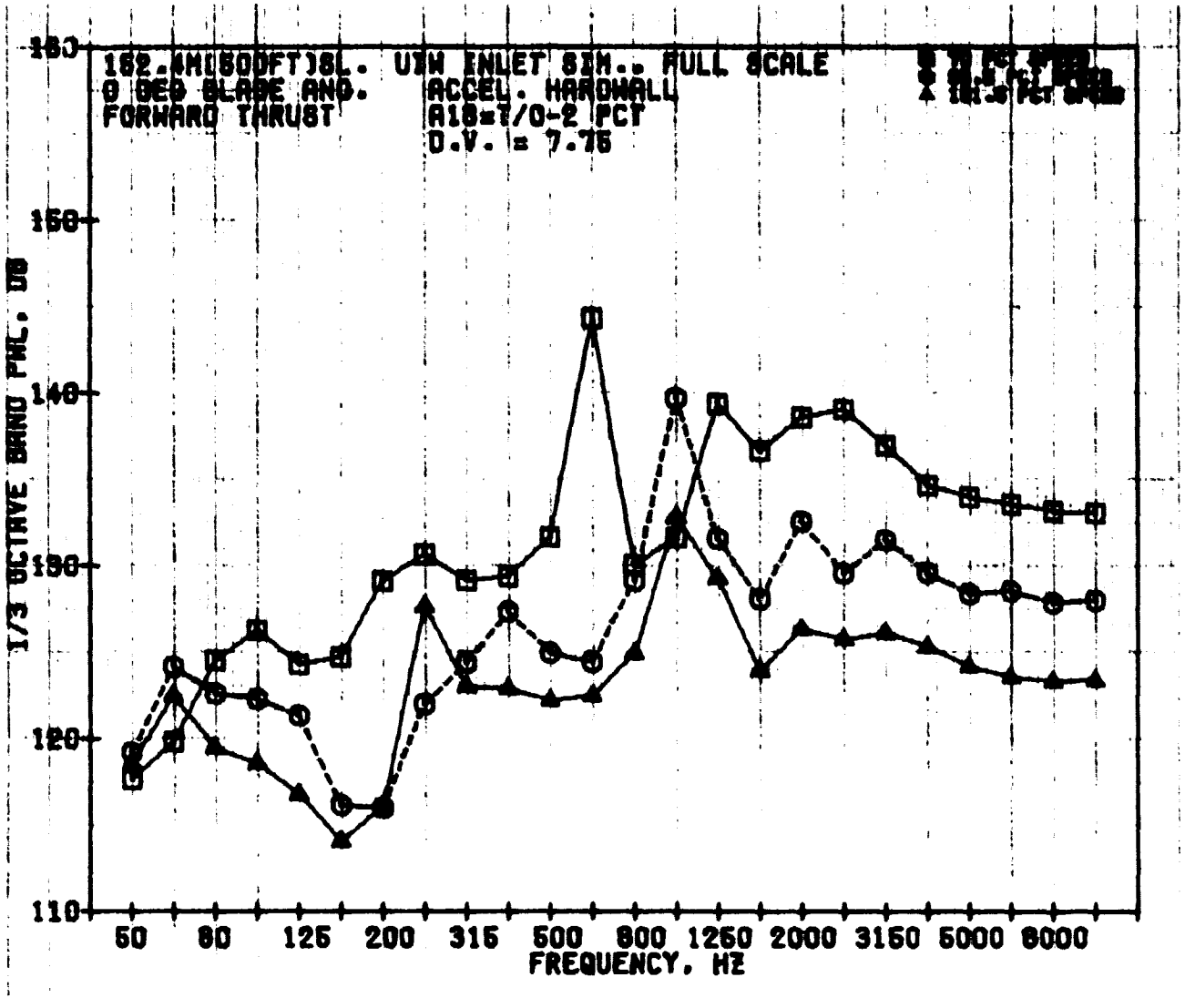

Figure 64. Forward-Thrust, 1/3-Octave-Band, PWL Spectra for the Accelerating, Hard-Wall Inlet at 70%, 98.5%, and 101.5% N_{FC}.

A comparison between the baseline bellmouth and the hard-wall, accelerating inlet is shown at 101.5% speed in Figures 65 through 69. The spectra at the peak angle, 60° to the inlet, show suppression over the entire frequency range. The origin of the spikes in both spectra at 250 Hz is a fan four-per-rev signal. One of the interesting phenomena seen with the bellmouth inlet is the significant levels of MPT's at frequencies higher than the BPF, seen in Figure 69. The 1/3-octave-band levels shown along with the 20-Hz narrowband do indicate that, with the bellmouth inlet, the MPT's controlled the 1/3-octave-band level below the BPF, but above the BPF the broadband noise controlled the 1/3-octave-band levels. The accelerating-inlet spectra that are superimposed show strong suppression of the MPT's over the entire frequency range in addition to suppressing the BPF and the second harmonic of the BPF.

9.2.3.2 Effectiveness of Accelerating-Inlet Treatments

The hard-wall- and the suppressed-accelerating-inlet PNL's for forward-thrust operation are given in Figure 70 as a function of fan speed. The results shown were extrapolated to a 152-m (500-ft) sideline distance at 60° relative to the fan inlet and are for a 0° blade angle.

Suppressed noise levels are given in Figure 70 for two inlet-treatment configurations, D and B. The other inlet configurations, A and C, were not run in the forward-thrust mode due to constraints on available test time. Treatment B was selected on the basis of previous test data (Reference 9) that showed good suppression with liner designs having 10% faceplate porosity. The selection of treatment D for forward-thrust testing was based on the good suppression characteristics exhibited in reverse-thrust tests (which will be discussed later).

The comparison of treatments D and B indicate that the latter shows increased suppression relative to the hard-wall, accelerating inlet at the higher fan speeds, whereas treatment D shows an increase in the noise level relative to hard wall. For a throat Mach number of 0.79, the inlet B treatment gives an additional 3 PNdB suppression. Comparing inlet D to the hard-wall at 0.79 throat Mach number shows that the noise level increased with the acoustic treatment by about 1.0 PNdB. Performance of these inlets at high throat Mach numbers will be discussed in more detail in Section 9.3.3.3.

Treatment B also gives more suppression than inlet D at the lower fan speeds. The suppression measured at 70% N_{FC} for treatment B is 6 PNdB; for inlet D, the suppression is approximately 4.0 PNdB.

The forward-radiated fan noise levels, PNL, versus acoustic angle, are shown in Figure 71 for the hard-wall accelerating inlet and treatments B and D. The data are for a 0.79 throat Mach number on a 152.4-m (500-ft) sideline. The unsuppressed noise peaks at an acoustic angle of 60°. The suppressed noise for all inlets also peaks at or near the 60° acoustic angle. The additional noise reduction with the treatment B configuration is seen to be independent of acoustic angle.

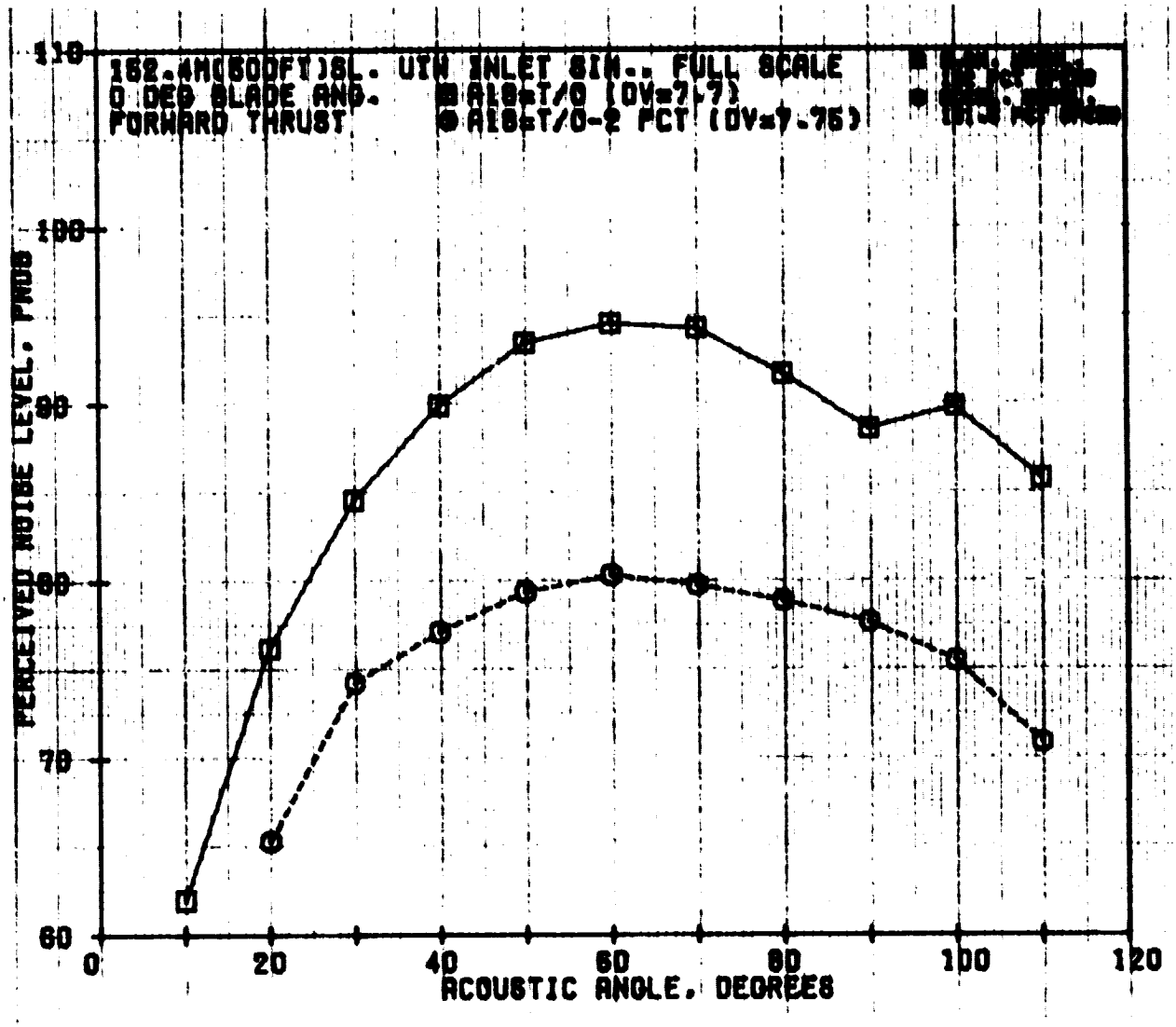

Figure 65. Forward-Thrust, PNL Directivity for the Baseline Bellmouth and Accelerating, Hard-Wall Inlets at 101.5% N_{FC}.

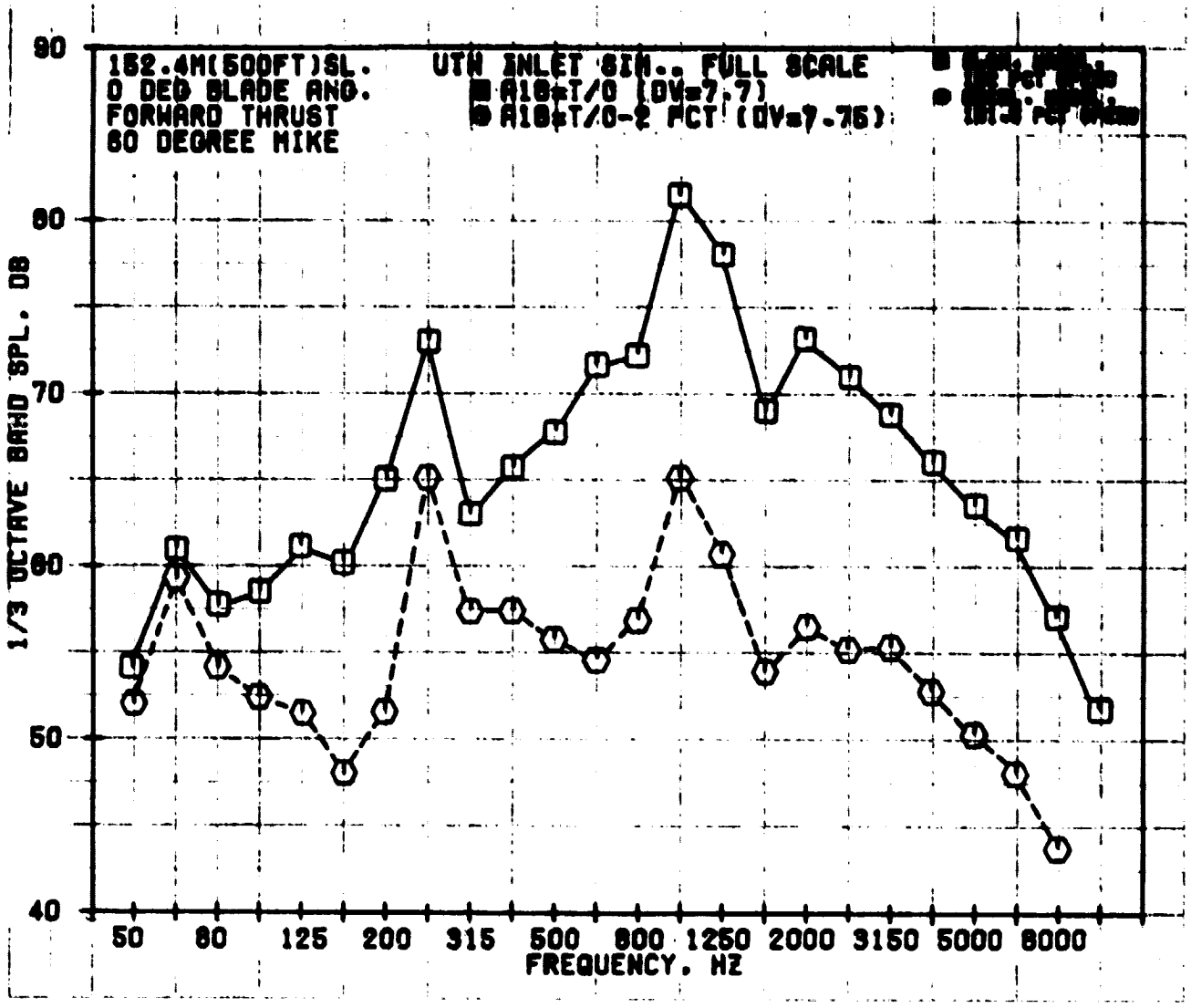

Figure 66. Forward-Thrust, 1/3-Octave-Band, SPL Spectra for the Baseline Bellmouth and Accelerating, Hard-Wall Inlets at 101.5% N_{FC} at 60°.

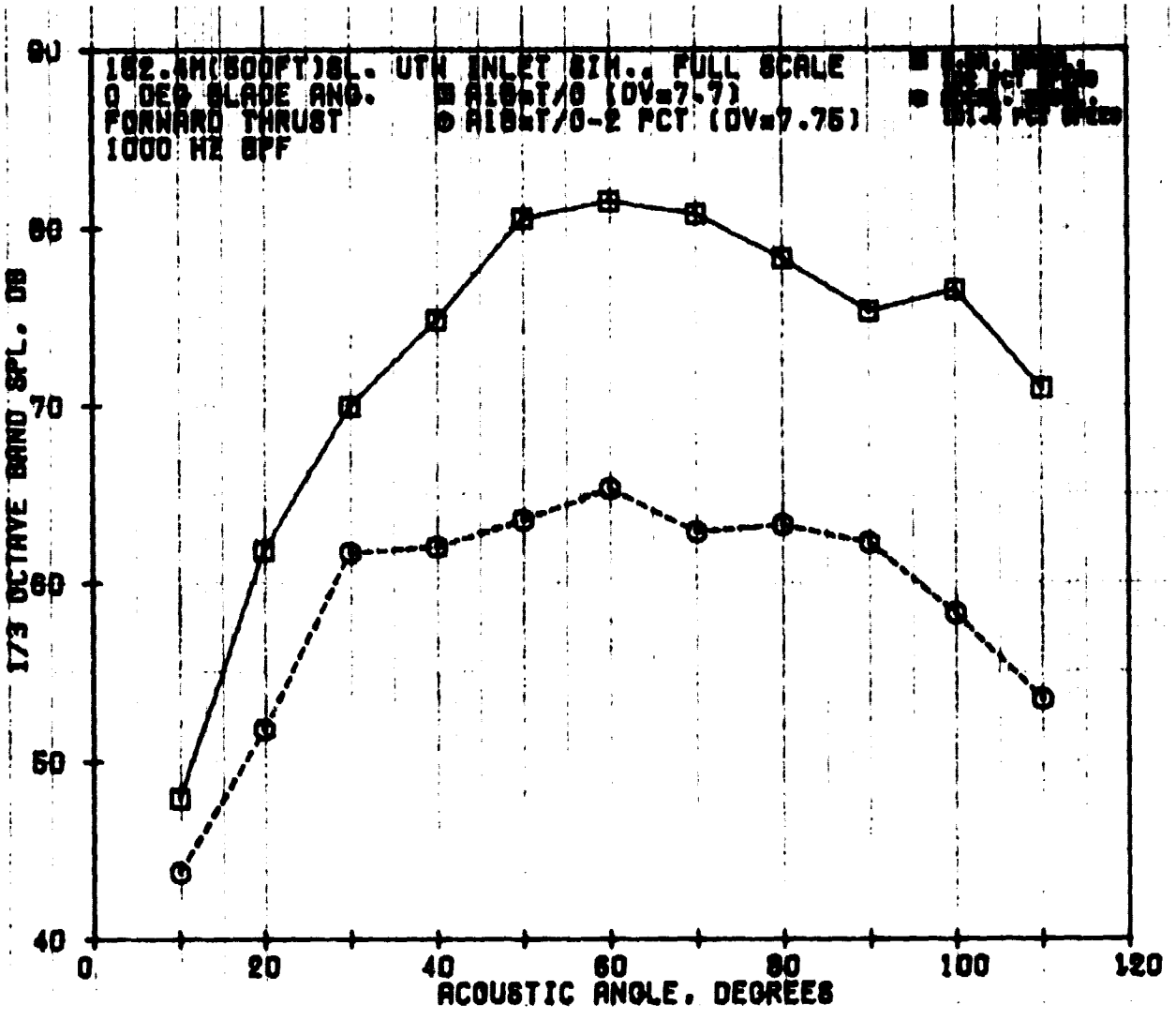

Figure 67. Forward-Thrust, 1/3-Octave-Band, SPL Directivity of Blade Passing Frequency for the Baseline Bellmouth and Accelerating, Hard-Wall Inlets at 101.5% N_{FC}.

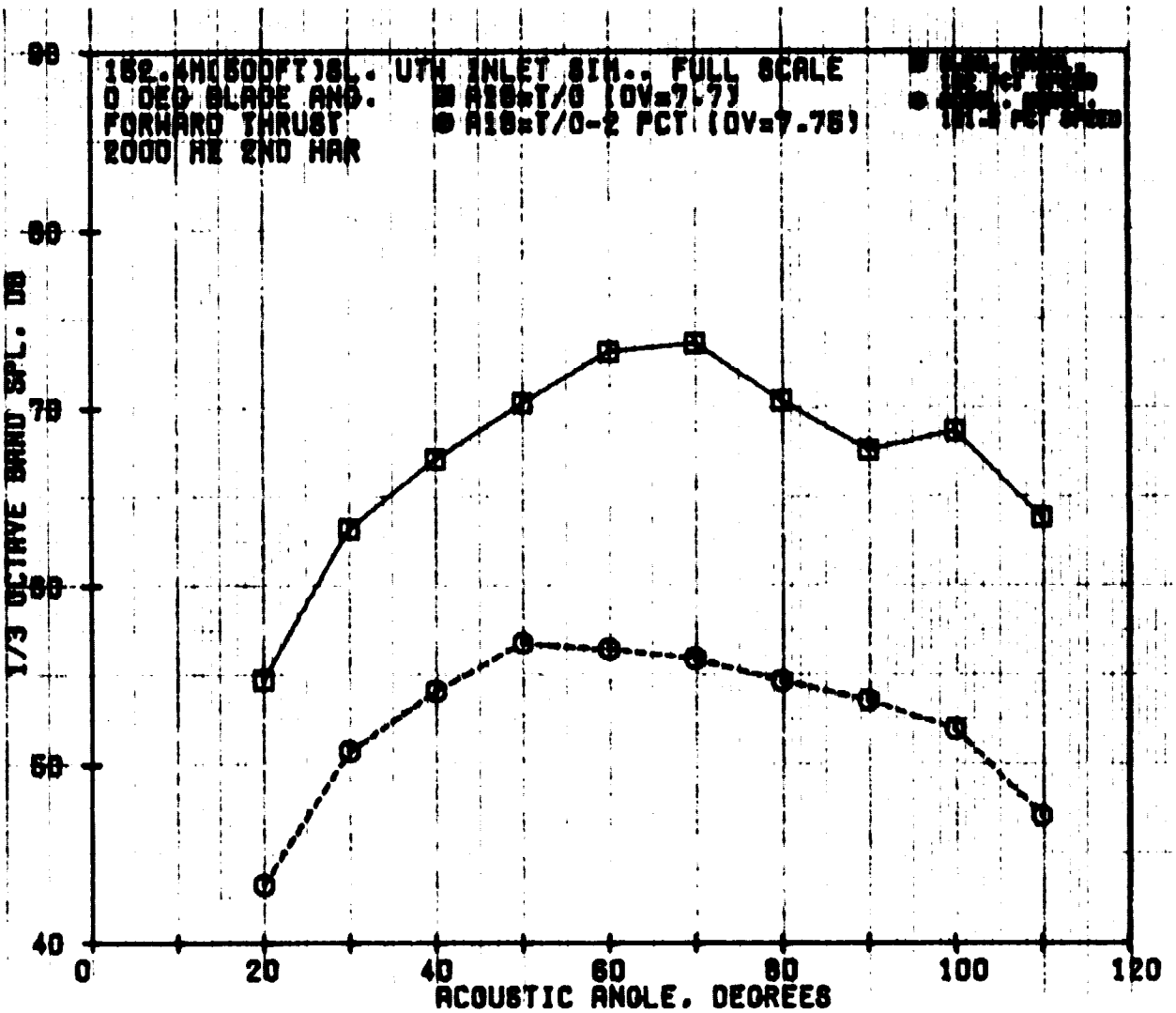

Figure 68. Forward-Thrust, 1/3-Octave-Band, SPL Directivity of Second Harmonic for the Baseline Bellmouth and Accelerating, Hard-Wall Inlets at 105% N_{FC}.

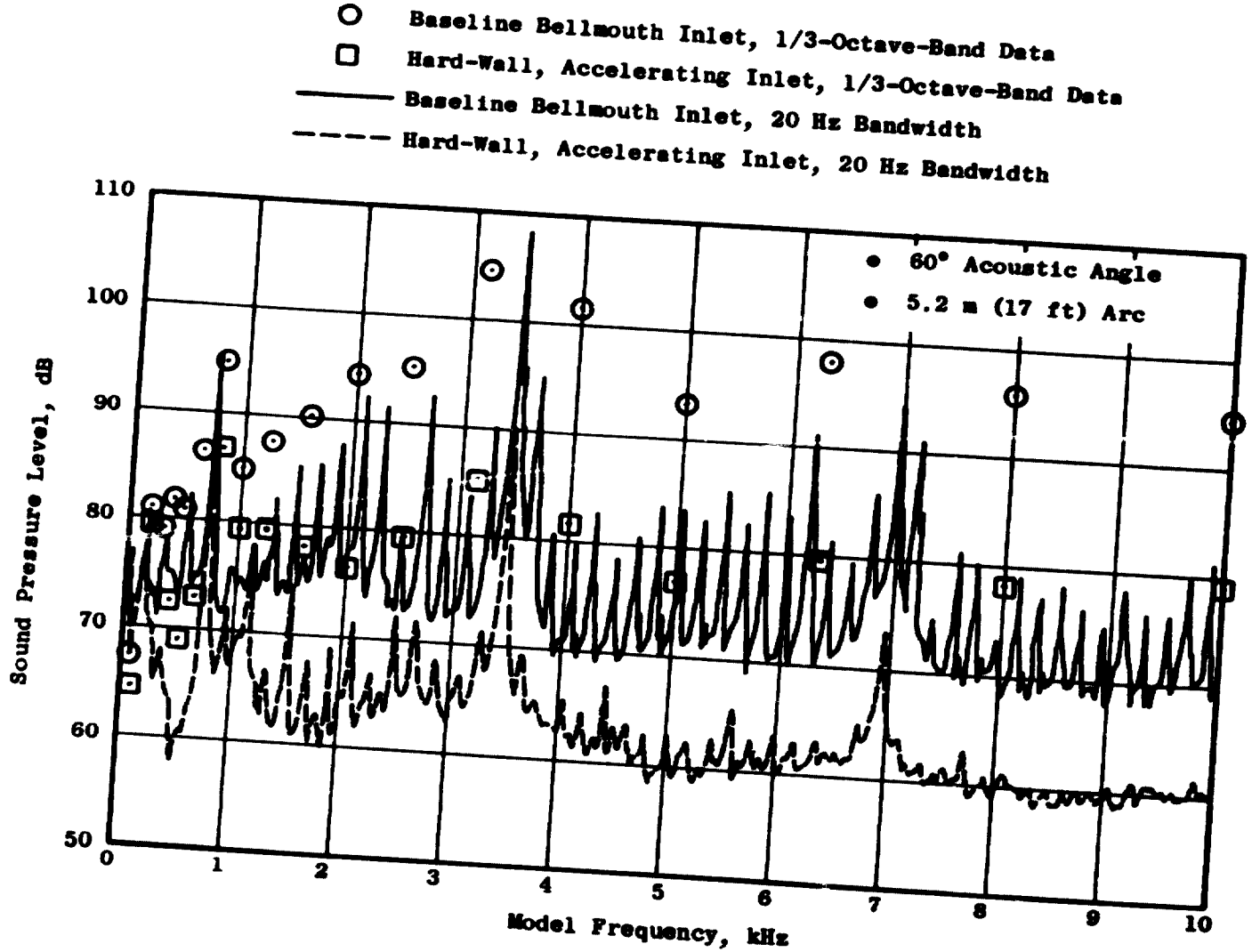

Figure 69. Narrowband SPL Spectra for the Baseline Bellmouth and Hard-Wall, Accelerating Inlet at 101.5% N_{FC}.

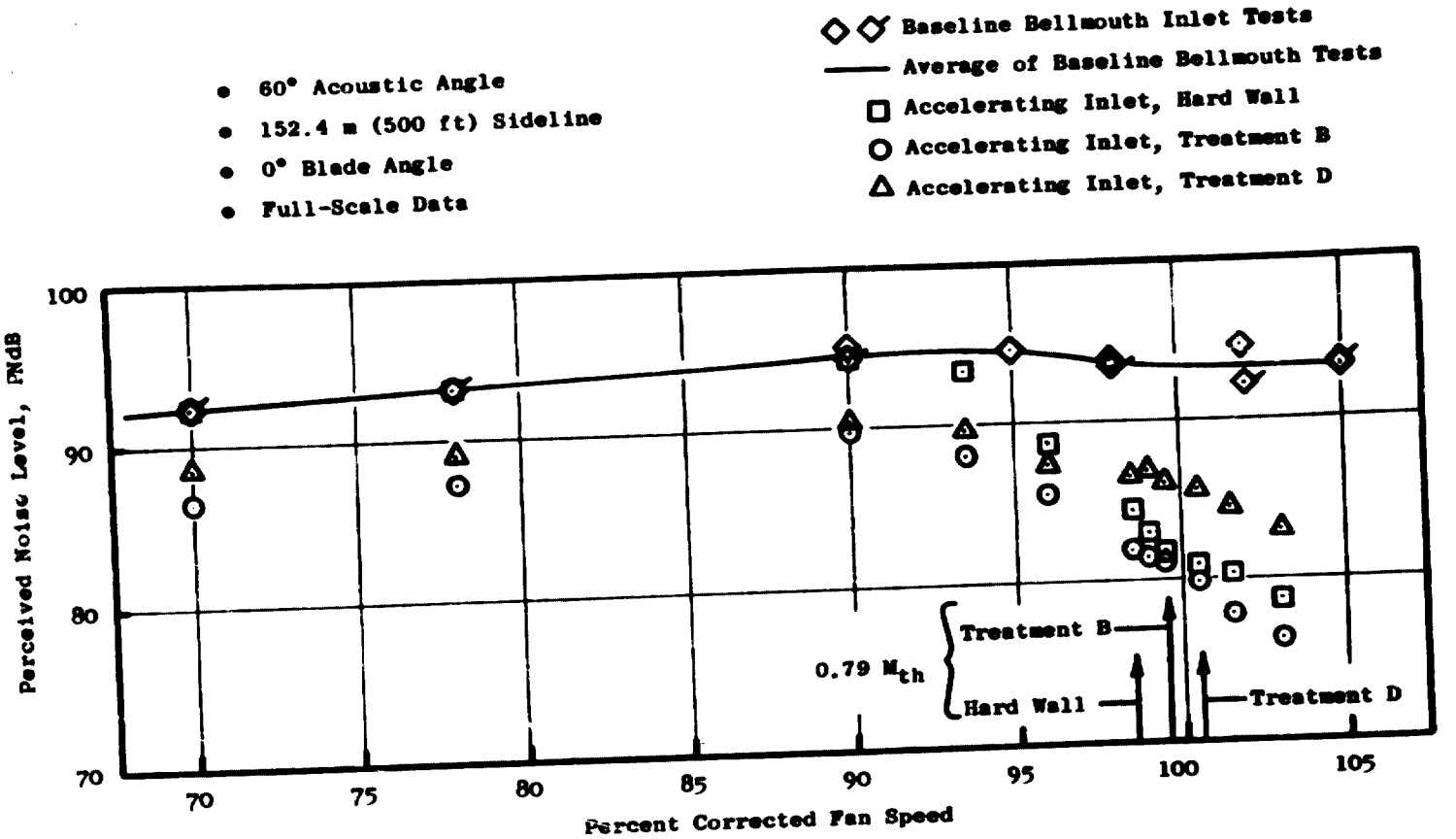

Figure 70. Forward-Thrust PNL Vs. Fan Speed for Baseline Bellmouth Inlets and Accelerating Inlets - Hard-Wall, Treatments B and D.

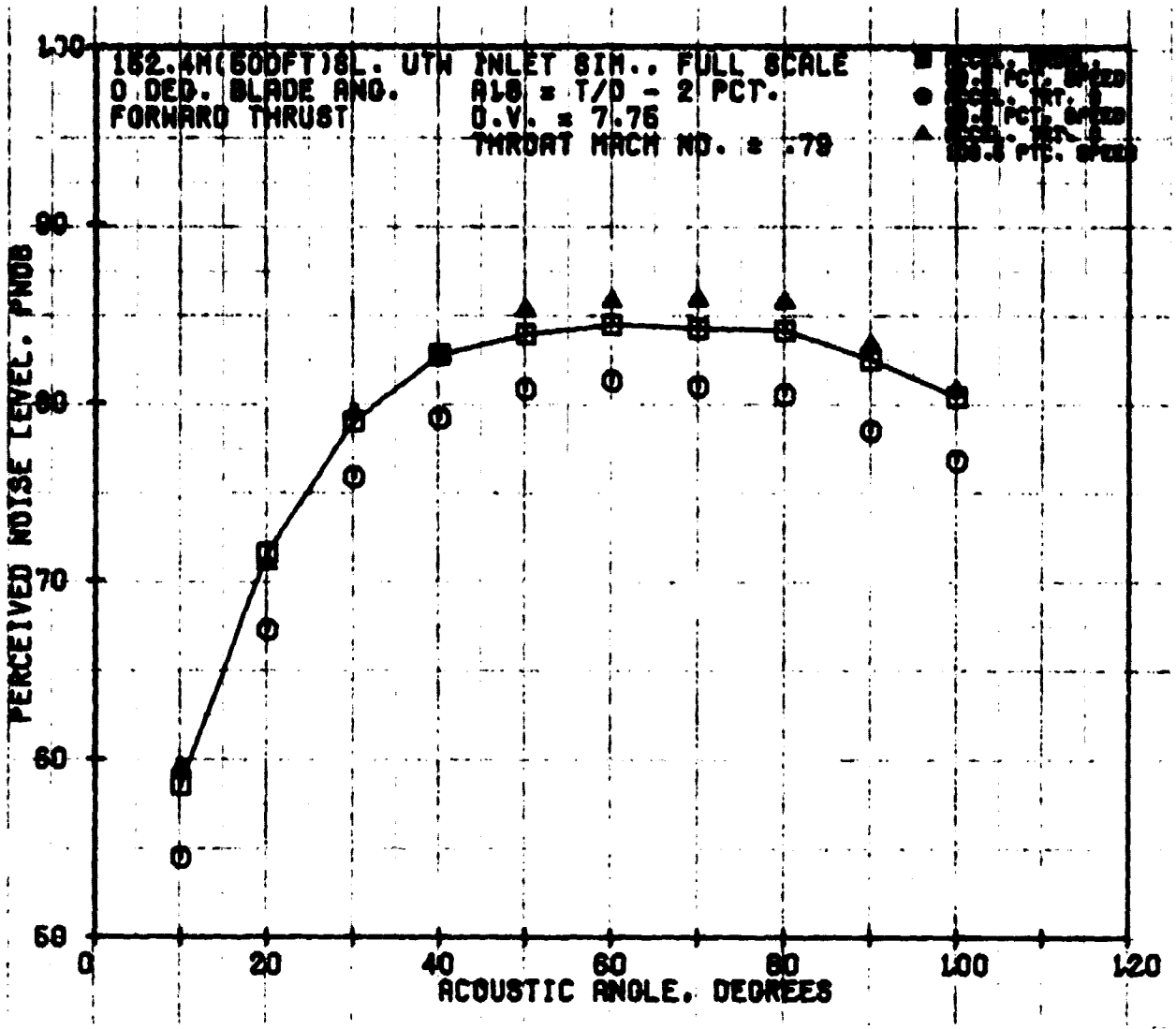

Figure 71. Forward-Thrust, PNL Directivity for the Accelerating Inlet: Hard-wall and Treatments B and D at 0.79 Throat Mach Number.

Spectral comparisons, at 0.79 throat Mach number, are shown in Figure 72 for the hard-wall accelerating inlet, and treatments B and D. The data are for an acoustic angle of 60° on a 152.4-m (500-ft) sideline. A noticeable reduction in noise is seen for the treatment B configuration relative to the other inlets in the frequencies ranging from the fan blade passing frequency (1,000 Hz) through 10,000 Hz. No particular trend in suppression is evident for frequencies below 1,000 Hz for any of the configurations. The hard-wall, accelerating inlet and treatment D have about the same noise levels at all frequencies except those below 1,250 Hz; in that range treatment D is about 6 dB higher. This increase undoubtedly contributes significantly to the 1.0 PNdB level increase measured on inlet D over the hard-wall, accelerating inlet.

The inlet B configuration gives a total 1/3-octave-band tone-suppression level of approximately 20 dB at 1000 Hz relative to the baseline bellmouth. Here 8 dB of the 20 dB suppression are from the acoustic treatment as shown in Figure 72. Comparatively, treatment D gives a total suppression of 15 dB of which only 3 dB result from the addition of acoustic treatment.

Figures 73 and 74 give the spectra, as discussed above, for the 70° and 50° acoustic angles. The suppression characteristics as noted in Figure 71 are found to be independent of acoustic angle between 50° and 70°.

Figure 75 gives PNL directivities at 70% speed for the hard-wall configuration and treatments B and D. The unsuppressed noise is shown peaking at 60° with sharp decreases in level for all other forward-quadrant angles. The suppressed noise level also peaks at 60°; however, the directivity pattern is somewhat flatter than that of the unsuppressed noise levels. The suppression as a function of angle is rather constant for angles of 50° and greater but decreases significantly for angles less that 50°.

Figure 76 gives the spectral comparisons at 60° to the inlet for 70% speed. The low fan speed results in no suppression from inlet Mach number. The spectral results for treatments B and D show that the treatment B configuration suppression levels at frequencies of 800 Hz through 3150 Hz are significantly higher than for inlet D. Tone suppression-level comparisons at 630 Hz, 1250 Hz, and 2500 Hz show treatment B giving from 1 dB to 5 dB more suppression. The suppression at frequencies greater than 4000 Hz is small, and little difference is seen for either treatment configuration.

Spectra for the hard-wall and the treated inlets at 70% fan speed are given in Figure 77 for 50° and Figure 78 for 70°. These data show no significant changes in the spectral suppression characteristics with respect to acoustic angle in the range of 50° to 70°.

Figures 79 through 82 compare suppression spectra for treatments B and D for fan speeds of 70%, 78%, 90%, and for the fan speed corresponding to 0.79 throat Mach number. All data are for an acoustic angle of 60°. At 70% speed, treatment D has both broadband and tone suppression improvement relative to treatment B. A similar difference is also seen in Figure 80 for a

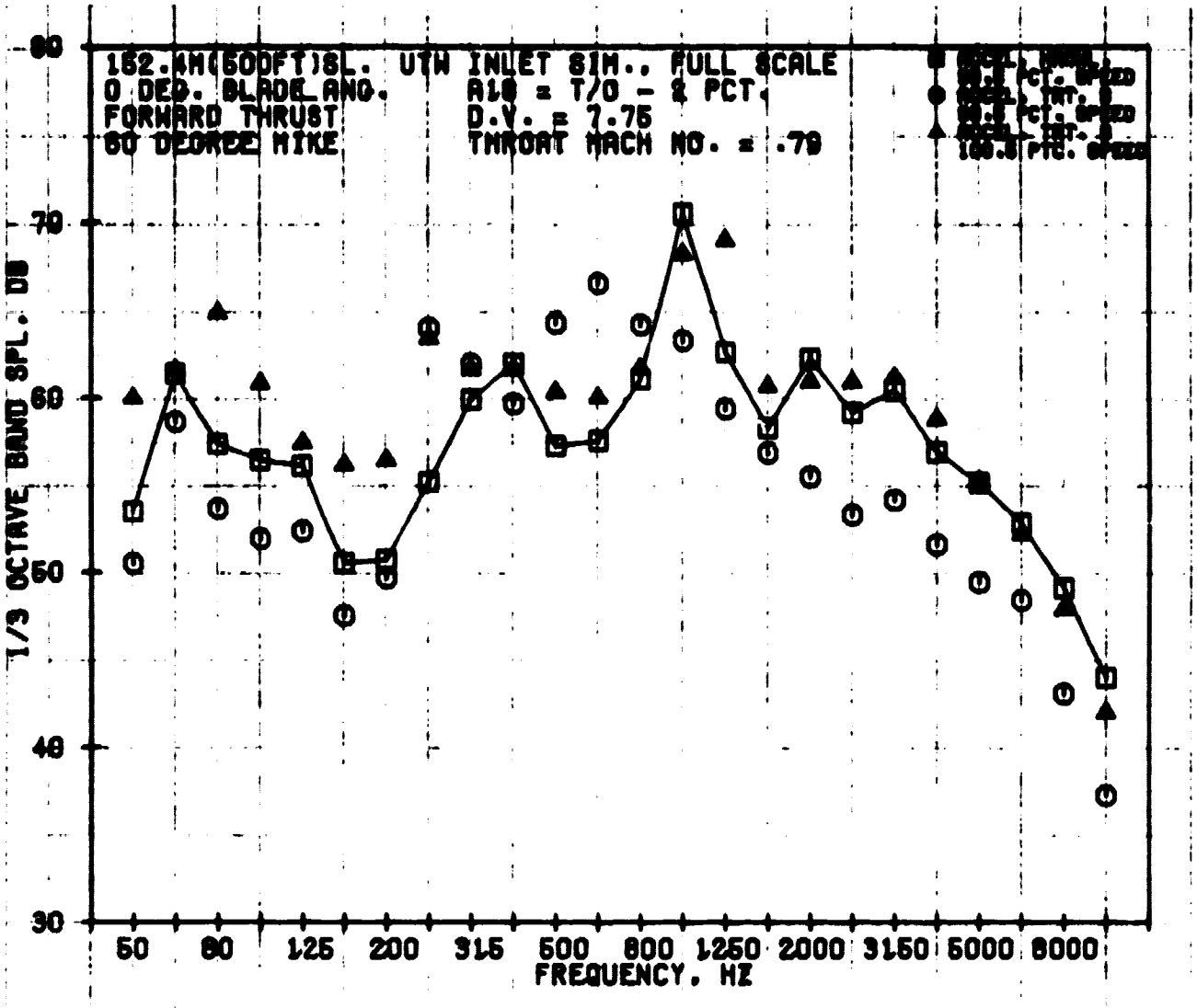

Figure 72. Forward-Thrust, 1/3-Octave-Band, SPL Spectra for the Accelerating Inlet: Hard-Wall and Treatments B and D at 0.79 Throat Mach Number at 60°.

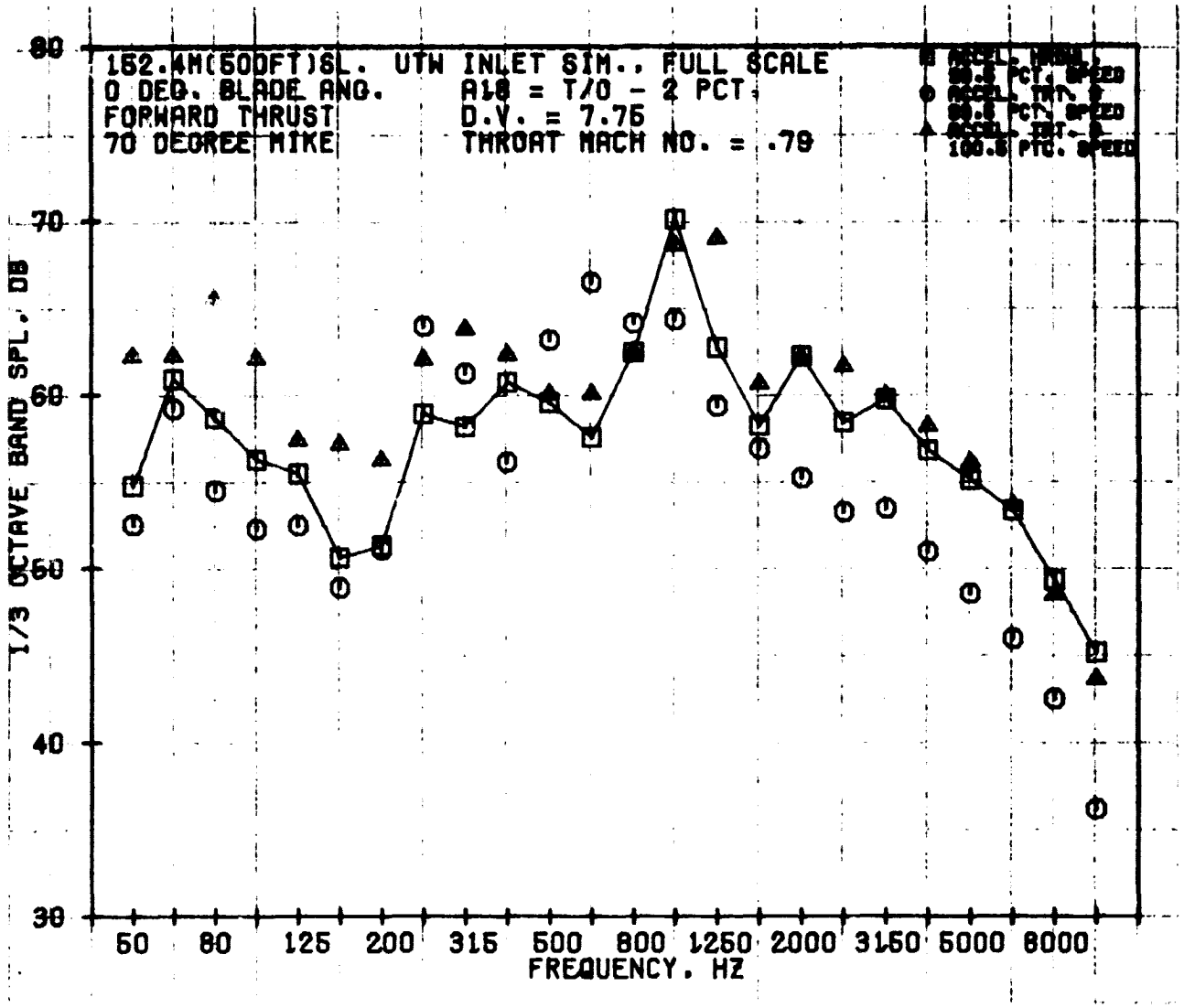

Figure 73. Forward-Thrust, 1/3-Octave-Band, SPL Spectra for the Accelerating Inlet: Hard-Wall and Treatments B and D at 0.79 Throat Mach Number at 70°.

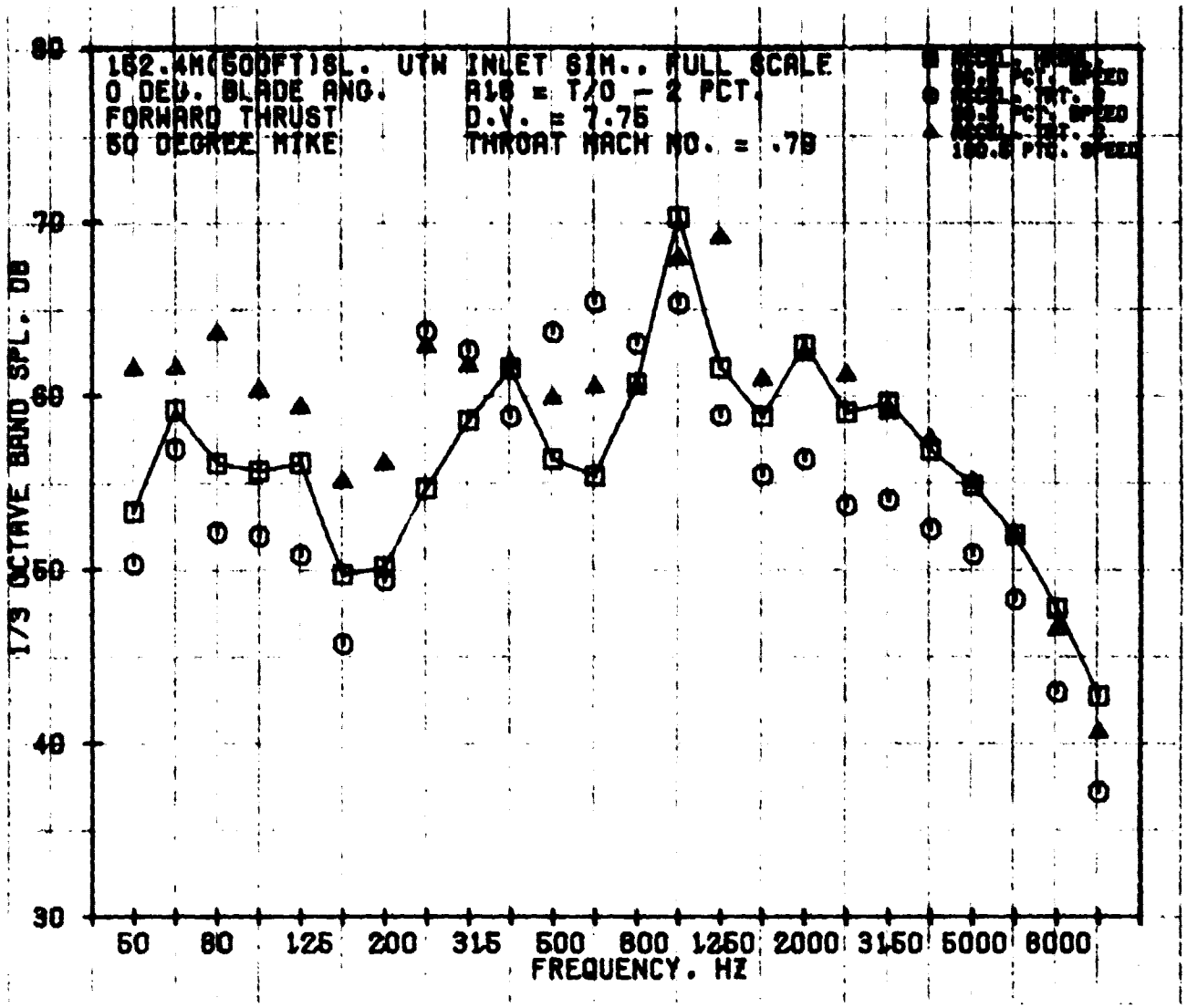

Figure 74. Forward-Thrust, 1/3-Octave-Band, SPL Spectra for the Accelerating Inlet: Hard-Wall and Treatments B and D at 0.79 Throat Mach Number at 50°.

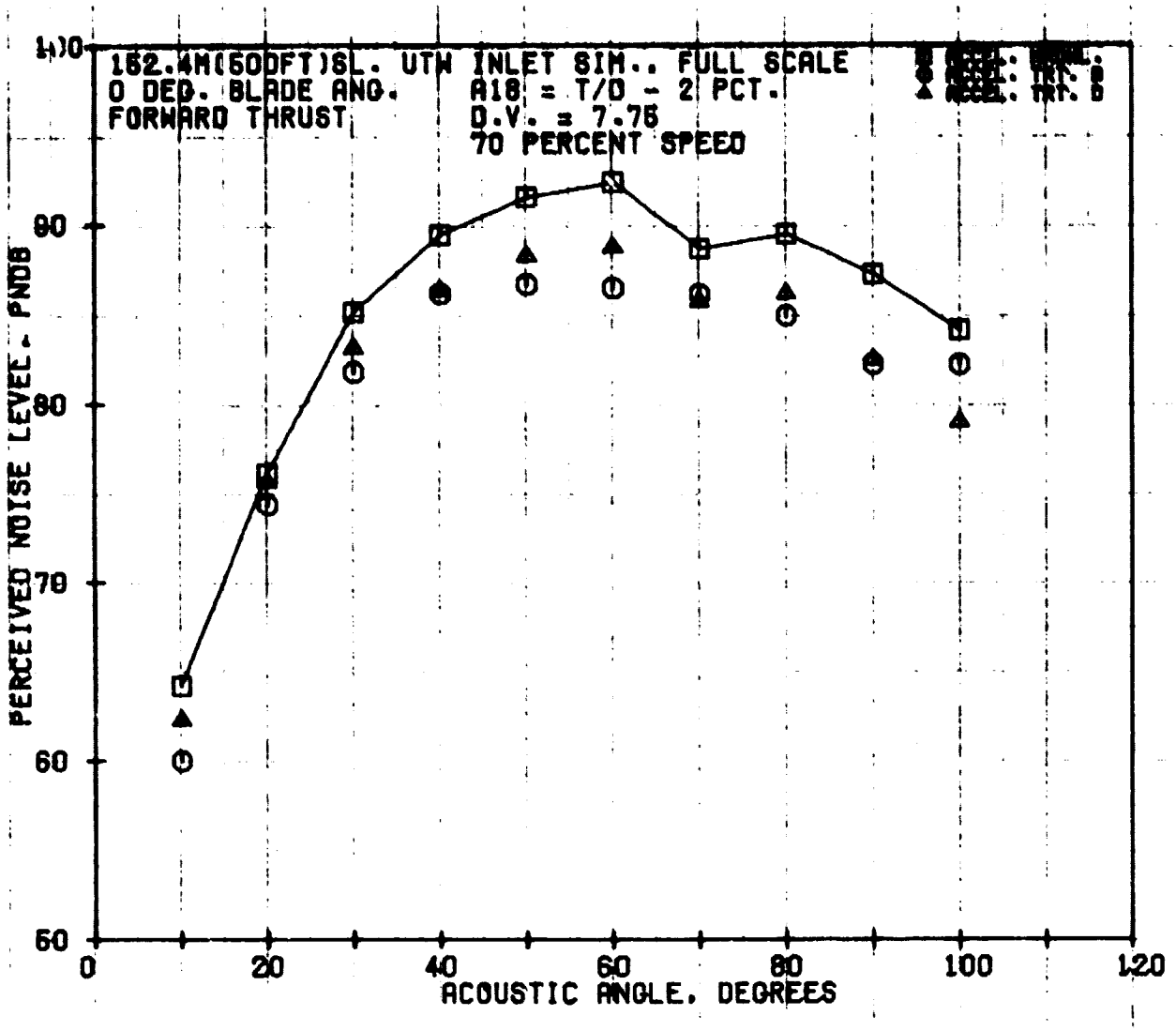

Figure 75. Forward-Thrust, PNL Directivities for the Accelerating Inlet: Hard-Wall and Treatments B and D at 70% N_{FC}.

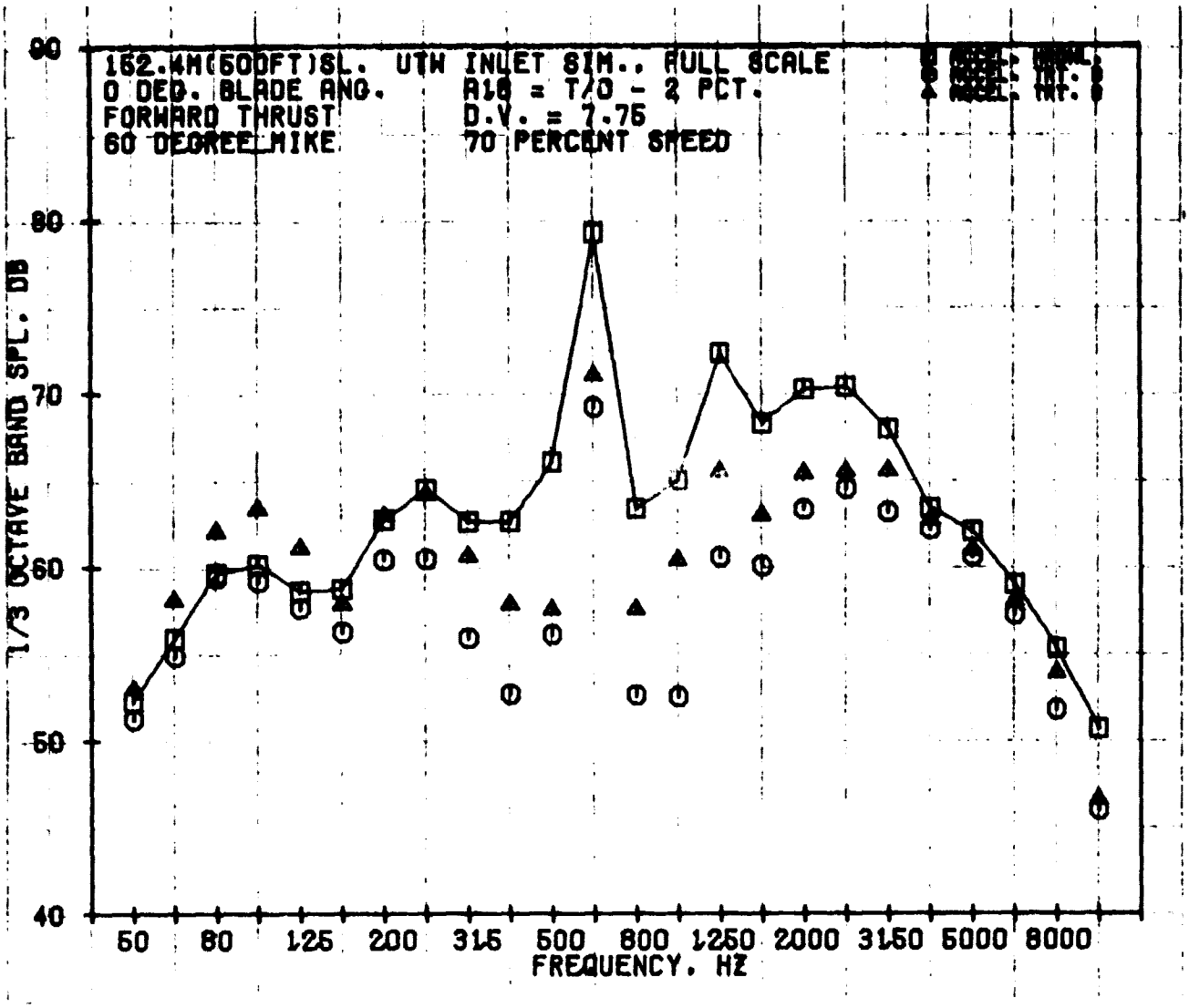

Figure 76. Forward-Thrust, 1/3-Octave-Band, SPL Spectra for the Accelerating Inlet: Hard-Wall and Treatments B and D at 70% N_{FC} at 60°.

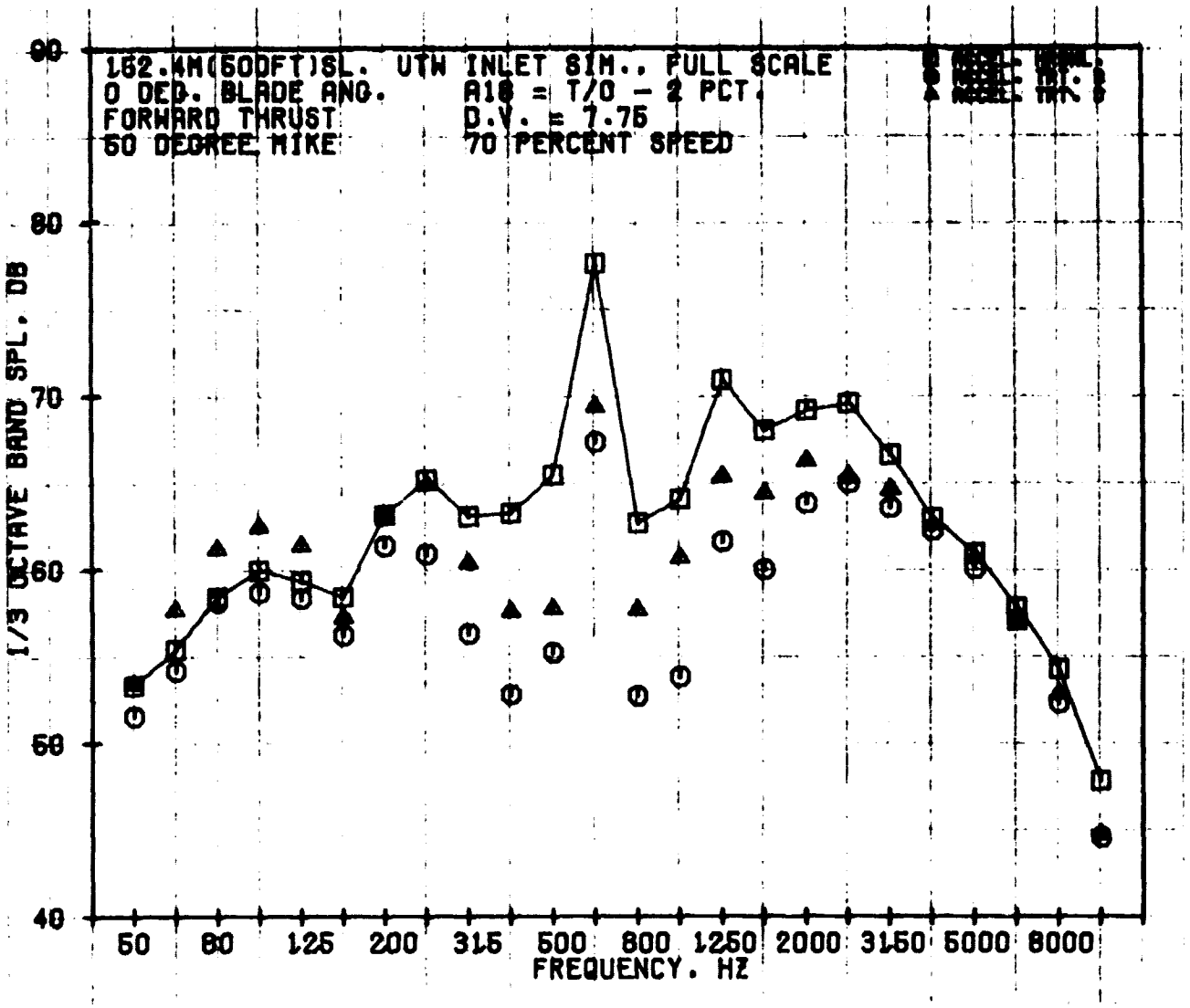

Figure 77. Forward-Thrust, 1/3-Octave-Band, SPL Spectra for the Accelerating Inlet: Hard-Wall and Treatments B and D at 70% N_{FC} at 50°.

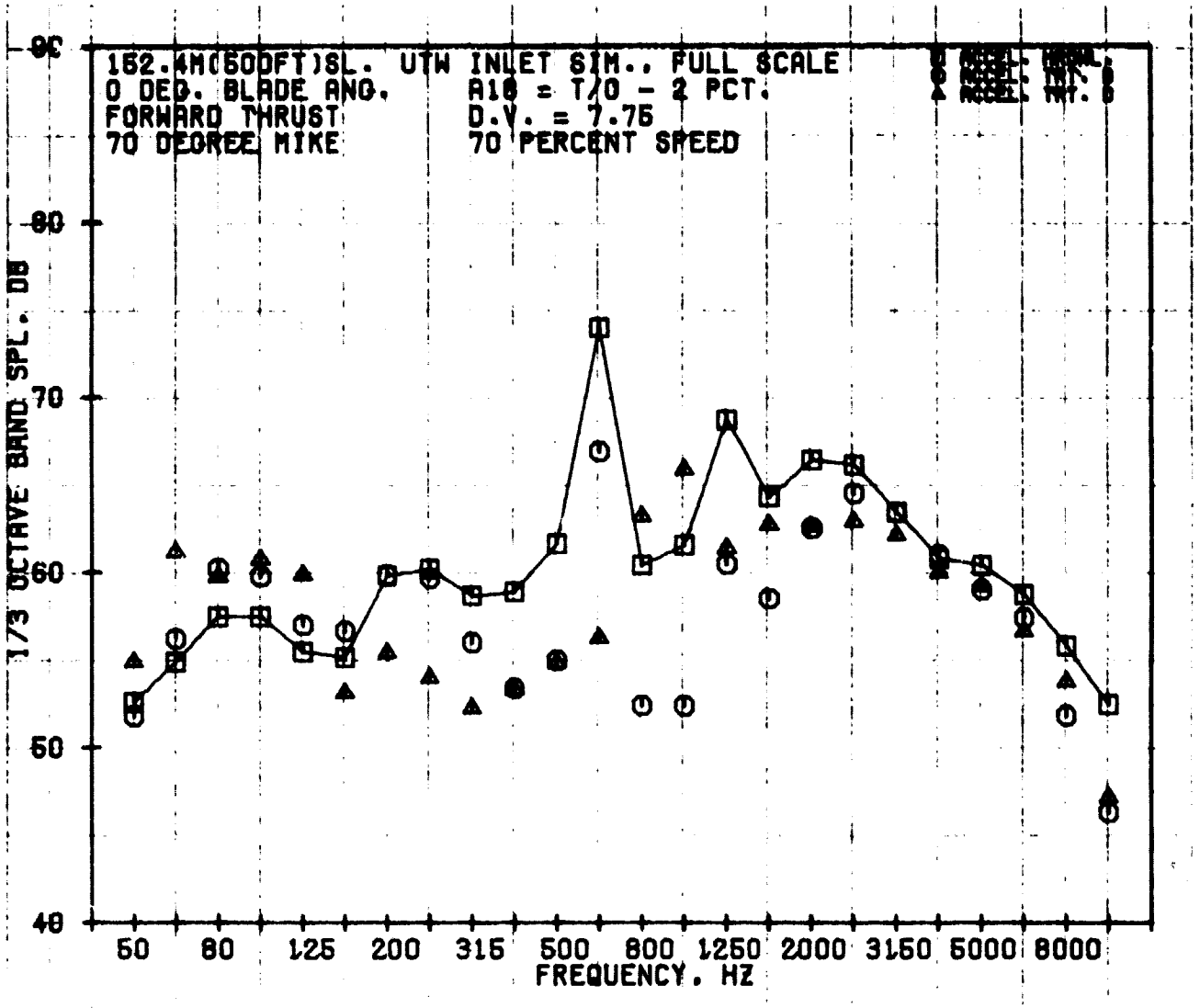

Figure 78. Forward-Thrust, 1/3-Octave-Band, SPL Spectra for the Accelerating Inlet: Hard-Wall and Treatments B and D at 70% N_{FC} at 70°.

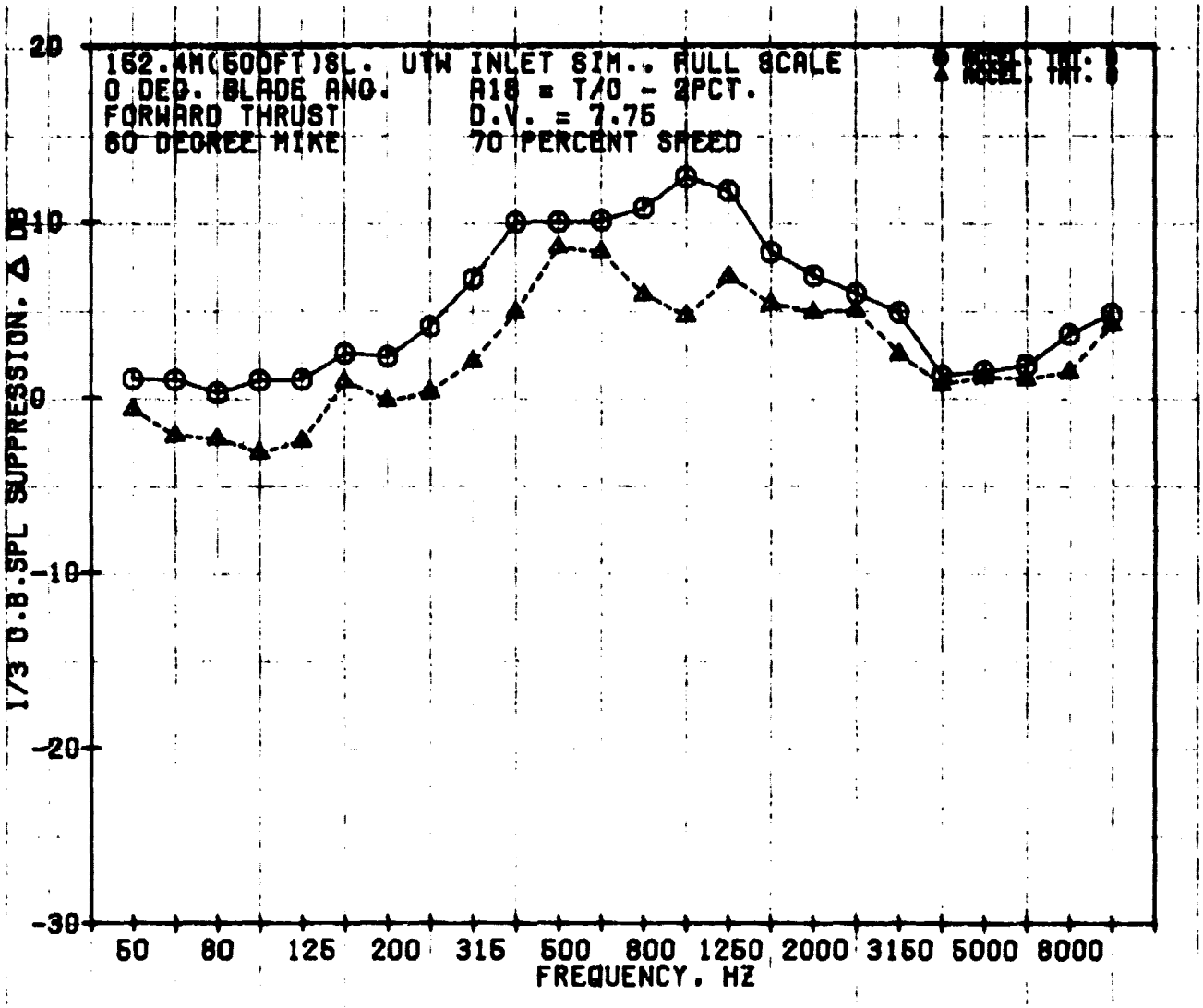

Figure 79. Forward-Thrust, 1/3-Octave-Band, SPL Suppression Spectra (Relative to Hard-Wall, Accelerating Inlet) for Treatments B and D at 70% N_{FC}.

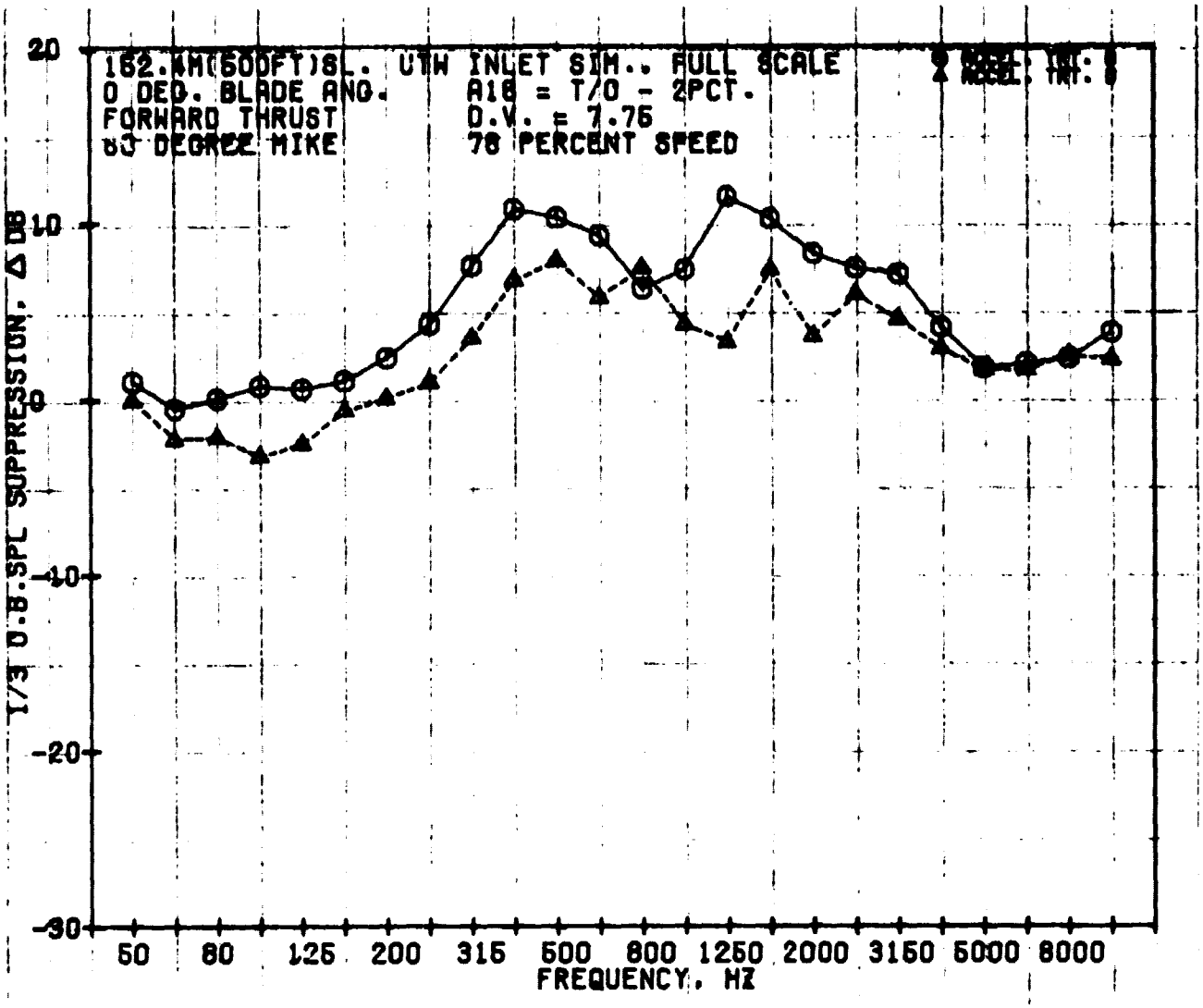

Figure 80. Forward-Thrust, 1/3-Octave-Band, SPL Suppression Spectra (Relative to Hard-Wall, Accelerating Inlet) for Treatments B and D at 78% N_{FC}.

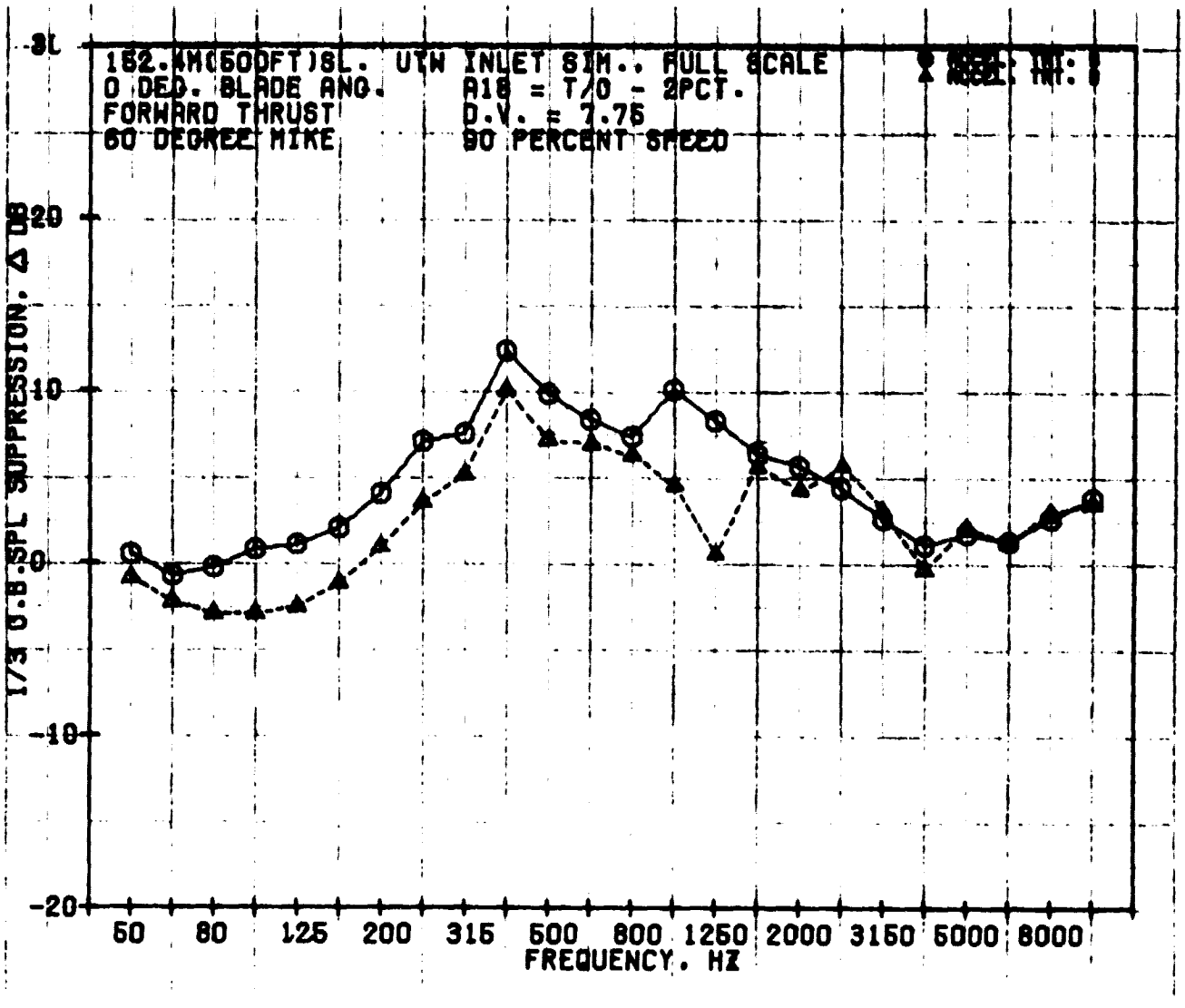

Figure 81. Forward-Thrust, 1/3-Octave-Band, SPL Suppression Spectra (Relative to Hard-Wall, Accelerating Inlet) for Treatments B and D at 90% N_{FC}.

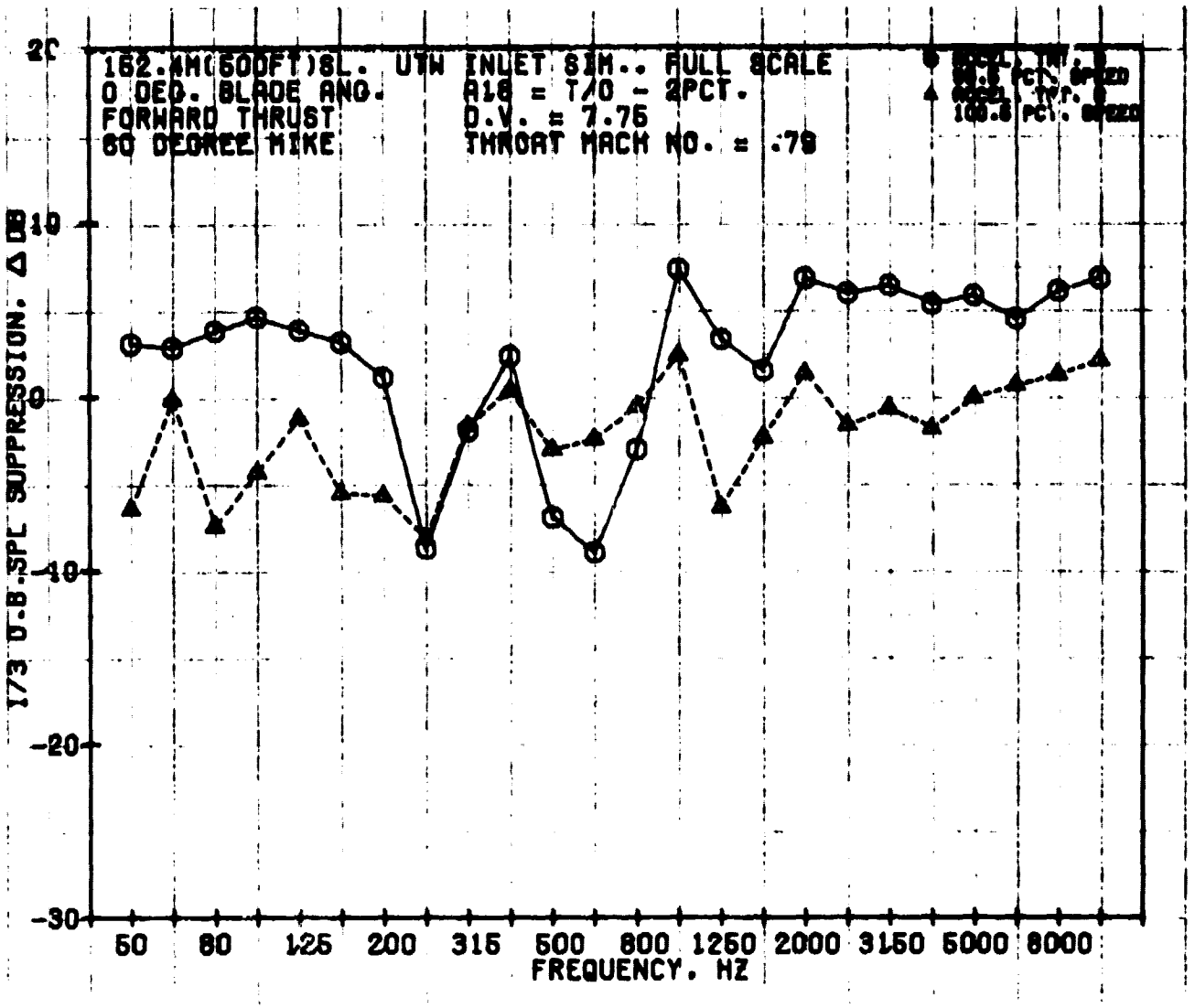

Figure 82. Forward-Thrust, 1/3-Octave-Band, SPL Suppression Spectra (Relative to Hard-Wall, Accelerating Inlet) for Treatments B and D at 0.79 Throat Mach Number.

78% speed. Spectra for 0.79 throat Mach number are shown in Figure 82. Treatment B is seen to consistently give suppression relative to the hard-wall, accelerating inlet at frequencies above 800 Hz. Treatment D results indicate an increase in noise level relative to the hard-wall, accelerating inlet at most of the 1/3-octave-band frequencies. This increase accounts for the higher PNL level seen in the earlier data.

Figure 83 compares suppression spectra for treatment B for fan speeds of 70%, 78%, and 90% speed. This comparison shows that the overall suppression decreases with increasing speed. Figure 84 gives the same set of data for treatment D. No significant suppression differences are seen for the three fan speeds.

9.2.3.3 Performance of Accelerating Inlet D at High Throat Mach Numbers

Treatment D consisted of three segments in tandem, each with a different open area - 7.2%, 14.4%, and 28%; treatment B had the same open area, 9.2%, in all three segments. In reverse-thrust tests, for which all the treatments had been designed, treatment D provided slightly more suppression than treatment B. Hence treatment D was also run in the forward mode to compare with B in order to select the better treatment for both forward- and reverse-thrust modes.

The full-size, 152.4-m (500-ft) sideline (60° microphone), PNL values versus percent corrected fan speed for the baseline bellmouth, hard-wall accelerating inlet, and treated accelerating inlets B and D were shown in Figure 70. Figure 85 is a crossplot of Figures 70 and 40 to give PNL versus throat Mach number. The speeds were matched for the bellmouth and inlet B in Figure 85. It may be noted from Figure 70 that at 90% speed, inlet D starts diverging from inlet B and providing less suppression. Figure 40 shows an apparent loss of flow recovery compared to inlet B beyond this speed. Figures 70 and 85 show that, beyond this speed, inlet D even provides less suppression than the hard-wall, accelerating inlet. The effect is less pronounced in Figure 85 due to suppression being plotted against flow (M_{th}).

In order to examine the deterioration of the performance of the D inlet, the measured wall Mach number data are presented along with acoustic data. The axial distribution of wall Mach numbers (obtained from a series of wall static taps) is shown in Figure 86 for inlets B and D at 93.5% speed, at which the average throat Mach number for both inlets is 0.69. Operation of the two inlets generally appears similar, but the higher corrected fan-face Mach number with inlet D indicates a recovery loss. Since inlet D was tested after some blade-angle changes, it is also possible that small errors during resetting of blade angles could have contributed to a difference in corrected fan-face flow. Figures 87 through 93 show the acoustic data for hard wall and treatments B and D at 93.5% corrected speed. The data indicate slightly better suppression from treatment B.

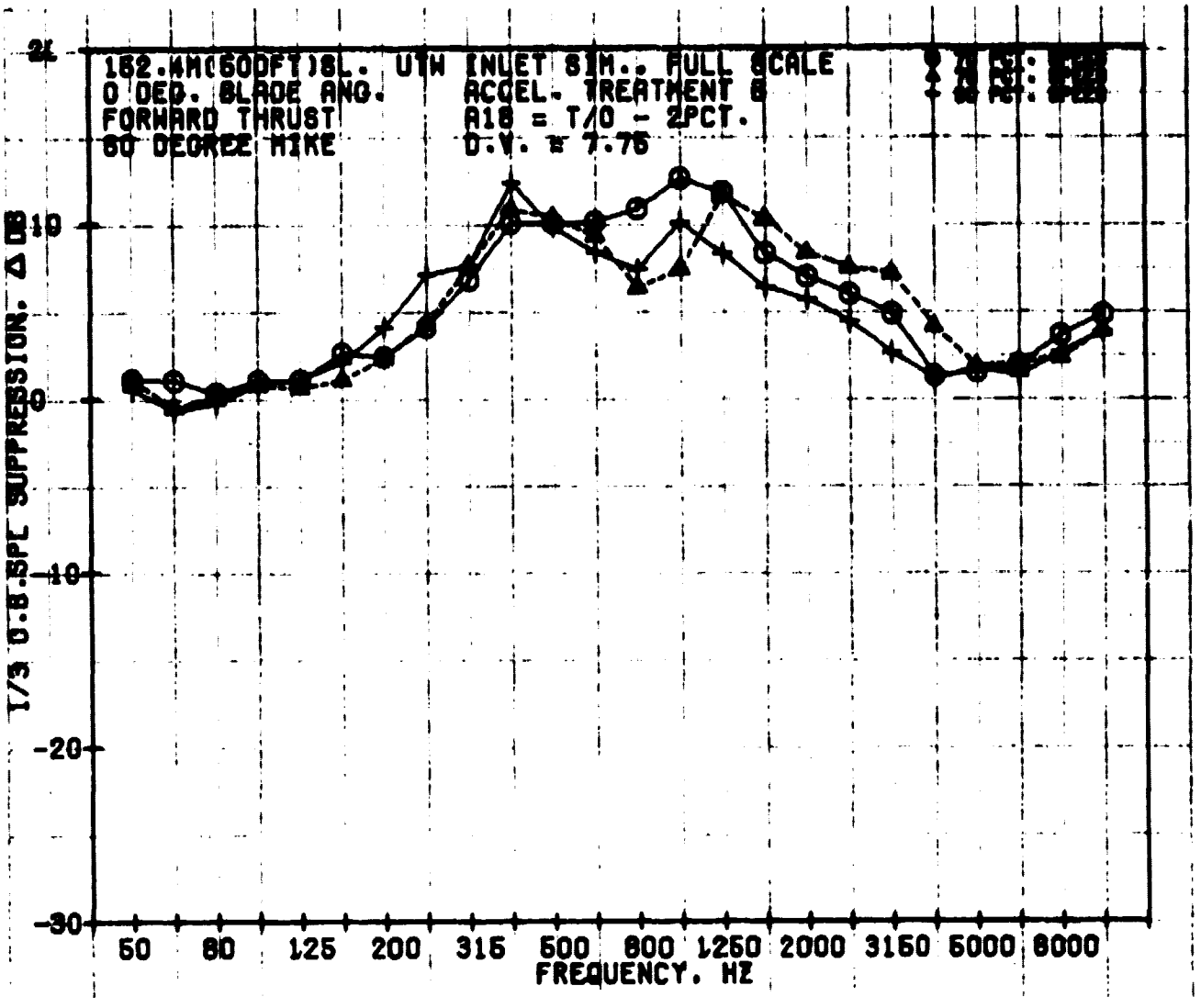

Figure 83. Forward-Thrust, 1/3-Octave-Band, SPL Suppression Spectra (Relative to Hard-Wall, Accelerating Inlet) for Treatment B at 70%, 78%, and 90% N_{FC}.

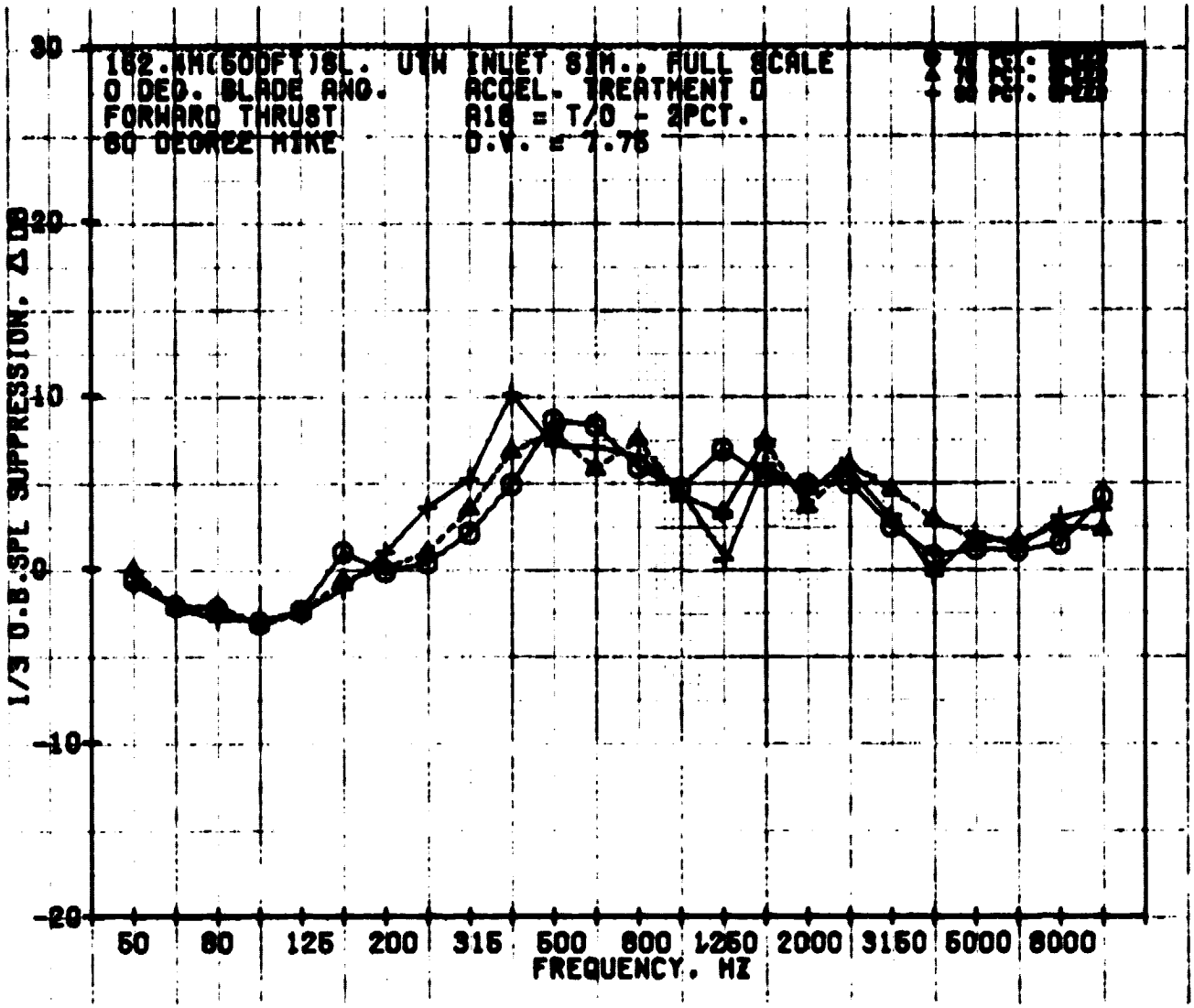

Figure 84. Forward-Thrust, 1/3-Octave-Band, SPL Suppression Spectra (Relative to Hard-Wall, Accelerating Inlet) for Treatment D at 70%, 78%, and 90% N_{FC}.

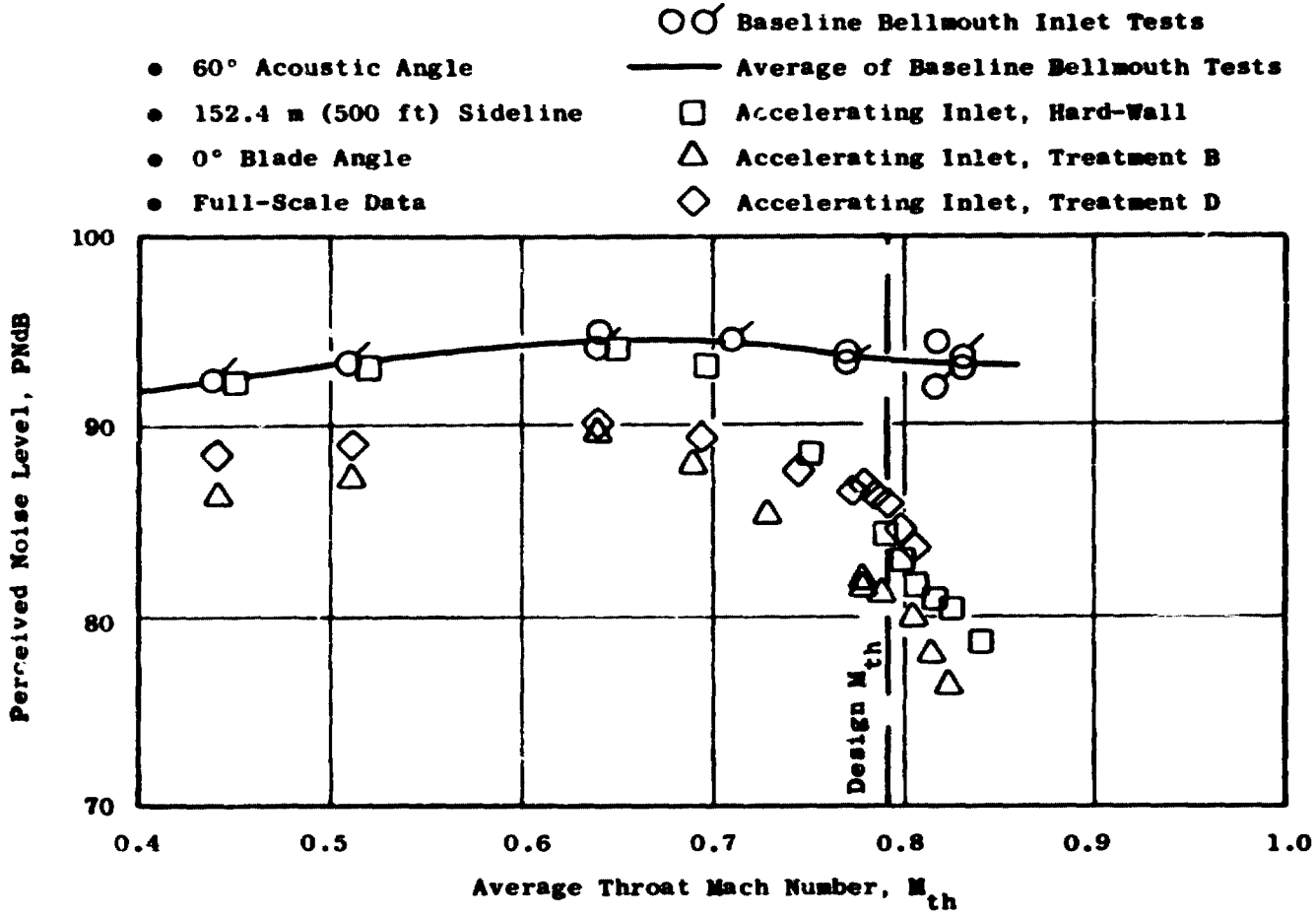

Figure 85. PNL Vs. Throat Mach Number for the Baseline Bellmouth and Accelerating Inlets.

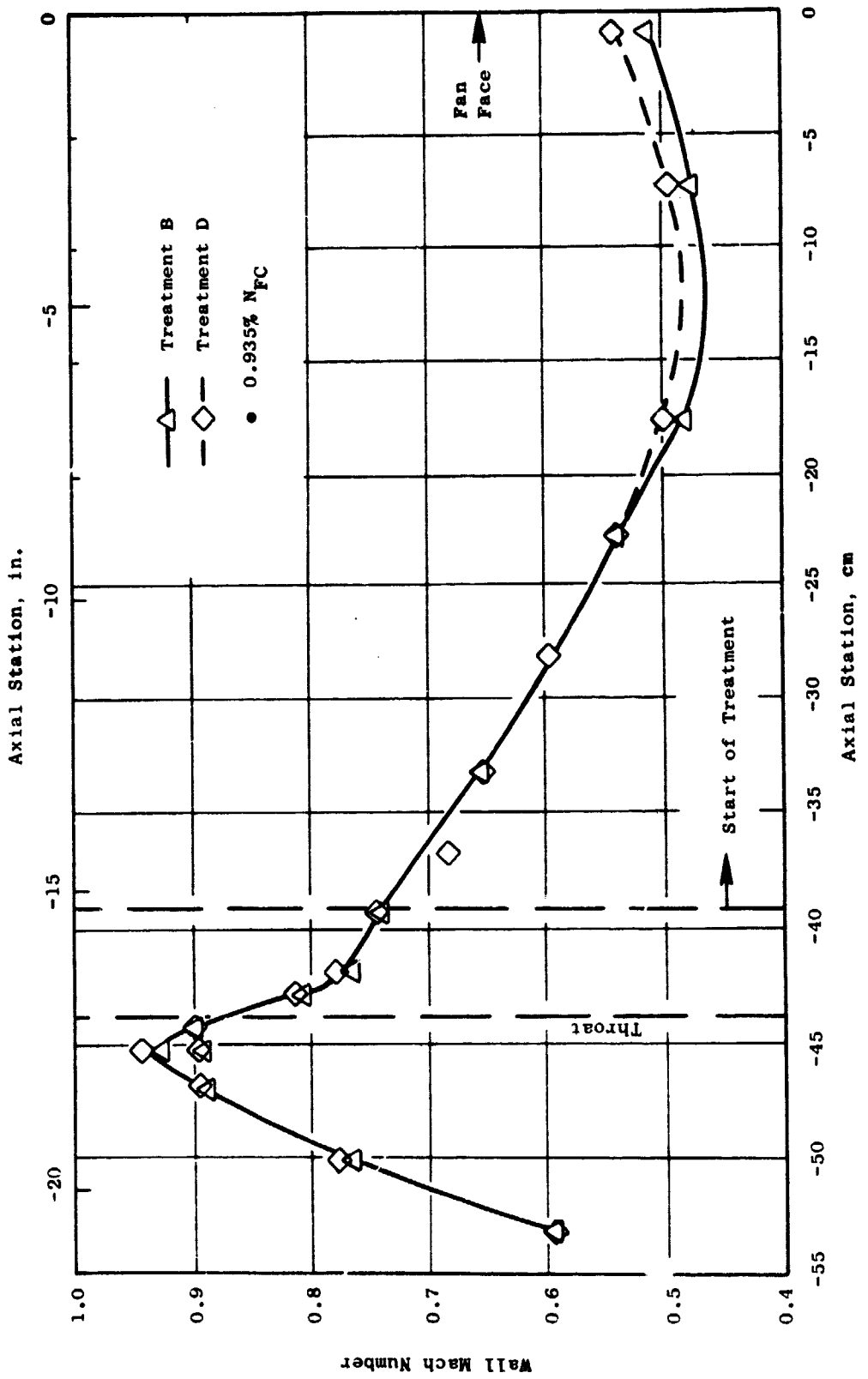

Figure 86. Measured Wall Mach Number Distributions for Accelerating Inlet Treatments B and D at 0.69 Throat Mach Number.

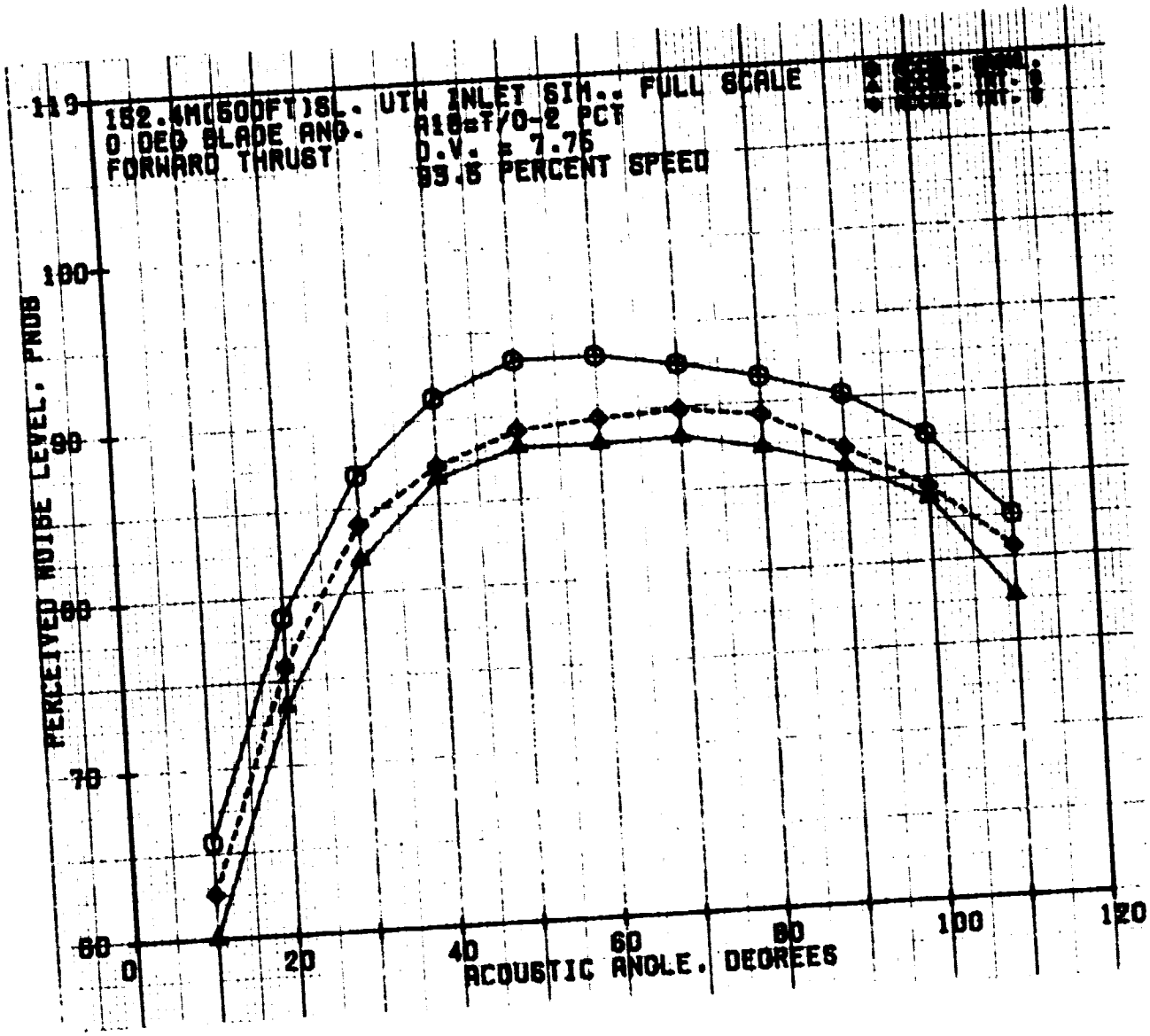

Figure 87. Forward-Thrust, PNL Directivities for Accelerating Inlets at 93.5% N_{FC}.

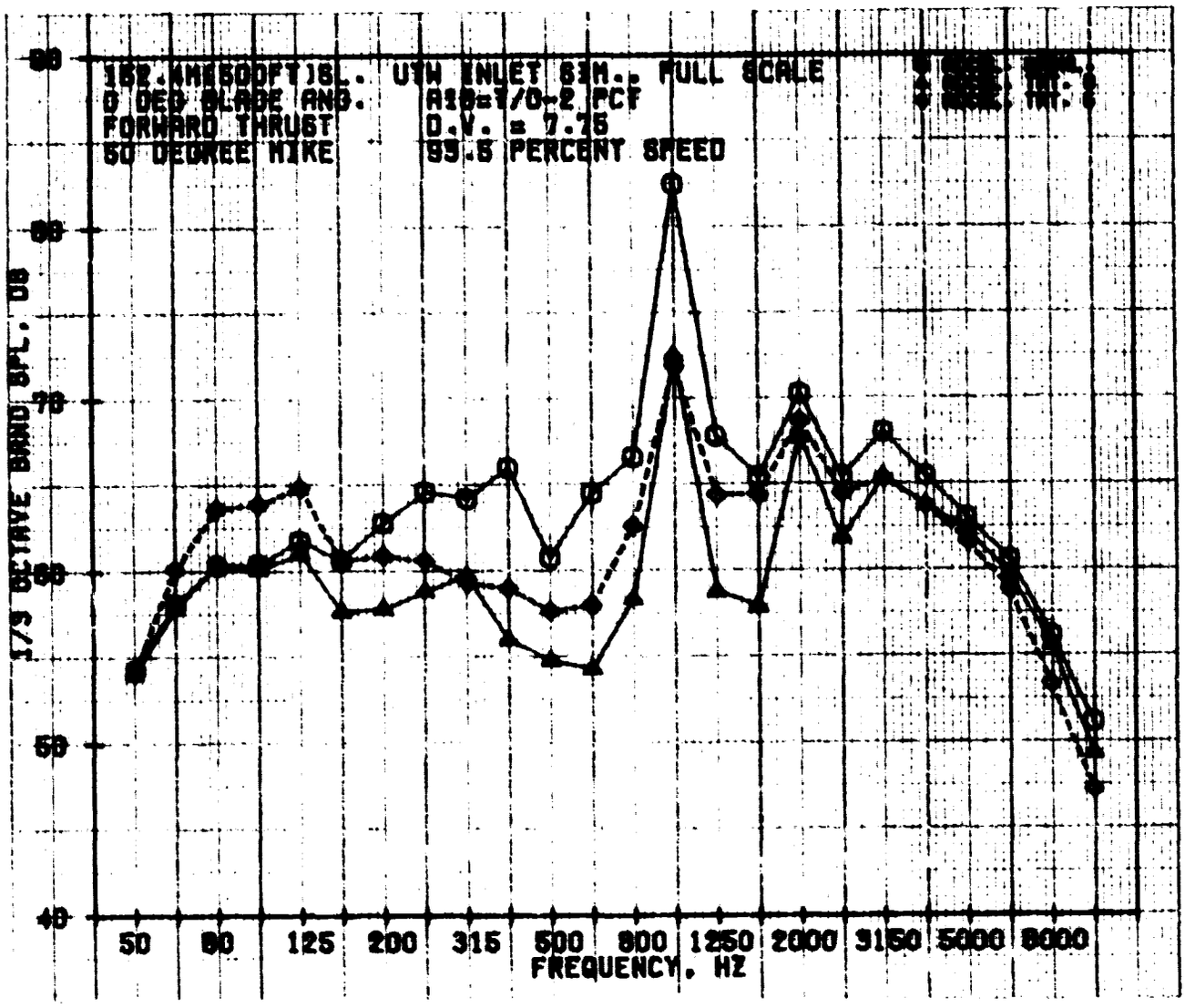

Figure 88. Forward-Thrust, 1/3-Octave-Band, SPL Spectra for Accelerating Inlets at 93.5% N_{FC} at 50°.

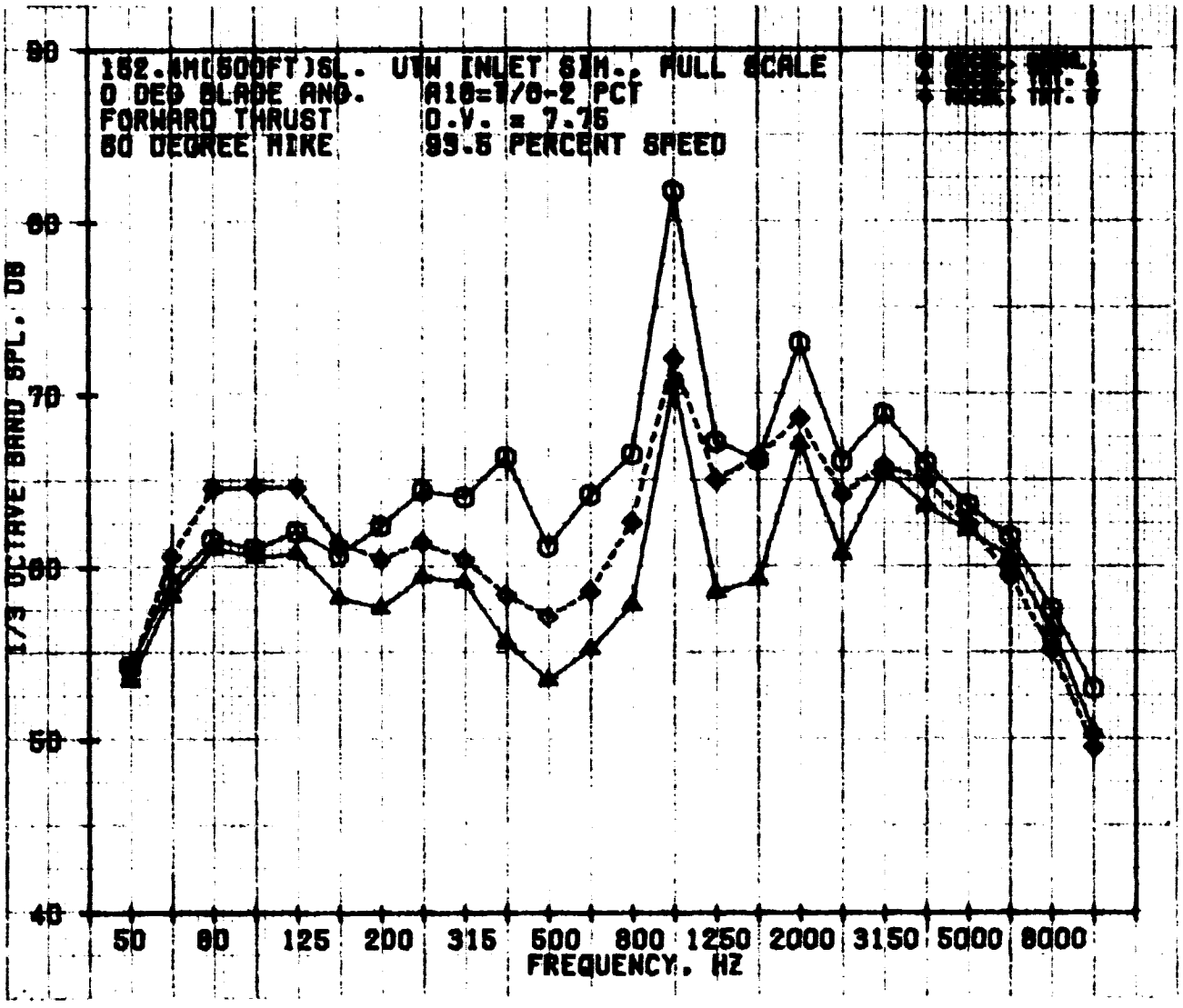

Figure 89. Forward-Thrust, 1/3-Octave-Band, SPL Spectra for Accelerating Inlets at 93.5% N_{FC} at 60°.

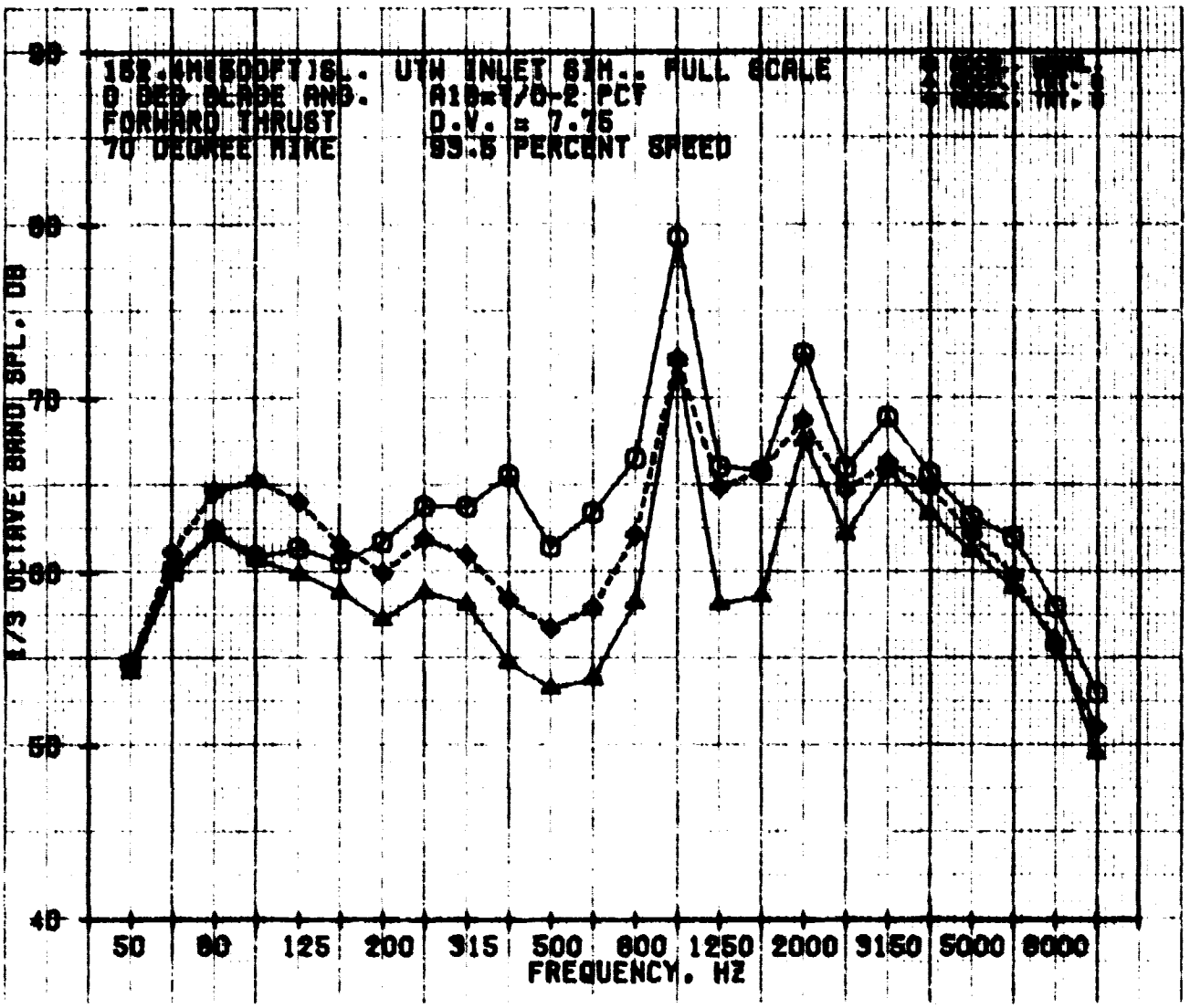

Figure 90. Forward-Thrust, 1/3-Octave-Band, SPL Spectra for Accelerating Inlets at 93.5% N_{FC} at 70°.

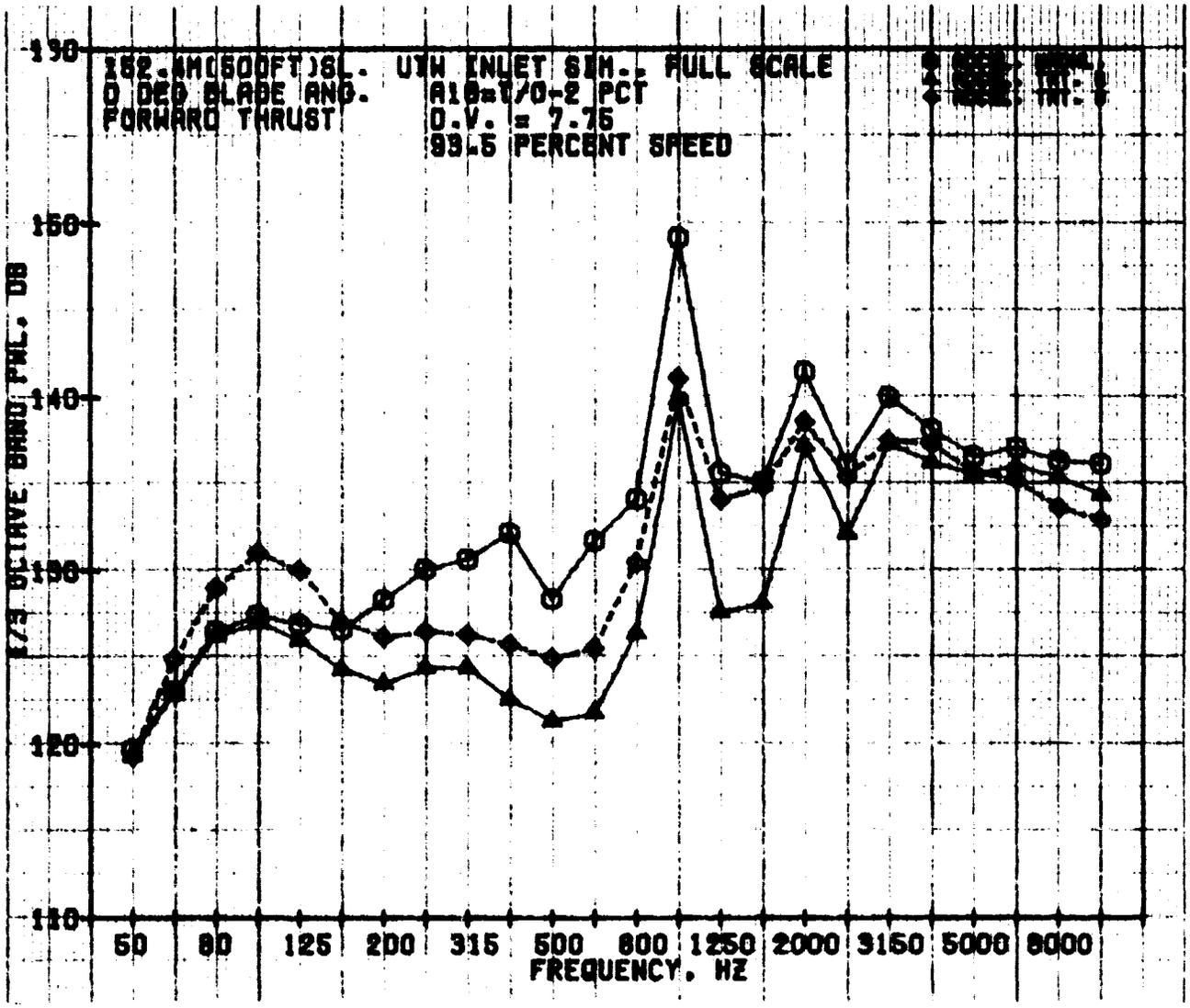

Figure 91. Forward-Thrust, 1/3-Octave-Band, PWL Spectra for Accelerating Inlets at 93.5% N_{FC}.

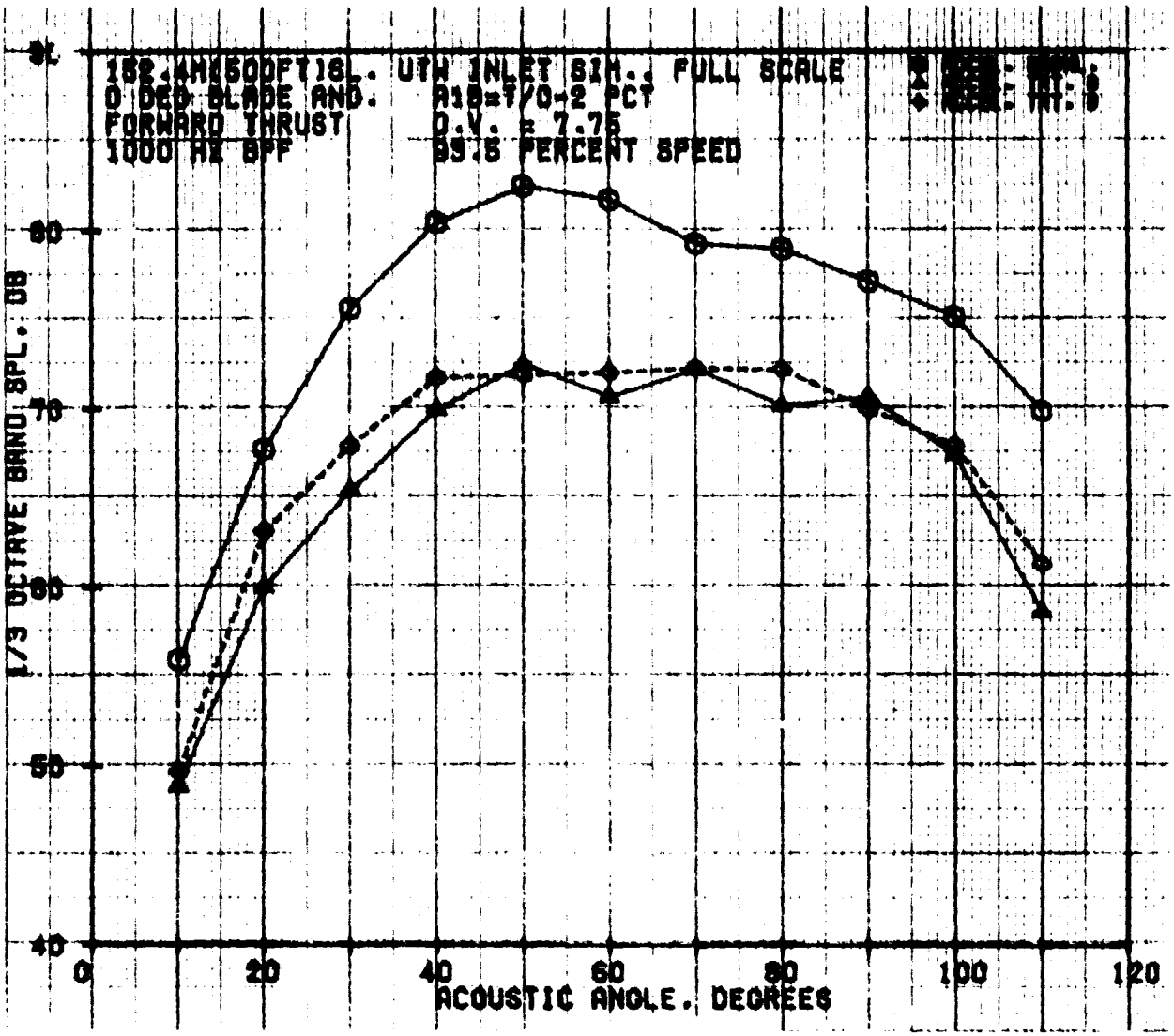

Figure 92. Forward-Thrust, 1/3-Octave-Band, SPL Blade Passing Frequency Directivities of Accelerating Inlets at 93.5% N_{FC}.

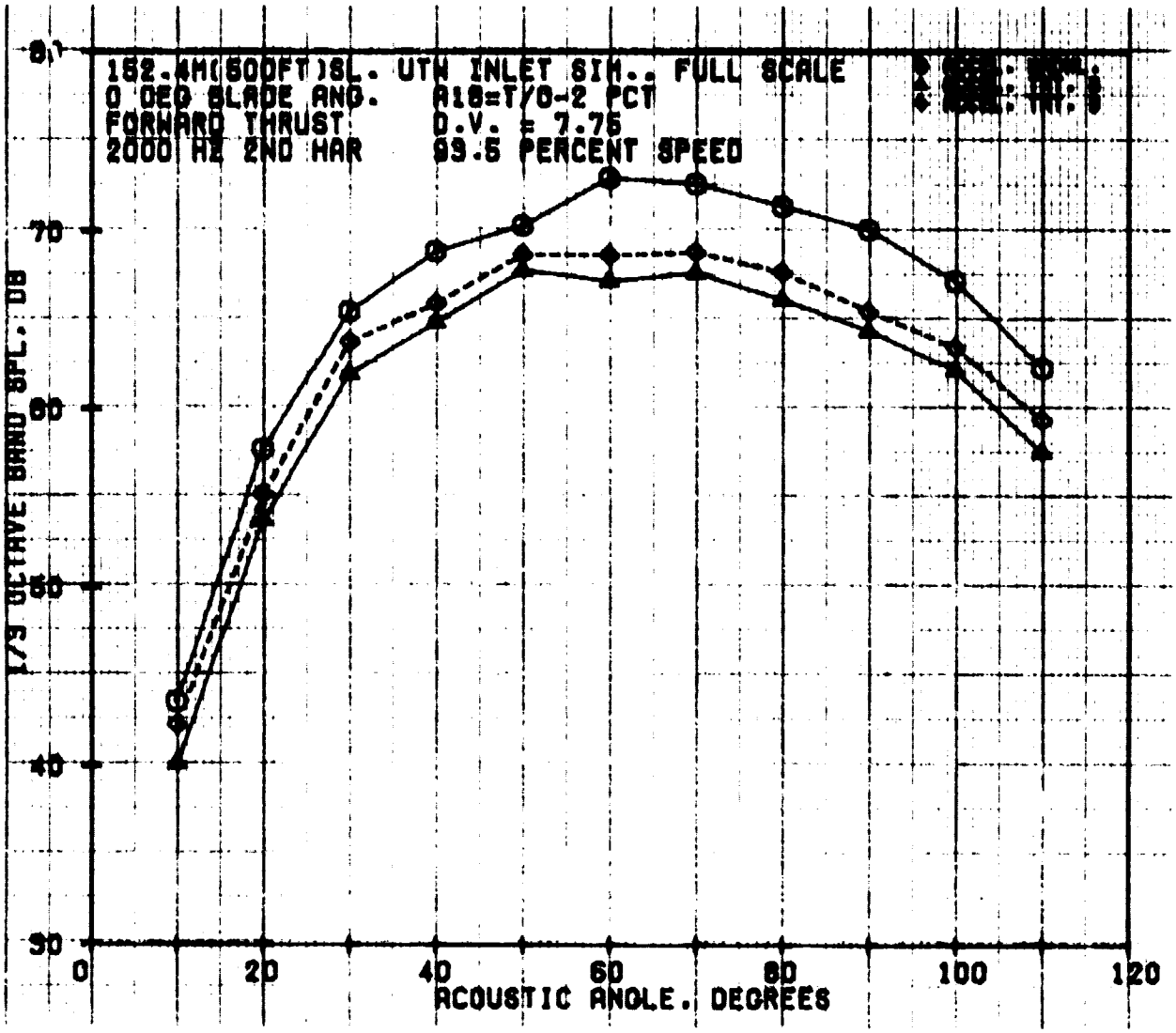

Figure 93. Forward-Thrust, 1/3-Octave-Band, SPL Second-Harmonic Directivities of Accelerating Inlets at 93.5% N_{FC}.

Figure 94 shows axial distribution of wall Mach numbers for the two treated inlets at 98.5% fan speed. At this speed, it can be seen from Figure 85 that the aerodynamic performance of treatment D has begun to deteriorate. The wall Mach number distribution in Figure 94 also shows a second peak, downstream of the throat, at Station -14.4. This peak was not observed in the 93.5% speed data shown earlier and is seen to be more pronounced in the M_{th} = 0.8 data shown in Figure 95. It may be noted that M_{th} = 0.8 was achieved at 100.5% speed with treatment B and 103.5% speed with treatment D.

Ordinarily, the unusually high wall Mach number observed with treatment D might be attributed to an instrumentation problem. The problem, however, is not one of instruments but of flow in the treated diffuser. This conclusion is supported by the fact that the spike does not appear until the inlet performance (as inferred from Figure 85) begins to deteriorate, introducing higher noise levels.

No positive conclusion could be reached regarding the poor aerodynamic performance and diffuser velocity spike of the treatment D inlet. Several possible explanations can be postulated. The most significant design difference between the two treated diffusers is the much higher faceplate pososity starting 4.4 cm (1.75 in.) aft of the throat in the treatment D diffuser (28% open area compared to 9.2% porosity with treatment B); this porosity could lead to higher boundary-layer momentum losses. Other explanations include (1) poor alignment of the lip and diffuser inlet components at the throat, (2) secondary airflow circulating forward under the treatment faceplate (the faceplate should be sealed, however), and (3) poor model fabrication. A visual inspection of the model failed to provide any conclusive evidence of mechanical defects which could have caused the poor inlet performance for treatment D.

Figures 96 through 102 compare acoustic data from the hard-wall and the treated inlets at 98.5% speed. The treatment D fared worse than even the hard-wall case at this speed, almost in the entire frequency range of interest except at the 1000-Hz BPF (Figure 101).

9.2.3.4 Flight Lip Versus Aero-Acoustic Lip: Comparison of Acoustic and Aerodynamic Performance

It was shown earlier that the flight lip and the aero-acoustic lip used on accelerating inlet B were quite similar in aerodynamic behavior. The only major difference observed was an apparently reduced flow with the flight lip. This was shown to be attributable to the tolerances in blade-angle setting and DV setting repeatabilities.

Full-size, 152.4-m (500-ft) sideline, PNL versus throat Mach number for the two configurations is compared in Figure 103. Using this type of comparison, the two lips performed similarly. Figures 104 through 108 show detailed comparisons at M_{th} = 0.69. It should be noted that the speeds at which this M_{th} was achieved were different for the two configurations. Figure 104 shows

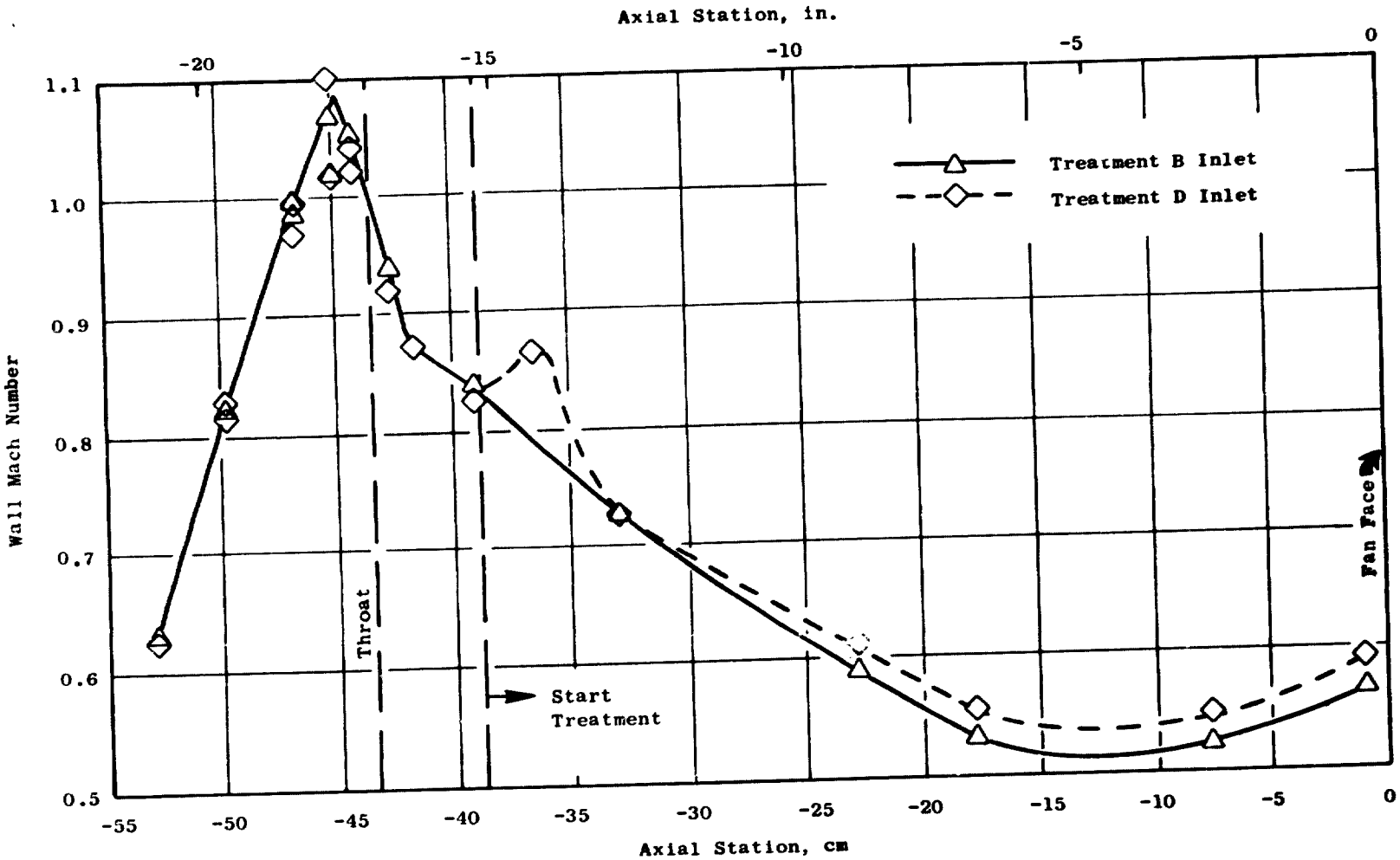

Figure 94. Measured Wall Mach Number Distributions for Accelerating Inlet Treatments B and D at 0.775 Throat Mach Number.

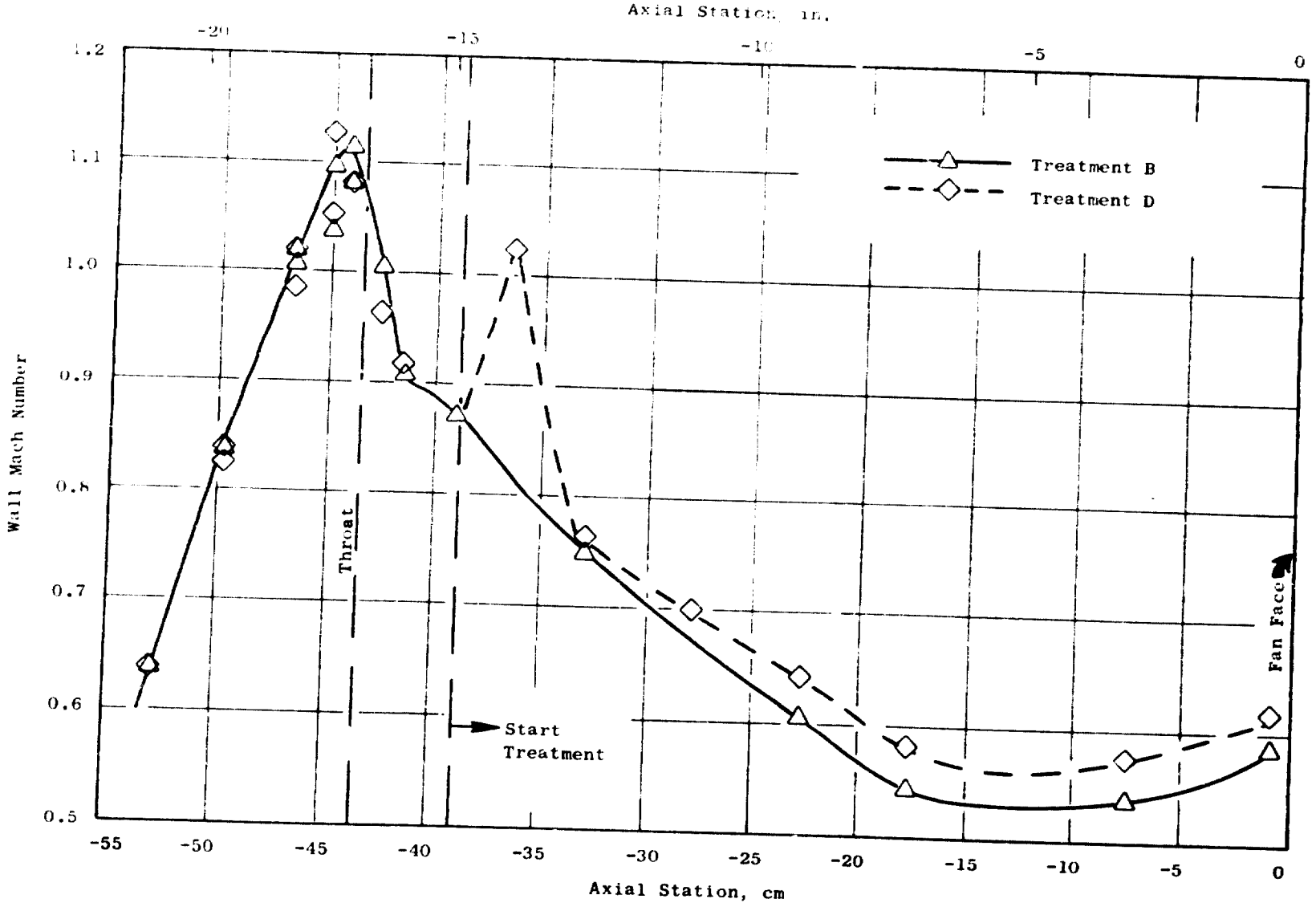

Figure 95. Measured Wall Mach Number Distributions for Accelerating Inlet Treatments B and D at 0.8 Throat Mach Number.

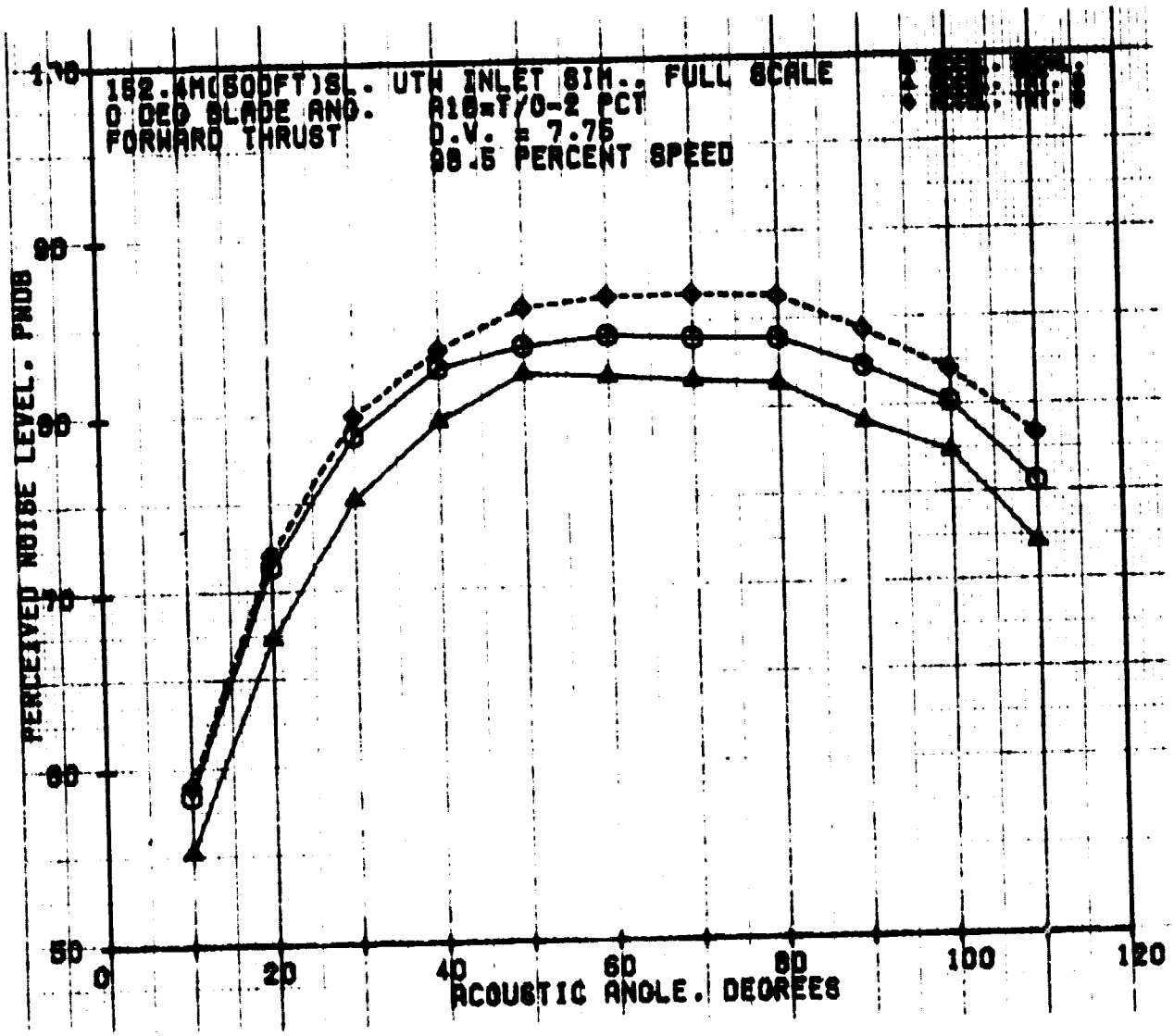

Figure 96. Forward-Thrust, PNL Directivities of Accelerating Inlets at 98.5% N_{FC}.

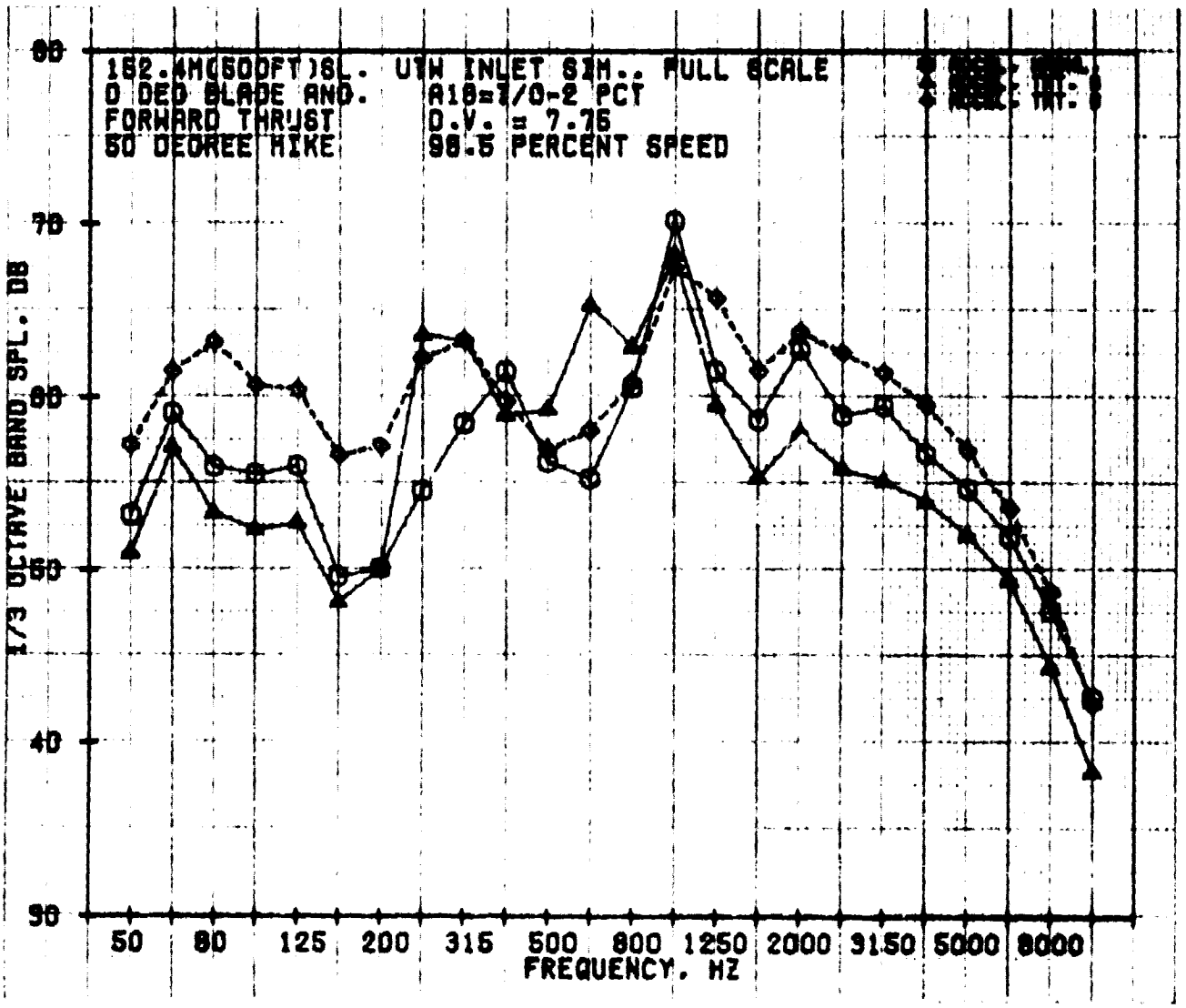

Figure 97. Forward-Thrust, 1/3-Octave-Band, SPL Spectra of Accelerating Inlets at 98.5% N_{FC} at 50°.

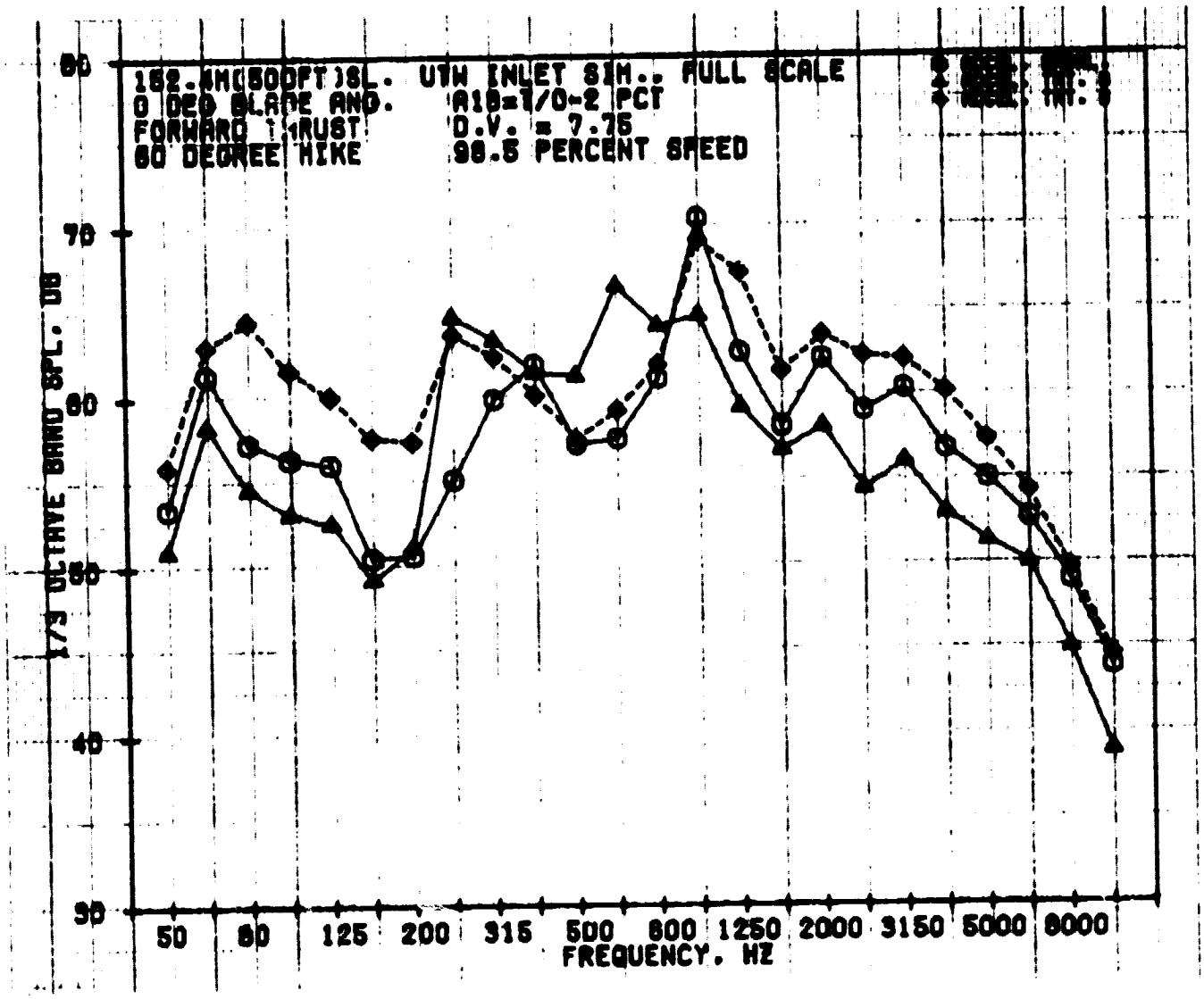

Figure 98. Forward-Thrust, 1/3-Octave-Band, SPL Spectra of Accelerating Inlets at 98.5% N_{FC} at 60°.

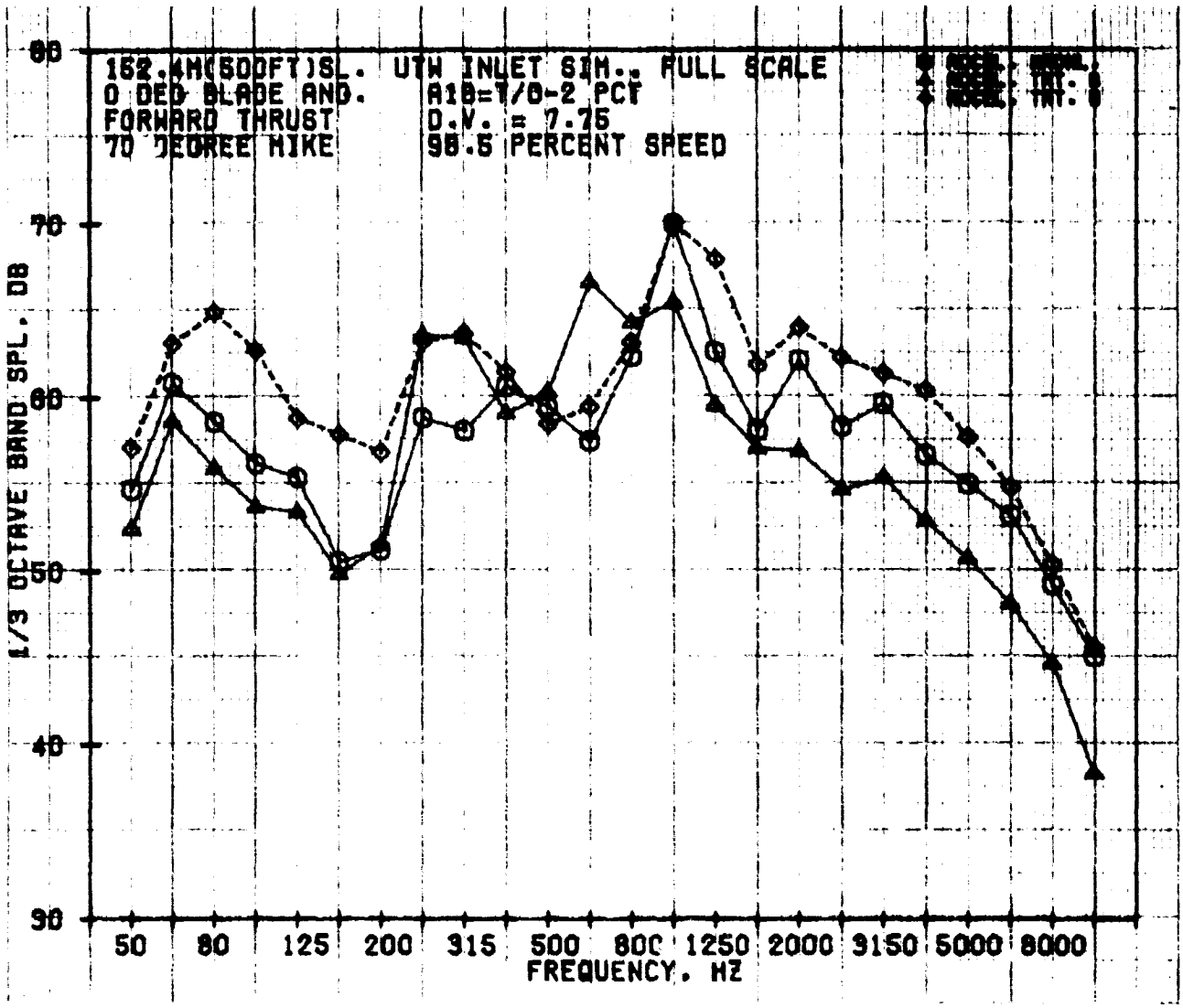

Figure 99. Forward-Thrust, 1/3-Octave-Band, SPL Spectra of Accelerating Inlets at 98.5% N_{FC} at 70°.

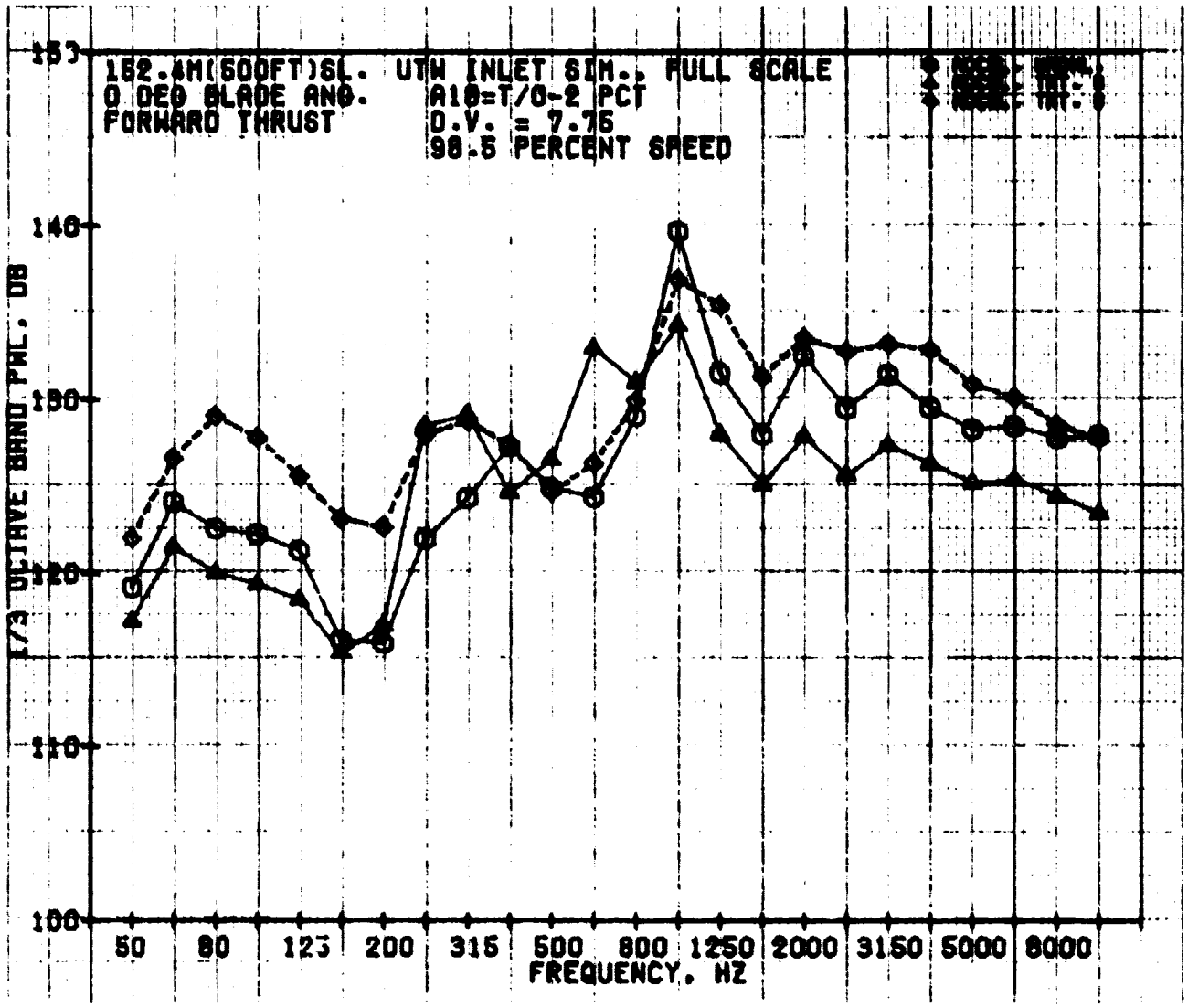

Figure 100. Forward-Thrust, 1/3-Octave-Band, PWL Spectra of Accelerating Inlets at 98.5% N_{FC}.

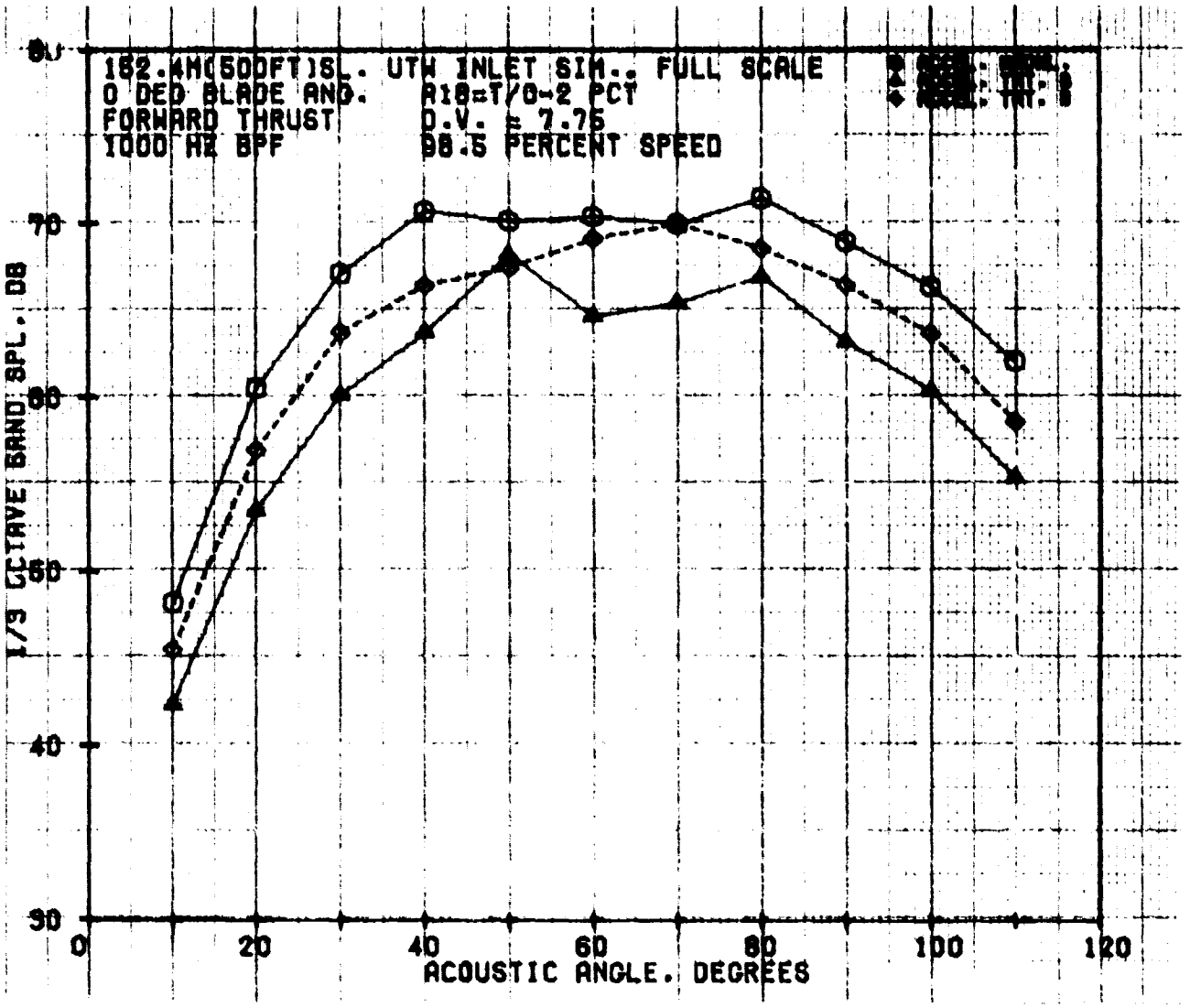

Figure 101. Forward-Thrust, 1/3-Octave-Band, SPL Blade Passing Frequency Directivities of Accelerating Inlets at 98.5% N_{FC}.

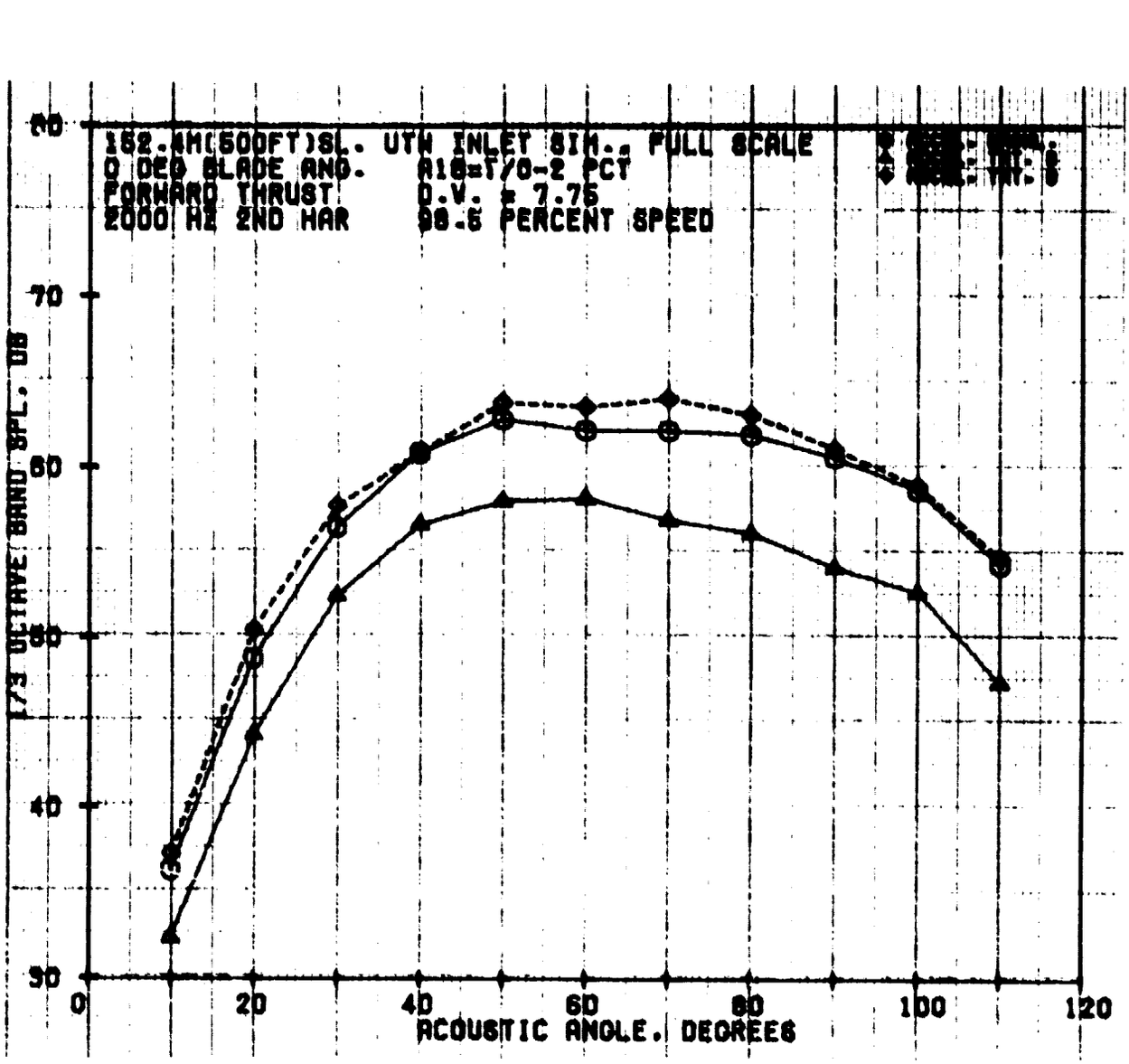

Figure 102. Forward-Thrust, 1/3-Octave-Band, SPL Second-Harmonic Directivities of Accelerating Inlets at 98.5% N_{FC}.

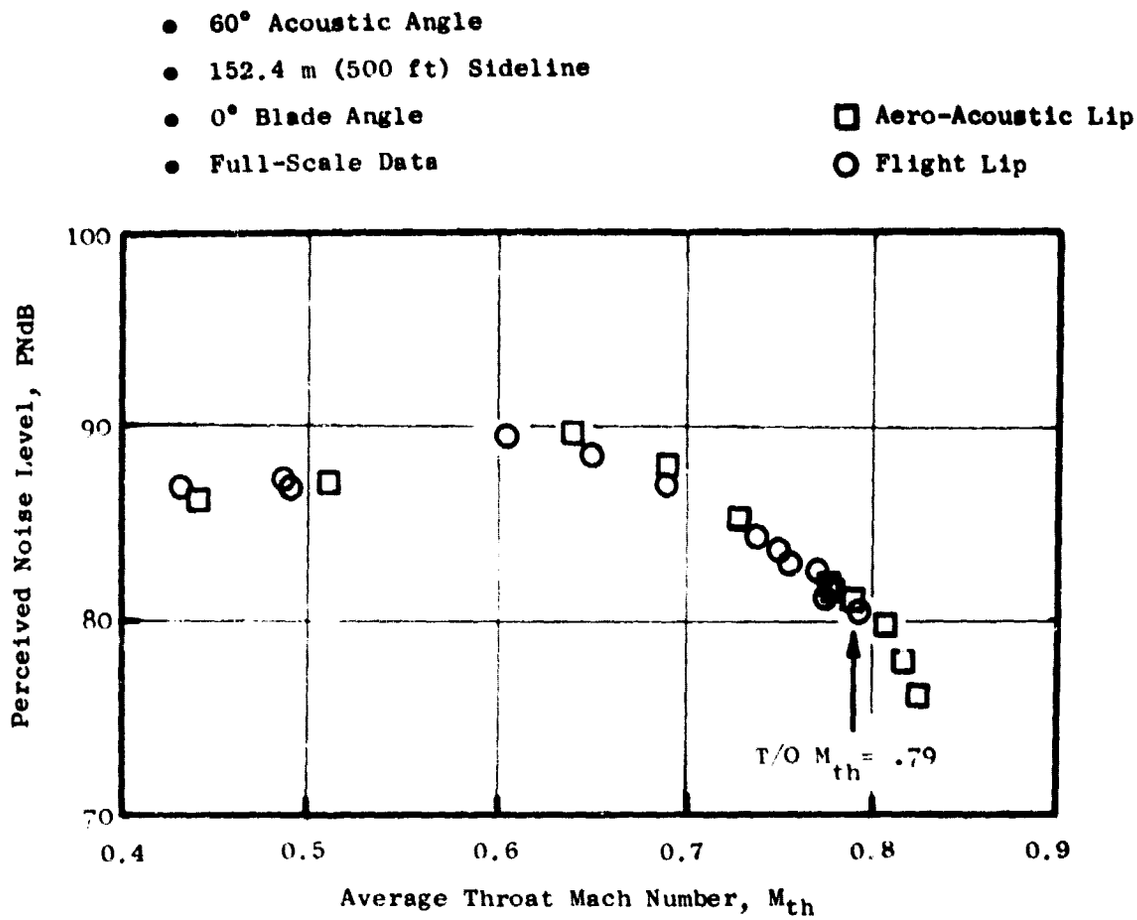

Figure 103. PNL Vs. Throat Mach Number for Aero-Acoustic and Flight Lips on Accelerating Inlet, Treatment B.

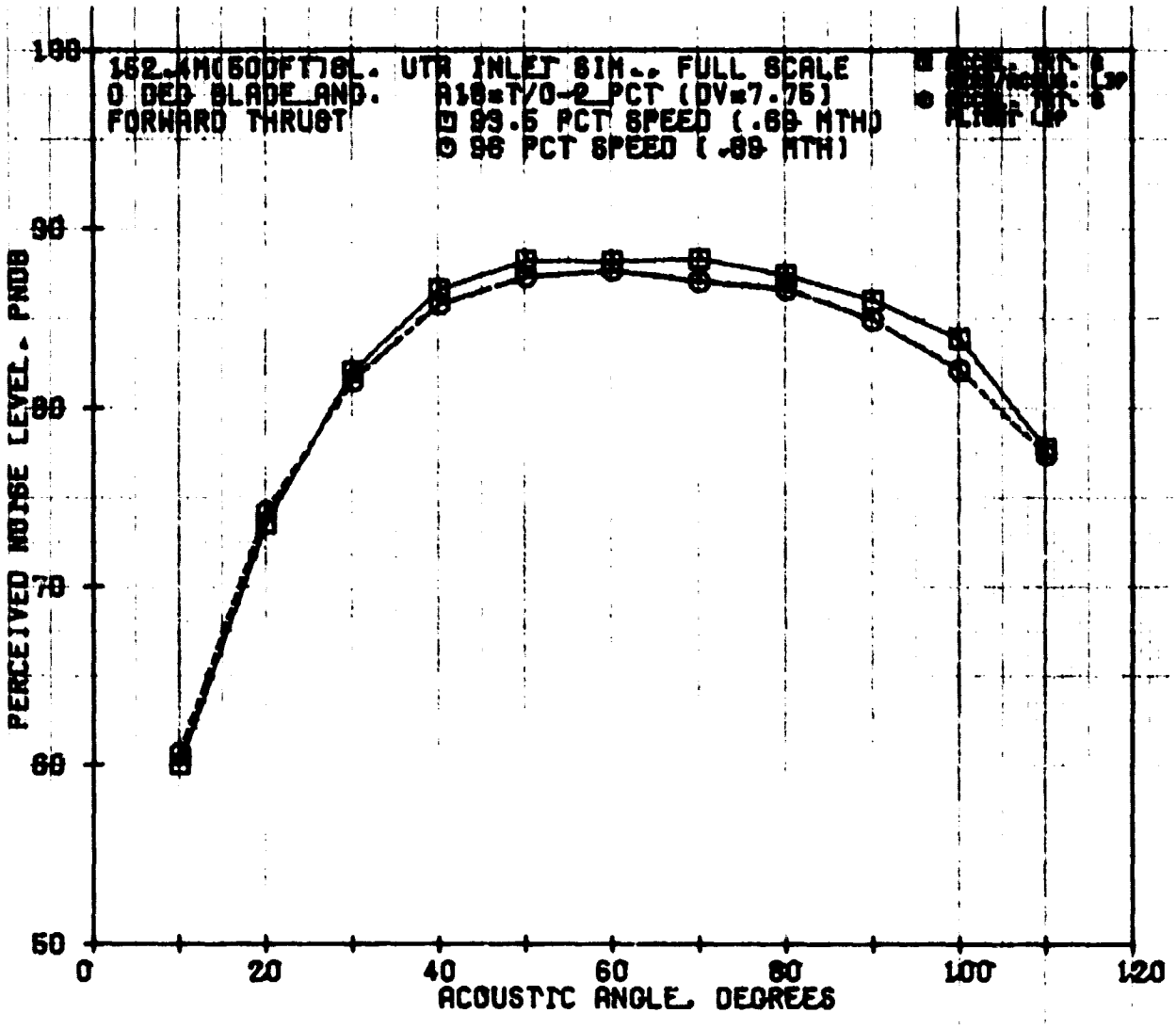

Figure 104. Forward-Thrust, PNL Directivities of Aero-Acoustic and Flight Lips on Accelerating Inlet, Treatment B at 0.69 Throat Mach Number.

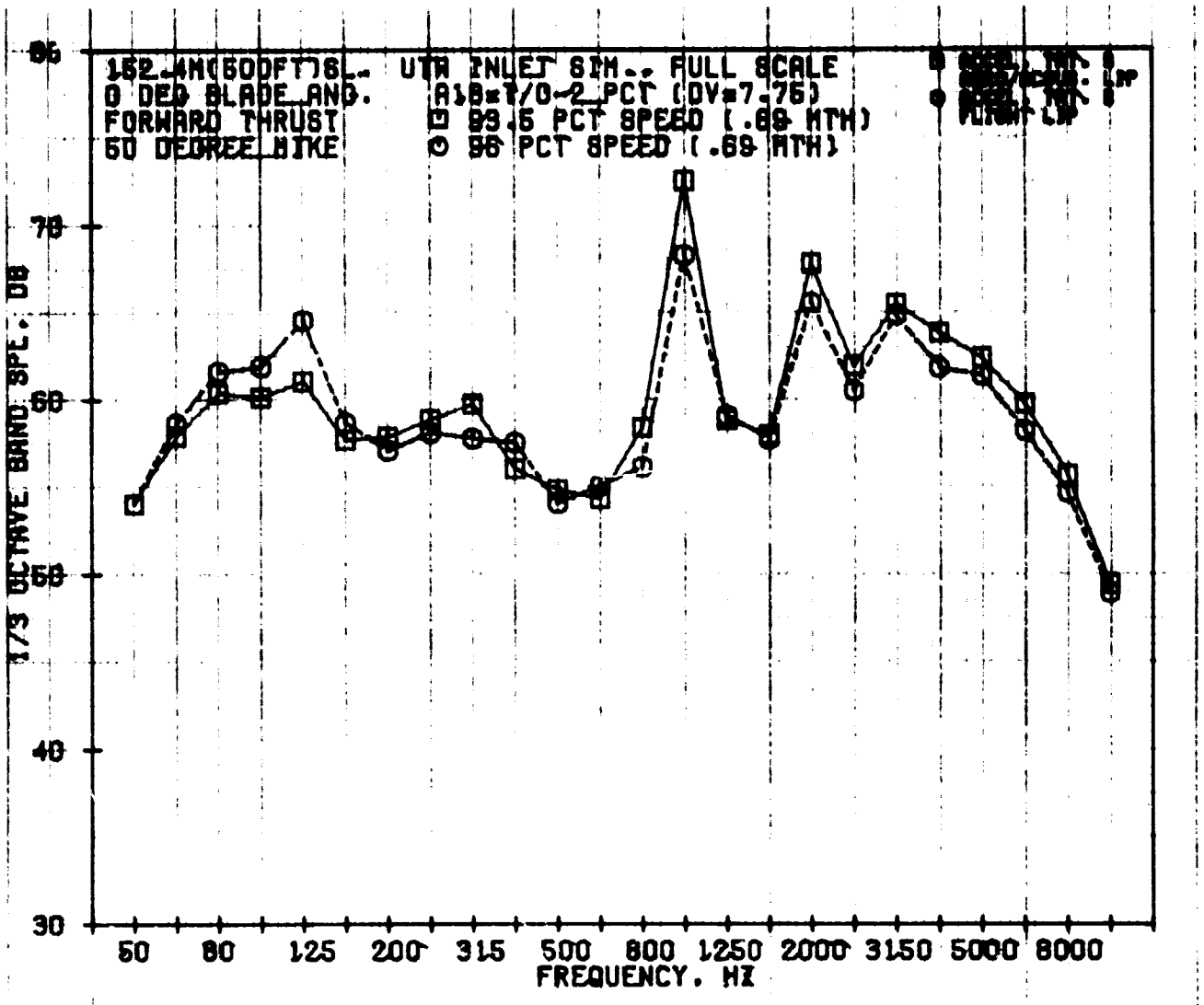

Figure 105. Forward-Thrust, 1/3-Octave-Band, SPL Spectra for Aero-Acoustic and Flight Lips on Accelerating Inlet, Treatment B at 0.69 Throat Mach Number at 50°.

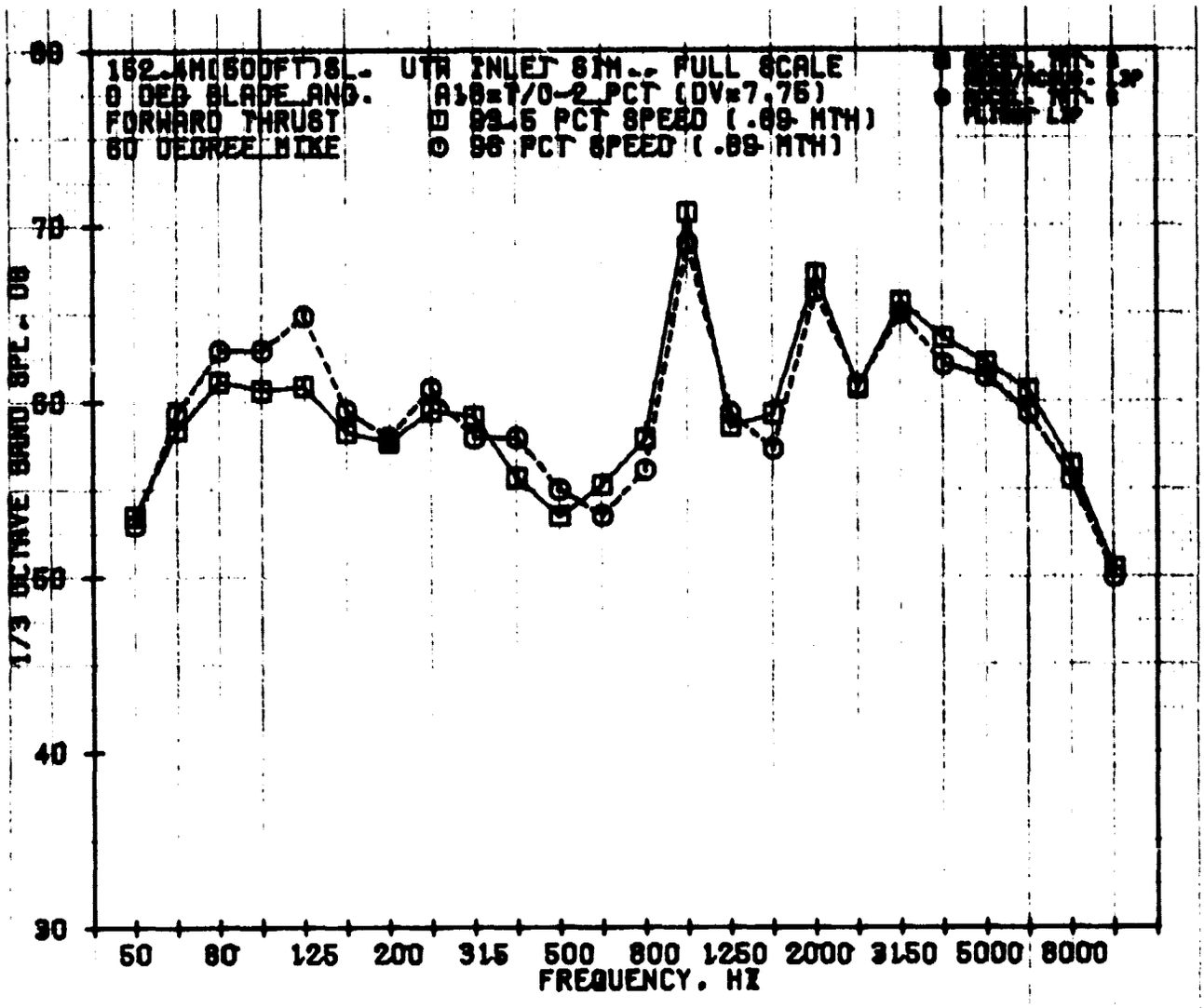

Figure 106. Forward-Thrust, 1/3-Octave-Band, SPL Spectra of Aero-Acoustic and Flight Lips on Accelerating Inlet, Treatment B at 0.69 Throat Mach Number at 60°.

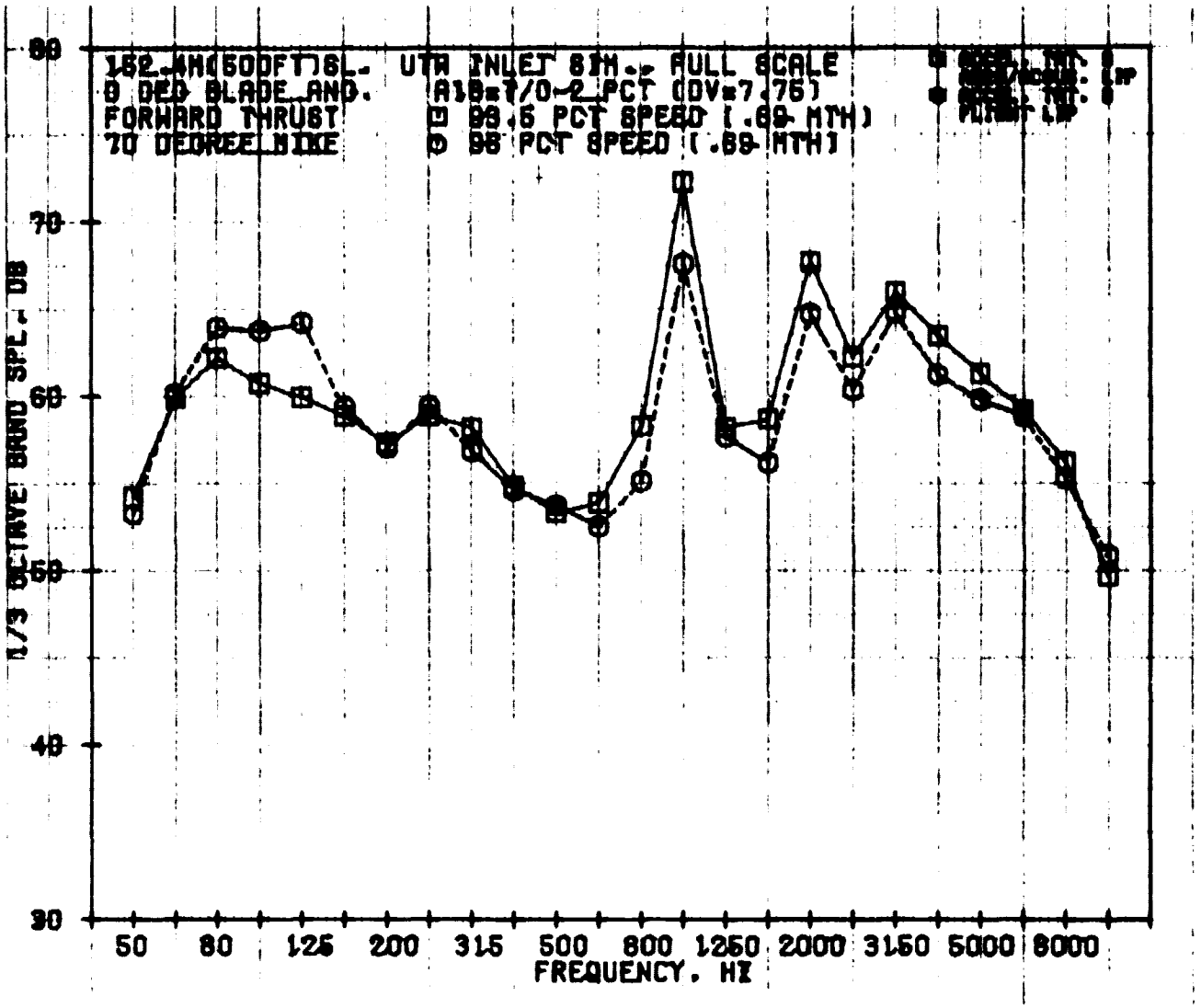

Figure 107. Forward-Thrust, 1/3-Octave-Band, SPL Spectra of Aero-Acoustic and Flight Lips on Accelerating Inlet, Treatment B at 0.69 Throat Mach Number at 70°.

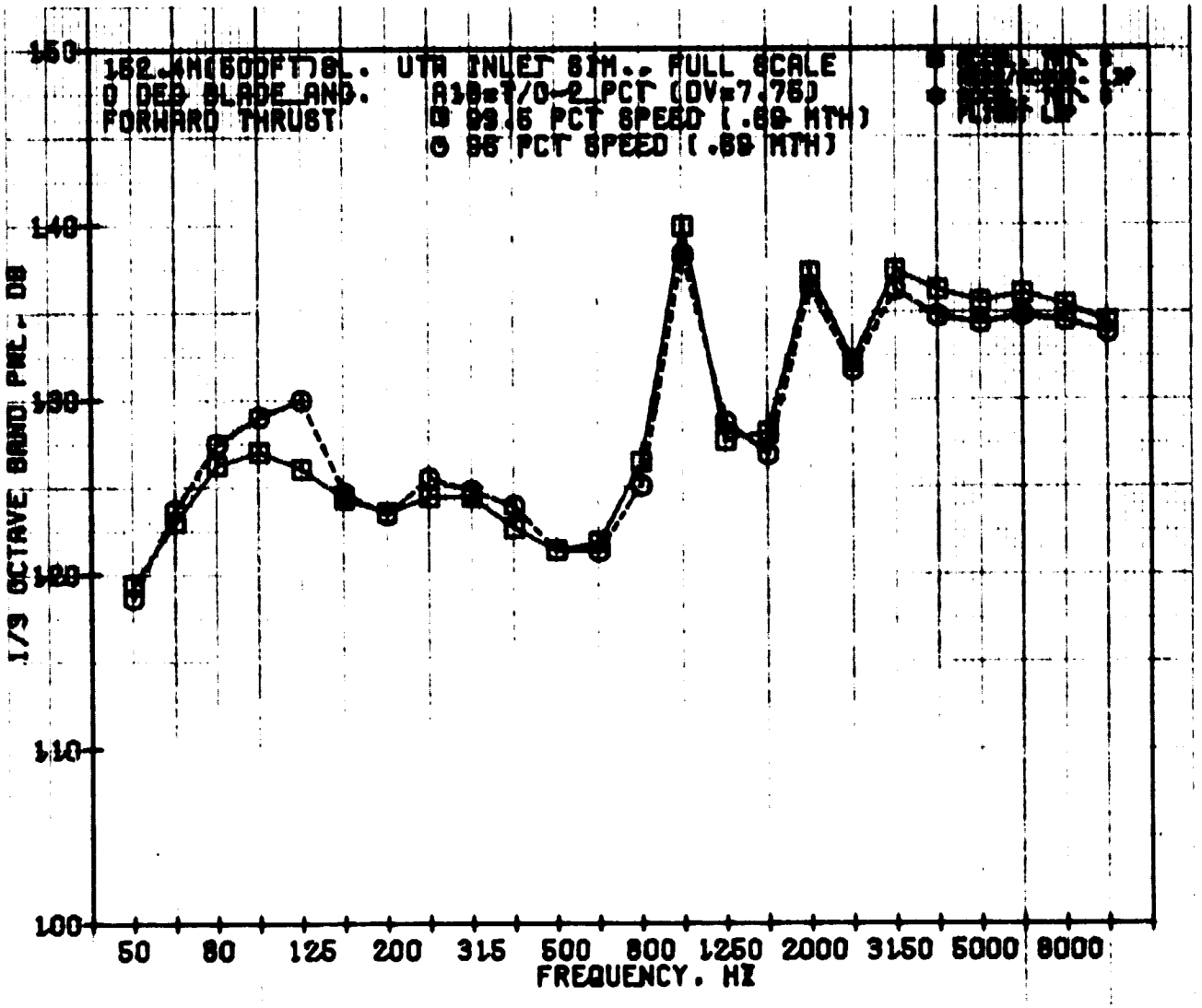

Figure 108. Forward-Thrust, 1/3-Octave-Band, PWL Spectra of Aero-Acoustic and Flight Lips on Accelerating Inlet, Treatment B at 0.69 Throat Mach Number.

that both the levels and the shapes of the PNL directivities for the two configurations were nearly identical at M_{th} = 0.69. The 1/3-octave-band spectra shown at 50°, 60°, and 70° in Figures 105, 106, and 107 also present essentially the same picture although the flight-lip spectrum at 70° appears to be at a slightly lower level. The 1/3-octave-band PWL spectra compared in Figure 108 show the similarity of the acoustic signatures of the two lips.

At higher speeds (and higher M_{th}), some differences are noticeable. At a throat Mach number of approximately 0.775, we see that while the PNL directivities (Figure 109) are quite comparable, the 1/3-octave-band SPL spectra at 50°, 60°, and 70° (Figures 110, 111, and 112) and the 1/3-octave-band PWL spectra (Figure 113) show a considerably higher level of low-frequency (below BPF) noise with the aero-acoustic lip. On a PNL basis, this higher level of low-frequency noise appears to have compensated for the very slightly higher level of high-frequency noise with the flight lip. A similar picture emerges at M_{th} = 0.79 from the comparisons shown in Figures 114 through 118. Narrowband analysis (20-Hz bandwidth) of the data from the 60° microphones at M_{th} = 0.775 (Figure 119) and at M_{th} = 0.79 (Figure 120) show that, at frequencies below BPF, the aero-acoustic lip configuration exhibited some inexplicably high levels of SPL. The source of this behavior is not obvious at this point. However, there is a strong, four-per-rev signal in the aero-acoustic lip narrowbands similar to that observed with the baseline bellmouth and the hard-wall, accelerating inlet in Figure 69. In Figures 119 and 120 the aero-acoustic lip narrowbands exhibit a strong, ten-per-rev signal which corresponds to the peak observed in the 630-Hz, 1/3-octave band in the full-scale data (Figure 116).

9.3 LOW MACH INLETS AT NOMINAL PITCH

9.3.1 Inlet Aerodynamics

Aero-acoustic testing of the low Mach inlet in the forward-thrust mode was conducted only with the aero-acoustic lip. A total of four inlet configurations was examined: a hard-wall diffuser and three treated diffusers. Figure 121 compares wall Mach number data for the four inlets at approximately the design throat Mach number (M_{th} = 0.60). All of the inlet wall Mach number distributions compared reasonably well to the predictions. It was observed after the test that several static pressure lines had been crimped during testing. This could explain the high pressures (low Mach numbers) indicated at stations -14, -15, and -16.2 (only for the hard-wall inlet).

In the low Mach inlet, flow approaching the fan appeared to accelerate a great deal more than in the accelerating inlet. The 13.99-m (5.50-in.) spool piece in the low Mach inlet permitted the flow to diffuse to a much lower Mach number prior to the acceleration induced by the hub (spinner). Figure 39 indicated that the lowest wall Mach number reached in the accelerating inlet was 0.53 compared to a 0.43 minimum in the low Mach inlet from

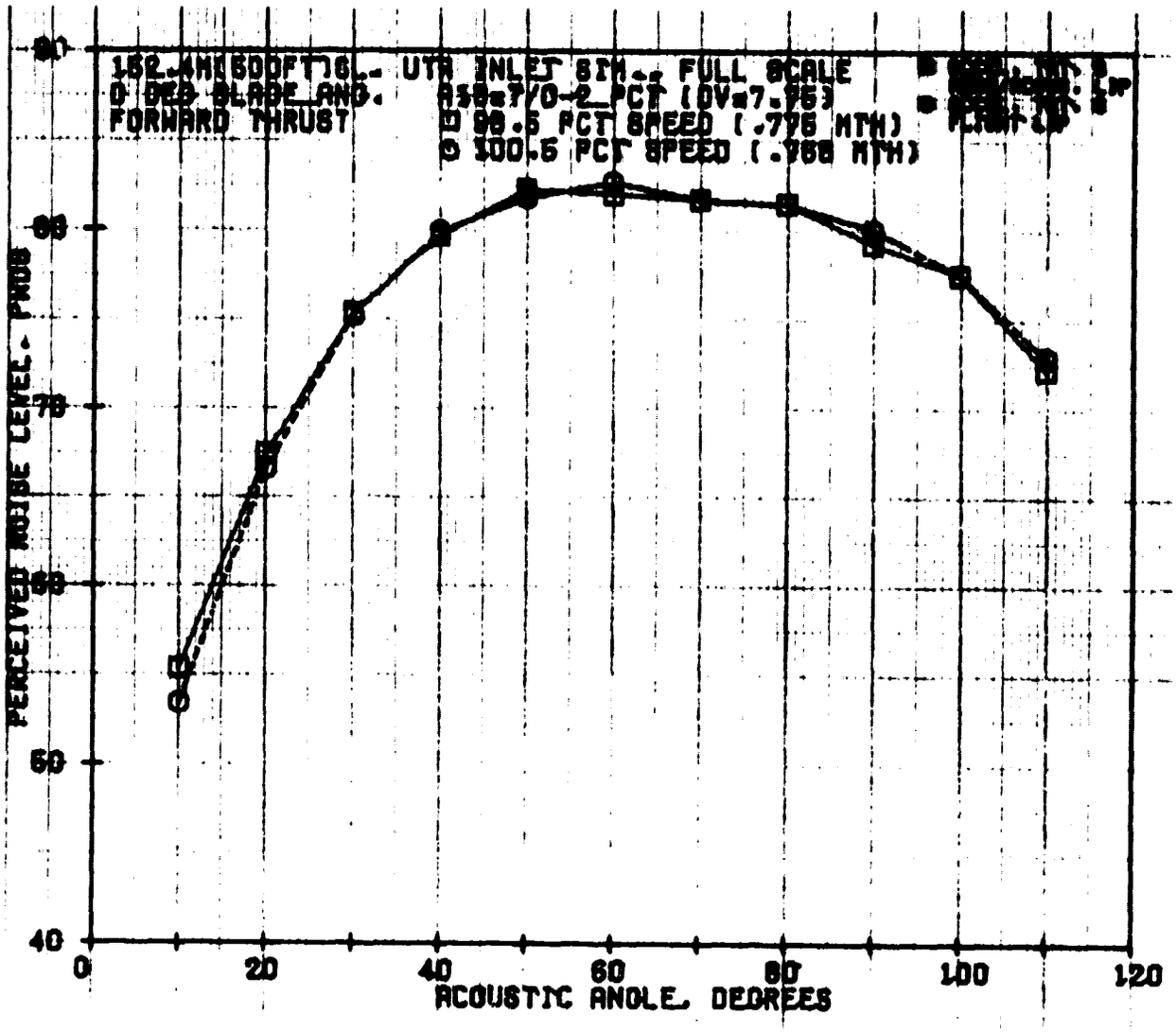

Figure 109. Forward-Thrust, PNL Directivities of Aero-Acoustic and Flight Lips on Accelerating Inlet, Treatment B at 0.775 Throat Mach Number.

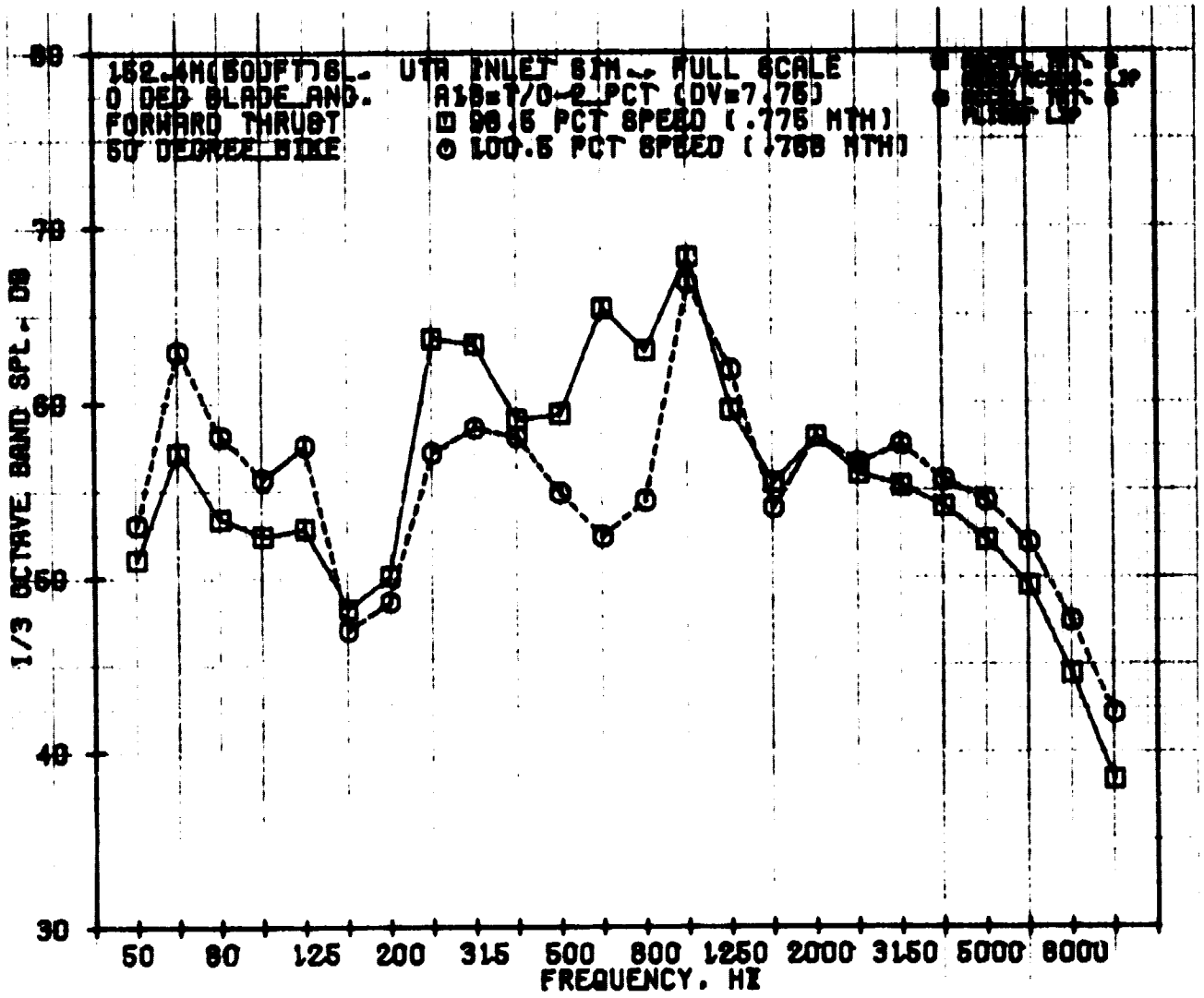

Figure 110. Forward-Thrust, 1/3-Octave-Band, SPL Spectra of Aero-Acoustic and Flight Lips on Accelerating Inlet, Treatment B at 0.775 Throat Mach Number at 50°.

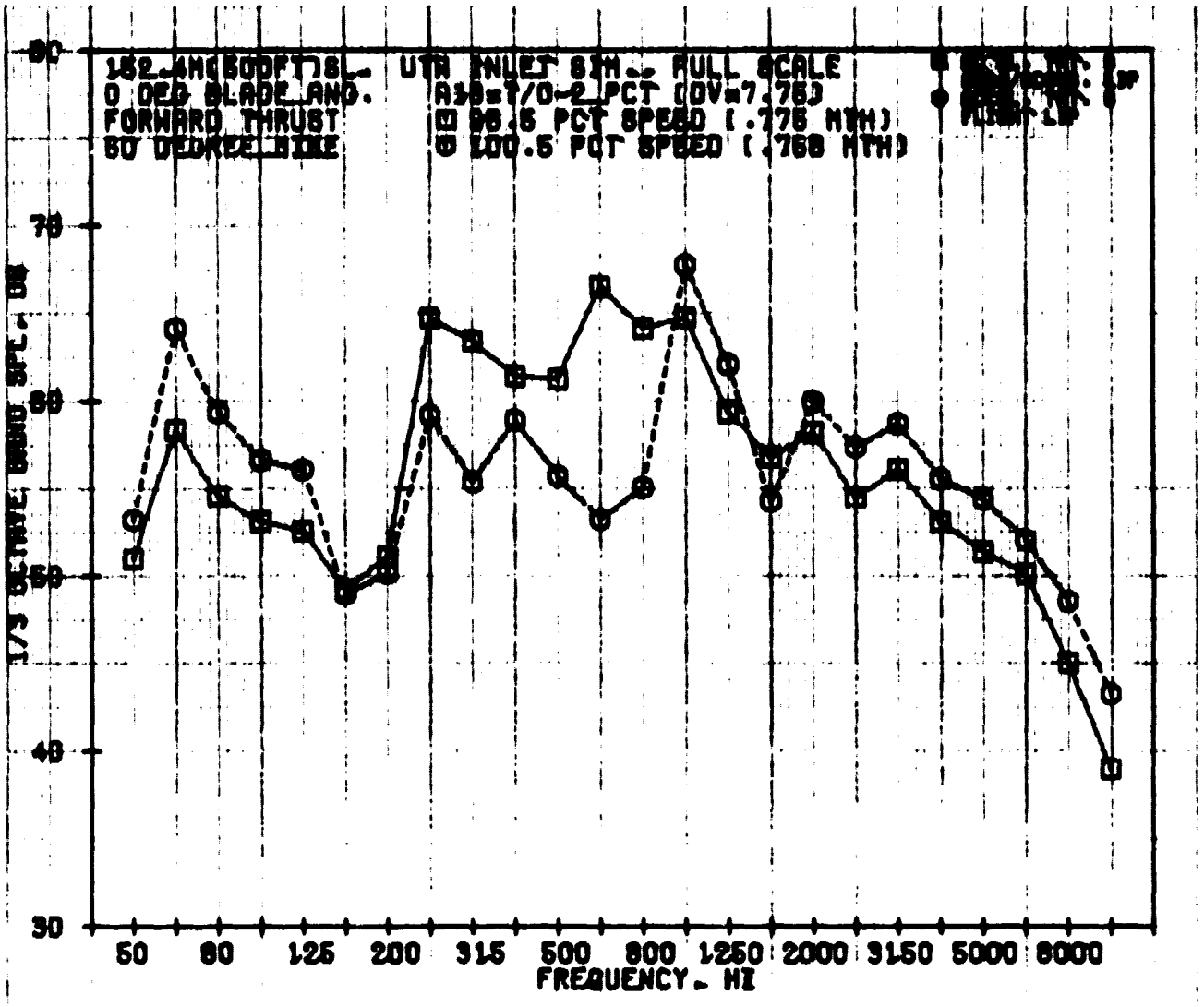

Figure 111. Forward-Thrust, 1/3-Octave-Band, SPL Spectra of Aero-Acoustic and Flight Lips on Accelerating Inlet, Treatment B at 0.775 Throat Mach Number at 50°.

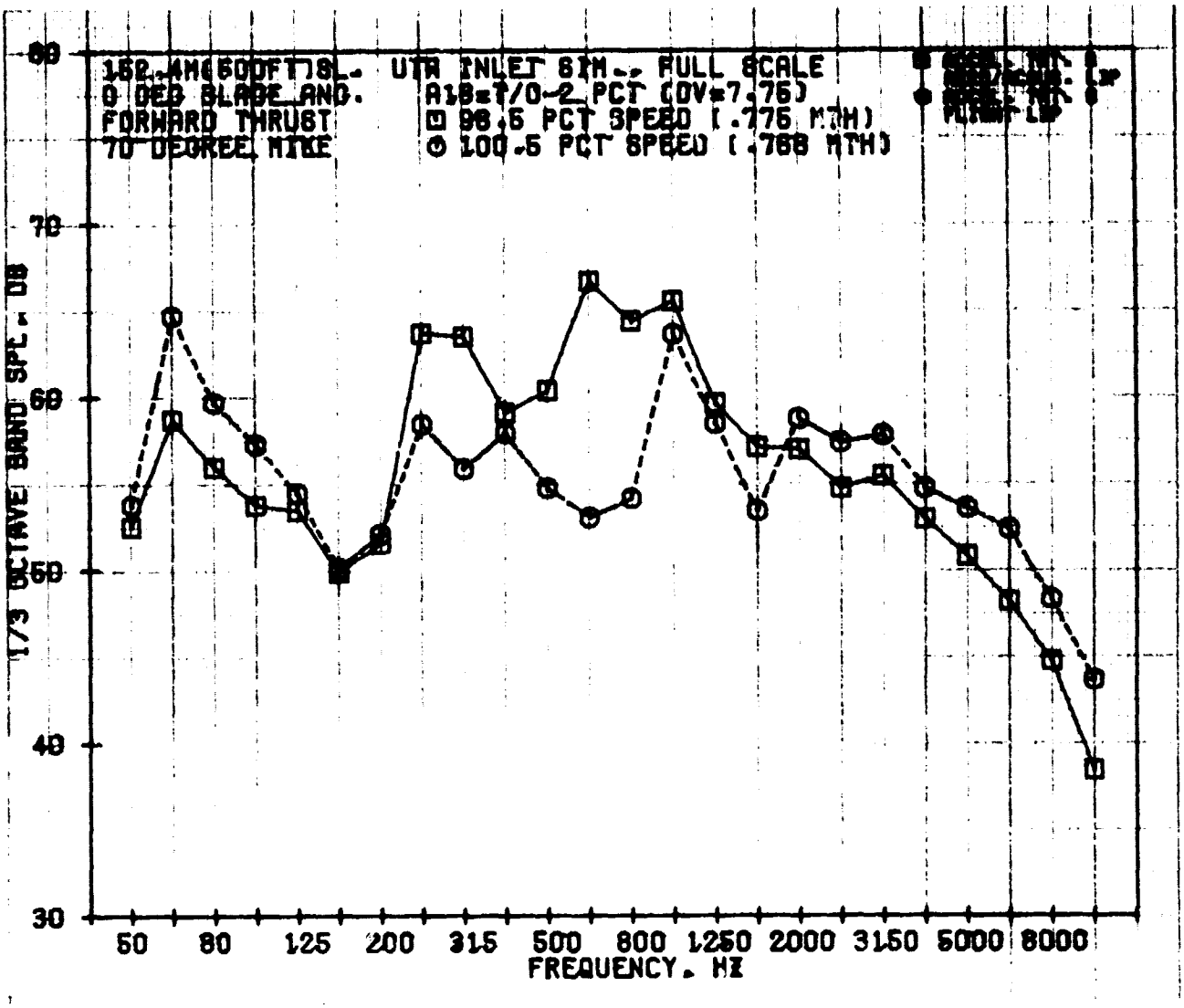

Figure 112 Forward-Thrust, 1/3-Octave-Band, SPL Spectra of Aero-Acoustic and Flight Lips on Accelerating Inlet, Treatment B at 0.775 Throat Mach Number at 60°.

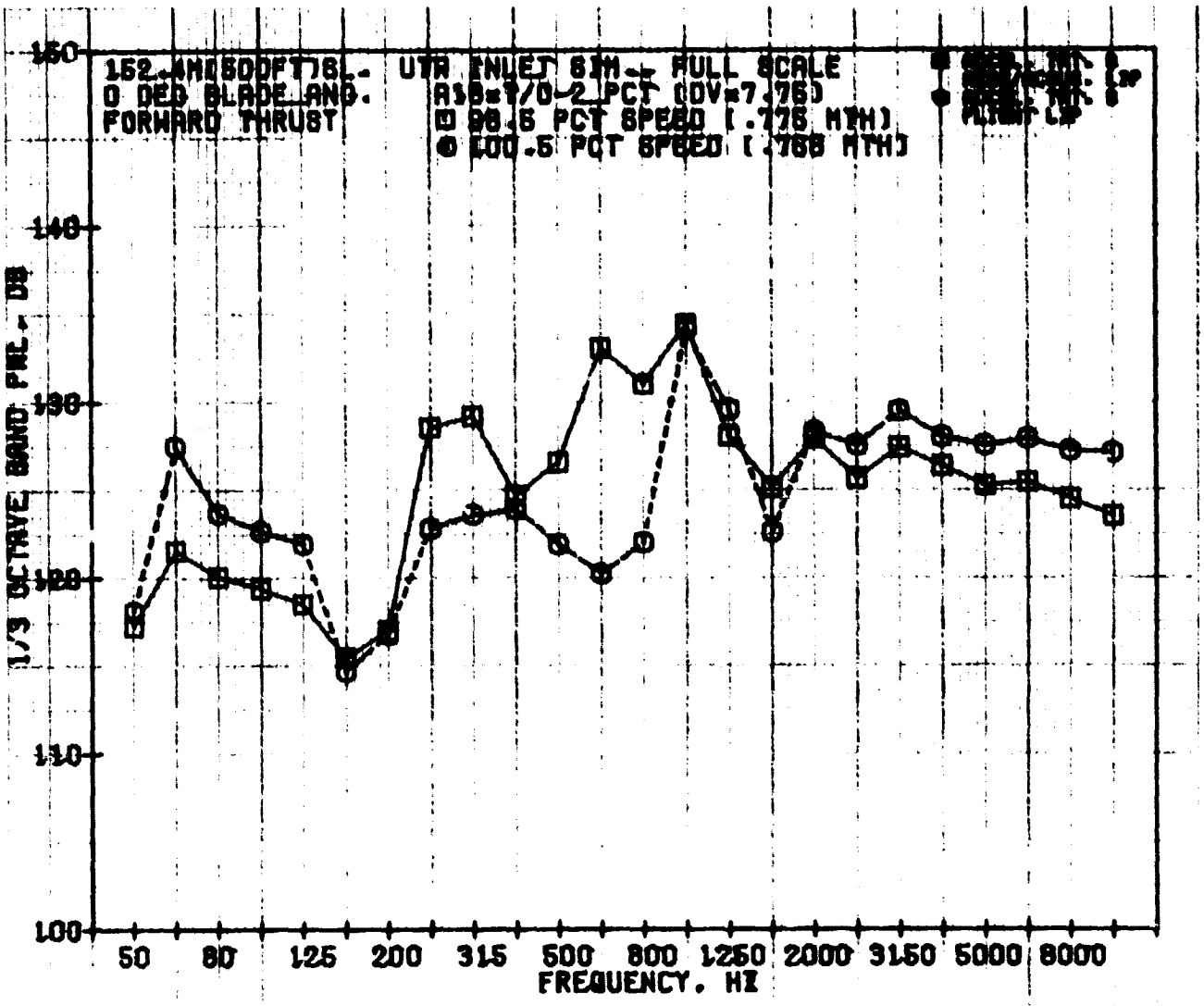

Figure 113. Forward-Thrust, 1/3-Octave-Band, PWL Spectra of Aero-Acoustic and Flight Lips on Accelerating Inlet, Treatment B at 0.775 Throat Mach Number.

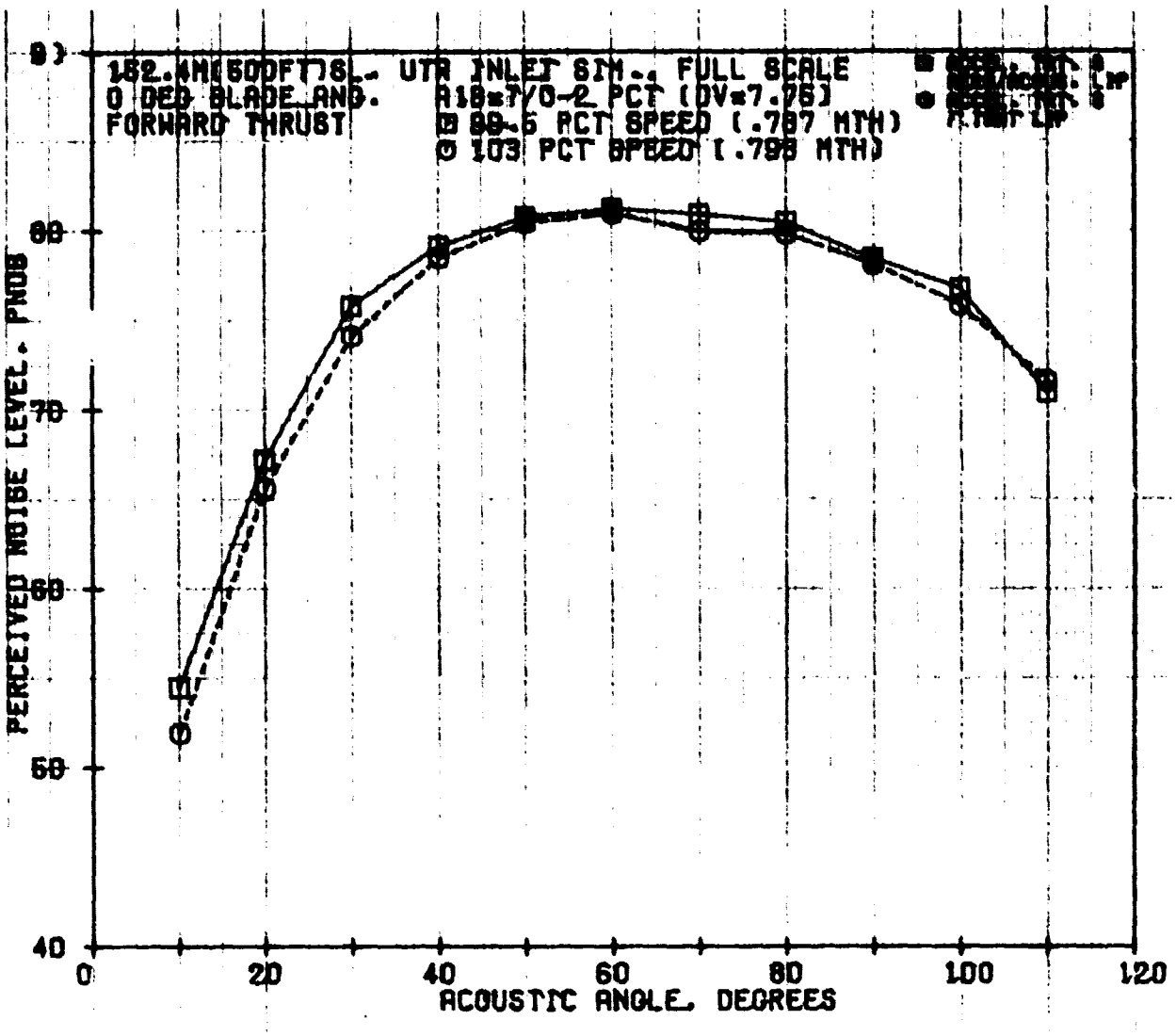

Figure 114. Forward-Thrust, PNL Directivities of Aero-Acoustic and Flight Lips on Accelerating Inlet, Treatment B at 0.79 Throat Mach Number.

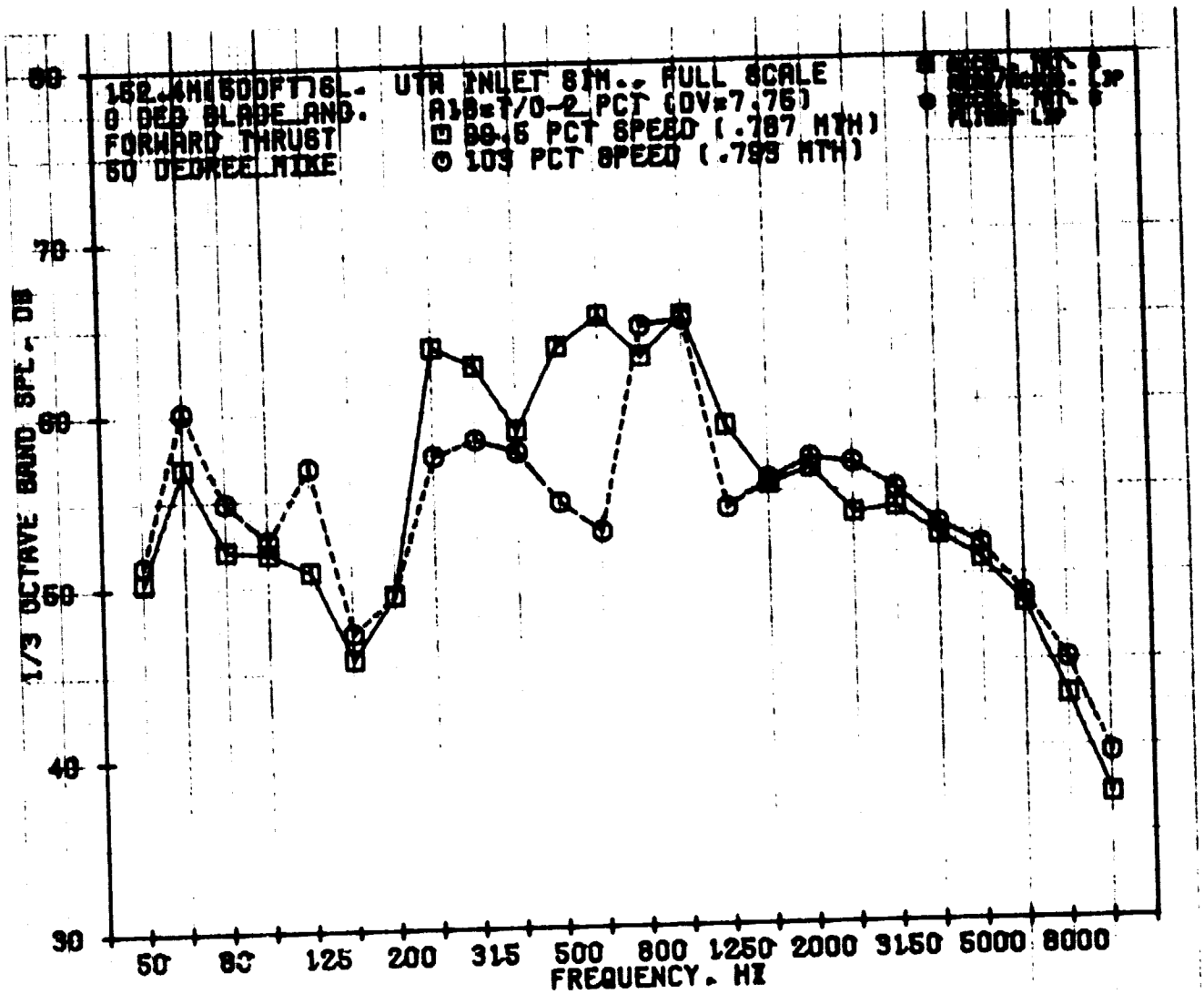

Figure 115. Forward-Thrust 1/3-Octave-Band, SPL Spectra of Aero-Acoustic and Flight Lips on Accelerating Inlet, Treatment B at 0.79 Throat Mach Number at 50°.

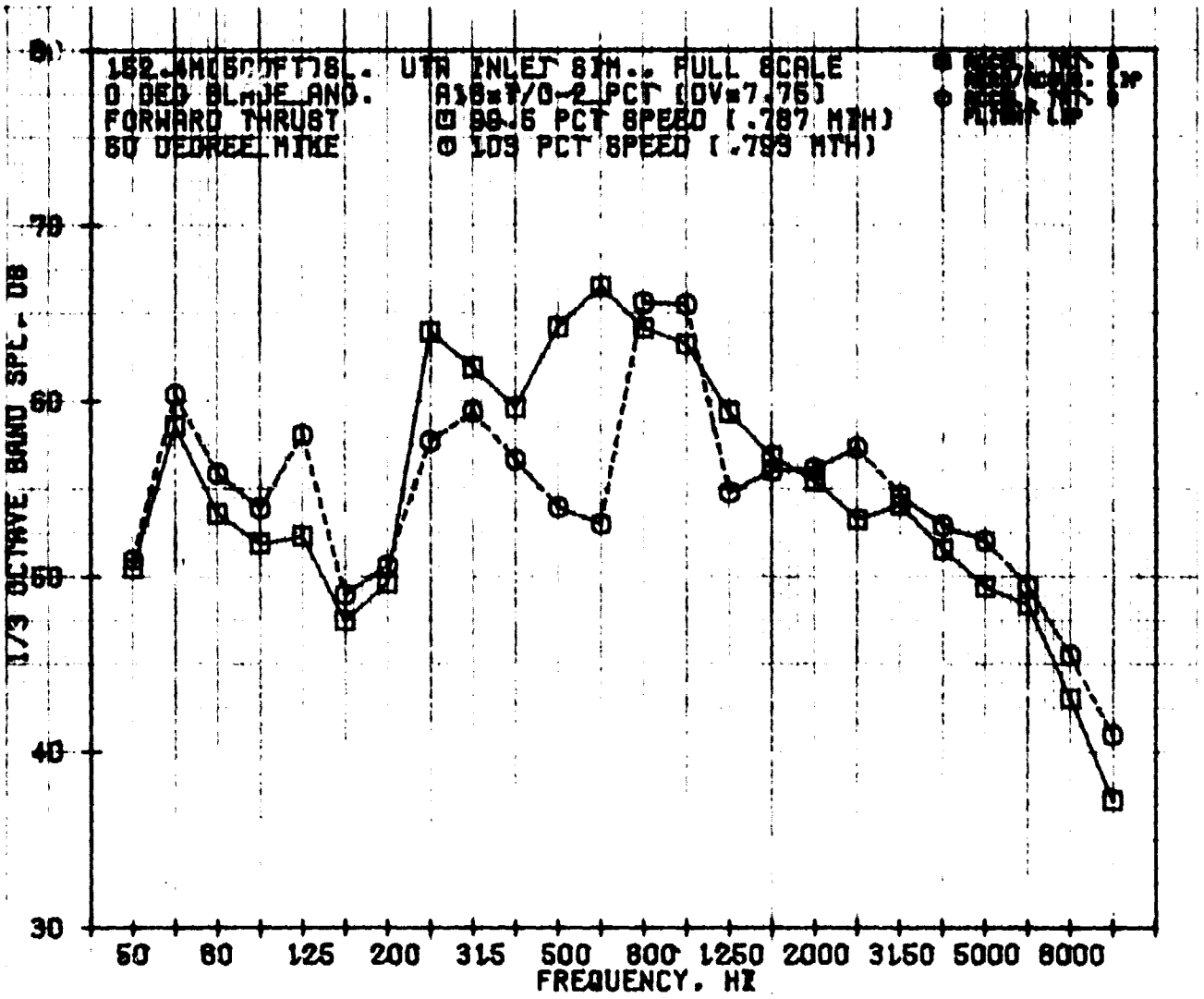

Figure 116. Forward-Thrust, 1/3-Octave-Band, SPL Spectra of Aero-Acoustic and Flight Lips on Accelerating Inlet, Treatment B at 0.79 Throat Mach Number at 60°.

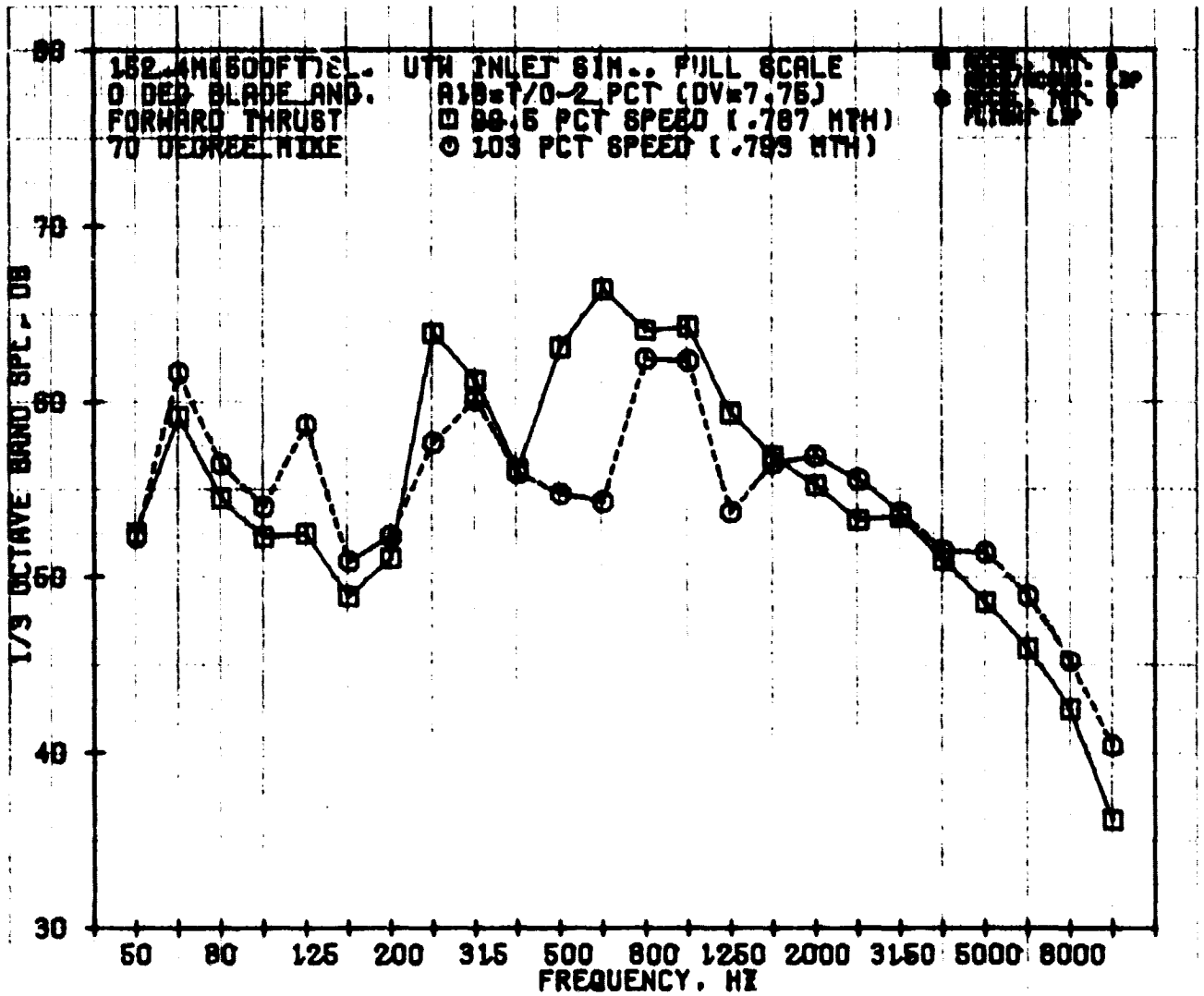

Figure 117. Forward-Thrust, 1/3-Octave-Band, SPL Spectra of Aero-Acoustic and Flight Lips on Accelerating Inlet, Treatment B at 0.79 Throat Mach Number at 70°.

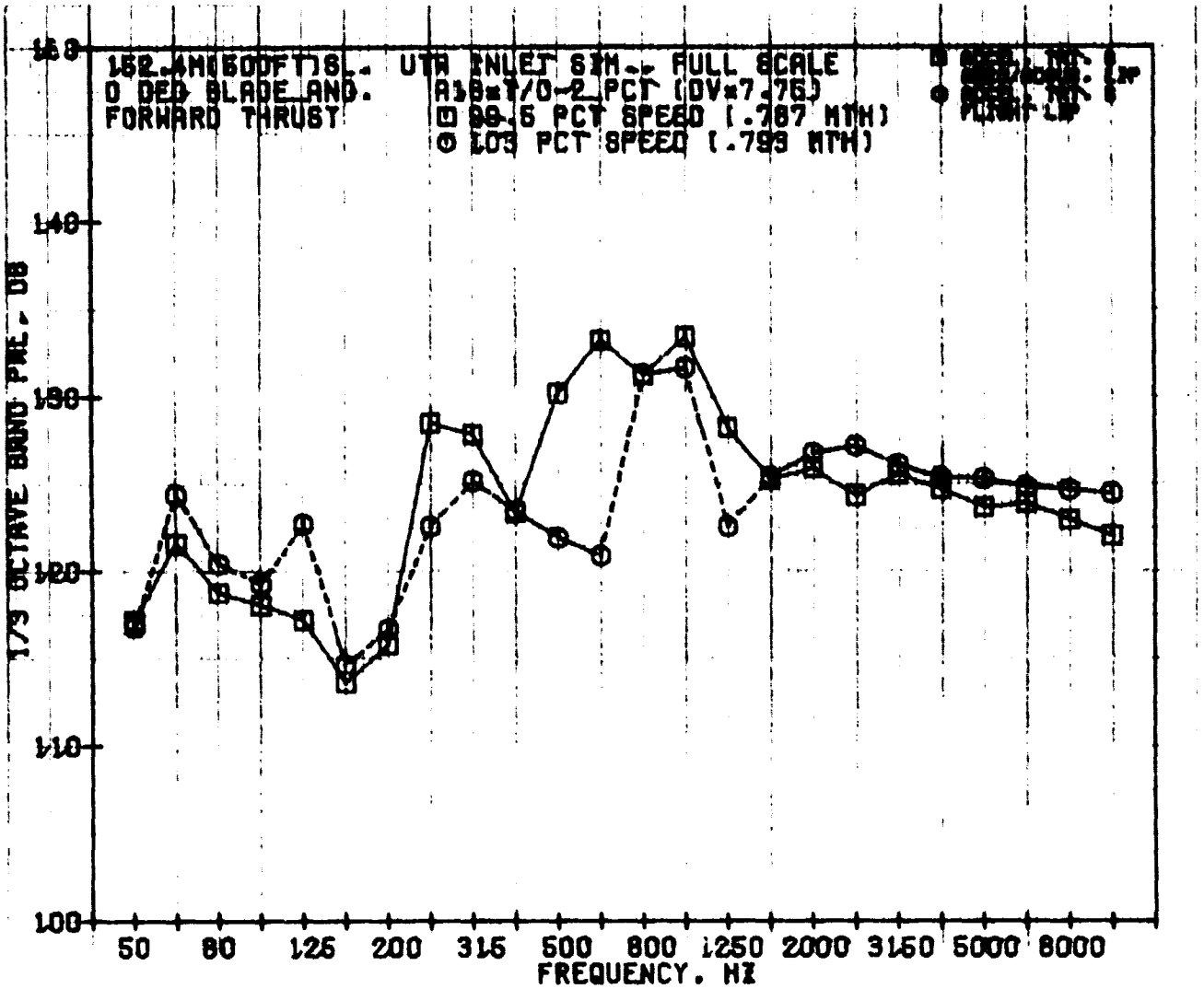

Figure 118. Forward-Thrust, 1/3-Octave-Band, PWL Spectra of Aero-Acoustic and Flight Lips on Accelerating Inlet, Treatment B at 0.79 Throat Mach Number.

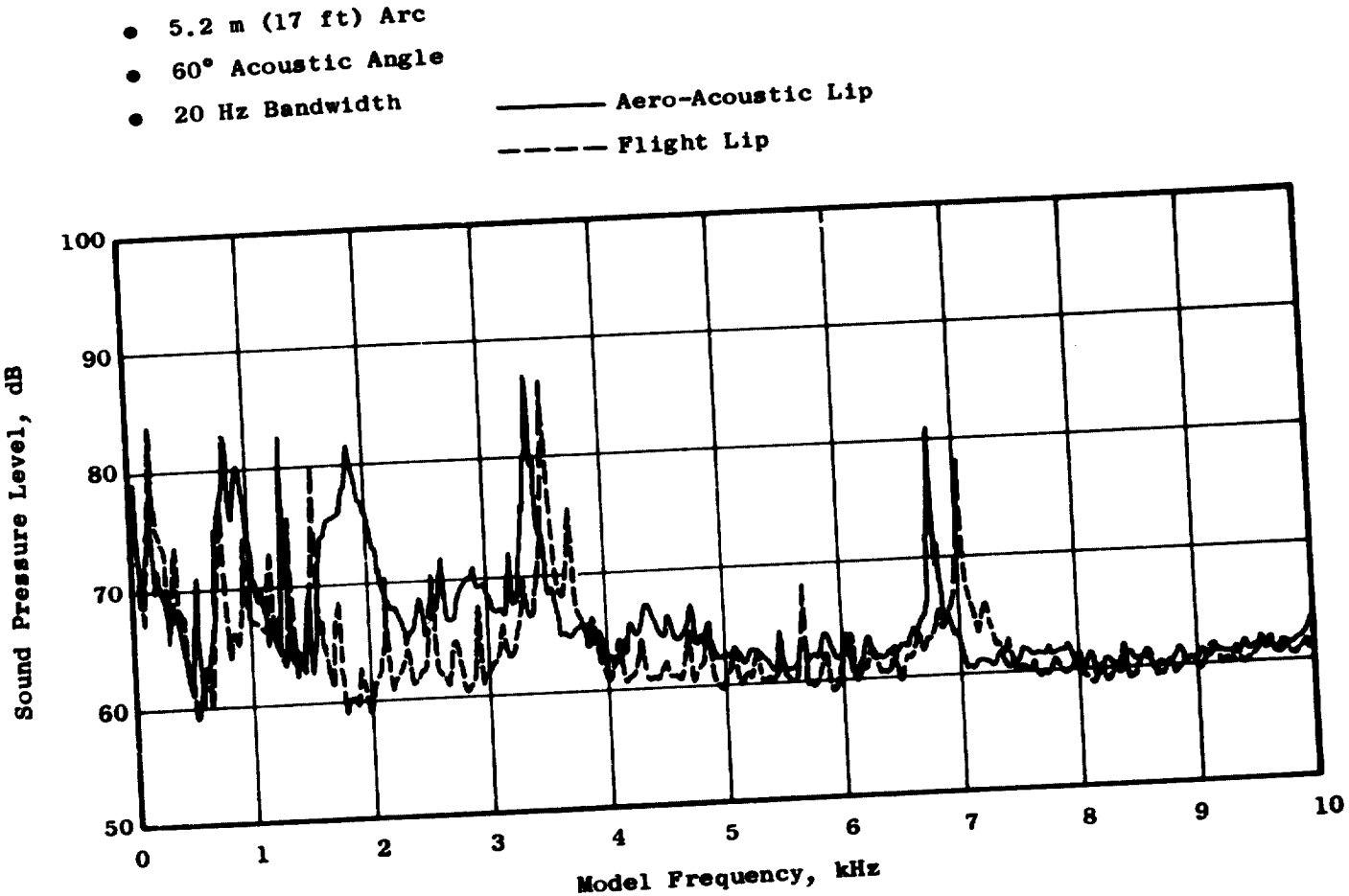

Figure 119. Narrowband SPL Spectra of Aero-Acoustic and Flight Lips on Accelerating Inlet, Treatment B at 0.775 Throat Mach Number.

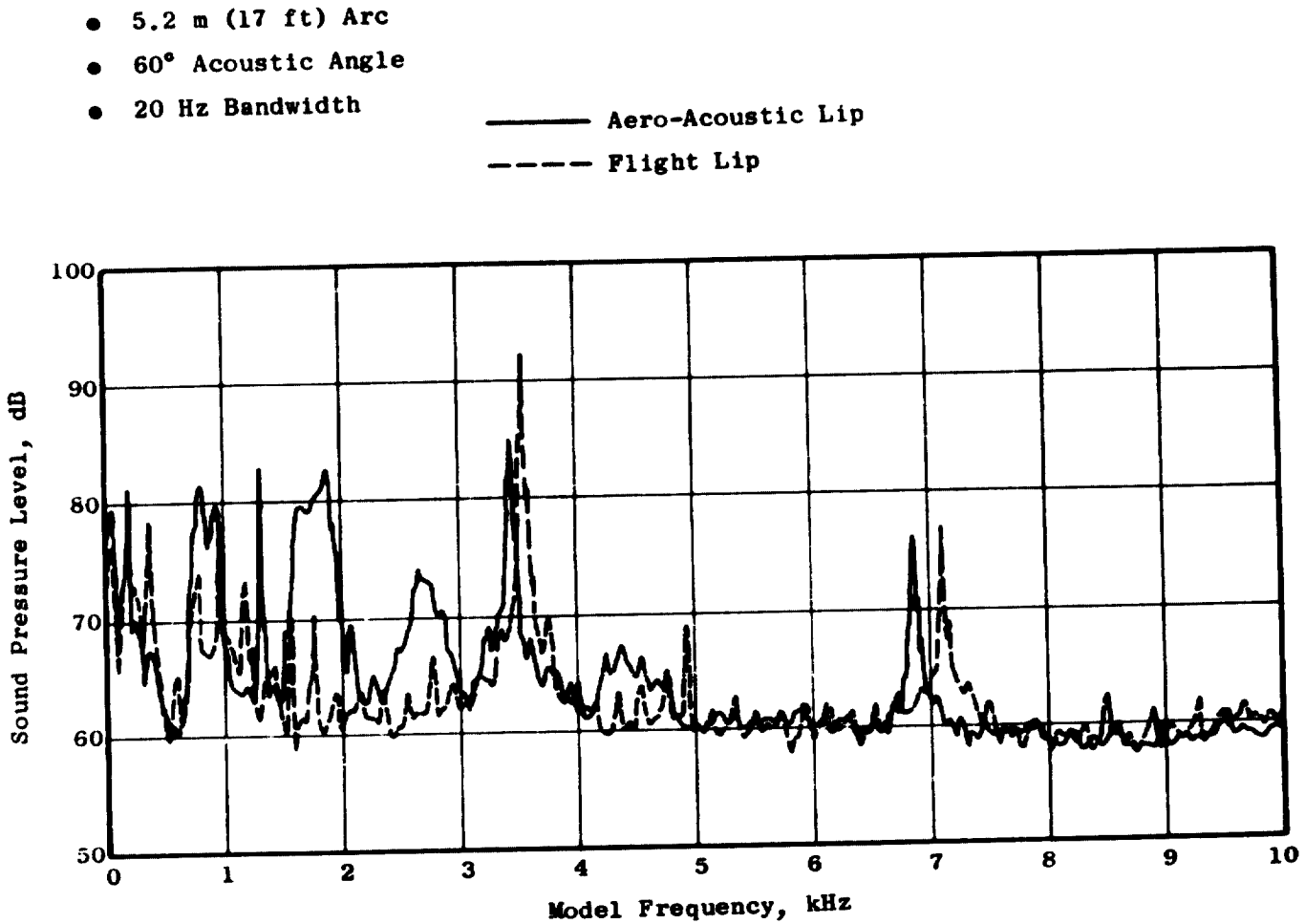

Figure 120. Narrowband SPL Spectra of Aero-Acoustic and Flight Lips on Accelerating Inlet, Treatment B at 0.79 Throat Mach Number.

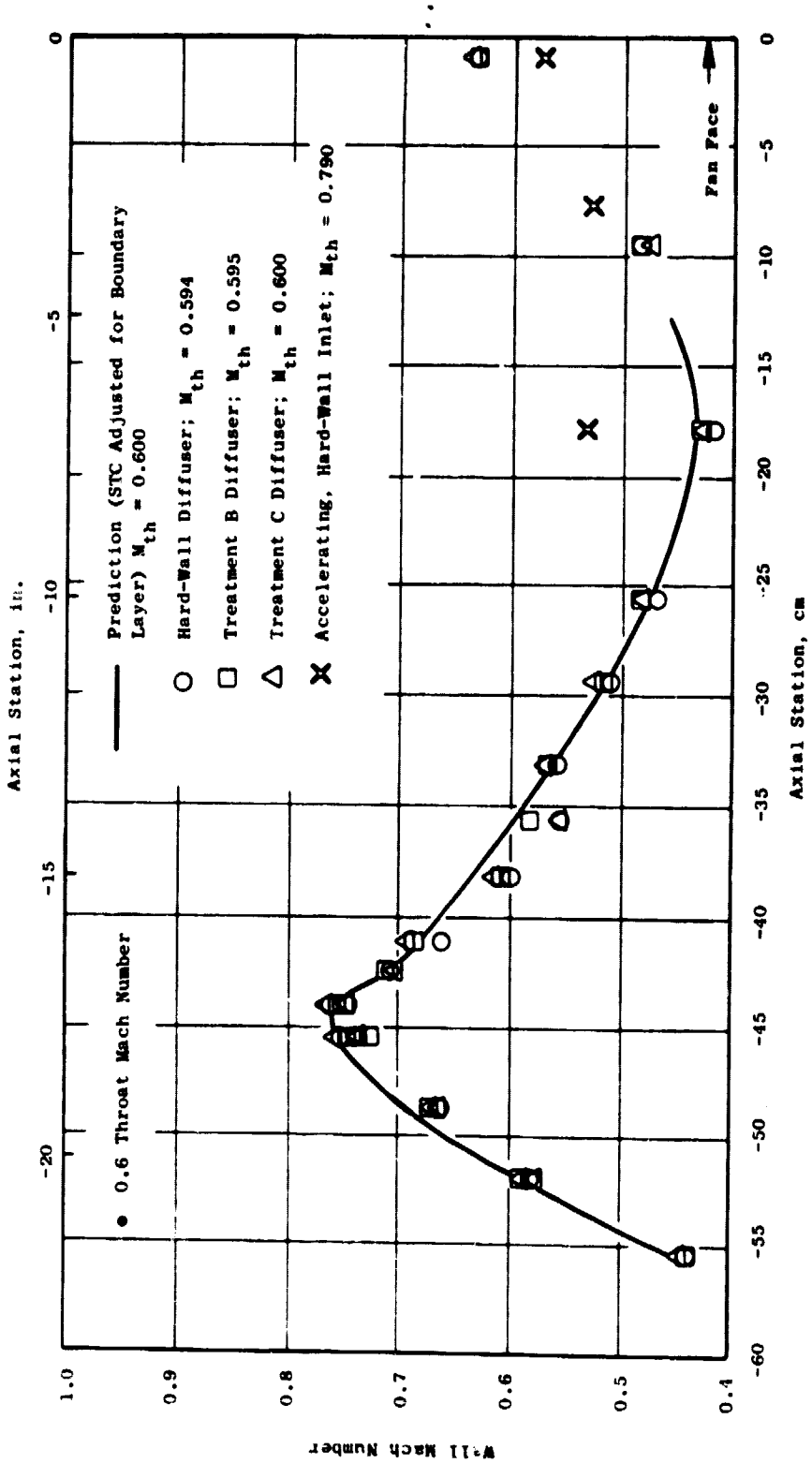

Figure 121. Low Mach Inlet Wall Mach Number Distributions at 99.6% N_{FC}.

Figure 120 at the design takeoff condition. Nevertheless, the low Mach number inlet accelerated the flow to a higher velocity at the fan face. It has not been determined whether the low Mach inlet static pressure data at station -14 are realistic. The STC predictions near the fan face were considered invalid since the inlet geometry analyzed included an additional 3.3-cm (1.3-in.) spool piece (similar to the instrumentation section planned for an upcoming wind tunnel test but not installed for the simulator test).

Figure 122 shows the low Mach inlet fan-speed relationship to throat Mach number. All configurations were tested at the same fan blade angle (unlike the tests for the accelerating inlet configurations). Results indicate similar aerodynamic performance for all three inlets regardless of treatment design.

9.3.2 Inlet Acoustics

9.3.2.1 Hard-Wall, Low Mach Inlet

The hard-wall, low Mach inlet should be expected to have acoustic characteristics roughly similar to the baseline bellmouth inlet. Figure 123 shows this to be true with a comparison of full-size, 152.4-m (500-ft) or sideline PNL, at 60° to inlet, plotted against percent corrected fan speed. A comparison of PNL directivity at 98.5% speed (corresponding to takeoff M_{th} with hard-wall, accelerating inlet) between the baseline bellmouth, hard-wall low Mach, and hard-wall accelerating inlets (Figure 124) shows that, whereas no suppression was achieved with the hard-wall low Mach inlet, a considerable amount (9.5 PNdB at 60°) of suppression was realized, as expected, with the use of the accelerating inlet. Figures 125 through 127 give the 1/3-octave-band SPL spectra for the three inlets at 98.5% speed at 50°, 60°, and 70° to the inlet. The low Mach inlet appears to have been influenced more strongly by MPT's below BPF than was the baseline bellmouth, with a corresponding small decrease in BPF tone level. The hard-wall, accelerating inlet, on the contrary, suppressed the MPT's as well as high-frequency, broadband noise. The small decrease in BPF with the low Mach inlet can be seen in Figure 128, which compares the 1/3-octave-band BPF directivity for the three inlets; Figure 129 compares the second-harmonic levels, and Figure 130 compares 1/3-octave-band PWL spectra. The general message appears to be that the low Mach inlet has a stronger MPT content below BPF and a corresponding, slightly reduced, BPF level. In terms of PNL, the hard-wall, low Mach inlet behavior is identical to that of the baseline bellmouth inlet. Hence, in order to meet the takeoff suppression goal of 13 PNdB, all the suppression would be expected to come from wall treatment.

9.3.2.2 Effectiveness of Low Mach Inlet Treatments

The low Mach inlet configuration, hard-wall and treated, forward-thrust PNL is given in Figure 131 as a function of percent fan speed. The data are for a 0° blade-angle setting.

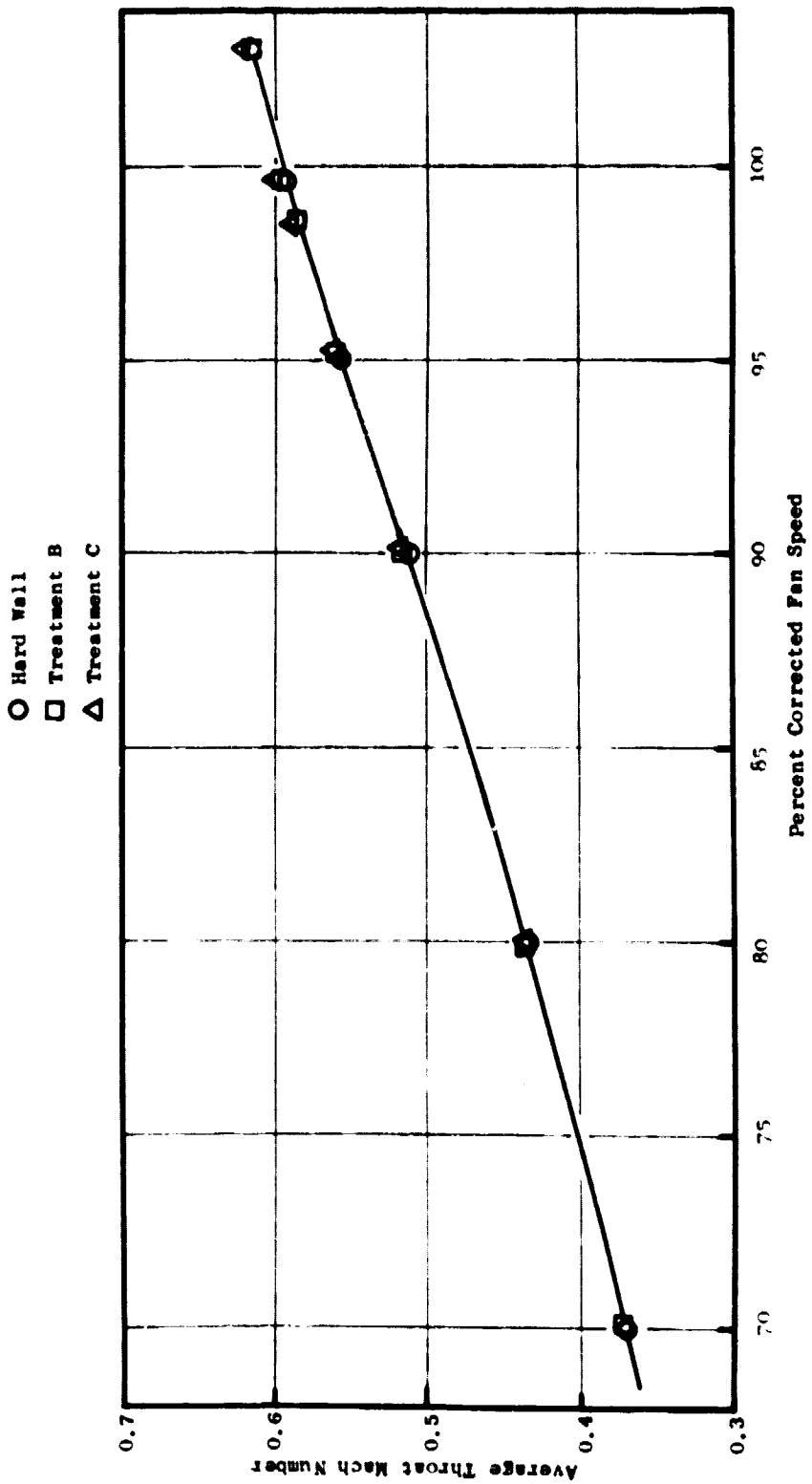

Figure 122. Low Mach Inlet Throat Mach Number Characteristics.

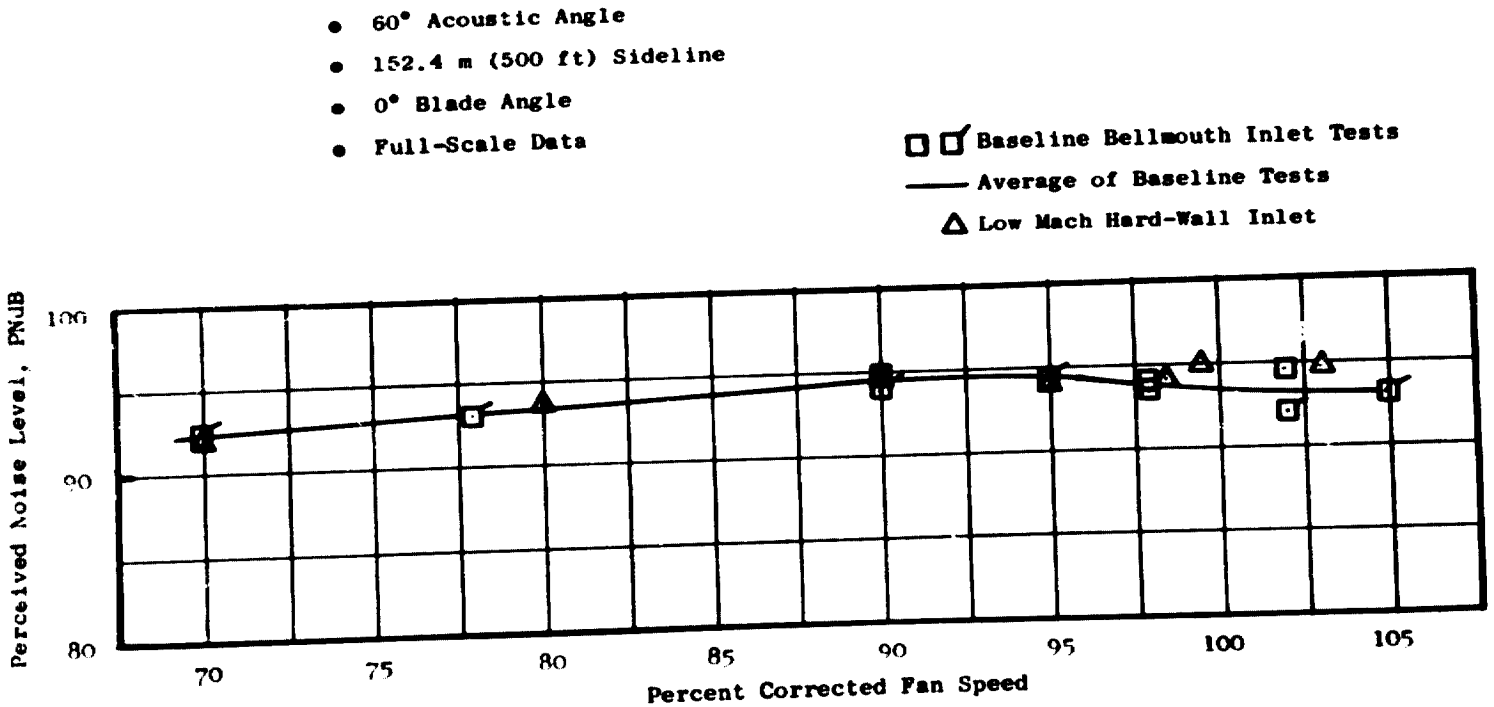

Figure 123. Forward-Thrust PNL Vs. Fan Speed - Baseline Bellmouth and Low Mach, Hard-Wall Inlets.

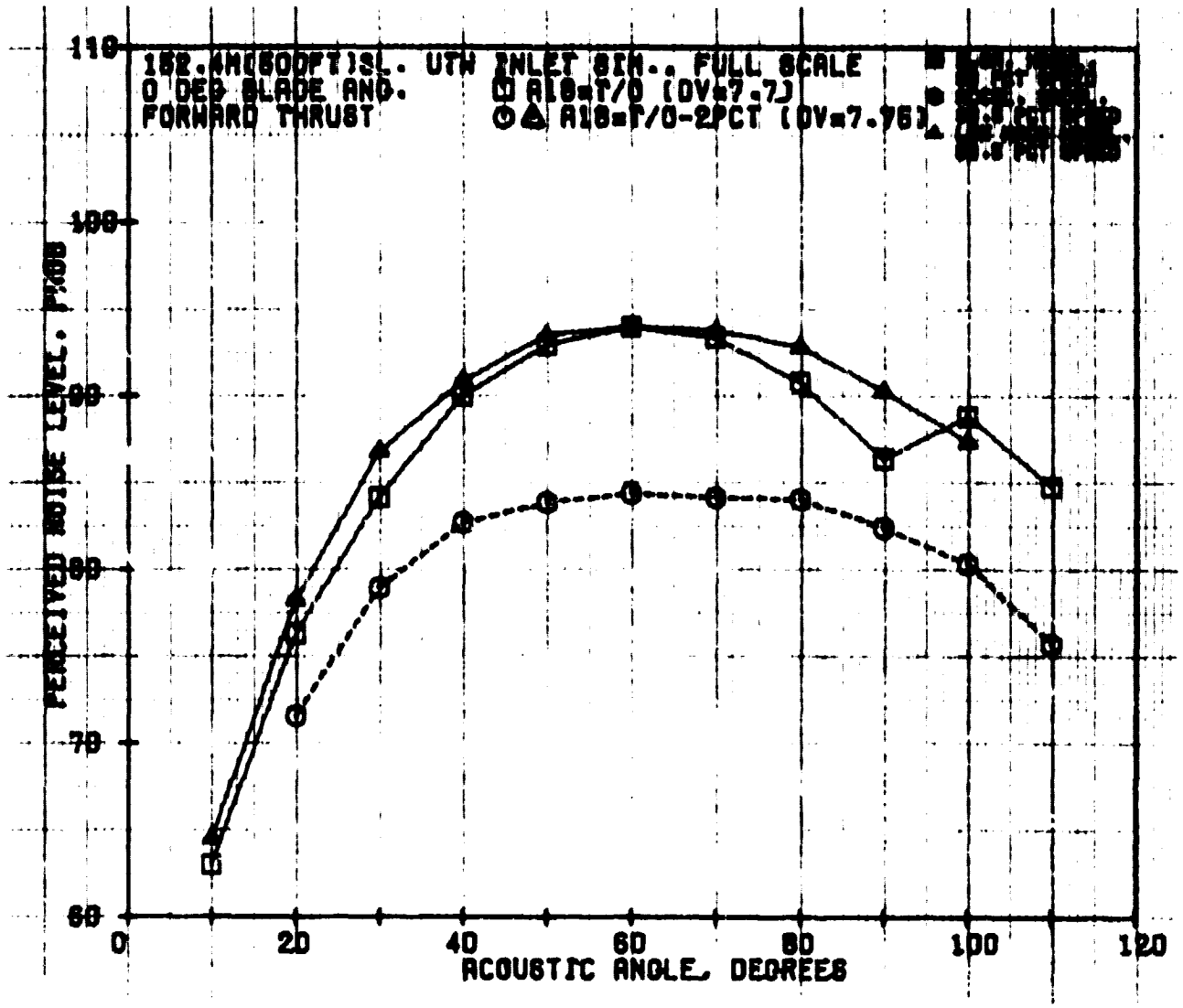

Figure 124. Forward-Thrust, PNL Directivity - Baseline Bellmouth, Accelerating Hard-Wall, and Low Mach Hard-Wall Inlets at 98.5% N_{FC}.

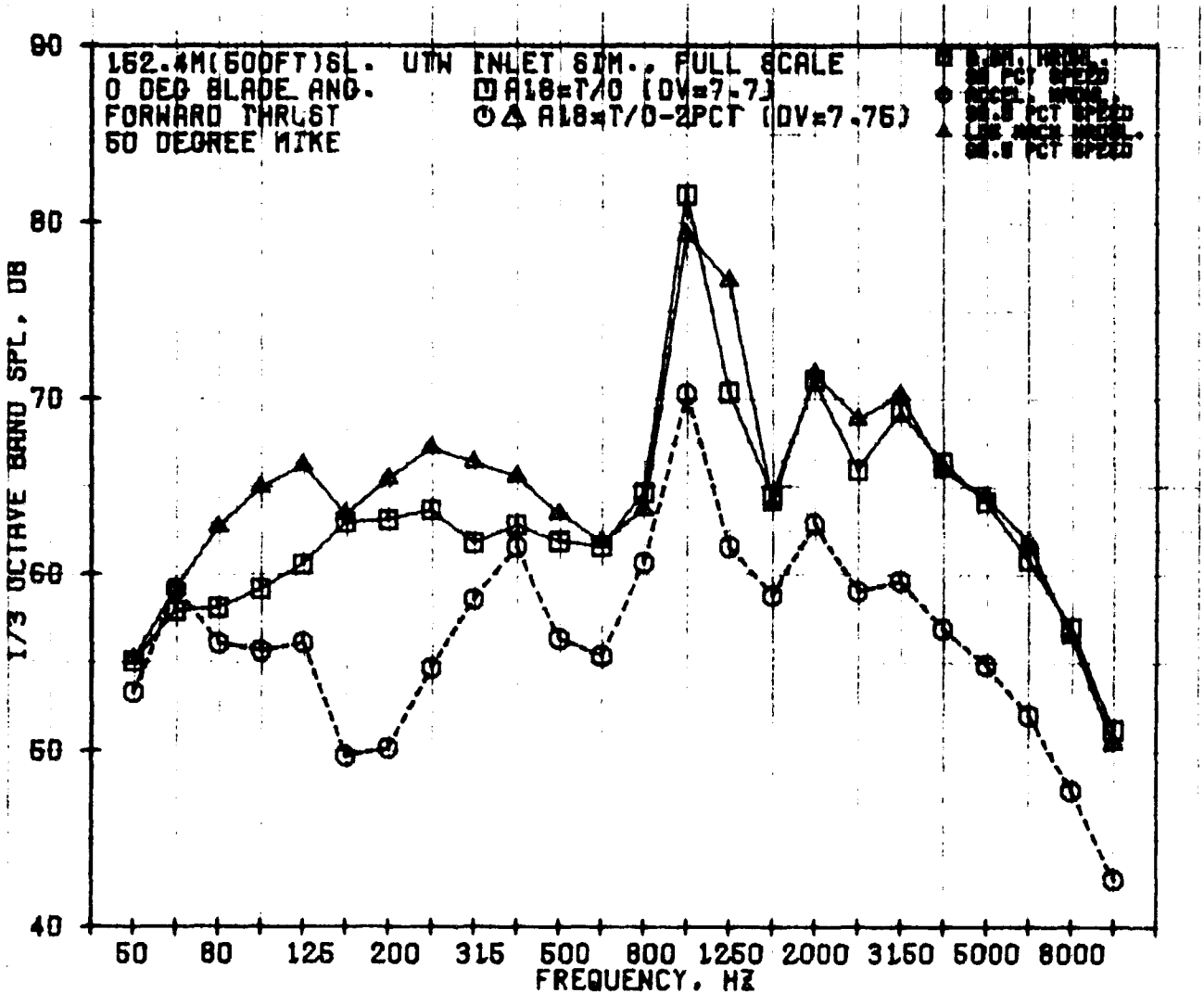

Figure 125. Forward-Thrust, 1/3-Octave-Band, SPL Spectra - Baseline Bellmouth, Accelerating Hard-Wall, and Low Mach Hard-Wall Inlets at 98.5% N_{FC}; 50° to Inlet.

C-3

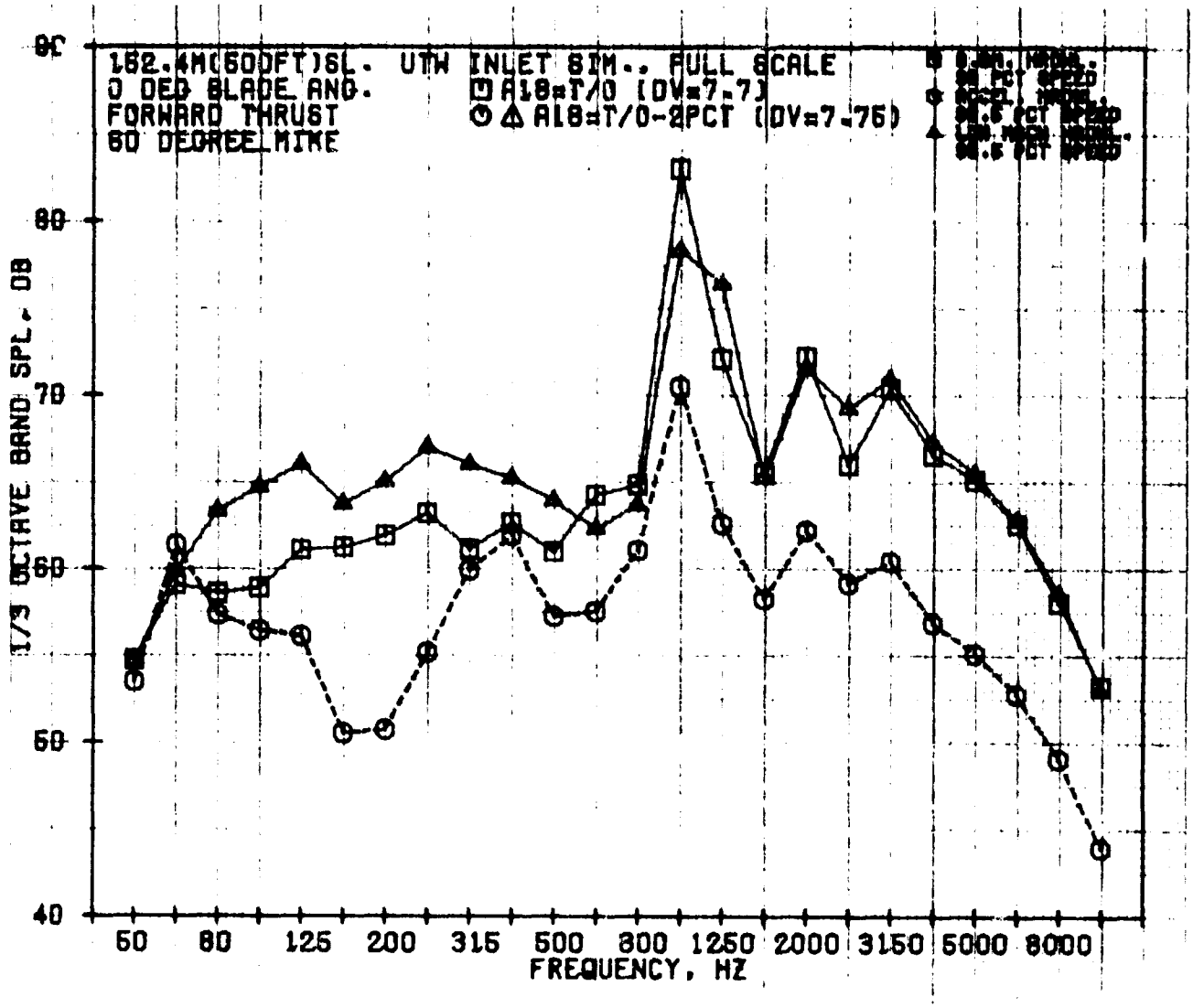

Figure 126. Forward-Thrust, 1/3-Octave-Band, SPL Spectra - Baseline Bellmouth, Accelerating Hard-Wall, and Low Mach Hard-Wall Inlets at 98.5% N_{FC}; 60° to Inlet.

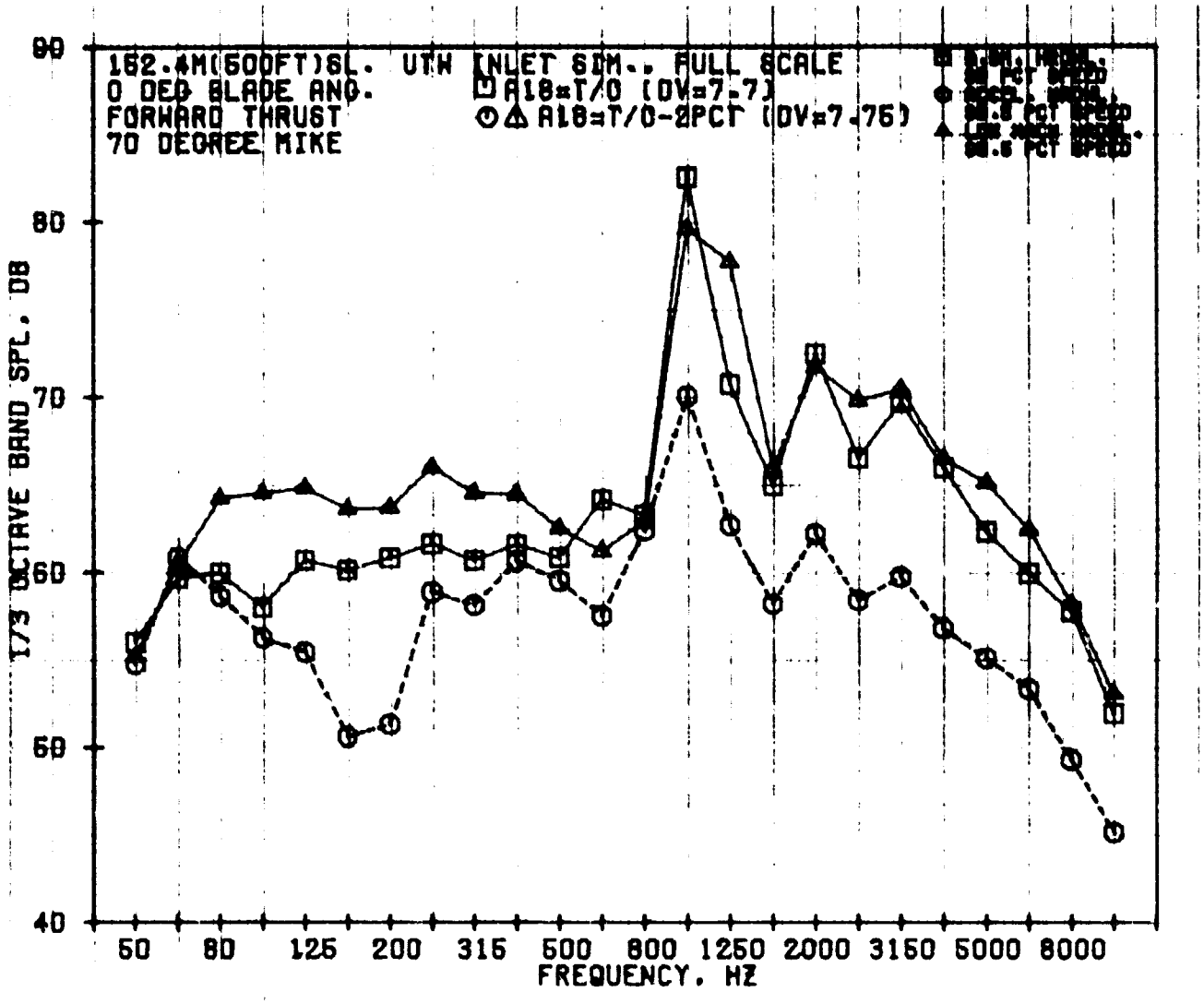

Figure 127. Forward-Thrust, 1/3-Octave-Band, SPL Spectra - Baseline Bellmouth, Accelerating Hard-Wall, and Low Mach Hard-Wall Inlets at 98.5% N_{FC}; 70° to Inlet.

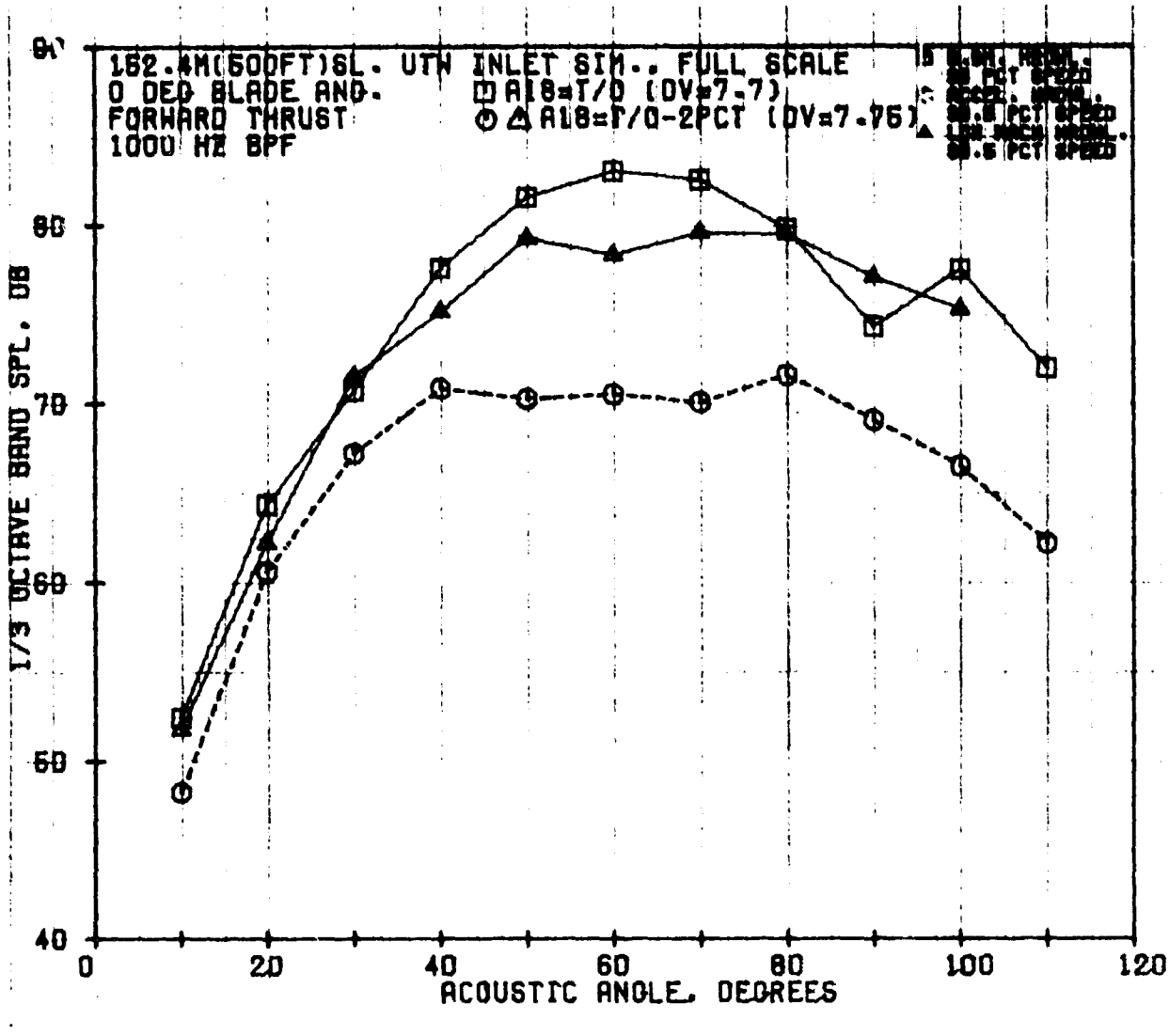

Figure 128. Forward-Thrust, 1/3-Octave-Band, SPL Directivity of Blade Passing Frequency - Baseline Bellmouth, Accelerating Hard-Wall, and Low Mach Hard-Wall Inlets at 98.5% N_{FC}.

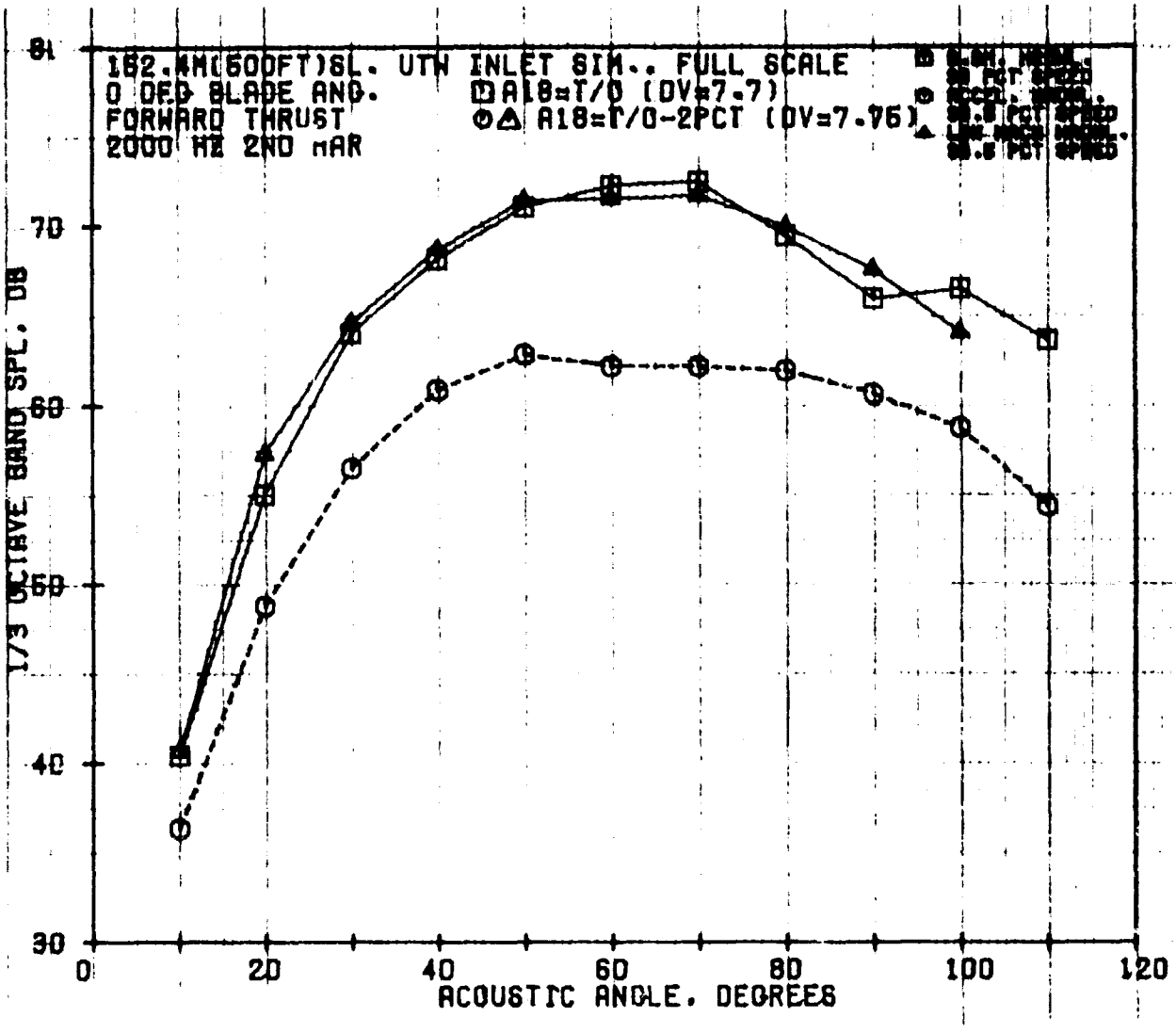

Figure 129. Forward-Thrust, 1/3-Octave-Band, SPL Directivity of Second Harmonic - Baseline Bellmouth, Accelerating Hard-Wall, and Low Mach Hard-Wall Inlets at 98.5% N_{FC}.

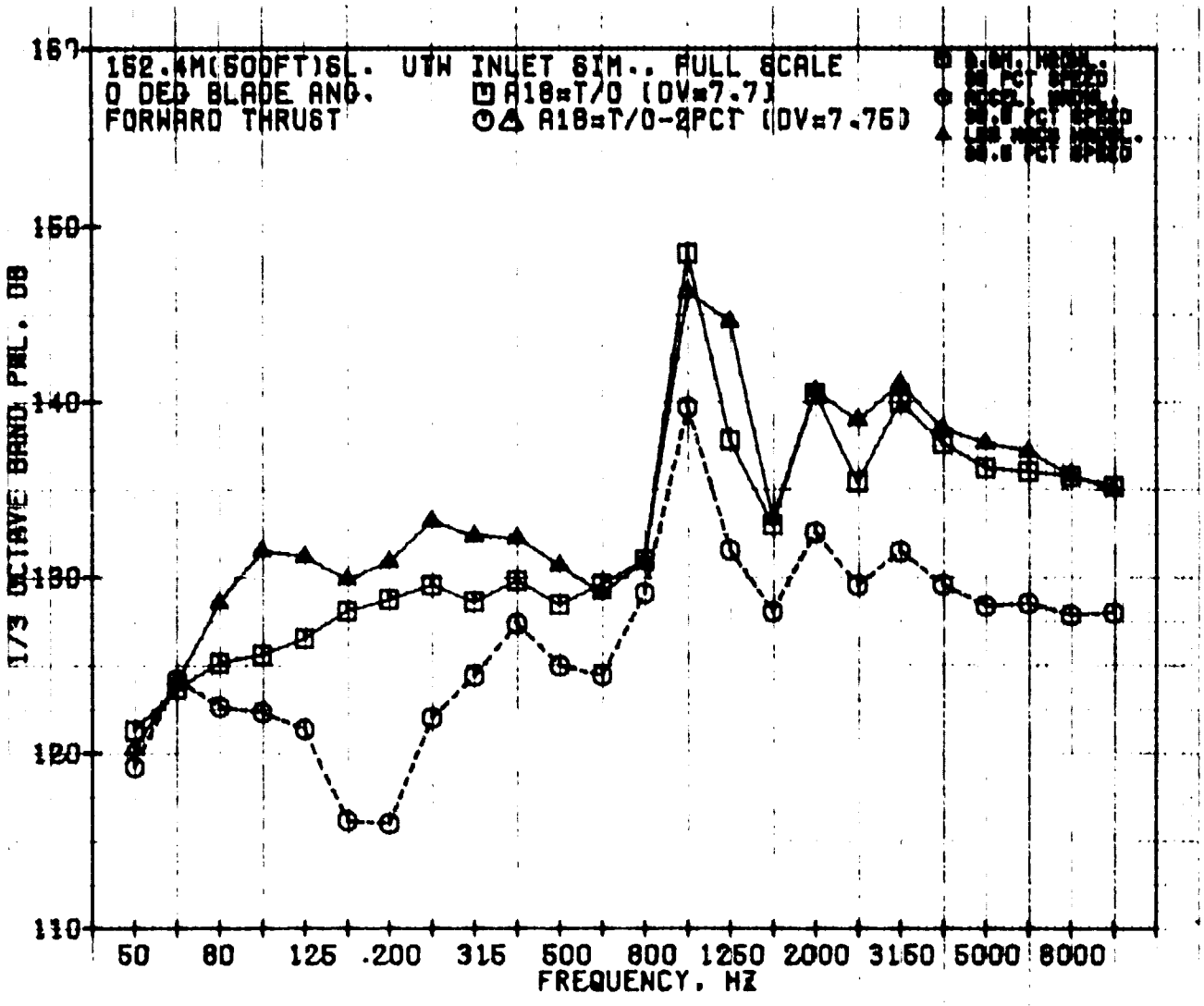

Figure 130. Forward-Thrust, 1/3-Octave-Band, PWL Spectra - Baseline Bellmouth, Accelerating Hard-Wall, and Low Mach Hard-Wall Inlets at 98.5% N_{FC}.

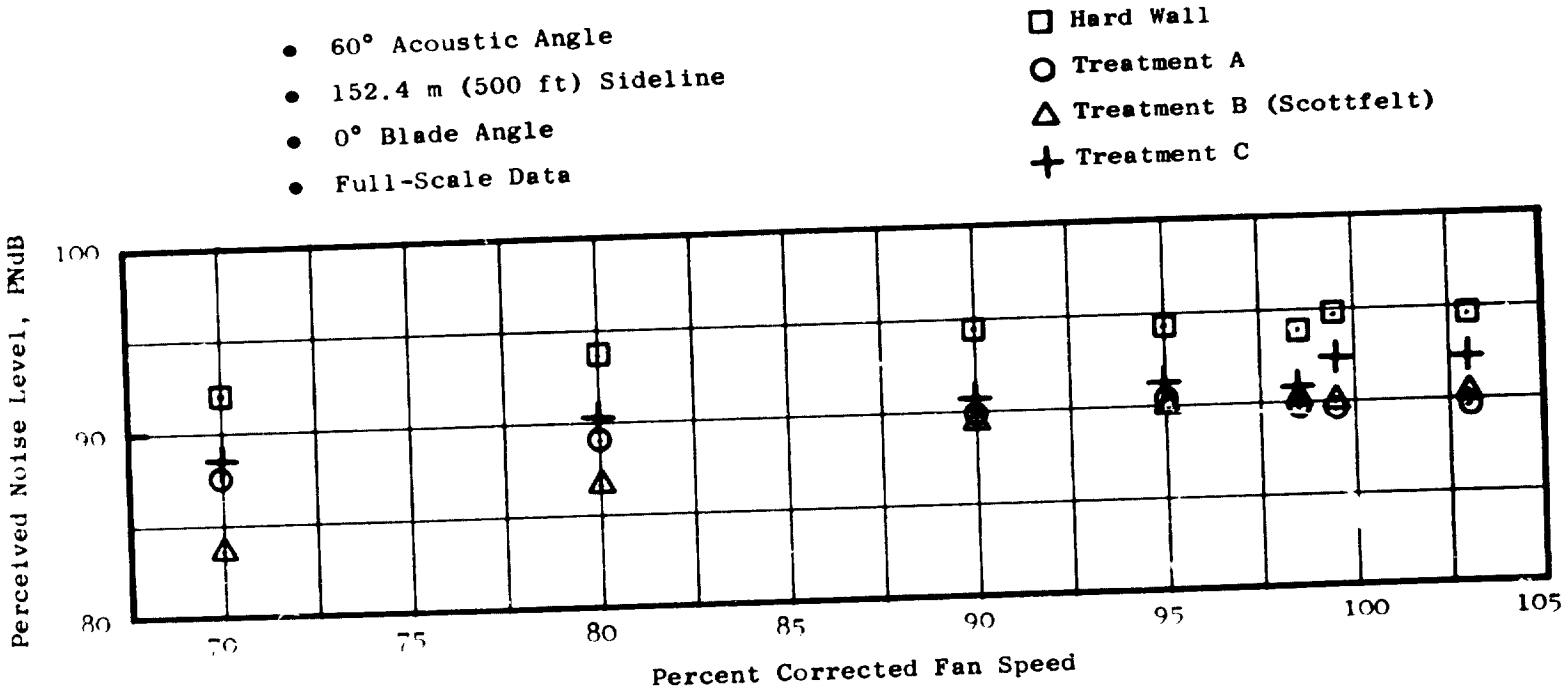

Figure 131. Forward-Thrust PNL Vs. Fan Speed - All Low Mach Inlets.

The bulk-absorber inlet treatment is seen to give significantly more suppression than the two resonator treatments at the 70% and 80% speed points. At 70% N_{FC} the bulk absorber, treatment B, gives about 8.5 PNdB suppression relative to the hard-wall inlet. Treatments A and C give about 4 dB at this fan speed. At the higher fan-speed points, 90% to 100%, the advantage of the bulk absorber relative to the resonator-type configurations decreases, and the level of suppression for inlet B is reduced to about 4.5 PNdB at the 95% fan speed. Thus the bulk-absorber, inlet-suppression performance decreases for increasing fan speed while the suppression level for the other two inlets is less influenced by fan speed.

The hard-wall and the suppressed-inlet noise levels in PNL versus acoustic angle are given in Figure 132 for 70% speed. The hard-wall level peaks at 60°. Treatments A and C also peak at 60°, but for treatment B the peak is shifted to 50°. The suppression is rather constant for angles of 60° and greater, but it decreases for lower acoustic angles. At 20°, inlets A and C show no suppression, whereas inlet B gives about 3 PNdB reduction.

Figures 133 through 135 show the hard-wall and suppressed spectra for acoustic angles of 50°, 60°, and 70° for 70% fan speed. The treatment B suppressed level is lower than the other inlet levels at all the 1/3-octave-band frequencies; thus, increased tone and broadband suppression is indicated relative to the resonator treatments. The maximum tone suppression occurs at the second fan harmonic; 12 dB is measured. Suppression at the fan fundamental tone is 8 dB.

In comparing the two resonator-treatment inlets, A and C, the spectral data indicate that inlet A, with the 10% faceplate porosity, gives much higher suppression at most of the 1/3-octave-band frequencies. The data at frequencies greater than 4000 Hz show that no suppression was measured for either inlet A or C and are seen not to be a function of acoustic angle.

Data for 98.5% fan speed are given in Figures 136 through 139. Figure 136 compares the hard-wall and the suppressed-inlet PNL directivities. The hard-wall and the suppressed directivity patterns are rather flat for angles of 50° to 70°; the unsuppressed and suppressed levels peak at 60°. Suppression level versus acoustic angle is constant for all the treated inlets at angles equal to or greater than 60°; however, for angles less than 60°, the suppression level decreases. This characteristic was also noted for the lower fan speeds discussed above.

Figures 137 through 139 give the hard-wall and suppressed spectra for angles of 50°, 60°, and 70°. Here the treatment B, as evaluated at the lower fan speed, gives more suppression at most of the 1/3-octave-band frequencies. At frequencies of 5000 Hz through 10000 Hz; however, no suppression is measured for any of the inlets.

Figures 140 through 143 are suppression spectra for all the treated inlets at fan speeds of 70%, 80%, 90%, and 99.5% respectively at an acoustic

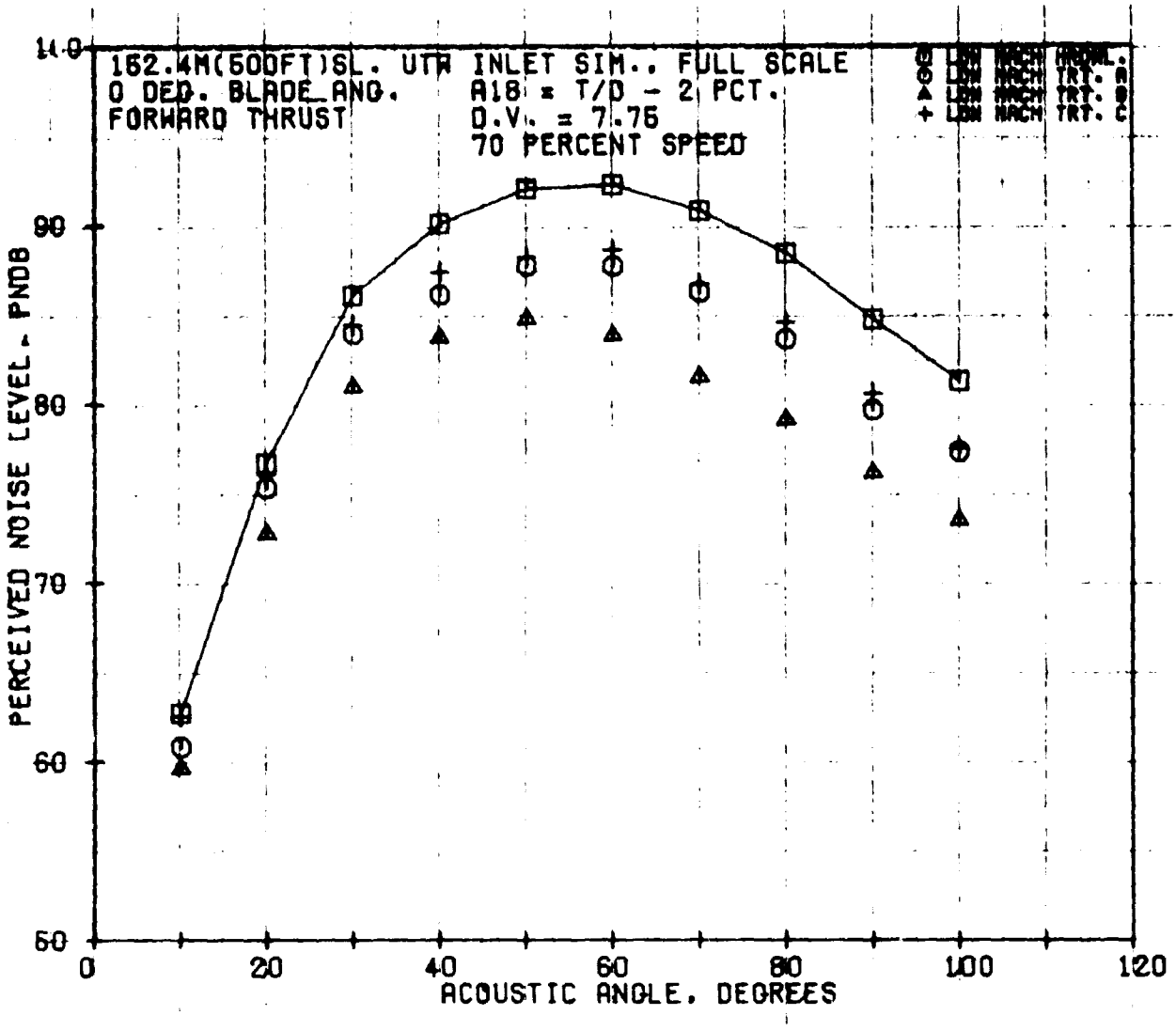

Figure 132. Forward-Thrust, PNL Directivity - All Low Mach Inlets at 70% N_{FC}.

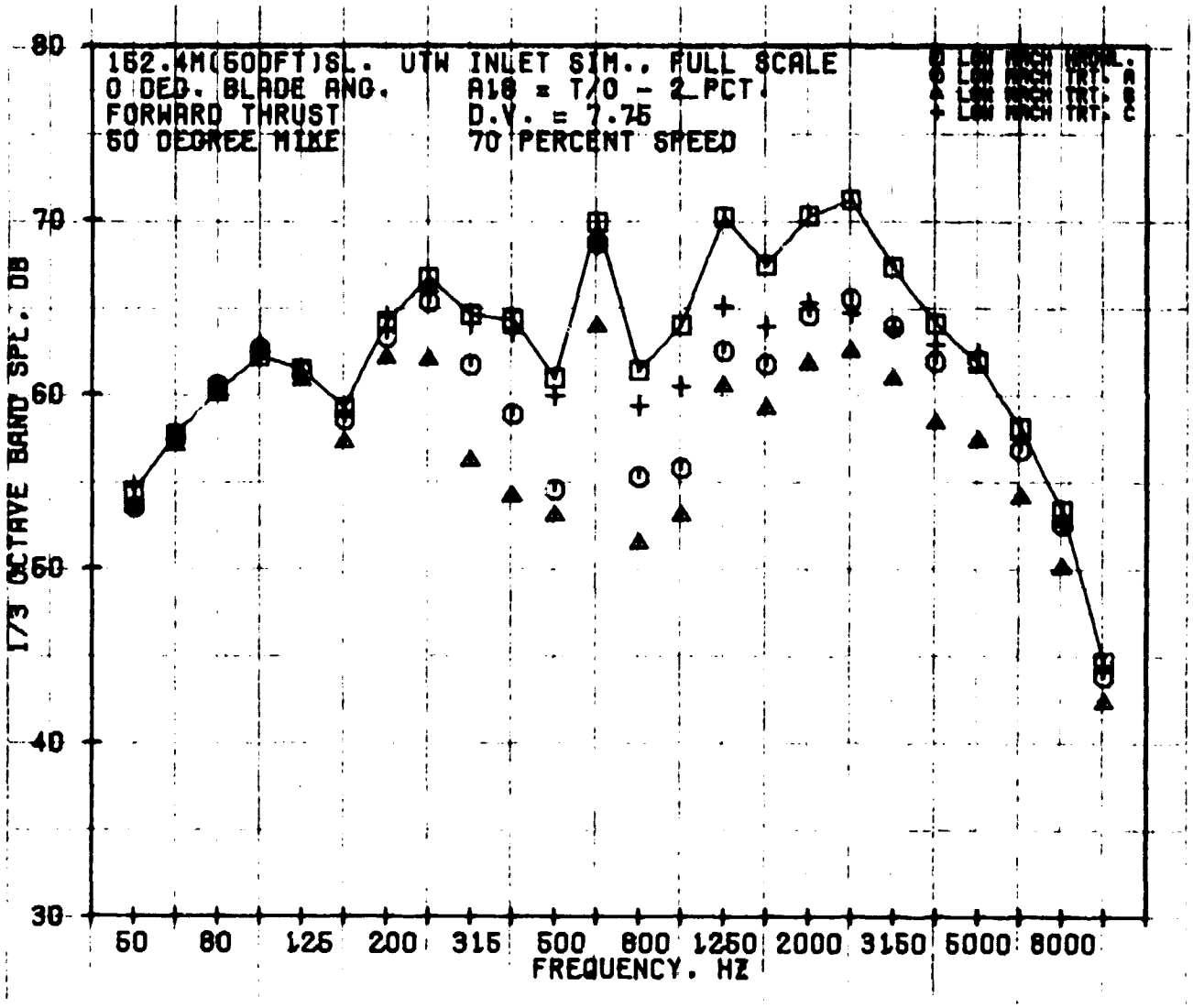

Figure 133. Forward-Thrust, 1/3-Octave-Band, SPL Spectra - All Low Mach Inlets at 70% N_{FC}; 50° to Inlet.

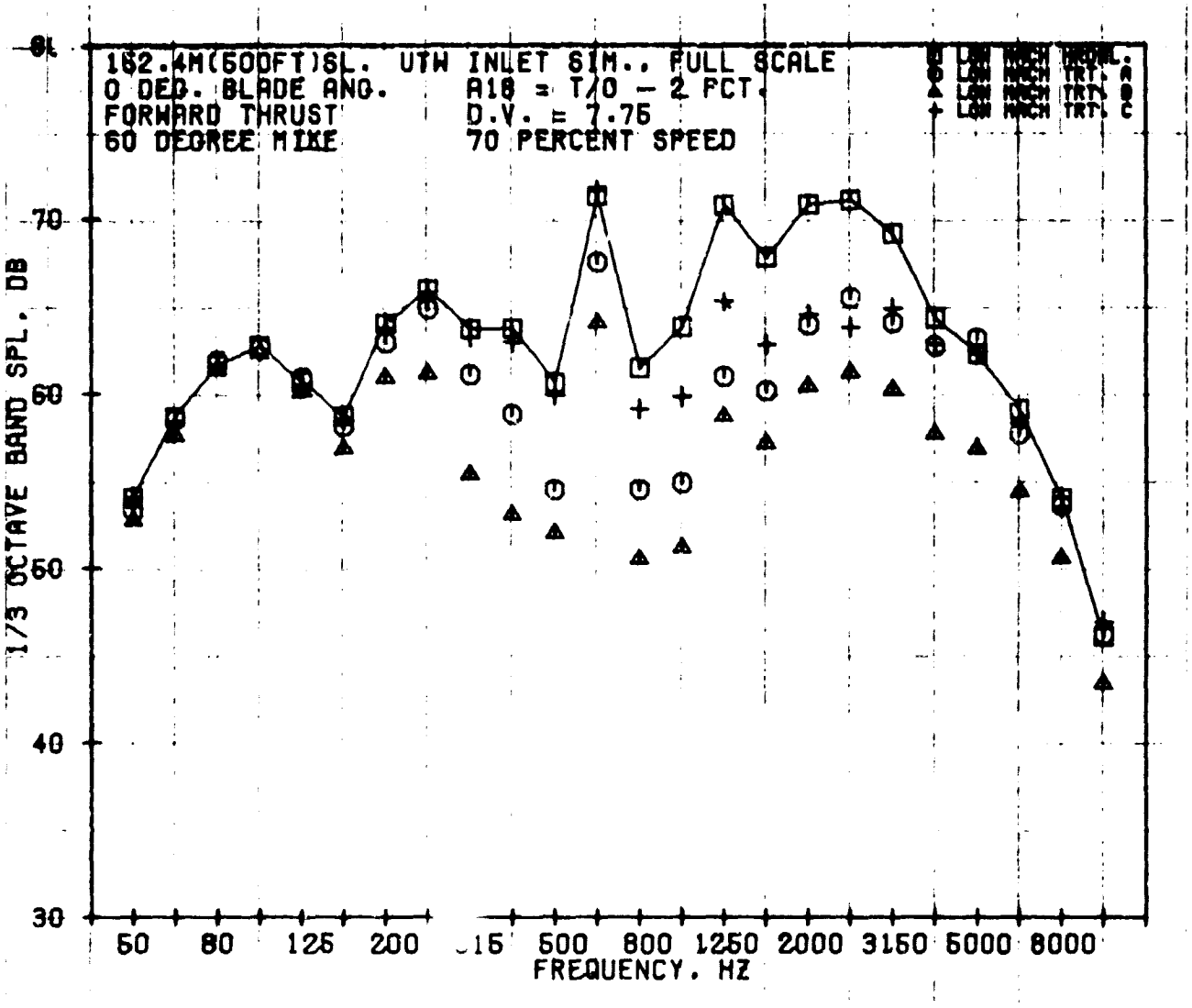

Figure 134. Forward-Thrust, 1/3-Octave-Band, SPL Spectra - All Low Mach Inlets at 70% N_{FC}; 60° to Inlet.

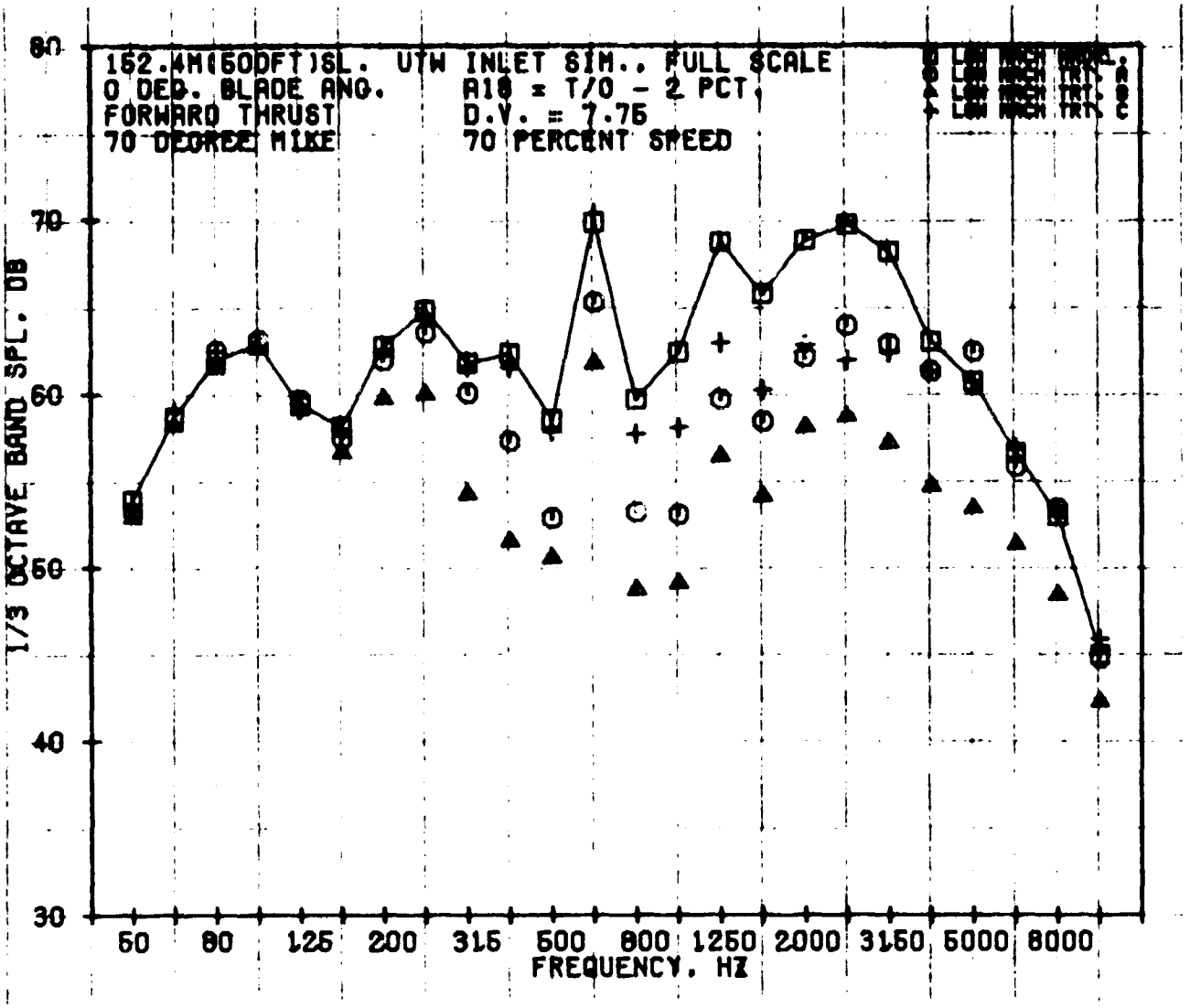

Figure 135. Forward-Thrust, 1/3-Octave-Band, SPL Spectra - All Low Mach Inlets at 70% N_{FC}; 70° to Inlet.

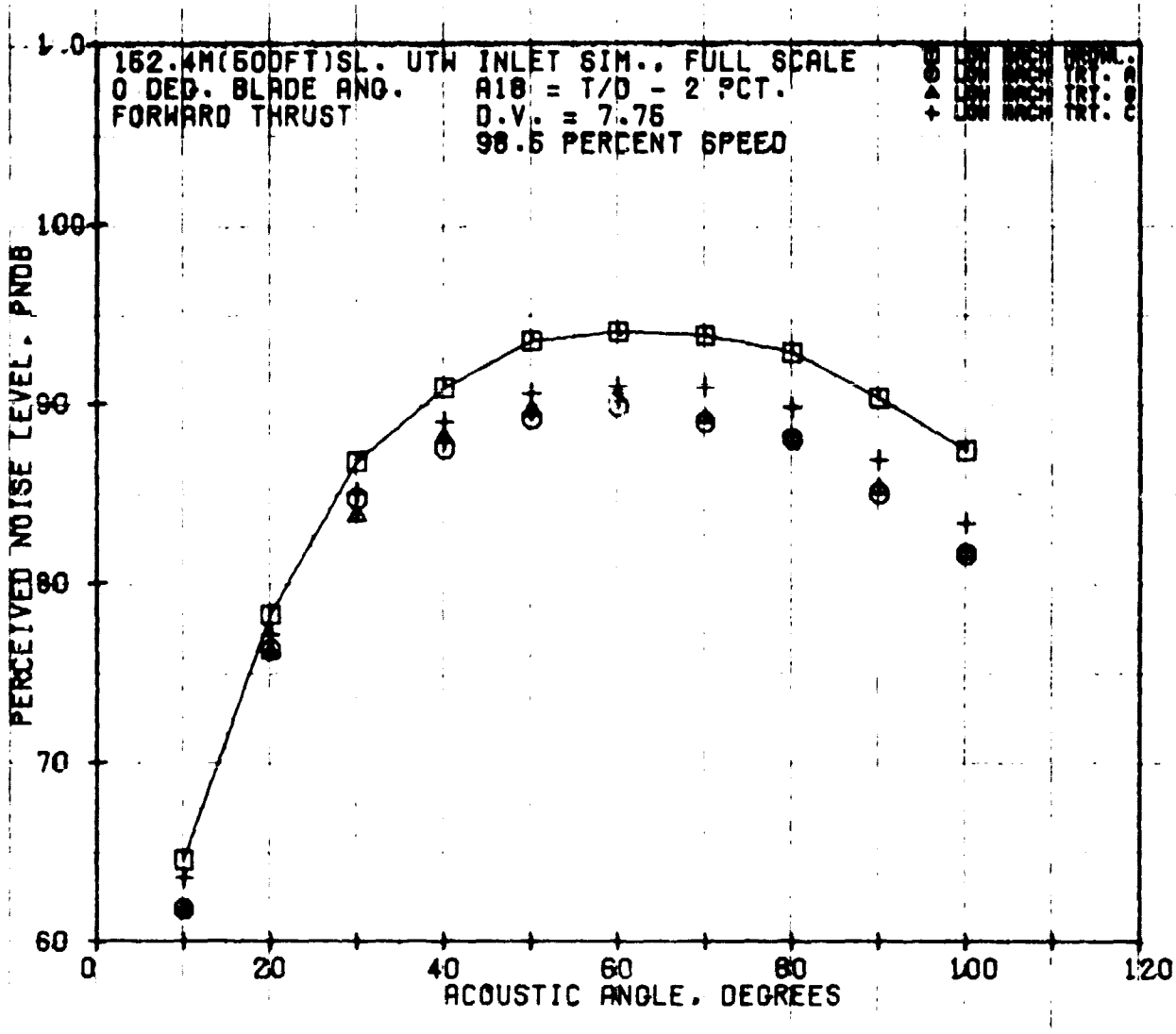

Figure 136. Forward-Thrust, PNL Directivity - All Low Mach Inlets at 98.5% N_{FC}.

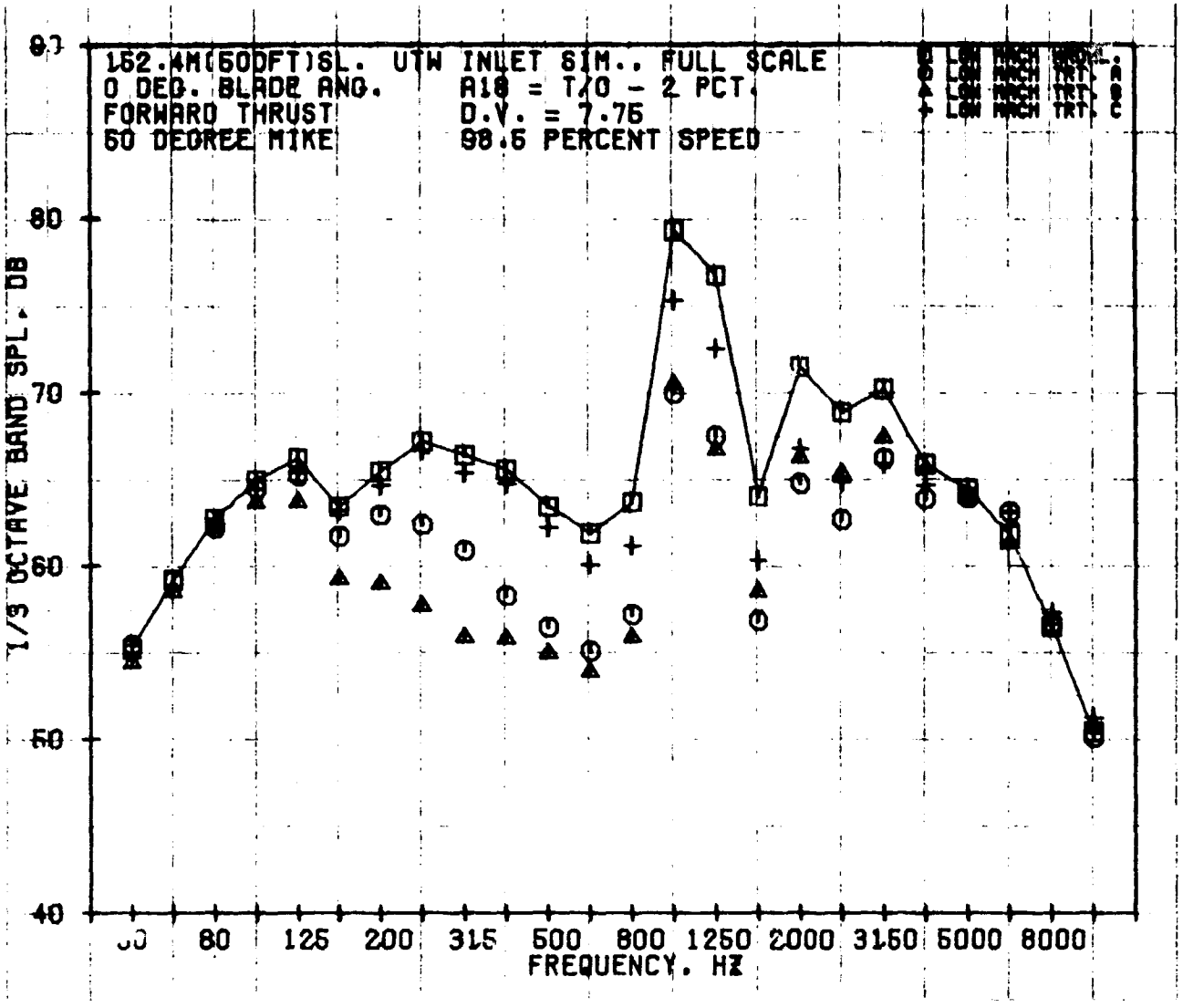

Figure 137. Forward-Thrust, 1/3-Octave-Band, SPL Spectra - All Low Mach Inlets at 98.5% N_{FC}; 50° to Inlet.

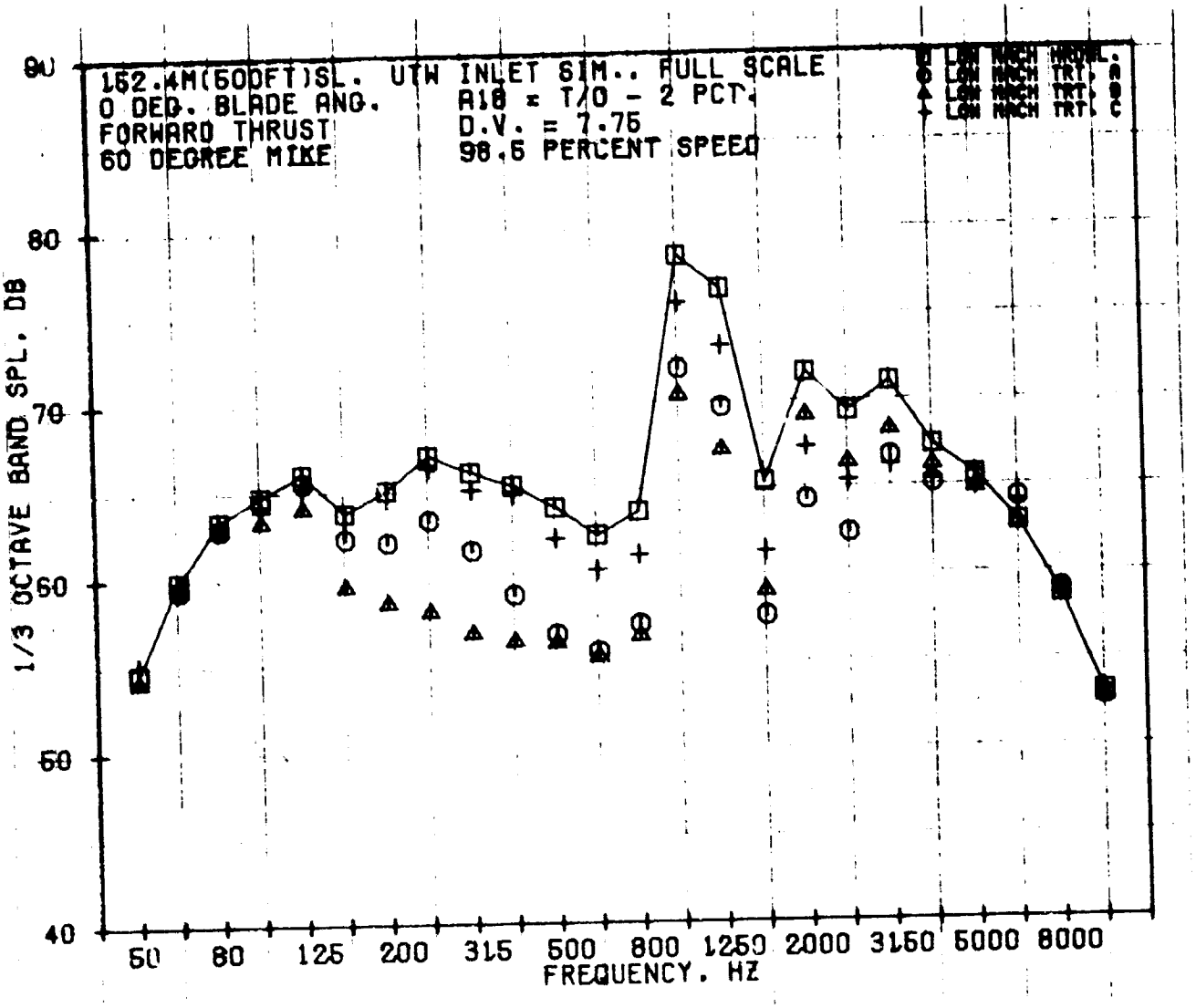

Figure 138. Forward-Thrust, 1/3-Octave-Band, SPL Spectra - All Low Mach Inlets at 98.5% N_{FC}; 60° to Inlet.

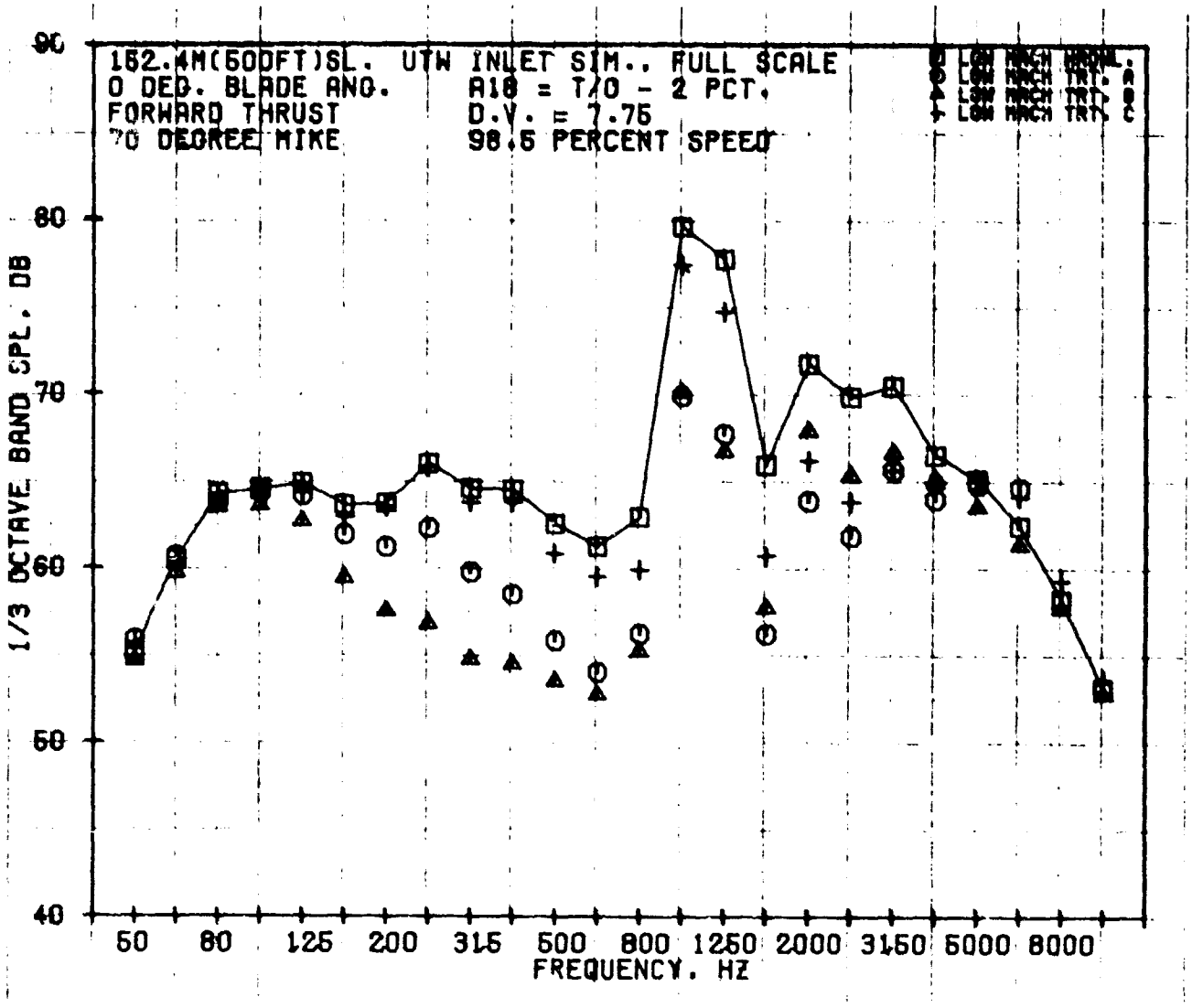

Figure 139. Forward-Thrust, 1/3-Octave-Band, SPL Spectra - All Low Mach Inlets at 98.5% N_{FC}; 70° to Inlet.

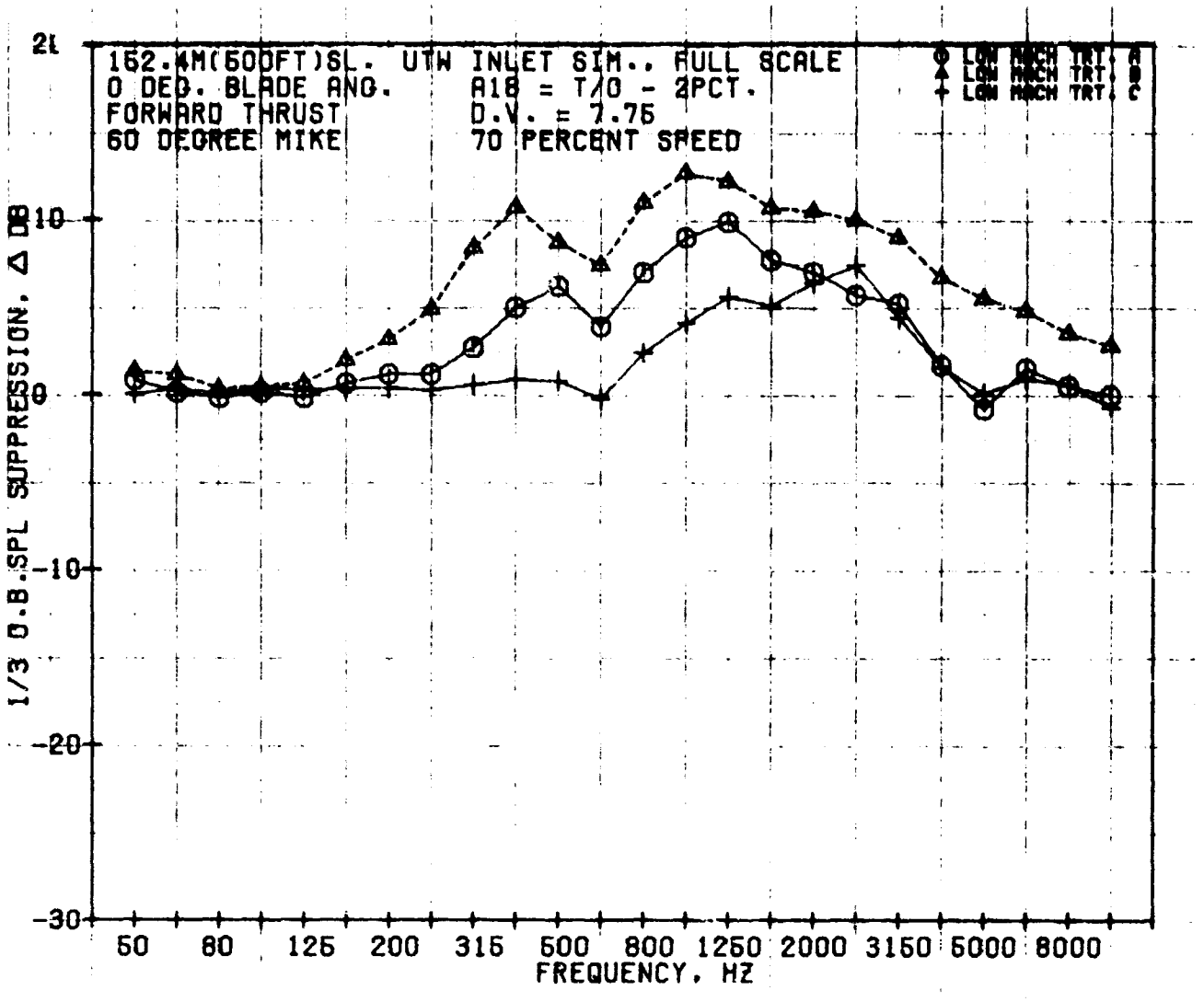

Figure 140. Forward-Thrust, 1/3-Octave-Band, SPL Suppression Spectra - Low Mach Inlet Treatments A, B, and C at 70% N_{FC}.

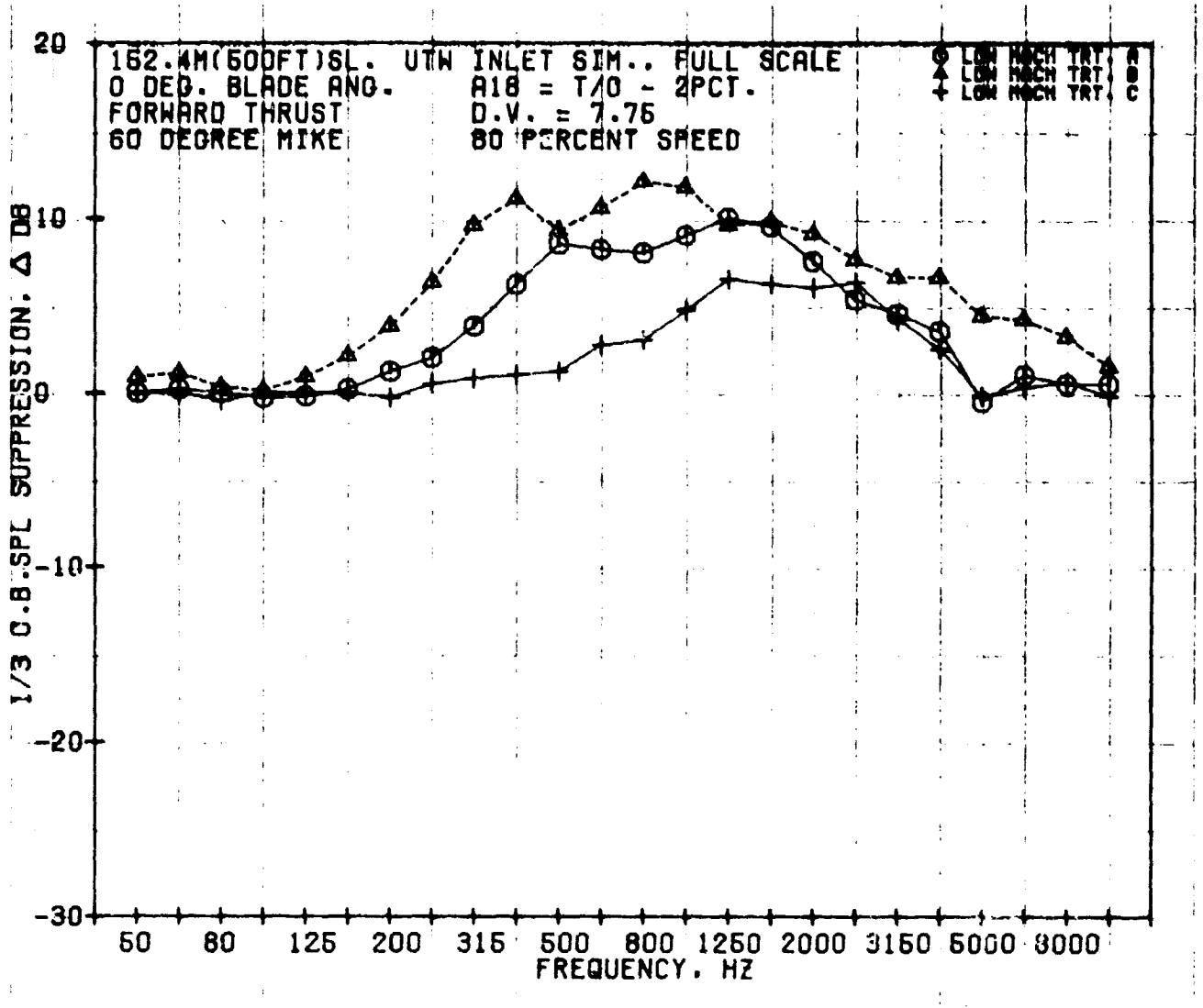

Figure 141. Forward-Thrust, 1/3-Octave-Band, SPL Suppression Spectra - Low Mach Inlet Treatments A, B, and C at 80% N_{FC}.

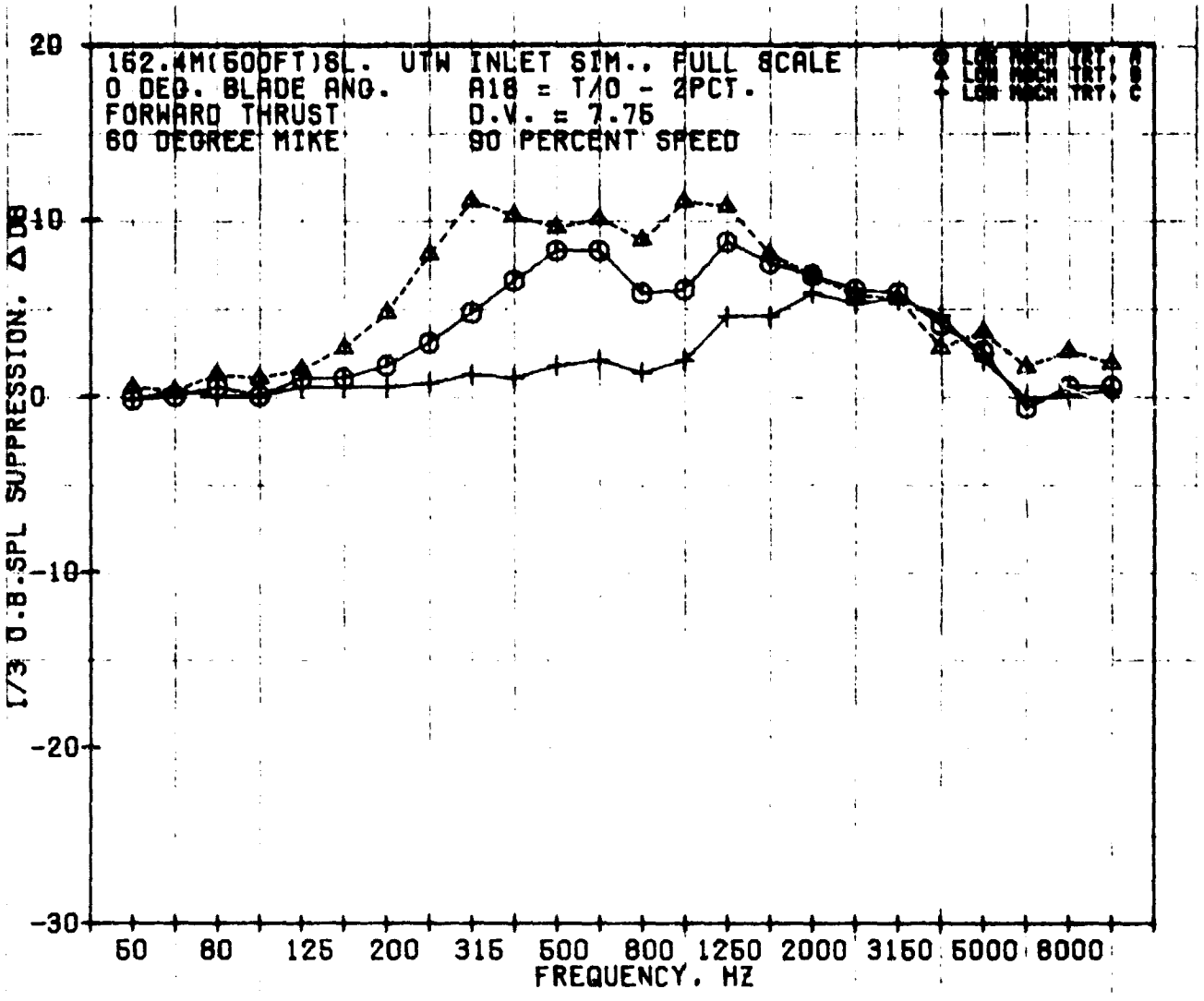

Figure 142. Forward-Thrust, 1/3-Octave-Band, SPL Suppression Spectra - Low Mach Inlet Treatments A, B, and C at 90% N_{FC}.

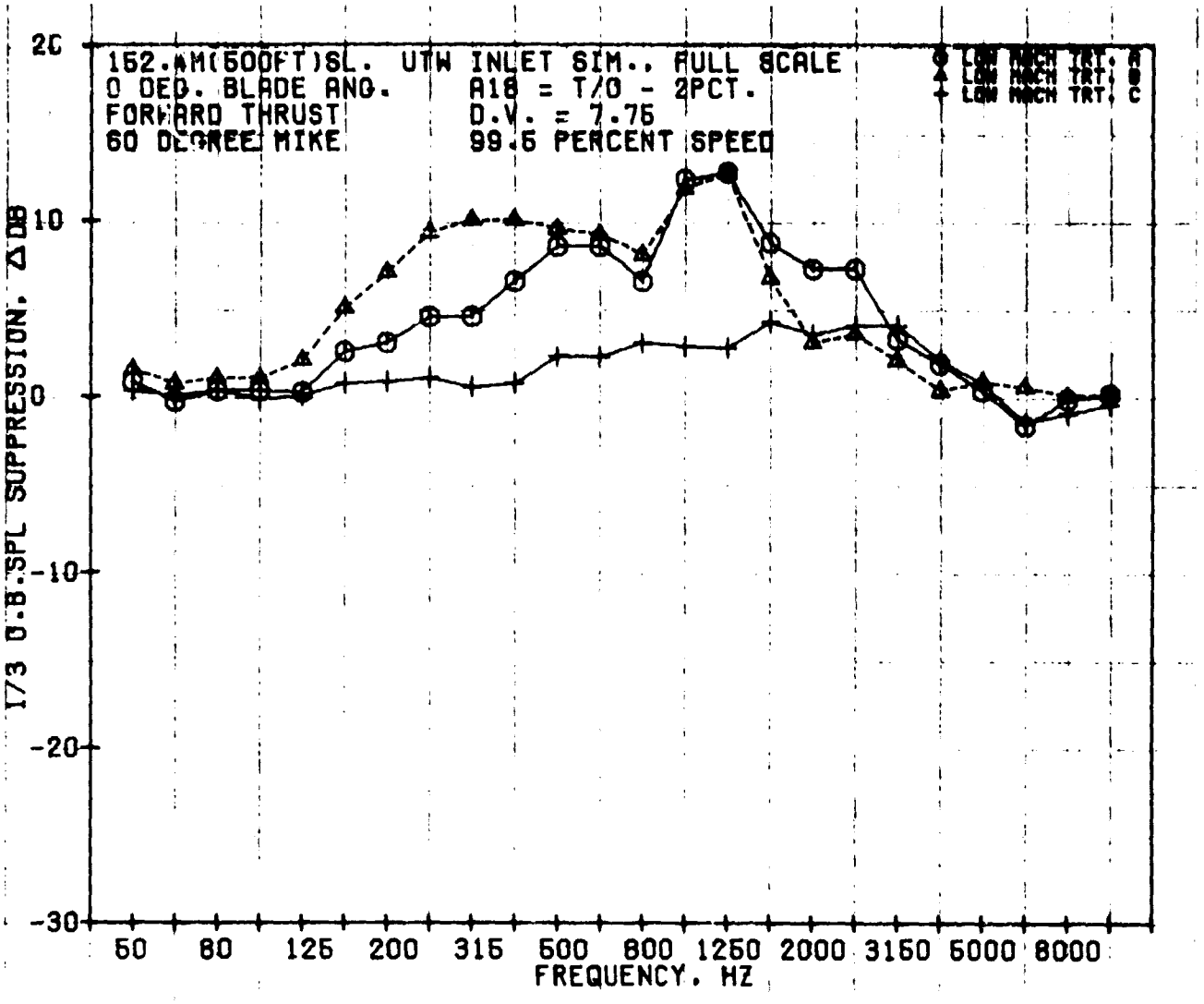

Figure 143. Forward-Thrust, 1/3-Octave-Band, SPL Suppression Spectra - Low Mach Inlet Treatments A, B, and C at 99.5% N_{FC}.

angle of 60°. As seen in earlier comparisons, the inlet B treatment has the highest suppression levels. However, at the 99.5% fan speed point in Figure 143, the peak suppression for inlet A is equal to that measured for inlet B.

Comparing inlet A suppression with fan speed shows that as the fan speed increases so does the peak suppression. Peak suppression for inlet B, on the other hand, stays constant, and for inlet C it decreases.

Figures 142 and 143 both show the poor high-frequency suppression performance for all the inlets at 90% and 99.5% fan speeds. This trend in suppression is rather unusual and certainly unexpected from the bulk-absorber inlet configuration.

9.4 APPROACH-CONDITION ANALYSIS

To evaluate inlet-noise levels of the UTW engine for the approach condition, acoustic tests with the UTW simulator were conducted at 0° and +5° (closed) blade-angle settings with the baseline bellmouth and the accelerating inlet B. The approach condition was defined as 65% of takeoff thrust; this could be achieved at several combinations of fan pressure ratio, weight flow, fan speed, rotor-pitch setting, and nozzle areas. A constant-thrust line can be established as a function of pressure ratio and weight flow on the fan map. At a given pressure ratio, flow, and area condition, a speed/blade-angle combination can be selected. To reduce engine response time under conditions where quick thrust changes are desirable, it is considered good operating technique to keep the engine rpm high. This can be accomplished with a variable-pitch fan by selecting a closed rotor-pitch setting at a higher speed and maintaining constant approach thrust. From an acoustic standpoint, it is important to determine the influence of higher speed and closed rotor-blade-angle setting on the inlet-radiated noise, both unsuppressed and suppressed. With this objective in mind, a wide range of DV/speed conditions was chosen at 0° and +5° blade-angle settings to bracket constant-thrust approach conditions.

For the several nozzle areas and the two blade angles chosen for the tests, 0° and +5°, the cycle deck - revised in light of the aerodynamic results of Reference 2 - was used to obtain the fan speed needed to provide the required approach thrust. The relationship thus obtained between nozzle area, fan speed, and rotor-pitch setting at the constant-thrust approach condition is plotted in Figure 144. This is valid for both inlets. Figure 145 shows plots of scaled, 152.4-m (500-ft) sideline, PNL versus percent fan speed at 0° and +5° pitch settings for the baseline bellmouth inlet at different nozzle areas at which acoustic tests were run. For each tested area, the required speed for approach thrust was obtained from Figure 144, and these constant-thrust points are shown in Figure 145. Figure 146 shows similar plots for the accelerating inlet B. Figure 146 between 90% and 100% speeds indicates the effect of an increase in throat Mach number on the suppression due to acceleration.

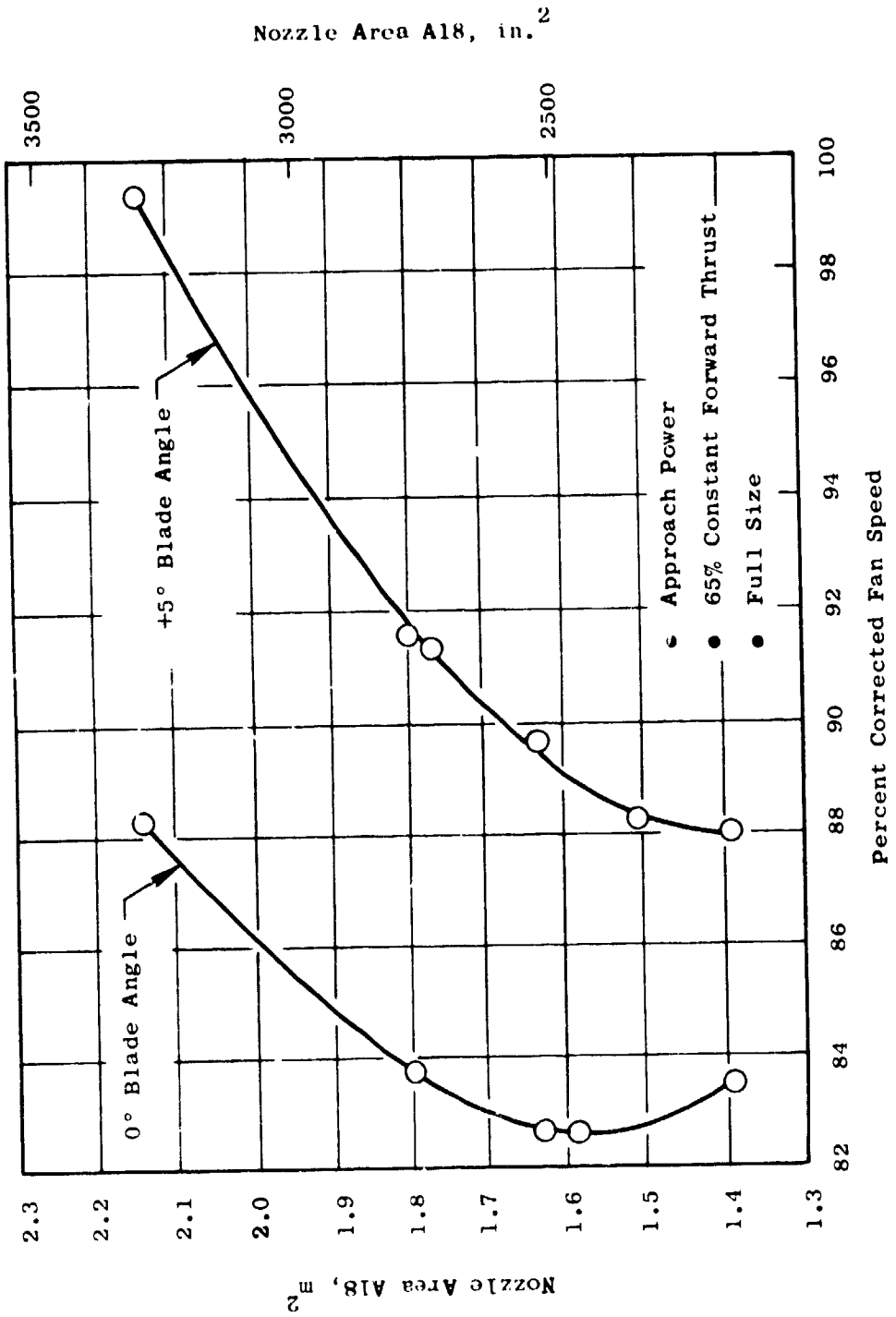

Figure 144. Nozzle Area Vs. Fan Speed at the Approach Thrust Condition.

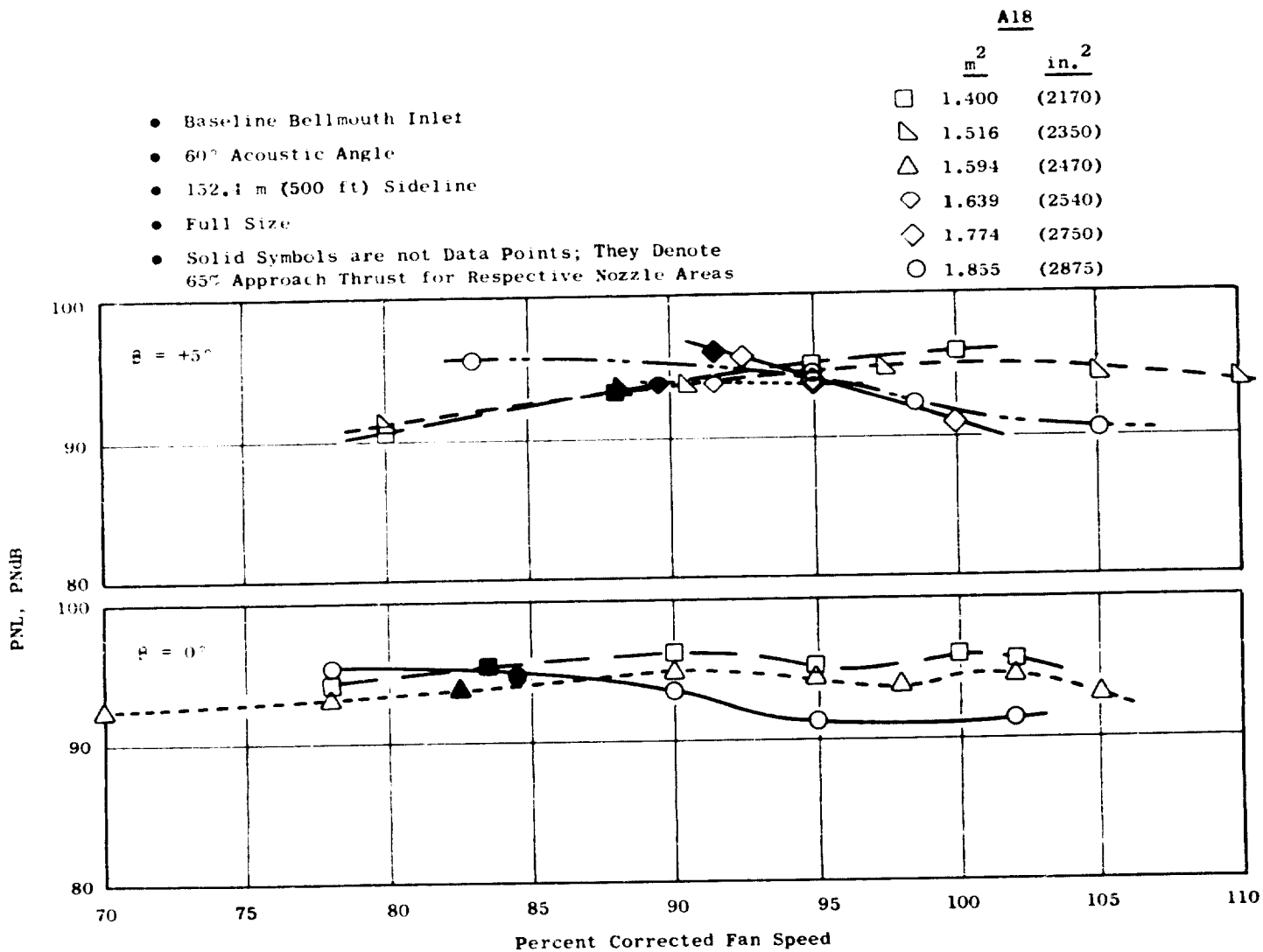

Figure 145. Baseline Bellmouth Inlet PNL Vs. Fan Speed.

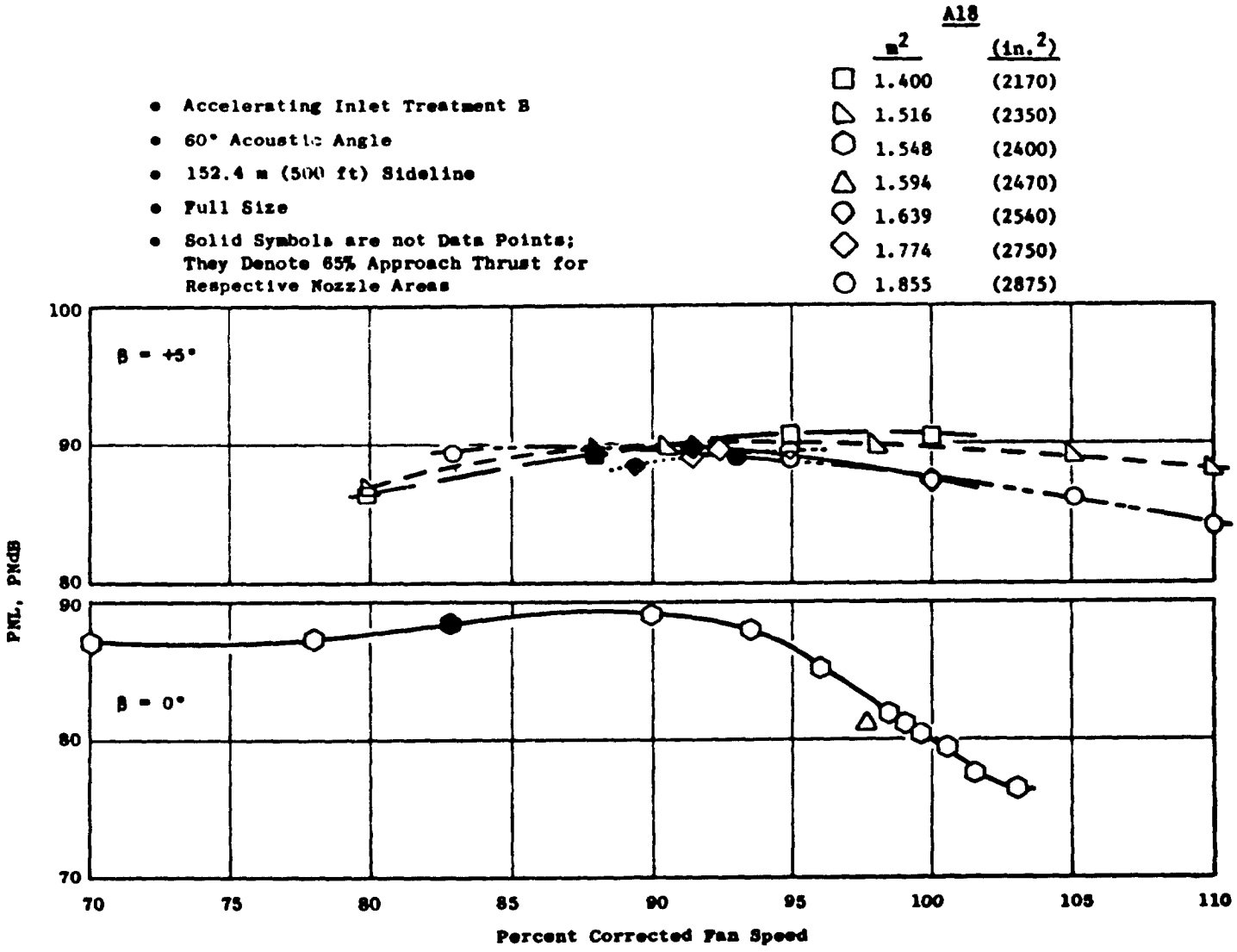

Figure 146. Accelerating Inlet Treatment B PNL Vs. Fan Speed.

In order to interpret these data at constant thrust, the PNL's from Figures 145 and 146 at the constant-thrust points are plotted against speed in Figure 147 and against nozzle area in Figure 148. With the bellmouth inlet there was a tendency for the noise to increase with speed both at 0° and at +5°. However, Figure 148 indicates that with the bellmouth inlet there is a minimal-noise area both at 0° and +5°. At +5°, a minimal-noise point is indicated at a low-speed/low-nozzle-area condition. With the accelerating inlet at +5° rotor pitch, a combination of treatment and acceleration suppression at higher speeds offsets the noise increase exhibited at higher speeds by the bellmouth inlet, resulting in a flat or nearly constant noise level along a constant-thrust-approach line. Even though only one point is available at 0°, it appears reasonable to predict that operation (with accelerating inlet B) between 0° and +5° along a constant-thrust-approach line would result in a PNL of 88.0 to 89.5 PNdB on a 152.4-m (500-ft) sideline. Thus, there is no optimum or low-noise point to select for approach with accelerating inlet B. From a systems standpoint, however, high-speed/open-nozzle operation is better because of lower jet/flap noise and better engine response.

9.5 RESULTS FROM SOUND-SEPARATION PROBE DATA

When acoustic measurements are made in ducts, a problem exists in discriminating between true noise and turbulence. A technique for separating the two noise sources has been developed and was demonstrated during this program. The technique incorporates a new type of probe referred to as a "sound-separation probe," rather than the standard waveguide probe, to acquire the data for the discrimination analysis. A description of the probe is given in the instrumentation section of this report.

The sound-separation probe was used during testing of the accelerating inlet with treatment B. Data were acquired at 90.5%, 92.5%, 98%, and 110% fan speeds at five immersions across the inlet just aft of the throat (as shown in Figure 17).

The first portion of the analysis involves determination of the spectra for the upstream sensor on the probe. The very narrowband (2.5 Hz) spectra, from 0 to 5000 Hz for the 90.5% and 98% fan speed conditions, is shown in Figures 149 and 150. There are two regions of the spectra that will be discussed with regard to the type of pressure fluctuations being measured. Those are the very low frequencies (0 to 300 Hz) and the frequency band from 500 to 5000 Hz. Note that the broadband level between 500 and 5000 Hz decreases and the tone levels at the very low frequencies remain about the same at all immersions. The discrimination analysis of the sound-separation-probe data will provide the explanation for these features in the spectra.

The acoustic discrimination technique described in Reference 12 computes the crosscorrelation between the signals from the two sensors on the probe. The result is a crosscorrelogram that has separate peaks for each of the components of the broadband signal. As discussed in Reference 12, there can be

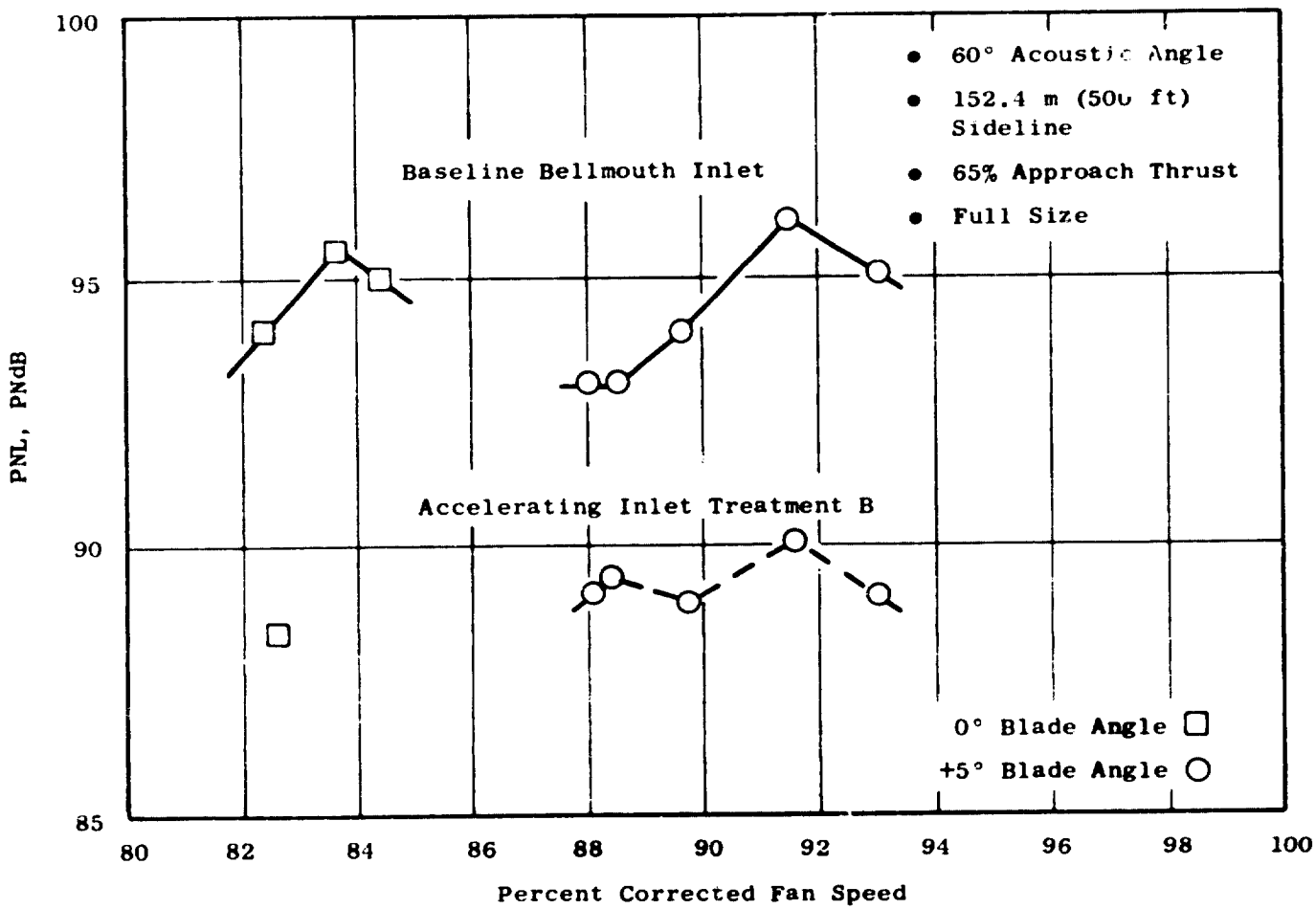

Figure 147. PNL Vs. Fan Speed at Constant-Thrust Approach.

- 60° Acoustic Angle
- 152.4 m (500 ft) Sideline
- 65% Approach Thrust
- Full Size

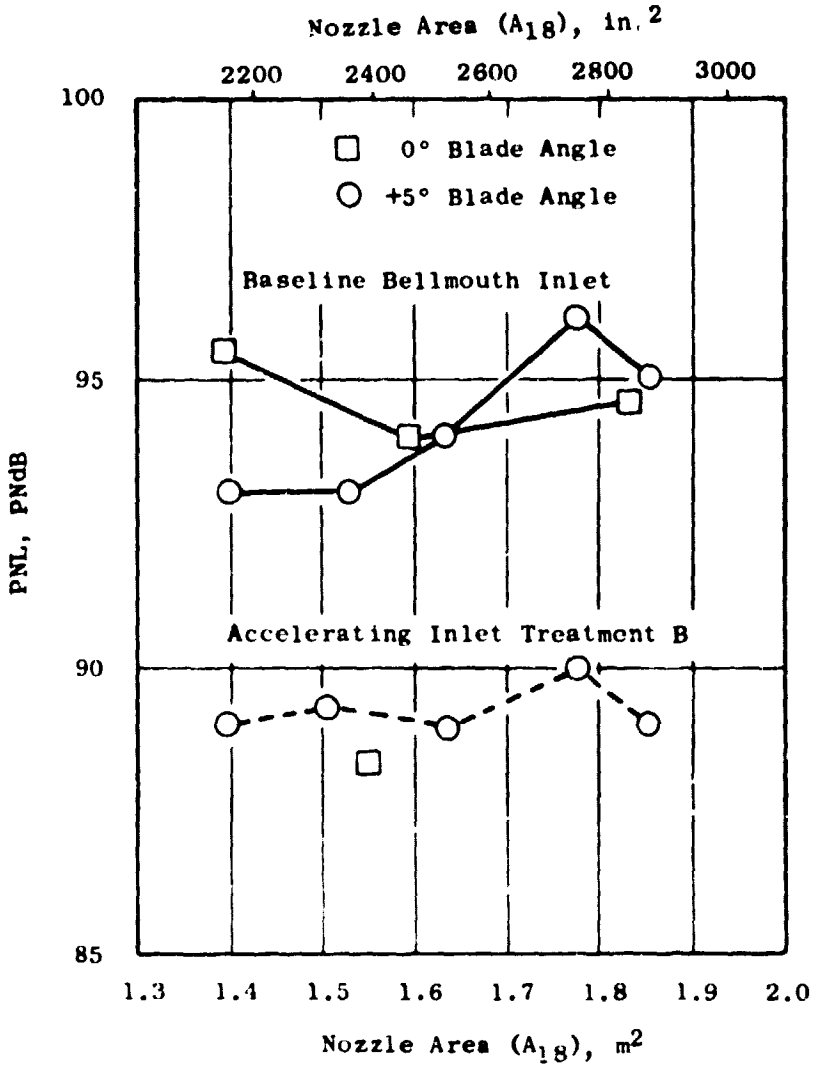

Figure 148. PNL Vs. Nozzle Area at Constant-Thrust Approach.

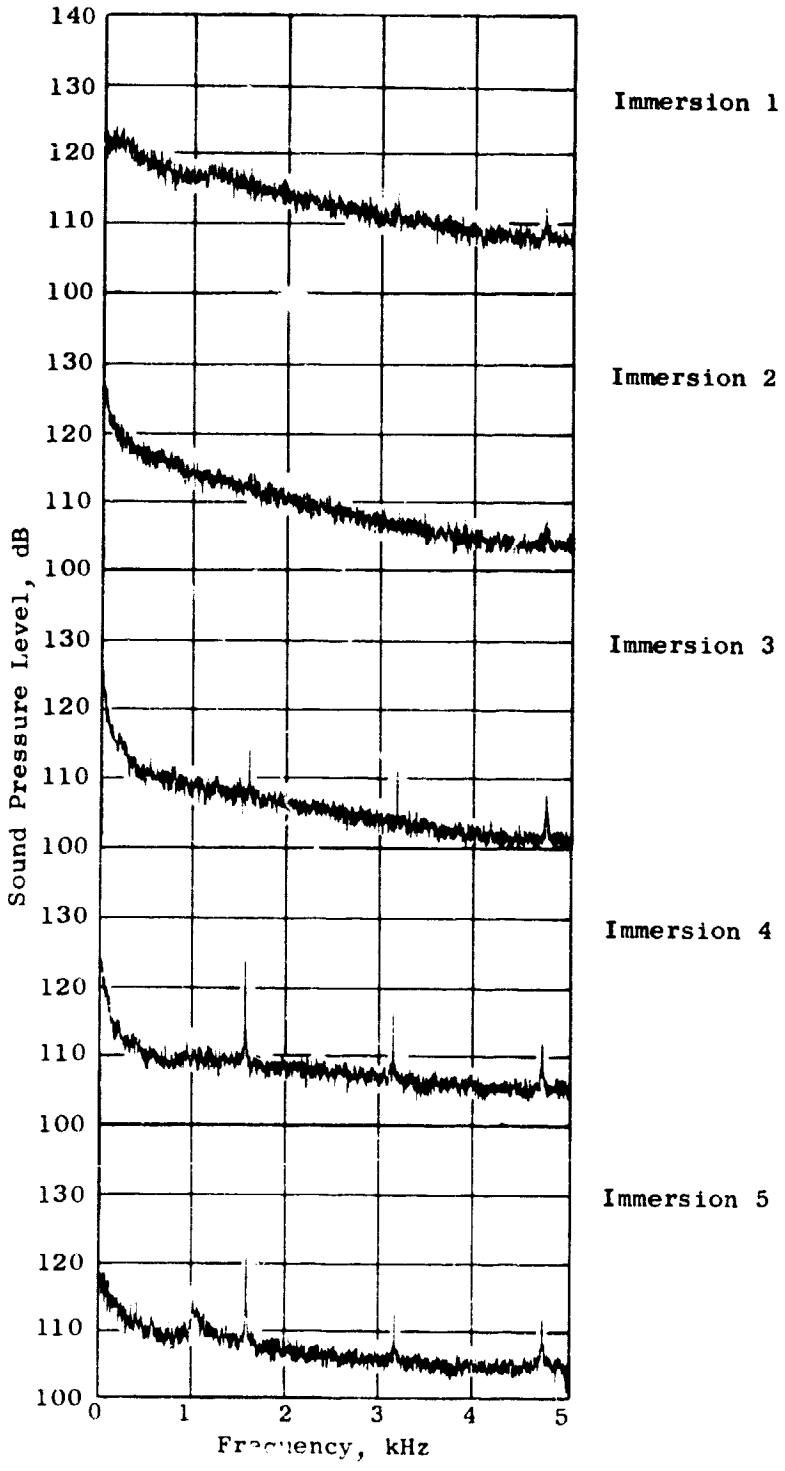

Figure 149. Narrowband (2.5 Hz) Spectra for Upstream Sensor at 90.5% Fan Speed.

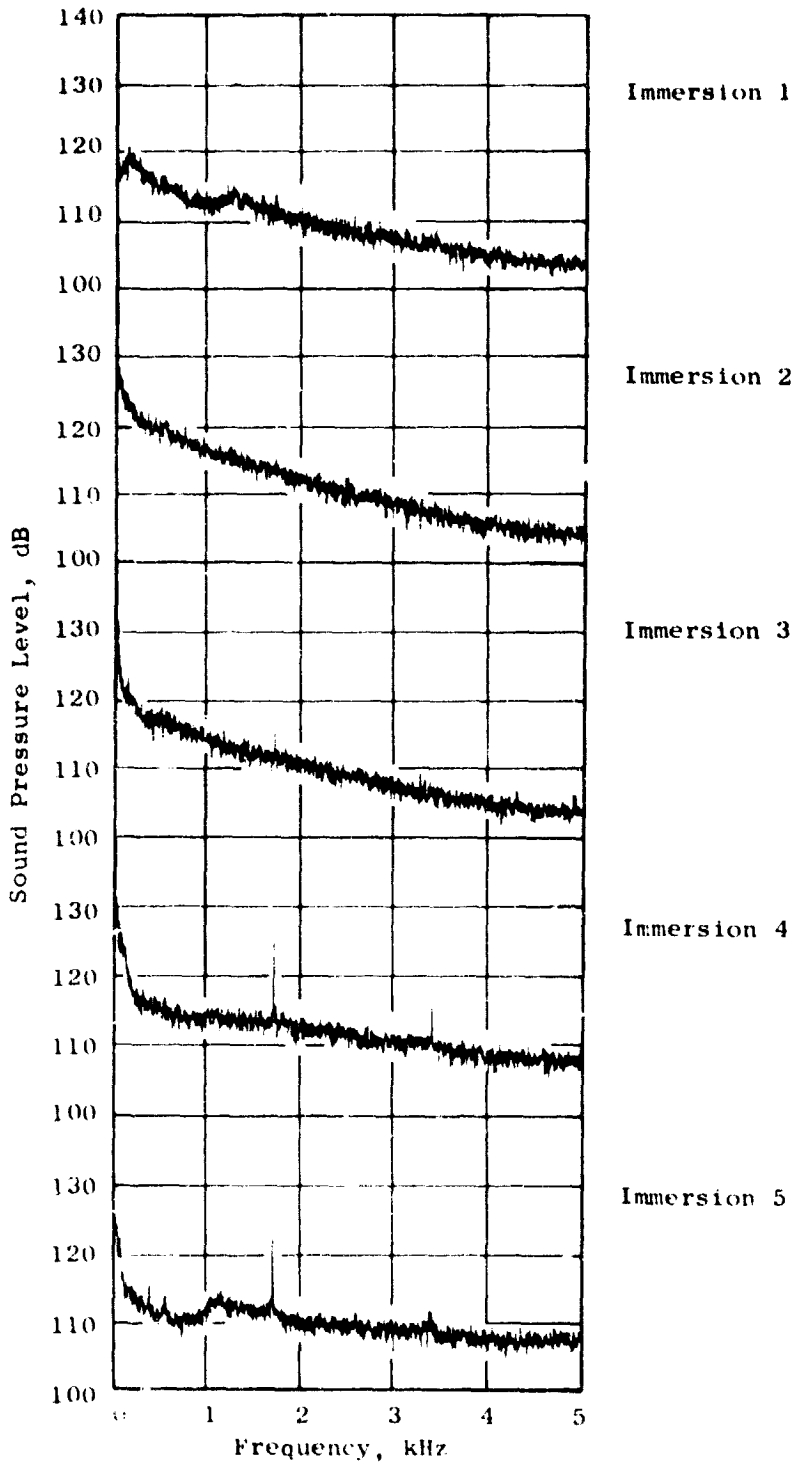

Figure 150. Crosscorrelograms for Sound Separation at 98% Fan Speed.

up to three peaks in the crosscorrelogram of the broadband signals. For measurements in the fan exhaust duct, the two peaks at positive time delay are due to sound and turbulence travelling with the flow; the peak at negative time delay is due to sound travelling against the flow. For measurements in the fan inlet duct there are only two peaks: one at positive time delay due to turbulence travelling with the flow, and one at negative time delay due to sound propagating upstream from the fan rotor.

Since the sound-separation analysis is only applicable to broadband, random signals, the tone levels must be removed prior to computation of the crosscorrelation so that the periodicity from the tones does not contaminate the crosscorrelograms. This is a relatively easy task involving modifying the cross-spectrum between the two probe-sensor signals prior to taking the Fourier transform to convert it to the crosscorrelation. It was demonstrated in Reference 12 that linear interpolation of the levels in the real (co) and imaginary (quad) parts of the cross-spectrum in the frequency range of the tones leaves only the broadband portion of the energy for transformation to the crosscorrelation.

The crosscorrelograms with the tones removed for the five immersions at 98% fan speed are shown in Figure 151. Note that the signal is predominatly sound for the outer three immersions indicated by the peak at $\tau \approx -0.0006$ sec. However, for the inner two immersions the buildup of turbulence in addition to sound becomes evident as indicted by the peak at $\tau \approx 0.0005$ sec. Also observed in the crosscorrelograms is the difference in the shape of the peak due to sound and that due to turbulence. Very sharp peaks in correlation functions indicate a broad band of random energy in the spectrum, and broad peaks indicate a relatively narrow band of energy in the spectrum.

The crosscorrelation information can now be used to determine which portions of the spectra are due to sound and which to turbulence. As indicated above, the sharp peak due to sound represents a very wide band of random noise. It is also safe to assume that the tones are due to blade interactions radiating forward in the inlet as sound. Therefore, the portion of the spectra shown in Figure 151 due to sound is the entire spectrum from the very low frequencies to 5000 Hz. This assumption is further supported by the fact that the peaks in the crosscorrelations due to turbulence indicate that a very narrow band of energy is present.

The crosscorrelogram also provides information about the relative, overall level of the two portions of the signal. At the outer three immersions the turbulence is much lower than the sound, as indicated by the lack of a peak at positive time delay. The turbulence in the inner immersions becomes equal in level to the scund, as indicted by the presence of nearly equal levels of the two peaks.

Using the above information, the separated spectra were constructed and are shown in Figure 152 for the five immersions at 98% fan speed. The turbulence spectrum is nearly constant for all five immersions. However, the

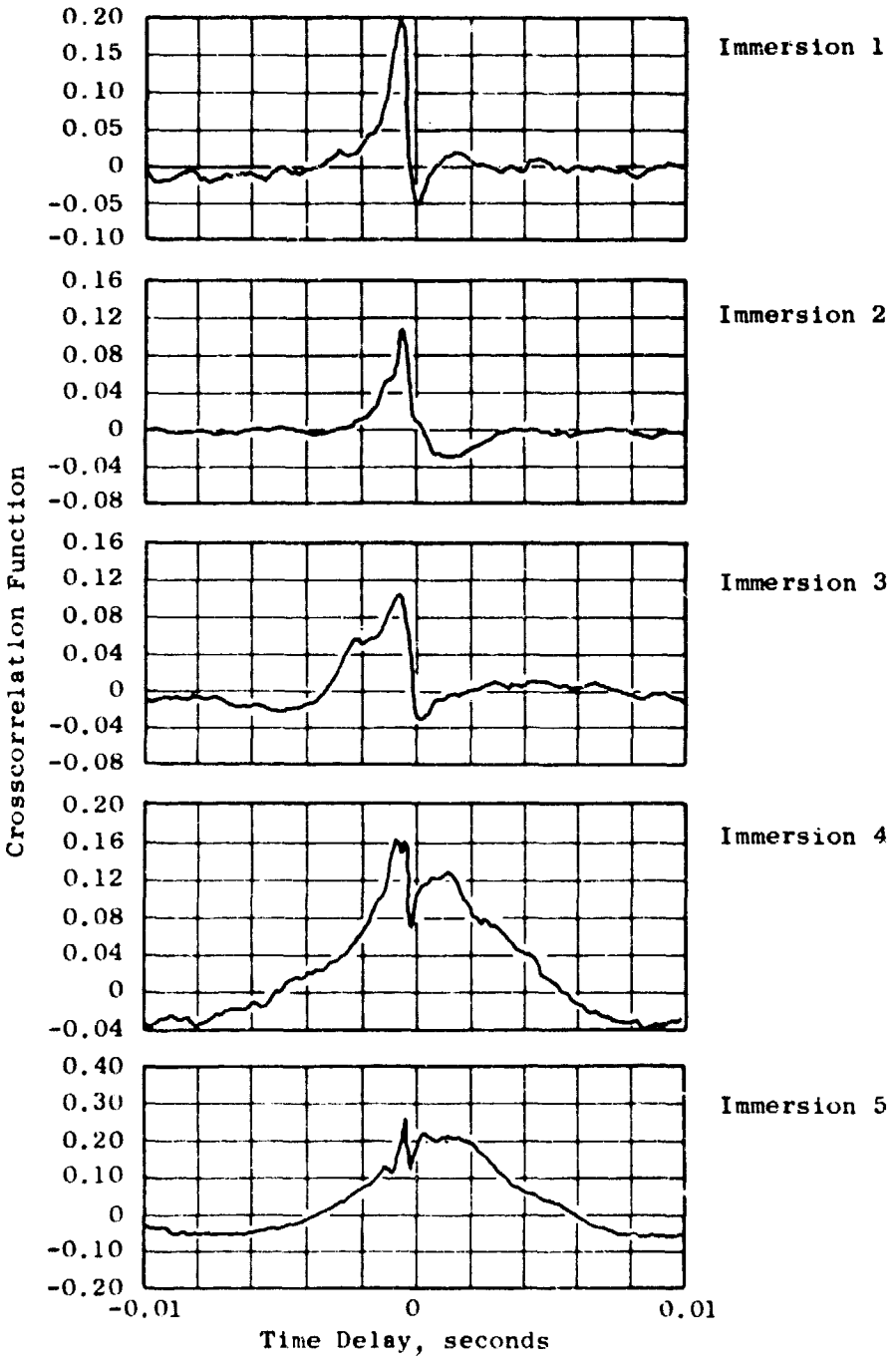

Figure 151. Narrowband (2.5 Hz) Spectra for Upstream Sensor at 98% Fan Speed.

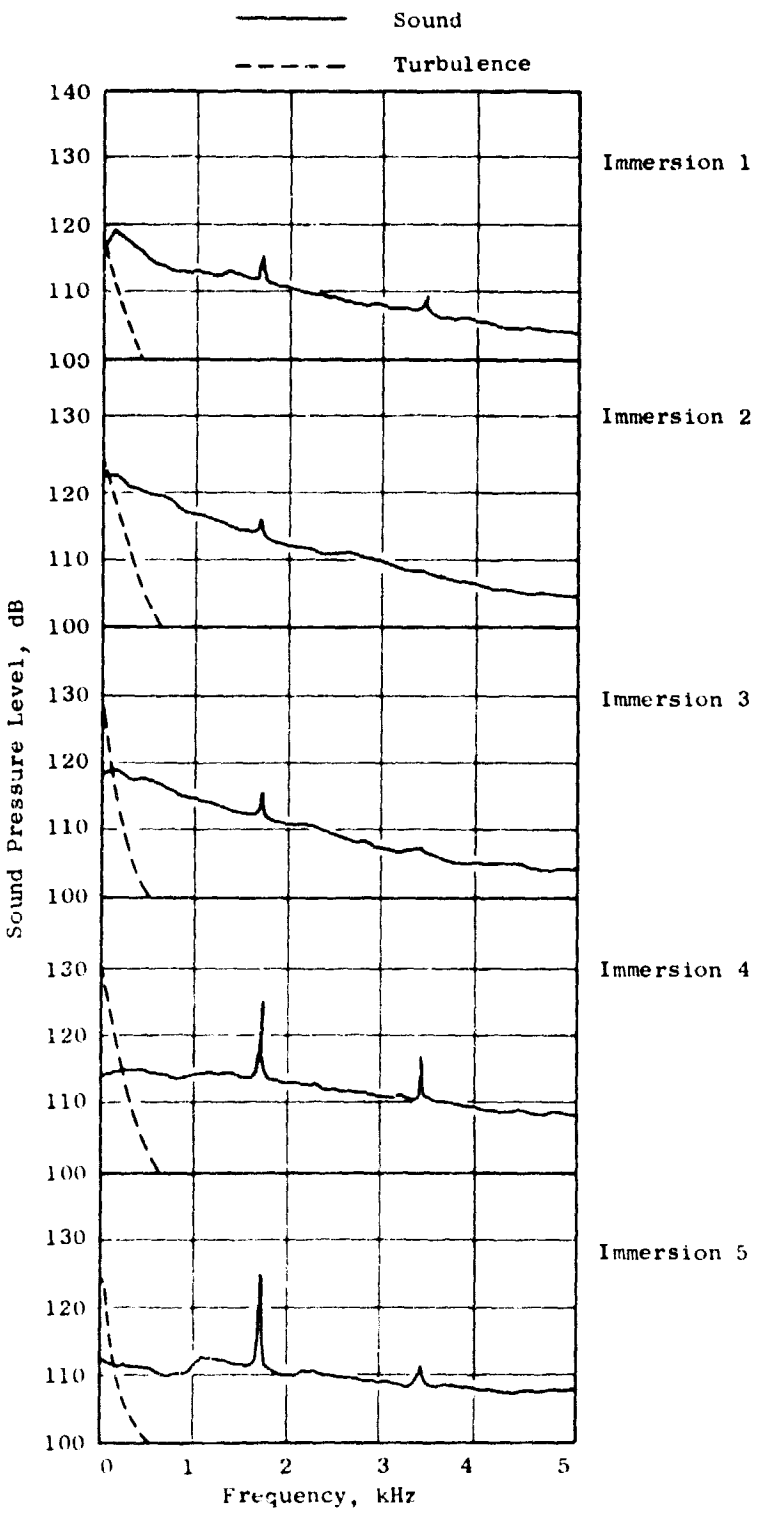

Figure 152. Sound and Turbulence Separated for 98% Fan Speed.

sound spectrum changes quite a bit in level and relative energy in tones compared to broadband. There is a decrease in the tone levels and an increase in broadband level near the outer wall of the duct.

The above results are examples of the added information provided by the sound-separation probe for the treated, accelerating inlet. Further data comparisons are not possible because the probe was not used on any other configuration during the tests. Another reason the sound-separation-probe results are limited in scope is the fact that a direct method for separating sound and turbulence into respective spectra is not completely developed. However, the use of the sound-separation probe in the inlet demonstrated the potential to be obtained from development of more advanced acoustic-measurement-analysis techniques.

10.0 REVERSE-THRUST RESULTS

Reverse-thrust testing was an important segment of the program both from aerodynamic and acoustic-performance points of view. From an aerodynamic standpoint, it was necessary to determine (1) whether the reverse-thrust objective (35% gross forward design thrust) was achievable at the selected reverse-through-stall- and reverse-through-flat-pitch settings (and, if so, at what blade angles and speeds), and (more fundamentally) (2) to assess the "starting phenomenon" in reverse thrust. The starting phenomenon refers to the establishment of useful reverse-thrust flow from the fully stalled regime which existed with initiation of rotor rotation. Another major aerodynamic interest was core flow recovery. The measured flow conditions at the transition duct discharge plane are representative of core compressor inlet conditions during engine operation. The recovery of this flow directly affects the power available to drive the fan.

From an acoustic standpoint, the tests were designed to estimate (1) the unsuppressed PNL at 152.4-m (500-ft) sideline for the full-size QCSEE at the objective reverse-thrust condition, and (2) the suppression provided by the various treatments in reverse thrust (for which they were initially designed). The next objective was to select the optimum treatment design for adequate suppression at takeoff, approach, and reverse modes of operation. But the most important acoustic objective was to determine whether the system noise goal of 100 PNdB on a 152.4-m (500-ft) sideline could be met in the reverse-thrust mode of operation.

With these basic objectives, a series of fan aerodynamic tests were first performed with the accelerating inlet B. The accelerating inlet was chosen since this, rather than the bellmouth inlet, represented the inlet that would be tested on the engine.

10.1 FAN AERODYNAMIC PERFORMANCE

Aerodynamic testing in the reverse mode of operation was performed, with the high Mach number inlet only, at open pitch-angle settings of -95°, -100°, and -105° in the reverse-through-stall-pitch direction and at closed pitch-angle settings of +73° and +78° in the reverse-through-flat-pitch direction. The bypass discharge valve (DV) was set at 6.37 for all tests. The method for determining this DV setting is discussed in Reference 2.

The overall reverse-thrust-mode performance of the fan is shown in Figure 153. These results represent measured test data adjusted by the methods described in Reference 2. Except for the flagged symbols, for which the discharge valve was fully open, the vehicle geometry was fixed for a given pitch setting.

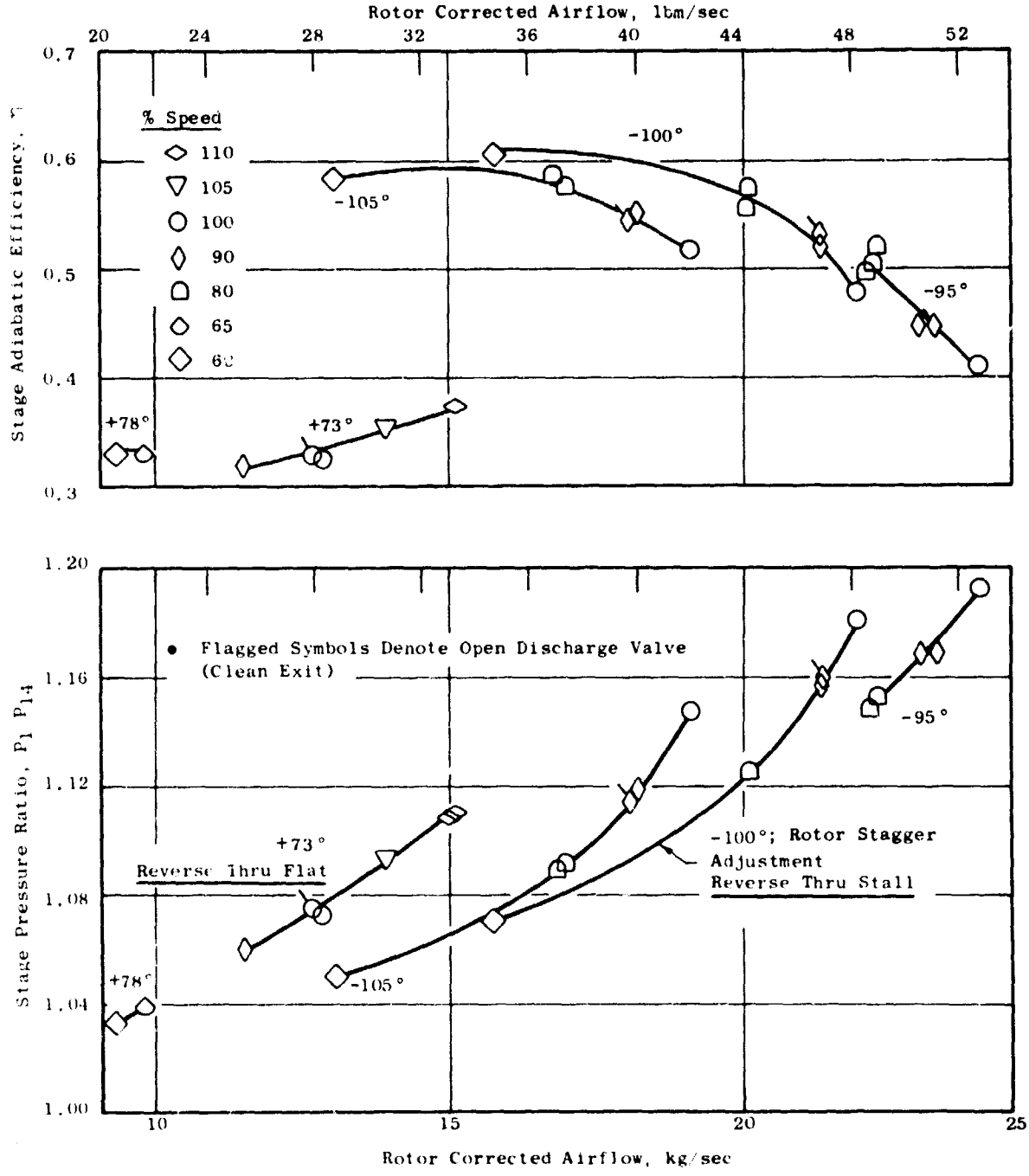

Figure 153. Reverse-Thrust-Mode Fan Performance.

In the reverse-through-stall-pitch settings, the reductions in flow, at speed, with more open pitch setting, is consistent with expectations. However, the rather dramatic change in operating line was not expected. The primary trend noted in adiabatic efficiency is a fall-off with increasing flow. A smaller but noticeable effect of pitch angle is observed. In the reverse-through-flat-pitch settings, the vehicle was restricted to a maximum speed of 65% at a pitch setting of +78° by high rotor stress. Flow and pressure ratio, and therefore reverse thrust, at the +73° setting are remarkedly reduced from the values obtained in the reverse-through-stall-pitch direction. Angle settings less than +73° were expected to result in even lower values. Since the +73° setting resulted in reverse-thrust levels less than objective, further aerodynamic testing in the reverse-through-flat-pitch direction was terminated. For the same reason no acoustic tests were performed in the reverse-through-flat-pitch settings.

The reverse-mode, flow-speed relationship is shown in Figure 154. The fan gross reverse thrust, consistent with the overall performance maps, is presented in Figure 155. The approximate, scaled-engine, fan-gross-thrust objective is also shown. In the reverse-through-stall-pitch direction the objective reverse thrust can be achieved, with the appropriate fan speed, for each of the three pitch settings tested. A line of constant gross thrust, equal to the appropriate objective, is shown in Figure 154. As the pitch setting is changed from (open) -95° to -105° it is noted that the speed increases but flow decreases. The implications of these trends on fan efficiency, core engine recovery, and overall engine operation must all be examined before the "optimum" pitch setting can be determined. From the standpoint of fan efficiency at objective-gross-thrust condition, a -100° pitch setting at 86% speed would appear to be a good operating condition.

Details on the starting phenomenon and the core engine recovery at the different pitch settings and speeds are discussed in detail in Reference 2.

10.2 ACOUSTIC PERFORMANCE OF ACCELERATING INLETS

The hard-wall, accelerating inlet and all four treated, accelerating inlets were tested in reverse-thrust mode with rotor-pitch setting at open 100° (which was deemed adequate for obtaining 35% of design thrust in reverse mode). The tests were performed at 60, 75, 80, 83, 86, 90, and 100% corrected speeds. The treated inlet D and the hard-wall inlet were also tested at -95° and -105°, at which angles the fan-performance tests indicated that the objective gross thrust was achievable.

The variation of PNL [full size, 152.4-m (500-ft) sideline] with corrected speed at -100° pitch is shown in Figure 156 for all five inlets. All the inlets showed increasing PNL with speed; treatments B and D gave the highest suppression of the four treatments tested. At the objective reverse-thrust condition corresponding to 86% speed at the -100°

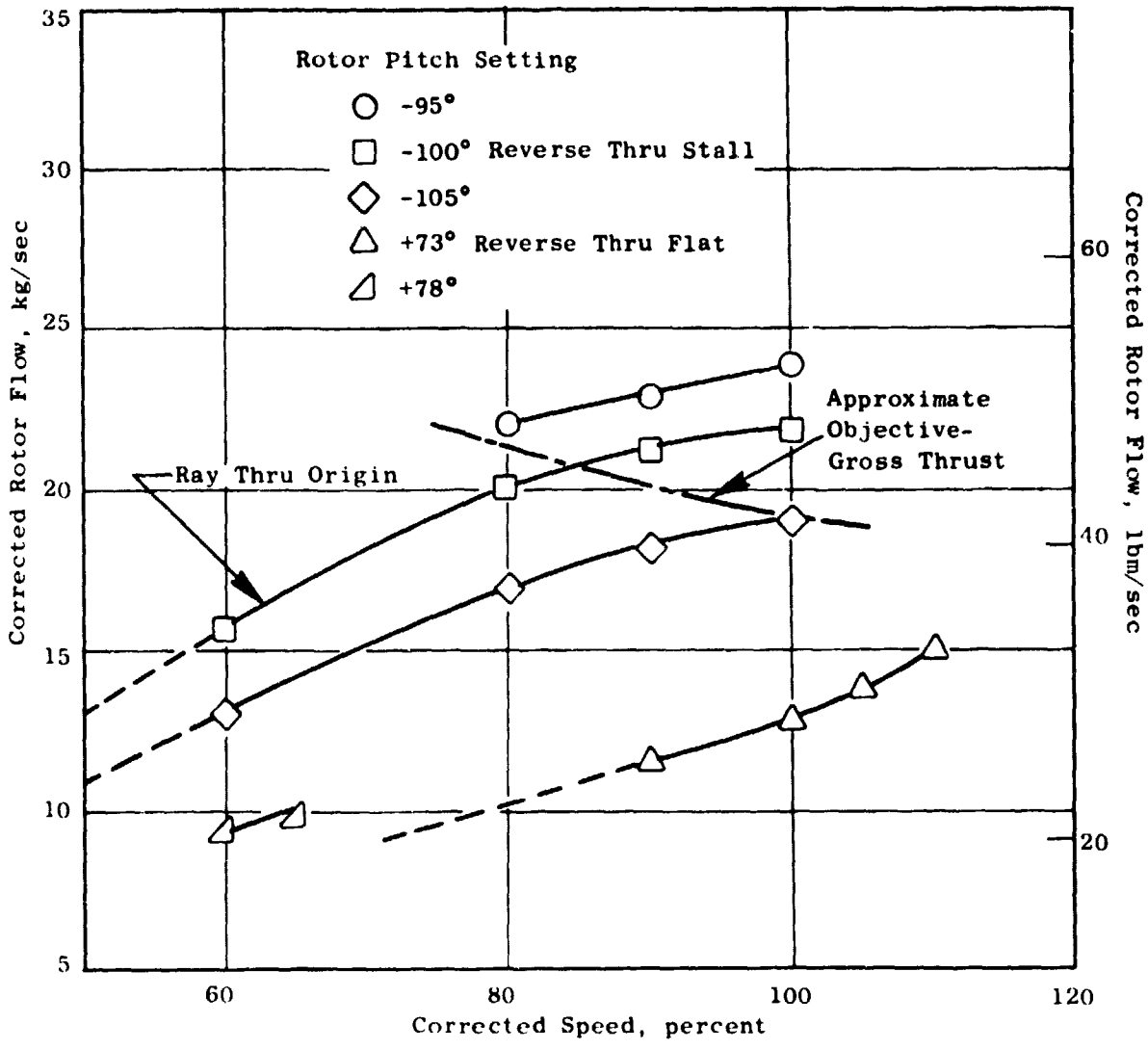

Figure 154. Reverse-Thrust Mode Flow/Speed Relationship.

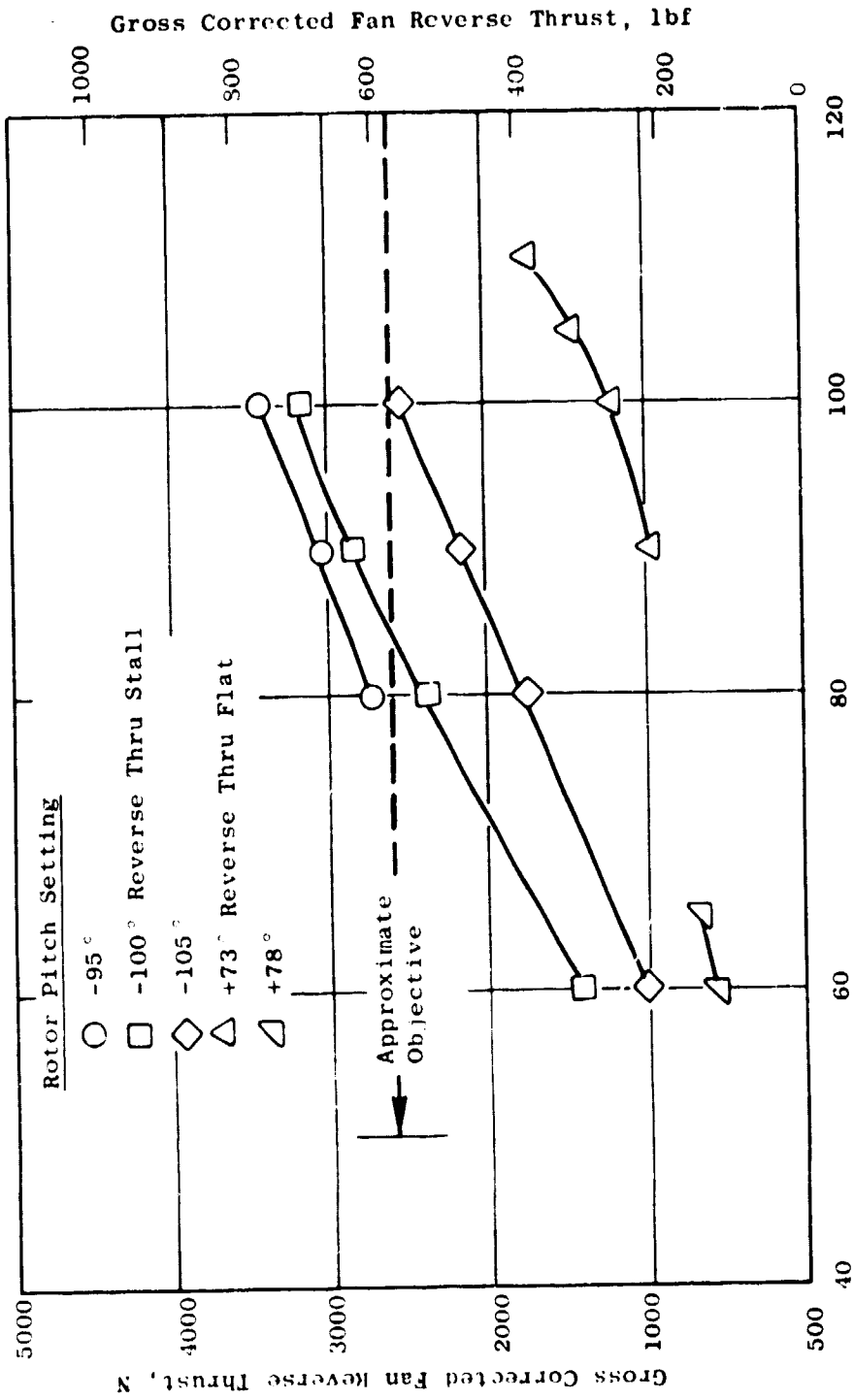

Figure 155. UTW Simulator Gross Reverse Thrust.

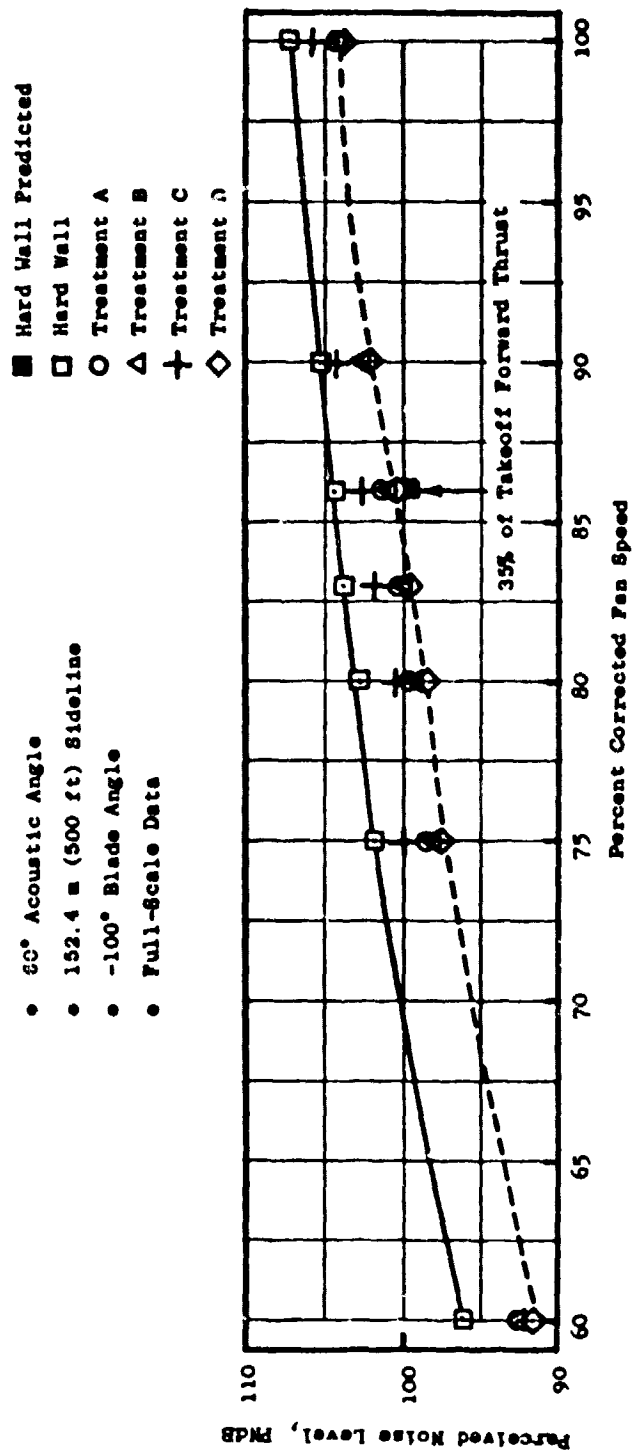

Figure 156. Reverse-Thrust PNL Vs. Fan Speed for All Accelerating Inlets.

setting, inlets B and D showed respective suppression levels of 3.9 and 4.2 PNdB. The same suppression trends are also observed at higher speeds up to 100% speed. The estimated hard-wall reverse thrust PNL is shown at the objective point of 35% reverse thrust in Figure 156. It is evident that the measured hard-wall level is about 6 PNdB higher than estimated.

The effectiveness of accelerating-inlet treatments specifically at the objective gross-reverse-thrust condition (86% speed) is discussed in Section 10.3. Data at other representative speeds are presented below.

PNL directivities for the five inlets at 80% speed are presented in Figure 157. A peak-angle suppression (relative to hard wall) of 4.5 dB and 3.5 dB is indicated, respectively, for inlets D and B; treatment C provided the least suppression. The 1/3-octave-band SPL spectra for all inlets at 50° and 60° to the inlet at 80% speed are presented in Figures 158 and 159. The SPL suppression (ΔSPL relative to hard wall) spectra for treatments B and D are shown in Figures 160 and 161 both at 50° and at 60° to the inlet. The 1/3-octave-band PWL spectra for inlets B and D are shown in Figure 162. The overall observation is that treatment D appears to be very slighly superior to treatment B in reverse-thrust suppression at this speed. Figures 163 through 168 present similar data at 83% speed and Figures 169 through 174 at 90% speed. One interesting point, as the speed is increased, is the considerably higher suppression (as high as 12 dB) of the blade passing frequency and harmonics.

All the data shown above indicate that inlets B and D were quite comparable in acoustic characteristics. Due to slightly better suppression characteristics, inlet D was selected for further tests at -95° and -105° pitch settings. It was noted earlier (Figure 155) that the objective gross thrust can also be achieved at about 78% corrected fan speed at -95° pitch setting and at 100% speed at -105° pitch setting. PNL directivity and 1/3-octave-band spectra at 50°, 60°, and 70° for -95° pitch setting for the hard wall and the treatment D configurations are shown as follows: Figures 175 through 178 at 75% speed, Figures 179 through 182 at 80% speed, and Figures 183 through 186 at 85% speed. Similar plots are presented in Figures 187 through 194 for -105° pitch setting at 90% and 100% speeds.

The variation of inlet D PNL with fan speed at 60°, on a 152.9-m (500-ft) sideline, at all three pitch angles (Figure 195), indicates that the levels do not vary much at the constant-thrust setting; however, a slight bottoming of the PNL at -100° (about 1 dB less than at the other two angles) is noted. It may also be noted from Figure 153 that a combination of -100° and 86% speed provides the best fan efficiency. Although it appears from these results that, both aerodynamically and acoustically, the reverse-thrust operation is feasible and acceptable at any point along the constant-thrust line between -95° and -105° (subject to core recovery considerations), the 86% speed at -100° setting appears to be slightly more advantageous.

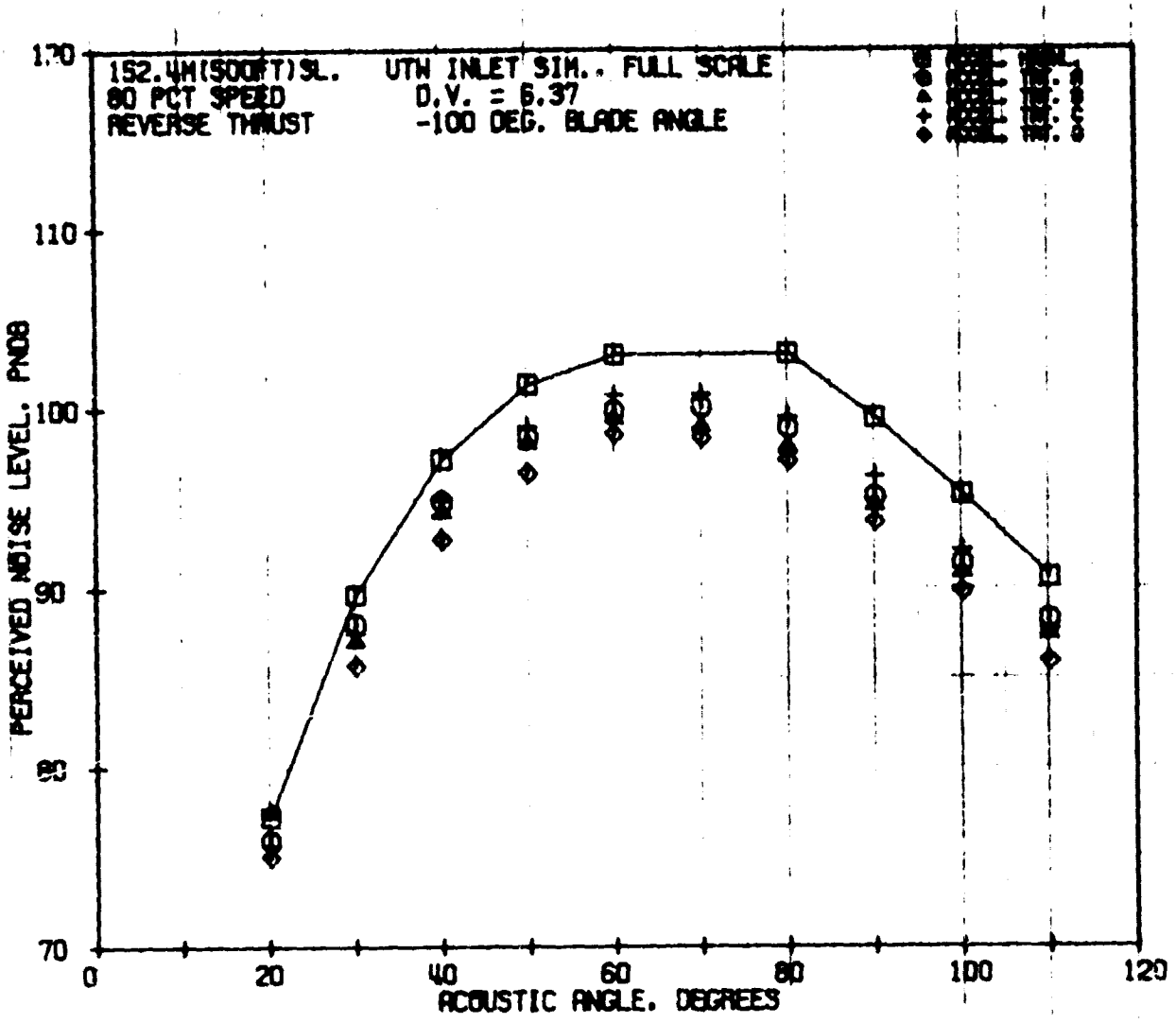

Figure 157. Reverse-Thrust, PNL Directivities of Axi1 Accelerating Inlets at 80% N_{FC}.

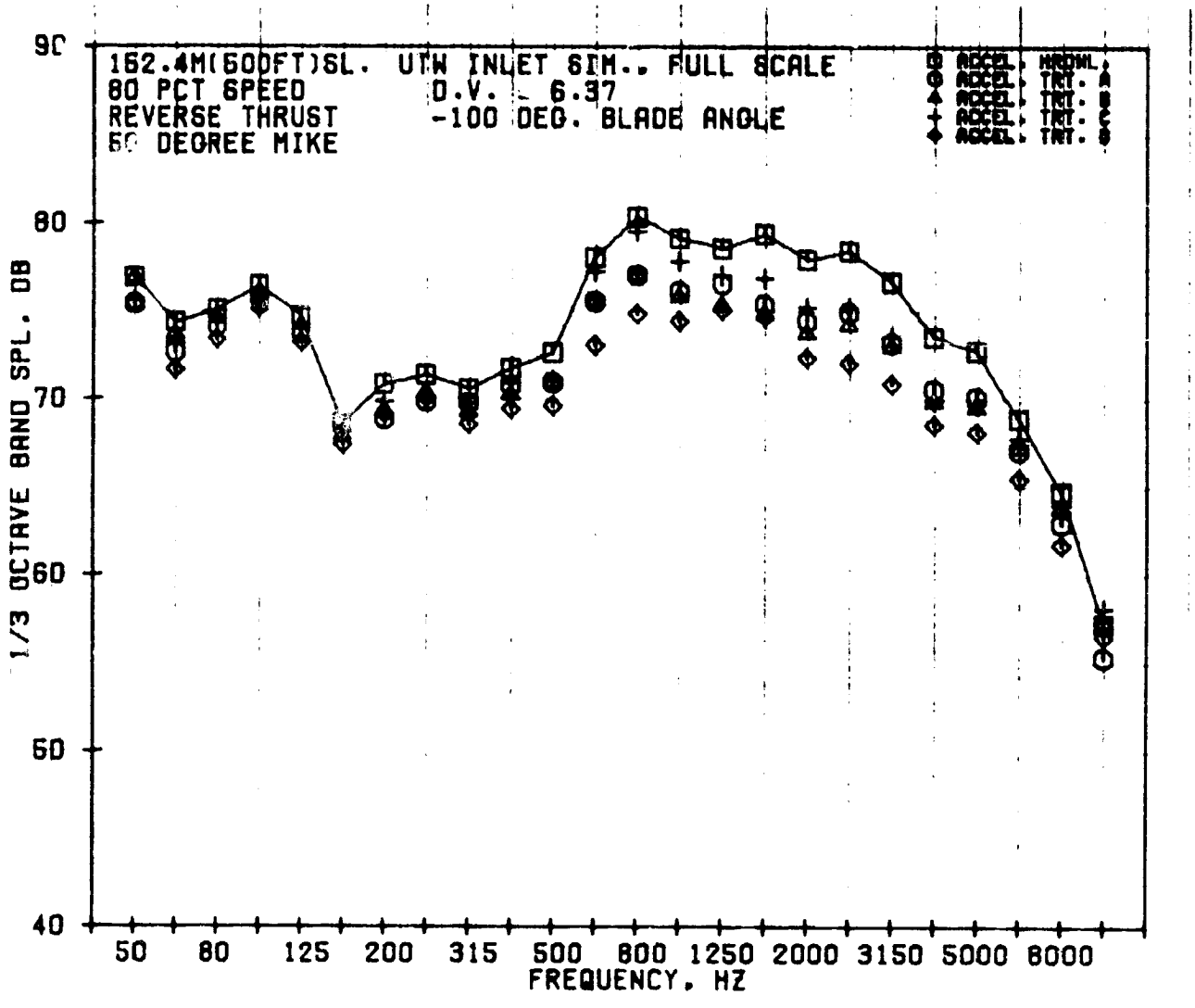

Figure 158. Reverse-Thrust, 1/3-Octave-Band, SPL Spectra of All Accelerating Inlets at 80% N_{FC} at 50°.

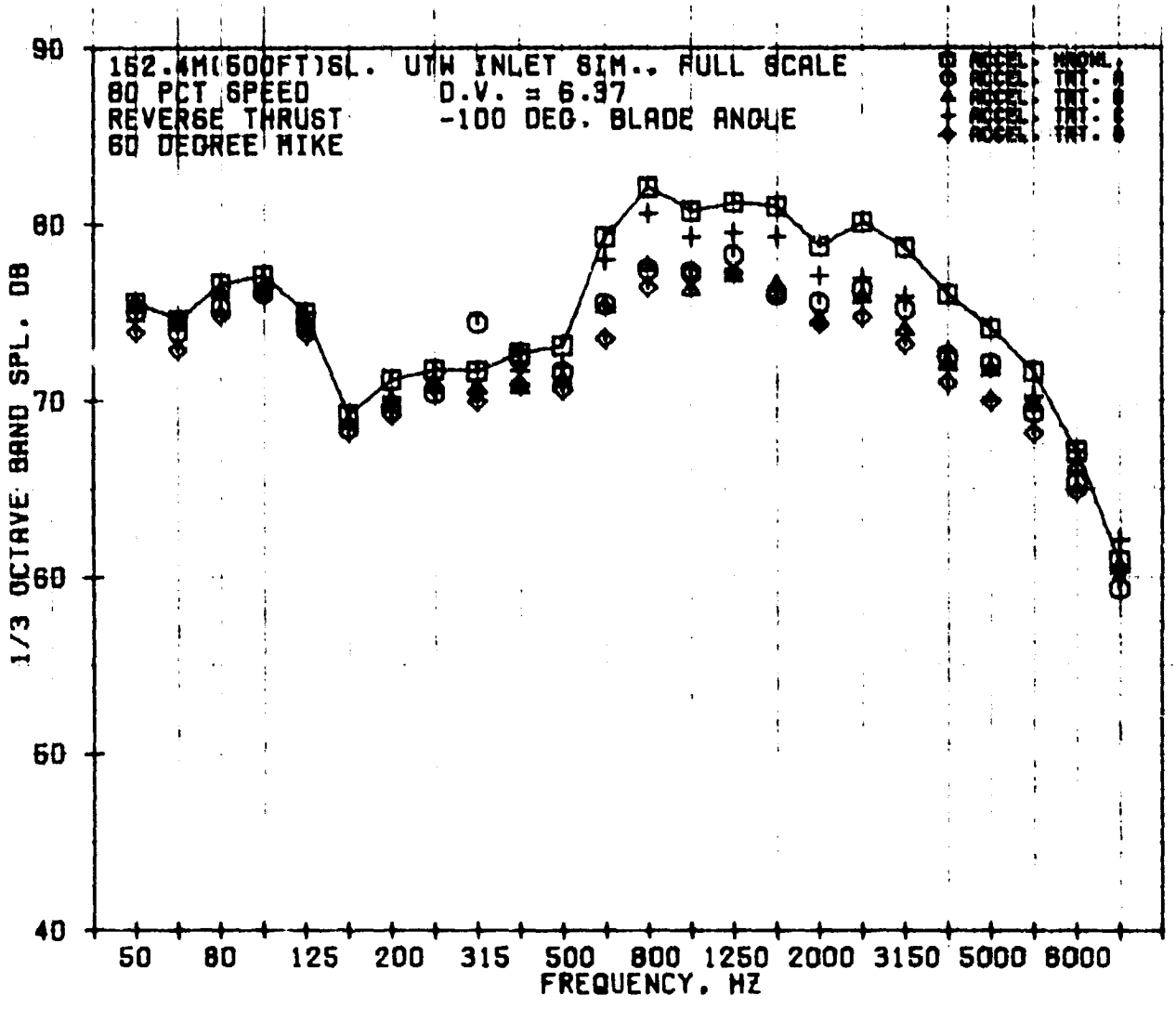

Figure 159. Reverse-Thrust, 1/3-Octave-Band, SPL Spectra of All Accelerating Inlets at 80% N_{FC} at 60°.

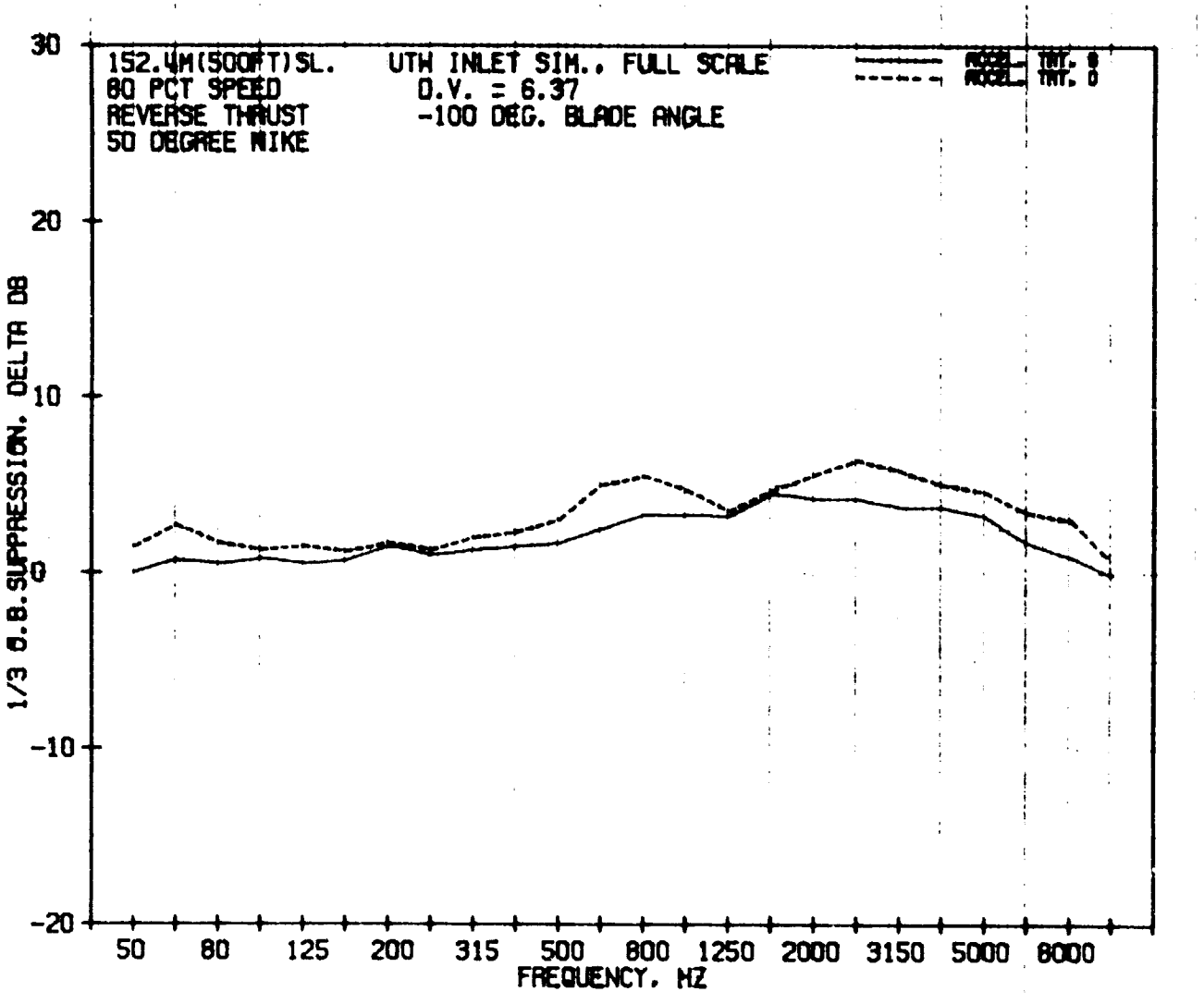

Figure 160. Reverse-Thrust, 1/3-Octave-Band, SPL Suppression Spectra for Accelerating-Inlet Treatments B and D at 80% N_{FC} at 50°.

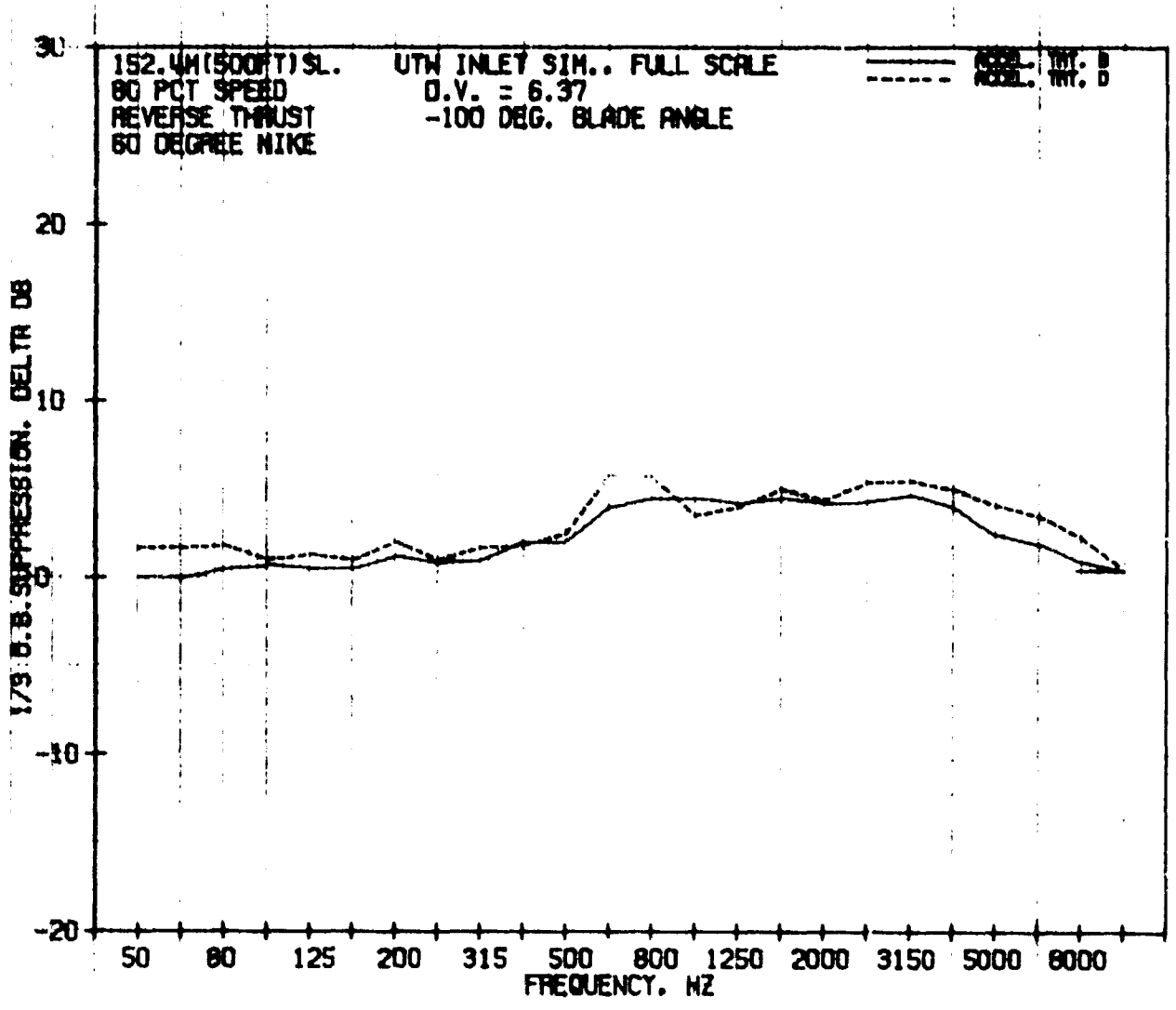

Figure 161. Reverse-Thrust, 1/3-Octave-Band, SPL Suppression Spectra for Accelerating-Inlet Treatments B and D at 80% N_{FC} at 60°.

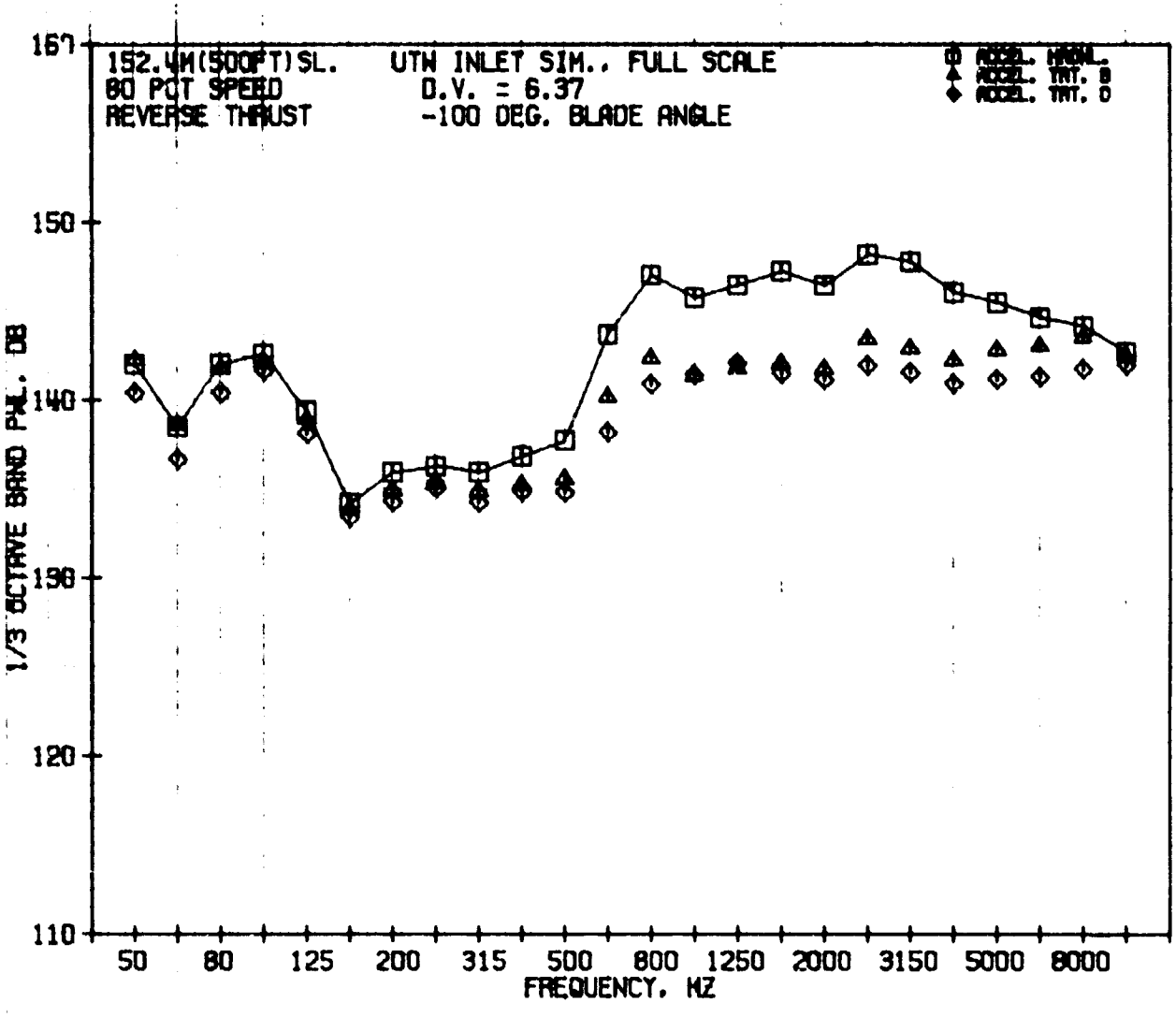

Figure 162. Reverse-Thrust, 1/3-Octave-Band, PWL Spectra for Accelerating Inlets - Hard-Wall and Treatments B and D at 80% N_{FC}.

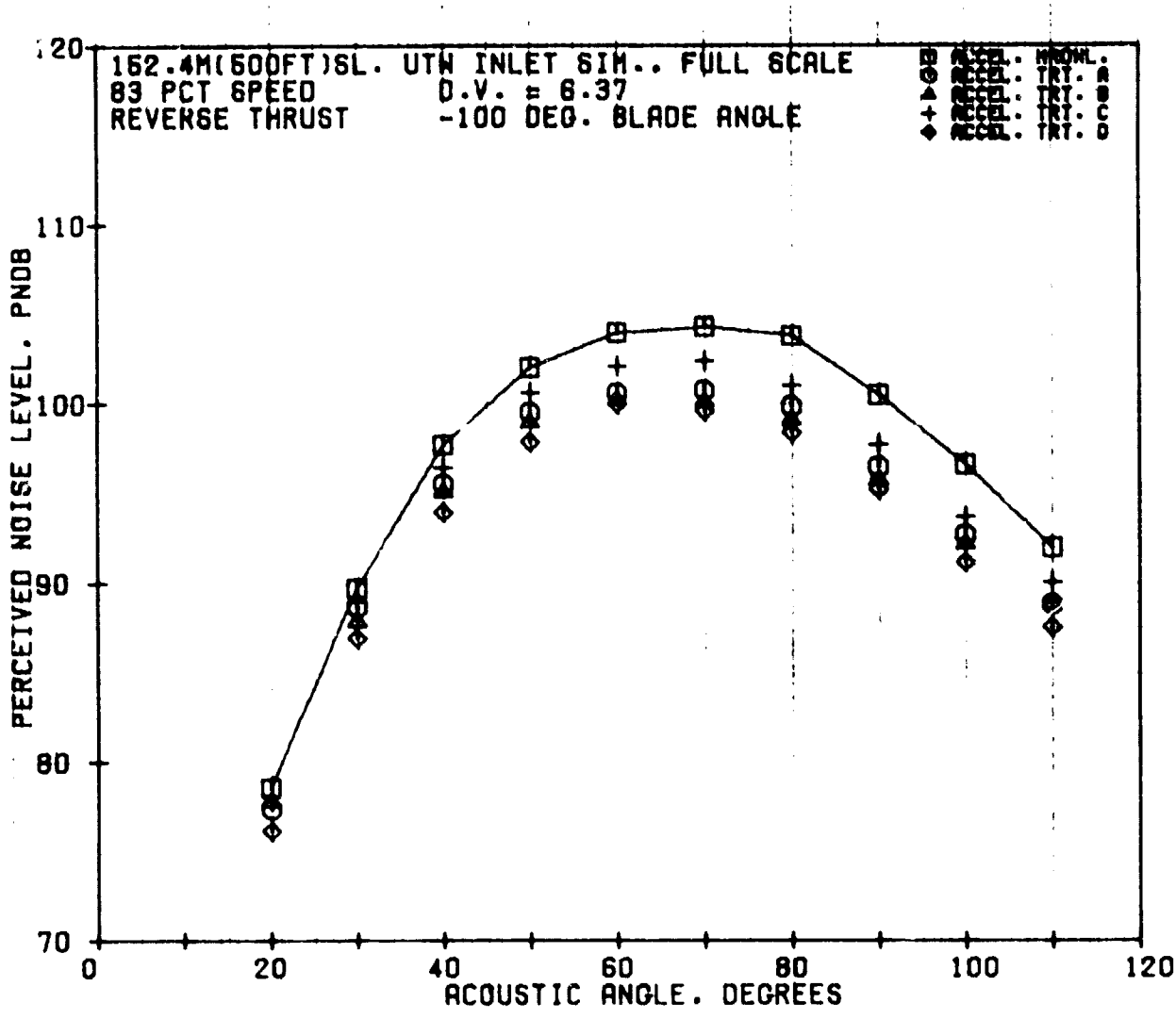

Figure 163. Reverse-Thrust, PNL Directivities for All Accelerating Inlets at 83% N_{FC}.

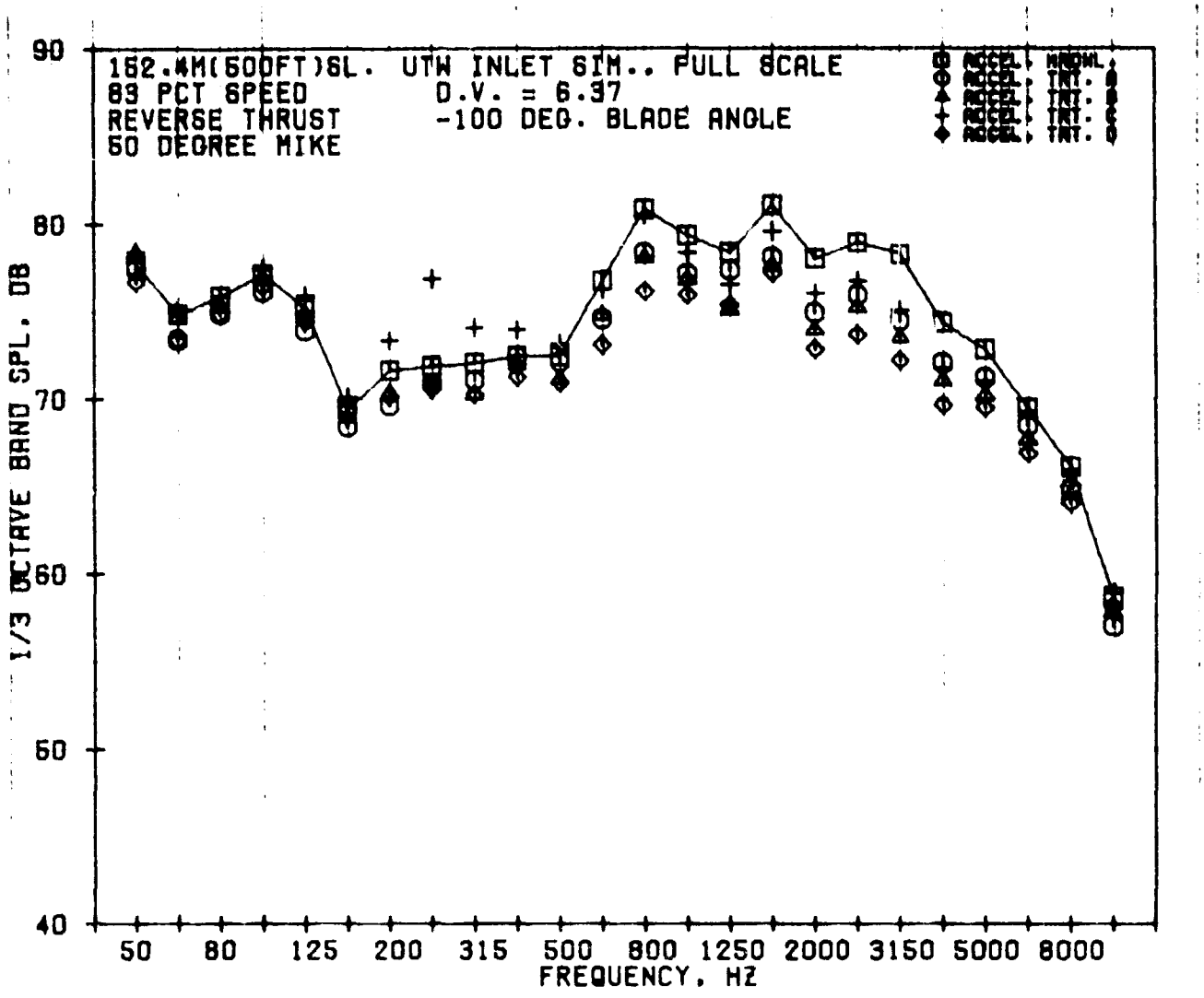

Figure 164. Reverse-Thrust, 1/3-Octave-Band, SPL Spectra of All Accelerating Inlets at 83% N_{FC} at 50°.

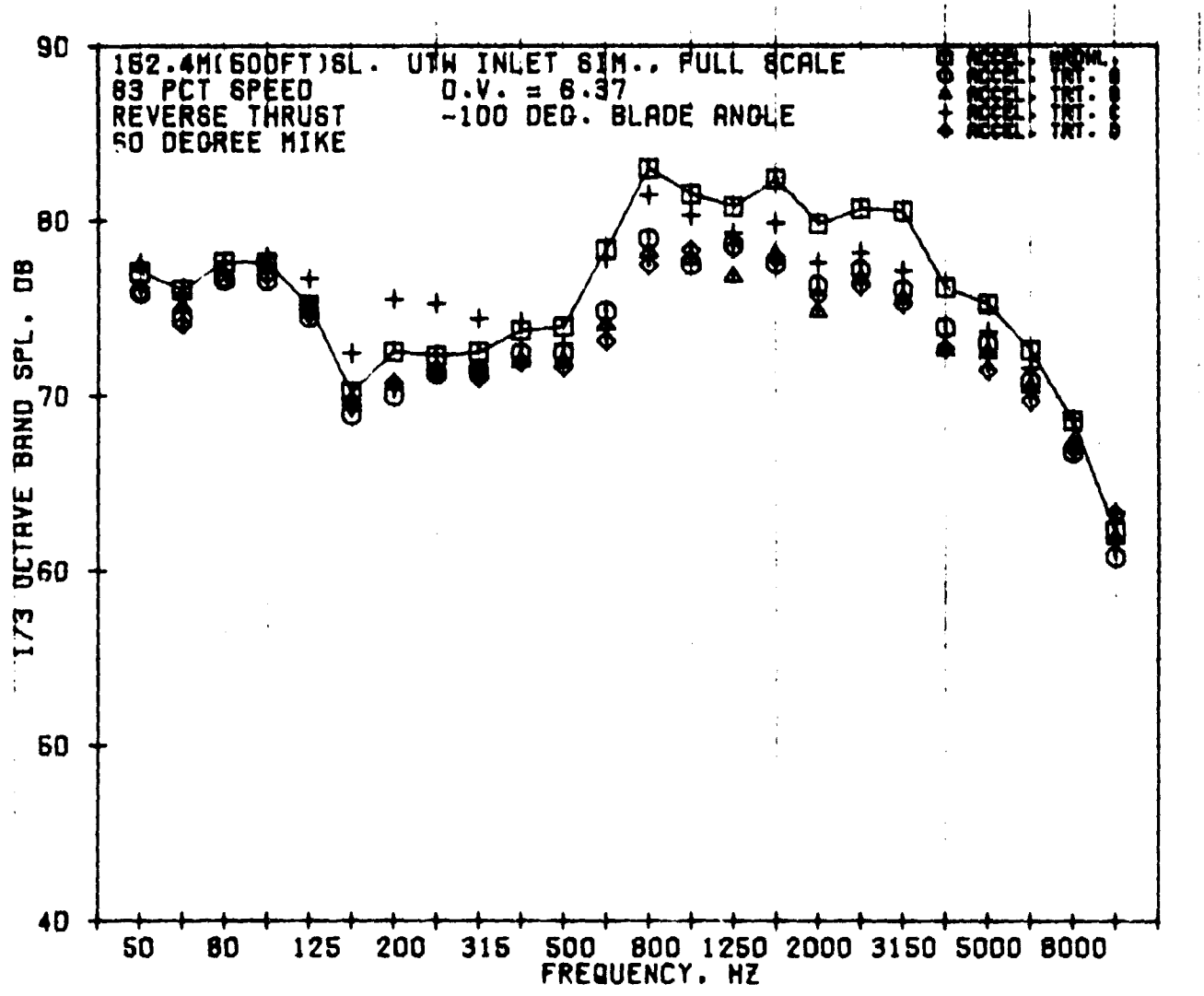

Figure 165. Reverse-Thrust, 1/3-Octave-Band, SPL Spectra of All Accelerating Inlets at 83% N_{FC} at 60°.

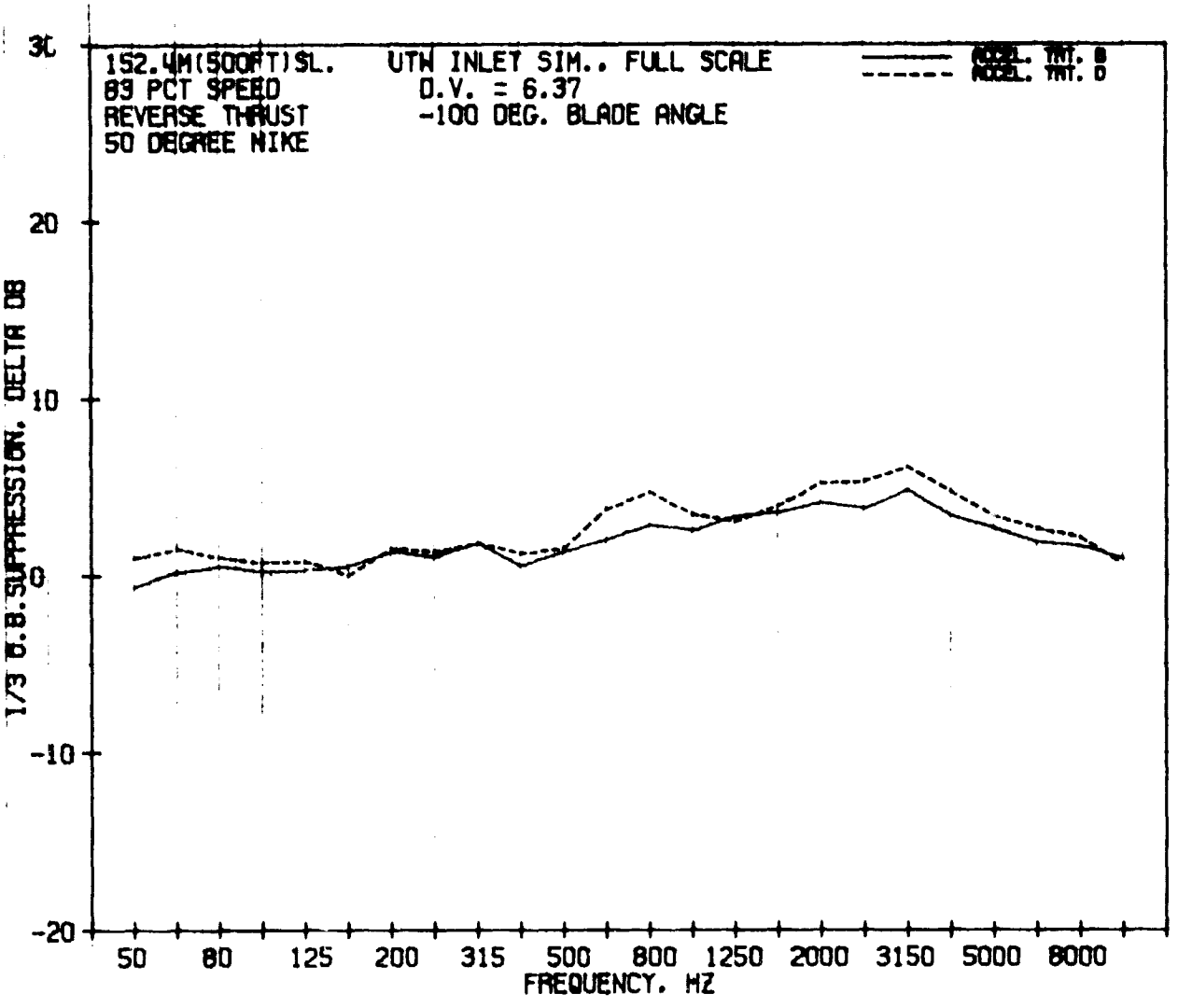

Figure 166. Reverse-Thrust, 1/3-Octave-Band, SPL Suppression Spectra of Accelerating-Inlet Treatments B and D at 83% NFC at 50°.

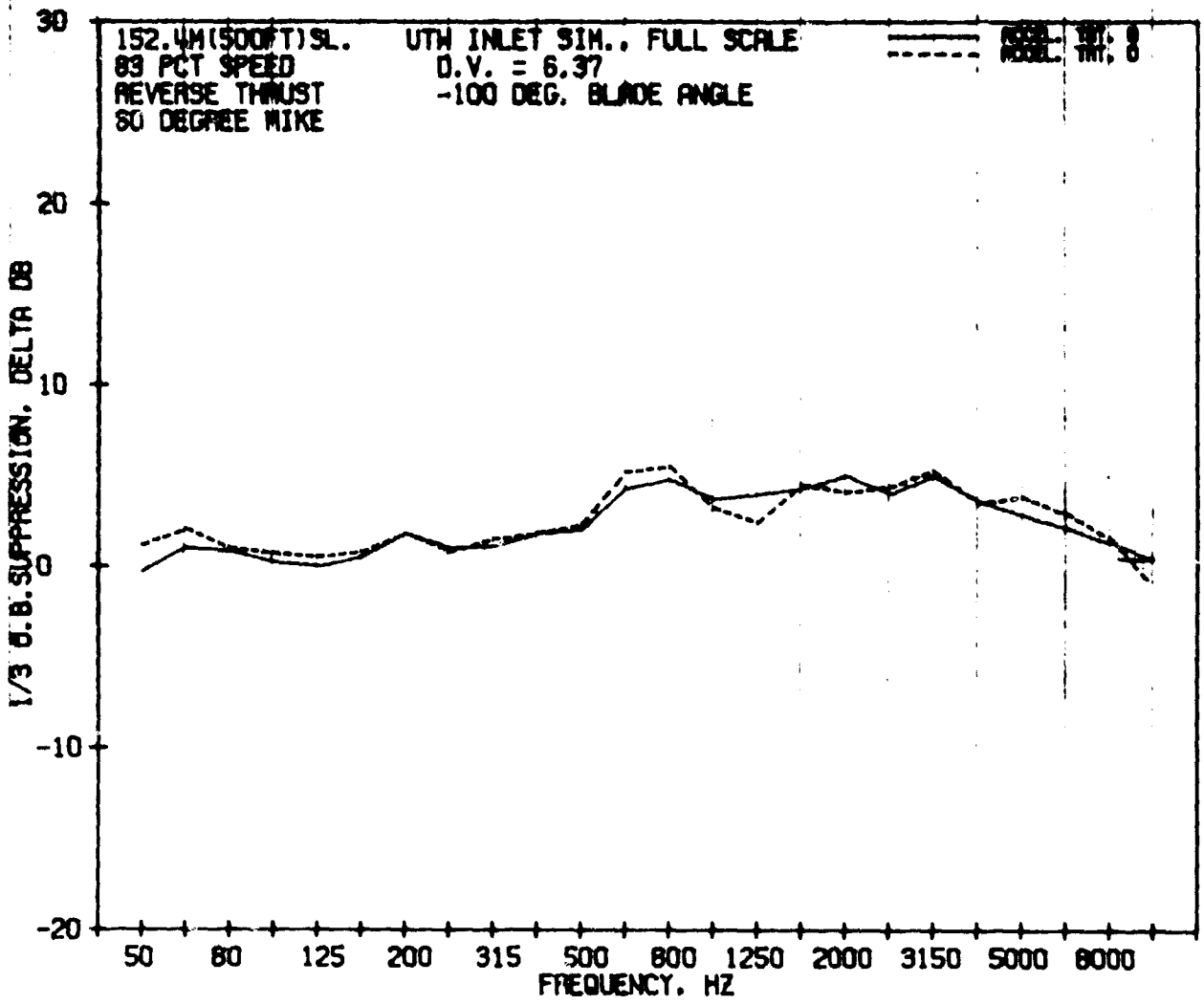

Figure 167. Reverse-Thrust, 1/3-Octave-Band, SPL Suppression Spectra of Accelerating-Inlet Treatments B and D at 83% N_{FC} at 60°.

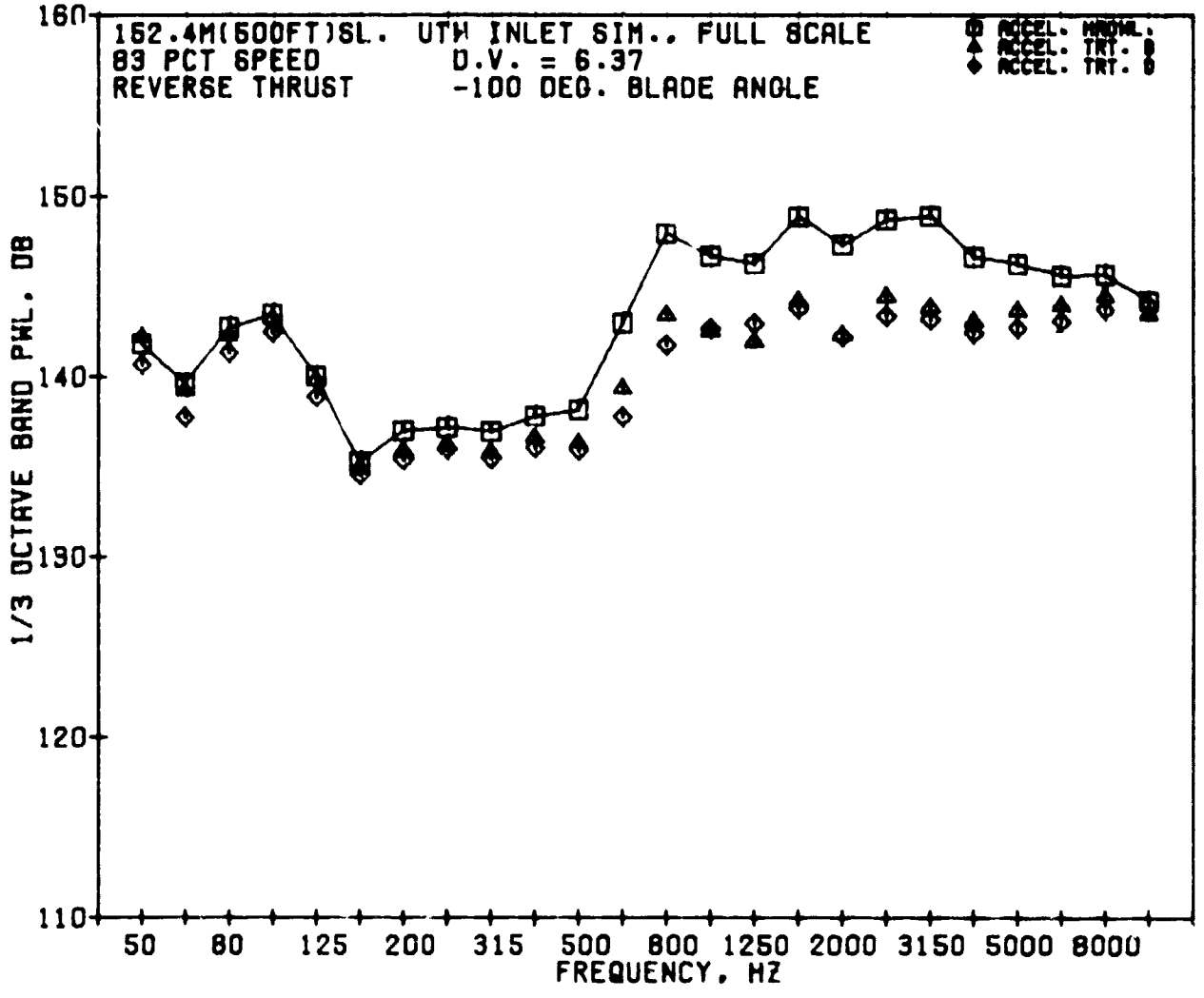

Figure 168. Reverse-Thrust, 1/3-Octave-Band, PWL Spectra of Accelerating Inlets - Hard-Wall and Treatments B and D at 83% N_{FC}.

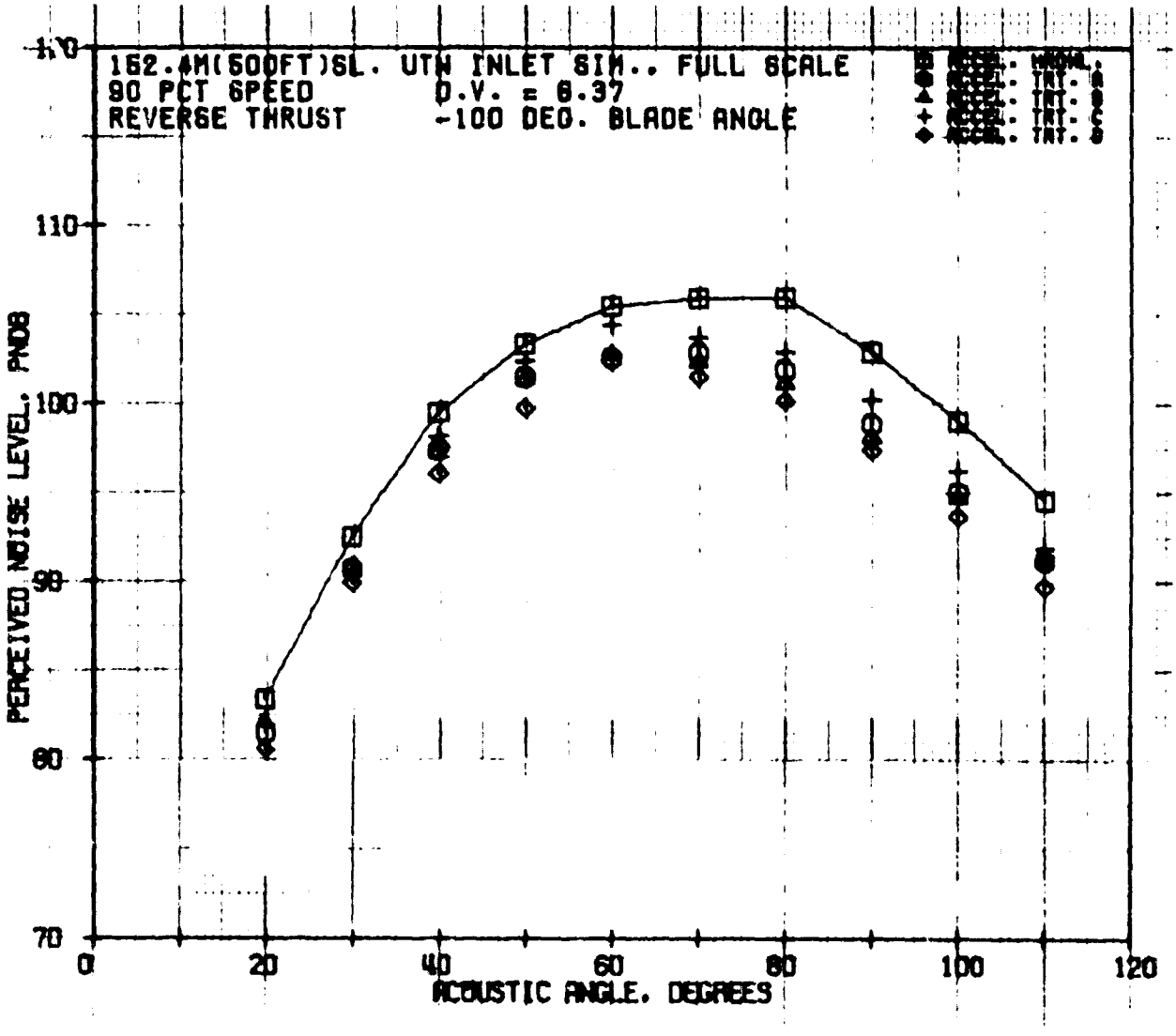

Figure 169. Reverse-Thrust, PNL Directivities of All Accelerating Inlets at 90% N_{FC}.

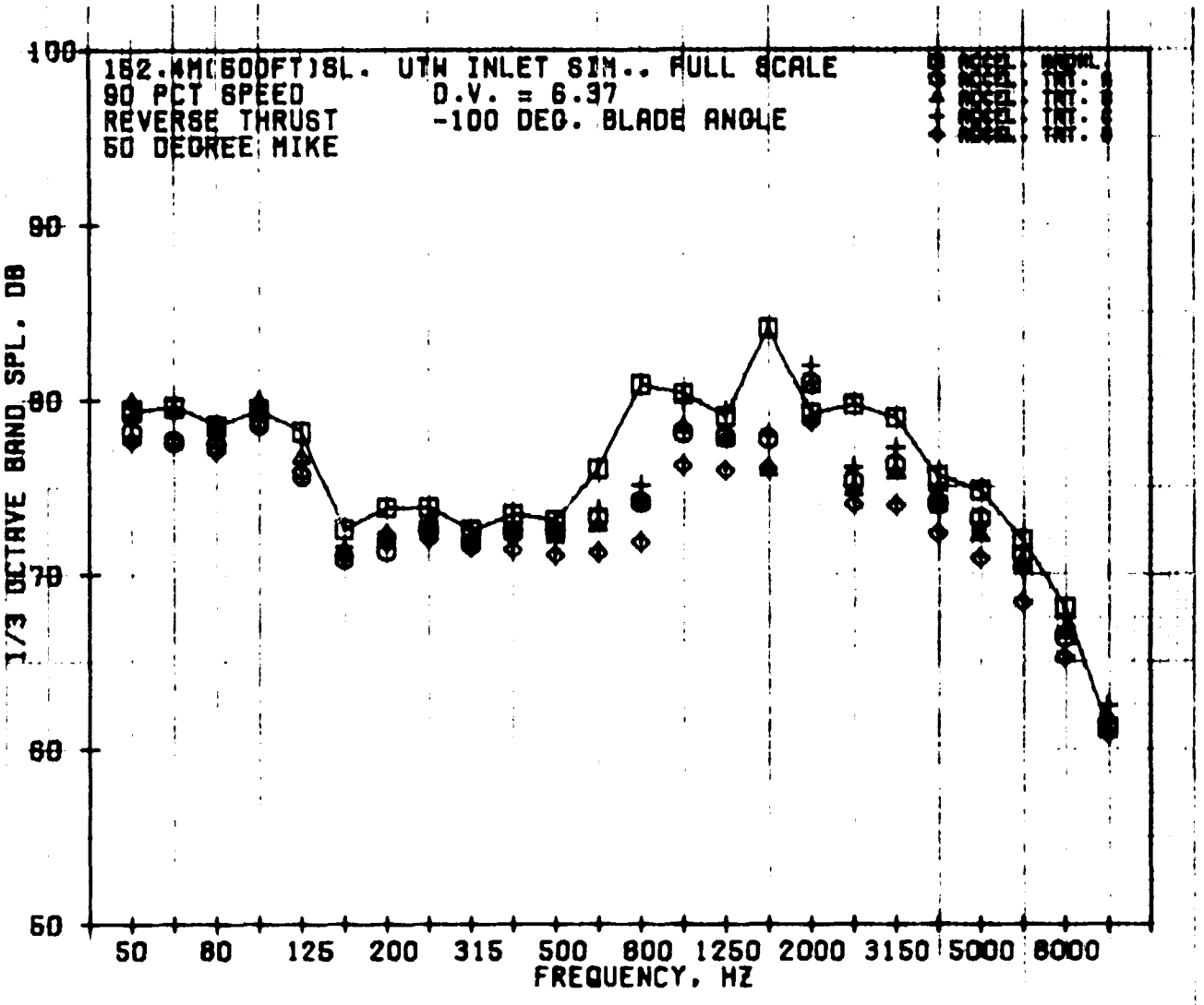

Figure 170. Reverse-Thrust, 1/3-Octave-Band, SPL Spectra of All Accelerating Inlets at 90% N_{FC} at 50°.

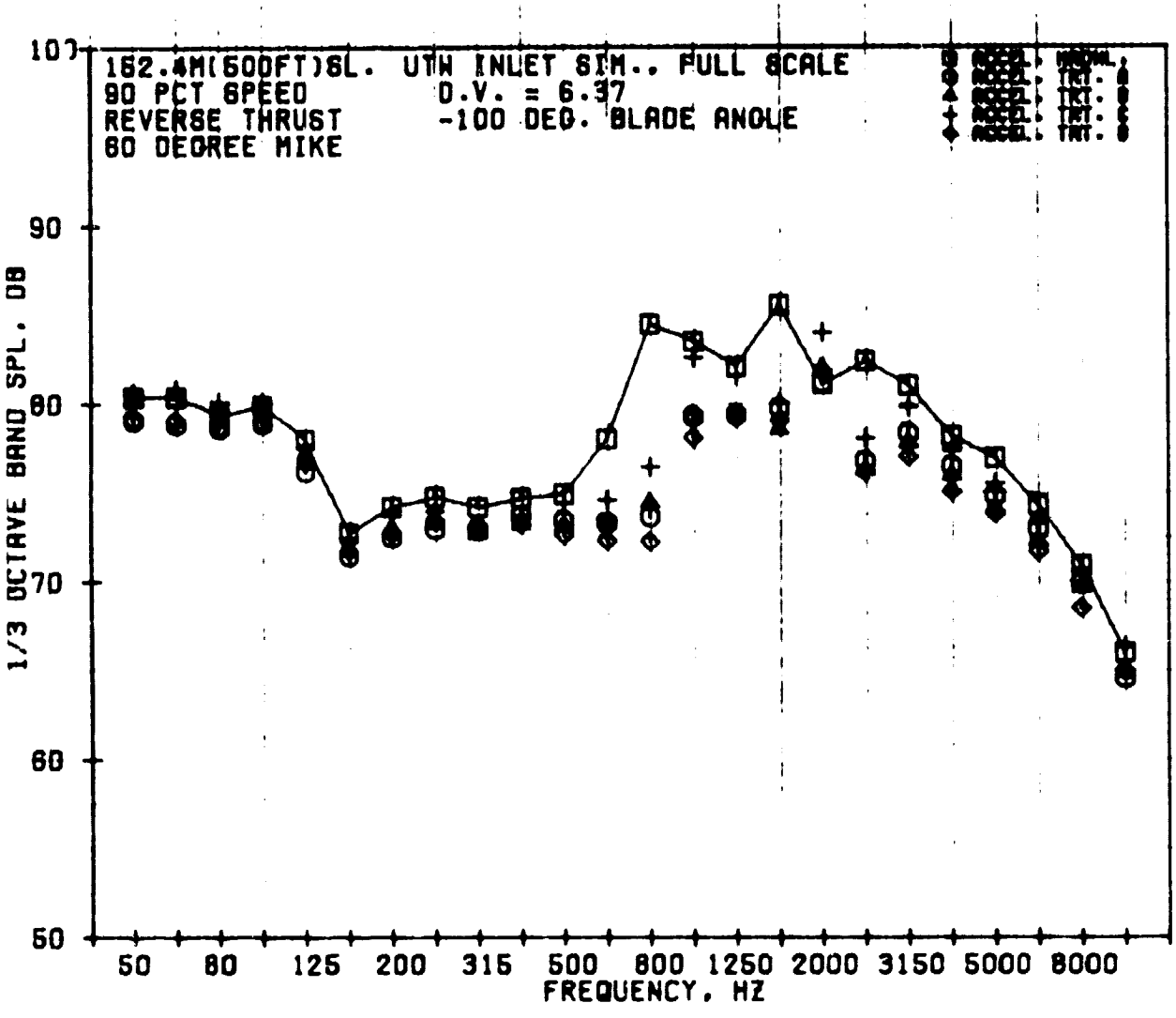

Figure 171. Reverse-Thrust, 1/3-Octave-Band, SPL Spectra of All Accelerating Inlets at 90% N_{FC} at 60°.

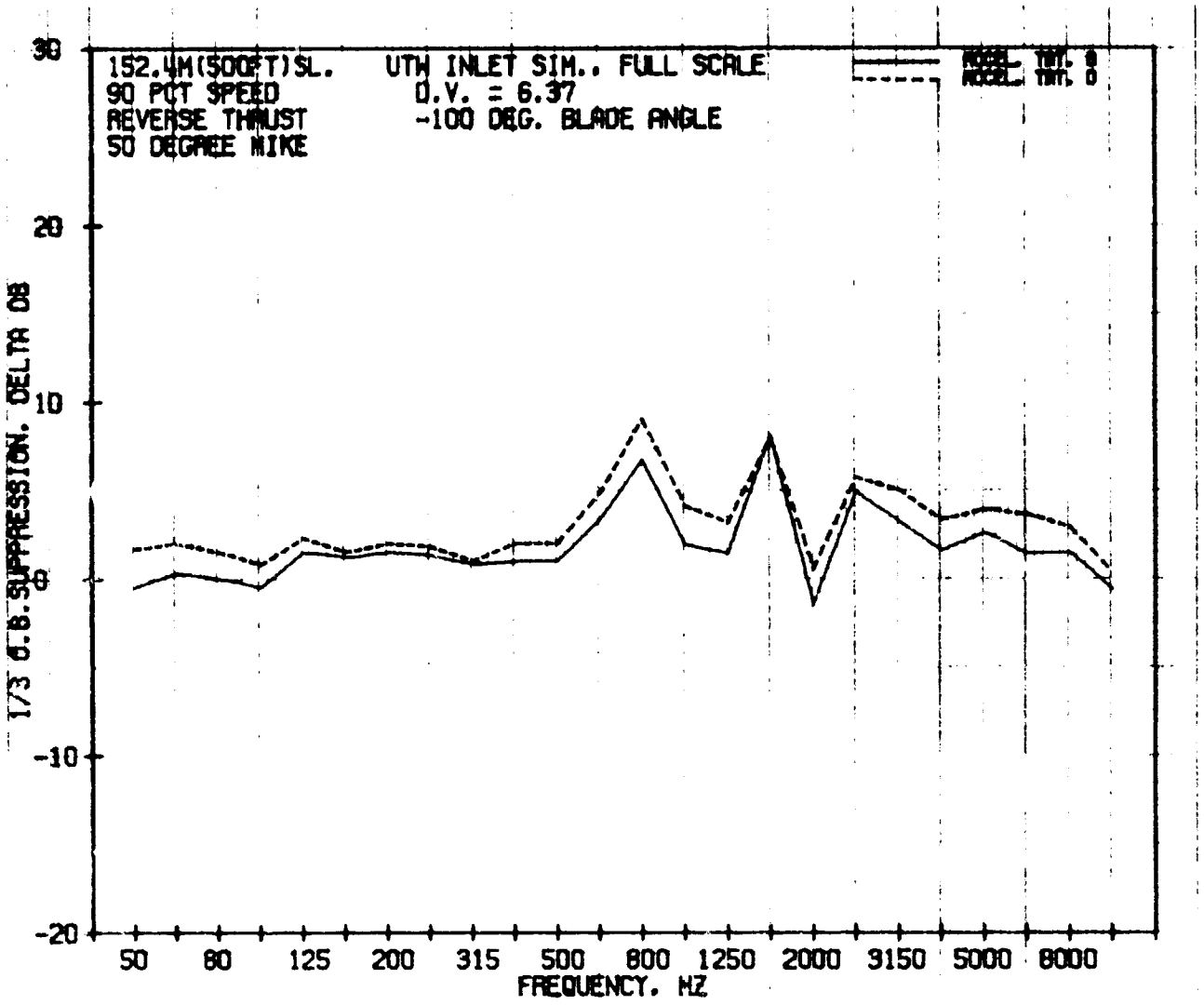

Figure 172. Reverse-Thrust, 1/3-Octave-Band, SPL Suppression Spectra of Accelerating-Inlet Treatments B and D at 90% N_{FC} at 50°.

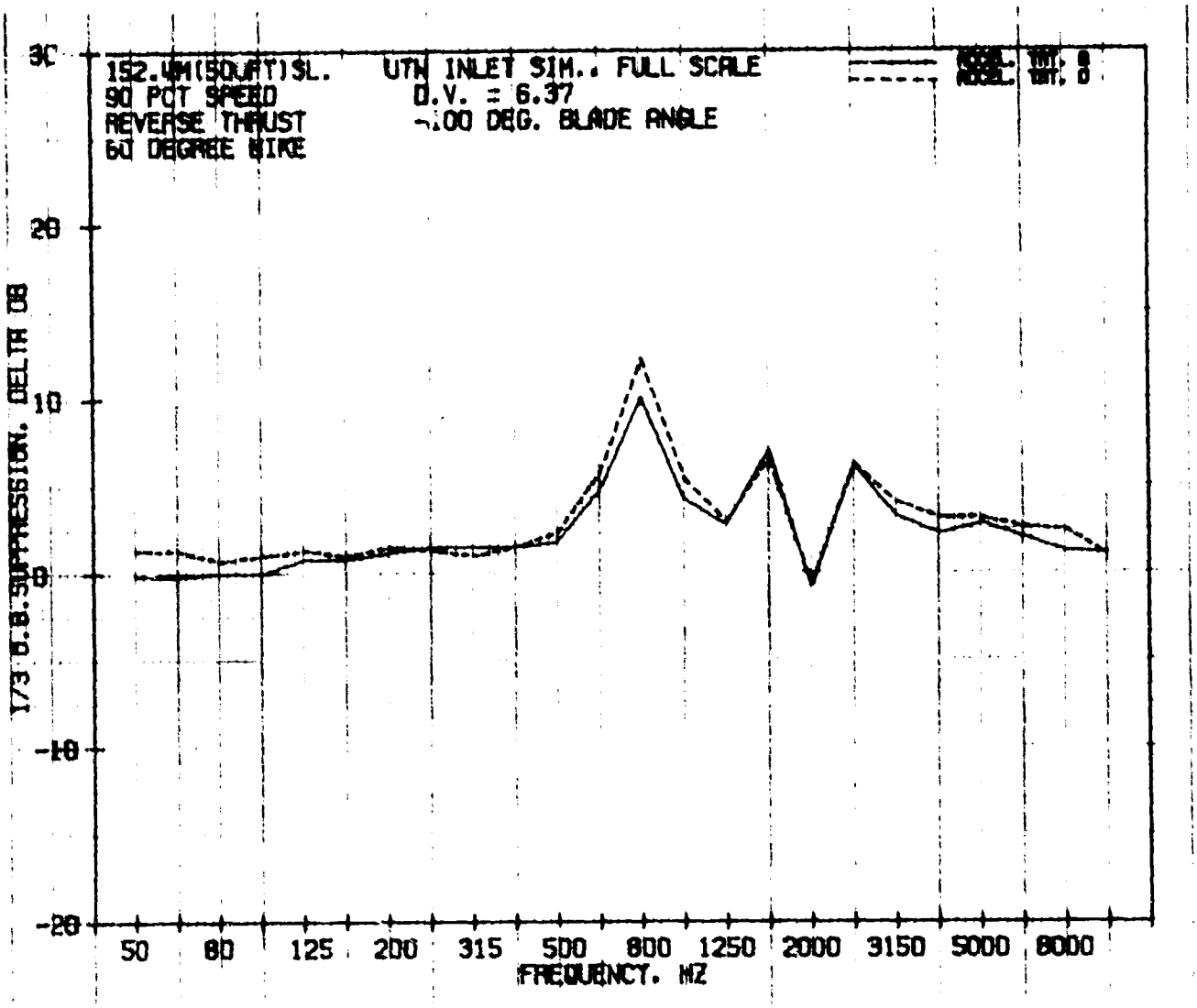

Figure 173. Reverse-Thrust, 1/3-Octave-Band, SPL Suppression Spectra of Accelerating-Inlet Treatments B and D at 90% N_{FC} at 60°.

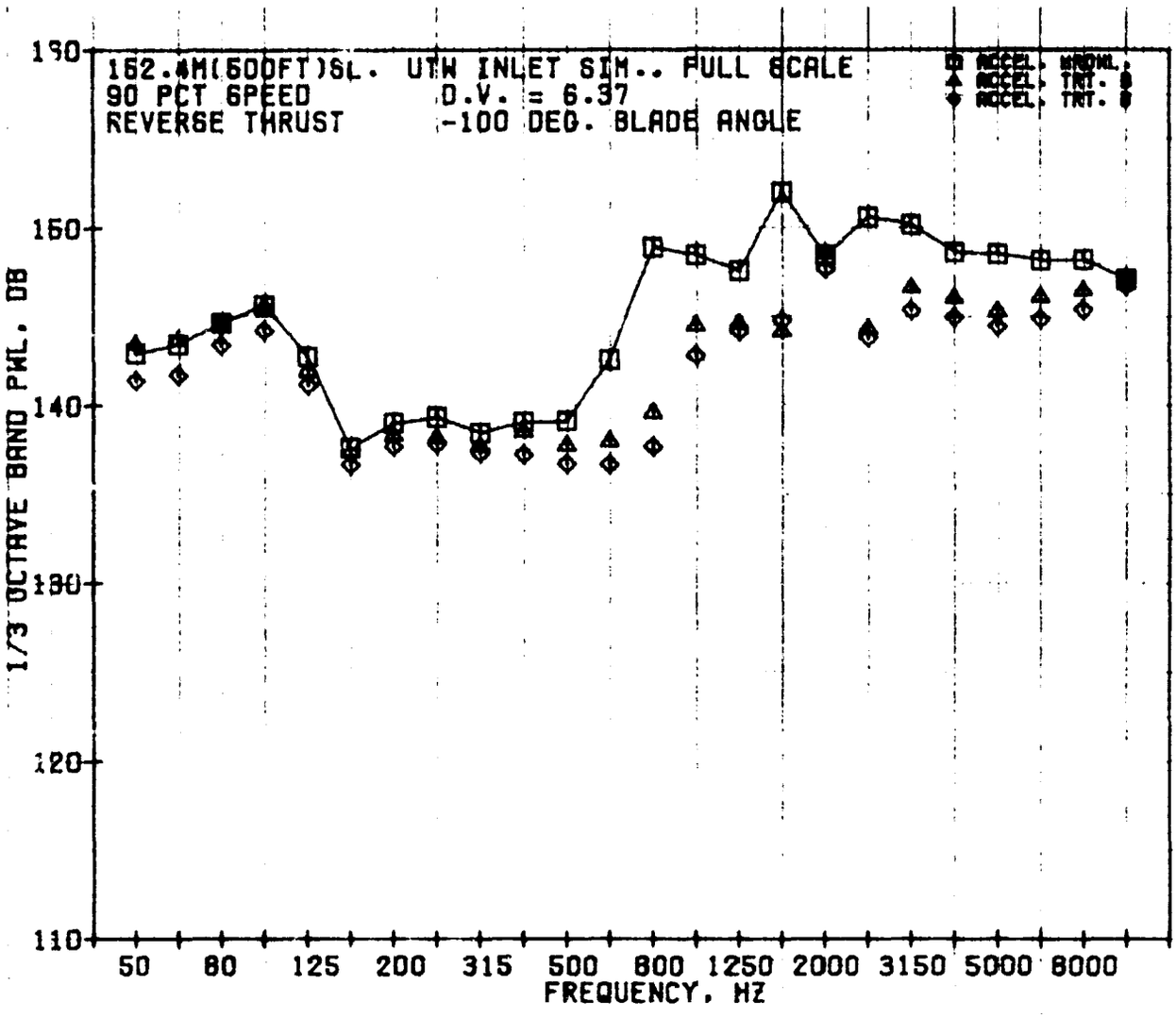

Figure 174. Reverse-Thrust, 1/3-Octave-Band, PWL Spectra of Accelerating Inlets, Hard-Wall and Treatments B and D at 90% N_{FC}.

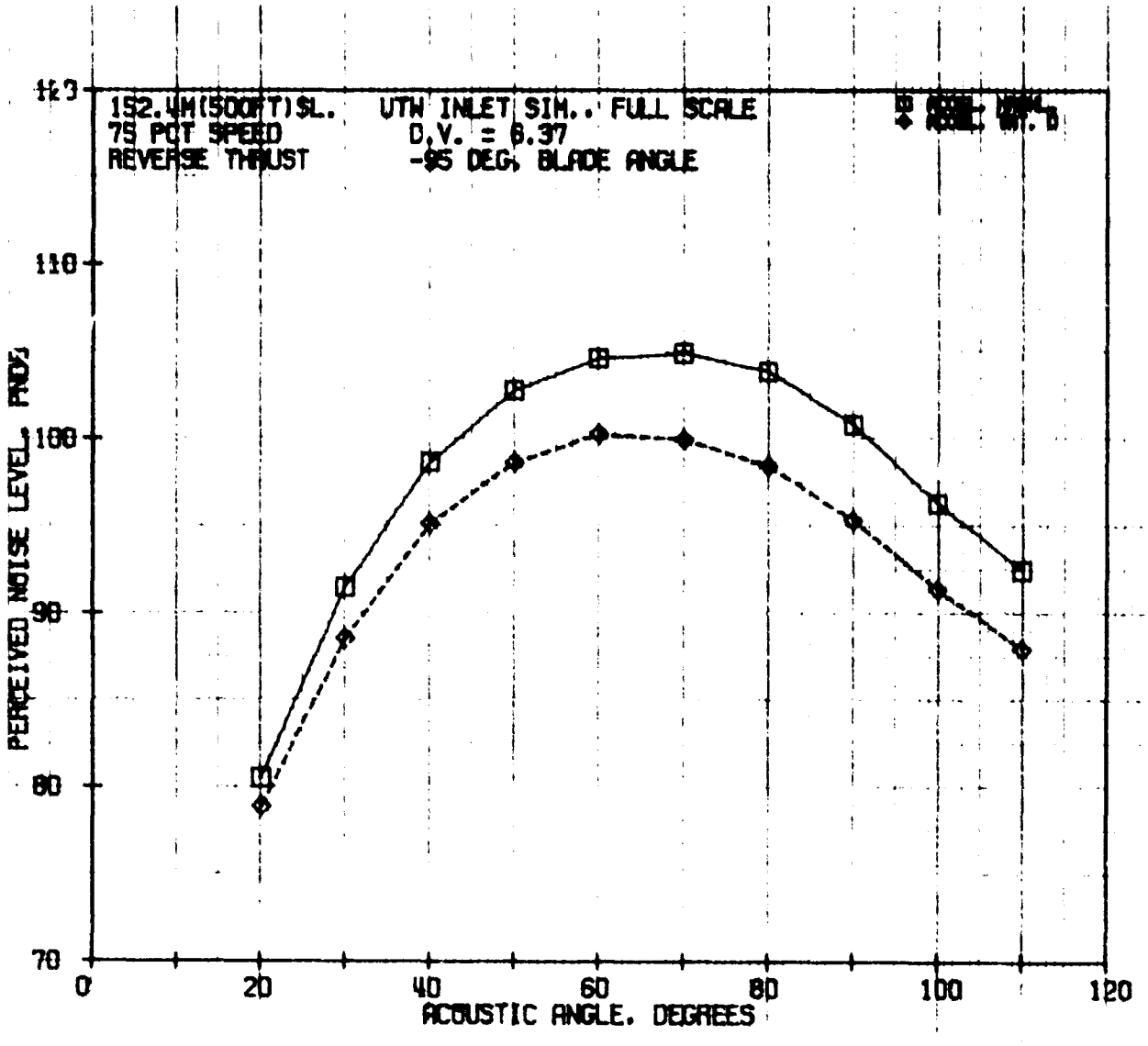

Figure 175. Reverse-Thrust, PNL Directivities of Hard-Wall and Treatment D Accelerating Inlets at -95° Blade Angle and 75% N_{FC}.

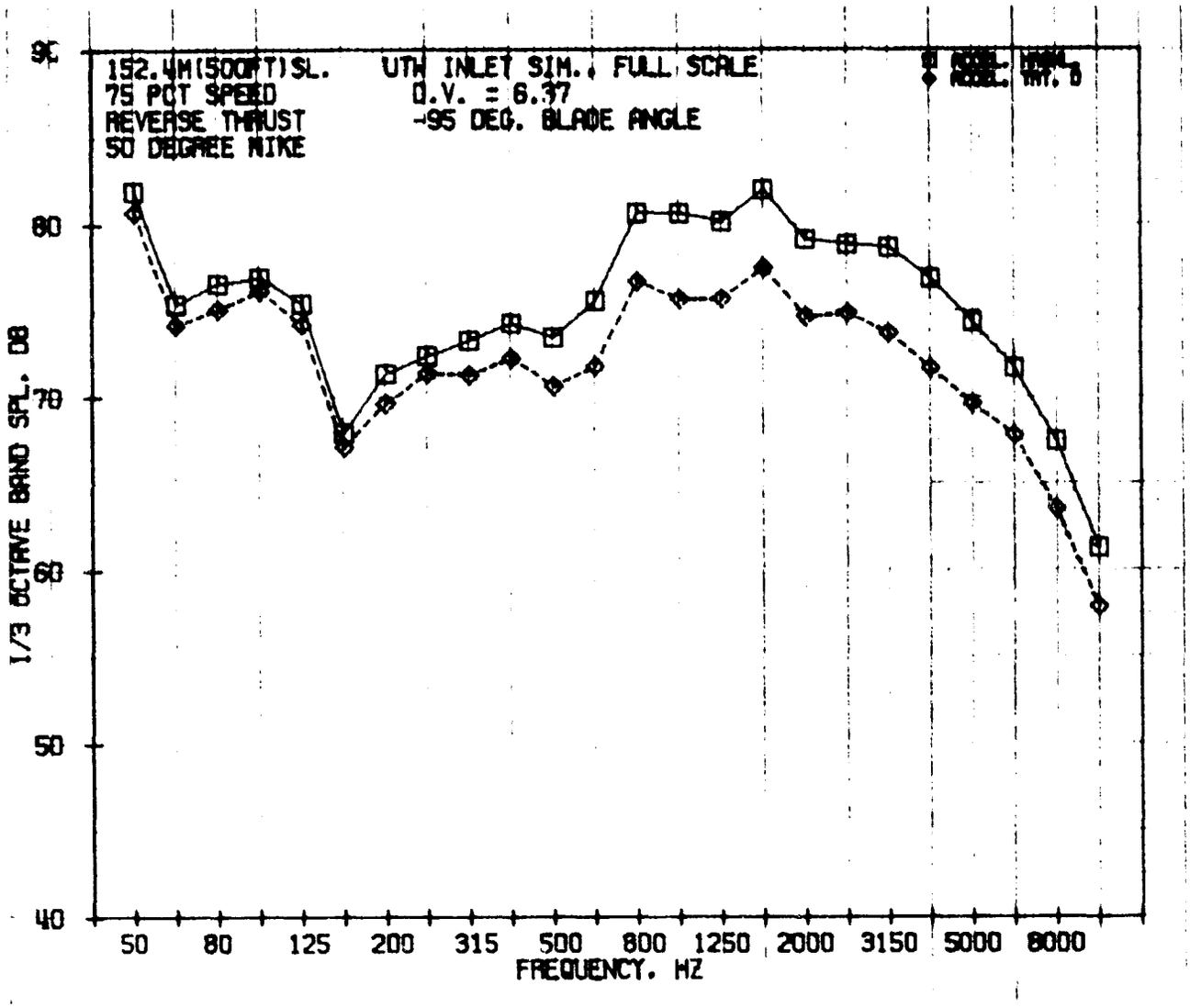

Figure 176. Reverse-Thrust, 1/3-Octave-Band, SPL Spectra of Hard-Wall and Treatment D Accelerating Inlets at -95° Blade Angle and 75% N_{FC} at 50°.

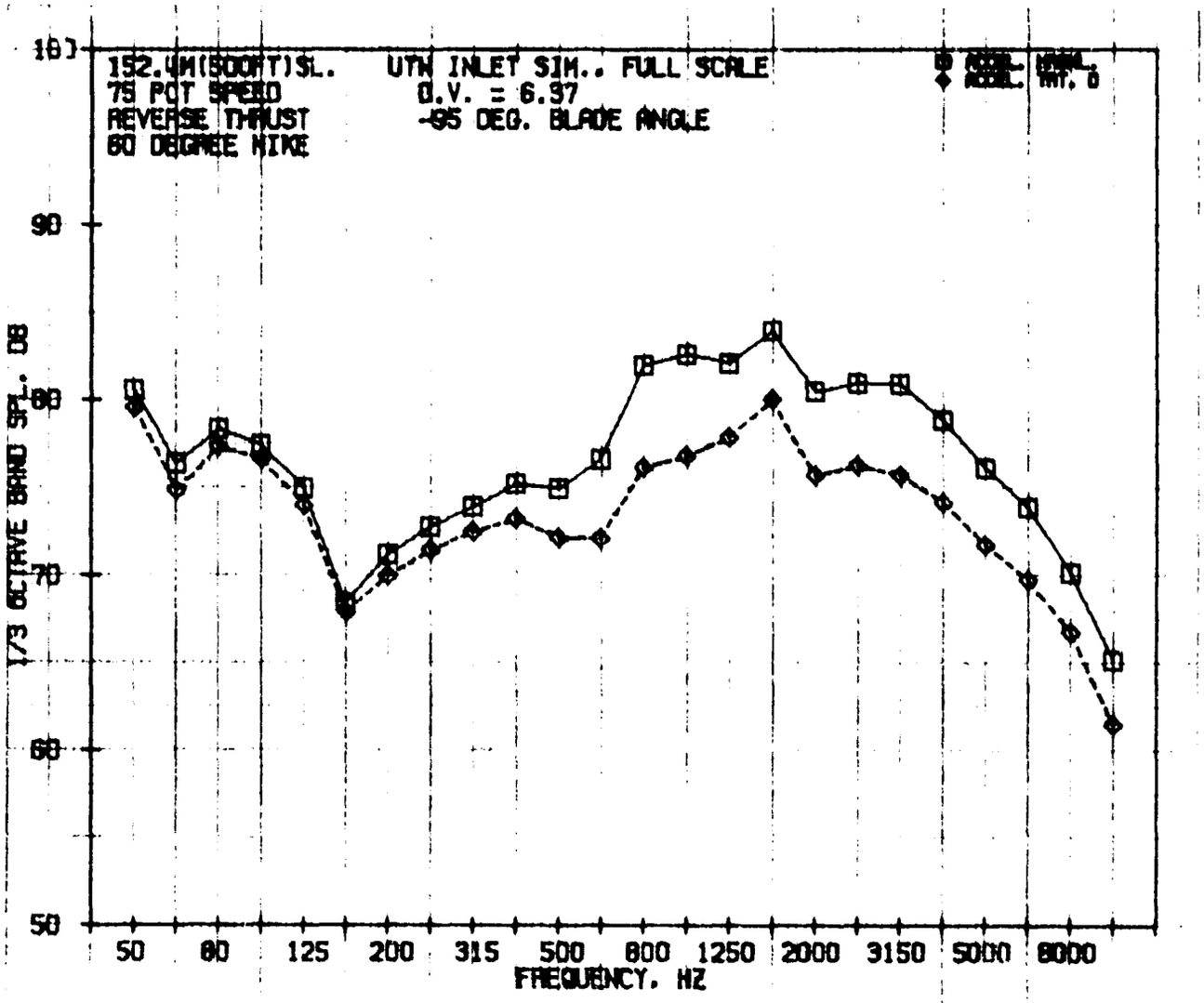

Figure 177. Reverse-Thrust, 1/3-Octave-Band, SPL Spectra of Hard-Wall and Treatment D Accelerating Inlets at -95° Blade Angle and 75% N_{FC} at 60°.

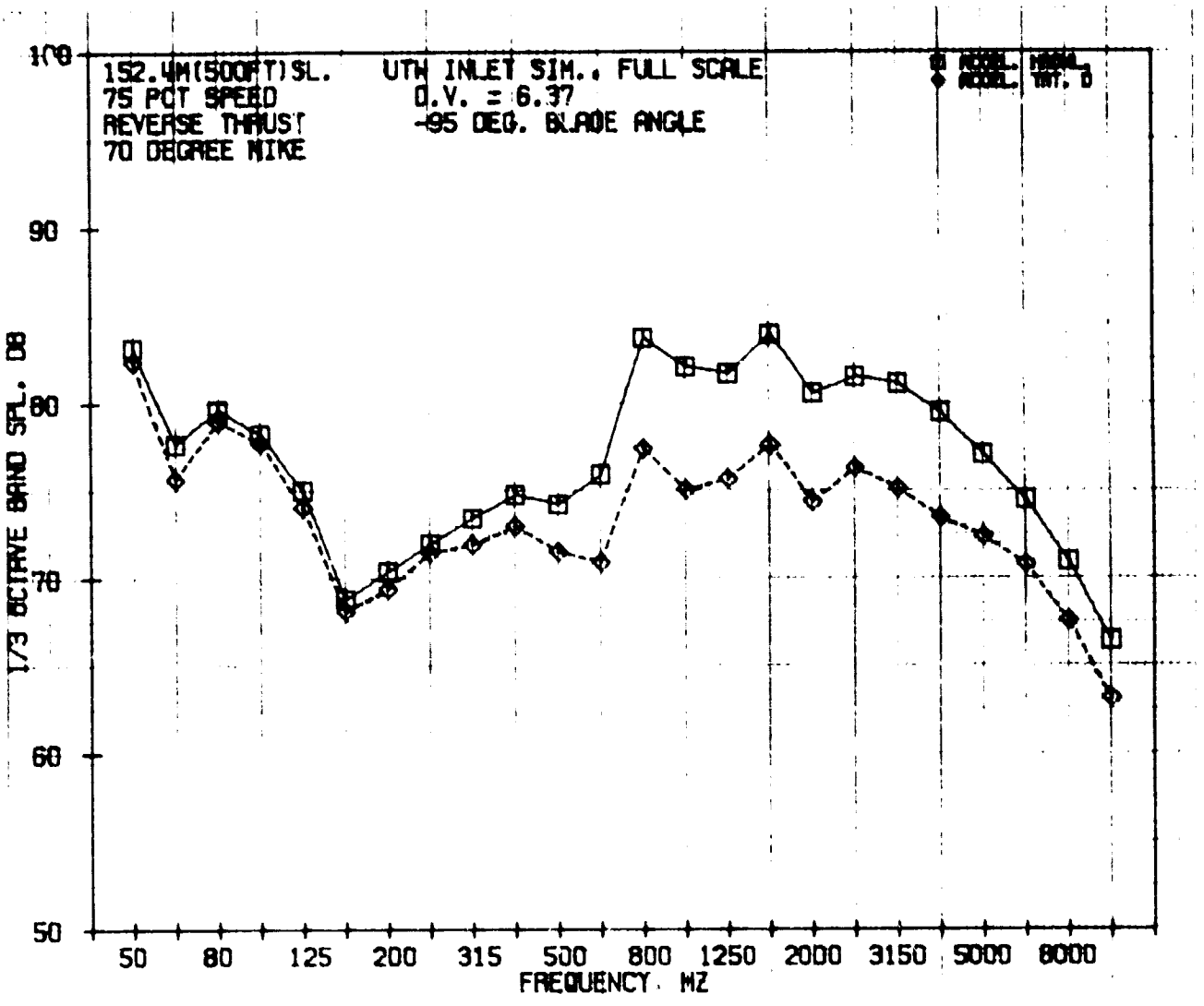

Figure 178. Reverse-Thrust, 1/3-Octave-Band, SPL Spectra of Hard-Wall and Treatment D Accelerating Inlets at -95° Blade Angle and 75% N_{FC} at 70°.

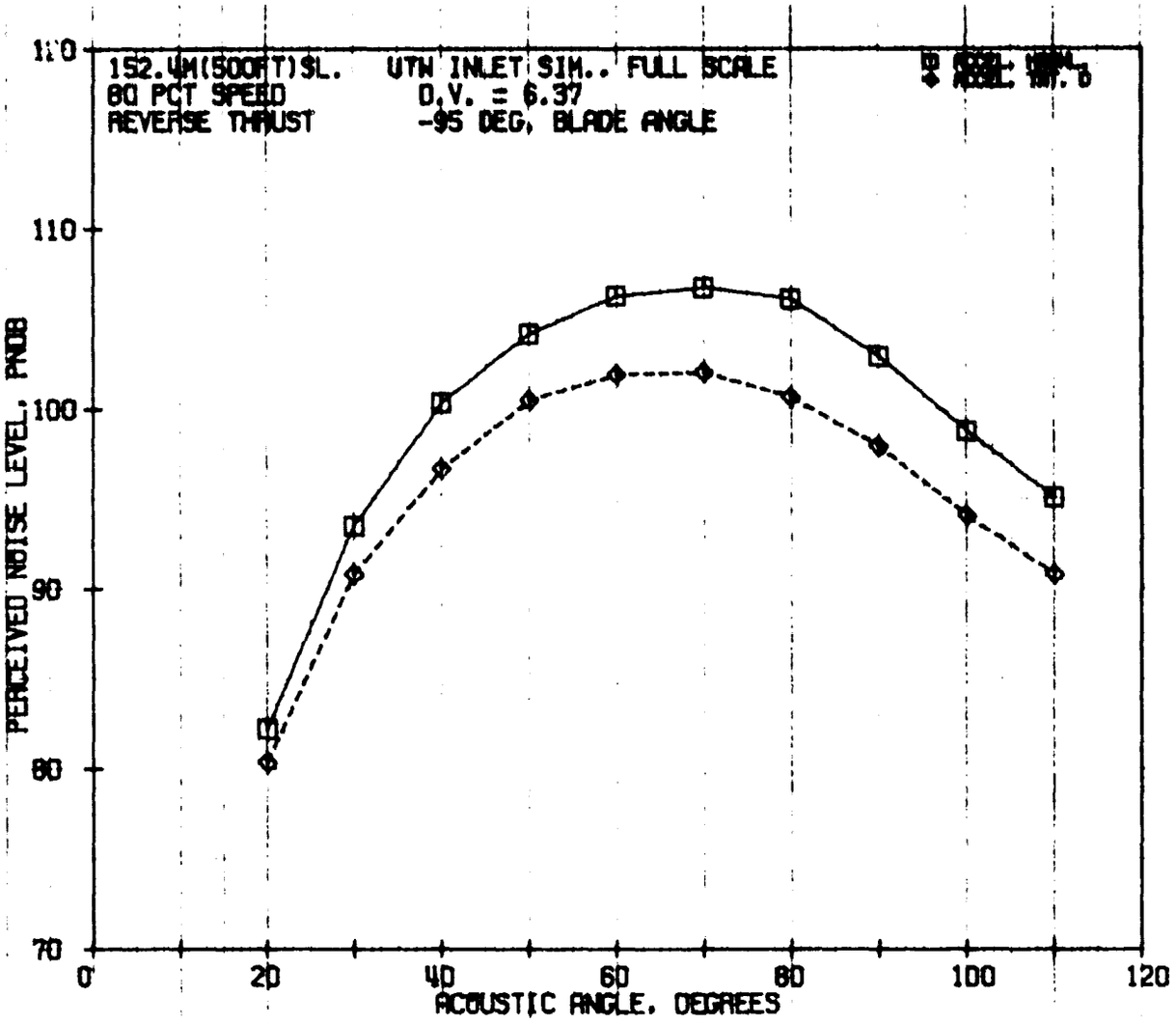

Figure 179. Reverse-Thrust, PNL Directivities of Hard-Wall and Treatment D Accelerating Inlets at -95° Blade Angle and 80% N_{FC}.

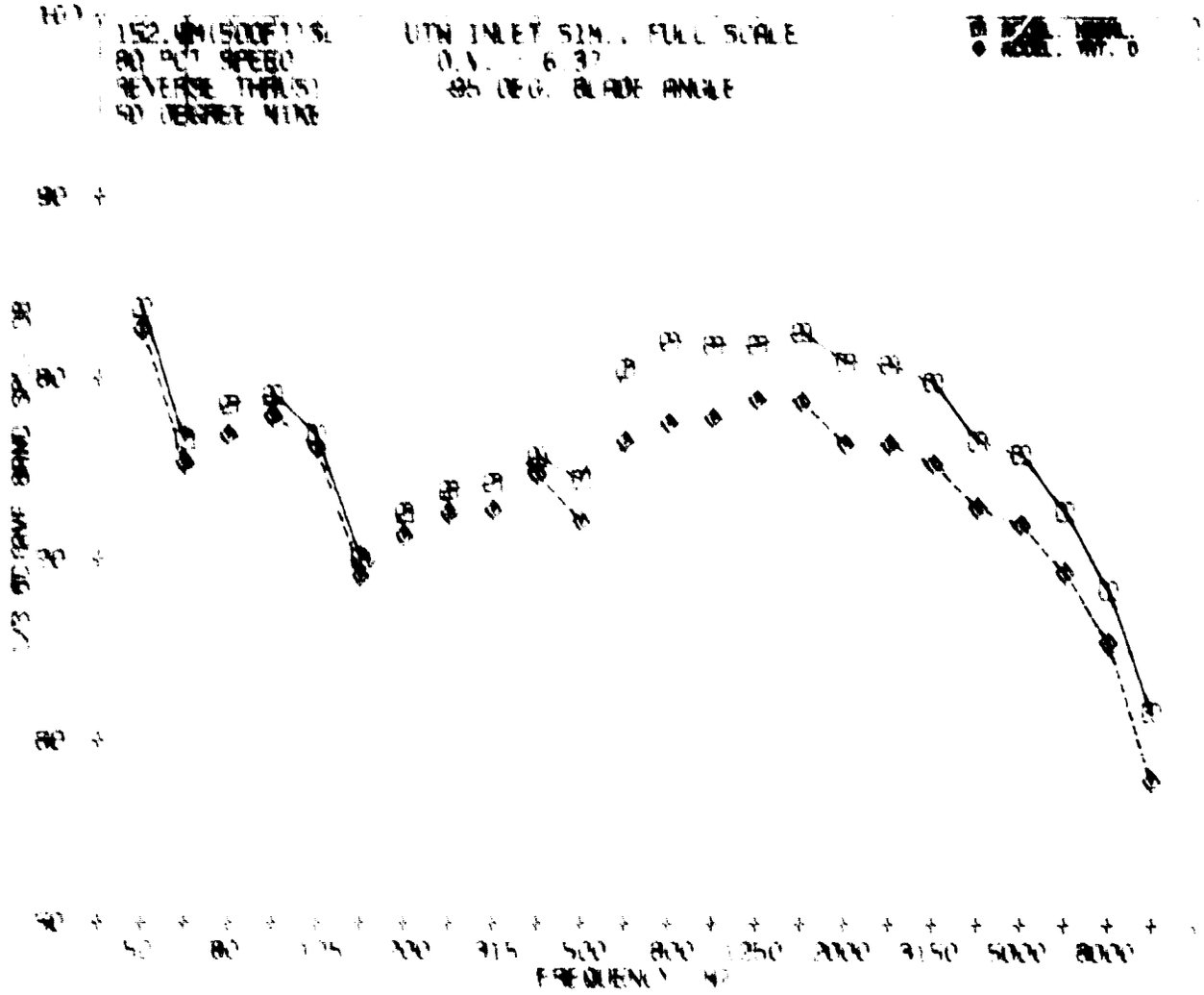

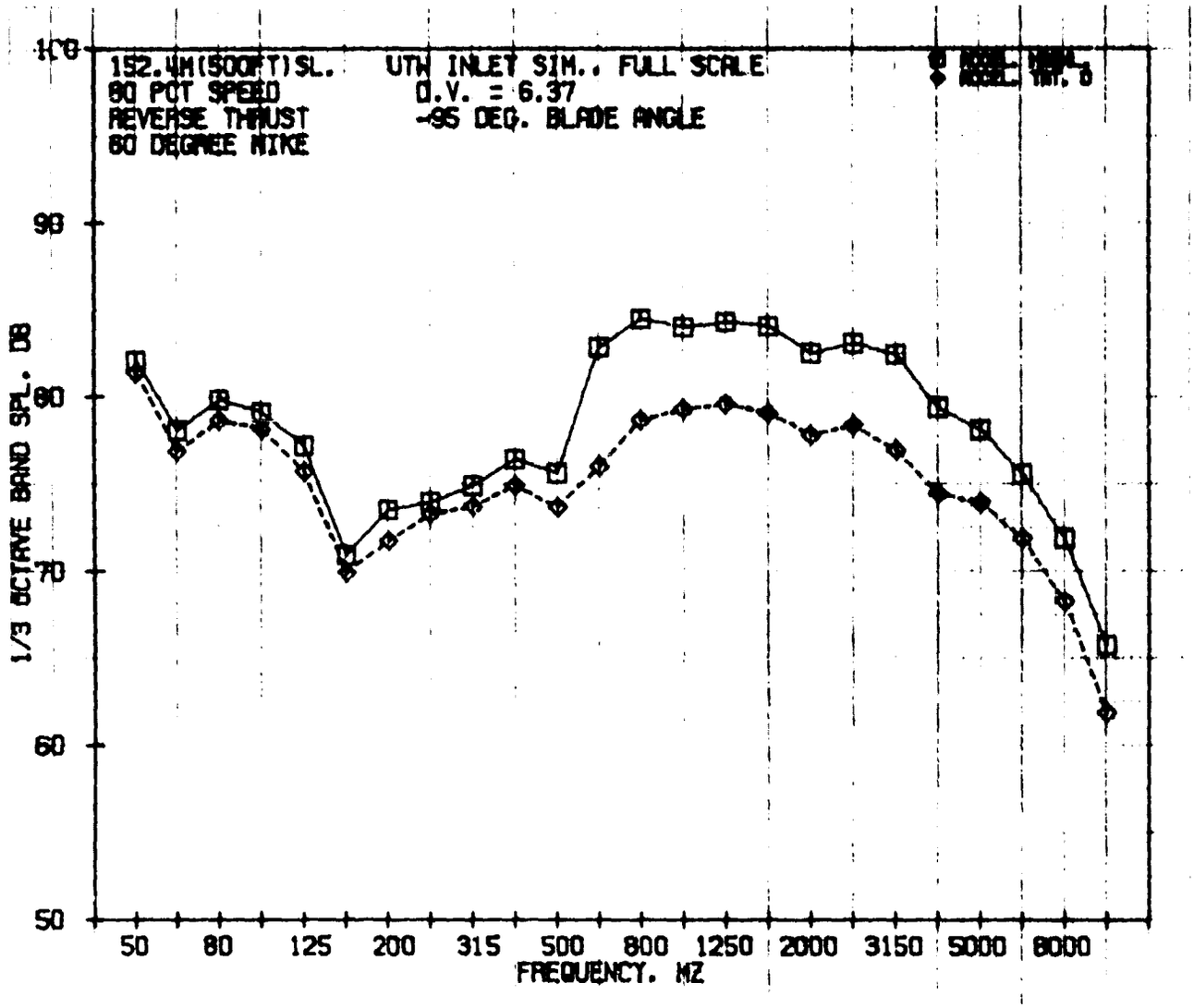

Figure 181. Reverse-Thrust, 1/3-Octave-Band, SPL Spectra of Hard-Wall and Treatment D Accelerating Inlets at -95° Blade Angle and 80% N_{FC} at 60°.

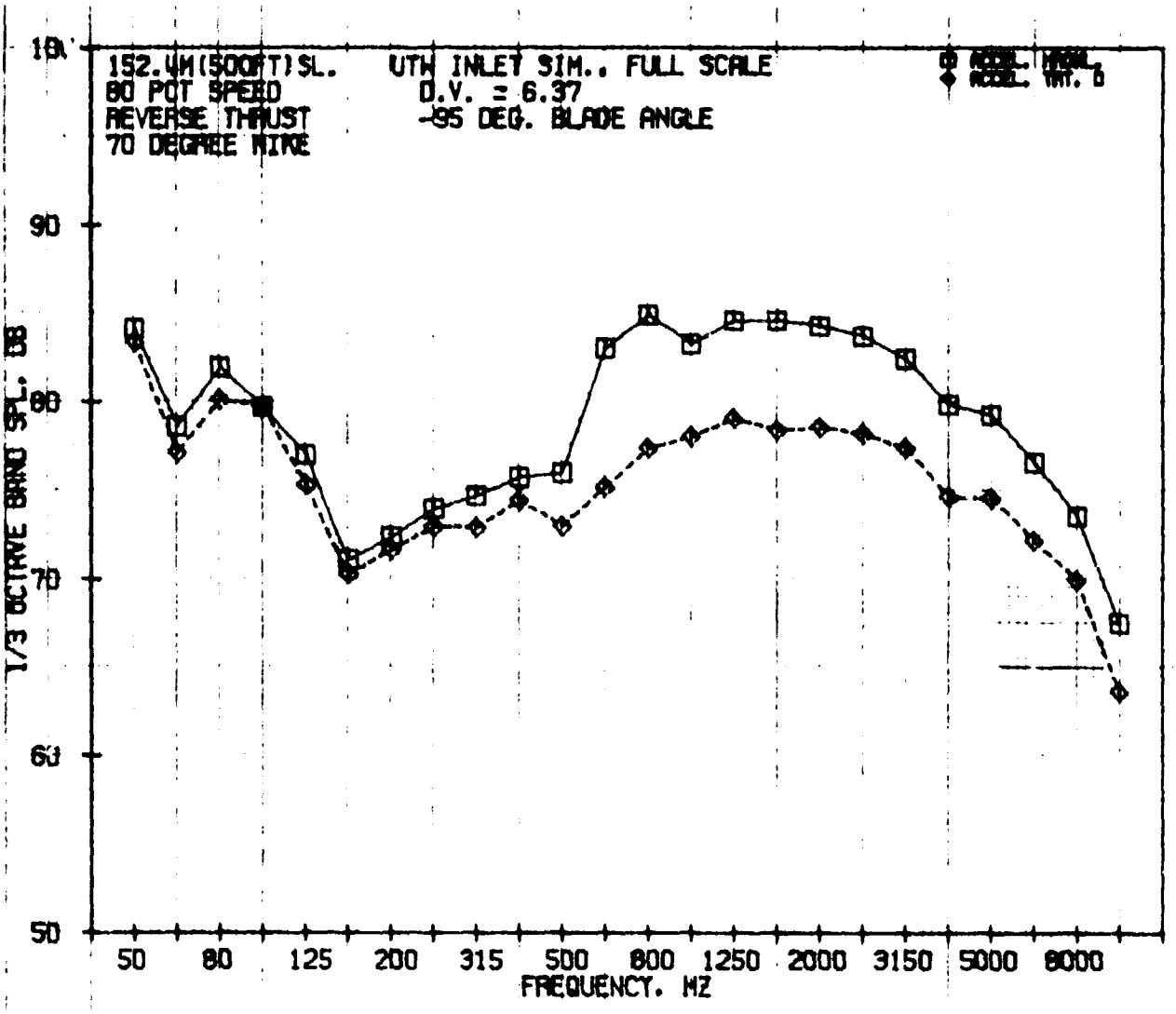

Figure 182. Reverse-Thrust, 1/3-Octave-Band, SPL Spectra of Hard-Wall and Treatment D Accelerating Inlets at -95° Blade Angle and 80% N_{FC} at 70°.

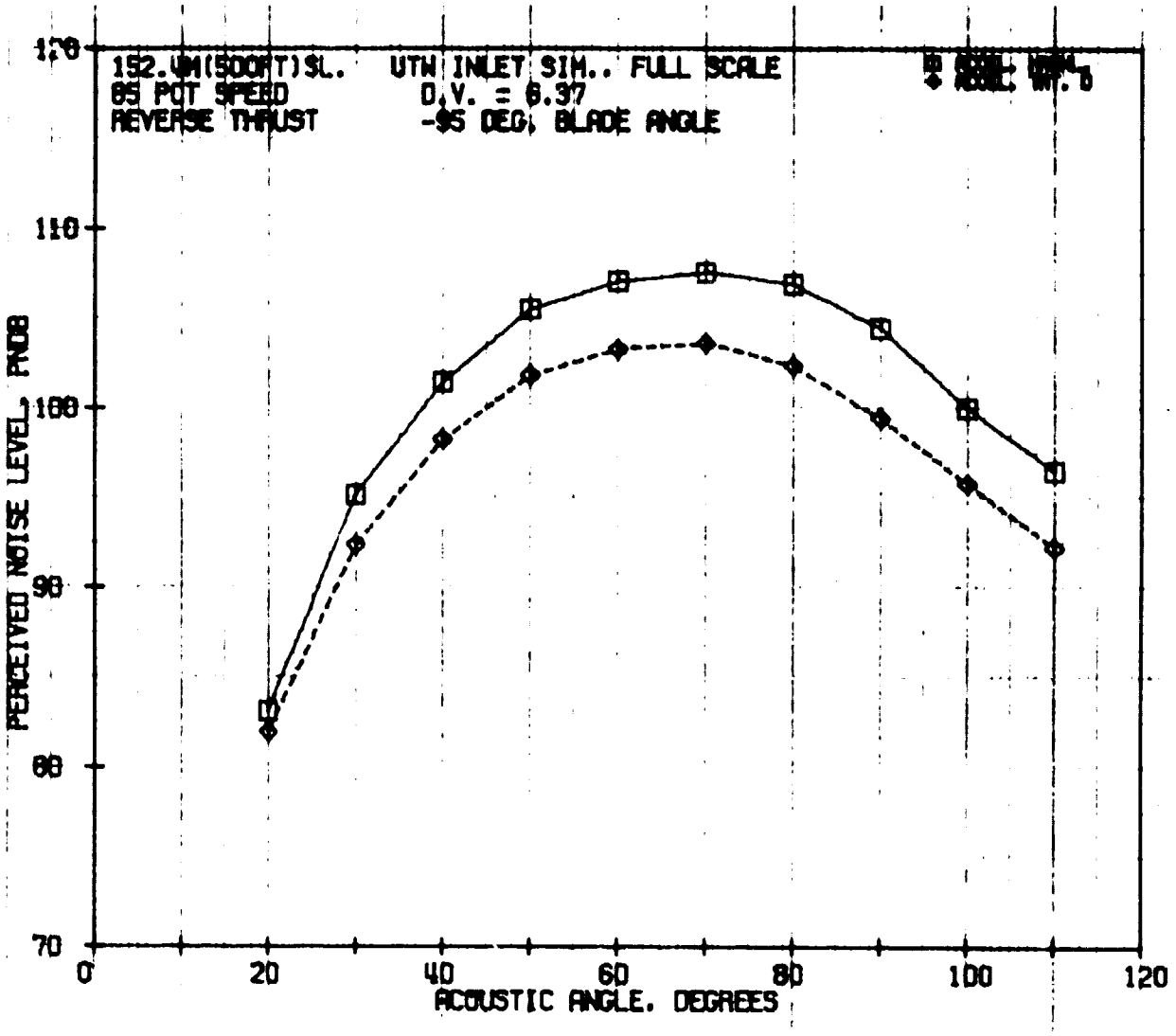

Figure 183. Reverse-Thrust, PNL Directivities of Hard-Wall and Treatment D Accelerating Inlets at -95° Blade Angle and 85% N_{FC}.

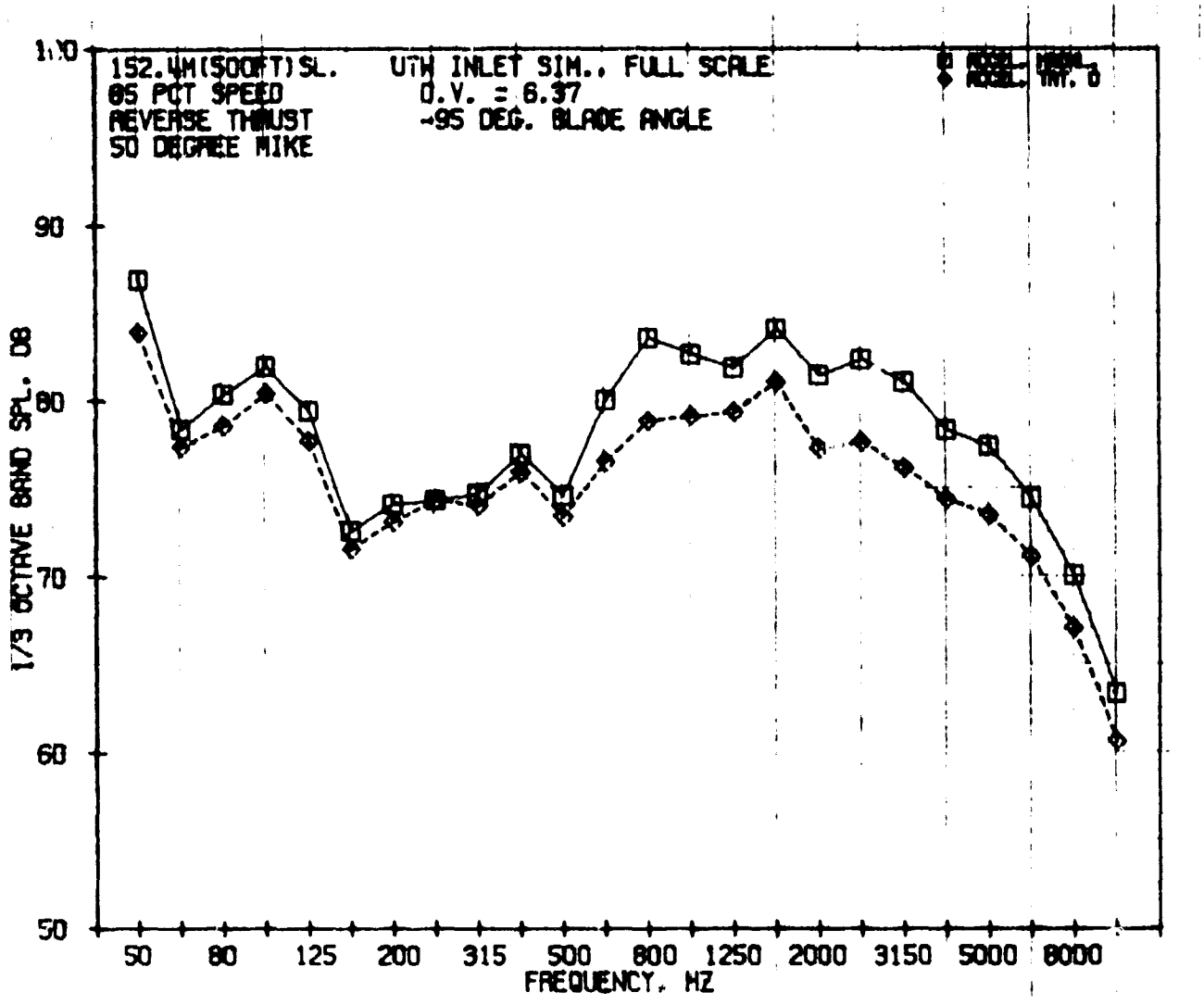

Figure 184. Reverse-Thrust, 1/3-Octave-Band, SPL Spectra of Hard-Wall and Treatment D Accelerating Inlets at -95° Blade Angle and 85% N_{FC} at 50°.

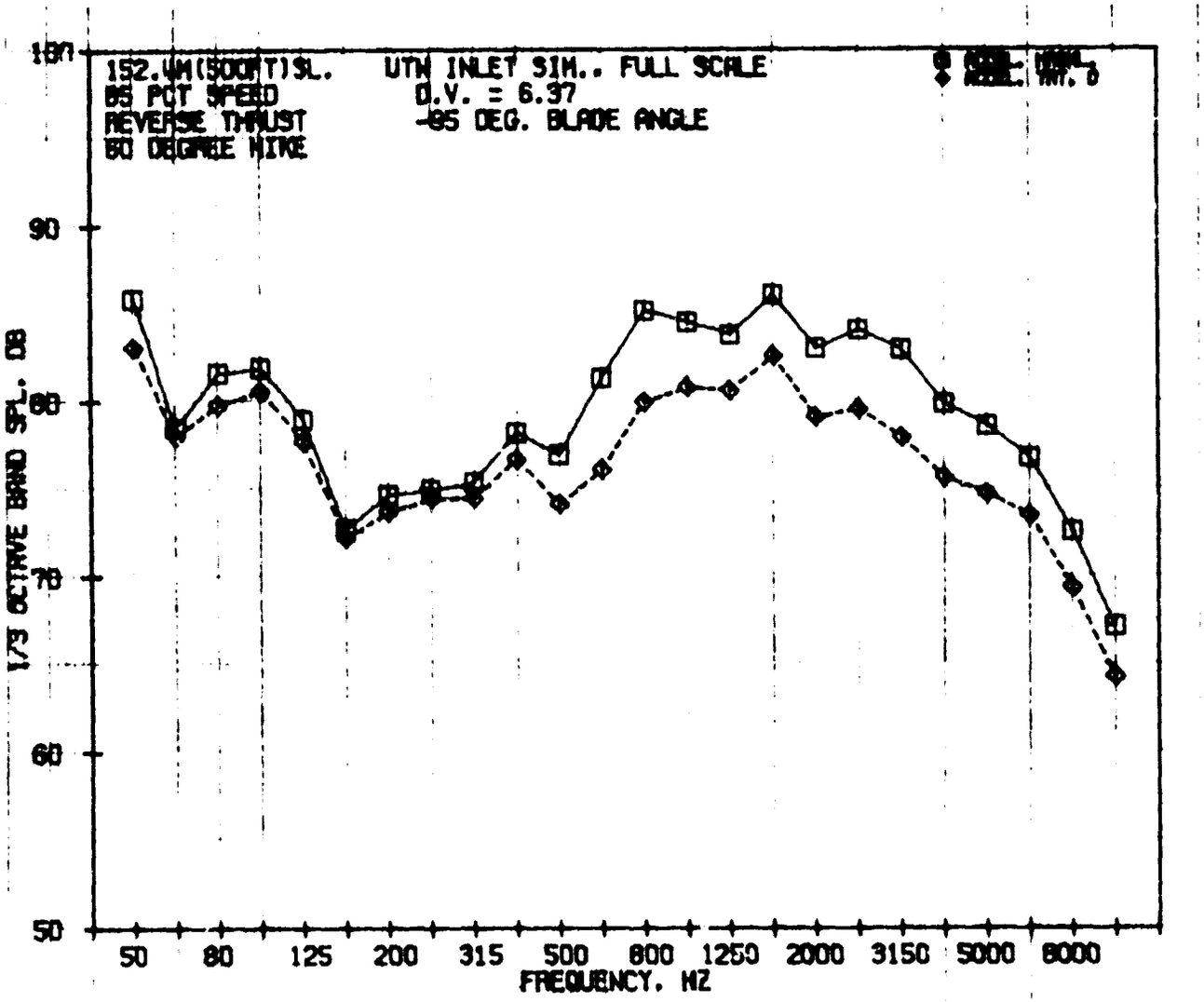

Figure 185. Reverse-Thrust, 1/3-Octave-Band, SPL Spectra of Hard-Wall and Treatment D Accelerating Inlets at -95° Blade Angle and 85% N_{FC} at 60°.

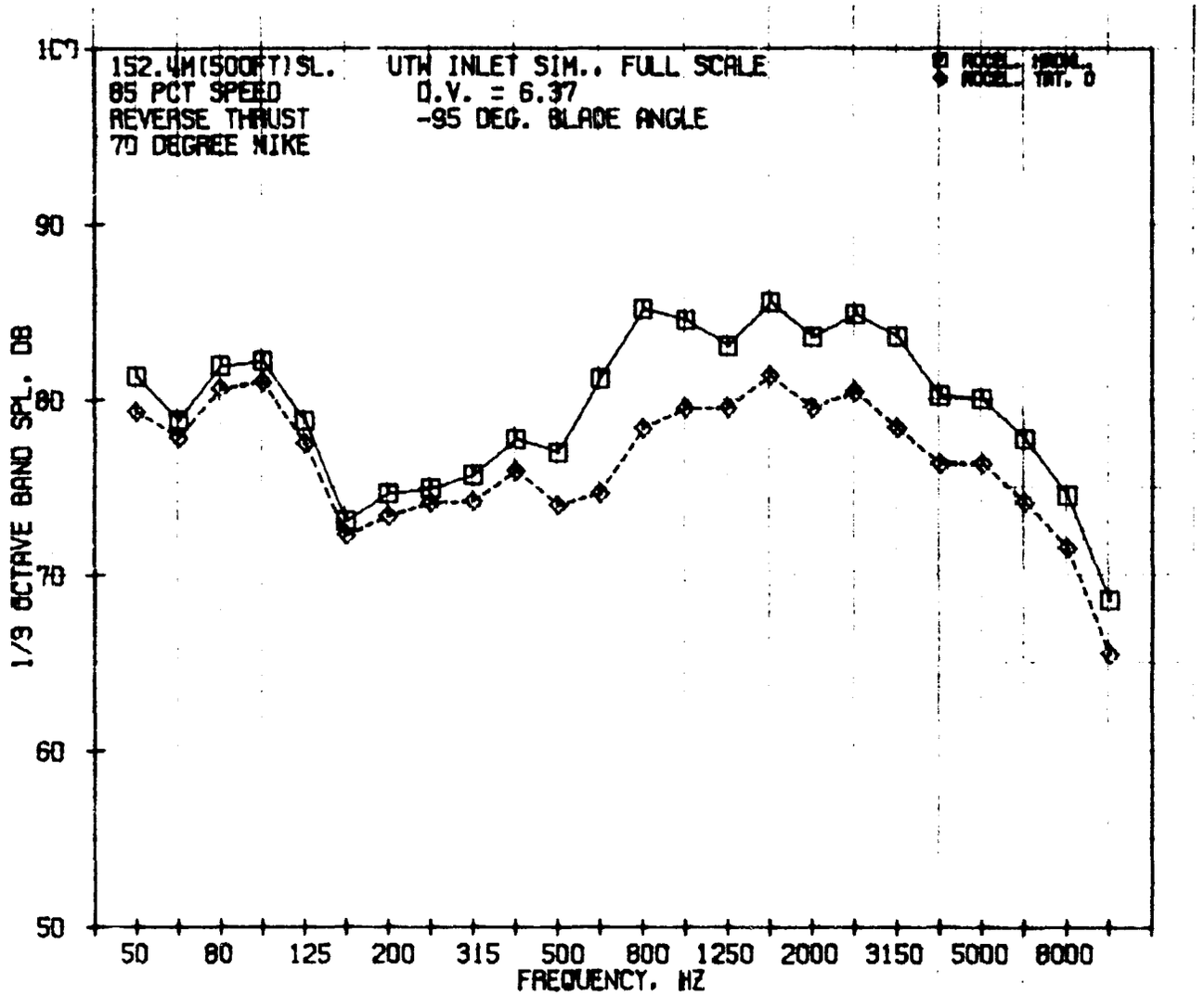

Figure 186. Reverse-Thrust, 1/3-Octave-Band, SPL Spectra of Hard-Wall and Treatment D Accelerating Inlets at -95° Blade Angle and 85% N_{FC} at 70°.

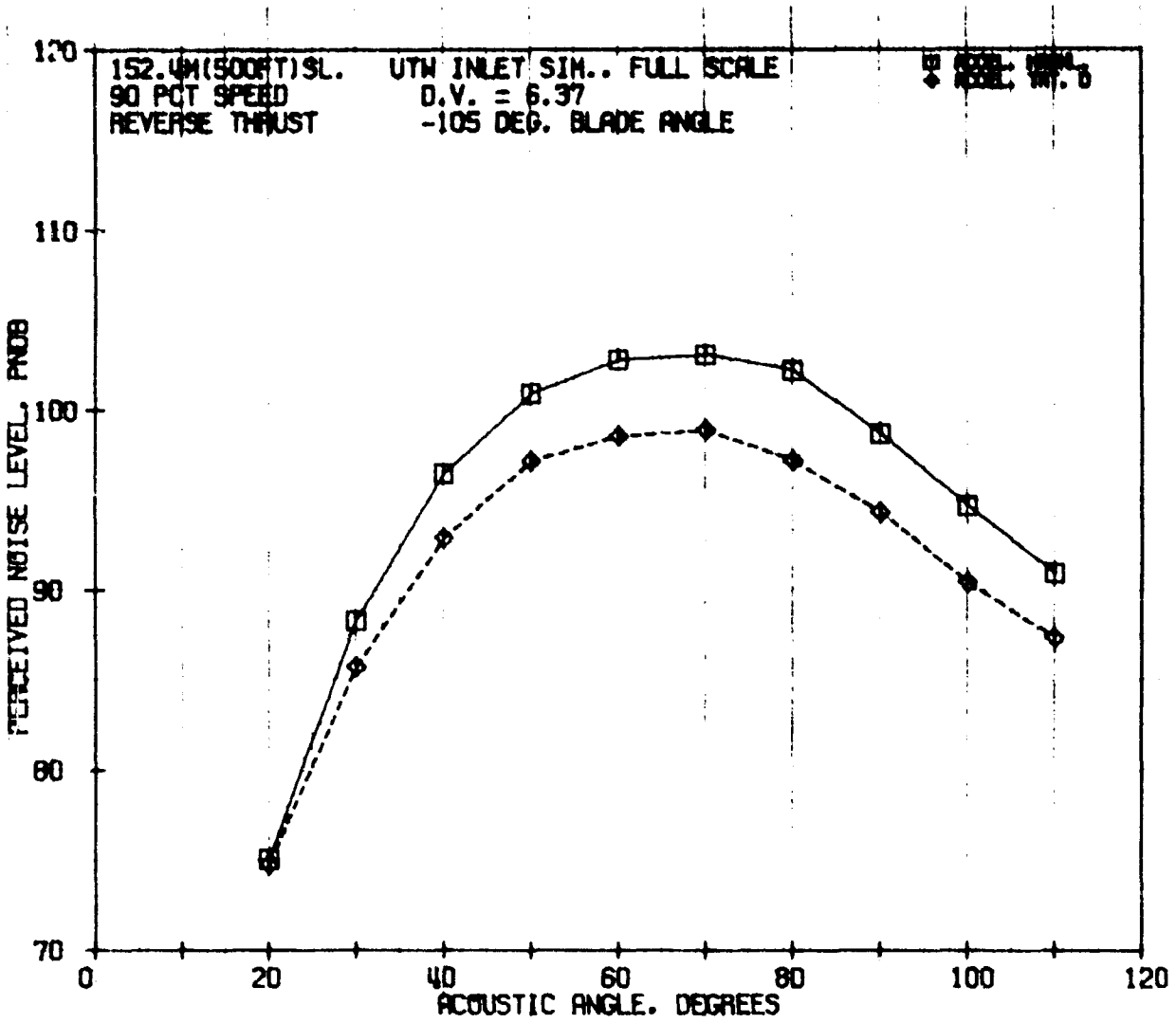

Figure 187. Reverse-Thrust, PNL Directivities of Hard-Wall and Treatment D Accelerating Inlets at -105° Blade Angle and 90% N_{FC}.

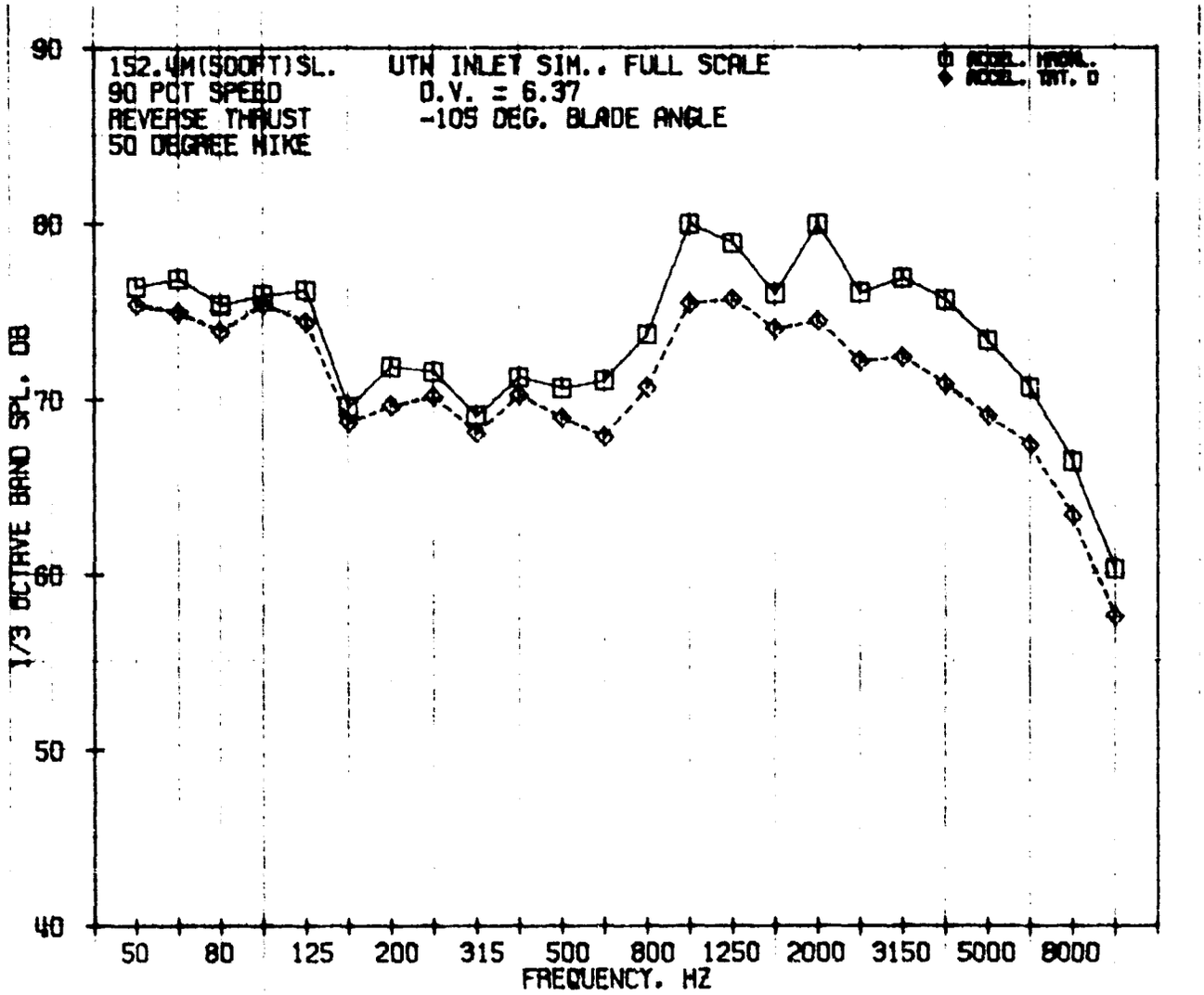

Figure 188. Reverse-Thrust, 1/3-Octave-Band, SPL Spectra of Hard-Wall and Treatment D Accelerating Inlets at -105° Blade Angle and 90% N_{FC} at 50°.

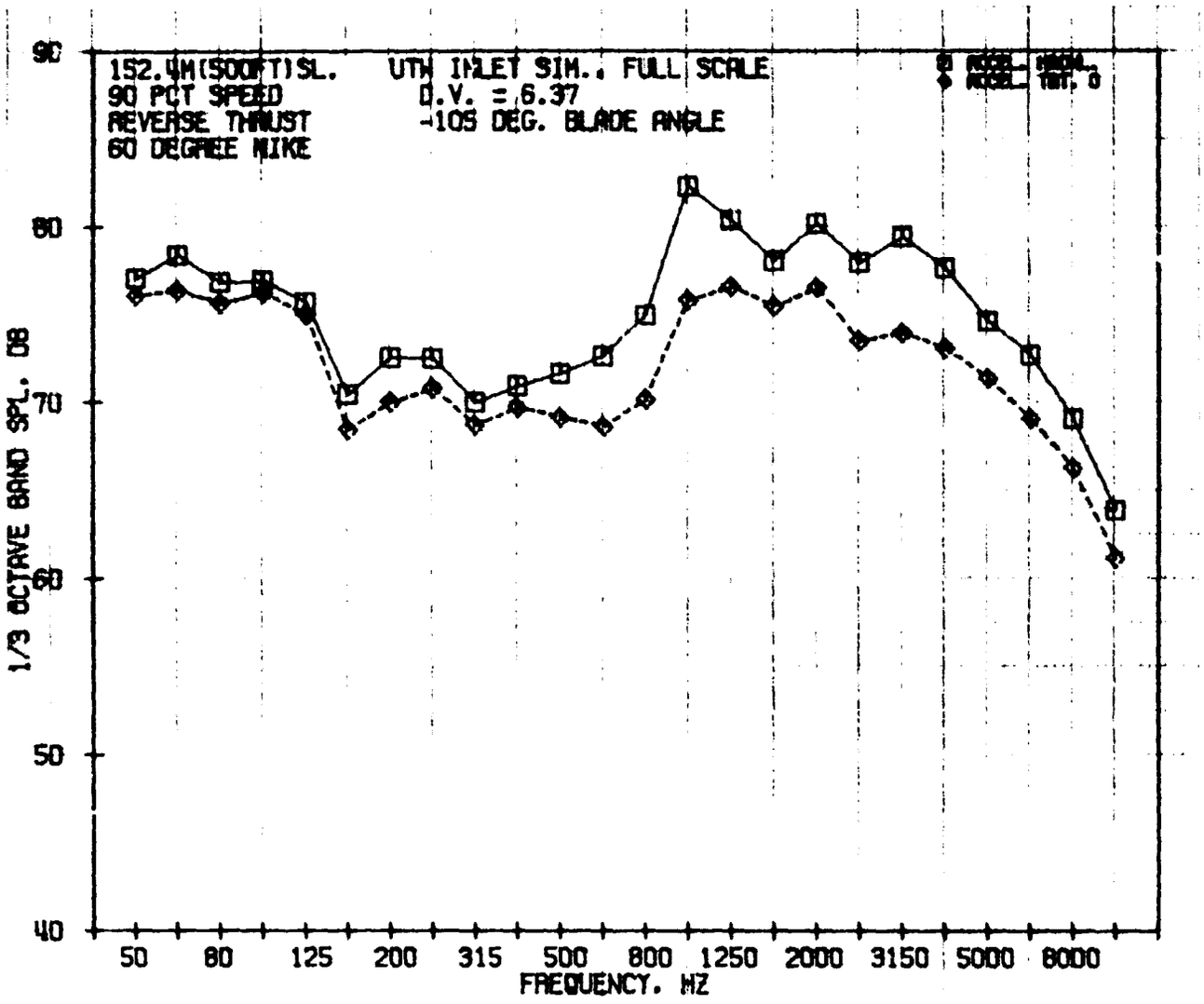

Figure 189. Reverse-Thrust, 1/3-Octave-Band, SPL Spectra of Hard-Wall and Treatment D Accelerating Inlets at -105° Blade Angle and 90% N_{FC} at 60°.

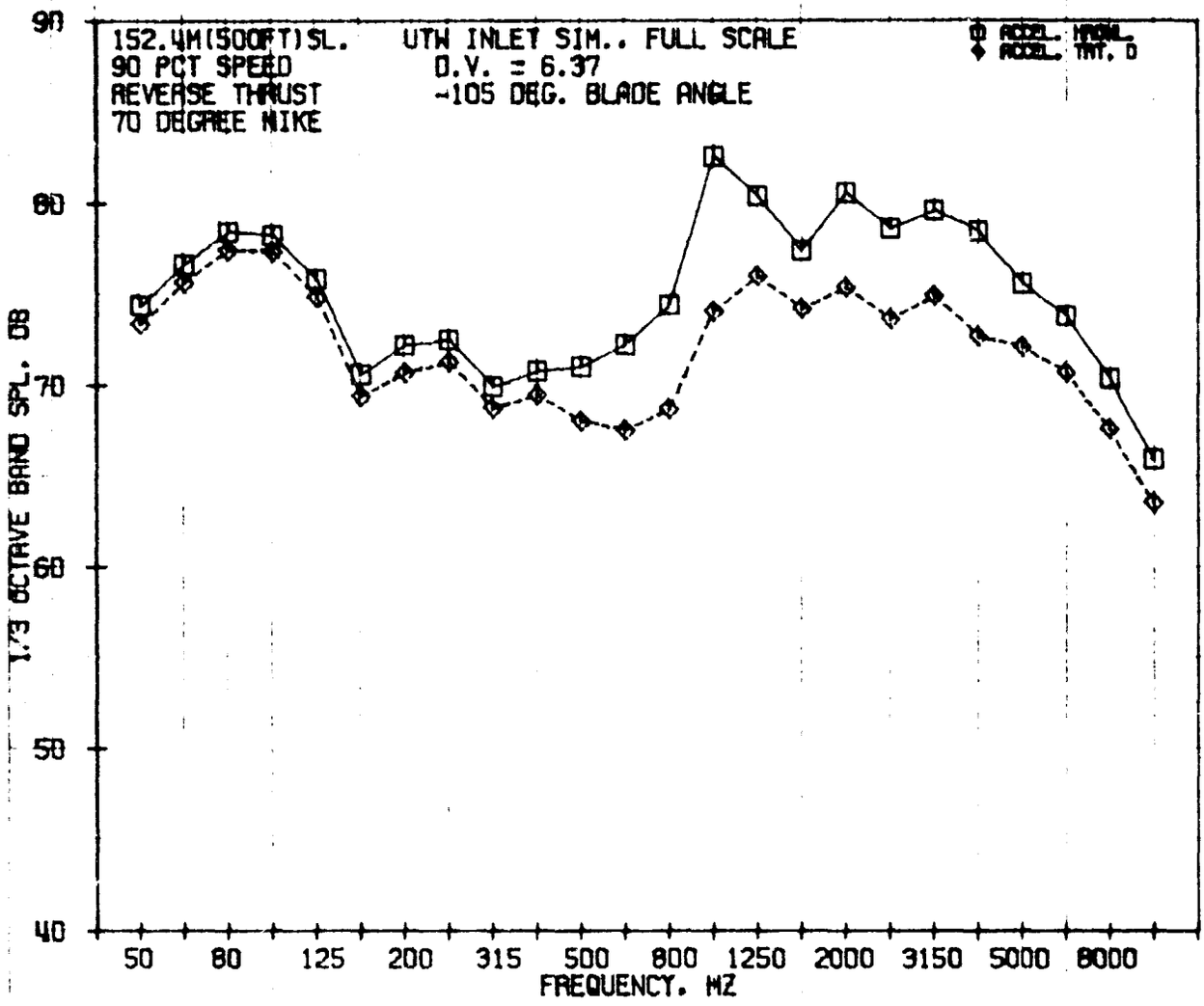

Figure 190. Reverse-Thrust, 1/3-Octave-Band, SPL Spectra of Hard-Wall and Treatment D Accelerating Inlets at -105° Blade Angle and 90% N_{FC} at 70°.

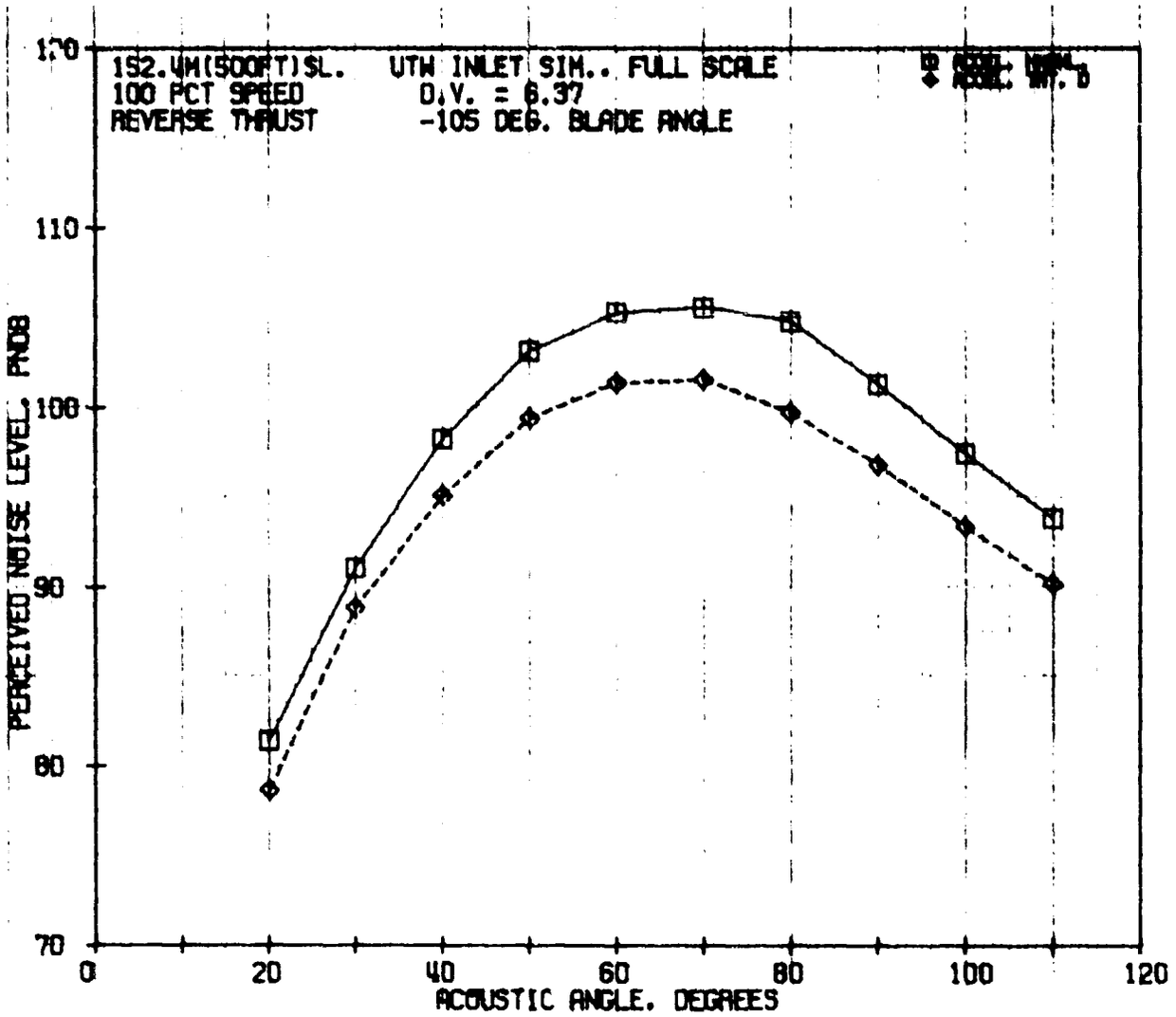

Figure 191. Reverse-Thrust, PNL Directivities of Hard-Wall and Treatment D Accelerating Inlets at -105° Blade Angle and 100% N_{FC}.

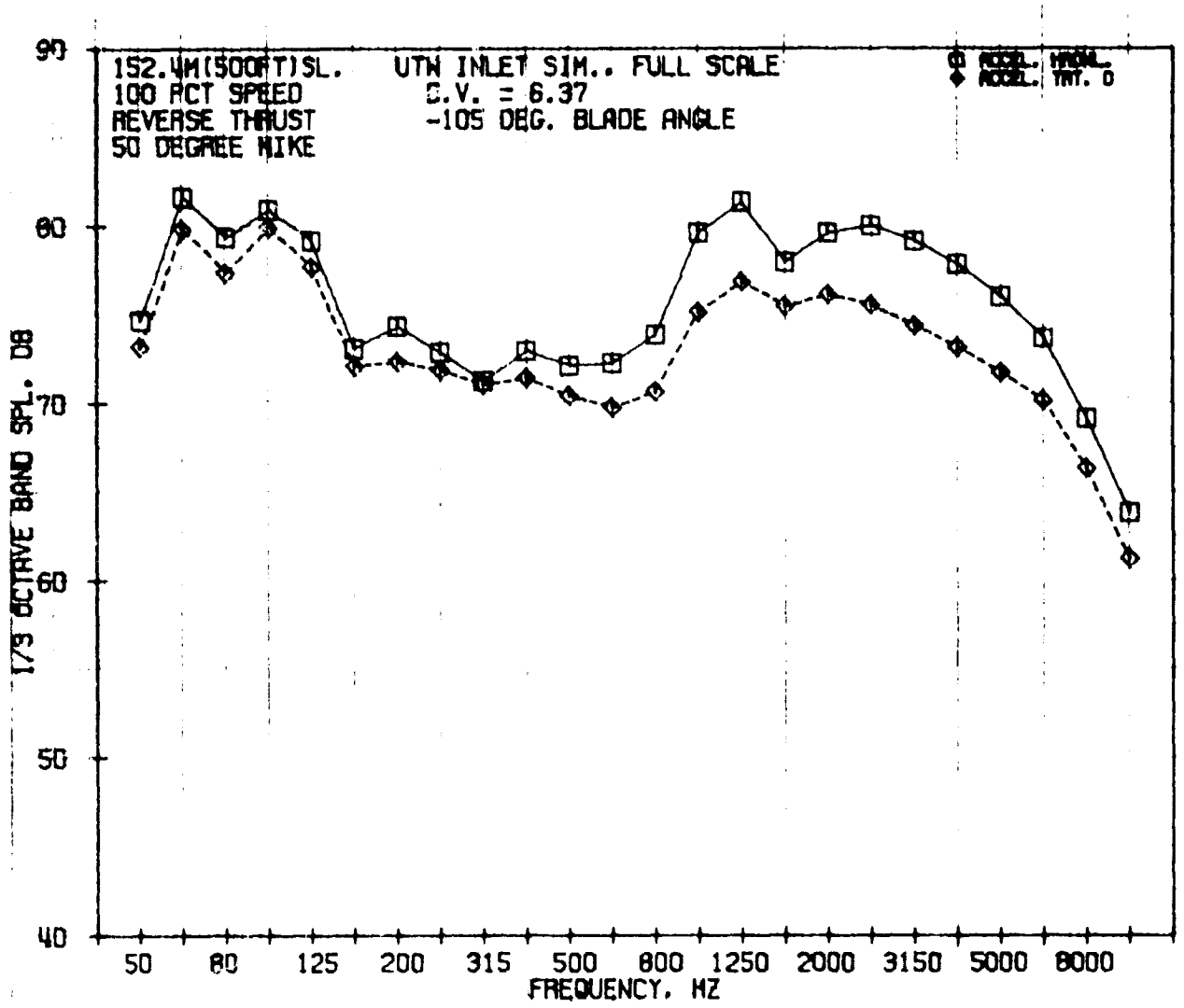

Figure 197. Reverse-Thrust, 1/3-Octave-Band, SPL Spectra of Hard-Wall and Treatment D Accelerating Inlets at -105° Blade Angle and 100% N_{FC} at 50°.

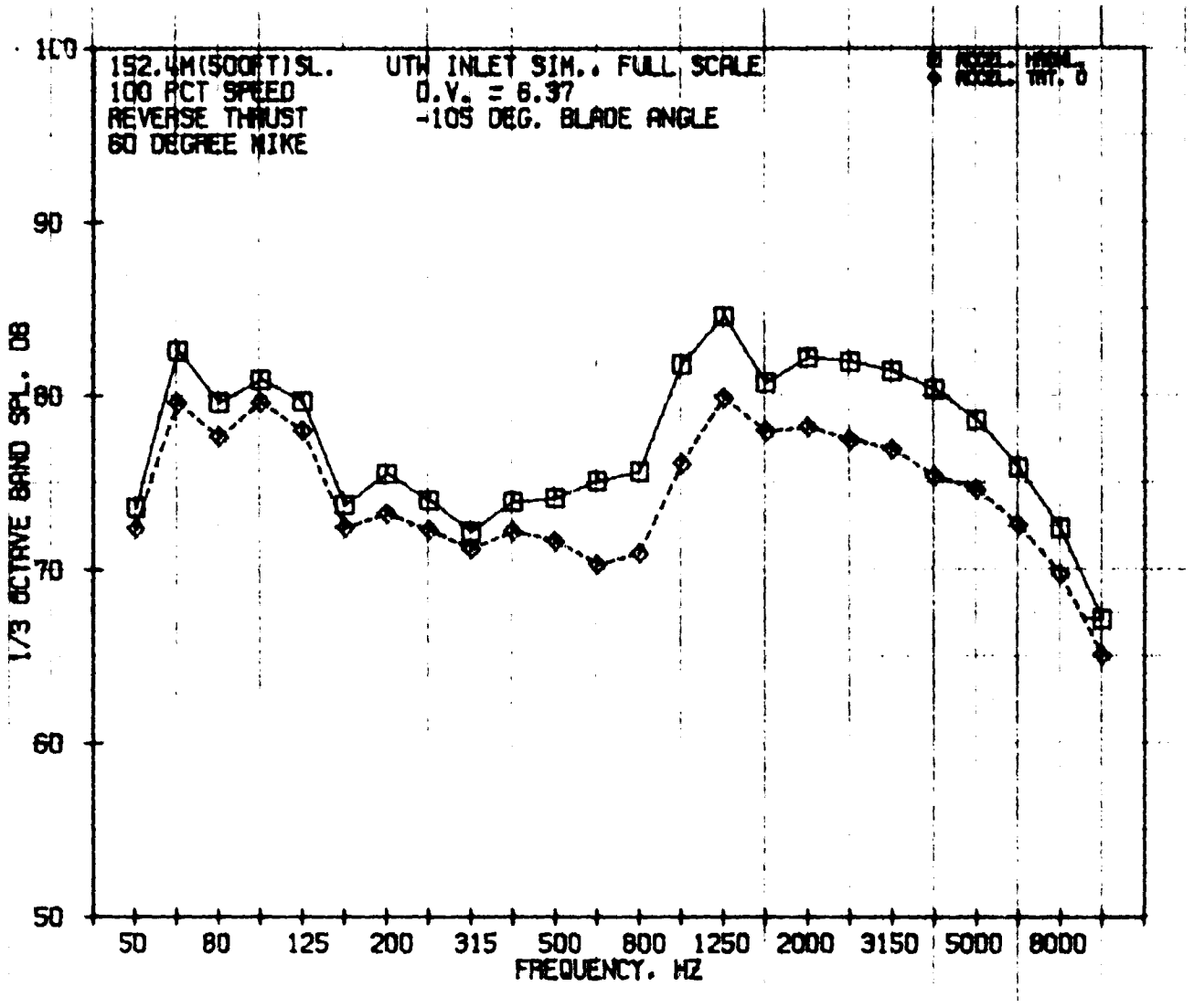

Figure 193. Reverse-Thrust, 1/3-Octave-Band, SPL Spectra of Hard-Wall and Treatment D Accelerating Inlets at -105° Blade Angle and 100% N_{FC} at 60°.

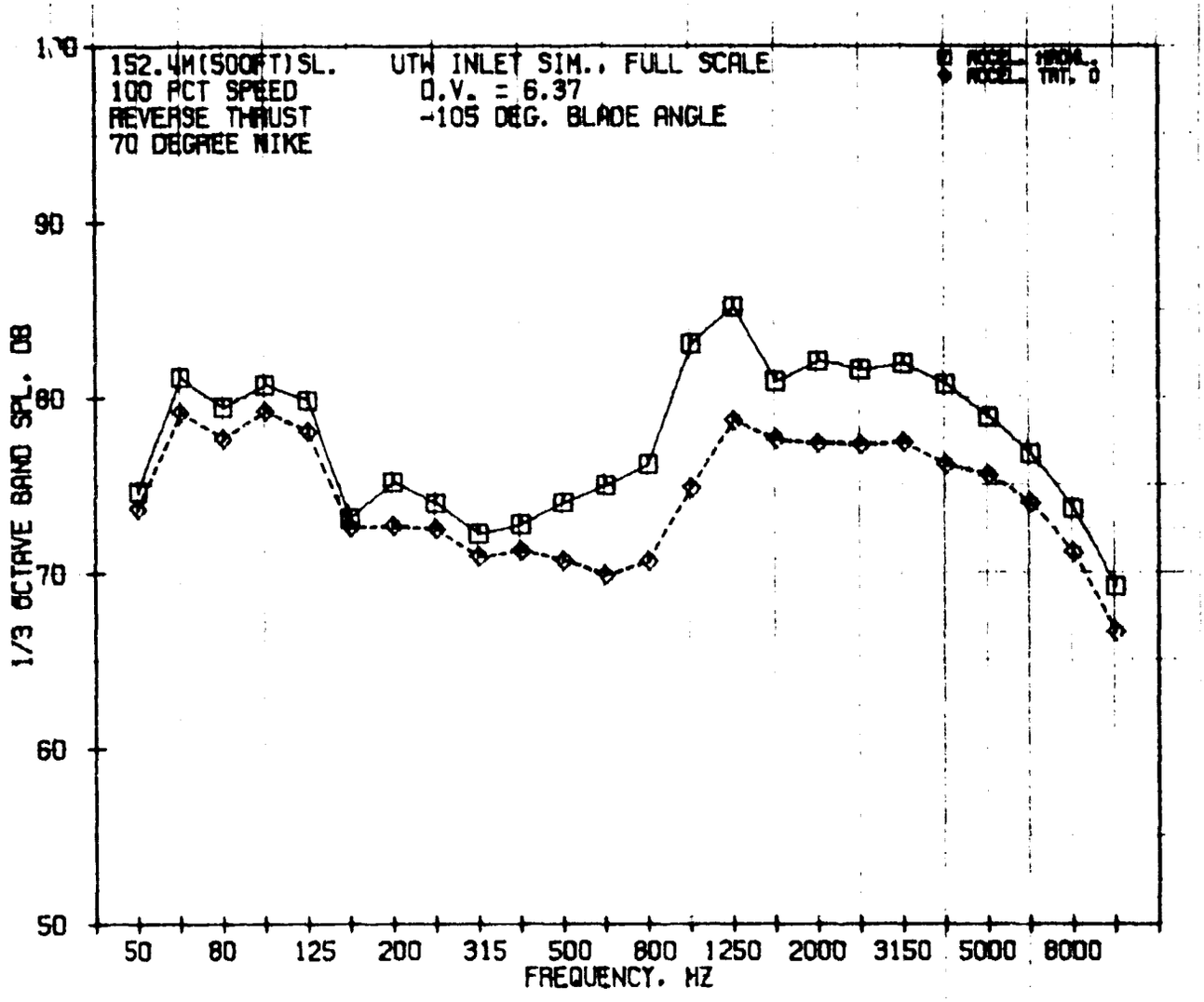

Figure 194. Reverse-Thrust, 1/3-Octave-Band, SPL Spectra of Hard-Wall and Treatment D Accelerating Inlets at -105° Blade Angle and 100% N_{FC} at 70°.

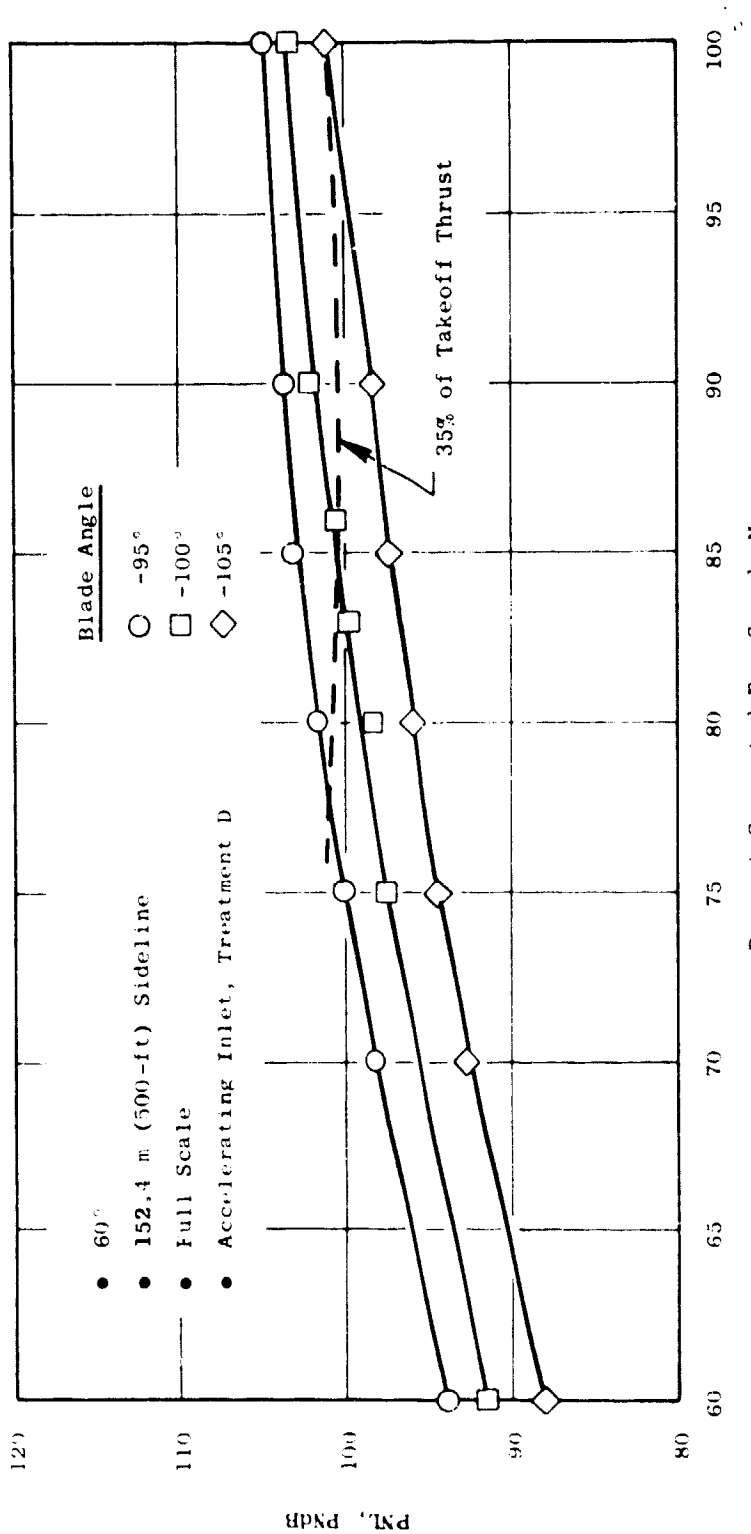

Figure 195. Reverse Thrust PNL Vs. Fan Speed for Treatment D.

10.3 EFFECTIVENESS OF ACCELERATING-INLET TREATMENTS

10.3.1 Measured Suppression Results

The measurement hard-wall and treated-inlet PNL directivities at 86% speed and -100° blade-angle setting are given in Figure 196. Treatments D and B have the highest suppression at all acoustic angles. The directivity pattern for the hard-wall inlet is rather flat from 60° through 80°, with the treated inlet noise peaking at 60°. Thus, the suppression levels at 70° and 80° are somewhat higher (~ 1.0 PNdB) than the suppression measured at 60°.

The hard-wall and suppressed spectra are shown in Figure 197 for reverse thrust at 35% Fn and 86% N_{FC}. The data are for a 60° acoustic angle on a 152.4-m (500-ft) sideline. The presence of a strong fan fundamental tone at 800 Hz, plus the second and third harmonics, are indicated in the hard-wall spectrum. Suppressed spectra indicate (as seen in the earlier comparison of the PNL's) that the treatment D configuration gives the highest level of suppression at most of the 1/3-octave-band frequencies. The peak suppression for treatment D occurs at the 1/3-octave-band frequency containing the fan fundamental frequency; a suppression level of approximately 8 dB is found. The spectra comparison show a broad suppression bandwidth with an average suppression of about 5 dB from 1000 Hz through 6300 Hz. However, the treatment B configuration suppression is, on the average, about 1 dB better than the suppression measured for treatment D, except at the fan fundamental tone where treatment D gives 2 dB to 2.5 dB more suppression. The remaining two treatments, A and C, both give significantly less suppression than treatments D and B; of these two inlets, however, treatment A gives the better suppression. This indicates that the inlet A treatment with a faceplate porosity of 24% offers an acoustic resistance value nearer the optimum value for these inlet conditions than inlet C. Inlet C, with a much lower porosity of 3.6%, undoubtedly has a resistance exceeding the required value at these conditions. Figure 198 and Figure 199 give the hard-wall and suppressed spectra for acoustic angles of 50° and 70° respectively for 86% N_{FC} (that is, 35% thrust), The PNL suppression increases at the 70° angle, as was noted in Figure 196; however, the relative performance of each inlet is similar to that observed for all other angles.

10.3.2 Predicted Versus Measured Suppression

A comparison of the reverse-thrust, suppression spectra for treatments D and B versus the estimated suppression is shown in Figure 200. The suppression estimate is based on previous, forward-thrust, suppression spectra with corrections for the reverse-flow condition. The understanding of treatment performance in the reverse-thrust mode had been limited due to lack of test data. This series of tests has, therefore, provided valuable data in this respect.

The comparison shows that the broadband suppression levels in the higher 1/3-octave frequency bands are somewhat higher than estimated; however, the peak suppression occurs at a lower frequency than predicted. The

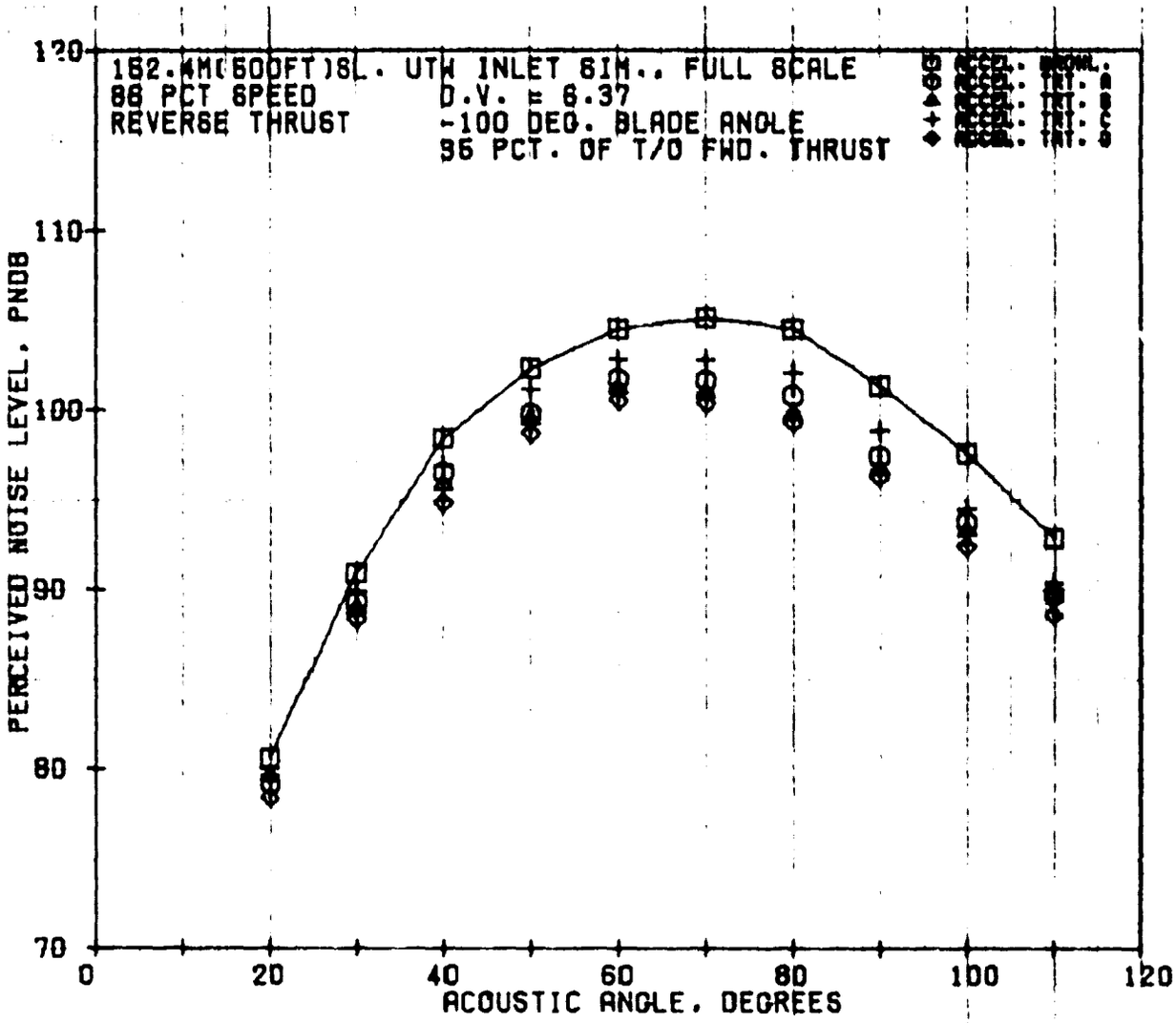

Figure 196. Reverse-Thrust, PNL Directivities for All Accelerating Inlets at 86% N_{FC}.

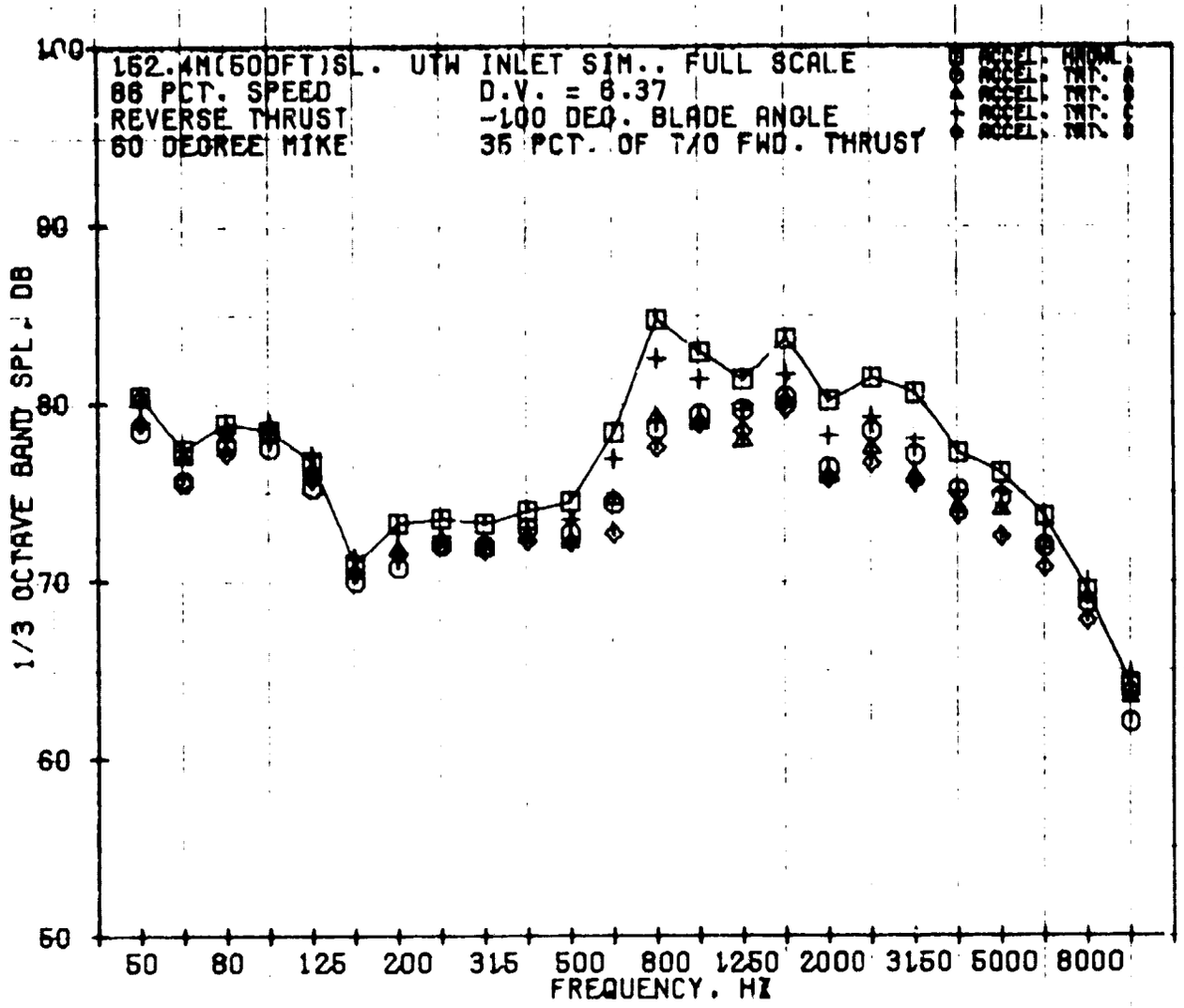

Figure 197. Reverse-Thrust, 1/3-Octave-Band, SPL Spectra for All Accelerating Inlets at 86% N_{FC} and 60°.

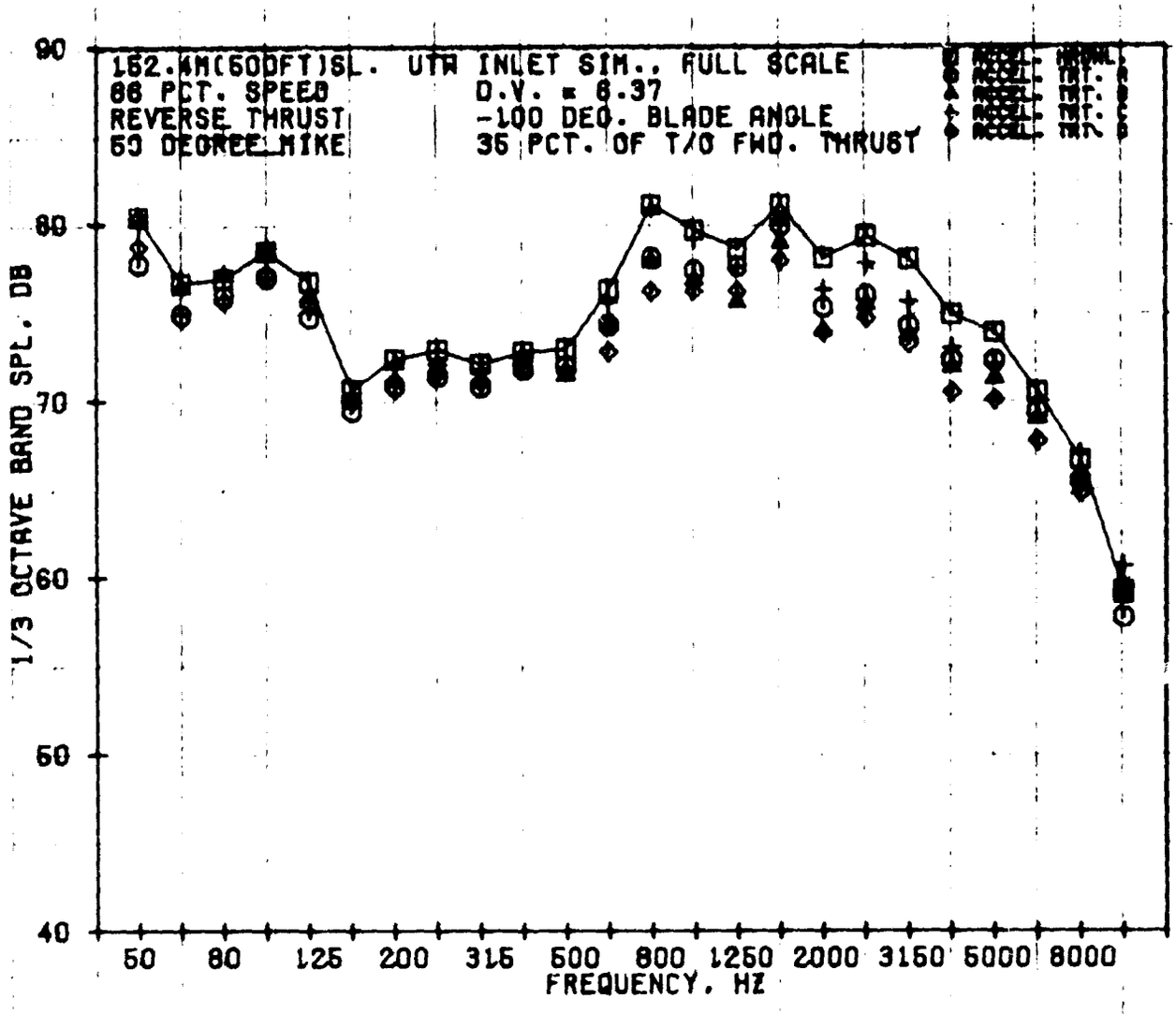

Figure 198. Reverse-Thrust, 1/3-Octave-Band, SPL Spectra of All Accelerating Inlets at 86% N_{FC} and 50°.

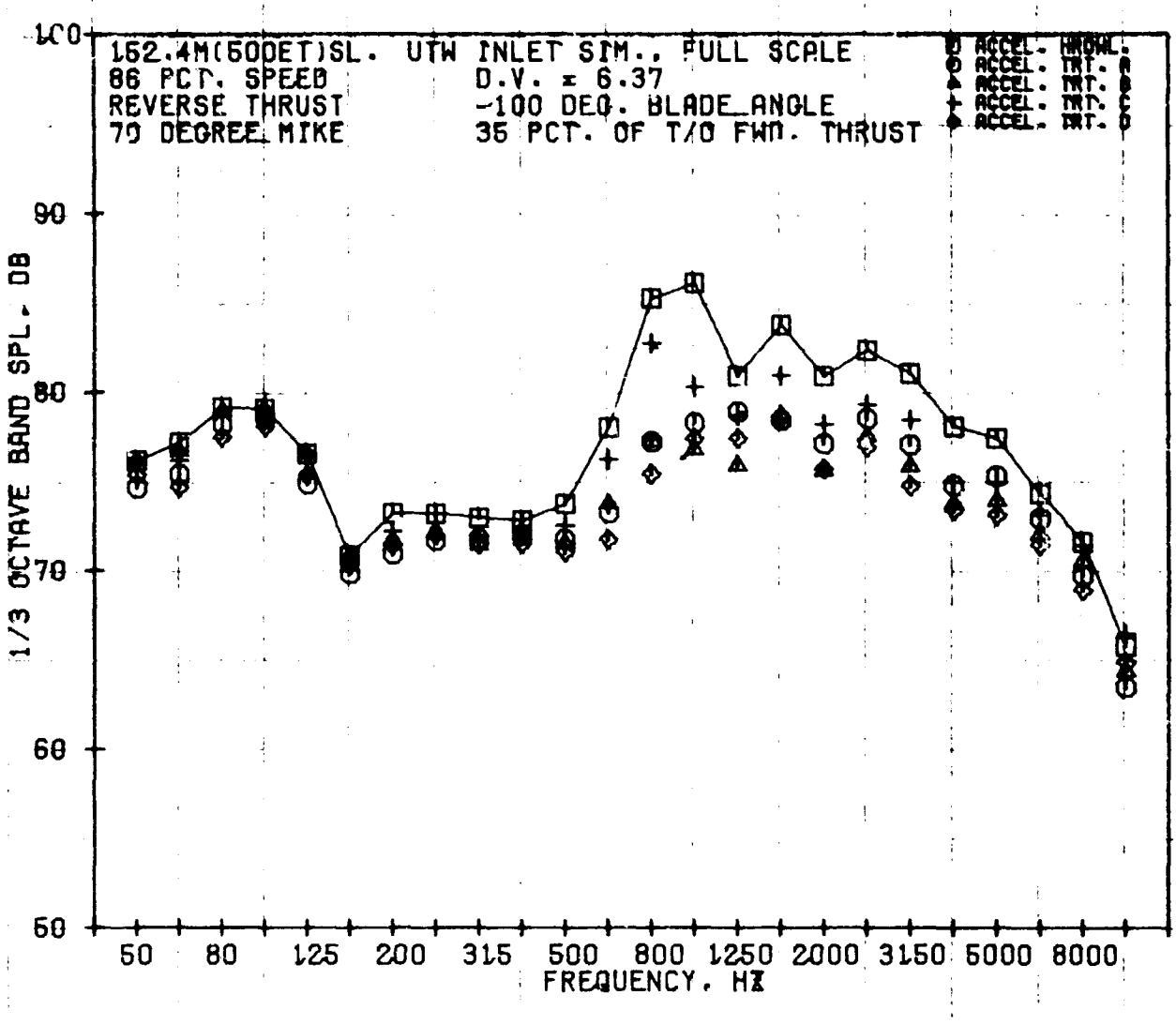

Figure 199. Reverse-Thrust, 1/3-Octave-Band, SPL Spectra of All Accelerating Inlets at 86% N_{FC} and 70°.

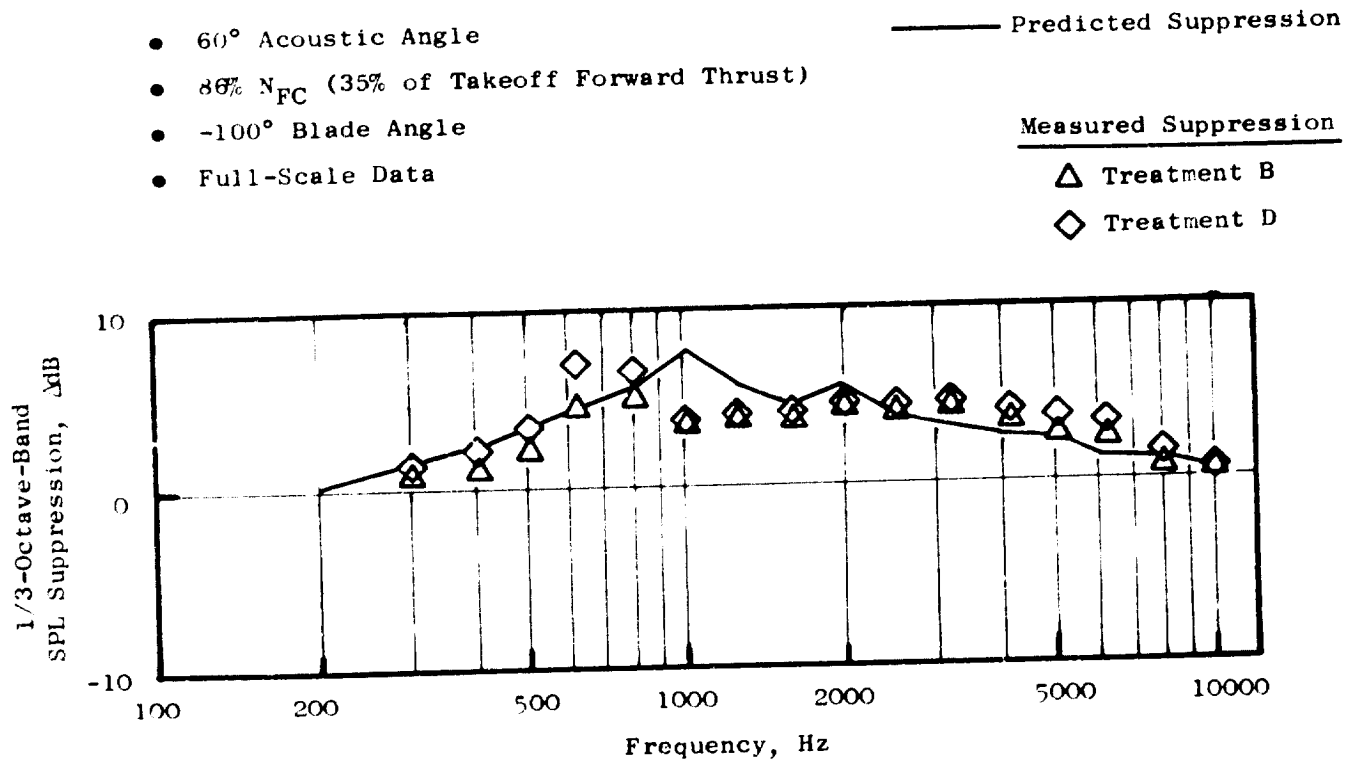

Figure 200. Reverse-Thrust, Predicted Vs. Measured Suppression Spectra for Accelerating Inlet Treatments B and D at 86% N_{FC}.

predicted PNL suppression determined by applying the suppression spectrum to the estimated hard-wall spectrum, was 3 PNdB. The measured suppression as previously presented showed treatments D and B giving suppression levels of 4.2 and 3.9 PNdB. Therefore, the treatments were somewhat more effective than was predicted.

The effectiveness of the treatment D configuration relative to treatment B is seen to be most significant at the 630-Hz and 800-Hz 1/3-octave-band frequencies. The treatment D configuration also gives more suppression, approximately 1 to 1.5 dB more, in the 2500- to 8000-Hz frequency range. This increase in treatment effectiveness can be attributed to the variable faceplate porosity used in this design rather than the constant porosity used with treatment B. However, in forward thrust the order of the treatment D faceplate porosities is opposite to what it should be for flow in this direction, whereas inlet B with the constant 10% porosity has the better overall-average acoustic resistance for both forward and reverse-thrust performance. The porosity for each section of treatment in inlet D was selected using analytical methods to optimize the acoustic resistance based on the tuning frequency of each treatment section and assuming reverse flow.

The reverse-thrust PNL suppressions are shown in Figure 201 as a function of faceplate porosity at 35% Fn and 86% N_{FC}. The suppression measured for treatment D is plotted at a porosity value of 14.4%, which is an average of the three porosities in the design (compared to the other configurations which have constant-porosity values as indicated). However, by plotting the data in this form, a trend in the suppression levels is indicated and suggests that the low-porosity (3.6%) and the high-porosity (24%) designs have nonoptimum acoustic-resistance values.

10.4 EFFECTIVENESS OF LOW MACH INLET TREATMENTS

Acoustic tests on the hard-wall and the three treated low Mach inlets were conducted at -100° blade-angle setting (reverse thrust) in the speed range of 60 to 100% N_{FC}. The low Mach inlet hard-wall and suppressed noise levels as functions of fan speed at a -100° blade-angle setting are given in Figure 202. This comparison shows that the bulk-absorber (Scottfelt 3-900) treatment B configuration gives the highest suppression at all fan speeds relative to the two configurations having resonator-type treatments. The suppression level is ≈ 6 dB at 60% N_{FC} for the bulk absorber as compared to about 3.5 dB for the best resonator design. The suppression decreases to about 5 dB as the fan speed is increased to 100% N_{FC}. However, the resonator design in treatment A gives approximately the same suppression as measured at the lower fan-speed point. Suppression measured at 86% N_{FC}, which gives the required reverse thrust (assuming reverse-thrust performance with the low Mach inlet is essentially the same as the high Mach inlet), is 5 PNdB for the bulk-absorber inlet versus 3.5 for treatment A.

The resonator-inlet configurations A and C have different faceplate porosity values. The results here show that treatment A, with a 10% porosity faceplate, gives significantly more suppression at all fan speeds

- 60° Acoustic Angle
- 86% N_{FC} (35% of Takeoff Forward Thrust)
- -100° Blade Angle
- Full-Scale Data

○ Treatment A
△ Treatment B
+ Treatment C
◇ Treatment D (Mixed Porosity, 7.2%, 14.4%, and 28%)

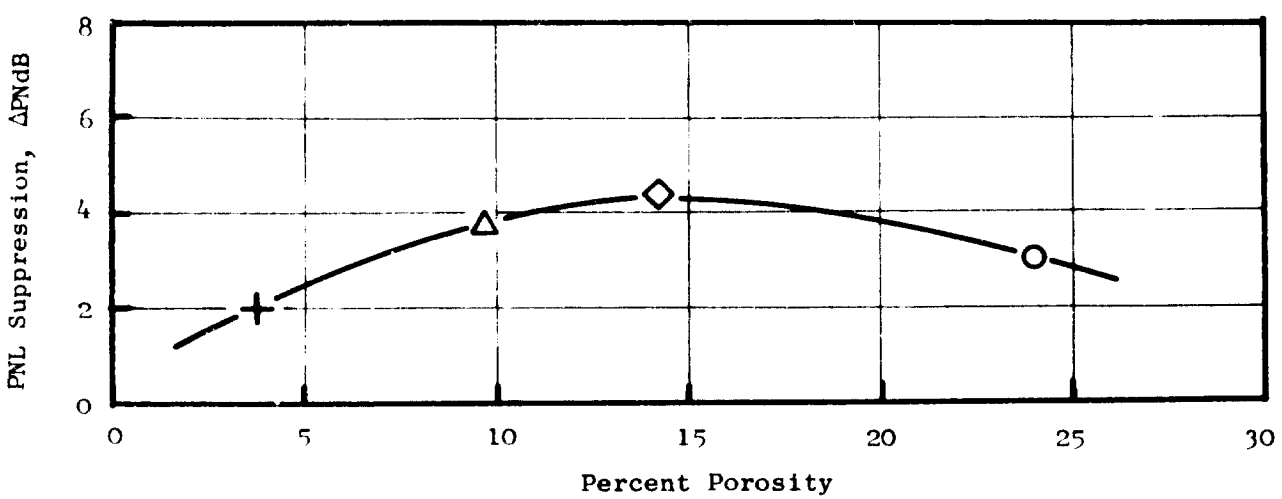

Figure 201. Reverse-Thrust, PNL Suppression Vs. Porosity for Treated Accelerating Inlets at 86% N_{FC}.

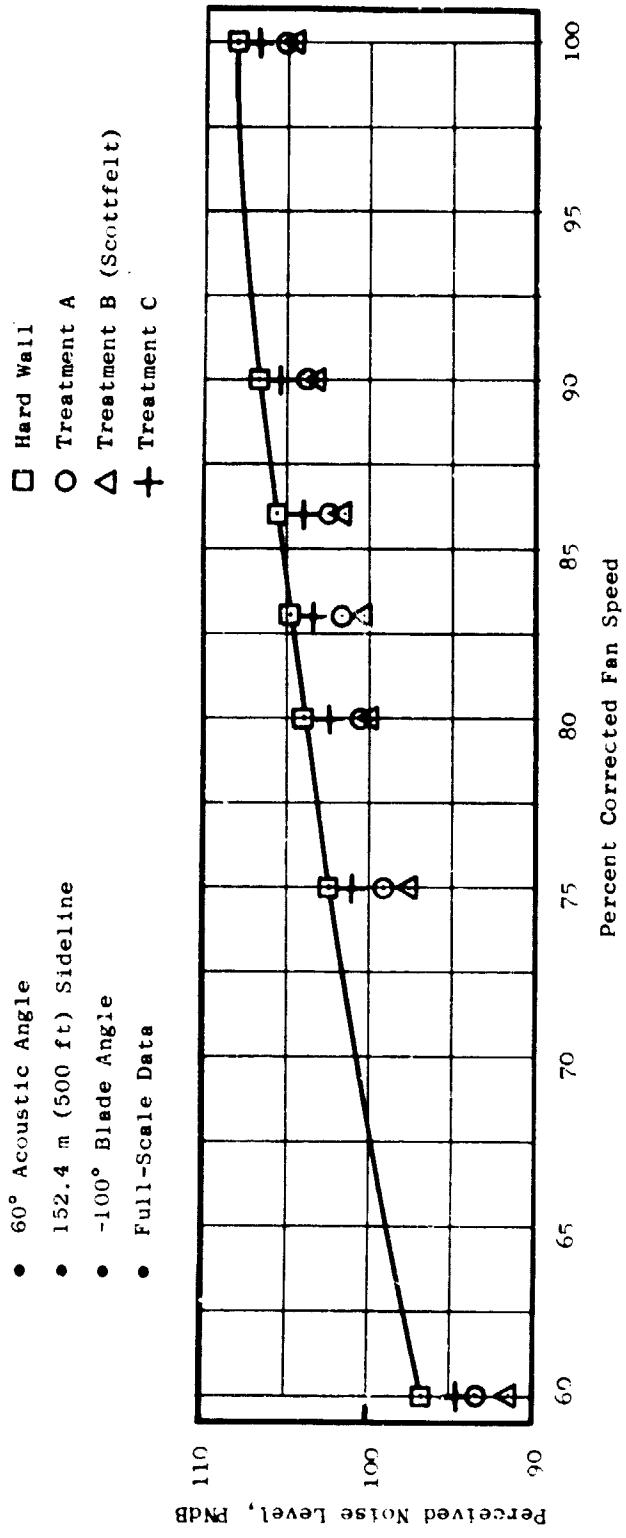

Figure 202. Reverse-Thrust PNL Vs. Fan Speed for All Low Mach Inlets.

than treatment C, with a 3.6% porosity faceplate. Thus, the lower porosity has an acoustic resistance much higher than optimum for reverse-thrust conditions.

Figure 203 gives the low Mach hard-wall and treated-inlet PNL directivities for 86% fan speed (35% of design forward thrust). The peak unsuppressed and suppressed noise levels occur at 60°. The suppression versus acoustic angle is seen to increase by a small amount for angles greater than 60° but decreases at angles less than 60°.

The measured spectra for the hard-wall and the treated-inlet configurations are shown in Figure 204. The spectra are for 86% speed (35% thrust) at an acoustic angle of 60° on a 152.4-m (500-ft) sideline. The bulk-absorber inlet configuration suppressed levels are lower at all the 1/3-octave-band frequencies relative to the two resonator-inlet configurations. Inlet A, which has the 10% faceplate porosity, gives suppression over a wide range of frequencies, whereas treatment C, with the 3.6% porosity, gives little suppression at frequencies below 2000 Hz. Neither of these two inlets gives suppression at the 8,000 Hz and the 10,000 Hz 1/3-octave-band frequencies. Figures 205 and 206 give the same spectral comparisons at acoustic angles of 50° and 70°. The same suppression trends are observed for these two angles; however, the level of suppression for each inlet increases at 70° and decreases at 50° relative to the 60° data. The hard-wall configuration tone level is observed to change significantly as a function of acoustic angle; the fan fundamental tone level increases as the acoustic angle increases. This increase in the unsuppressed tone level relative to the broadband noise is a significant factor in the increased suppression levels at the higher angles because tones are generally suppressed more effectively than broadband noise.

Figures 207 and 208 give spectral comparisons for the hard-wall and treated-inlet configurations for fan speeds of 60% and 100% at an acoustic angle of 60°. The 60% speed results show the same spectral characteristics previously observed for 86% speed. However, the results for 100% speed in Figure 206 show the bulk-absorber inlet giving little suppression at the higher fan speed. The suppression at almost all the frequency bands, including tones, is significantly reduced relative to the suppression at the 60% fan speed.

The suppressed spectra for all the inlet configurations indicate that additional PNL suppression would require more high-frequency suppression. In fact, even the large amount of low-frequency suppression, measured for each of the inlets tested, contributed little toward reducing the PNL. Therefore, a design with more of the treatment length tuned to the higher 1/3-octave-band frequencies would be desirable.

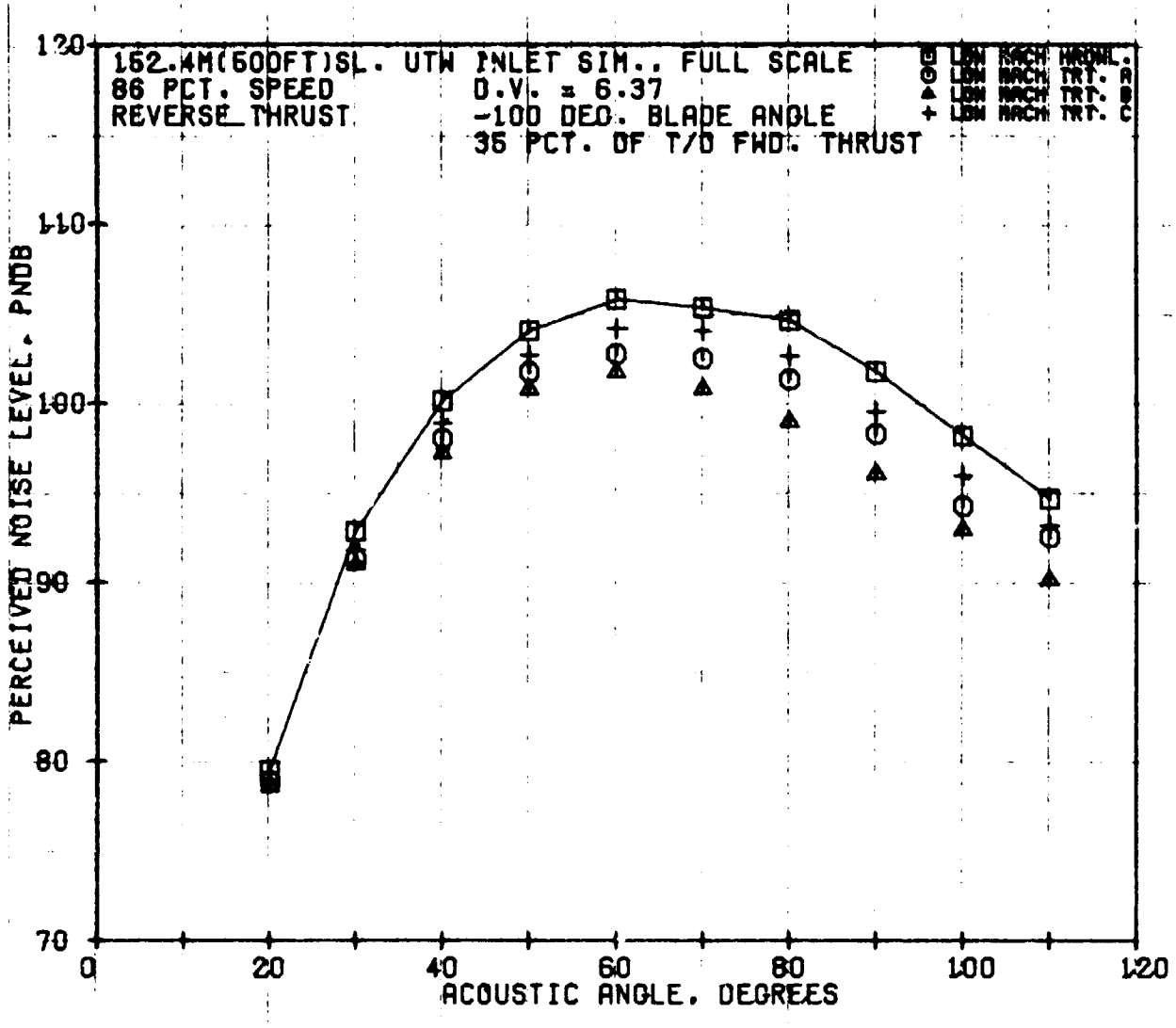

Figure 203. Reverse-Thrust, PNL Directivities for All Low Mach Inlets at 86% N_{FC}.

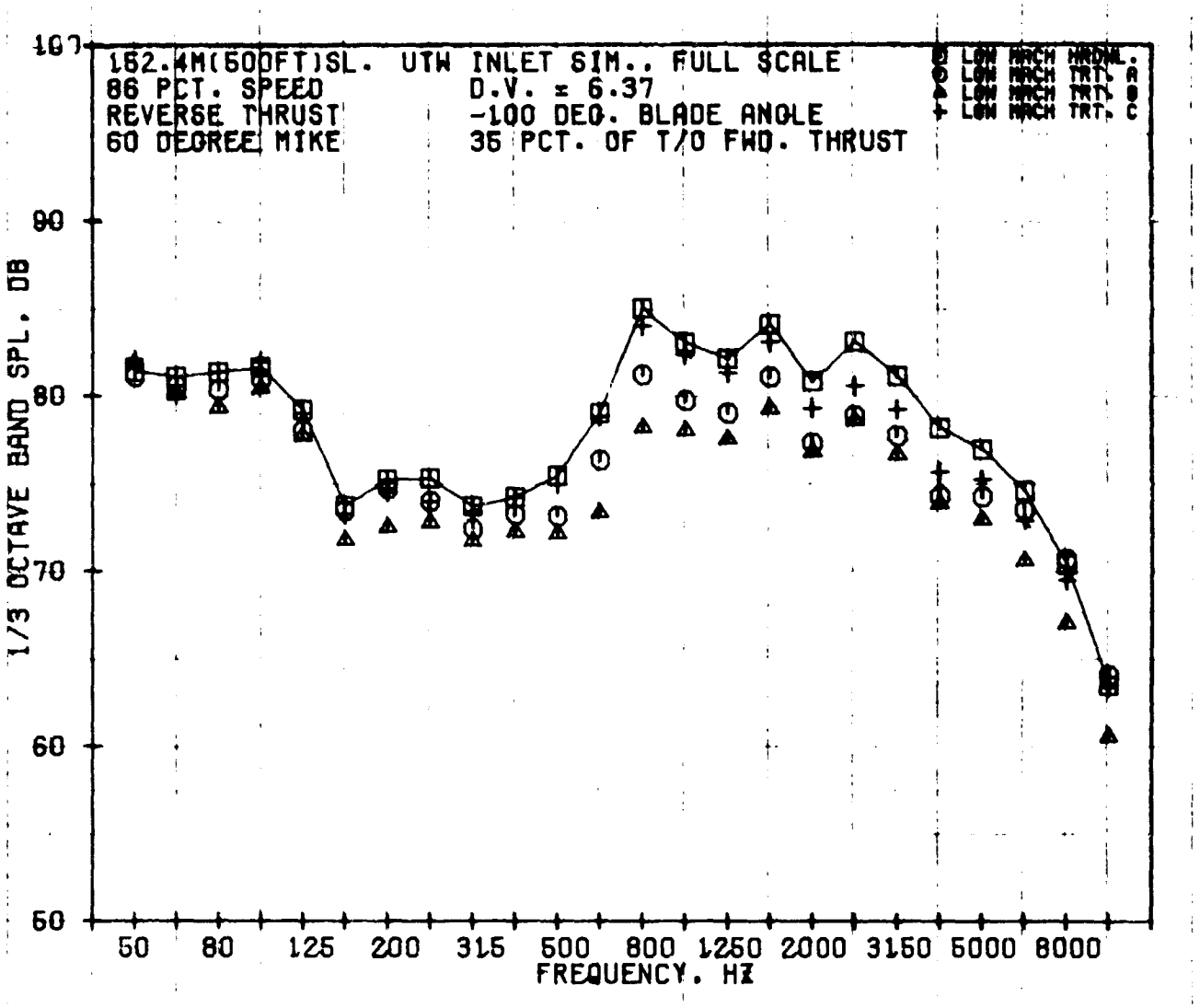

Figure 204. Reverse-Thrust, 1/3-Octave-Band, SPL Spectra for All Low Mach Inlets at 86% N_{FC} and 60°.

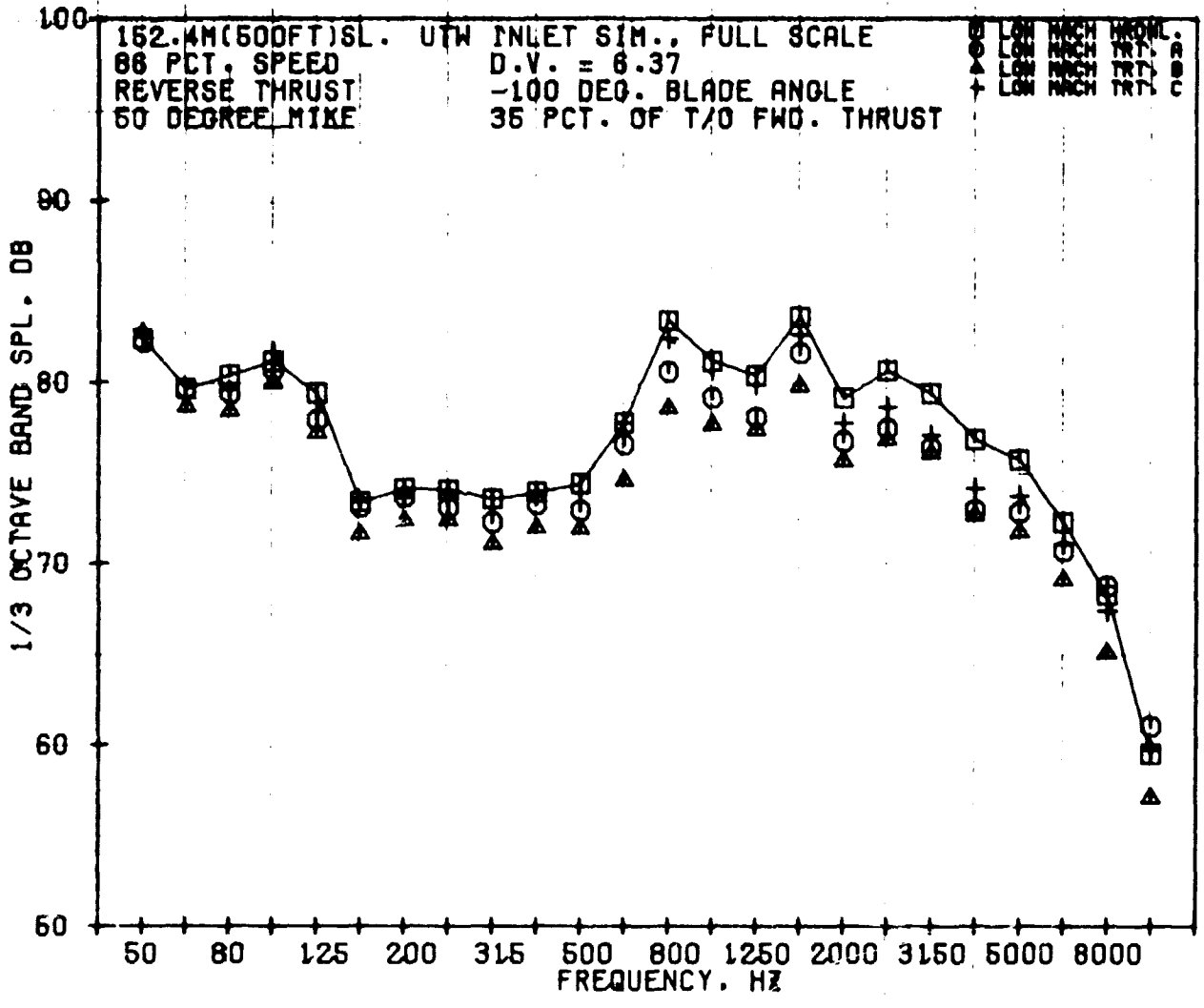

Figure 205. Reverse-Thrust, 1/3-Octave-Band, SPL Spectra for All Low Mach Inlets at 86% N_{FC} and 50°.

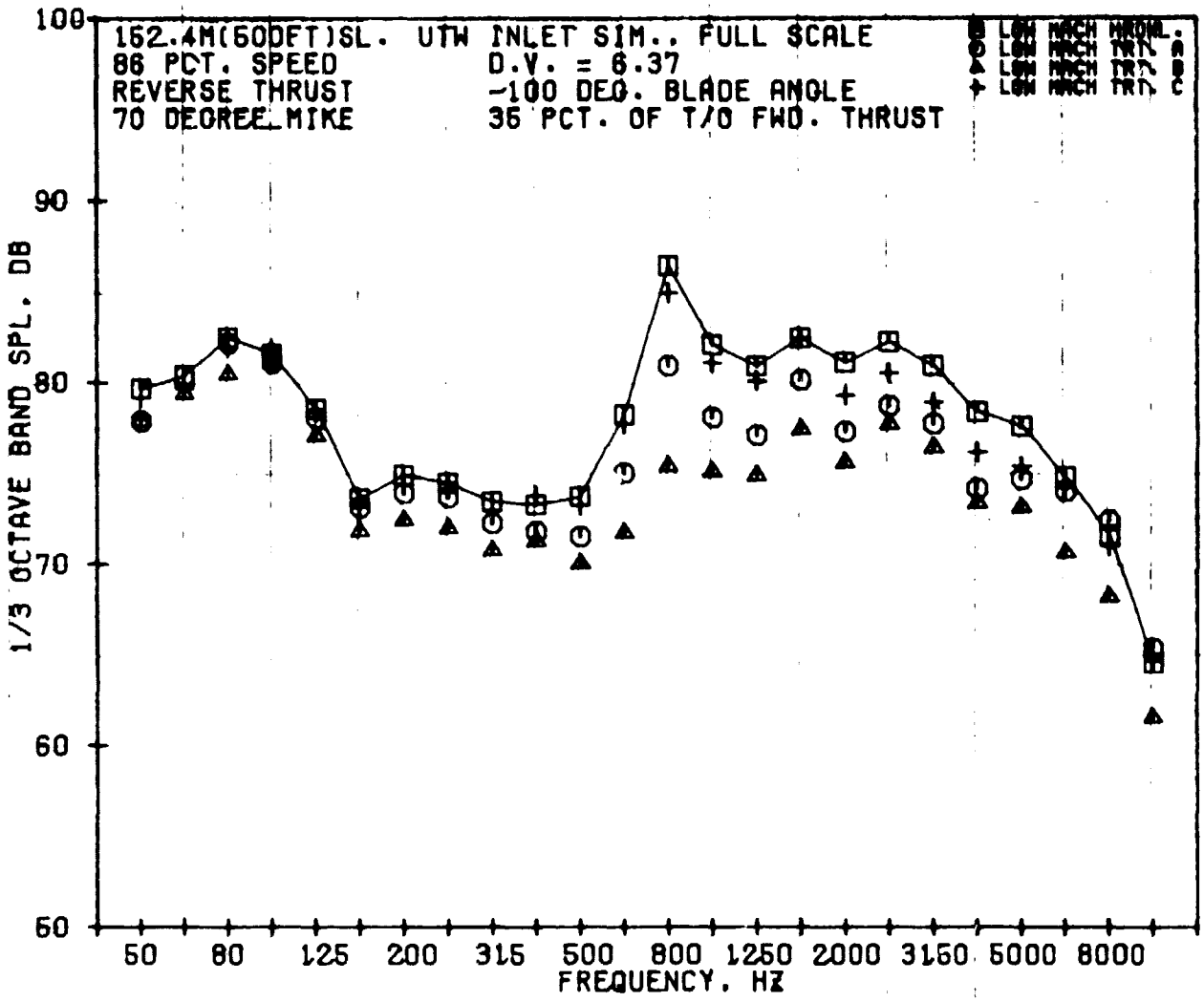

Figure 206. Reverse-Thrust, 1/3-Octave-Band, SPL Spectra for All Low Mach Inlets at 86% N_{FC} and 70°.

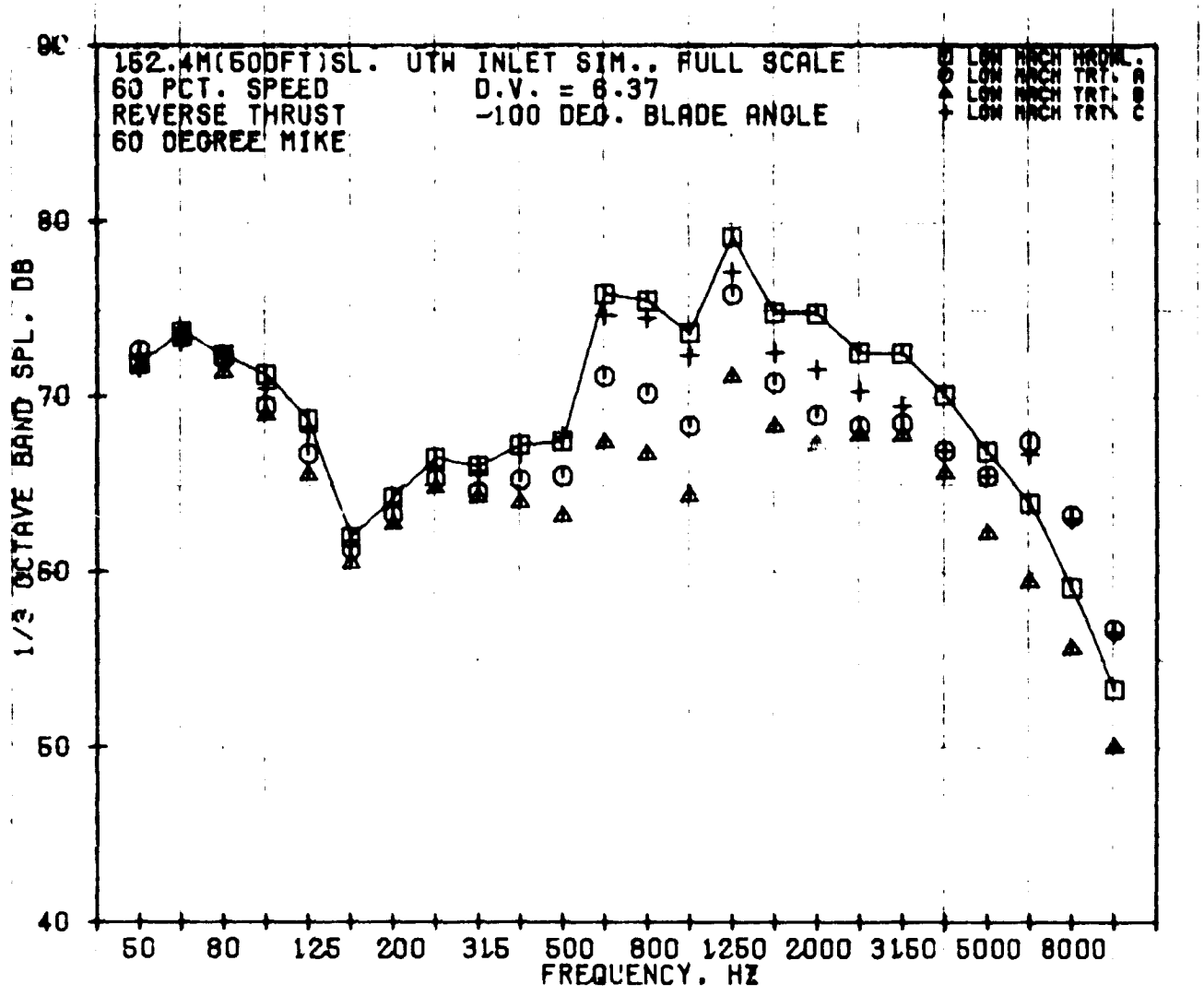

Figure 207. Reverse-Thrust, 1/3-Octave-Band, SPL Spectra for All Low Mach Inlets at 60% N_{FC}.

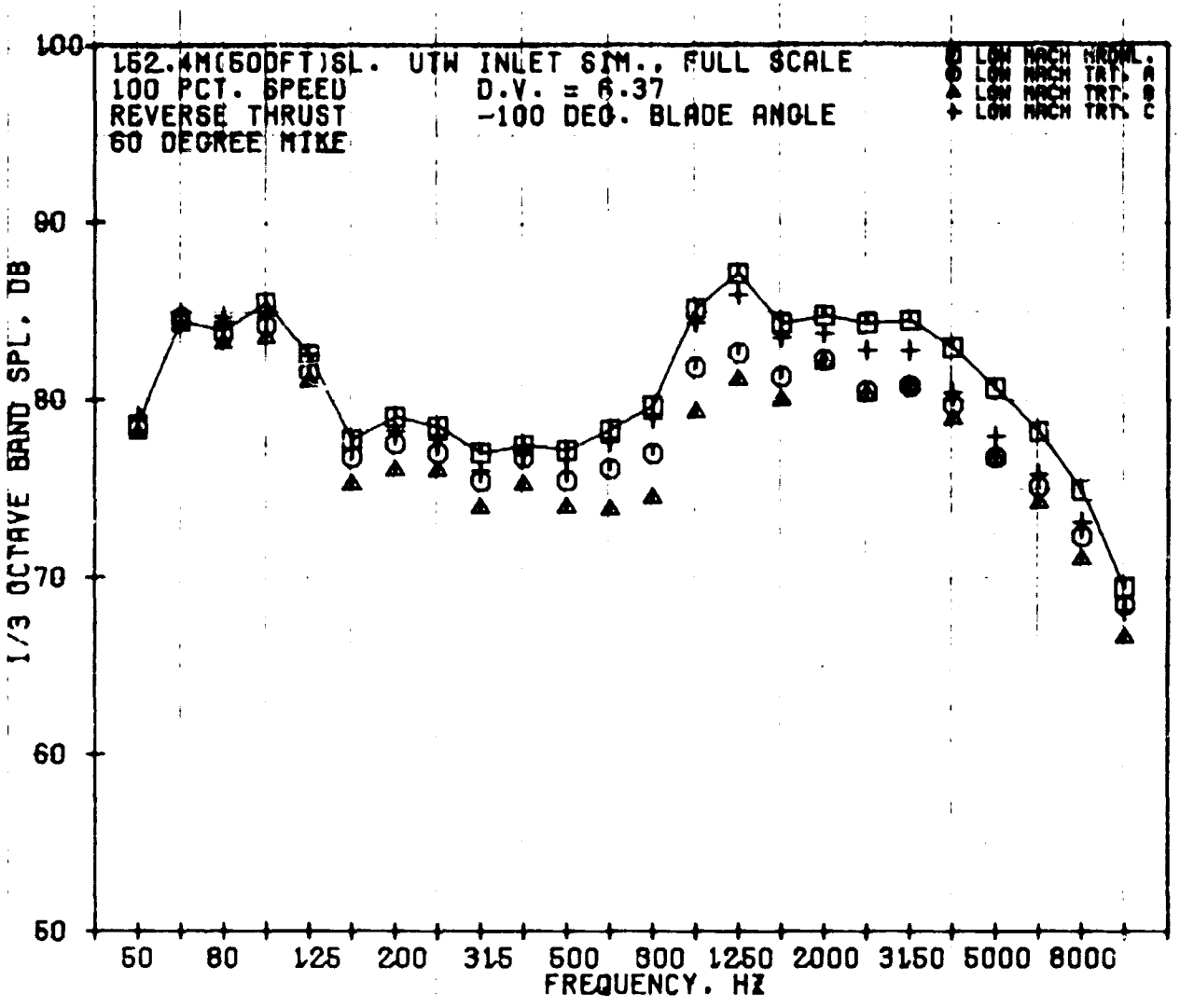

Figure 208. Reverse-Thrust, 1/3-Octave-Band, SPL Spectra for All Low Mach Inlets at 100% N_{FC}.

11.0 CONCLUSIONS AND OBSERVATIONS

Acoustic tests of inlet-radiated noise were conducted on a scale-model (1:3.5) fan [50.8-cm (20-in.) diameter] of the under-the-wing QCSEE inlet and fan stage in forward and reverse thrust modes. A baseline bellmouth inlet, five accelerating inlets (one hard-wall and four treated), and four low Mach inlets (one hard-wall and three treated) were tested. Unsuppressed and suppressed inlet-radiated noise levels were measured at conditions representative of QCSEE-UTW takeoff, approach, and reverse thrust operations. The suppression effectiveness of inlet wall treatments in forward and reverse thrust modes was measured.

The tabulation below summarizes the predicted and achieved perceived noise levels. The values are for scaled-to-QCSEE size on a 152.4-m (500-ft) sideline.

Summary of Inlet Noise Levels

Full QCSEE Size, 152.4-m (500-ft) Sideline PNL

Condition	Predicted	Measured
Takeoff		
Unsuppressed Level	94.0	93.5
Suppressed Level	81.0	81.0
Suppression	13.0	12.5
Approach		
Unsuppressed Level	90.4	94.4
Suppressed Level	82.4	88.7
Suppression	8.0	5.7
Reverse Thrust		
Unsuppressed Level	98.9	105.0
Suppressed Level	95.9	100.7
Suppression	3.0	4.3

As can be seen from the above tabulation, the measured unsuppressed level at takeoff was slightly lower than predicted, while at approach and reverse thrust the unsuppressed levels were 4 and 6.1 PNdB higher than predicted, respectively. Suppression at approach was 2.3 PNdB lower than predicted while at reverse thrust the suppression was about 1.3 PNdB higher than predicted. As a result, the suppressed levels at approach and reverse thrust are somewhat higher than predicted.

At approach thrust, blade angles of 0° and +5° gave nearly the same unsuppressed and suppressed noise levels. At both blade angles, for increasing

fan speed and increasing fan nozzle area to hold constant thrust, there was an increase in noise with a slight rolloff of about 1 PNdB at the maximum speed for each blade angle.

Summaries of suppression results of accelerating and low Mach inlets in forward and reverse thrust follow.

Accelerating-Inlet, Forward-Thrust Suppression

- Suppression measured from inlet B is higher than that measured for inlet D at all fan speeds.
- The inlet D PNL at the 0.79 throat Mach number is higher than the noise level measured for the hard-wall, accelerating inlet.
- Suppression level is sensitive to the liner faceplate porosity. Inlet B with the constant 10% porosity results in a better compromise for both forward- and reverse-thrust performance than does inlet D with the mixed-porosity design optimized for the reverse-thrust mode.
- The poor performance of inlet D treatment at the 0.79 throat Mach number suggests that the positioning of treatment with a high faceplate porosity (inlet D - 28%) near the throat area in a high Mach inlet may degrade the acoustic performance of hybrid inlets.

Accelerating-Inlet, Reverse-Thrust Suppression

- Treatments B and D gave the highest suppression levels of the four inlets tested. Inlet D gave 4.2 PNdB suppression while inlet B gave 3.9 PNdB suppression at the reverse thrust-design point (86% fan speed, which gives 35% of design takeoff thrust).
- Suppression improvement was measured for the mixed-porosity design, inlet D, relative to the best constant-porosity design, inlet B.
- Inlets B and D both gave suppression levels higher than predicted.
- The suppression performance of inlets A and C indicates that each have nonoptimum porosity values; inlet A at 24% porosity is too high, and inlet C with 3.6% is too low.

Low Mach Inlet, Forward-Thrust Suppression

- The constant-depth, bulk-absorber treatment (inlet B) gave more suppression at most fan speeds than did the inlets with resonator-type treatment.

- The inlet A treatment with a faceplate porosity of 10% gave higher suppression than the inlet C treatment with the lower (3.6%) faceplate porosity.

- The suppression performance of the bulk-absorber inlet treatment decreased with increased fan speeds while resonator-treatment suppression was not influenced by fan speed.

- None of the inlet-treatment configurations gave suppression in the higher 1/3-octave-band frequencies for fan speeds at and above 90%.

- The lower suppression for the two resonator-type treatment configurations relative to the suppression measured for the bulk-absorber treatment indicates that the resonator-treatment designs were nonoptimum.

Low Mach Inlet, Reverse-Thrust Suppression

- The constant-depth, bulk-absorber treatment gave higher suppression than did either of the two resonator-treatment designs. At the reverse-thrust design point, the bulk absorber gave an increase of 1.5 PNdB relative to the best resonator treatment. This suppression is 0.8 PNdB better than the best accelerating-inlet treatment designed for reverse thrust.

- The inlet A resonator design with a 10% porosity gave significantly more suppression than inlet C with a 3.6% faceplate porosity.

- The suppession level for the bulk-absorber treatment decreased with increasing fan speed. The best resonator design suppression was constant with fan speed.

- PNL suppression can be improved with more of the overall treated length tuned to the higher frequencies.

Sound-Separation Probe

The sound-separation probe was traversed across the inlet throat for the accelerating, treated inlet. The sound-separation technique was used to confirm that the spectrum levels from 500 to 5500 Hz were due to sound propagating from the inlet and that those below 500 Hz were due to turbulence. Unfortunately, no information relative to treatment effectiveness or design could be derived since there were no sound-separation-probe measurements made with the hard-wall or other inlets for comparison.

Aerodynamic Performance - Accelerating Inlet

Wall static pressure data at 0.79 throat Mach number agreed very well with the predicted distribution obtained from a stream-tube curvature (STC) computer program analysis. The aeroacoustic lip and the flight lip were found to have similar wall Mach number distributions in terms of both the peak wall Mach number and the rate of diffusion.

APPENDIX - QCSEE INLET THROAT MACH NUMBER DETERMINATION

Determining weight flow has always been a problem in evaluating inlet aerodynamic performance. The usual methods of flow measurement include a vehicle-discharge venturi, discharge total pressure rakes, and flow-measuring bellmouths. These tests establish fan speed/flow characteristics (i.e., fan operating lines) important in designing the inlet for good cruise performance. Due to the sensitivity of acoustic suppression to throat Mach number, the advent of accelerating inlets for noise suppression has increased the significance of accurate weight-flow determination.

During the QCSEE 50.8-cm (20-in.) inlet tests at Schenectady, there were no means available to directly measure inlet weight flow. Calibration of flow/speed relationships using a flow-measuring bellmouth was attempted, but the blade-angle repeatability of the QCSEE fan compromised the results of this method since blade angle settings were only repeatable to within ±0.5°. An accurate evaluation of acoustic-suppression data requires a more accurate indication of inlet flow (i.e., inlet throat Mach number).

In view of difficulties associated with direct inlet-flow measurements for the QCSEE 50.8-cm (20-in.) model tests, General Electric utilized a previously developed method of determining the inlet flow using analytical predictions and measured inlet-wall static pressures. Prior to testing, the General Electric Streamtube Curvature (STC) flow-analysis program (Reference 11) was utilized to calculate inviscid inlet-wall static pressure distributions both for the accelerating inlet and for the low Mach inlet. The analysis included each inlet with both a flight lip and an aero/acoustic bellmouth lip. The effects of diffuser-wall treatment and the associated total pressure loss were not considered in the analysis. Upstream of the peak wall Mach number, which usually occurred slightly ahead of the inlet throat, the inviscid solution was considered valid. Aft of the peak, diffusion of the flow causes a rapid growth in the boundary layer which affects the measured wall pressures. To compensate for the viscous effects, the inviscid wall pressures were adjusted according to the blockage of the calculated boundary layer displacement thickness. Boundary layer characteristics were obtained from the Stratford and Beavers solution (SABBL: Reference 11), an option of the STC program. The following steps describe the method of adjusting the wall static pressure for viscosity.

(1) $$\left(P_S/P_T\right)_{\text{inviscid}} \Rightarrow \left(\frac{W\sqrt{\theta}}{\delta A}\right)_{\text{inviscid}}$$

(2) $$\left(\frac{W\sqrt{\theta}}{\delta A}\right)_{\text{inviscid}} \left(\frac{R}{R-\delta^*}\right)^2 = \left(\frac{W\sqrt{\theta}}{\delta A}\right)_{\text{effective}}$$

(3) $\left(\frac{W\sqrt{\theta}}{\delta A}\right)_{effective}$ ⇨ $(P_S/P_T)_{inviscid}$

In Step 1, the imaginary specific flow was inferred from the predicted, normalized, static pressure (at a given position on the diffuser wall) using compressible-flow tables. The specific flow was then corrected for boundary layer blockage on a one-dimensional area basis (Step 2). Step 3 reversed the process of step 1 to identify the predicted, viscous, wall pressure. The procedure was repeated at a number of stations along the diffuser duct.

Having calculated the viscous wall pressures for a range of different inlet weight flows, the results were plotted for each inlet configuration (see Figures 209 through 212). High flow rates in the accelerating inlet resulted in supersonic wall velocities near the throat, leading (in some cases) to a local instability in the STC solution. Also, transonic velocities invalidated the method of adjusting for boundary layer blockage. However, boundary layer blockage corrections were only applied to subsonic wall Mach number regions downstream of the peak wall Mach number, for it is in these regions that blockage begins to have a significant effect due to the rapid growth in boundary layer thickness. Portions of the predicted wall-pressure distributions considered invalid for either of these reasons are indicated by dashed lines on the curves in Figures 209 through 212.

For several static pressure tap locations (chosen locations shown in Figures 209 through 212), the predicted normalized pressure was cross-plotted against inlet throat Mach number. Throat Mach number was determined from corrected weight flow (an input for the STC analysis), inlet physical throat area, and one-dimensional compressible-flow relationships. The resulting plots for several tap locations are contained in Figures 213 through 216. The selected flow-correlating taps were located in the forward part of the inlet where experience has indicated better agreement between data and predictions and where the acoustic treatment has a minimal effect on the data. Although the taps near the throat are extremely sensitive to small changes in inlet airflow, usefulness is limited because the analytical solution is unreliable in the throat region. This problem is only encountered with the accelerating inlet at high flow rates as already discussed. Therefore, some existing taps located in the throat were not used for the weight-flow correlation.

During testing of a particular inlet configuration, wall static pressure data were acquired for a number of different fan speeds. For each data point, the selected, normalized pressures were plotted on the appropriate plot from Figures 213 through 215. Data should be distributed vertically on the plot with all taps indicating the identical throat Mach number. Test data at the apparent design flow are included in Figures 213 through 215 for each of the inlet configurations tested. A modest amount of data scatter results from the

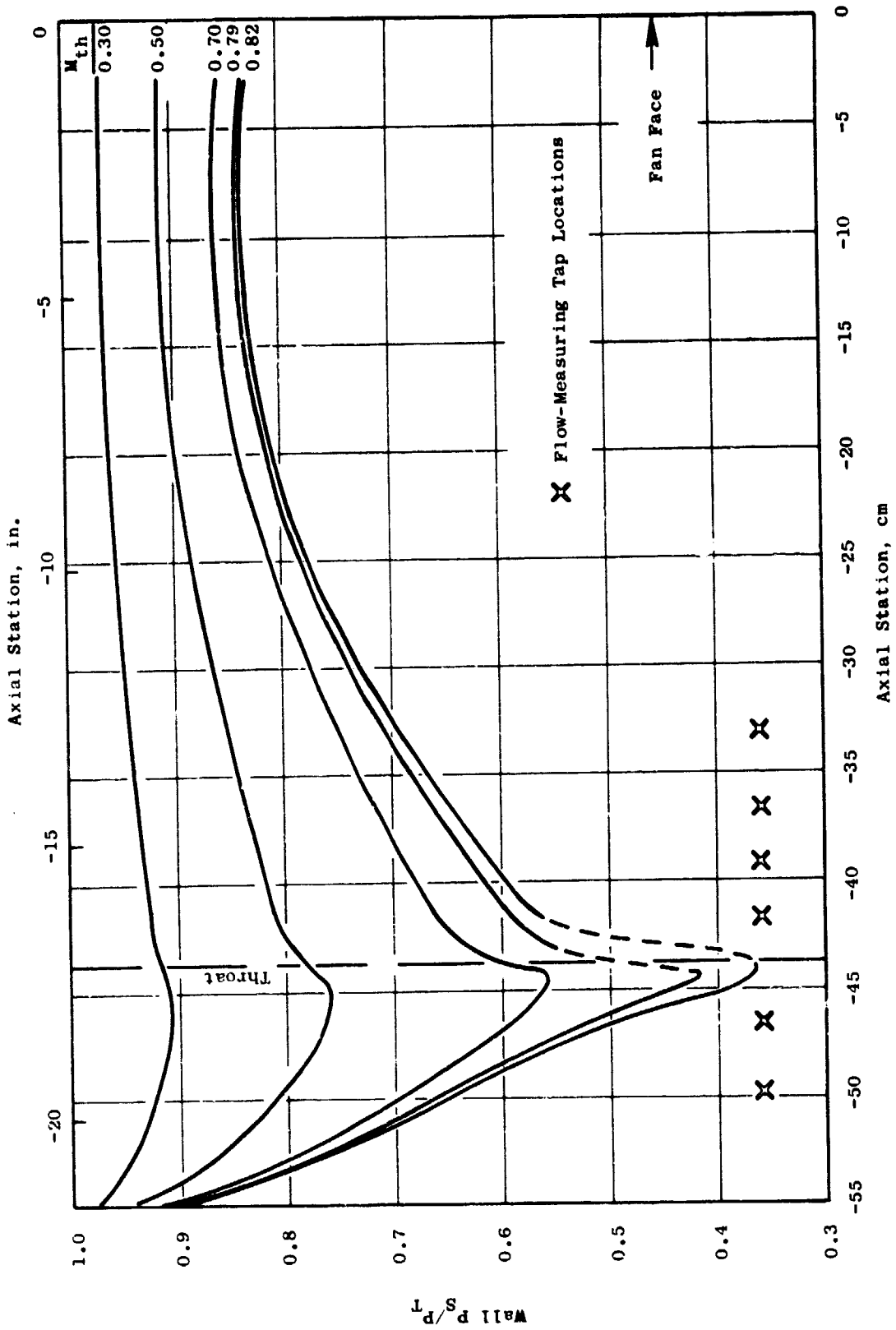

Figure 209. Aero-Acoustic Lip, Accelerating-Inlet, Predicted Wall-Pressure Gradients.

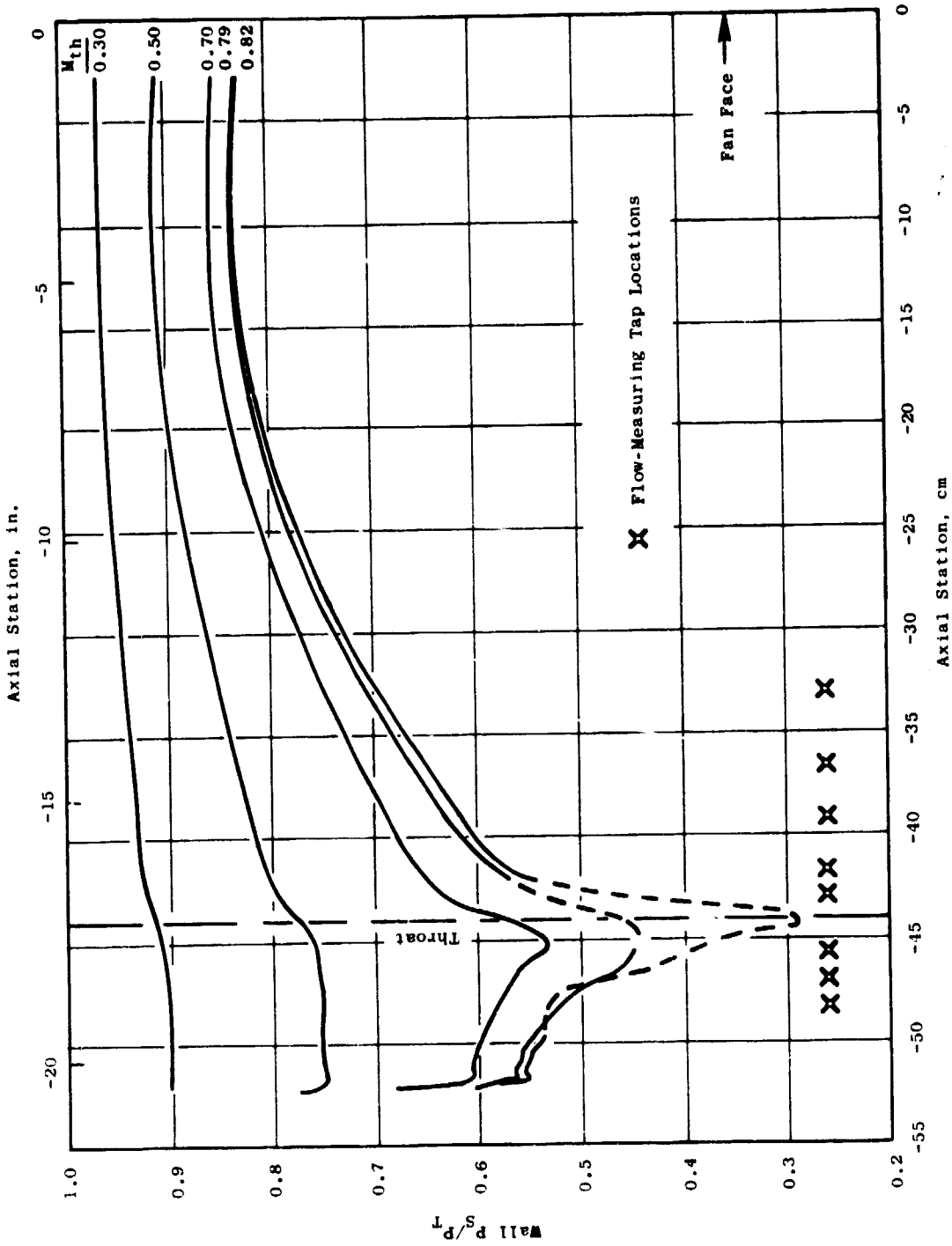

Figure 210. Flight Lip, Accelerating-Inlet, Predicted Wall-Pressure Gradients.

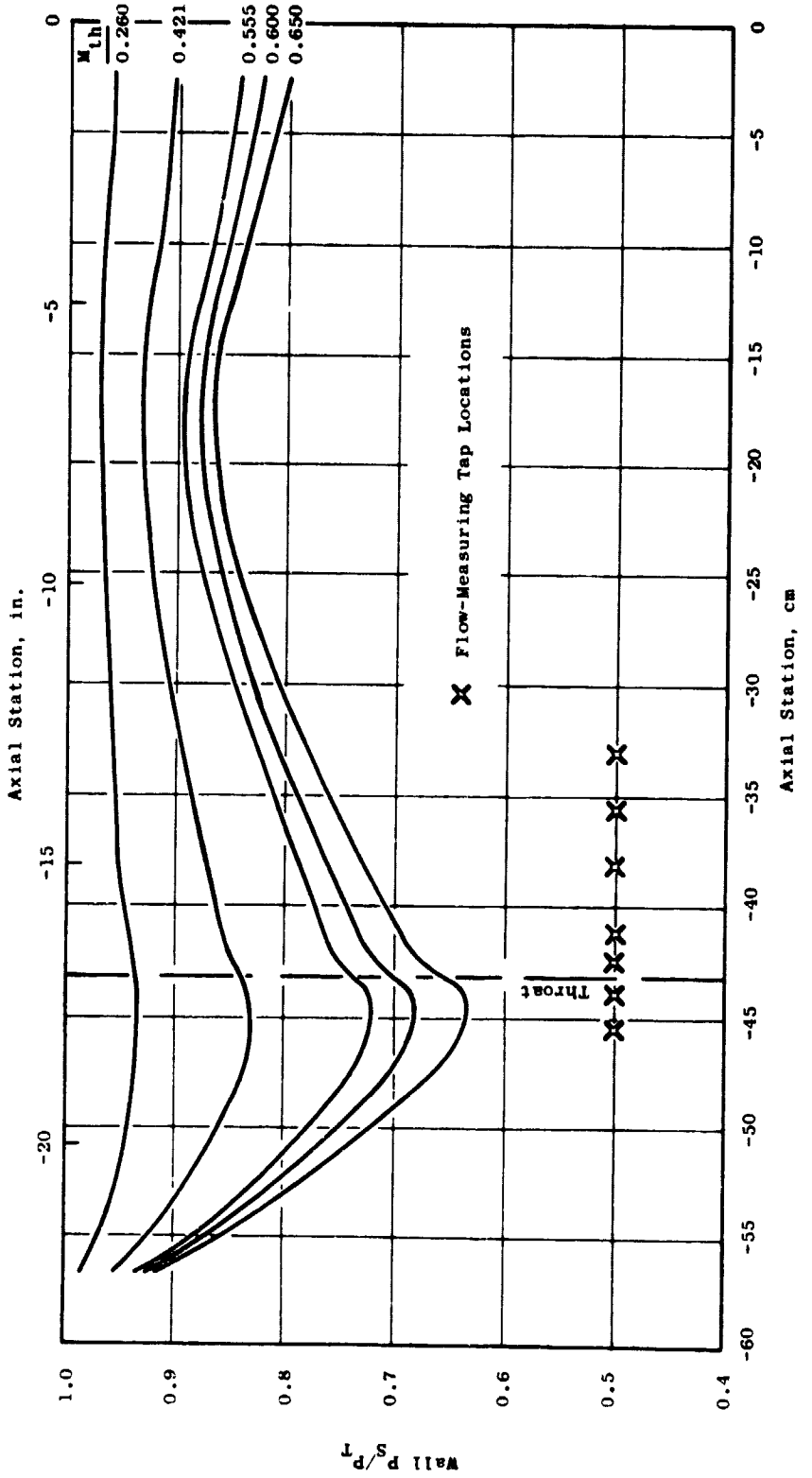

Figure 211. Aero-Acoustic Lip, Low Mach Inlet, Predicted Wall-Pressure Gradients.

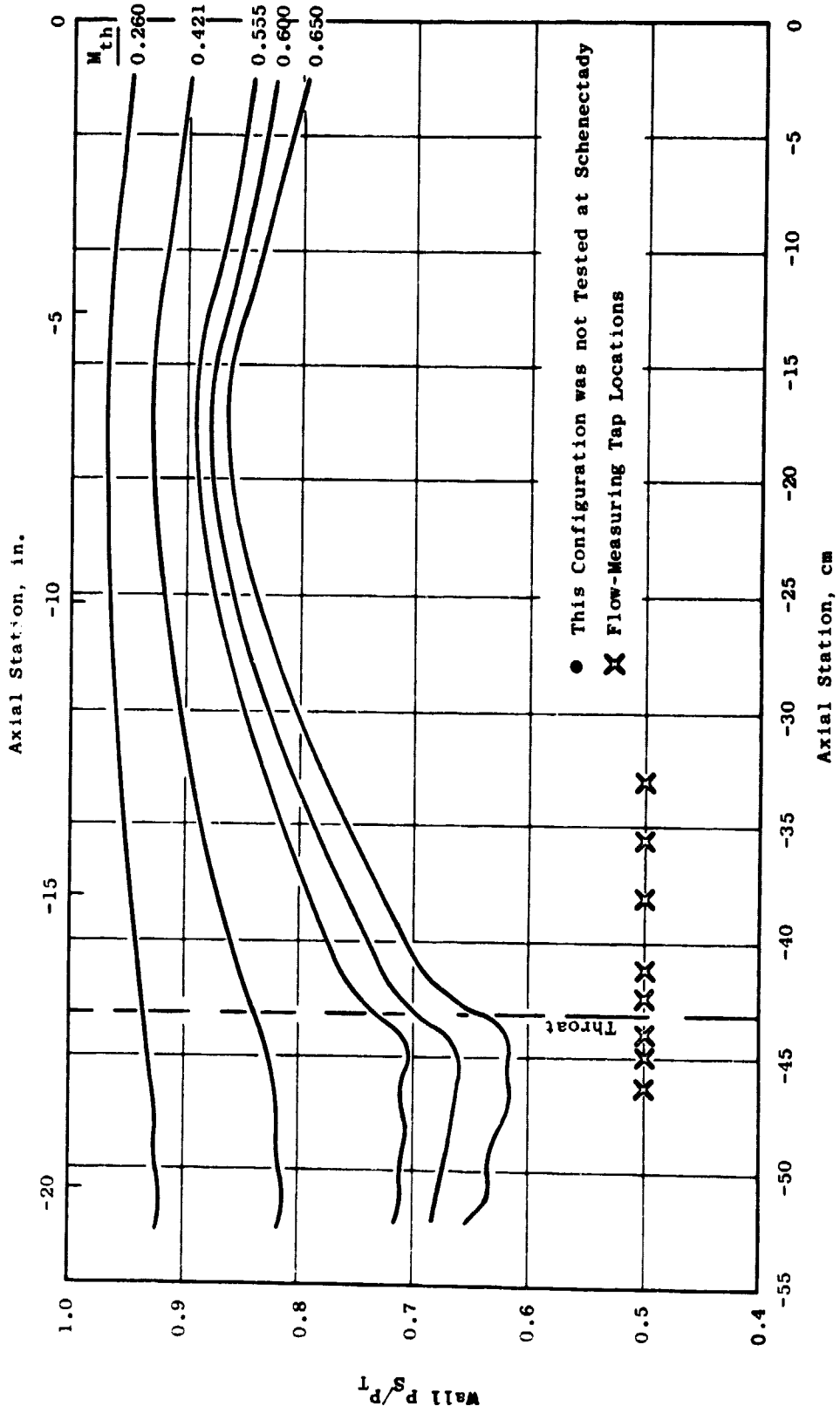

Figure 212. Flight Lip, Low Mach Inlet, Predicted Wall-Pressure Gradients.

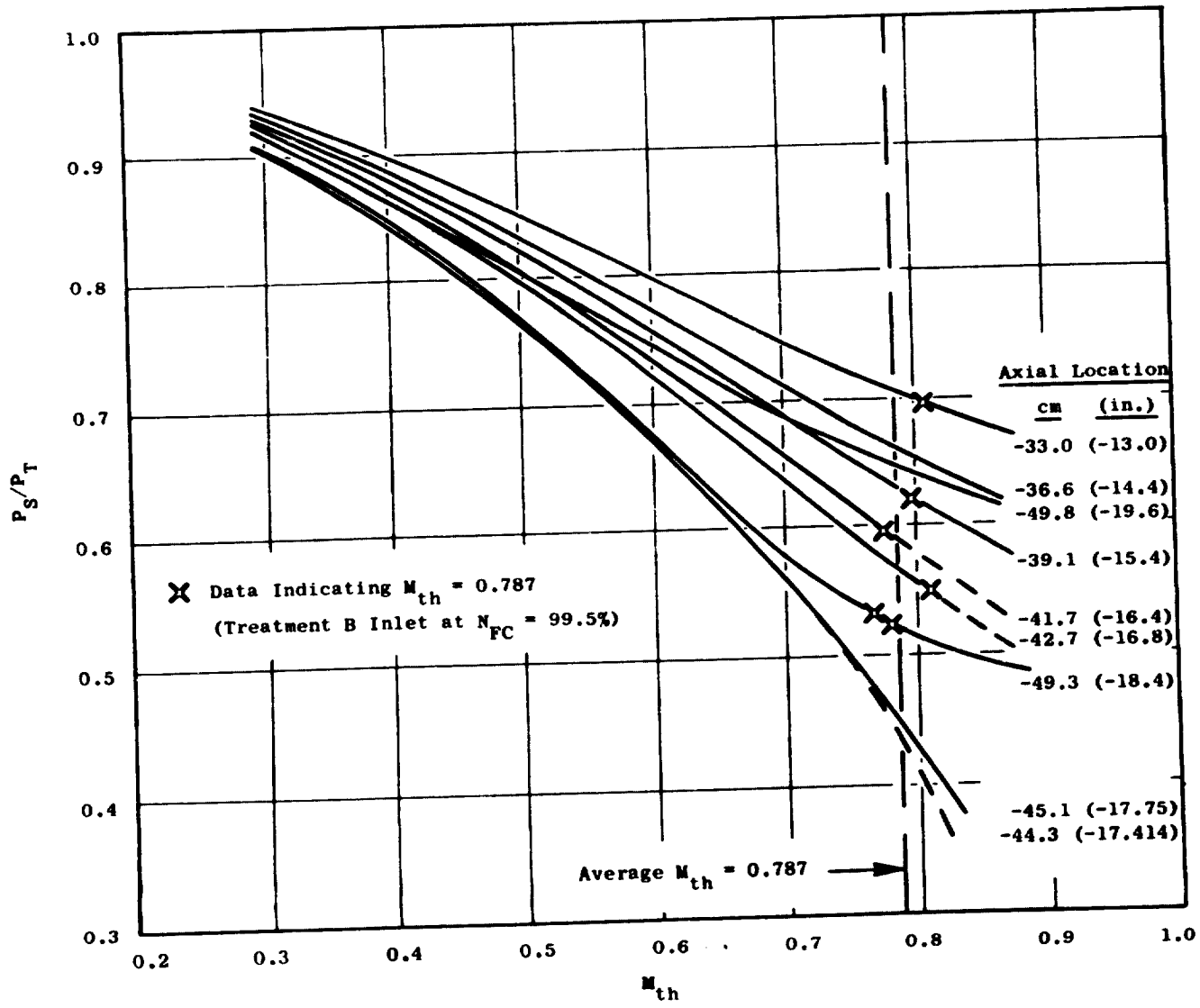

Figure 213. Accelerating-Inlet, Aero-Acoustic Lip, STC Flow Correlations.

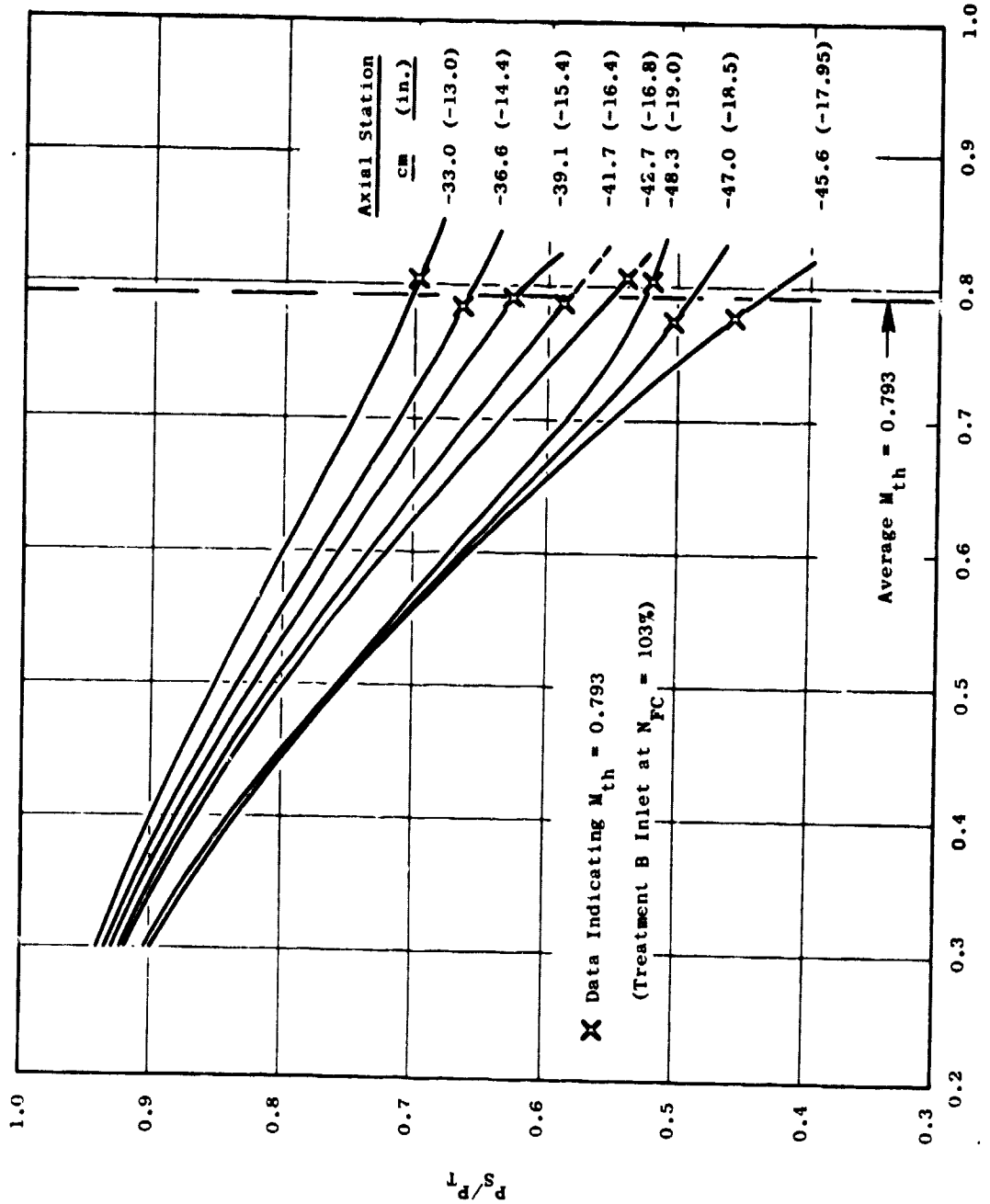

Figure 214. Accelerating-Inlet, Flight Lip, STC Flow Correlations.

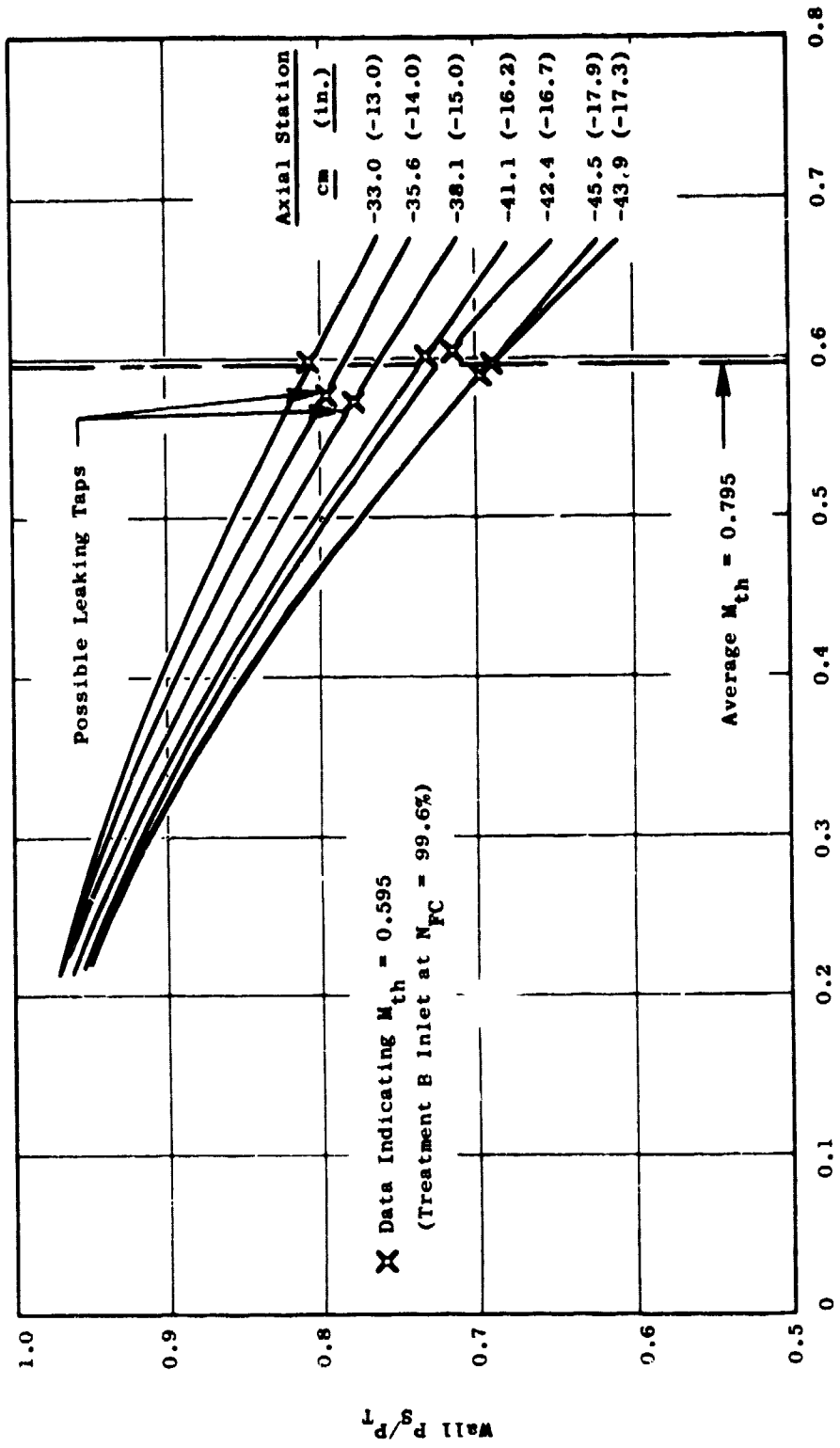

Figure 215. Aero-Acoustic Lip, Low Mach Inlet, STC Flow Correlations.

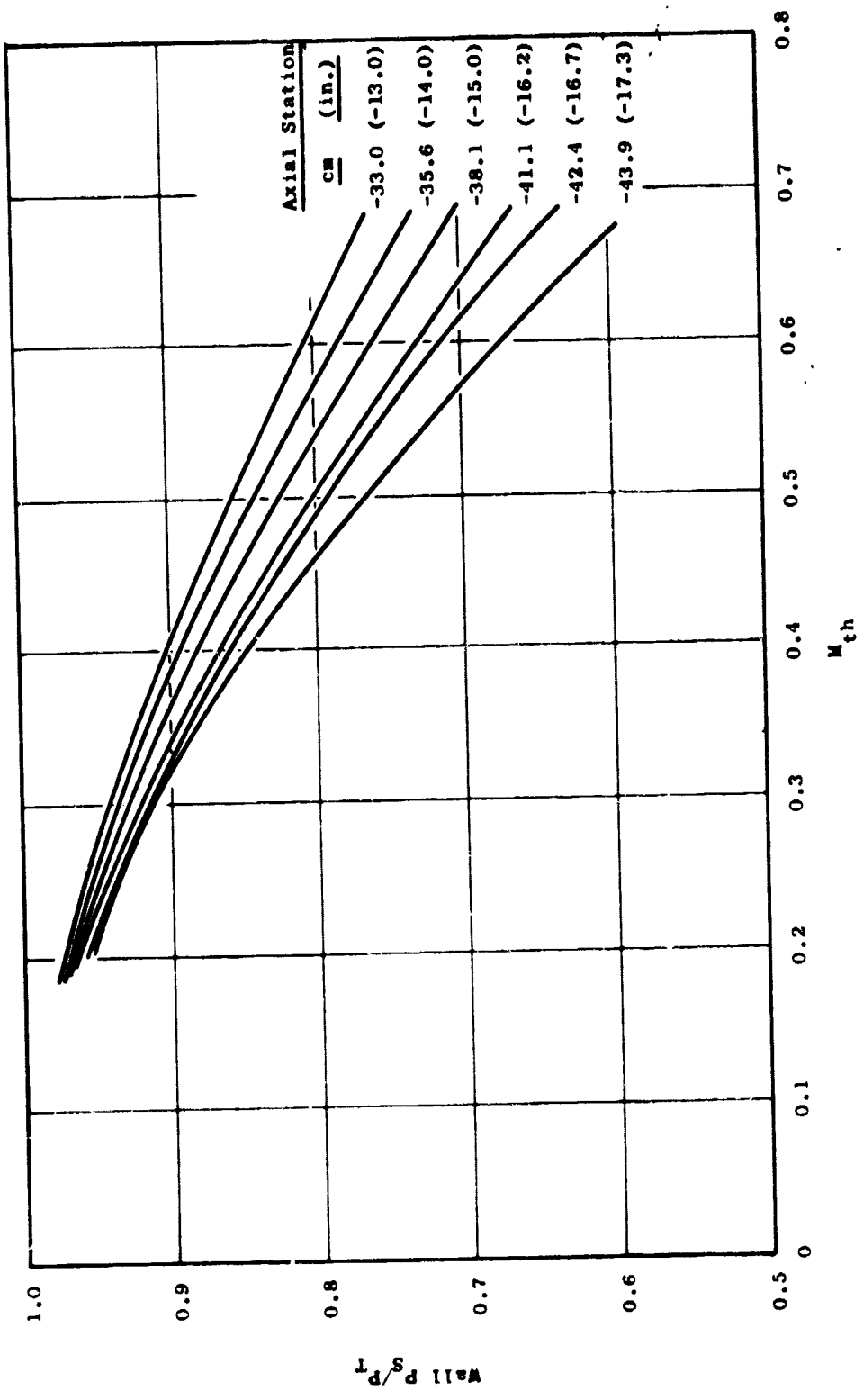

Figure 216. Flight Lip, Low Mach Inlet, STC Flow Correlations.

usual causes (model-contour inaccuracies, inprecise tap installations, or undetected pressure leaks in the static pressure lines). Inlet throat Mach number was determined by averaging the inlet Mach numbers indicated by all of the selected flow-correlation static pressure taps. Throat Mach number versus fan-speed results are contained in Figures 40 and 122 for the accelerating and the low Mach inlet, respectively. For the flight lip, Figure 216, test data were not obtained and only predicted results are shown.

Having determined the inlet throat Mach number (i.e., inlet corrected flow) via the foregoing discussion, it is possible to estimate the fan-face corrected flow as follows:

$$\frac{W\sqrt{\theta}}{\delta_2} = \left(\frac{W\sqrt{\theta}}{\delta_A}\right)_{\text{throat}} \left(\frac{A_{th}}{n}\right)$$

where

$\left(\frac{W\sqrt{\theta}}{\delta A}\right)_{\text{throat}}$ is the specific flow at the throat corresponding to the calculated throat Mach number,

A_{th} is the inlet physical throat area,

n is the diffuser total pressure recovery, P_{T_2}/P_{T_0}.

Inlet recovery (P_{T_2}/P_{T_0}) must be determined from fan-face total pressure rake data. In the Schenectady 50.8-cm (20-in.) inlet test program, adequate rake data were not available; however, representative recovery data had been previously obtained for scaled inlet [30.5-cm (12-in.)] models. Figure 217 relates the inlet-throat Mach number to 50.8-cm (20-in.) inlet fan-face corrected flow ($W\sqrt{\theta}/\delta 2$) based on the measured 30.5-cm (12-in.) recoveries. It is assumed that the difference in Reynolds number between the 30.5-cm (12-in.) and 50.8-cm (20-in.) inlets has a negligible effect on inlet recovery. The expected flight lip and aero-acoustic bellmouth inlet recoveries (solid and dashed curves) were evaluated by testing the 30.5-cm (12-in.) flight lip inlet at $V_0 = 0$ and $V_0 = 41.2$ m/sec (80 knots), respectively. No 30.5-cm (12-in.) inlet tests were conducted with an aero-acoustic bellmouth lip or a low Mach inlet.

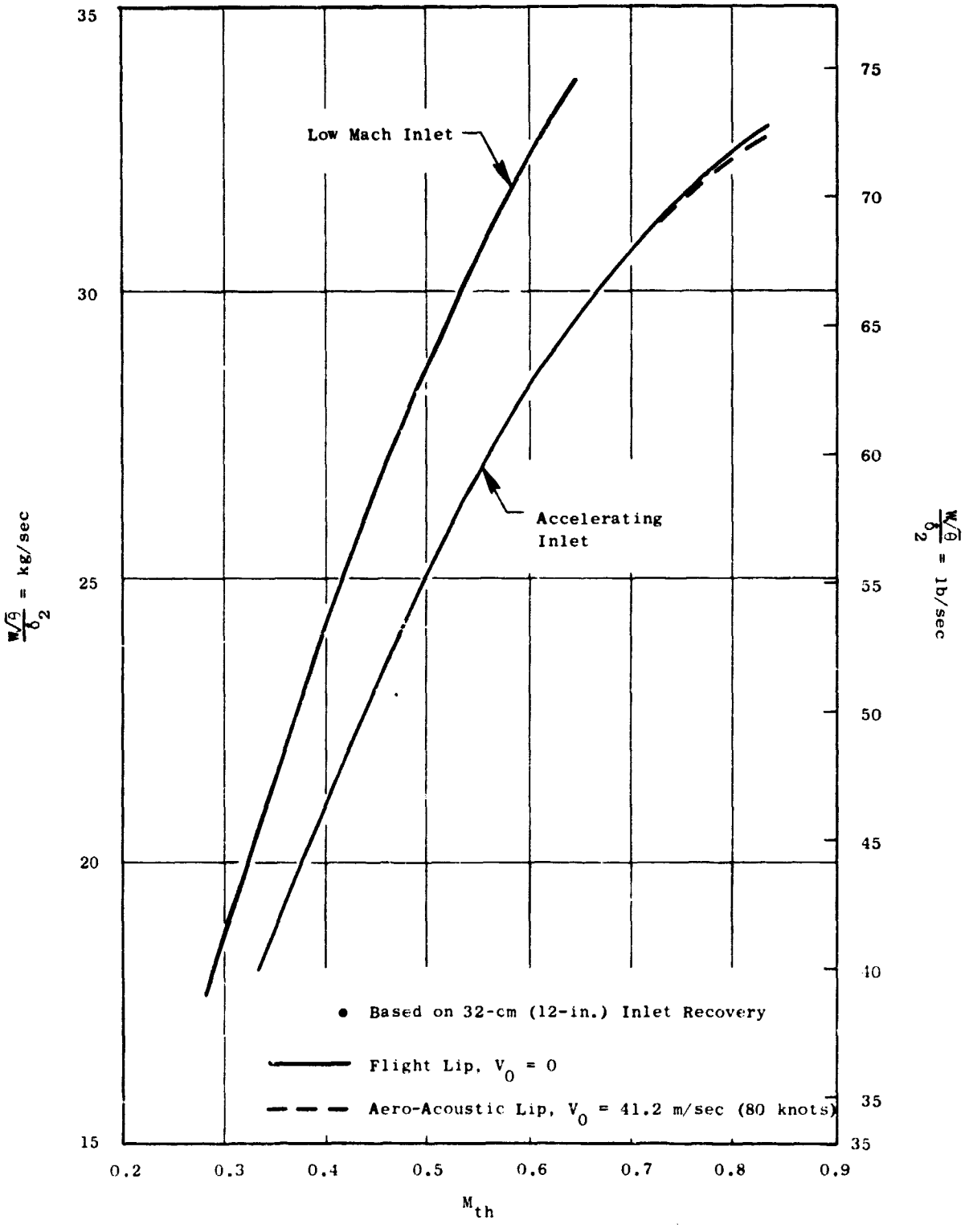

Figure 217. Relationship of Inlet Flow and Mach Number.

REFERENCES

1. Adamson, A.P., "Quiet Clean Short-Haul Experimental Engine (QCSEE) Design Rationale," Society of Automotive Engineers, Air Transportation Meeting, May 1975, Paper No. 750605.

2. Giffin, R.G., McFalls, R.A., and Beacher, B.F., "Aerodynamic and Aeromechanical Performance of a 50.8 cm (20 inch) Diameter 1.34 PR Variable-Pitch Fan with Core Flow," NASA CR-135017, March 1977.

3. "Quiet Clean Short-Haul Experimental Engine (QCSEE) Under-The-Wing (UTW) Final Design Report," NASA CR-134847, May 1978.

4. Clemons, A., and Motsinger, R.E., "Quiet Clean Short-Haul Experimantal Engine (QCSEE) Acoustic Treatment Development and Design," NASA CR-135266, May 1978.

5. Paul, D.L., "Quiet Clean Short-Haul Experimental Engine (QCSEE) Aerodynamic Characteristics of a 30.5 cm Diameter Inlet," NASA CR-134866, August 1975.

6. Glaser, F.W., Wazyniak, J.A., and Friedman, R., "Noise Data from Tests of a 1.83 m (6 ft) Diameter Variable Pitch, 1.2 Pressure Ratio Fan (QF9)," NASA TMX-3181, March 1975.

7. Rice, E.J., "Spinning Mode Sound Propagation in Ducts with Acoustic Treatment and Sheared Flow," NASA TMX-71672, March 1975.

8. Groeneweg, J.F., "Current Understanding of Helmholtz Resonator Arrays as Duct Boundary Conditions," NASA SP-207, 1969.

9. Dittmar, J.H., and Goeneweg, J.F., "Effect of Treated Length on Performance of Full-Scale Turbofan Inlet Noise Suppressors," NASA TN-D-7826, December 1974.

10. "UTW/OTW Preliminary Design Report," Volume I, NASA CR-134838, and Volume II, NASA CR-134839, December 1974.

11. Keith, J.S., et al., "Analytical Method for Predicting the Pressure Distribution About a Nacelle at Transonic Speeds," NASA CR-2217, July 1973.

12. Stimpert, D.L., and Clemons, A., "Acoustic Analysis of Aft Noise Reduction Techniques Measured on a Subsonic Tip Speed 50.8 cm (20 inch) Diameter Fan," NASA CR-134891, January 1977.